Craniodental Morphology and Phylogeny of Marsupials

ROBIN M.D. BECK, ROBERT S. VOSS,
AND SHARON A. JANSA

CRANIODENTAL MORPHOLOGY AND PHYLOGENY OF MARSUPIALS

ROBIN M.D. BECK

School of Science, Engineering and Environment

University of Salford, U.K.

School of Biological, Earth & Environmental Sciences

University of New South Wales, Australia

Division of Vertebrate Zoology (Mammalogy)

American Museum of Natural History

ROBERT S. VOSS

Division of Vertebrate Zoology (Mammalogy)

American Museum of Natural History

SHARON A. JANSA

Bell Museum and
Department of Ecology, Evolution, and Behavior

University of Minnesota

FRONTISPIECE. The honey opossum (*Tarsipes rostratus,* illustrated by Gould, 1863) has aptly been described as "a paragon of autapomorphic specialization" (Aplin and Archer, 1987).

CONTENTS

ABSTRACT

The current literature on marsupial phylogenetics includes numerous studies based on analyses of morphological data with limited sampling of Recent and fossil taxa, and many studies based on analyses of molecular data with dense sampling of Recent taxa, but few studies have combined both data types. Another dichotomy in the marsupial phylogenetic literature is between studies focused on New World taxa and those focused on Sahulian taxa. To date, there has been no attempt to assess the phylogenetic relationships of the global marsupial fauna based on combined analyses of morphology and molecular sequences for a dense sampling of Recent and fossil taxa. For this report, we compiled morphological and molecular data from an unprecedented number of Recent and fossil marsupials. Our morphological data consist of 180 craniodental characters that we scored for 97 terminals representing every currently recognized Recent genus, 42 additional ingroup (crown-clade marsupial) terminals represented by well-preserved fossils, and 5 outgroups (nonmarsupial metatherians). Our molecular data comprise 24.5 kb of DNA sequences from whole-mitochondrial genomes and six nuclear loci (*APOB*, *BRCA1*, *GHR*, *RAG1*, *RBP3* and *VWF*) for 97 marsupial terminals (the same Recent taxa scored for craniodental morphology) and several placental and monotreme outgroups. The results of separate and combined analyses of these data using a wide range of phylogenetic methods support many currently accepted hypotheses of ingroup (marsupial) relationships, but they also underscore the difficulty of placing fossils with key missing data (e.g., †*Evolestes*), and the unique difficulty of placing others that exhibit mosaics of plesiomorphic and autapomorphic traits (e.g., †*Yalkaparidon*). Unique contributions of our study are (1) critical discussions and illustrations of marsupial craniodental morphology including features never previously coded for phylogenetic analysis; (2) critical assessments of relative support for many suprageneric clades; (3) estimates of divergence times derived from tip-and-node dating based on uniquely taxon-dense analyses; and (4) a revised, higher-order classification of marsupials accompanied by lists of supporting craniodental synapomorphies. Far from the last word on these topics, this report lays the foundation for future research that may be enabled by the discovery of new fossil taxa, better-preserved material of previously described taxa, novel morphological characters (e.g., from the postcranium), and improved methods of phylogenetic analysis.

INTRODUCTION

Marsupialia (marsupials) comprises one of the three major extant mammalian clades, together with Placentalia (placentals) and Monotremata (monotremes). The name Marsupialia is now often used to refer to the crown clade—the last common ancestor of living marsupials and all its descendants (e.g., Rougier et al., 1998; Flynn and Wyss, 1999; Horovitz and Sánchez-Villagra, 2003; Sereno, 2006; Asher et al., 2007; Sánchez-Villagra et al., 2007; Horovitz et al., 2008, 2009; Forasiepi, 2009; Williamson et al., 2012, 2014; O'Leary et al., 2013; Beck et al., 2014; Forasiepi et al., 2014a; Wilson et al., 2016; Velazco et al., 2022). However, other recent studies have used the name Marsupialia in a more inclusive sense by incorporating fossil taxa that

appear to lie outside the crown clade (e.g., Kielan-Jaworowska et al., 2004; Case et al., 2005; Fox and Naylor, 2006; Davis, 2007; Beck et al., 2008b). Beck et al. (2014) provided the following crown-based definition of Marsupialia, which will be followed here: the least inclusive clade containing *Didelphis marsupialis* Linnaeus, 1758; *Caenolestes fuliginosus* (Tomes, 1863); and *Phalanger orientalis* (Pallas, 1766).

Marsupialia sits within the more inclusive (total, or stem-based) clade Metatheria, which comprises marsupials together with all taxa more closely related to Marsupialia than to Placentalia (Sereno, 2006; O'Leary et al., 2013). We follow Sereno's (2006: table 10.1) stem-based phylogenetic definition of Metatheria, namely the most inclusive clade containing *Didelphis marsupialis* Linnaeus, 1758, but not *Mus musculus* Linnaeus, 1758.

Living marsupials include >400 currently recognized species (~6% of modern mammalian diversity; Burgin et al., 2018; Eldridge et al., 2019; Mammal Diversity Database, 2021) belonging to seven clades that are currently ranked as orders in the Linnean hierarchy (table 1; Aplin and Archer, 1987; Wilson and Reeder, 2005; Burgin et al., 2018; Eldridge et al., 2019): Didelphimorphia (opossums), Paucituberculata (shrew opossums), Microbiotheria (the monito del monte, *Dromiciops gliroides*), Dasyuromorphia (predominantly carnivorous forms such as quolls, antechinuses, dunnarts, the Tasmanian devil, the numbat, and the recently extinct thylacine), Diprotododontia (possums, gliders, kangaroos, wallabies, rat kangaroos, wombats, koalas, etc.), Notoryctemorphia (marsupial moles), and Peramelemorphia (bandicoots and bilbies).

Dromiciops gliroides (the sole extant microbiotherian) and the three genera of modern paucituberculatans (*Caenolestes*, *Lestoros,* and *Rhyncholestes*, all members of the family Caenolestidae) are exclusively South American in distribution (Gardner, 2008). Fossil members of both orders are known from South America (e.g., Marshall, 1980; Marshall, 1982; Abello, 2013; Goin and Abello, 2013; Goin et al., 2016), and fossil microbiotherians are also known from Antarctica (Goin and Carlini, 1995; Goin et al., 1999, 2007c; Gelfo et al., 2019).

Extant didelphimorphians (all of which belong to the family Didelphidae) are predominantly Neotropical in distribution (Gardner, 2008; Voss and Jansa, 2009; Castro et al., 2021), with the unique exception of *Didelphis virginiana*, whose range extends from Central America to southern Canada. Interpretation of the fossil record of didelphimorphians is complicated by the fact that numerous dentally plesiomorphic metatherians, including many Mesozoic taxa, have often been referred to "Didelphimorphia" (sensu lato) by various authors (e.g., Kielan-Jaworowska et al., 2004; Case et al., 2005; Martin et al., 2005; Davis, 2007). However, phylogenetic analyses consistently indicate that "Didelphimorphia" in this latter sense is nonmonophyletic

because it includes both marsupials and nonmarsupial metatherians (Rougier et al., 1998; Luo et al., 2003; Sánchez-Villagra et al., 2007; Horovitz et al., 2008, 2009; Luo et al., 2011; Williamson et al., 2012, 2014; Wilson et al., 2016; Maga and Beck, 2017; Bi et al., 2018).

By contrast, monophyly of Didelphidae (crown-clade Didelphimorphia; Voss and Jansa, 2009) is strongly supported by both morphological and molecular data (Jansa and Voss, 2000; Voss and Jansa, 2003, 2009; Steiner et al., 2005; Jansa et al., 2014; Amador and Giannini, 2016), and didelphids may have diversified only within the past 20–30 million years (Jansa et al., 2014; Beck and Taglioretti, 2020; but see Steiner, et al., 2005; Mitchell, et al., 2014; Vilela, et al., 2015). Fossil didelphids are known almost exclusively from South America (Goin and Pardiñas, 1996; Goin, 1997a, 1997b; Cozzuol et al., 2006; Goin et al., 2009b, 2013; Voss and Jansa, 2009; Goin and de los Reyes, 2011; Antoine et al., 2013, 2016, 2017; Suárez Gómez, 2019; Beck and Taglioretti, 2020; Castro et al., 2021), with the exception of fossil remains of *Didelphis* from Pleistocene sites in North America (Bell et al., 2004; Morgan, 2018). South American fossil "sparassocynids" have also been generally accepted members of Didelphimorphia sensu stricto (i.e., more closely related to didelphids than to any other Recent family; Goin, 1991, 1995; Forasiepi et al., 2009; Engelman and Croft, 2014). However, Beck and Taglioretti (2020) concluded that "sparassocynids" fall within Didelphidae, as a lineage sister to *Monodelphis*, and assigned them tribal status (as Sparassocynini), which we follow here (table 2).

Of the remaining four modern orders, species of Dasyuromorphia, Diprotodontia, and Peramelemorphia today occur in mainland Australia, Tasmania, New Guinea, and surrounding islands, but the two extant notoryctemorphian species (*Notoryctes caurinus* and *N. typhlops*) occur only in the deserts of mainland Australia (Flannery, 1995a, 1995b; Van Dyck and Strahan, 2008). The known fossil record of these four orders is likewise restricted to this region (Archer, 1984c; Archer et al., 1999; Long et al., 2002; Archer and

TABLE 1

Higher Classification and Geographic Distribution of Recent Marsupials[a]

	Genera	Species	Distribution
DASYUROMORPHIA			
Dasyuridae	21[b]	77	Australia, New Guinea, and surrounding islands
Myrmecobiidae	1	1	Australia
Thylacinidae	1	1	Australia and New Guinea
DIDELPHIMORPHIA			
Didelphidae[c]	18	125	North and South America
DIPROTODONTIA			
Acrobatidae	2	3	Australia and New Guinea
Burramyidae	2	5	Australia and New Guinea
Hypsiprymnodontidae	1	1	Australia
Macropodidae	13[d]	67	Australia, New Guinea, and surrounding islands
Petauridae	4[e]	14	Australia, New Guinea, and surrounding islands
Phalangeridae	6	31	Australia, New Guinea, and surrounding islands
Phascolarctidae	1	1	Australia
Potoroidae	4	12	Australia
Pseudocheiridae	6	20	Australia, New Guinea, and surrounding islands
Tarsipedidae	1	1	Australia
Vombatidae	2	3	Australia
MICROBIOTHERIA			
Microbiotheriidae	1	1[f]	South America
NOTORYCTEMORPHIA			
Notoryctidae	1	2	Australia
PAUCITUBERCULATA			
Caenolestidae	3	7	South America
PERAMELEMORPHIA			
Chaeropodidae	1	2	Australia
Peramelidae[g]	6	26	Australia, New Guinea, and surrounding islands
Thylacomyidae	1	2	Australia
TOTAL	96	402	

[a] Classification above the species level follows Wilson and Reeder (2005), except where noted. Species-level classification follows Burgin et al. (2018), with updates from Eldridge et al. (2019) and the American Society of Mammalogists' Mammal Diversity Database except as noted. Recently extinct species have also been included.

[b] *Phascomurexia* and *Murexechinus* recognized as distinct from *Murexia*, following Van Dyck (2002).

[c] Classification above the species level follows Voss and Jansa (2009). Number of species from Voss (2022).

[d] *Notamacropus, and Osphranter* recognized as separate genera from *Macropus* following Jackson and Groves (2015) and Celik et al. (2019).

[e] *Dactylonax* recognized as a separate genus from *Dactylopsila*, following Thomas (1910) and Helgen (2007).

[f] D'Elia et al. (2016) recognized three species of *Dromiciops*, as did Burgin et al. (2018) and the American Society of Mammalogists' Mammal Diversity Database (https://www.mammaldiversity.org; accessed March 3, 2022). Subsequent morphological (Valladares-Gómez et al., 2017; Martin, 2018) and molecular (Suárez-Villota et al., 2018) studies, however, support the recognition of a single species (but see Quintero-Galvis et al., 2021, 2022).

[g] Some authors (e.g., Travouillon and Phillips, 2018) recognize Peroryctidae (which includes predominantly New Guinean taxa) as a separate family from Peramelidae (which includes predominantly Australian taxa).

Hand, 2006; Black et al., 2012b), with the possible exception of isolated tarsals from the Eocene of southern Argentina that may be diprotodontian (Lorente et al., 2016).[1]

Most phylogenetic analyses published over the past 15 to 20 years, particularly those using molecular or total-evidence datasets, have supported monophyly of the supraordinal clade that Szalay (1982a; 1982b; 1994) named Australidelphia, which includes the four Australian orders together with Microbiotheria (e.g., Phillips et al., 2001, 2006; Amrine-Madsen et al., 2003b; Horovitz and Sánchez-Villagra, 2003; Asher et al., 2004; Nilsson et al., 2004; Beck, 2008a, 2012; Beck et al., 2008a; Nilsson et al., 2010; Meredith et al., 2011; Mitchell et al., 2014; Lorente et al., 2016; Duchêne et al., 2018). Other superordinal relationships have proven more difficult to resolve confidently (Eldridge et al., 2019). However, retroposon insertion studies by Nilsson et al. (2010) and Gallus et al. (2015a) found relatively strong support for a clade comprising the four Australian orders (Eomarsupialia sensu Beck et al., 2014) to the exclusion of Microbiotheria and for positioning the root between Didelphimorphia and the other six orders. Recent molecular-sequence analyses have also consistently supported a clade comprising the orders Dasyuromorphia, Peramelemorphia, and Notoryctemorphia (e.g., Beck, 2008a; Meredith et al., 2011; Mitchell et al., 2014; Duchêne et al., 2018), as have some total-evidence analyses (Beck et al., 2008a; 2014; 2016; Beck, 2017a; Maga and Beck, 2017); Beck et al. (2014) named this clade Agreodontia. Gallus et al. (2015a) found that different

retroposon insertions support different branching patterns within Agreodontia and suggested that the reason for this is that the three orders diverged in quick succession, with phenomena such as independent lineage sorting, hybridization, and/or gene flow resulting in conflicting phylogenetic signals. However, the recent phylogenomic study of Duchêne et al. (2018) found strong support for a sister-taxon relationship between Notoryctemorphia and Peramelemorphia to the exclusion of Dasyuromorphia.

Intraordinal relationships are also not fully resolved, with particular uncertainty surrounding the relationships among didelphid subfamilies (Voss and Jansa, 2009) and among phalangeridan diprotodontians (Phillips and Pratt, 2008; Duchêne et al., 2018). Another problem is that relatively few fossil taxa have been included in published phylogenies of higher-level marsupial relationships (Sánchez-Villagra, 2001; Sánchez-Villagra et al., 2007; Beck et al., 2008a, 2014, 2016; Horovitz et al., 2008, 2009; Abello and Candela, 2010, 2019; Beck, 2012, 2017a; Maga and Beck, 2017; Zimicz and Goin, 2020), limiting the usefulness of such phylogenies for comparative analyses of trait evolution (Slater et al., 2012), diversification (Rabosky, 2010, 2016), and biogeography (Crisp et al., 2011).

In contrast with the currently restricted distribution of Recent marsupials, fossil metatherians are known from every continent, including Antarctica (Weisbecker and Beck, 2015; Eldridge et al., 2019). The oldest metatherian was previously thought to be †*Sinodelphys szalayi*, from the Early Cretaceous (Barremian; ~126 Mya) of China (Luo et al., 2003), but this taxon has subsequently been reinterpreted as a eutherian (Bi et al., 2018). Thus, the oldest metatherian fossils currently known are fragmentary dental remains from the Aptian-Albian of North America (Davis et al., 2008; Davis and Cifelli, 2011; Williamson et al., 2014; Cifelli and Davis, 2015). However, the description of a probable eutherian, †*Juramaia sinensis*, from the Middle Jurassic of China suggests that the Eutheria-Metatheria split might be as old as 160 Mya (Luo et al., 2011), congru-

---

[1] †*Chulpasia* is the sole example of a genus-level marsupialiform taxon known from both South America and Australia: the type species, †*C. mattaueri*, is from the late Paleocene or earliest Eocene Laguna Umayo Fauna of Peru and a second species, †*C. jimthorselli*, has been described from the earliest Eocene Tingamarra Local Fauna of southeastern Australia, with both species represented by isolated molars (Crochet and Sigé, 1993; Sigé et al., 2004, 2009). However, the precise relationship of †*Chulpasia* and a second Tingamarran genus, †*Thylacotinga* (which has been referred to the same subfamily, Chulpasiinae), to other marsupialiforms and to crown-clade marsupials in particular is debated (Goin and Candela, 2004; Beck et al., 2008b; Sigé et al., 2009; Chornogubsky and Goin, 2015; Goin et al., 2016, 2020; Métais et al., 2018).

ent with several recent molecular estimates for this divergence (Meredith et al., 2011; dos Reis et al., 2012; Tarver et al., 2016).[2]

Current evidence suggests that many fossil metatherians are either stem taxa or only questionably members of Marsupialia (Rougier et al., 1998, 2004, 2015; Luo et al., 2003; Goin et al., 2006; Ladevèze and Muizon, 2007; Sánchez-Villagra et al., 2007; Beck et al., 2008a; Horovitz et al., 2008, 2009; Forasiepi, 2009; Ladevèze and Muizon, 2010; Luo et al., 2011; Beck, 2012, 2017a; Williamson et al., 2012, 2014; Engelman and Croft, 2014; Forasiepi et al., 2014a; Wilson et al., 2016; Carneiro and Oliveira, 2017a, 2017b; Maga and Beck, 2017; Bi et al., 2018; Carneiro, 2018, 2019; Carneiro et al., 2018; Engelman et al., 2020; Muizon et al., 2018; Ladevèze et al., 2020; Muizon and Ladevèze, 2020).[3] This is the case for all known Mesozoic forms (e.g., †*Asiatherium*, deltatheroidans, "alphadontids," "pediomyids," stagodontids), the predominantly Laurasian Cenozoic taxa traditionally referred to the families †Herpetotheriidae and †Peradectidae (neither of which was recovered as monophyletic in the phylogenetic analyses of Williamson et al., 2012, 2014), and South American Cenozoic groups such as pucadelphyids, protodidelphids, caroloameghiniids, derorhynchids, sparassodontans, and polydolopimorphians (Eldridge et al., 2019). Definitive (crown-clade) marsupials are known only from the Cenozoic and (with the exception of living North American species descended from South American immigrants; Jansa et al., 2014) are entirely Gondwanan in distribution (Beck, 2017a). Of these, nearly all can

be identified as belonging to one or another of the seven Recent orders, with a handful of exceptions (Beck et al., 2008a, 2014; Beck, 2012).

To date, available morphological and total-evidence phylogenies focusing on the higher-level relationships of Marsupialia have suffered from limited taxon sampling (Horovitz and Sánchez-Villagra, 2003; Asher et al., 2004; Beck et al., 2008a, 2014, 2016; Horovitz et al., 2008, 2009; Beck, 2012, 2017a; Maga and Beck, 2017), whereas molecular phylogenies, some of which are taxonomically densely sampled (e.g., Kirsch et al., 1997; Meredith et al., 2009a; Mitchell et al., 2014; May-Collado et al., 2015; Álvarez-Carretero et al., 2021), are necessarily restricted to extant or recently extinct species. Thus, our understanding of the evolution and biogeography of marsupials has been hampered by the absence of a reasonably comprehensive, quantitative, character-based phylogeny of the group that includes a diverse sampling of extant and fossil taxa.

Estimates of divergence times are necessary to compute metrics such as absolute rates of lineage diversification and trait evolution from molecular phylogenies, and such estimates typically require the use of fossil evidence for calibration purposes (Ho and Phillips, 2009). Unfortunately, many marsupial fossils used for molecular node-dating (sensu Ronquist et al., 2012a; O'Reilly et al., 2015; O'Reilly and Donoghue, 2016) have not had their evolutionary relationships tested by formal phylogenetic analysis (e.g., some of those used by Beck, 2008a; Meredith et al., 2008b, 2009a, 2009c, 2011; Mitchell et al., 2014; Duchêne et al., 2018; Álvarez-Carretero et al., 2021). Tip-dating and tip-and-node dating are promising alternatives to traditional node-dating (but see O'Reilly et al., 2015) that involve simultaneous analyses of character and temporal data from Recent and fossil taxa (Ronquist et al., 2012b; O'Reilly and Donoghue, 2016; Zhang et al., 2016). Tip-and-node dating has been implemented on reasonably comprehensive total-evidence datasets for the marsupial orders Dasyuromorphia (Kealy

---

[2] Note, however, that the reported age of †*Juramaia* has been questioned (Meng, 2014; Sullivan et al., 2014; Bi et al., 2018), and that the molecular-clock study of Álvarez-Carretero et al. (2021)—which used †*Sinodelphys*, not *Juramaia*, to provide a minimum bound on the age of the Eutheria-Metatheria split—found that the divergence between eutherians and metatherians might be as young as 123 Mya.

[3] The recent study of Velazco et al. (2022) is a notable exception, suggesting that †*Deltatheridium* from the Late Cretaceous of Mongolia and †*Pucadelphys* from the Paleocene of Bolivia (see the account for †*Pucadelphys* in appendix 2) are both marsupials, rather than nonmarsupial metatherians (as in the other studies cited here).

and Beck, 2017), Peramelemorphia (Travouillon and Phillips, 2018), and Didelphimorphia (Beck and Taglioretti, 2020), but previously published tip-and-node dated phylogenetic analyses of total-evidence datasets for Marsupialia as a whole are characterized by sparse taxon sampling (Beck et al., 2016; Maga and Beck, 2017), limiting their usefulness.

The current study attempts to remedy such shortcomings. Our phylogenetic dataset includes 24.5 kb of DNA sequence data from whole mitochondrial genomes and six nuclear loci (*APOB*, *BRCA1*, *GHR*, *IRBP*, *RAG1*, and *VWF*) for 97 ingroup (marsupial) terminals representing at least one member of every currently recognized Recent genus. We analyze these DNA data separately and in combination with 180 craniodental characters. In the process of describing our craniodental characters, we provide a detailed overview of the comparative craniodental morphology of marsupials, including discussion of additional morphological variation that we were unable to consistently parse into discrete characters. Similar to the DNA dataset, we scored this craniodental dataset for 97 ingroup (marsupial) terminals representing at least one member of every currently recognized Recent genus, as well as a further 42 fossil ingroup terminals and five fossil outgroup terminals. We analyzed these data using maximum parsimony (craniodental dataset only), undated Bayesian (DNA, craniodental, and combined DNA and craniodental datasets), and Bayesian tip-and-node dating (combined DNA and craniodental dataset) approaches. Our results effectively summarize the evidence at hand for inferring marsupial relationships and provide a basis for future studies of metatherian evolution and biogeography.

MATERIALS AND METHODS

Ingroup Taxon Sampling

The designated ingroup for our study is Marsupialia, including the seven currently recognized extant orders together with crown-clade fossil taxa (table 2). To ensure a comprehensive sampling of Recent marsupials, we included at least one representative of every Recent marsupial genus recognized by Wilson and Reeder (2005), with exceptions as noted in the footnotes to table 2. To avoid future nomenclatural confusion in the event of future taxonomic splitting, we tried to score data from the type species of each genus.

In general, we avoided combining morphological data from multiple species, with three exceptions (see table S1 in the online supplement: https://doi.org/10.5531/sd.sp.54): (1) We scored morphological characters for *Caenolestes* based on specimens of *C. fuliginosus* (the type species of *Caenolestes*), *C. caniventer*, *C. convelatus*, and unidentified material that preserves important morphological features (notably the deciduous dentition; see also Luckett and Hong, 2000) that were missing in all *C. fuliginosus* individuals examined; monophyly of *Caenolestes* relative to other extant caenolestids is strongly supported by both mitochondrial sequence data and combined mitochondrial and morphological data (Ojala-Barbour et al., 2013). (2) Morphological data for *Chaeropus* were obtained from specimens of *C. ecaudatus*, but also from specimens that were subsequently described as a second species, *C. yirratji* (see Travouillon et al., 2019). (3) Morphological data for *Phalanger* were obtained from specimens of *P. orientalis* (the type species of *Phalanger*), *P. intercastellanus*, and *P. mimicus*, which collectively appear to comprise a closely related species complex (Colgan et al., 1993; Norris and Musser, 2001; Kealy et al., 2019).

In compiling DNA data for our analyses, the following Recent terminals represent composites of more than one congeneric species (see table S1 in the online supplement): the didelphids *Caluromys*, *Didelphis*, *Gracilinanus*, *Marmosops*, *Monodelphis*, *Philander*, and *Thylamys*; the dasyurids *Antechinus*, *Dasyurus*, *Myoictis*, *Ningaui*, and *Planigale*; the peramelid *Echymipera*; the burramyid *Cercartetus*; the macropodoids *Bettongia*, *Dendrolagus*, *Dorcopsis*,

TABLE 2

Assumed Classification of Marsupial Ingroup Genera Scored for Phylogenetic Analysis[a]

DIDELPHIMORPHIA
    Didelphidae[b]
        Caluromyinae
            Caluromys
            Caluromysiops
        Didelphinae
            Didelphini
                Chironectes
                Didelphis
                Lutreolina
                Philander
                †*Thylophorops*
            Marmosini
                Marmosa
                Tlacuatzin[c]
            Metachirini
                Metachirus
            Monodelphini
                Monodelphis
                †*Thylatheridium*
            †Sparassocynini
                †*Hesperocynus*
                †*Sparassocynus*
            Thylamyini
                Chacodelphys
                Cryptonanus
                Gracilinanus
                Lestodelphys
                Marmosops
                Thylamys
        Glironiinae
            Glironia
         Hyladelphinae
            Hyladelphys

PAUCITUBERCULATA[d]
    Caenolestoidea
        Caenolestidae
            Caenolestes
            Lestoros
            Rhyncholestes
            †*Stilotherium*
    †Palaeothentoidea
        †Palaeothentidae
            Acdestinae
                †*Acdestis*
            Palaeothentinae
                †*Palaeothentes*
        †Pichipilidae
            †*Pichipilus*
    incertae sedis
        †*Evolestes*

TABLE 2 *continued*

MICROBIOTHERIA
        Microbiotheriidae
                Dromiciops

NOTORYCTEMORPHIA
        Notoryctidae
                Notoryctes

DASYUROMORPHIA[e]
        Dasyuridae
                Dasyurinae
                        Dasyurini[f]
                                Dasycercus
                                Dasykaluta
                                Dasyuroides
                                Dasyurus
                                Myoictis
                                Neophascogale
                                Parantechinus
                                Phascolosorex
                                Pseudantechinus
                                Sarcophilus
                        Phascogalini[f]
                                Antechinus
                                Micromurexia
                                Murexia
                                Murexichinus
                                Paramurexia
                                Phascogale
                                Phascomurexia
                Sminthopsinae
                        Planigalini[f]
                                Planigale
                        Sminthopsini[f]
                                Antechinomys
                                Ningaui
                                Sminthopsis
        Myrmecobiidae
                Myrmecobius
        Thylacinidae
                †*Nimbacinus*
                Thylacinus
        ?Thylacinidae
                †*Badjcinus*[g]
        incertae sedis
                †*Barinya*[h]
                †*Mutpuracinus*[i]

PERAMELEMORPHIA[j]
        Perameloidea
                Chaeropodidae
                        Chaeropus
                Peramelidae
                      Peramelinae
                              Isoodon
                              Perameles
                      Echymiperinae

TABLE 2 *continued*

> > > > *Echymipera*
> > > > *Microperoryctes*
> > > > *Rhynchomeles*
> > > Peroryctinae
> > > > *Peroryctes*
> > Thylacomyidae
> > > *Macrotis*
> †Yaraloidea
> > †Yaralidae
> > > †*Yarala*
> incertae sedis
> > > †*Bulungu*
> > > †*Galadi*

DIPROTODONTIA[k]
> Vombatiformes
> > Phascolarctidae
> > > †*Litokoala*
> > > †*Nimiokoal*a
> > > *Phascolarctos*
> > Vombatidae
> > > *Lasiorhinus*
> > > *Vombatus*
> > > †*Warendja*
> > †Diprotodontidae
> > > †*Neohelos*
> > > †*Ngapakaldia*
> > > †*Nimbadon*
> > > †*Silvabestius*
> > †Thylacoleonidae
> > > †*Priscileo*
> > > †*Thylacoleo*
> > > †*Wakaleo*
> > †Ilariidae
> > > †*Ilaria*
> > †Wynyardiidae
> > > †*Muramura*
> > > †*Namilamadeta*

Vombatomorphia

> Phalangerida[l]
> > Burramyidae
> > > *Burramys*
> > > *Cercartetus*
> > Phalangeridae
> > > Ailuropinae
> > > > *Ailurops*
> > > > *Strigocuscus*
> > > Phalangerinae
> > > > *Phalanger*
> > > > *Spilocuscus*
> > > Trichosurinae
> > > > *Trichosurus*
> > > > *Wyulda*
> > > incertae sedis
> > > > †*Onirocuscus*[m]
> > > > "*Trichosurus*" †*dicksoni*[m]

TABLE 2 *continued*

Pseudocheiridae

    Pseudocheirinae

        Pseudocheirus

        Pseudochirulus

    Pseudochiropsinae

        Pseudochirops[n]

        Petropseudes[n]

    Hemibelideinae

        Hemibelideus

        Petauroides

Petauridae

    Dactylopsilinae

        Dactylonax[o]

        Dactylopsila

    Petaurinae

        Petaurus

    incertae sedis

        Gymnobelideus[p]

Tarsipedidae

        Tarsipes

Acrobatidae

        Acrobates

        Distoechurus

Petauroidea

Macropodiformes[q]

    Hypsiprymnodontidae

        Hypsiprymnodon

    Macropodidae

        Macropodinae

            Dendrolagini

                †*Bohra*

                Dendrolagus

                Petrogale

                Thylogale

            Dorcopsini

                Dorcopsis

                Dorcopsulus

            Macropodini

                Lagorchestes

                Macropus

                Notamacropus[s]

                Osphranter[s]

                Wallabia

            Setonichini

                Setonix

            incertae sedis

                Onychogalea

        Lagostrophinae

            Lagostrophus

        †"Bulungamayinae"[r]

            †*Ganguroo*

        Sthenurinae

            †*Hadronomas*

            †*Rhizosthenurus*

    Potoroidae

        Bettongini

            Aepyprymnus

TABLE 2 *continued*

$$\begin{array}{l}
\qquad\qquad\qquad\qquad \textit{Bettongia} \\
\qquad\qquad\quad \text{Potoroini} \\
\qquad\qquad\qquad\qquad \textit{Potorous} \\
\qquad\qquad\quad \text{incertae sedis} \\
\qquad\qquad\qquad\qquad \text{?}\textit{Bettongia} \dagger\textit{moyesi}^{\text{s}} \\
\qquad\qquad\qquad\qquad \textit{Caloprymnus}^{\text{t}}
\end{array}$$

        †Balbaridae
                †*Balbaroo*
                †*Ganawamaya*
        incertae sedis
                †Propleopinae[u]
                        †*Ekaltadeta*

†YALKAPARIDONTIA[v]
        †Yalkaparidontidae
                †*Yalkaparidon*

---

[a] Classification of Recent genera follows Wilson and Reeder (2005) and Jackson and Groves (2015) except where noted. Classification of fossil genera indicated where relevant.

[b] Classification follows Voss and Jansa (2009), except that we follow Beck and Taglioretti (2020) in also recognizing the tribes Monodelphini and †Sparassocynini (but see Voss, 2022: appendix 1).

[c] *Tlacuatzin* is here included within Marmosini following Voss and Jansa (2009), although it may warrant tribal distinction (Beck and Taglioretti, 2019; but see Voss, 2022).

[d] Classification of fossil genera follows Goin et al. (2009a: table 3) and Abello (2013).

[e] Classification follows Kealy and Beck (2017).

[f] Recognized as a subfamily by Jackson and Groves (2015).

[g] Described as a thylacinid by Muirhead and Wroe (1998), but not consistently recovered as a thylacinid by Kealy and Beck (2017).

[h] Described as a dasyurid by Wroe (1999), but not recovered as a dasyurid by Kealy and Beck (2017) or Rovinsky et al. (2019).

[i] Described as a thylacinid by Murray and Megirian (2000, 2006a), but not recovered as a thylacinid by Kealy and Beck (2017) or Rovinsky et al. (2019).

[j] Classification of fossil genera follows Warburton and Travouillon (2016: table 1).

[k] Classification of fossil genera follows Aplin and Archer (1987) and Long et al. (2002), except where noted.

[l] Definition of Phalangerida follows Aplin and Archer's (1987) original usage; Jackson and Groves (2015) instead recognized Phalangerida as comprising Phalangeridae, Burramyidae, and Petauroidea only, with Macropodiformes as a separate suborder.

[m] †*Onirocuscus reidi* (originally named "*Strigocuscus*" †*reidi*) and "*Trichosurus*" †*dicksoni* were both referred to extant genera in their original descriptions by Flannery et al. (1987), but this was rejected by Crosby (2007; see especially figure 7 of that paper). Both Flannery et al.'s (1987) and Crosby's (2007: fig. 7) proposed phylogenies of Phalangeridae are strongly incongruent with current molecular evidence (reviewed by Eldridge et al., 2019: 811), and so we consider that relationships of †*Onirocuscus* and "*Trichosurus*" †*dicksoni* to the modern phalangerid subfamilies uncertain.

[n] *Pseudochirops* has been consistently recovered as paraphyletic with respect to *Petropseudes* in recent molecular phylogenetic analyses (Meredith et al. 2009a; 2009b; Mitchell et al., 2014; May-Collado et al., 2015).

[o] Recognized as a separate genus by Thomas (1910) and Helgen (2007) but included within *Dactylopsila* by Jackson and Groves (2015).

[p] Placed within Dactylopsilinae by Groves and Jackson (2015), but its precise relationship to other petaurids remains unclear (Eldridge et al., 2019: 811).

[q] We follow den Boer and Kear (2018) in referring to the crown clade as Macropodoidea and the total clade as Macropodiformes.

[r] †"Bulungamayinae" appears to be paraphyletic relative to living crown-clade macropodids (Cooke, 1999; Prideaux and Warburton, 2010).

[s] Referred to the modern genus *Bettongia* by Flannery and Archer (1987; see also Flannery, 1989), but does not form a clade with extant *Bettongia* in several recent phylogenetic analyses (e.g., Butler et al., 2018; den Boer and Kear, 2018: supplementary data; Travouillon et al., 2022).

[t] On morphological grounds, most (but not all) authors have placed *Caloprymnus* within Bettongini (see Kear and Cooke, 2001: 90), but limited mitochondrial DNA data place it within Potoroini (Westerman et al., 2004).

[u] †*Ekaltadeta* and other propleopines have been referred to Hypsiprymnodontidae by several authors (e.g., Kear and Cooke, 2001), but this relationship has not been consistently supported in recent phylogenetic analyses of macropodiform phylogeny (e.g., Butler et al., 2018; den Boer and Kear, 2018: supplementary data).

[v] Recognized as a distinct order following Archer et al. (1988) and Beck et al. (2014). Some published phylogenetic analyses place †*Yalkaparidon* within Australidelphia, but others place it in a clade with paucituberculatans (Beck et al., 2014; Beck et al., 2016; Beck, 2017a; Abello and Candela, 2019; Zimicz and Goin, 2020).

Macropus, *Notamacropus*, *Petrogale*, and *Thylogale*; the phalangerid *Phalanger*; and the vombatid *Lasiorhinus*. Recent phylogenetic analyses indicate that all sets of congeneric species combined to form these Recent terminals represent monophyletic clusters relative to our other Recent and fossil taxa (Meredith et al., 2009a, 2009b; Voss and Jansa, 2009; Westerman et al., 2012, 2016; Mitchell et al., 2014; Dodt et al., 2017; Kealy and Beck, 2017; Nilsson et al., 2018; Travouillon and Phillips, 2018).

Our fossil ingroup taxa include 42 terminals that have been consistently recovered as crown-clade marsupials in previous phylogenetic studies. To maximize the phylogenetic informativeness of included fossils, we chose plesiomorphic members of speciose clades—on the assumption that these would be more likely to subdivide otherwise long branches than highly derived representatives—and taxa represented by relatively complete specimens. Additionally, we included the early Eocene peradectid †*Mimoperadectes* and the early Oligocene herpetotheriid †*Herpetotherium*, whose relationships to Marsupialia are not fully resolved, although they usually fall close to, but outside, the crown clade (Sánchez-Villagra et al., 2007; Beck et al., 2008a; Horovitz et al., 2008, 2009; Beck, 2012, 2017a; Beck et al., 2014, 2016; Wilson et al., 2016; Carneiro and Oliveira, 2017a, 2017b; Maga and Beck, 2017; Carneiro, 2018, 2019; Carneiro et al., 2018; Muizon et al., 2018; Rangel et al., 2019; Ladevèze et al., 2020).

Insofar as possible, we scored each fossil terminal based on specimens of a single species (usually the type species of the genus; see appendix 1 and table S1 in the online supplement). However, the following terminals were scored based on individuals of multiple species, because we felt that the advantage of more complete character scoring outweighed the risk of potential nonmonophyly in these cases (see appendix 1 and table S1 in the online supplement): the paucituberculatans †*Acdestis* (†*A. maddeni*, †*A. oweni*, and †*A. spegazzinii*) and †*Palaeothentes* (†*P. lemoinei* and †*P. minutus*); the diprotodon-

tids †*Ngapakaldia* (†*N. tedfordi*, †*N. bonythoni*, and †*N.* sp.) and †*Silvabestius* (†*S. michaelbirti* and †*S. johnnilandi*); the phascolarctid †*Litokoala* (†*L. kutjamarpensis* and †*L. dicksmithi*); and the wynyardiids †*Muramura* (†*M. pinpensis* and †*M. williamsi*) and †*Namilamadeta* (†*N. albivenator*, †*N. crassirostrum*, and †*N. superior*). In fact, monophyly of each of these sets of congeneric species seems highly likely based on the evidence at hand (Pledge, 2003; 2005; Abello, 2007; Black, 2008; Black, 2010; Black et al., 2012a; Abello, 2013; Black et al., 2014a). Appendix 1 provides further details regarding our fossil ingroup terminals, including locality information and probable age(s) of the specimens from which we recorded data, and additional remarks regarding their significance.

Rooting and Outgroup Taxa

For our molecular analyses, we used the same outgroups as Mitchell et al. (2014): the extant monotremes *Ornithorhynchus anatinus* and *Tachyglossus aculeatus*, together with the extant placentals *Elephas maximus*, *Trichechus manatus*, *Bradypus tridactylus*, *Dasypus novemcinctus*, *Mus musculus*, *Homo sapiens*, *Bos taurus*, and *Canis lupus* (see table S1 in the online supplement).

However, monotremes differ markedly from marsupials and stem metatherians in many aspects of their craniodental morphology (with Recent monotremes entirely lacking functional dentitions; Archer et al., 1993b; Kielan-Jaworowska et al., 2004; Crompton et al., 2018), as do placentals and stem eutherians (albeit to a lesser extent; Kielan-Jaworowska et al., 2004; Wible et al., 2005). Therefore, adding monotremes, placentals, or stem eutherians to our morphological matrix would have required the inclusion of many additional morphological characters and character states to account for such differences. Doing so would also have raised several problematic issues of homology, for example, regarding postcanine dental loci in eutherians and metatherians (table 12; Averianov et al., 2010; O'Leary et al., 2013). For

this reason, we did not use monotremes, placentals, or stem eutherians as outgroups for our morphological or total-evidence matrices. Instead, we included three well-preserved Paleocene fossil metatherians: †*Pucadelphys andinus*, †*Mayulestes ferox*, and †*Allqokirus australis*. These three taxa consistently fall outside Marsupialia, and more distant from the crown clade than either †*Herpetotherium* or †*Mimoperadectes*, in most recent phylogenetic analyses (see Rougier et al., 1998, 2004, 2015; Luo et al., 2003; Ladevèze and Muizon, 2007; Sánchez-Villagra et al., 2007; Beck et al., 2008a, 2014; Horovitz et al., 2008, 2009; Forasiepi, 2009; Ladevèze and Muizon, 2010; Luo et al., 2011; Beck, 2012, 2017a; Williamson et al., 2012, 2014; Engelman and Croft, 2014; Forasiepi et al., 2014a; Suarez et al., 2015; Ni et al., 2016; Wilson et al., 2016; Carneiro and Oliveira, 2017a, 2017b; Maga and Beck, 2017; Bi et al., 2018; Carneiro et al., 2018; Engelman et al., 2020; Muizon et al., 2018; Abello and Candela, 2019; Carneiro, 2019; Rangel et al., 2019; Ladevèze et al., 2020).However, the phylogenetic analyses of Goin et al. (2006) and Velazco et al. (2022) are notable exceptions to this (see the account for †*Pucadelphys* in appendix 1). All three are represented by exceptionally complete cranial material (Muizon, 1994, 1998; Marshall and Muizon, 1995; Ladevèze and Muizon, 2007; Ladevèze et al., 2011; Muizon et al., 2018).

In our dated total-evidence analysis, calibrated nodes needed to be constrained as monophyletic. To calibrate deep divergences within Marsupialia, we constrained the root between Didelphimorphia and the rest of Marsupialia; five uncontradicted retroposon insertions provide statistically significant support for this rooting position (Nilsson et al., 2010; Gallus et al., 2015a). We also constrained †*Herpetotherium* (the relationships of which are unresolved in our morphological and undated total-evidence analyses) to fall outside Marsupialia, in agreement with the majority of published phylogenetic analyses (Beck et al., 2008a,

2014, 2016; Horovitz et al., 2008, 2009; Forasiepi et al., 2014a; Suarez et al., 2015; Lorente et al., 2016; Carneiro and Oliveira, 2017a, 2017b; Maga and Beck, 2017; Carneiro, 2018, 2019; Carneiro et al., 2018; Engelman et al., 2020; Muizon et al., 2018; Abello and Candela, 2019; Rangel et al., 2019; Ladevèze et al., 2020; Muizon and Ladevèze, 2020). A full justification for constraining and calibrating these and other nodes is given in appendix 2.

Morphological Character Selection and Scoring

The morphological characters used in this study are taken solely from the cranium, mandible, and dentition. Although the postcranium and soft tissues represent additional valuable sources of morphological characters (see, e.g., Szalay, 1982a; 1994; Szalay and Sargis, 2001, 2006; Horovitz and Sánchez-Villagra, 2003; Voss and Jansa, 2003, 2009; Flores, 2009; Kealy and Beck, 2017), most of the fossil taxa and some of the Recent terminals included in the current study are represented only by craniodental material, and hence would necessarily have to be scored as unknown for characters from other anatomical systems.

We initially identified a large pool of candidate craniodental characters by examining published morphological datasets focused on higher-level marsupial and metatherian relationships (e.g., Springer et al., 1997; Rougier et al., 1998; Sánchez-Villagra and Wible, 2002; Horovitz and Sánchez-Villagra, 2003; Luo et al., 2003; Goin et al., 2006; Sánchez-Villagra et al., 2007; Beck et al., 2008a; Horovitz et al., 2008, 2009; Beck, 2012), as well as those intended to resolve relationships among marsupial subclades such as macropodiforms (Prideaux, 2004; Kear et al., 2007), didelphids (Voss and Jansa, 2003; 2009), paucituberculatans (Abello, 2007; Goin et al., 2009a), peramelemorphians (Muirhead, 1994; Travouillon et al., 2010; Gurovich et al., 2014), dasyuromorphians (Wroe et al., 2000; Wroe and Musser, 2001; Murray and Megirian, 2006a), pseudocheirids (Roberts, 2008), phalangerids

(Crosby, 2002b), and vombatiforms (Gillespie, 2007; Black, 2008; Black et al., 2012a). Studies that did not carry out explicit phylogenetic analyses of morphological characters but that nevertheless provided morphological data bearing on marsupial phylogeny were also examined for potential characters; these included anatomical descriptions (e.g., Aplin, 1987; 1990; Wroe et al., 1998; Cooke, 2000; Wible, 2003) and reviews of marsupial phylogeny (e.g., Archer, 1984b, 1984c; Aplin and Archer, 1987; Marshall et al., 1990).

We evaluated this initial pool of characters against our own observations of relevant taxa and eliminated all that were poorly defined or otherwise unclear, that seemed to exhibit continuous variation that could not easily be parsed into discrete states, or that clearly overlapped with others. Many characters were retained essentially unchanged from these previous studies. However, others were significantly modified or redefined to better correspond with our own observations and hypotheses of homology and to take full account of the range of variation seen in our taxon set. We also identified additional morphological characters that—as far as we are aware—have not been used in previous studies of marsupial phylogeny. Our final morphological dataset of 102 craniomandibular and 78 dental characters is restricted to just those that we could score consistently and confidently over our entire taxon set and for which homologies appear to be relatively straightforward. Although our morphological character set might be considered scanty in comparison to the number of taxa in our study, we believe it preferable to use only characters that have been carefully evaluated and can be scored unambiguously for all taxa.

We made a deliberate attempt to identify and score autapomorphies for three main reasons (see also Voss and Jansa, 2003: 8): First, such autapomorphies may become synapomorphies with denser taxon sampling. Second, the inclusion of autapomorphies is important for analyses that use the Mk model and its variants for discrete morphological data, particularly those employing tip- and tip-and-node dating (Lewis,

2001; Müller and Reisz, 2006; Wright and Hillis, 2014; Lee and Palci, 2015; Matzke and Irmis, 2018). Third, the supposed correction to the Mk model implemented by MrBayes for datasets that include only parsimony-informative characters (Nylander et al., 2004; Ronquist et al., 2005; Allman et al., 2010; Ronquist et al., 2011) does not appear to be computationally feasible for nonbinary characters (which are used extensively here), and so is unlikely to function as intended (Koch and Holder, 2012; dos Reis et al., 2016; Matzke, 2016; Matzke and Irmis, 2018).

Wherever possible, we scored morphological characters from multiple specimens of each taxon, ideally including juveniles (with incompletely erupted dentitions), both young and old adults (distinguished largely based on the degree of ossification and tooth wear) and both males and females. This strategy allowed us to score characters that were ascertainable only during particular ontogenetic stages (for example, features of the deciduous dentition) and to assess the overall impact of ontogeny (for example, the increased ossification, sutural fusion, and tooth wear that typically accompany advancing age) and sexual dimorphism. However, such inclusive sampling was not possible for most fossil taxa, with the notable exceptions of the diprotodontid †*Nimbadon* (known from a large ontogenetic series; Black et al., 2010) and the stem taxon †*Pucadelphys* (known from multiple putative males and females; Ladevèze et al., 2011). For most other fossil taxa, the absence of ontogenetic series and/or information about sex dictated conservative scoring. For example, dental characters that can be confidently determined only from unworn or lightly worn teeth (such as the presence or absence of a posterior lobe on i3; char. 150) were not scored if the only available specimens exhibited substantial dental wear. By contrast, the morphology of the palatal vacuities (if present; chars. 35–39) and the presence or absence of a sagittal crest (char. 27) were scored based on adult specimens only, because these features are fully developed only in mature individuals (see, e.g., Flores et al., 2003, 2006, 2010,

2013; Black et al., 2010). Characters that we scored based on specimens of a particular ontogenetic stage (or stages) are indicated in our character list as appropriate. We examined damaged or disarticulated skulls, where available, in addition to intact specimens, to facilitate scoring of characters of regions that are often concealed in intact skulls, such as the middle ear. We scored all our terminals based on firsthand examination of specimens, with the exception of a single outgroup taxon, †*Allqokirus australis*, for which we relied upon the richly illustrated monograph of Muizon et al. (2018). A full list of the specimens we used for scoring purposes, together with institutional abbreviations, is given in table S2 in the online supplement (https://doi.org/10.5531/sd.sp.54).

Following Voss and Jansa (2009), we scored characters as polymorphic only when alternative states were about equally common among examined conspecific specimens. Otherwise, the taxon was scored based on the clearly modal condition. Polymorphisms were scored as variable (e.g., "0+1"), rather than as intermediate states (with transformations to and from the polymorphic state given a weight of 0.5—the "scaled" option of Wiens, 2000) to allow Bayesian analysis of our morphological dataset, because current versions of MrBayes do not allow the use of step matrices. In certain cases, a terminal could not be scored as exhibiting a specific state for a particular character, but at least one alternative state could be definitively ruled out (for example, a sagittal crest [char. 27] is clearly present in the phascolarctid †*Litokoala* and the dasyuromorphian †*Mutpuracinus*, but it is not clear based on available material whether this crest extended onto the frontals in either taxon; Murray and Megirian, 2006a; Louys et al., 2009); in such cases, we used uncertainty (either/or) coding, with all possible states scored (e.g., "1/2").

We elected not to score sexual dimorphism of particular features (for example, root number and the presence or absence of accessory cusps on the upper canines of the extant caenolestids *Caenolestes* and *Rhyncholestes*) as distinct char-

acter states because sample sizes for many of our terminals were insufficient to determine whether sexual dimorphism was present; instead, such sexually dimorphic traits were coded as polymorphisms (following Voss and Jansa, 2009).[4] Following standard practice in morphological phylogenetics, we coded missing/unknown data as "?" and inapplicable data as "-" although both were treated in the same way (as missing/unknown) in our phylogenetic analyses. As in Voss and Jansa (2009), characters representing putative morphoclines or transformation series were treated as ordered (additive) in all analyses (Wiens, 2001:691 presented a formal justification of this approach; but see Brocklehurst and Haridy, 2021).

Molecular Characters

We analyzed DNA sequences from the following six protein-coding nuclear loci (gene names and symbols follow the HUGO Gene Nomenclature Committee; Yates et al., 2017): exon 26 of apolipoprotein B (*APOB*); exon 11 of breast cancer 1, early onset (*BRCA1*); exon 10 of growth hormone receptor (*GHR*); exon 1 of retinol binding protein 3 interstitial (*RBP3*, also known as interphotoreceptor retinoid binding protein [*IRBP*] in other studies); the intronless recombination activating gene 1 (*RAG1*); and exon 28 of von Willebrand factor (*VWF*). We also analyzed sequence data from whole mitochondrial genomes, namely the 12 heavy-strand protein-coding genes, the light-strand protein-coding gene NADH-ubiquinone oxidoreductase chain 6 (*MT-ND6*), the mitochondrially encoded 12S (*MT-RNR1*) and 16S (*MT-RNR2*) ribosomal RNA genes, and 21 mitochondrially encoded tRNA genes (Janke et al., 1994). The mitochondrially encoded tRNA lysine gene (*MT-TK*) was excluded because it appears to be a pseudogene

---

[4] We appreciate that this approach is suboptimal, conflating true polymorphism (due to, for example, allelic variation segregating in a population) or intraspecific geographic variation with the result of sex-specific differences in development.

in marsupials (Janke et al., 1997; Dörner et al., 2001; Nilsson et al., 2003) and cannot be aligned with homologous nonmarsupial sequences.

For *APOB*, *BRCA1*, *RAG1*, *VWF*, and the mitochondrial genomes, DNA sequences were downloaded from GenBank (table S1 in the online supplement). Some *RBP3* and *GHR* sequences were also obtained from GenBank, but we also obtained many new marsupial sequences for these loci (table S1). For most new sequences of *GHR*, exon 10 was amplified using forward primer GHRF1alt-5′GCCATGACAGCTAYAAGCCTCA paired with reverse primer GHRendAlt-5′GATTTTGTTCAGTTGGTCTGTGCTCAC. For some taxa, the forward primer was replaced with GHRF1mon-5′TTCTAYARYGATGACTCYT GGGT. This full-length transcript was reamplified as two smaller overlapping segments by pairing the forward primer with GHR750R-5′GTAAGGCTTTCTGTGGTGATRTAA and the reverse primer with GHR50F-5′TTCTAYARY GATGACTCYTGGGT. For unknown reasons, we were unable to amplify exon 10 of *GHR* from any didelphin taxon using these primers.

New *RBP3* sequences were amplified from all non-dasyuromorphian taxa using forward primer IRBPA-5′ATGGCCAAGGTCCTCTTGGA TAACTACTGCTT paired with reverse primer IRBPD1-5′ CATCATCAAACCGCAGATAGC CCA. This fragment was reamplified as two smaller overlapping segments by pairing the forward primer with IRBPF-5′CTCCACT GCCCTCCCATGTCT and the reverse primer with IRBPE1-5′AGCCTACATCCTCAAGA AGATGCG. For dasyuromorphians, primer IRBPA was replaced with IRBP_DasyA-5′TGCAAGAAGCGATTGAACAAGC and IRBPD1 was replaced with IRBP_ KraB-5′ AGGTGCTCCGTGTCCTGAA.

All PCR amplifications used AmpliTaq Gold DNA polymerase (Thermo Fisher Scientific) with recommended reagent concentrations. For *GHR*, full-length amplifications were performed using a modified touchdown program in which annealing temperature started at 58° C and decreased by 2° every 5 cycles until 52° C. Ream-

plifications were done using 25 cycles at an annealing temperature of 52° C. For *IRBP*, touchdown protocols started at 64° C and decreased by 2° every 5 cycles until 58° C; reamplifications used an annealing temperature of 58° C or 60° C for 25 cycles. Resulting PCR products were Sanger sequenced on an Applied Biosystems 3730xl DNA Analyzer using ABI BigDye Terminator ver. 3.1 chemistry.

Given their essential roles in cellular respiration and mitochondrial protein translation respectively, the mitochondrial protein-coding genes and ribosomal and tRNA genes are expressed ubiquitously in eukaryotic cells. Voss and Jansa (2009) provided detailed information regarding the genes *BRCA1, RBP3, RAG1,* and *VWF*, demonstrating that these loci appear to exist as single copies, are unlinked in *Monodelphis domestica*, are expressed in different tissues, and have translated protein products with very different functions. Here we provide similar information regarding *APOB* and *GHR*.

Apolipoprotein B (APOB): The human apolipoprotein B gene (*APOB*) consists of 29 exons spanning about 45 kb on the short arm of chromosome 2 (Blackhart et al., 1986; Chen et al., 1986; Cladaras et al., 1986; Amrine-Madsen et al., 2003a). Meredith et al. (2009b: accessory publication) reported that *APOB* maps to chromosome 1 in *Monodelphis domestica*, and it appears to exist as a single copy in both *M. domestica* and *Macropus eugenii*. In humans, the gene is expressed primarily in the liver, where the gene product is a very large (4536 amino acids) protein (APOB100), and in the small intestine, where editing of the mRNA transcript results in a smaller isoform (2152 amino acids, APOB48; Chen et al., 1986; Cladaras et al., 1986). The same editing process has been shown to occur in the small intestine of *M. domestica* (Fujino et al., 1999). The two APOB isoforms are the major apolipoproteins of chylomicrons and low-density lipoproteins (Young, 1990).

APOB was first used to investigate mammalian phylogeny by Amrine-Madsen et al. (2003a;

2003b), who sequenced part of exon 26 (which contains putative binding sites for the LDL receptor; Hospattankar et al., 1986; Yang et al., 1986; Ebert et al., 1988; Maeda et al., 1988). Subsequent studies focusing on relationships within Marsupialia (Meredith et al., 2008a, 2008b, 2009a, 2009b, 2009c, 2010) sequenced exon 26 for 65 of the 97 Recent ingroup terminals included in our study (table S1 in the online supplement). We downloaded these sequences from Genbank and performed our own alignment (see below).

Growth Hormone Receptor (GHR): The human growth hormone receptor (*GHR*) gene consists of 10 exons spanning about 87 kb on the short arm of chromosome 5 (Godowski et al., 1989). In *Monodelphis domestica*, the homologous gene is present on chromosome 3. In humans, the full-length (638 amino acids) GHR gene product (isoform 1) is a type I cytokine receptor that acts as a transmembrane receptor for growth hormone, but multiple alternatively spliced transcript variants are known (Urbanek et al., 1992; Pantel et al., 2000). *GHR* was first used to investigate mammalian phylogeny by Adkins et al. (2001), who sequenced exon 10 in rodents and nonrodent outgroups. We amplified and sequenced part of exon 10 of *GHR* for 53 of our 97 Recent terminals (details above), to which we added additional marsupial sequences downloaded from GenBank (table S1 in the online supplement).

Sequence Alignment

DNA sequences for the protein-coding genes were aligned separately using MUSCLE (Edgar, 2004) for codons in MEGA 6.0 (Tamura et al., 2013) and then subsequently adjusted manually to maintain an open reading frame. *RBP3* is a pseudogene in *Notoryctes* (AF025385; see Springer et al., 1998) and *APOB* is a pseudogene in *Tarsipes* (FJ603116),[5] but all other sequences

for both genes could be aligned to an open reading frame. *MT-RNR1* and *MT-RNR2* were aligned manually with reference to the secondary structure model presented by Springer and Douzery (1996) and Burk et al. (2002), respectively, with stem and loop regions identified, and alignment-ambiguous regions removed. The tRNA genes were aligned using the reference alignments in the Mamit-tRNA database (Pütz et al., 2007). The final alignments are summarized in table 3. Each of our Recent terminals is represented by sequence data from at least one gene (table S1 in the online supplement), but we note that a few terminals do not overlap with others (e.g., the didelphid *Caluromysiops* is represented only by an *RBP3* sequence, whereas the peramelemorphian *Rhynchomeles* is represented only by a *MT-RNR1* sequence). The final alignments were concatenated into an alignment of mitochondrial genes (14,704 bases), an alignment of nuclear genes (9797 bases), and a single combined (mitochondrial and nuclear DNA) alignment (24,501 bases).

Total-Evidence Matrix

Concatenating our combined DNA and morphological matrices resulted in a total-evidence matrix comprising 24,681 characters (24,501 molecular, 180 morphological). The 10 nonmarsupial outgroup terminals used to root the molecular-only analyses were deleted from the total-evidence matrix, leaving an ingroup of 141 marsupial terminals (97 Recent, 42 fossil), plus †*Herpetotherium* and †*Mimoperadectes*, with †*Pucadelphys*, †*Mayulestes*, and †*Allqokirus* as the three fossil outgroup terminals. Relative completeness of all terminals is given in table 4.

---

[5] Meredith et al. (2009c) published this sequence but did not explicitly identify it as pseudogenic, nor have subsequent studies that have used it (e.g., Meredith et al., 2010; Mitchell

et al., 2014; Gallus et al., 2015a). However, the Genbank entry for FJ603116 states that it is a pseudogene and our *APOB* alignment indicates the presence of a 16 bp deletion in this sequence relative to other mammals, resulting in a frameshift mutation.

TABLE 3

Summary of Molecular Loci

Gene(s)	Type	Aligned Length (bp)
Apolipoprotein B (*APOB*) exon 26	nuclear protein-coding	2299
Breast cancer 1, early onset (*BRCA1*) exon 11	nuclear protein-coding	2217
Growth hormone receptor (*GHR*) exon 10	nuclear protein-coding	876
Recombination activating gene (*RAG1*)	nuclear protein-coding	2277
Retinol binding protein 3, interstitial (*RBP3*) exon 1[a]	nuclear protein-coding	1162
Von Willebrand factor (*VWF*) exon 28	nuclear protein-coding	966
12 mitochondrial "heavy-strand" protein-coding genes	mitochondrial protein-coding	10,857
NADH-ubiquinone oxidoreductase chain 6 (*MT-ND6*)	mitochondrial protein-coding	456
Mitochondrial 12S RNA (*MT-RNR1*), 16S RNA (*MT-RNR2*) and 21 tRNAs[b]	mitochondrial RNAs	3391

[a] Often referred to as "interphotoreceptor binding protein" (*IRBP*).
[b] Excluding tRNA lysine (*MT-TK*), which appears to be pseudogenic in marsupials (Janke et al., 1997; Dörner et al., 2001; Nilsson et al., 2003) and cannot be aligned with nonmarsupial sequences.

Online Data Archives

All the new molecular sequences produced for this study have been deposited in GenBank with accession numbers ON677544–ON677610 (for new *RBP3* sequences) and ON677611–ON677671 (for new *GHR* sequences); for a complete list of GenBank accession numbers of all analyzed sequences, old and new, see table S1 in the online supplement. All our datasets and associated trees have been deposited on Dryad (doi:10.5061/dryad.jdfn2z3dc).

Phylogenetic Analyses

Molecular: Phylogenetic analysis of the molecular matrix was carried out using Bayesian inference implemented in MrBayes 3.2.7a (Ronquist et al., 2011, 2012b) via the CIPRES Science Gateway (Miller et al., 2010). PartitionFinder v2.1.1 (Lanfear et al., 2017) was first used to identify an appropriate partitioning scheme and models for the molecular matrix. For the PartitionFinder analysis of our molecular matrix, we initially partitioned the nuclear protein-coding genes and *MT-ND6* by gene and codon position, but we treated our 12 mitochondrial heavy-strand genes as a single locus partitioned by codon position only, and we combined the rRNA and tRNA genes, which were partitioned into stems and loops (i.e., two partitions) only. The PartitionFinder analysis employed the "greedy" search algorithm (Lanfear et al., 2012), with the assumption of linked branch lengths among partitions (Duchêne et al., 2020). We used the Bayesian Information Criterion (BIC) to identify the partitioning scheme and models that best fit our sequence data. The BIC penalizes extra parameters more than either the Akaike Information Criterion or corrected Akaike Information Criterion (Sullivan and Joyce, 2005; Luo et al., 2010; Lanfear, 2016: 18; Duchêne et al., 2020), so it is likely to prefer a partitioning scheme with fewer partitions, less complex models, or both. This is desirable because fewer partitions and simpler models reduce the computational burden of subsequent analyses. Comparisons were restricted to models implemented by MrBayes, except that we did not test models that combined a gamma distribution for rate heterogeneity with

TABLE 4

Percentage Completeness of Terminal Taxa[a]

	Percent complete character data				
	Morphological	Mitochondrial	Nuclear	Combined DNA	Total Evidence
OUTGROUP					
Monotremata					
Tachyglossus aculeatus	n/a	100	55.6	82.3	n/a
Ornithorhynchus anatinus	n/a	100	71.0	88.4	n/a
Placentalia					
Bradypus tridactylus	n/a	99.9	94.4	97.7	n/a
Dasypus novemcinctus	n/a	100	88.1	95.2	n/a
Elephas maximus	n/a	100	99.7	99.9	n/a
Trichechus manatus	n/a	100	96.6	97.7	n/a
Bos taurus	n/a	100	100	100	n/a
Mus musculus	n/a	100	99.9	99.9	n/a
Homos sapiens	n/a	100	100	100	n/a
Canis lupus familiaris	n/a	100	100	100	n/a
Metatheria					
†*Mayulestes ferox*	72.8	n/a	n/a	n/a	0.5
†*Pucadelphys andinus*	87.2	n/a	n/a	n/a	0.6
†*Allqokirus australis*	77.2	n/a	n/a	n/a	0.6
INGROUP					
Metatheria (continued)					
†*Herpetotherium fugax*	73.3	n/a	n/a	n/a	0.5
†*Mimoperadectes* spp.	53.9	n/a	n/a	n/a	0.4
Didelphimorphia					
Caluromys spp.	95.6	99.4	99.9	99.6	99.6
Caluromysiops irrupta	91.1	n/a	11.9	4.8	5.4
Chacodelphys formosa	86.7	n/a	4.4	2.7	3.3
Chironectes minimus	95.6	17.4	67.6	37.5	37.9
Cryptonanus unduaviensis	95.0	18.3	67.4	38.0	38.4
Didelphis spp.	96.1	100	90.3	96.1	96.1
Glironia venusta	92.2	7.8	100	44.7	45.0
Gracilinanus spp.	96.1	29.2	67.4	44.5	44.9
Hyladelphys kalinowskii	94.4	7.8	76.6	35.3	35.7
Lestodelphys halli	93.9	19.5	22.5	20.7	21.2
Lutreolina crassicaudata	100	13.0	67.6	34.8	35.3

TABLE 4 *continued*

Marmosa murina	95.6	99.7	67.3	86.7	86.8
Marmosops spp.	96.7	26.7	67.6	43.1	43.5
Metachirus nudicaudatus	96.1	29.6	67.5	44.7	45.1
Monodelphis spp.	96.1	100	100	100	100.0
Philander spp.	96.1	99.5	67.6	86.7	86.8
Thylamys spp.	96.1	99.4	73.3	88.9	89.0
Tlacuatzin canescens	96.7	7.8	66.5	31.3	31.8
†*Hesperocynus dolgopolae*	55.6	n/a	n/a	n/a	0.4
†*Sparassocynus* spp.	89.4	n/a	n/a	n/a	0.7
†*Thylatheridium chapalmalensis*	86.7	n/a	n/a	n/a	0.6
†*Thylophorops cristatum*	68.3	n/a	n/a	n/a	0.5
Pauctuberculata					
Caenolestes spp.	90.6	100	96.4	98.6	98.5
Lestoros inca	83.3	11.9	20.9	15.5	16.0
Rhyncholestes raphanurus	86.7	100	95.8	98.3	98.2
†*Acdestis* spp.	60.0	n/a	n/a	n/a	0.4
†*Evolestes* spp.	29.4	n/a	n/a	n/a	0.2
†*Palaeothentes* spp.	56.7	n/a	n/a	n/a	0.4
†*Pichipilus* spp.	32.2	n/a	n/a	n/a	0.2
†*Stilotherium dissimile*	35.6	n/a	n/a	n/a	0.3
Microbiotheria					
Dromiciops gliroides	93.9	99.4	95.6	98.0	98.0
†*Microbiotherium tehuelchum*	62.2	n/a	n/a	n/a	0.5
Notoryctemorphia					
Notoryctes typhlops	65.0	99.6	96.3	98.3	98.1
Dasyuromorphia					
Antechinomys laniger	95.0	99.5	20.9	68.1	68.3
Antechinus spp.	95.6	99.8	56.7	82.6	82.7
Dasycercus cristicauda	91.1	99.5	20.9	68.1	68.3
Dasykaluta rosamondae	88.9	99.5	11.6	64.3	64.5
Dasyuroides byrnei	91.1	99.5	20.3	67.8	68.0
Dasyurus spp.	90.0	100	93.6	97.4	97.3
Micromurexia hageni	95.6	99.4	20.9	68.0	68.2
Murexia longicaudata	93.3	99.4	53.1	80.9	81.0
Murexichinus melanurus	96.1	100	20.6	68.2	68.4
Myoictis spp.	95.0	99.5	18.9	67.3	67.5
Myrmecobius fasciatus	83.3	100	79.4	91.7	91.6

TABLE 4 *continued*

Neophascogale lorentzi	95.0	100	20.7	68.3	68.5
Ningaui spp.	92.2	100	20.6	68.2	68.4
Paramurexia rothschildi	92.8	100	10.5	64.2	64.4
Parantechinus apicalis	82.2	99.5	11.6	64.3	64.4
Phascogale tapoatafa	96.1	100	65.0	86.0	86.1
Phascolosorex dorsalis	95.6	99.5	55.8	82.0	82.1
Phascomurexia naso	96.1	100	20.6	68.2	68.4
Planigale spp.	92.2	99.5	55.1	81.7	81.8
Pseudantechinus macdonnellensis	90.6	99.5	20.9	68.1	68.3
Sarcophilus harrisii	86.1	99.5	100	99.7	99.6
Sminthopsis crassicaudata	94.4	100	48.4	79.4	79.5
Thylacinus cynocephalus	93.3	100	n/a	60.0	60.2
†*Barinya wangala*	87.2	n/a	n/a	n/a	0.6
†*Badjcinus turnbulli*	62.2	n/a	n/a	n/a	0.5
†*Mutpuracinus archibaldi*	61.1	n/a	n/a	n/a	0.4
†*Nimbacinus dicksoni*	76.7	n/a	n/a	n/a	0.6
Peramelemorphia					
Chaeropus spp.	91.7	17.2	n/a	10.3	10.9
Echymipera spp.	95.6	100	87.4	94.9	94.9
Isoodon macrourus	95.0	100	96.4	98.6	98.6
Macrotis lagotis	93.3	99.0	94	97.0	97.0
Microperoryctes ornata	94.4	99.5	57.6	82.7	82.8
Perameles gunnii	92.2	99.3	57.4	82.6	82.7
Peroryctes raffrayana	95.6	99.5	57.6	82.7	82.8
Rhynchomeles prattorum	91.1	5.8	n/a	3.5	4.1
†*Bulungu palara*	75.0	n/a	n/a	n/a	0.5
†*Galadi speciosus*	79.4	n/a	n/a	n/a	0.6
†*Yarala burchfieldi*	73.9	n/a	n/a	n/a	0.5
Diprotodontia					
Acrobates pygmaeus	77.8	98.5	96.4	97.7	97.6
Aepyprymnus rufescens	86.7	100	96.2	98.5	98.4
Ailurops ursinus	83.9	99.5	70.2	87.8	87.8
Bettongia spp.	84.4	100	57.7	83.1	83.1
Burramys parvus	81.7	99.4	66.6	86.3	86.3
Caloprymnus campestris	83.3	13.6	n/a	8.2	8.7
Cercartetus spp.	86.1	99.7	91.9	96.5	96.4
Dactylonax palpator	82.8	99.5	66.7	86.4	86.4

TABLE 4 *continued*

Dactylopsila trivirgata	84.4	100	66.7	86.7	86.7
Dendrolagus spp.	85.0	100	59.2	83.7	83.7
Distoechurus pennatus	83.3	100	66.7	86.7	86.7
Dorcopsis spp.	87.8	99.5	66.7	86.4	86.4
Dorcopsulus vanheurni	89.4	99.7	57.7	82.9	82.9
Gymnobelideus leadbeateri	81.7	23.4	57.7	37.1	37.4
Hemibelideus lemuroides	83.3	n/a	66.7	26.7	27.1
Hypsiprymnodon moschatus	84.4	99.5	96.4	98.2	98.1
Lagorchestes conspicillatus	83.9	100	66.7	86.7	86.7
Lagostrophus fasciatus	82.2	100	66.3	86.5	86.5
Lasiorhinus spp.	80.6	100	57.7	83.1	83.1
Macropus spp.	86.1	99.5	66.7	86.4	86.4
Notamacropus spp.	87.2	100	66.7	86.7	86.7
Onychogalea unguifera	86.1	100	66.7	86.7	86.7
Osphranter robustus	86.7	100	65.9	86.4	86.4
Petauroides volans	87.2	99.8	66.7	86.5	86.5
Petaurus breviceps	87.8	100	95.9	98.4	98.3
Petrogale spp.	80.6	100	66.7	86.7	86.7
Petropseudes dahli	84.4	n/a	57.7	23.1	23.5
Phalanger spp.	86.1	99.4	62.0	84.4	84.4
Phascolarctos cinereus	89.4	100	96	98.4	98.3
Potorous tridactylus	86.1	100	70.2	88.1	88.1
Pseudocheirus peregrinus	88.3	99.7	61.2	84.3	84.3
Pseudochirops archeri	84.4	14.8	58.1	32.1	32.5
Pseudochirops cupreus	90.0	29.7	96.4	56.4	56.6
Pseudochirulus canescens	83.9	99.78	57.7	82.9	82.9
Setonix brachyurus	86.7	100	57.7	83.1	83.1
Spilocuscus maculatus	83.9	99.8	66.5	86.5	86.5
Strigocuscus celebensis	77.8	99.5	57.7	82.8	82.8
Tarsipes rostratus	51.7	100	96.3	98.5	98.2
Thylogale spp.	86.1	100	57.7	83.1	83.1
Trichosurus vulpecula	82.8	100	94.3	97.7	97.6
Vombatus ursinus	80.0	99.9	96	98.4	98.3
Wallabia bicolor	83.3	100	57.7	83.1	83.1
Wyulda squamicaudata	80.6	99.5	66.7	86.4	86.4
†*Balbaroo fangaroo*	67.8	n/a	n/a	n/a	0.5
?*Bettongia* †*moyesi*	45.6	n/a	n/a	n/a	0.3

TABLE 4 *continued*

†*Bohra illuminata*	72.2	n/a	n/a	n/a	0.5
†*Ekaltadeta ima*	75.6	n/a	n/a	n/a	0.6
†*Ganawamaya gillespieae*	68.3	n/a	n/a	n/a	0.5
†*Ganguroo* spp.	82.2	n/a	n/a	n/a	0.6
†*Hadronomas puckridgi*	50.0	n/a	n/a	n/a	0.4
Hypsiprymnodon †*bartholomaii*	46.7	n/a	n/a	n/a	0.3
†*Ilaria* spp.	44.4	n/a	n/a	n/a	0.3
†*Lekanoleo roskellyae*	71.7	n/a	n/a	n/a	0.5
†*Litokoala* spp.	67.8	n/a	n/a	n/a	0.5
†*Muramura* spp.	57.2	n/a	n/a	n/a	0.4
†*Namilamadeta* spp.	81.7	n/a	n/a	n/a	0.6
†*Neohelos stirtoni*	65.0	n/a	n/a	n/a	0.5
†*Ngapakaldia* spp.	62.8	n/a	n/a	n/a	0.5
†*Nimbadon lavarackorum*	77.2	n/a	n/a	n/a	0.6
†*Nimiokoala greystanei*	57.8	n/a	n/a	n/a	0.4
†*Onirocuscus reidi*	67.8	n/a	n/a	n/a	0.5
†*Rhizosthenurus flanneryi*	67.2	n/a	n/a	n/a	0.5
†*Silvabestius* spp.	66.7	n/a	n/a	n/a	0.5
†*Thylacoleo carnifex*	71.1	n/a	n/a	n/a	0.5
"*Trichosurus*" †*dicksoni*	50.0	n/a	n/a	n/a	0.4
†*Wakaleo vanderleuri*	63.9	n/a	n/a	n/a	0.5
†*Warendja wakefieldi*	38.3	n/a	n/a	n/a	0.3
†Yalkaparidontia					
†*Yalkaparidon* spp.	50.0	n/a	n/a	n/a	0.4
Mean completeness (all)	80.7	n/a	n/a	n/a	49.3
Mean completeness (Recent taxa)	88.2	86.2	65.7	75.1	72.3
Mean completeness (fossil taxa)	64.8	n/a	n/a	n/a	0.5

[a] Following Voss and Jansa (2009: table 2), terminal completeness was calculated as the number of filled (total minus empty) cells in the corresponding row of each data matrix, divided by the total number of cells (N = 180, 14704, 9797, 24501, and 24681 for morphological, mitochondrial, nuclear, combined DNA, and total evidence, respectively) × 100. For the morphological data, empty cells include those scored as missing ("?") and those scored as inapplicable ("-"). For the DNA data, only unsequenced bases were counted as missing "?"), and gaps ("-") were counted as filled data cells.

TABLE 5

Partitions for Bayesian Analysis Based on PartitionFinder Output[a]

	Subsets	Model[a]
1	concatenated 12 mitochondrial "heavy-strand" protein-coding genes, 1st codon position	GTR+G
2	concatenated 12 mitochondrial "heavy-strand" protein-coding genes, 2nd codon position	GTR+G
3	concatenated 12 mitochondrial "heavy-strand" protein-coding genes, 3rd codon position	GTR+G
4	*MT-ND6* 1st and 2nd codon positions	GTR+G
5	*MT-ND6* 3rd codon position	HKY+G
6	concatenated mitochondrial rRNAs and tRNAs, stem regions	GTR+G
7	concatenated mitochondrial rRNAs and tRNAs, loop regions	GTR+G
8	*APOB* 1st codon position	HKY+G
9	*APOB* 2nd codon position	GTR+G
10	*APOB* 3rd codon position, *RAG1* 3rd codon position, *VWF* 3rd codon position	GTR+G
11	*BRCA1* 1st and 2nd codon position	GTR+G
12	*BRCA1* 3rd codon position	HKY+G
13	*GHR* 1st codon position, *RBP3* 1st codon position, *VWF* 1st codon position	GTR+G
14	*GHR* 2nd codon position, *RAG1* 1st codon position	GTR+G
15	*GHR* 3rd codon position, *RBP3* 3rd codon position	GTR+G
16	*RAG1* 2nd codon position, *RBP3* 2nd codon position, *VWF* 2nd codon position	GTR+G

[a] Using the Bayesian Information Criterion for model selection and assuming linked branch lengths. Model comparisons in PartitionFinder were restricted to models implemented by MrBayes, excluding models that combine a gamma distribution for rate heterogeneity with a proportion of invariant sites following the recommendation of Stamatakis (2016; see also Yang, 2006: 113–114).

a proportion of invariant sites, following the recommendation of Stamatakis (2016; see also Yang, 2006: 113–114). The optimal partitioning schemes and models are given in table 5.

For our Bayesian analyses, we assumed linked branch lengths between partitions, with the number of gamma rate categories increased from the default number of four to eight (see Jia et al., 2014); the latter may be particularly important here as we did not use models that combined a gamma distribution for rate heterogeneity with a proportion of invariant sites (see above). The MrBayes analysis comprised four runs of four chains (each with one cold and three incrementally heated chains, with the temperature of the heated chains set at the default value of 0.1), which were run for 50×10^6 generations and sampling trees every 5000 generations. Stationarity and con-

vergence between chains was checked using Tracer 1.6 (Rambaut et al., 2014). Tracer was also used to determine the burnin for for each individual run, and effective sample sizes (ESSs) from the combined post-burnin samples were checked to make sure that they were greater than 200 for most parameters. The post-burnin trees were then concatenated into a single file using the Burntrees v.0.3.0 perl script (available from https://github.com/nylander/Burntrees) and then summarized using 50% majority rule consensus in MrBayes.

MORPHOLOGICAL: The morphological matrix was analyzed using maximum parsimony, as implemented in TNT 1.5 (Goloboff et al., 2008; Goloboff and Catalano, 2016), and Bayesian inference, as implemented in MrBayes 3.2.7a (Ronquist and Huelsenbeck, 2003; Ronquist et al., 2012b). We note here that TNT recognizes cases where a par-

ticular taxon is scored as multiple states for a particular character but does not distinguish between those due to observed polymorphism within a terminal and those due to uncertainty (treating both as cases of polymorphism; Watanabe, 2015), whereas MrBayes treats all such scorings as missing/unknown (Ronquist et al., 2011).

The TNT analysis comprised an initial New Technology search (which combined Sectorial Search, Ratchet, Drift, and Tree Fusing), which was terminated after the same minimum length was found 1000 times; this was followed by a Traditional search with tree-bisection reconnection (TBR) within the trees saved from the first stage, saving a maximum of 100,000 trees. Support values were calculated using 10,000 standard (sampling-with-replacement) bootstrap replicates with a traditional search, and the results were output as absolute frequencies. The consistency index and retention index for the most parsimonious trees were calculated using the "STATS.RUN" script provided with TNT 1.5.

The MrBayes analysis employed the Lewis (2001) Mk model for discrete morphological characters under the assumption that only variable characters have been scored (i.e., the Mkv variant). A lognormal distribution with eight rate categories was used to model rate heterogeneity across characters following Harrison and Larsson (2015). As for the molecular analysis using MrBayes, the morphological analysis comprised four runs of four chains each, run for 50×10^6 generations and sampling trees every 5000 generations. To reduce the time required for chains to reach stationarity and convergence, we randomly selected 16 mostparsimonious trees from the equivalent TNT analysis and used these as starting topologies for each of the 16 chains. Tracer was again used to check for stationarity and convergence between chains, to determine the burnin for each chain, and to check that ESSs were greater than 100 for most parameters. The post-burnin trees were again concatenated into a single file using Burntrees, and then summarized using 50% majority rule consensus in MrBayes.

Total Evidence: We used only Bayesian inference (implemented by MrBayes 3.2.7a) for our total-evidence analysis. We carried out an undated analysis and a "tip-and-node dated" analysis (sensu O'Reilly and Donoghue, 2016). For both analyses, we used the same models for the molecular and morphological partitions as for the molecular-only and morphological-only Bayesian analyses (see above; table 5) and assumed a single set of linked branch lengths across all partitions. To reduce the time taken to reach stationarity and convergence in the undated analysis, we first analyzed the total-evidence matrix in TNT with the same search settings used for analyzing the morphological matrix (see above) and then used 16 of the mostparsimonious trees from this analysis as starting topologies for each of the 16 chains.

For the dated analysis, we used the Independent Gamma Clock (IGR) model (Lepage et al., 2007; Ronquist et al., 2012a, 2012b; Zhang et al., 2016), with one IGR model applied to the molecular partition and one to the morphological partition (see Beck and Taglioretti, 2020). For both partitions, we specified a normally distributed clock rate prior with a mean of 0.01 and a standard deviation of 0.1. Each of our Recent terminals was assigned a fixed age of 0 Mya, whereas each fossil terminal was assigned a uniform prior age range based solely on the age(s) of the fossil specimens used to score it (see appendix 1), even if older specimens have been reported, following the recommendations of Püschel et al. (2020). We also specified uniform prior age ranges for the age of the root and for 24 nodes that could be calibrated based on available fossil and phylogenetic evidence; a full justification for these calibrations is given in appendix 2. We specified a fossilized birthdeath prior with sampled ancestors (Heath et al., 2014; Matzke and Wright, 2016; Zhang et al., 2016; Gavryushkina et al., 2017), and we assumed diversity sampling of our Recent terminals (which were selected to include at least one representative of each currently recognized Recent genus; Zhang et al., 2016). We included

TABLE 6

**Summary of Posterior Age Estimates for Calibrated Nodes in Dated Total-Evidence Analysis[a]
and Comparisons with the Results of Previous Molecular-Clock Studies**

	This study[b]	Meredith et al. (2009)[c]	Meredith et al. (2011)[d]	Mitchell et al. (2014)[e]	Duchene et al. (2018)[e]	Álvarez-Carretero et al. (2021)[e]
Root	72.3 (65.3-80.8)	N/A	N/A	N/A	N/A	N/A
†Pucadelphyda	66.8 (62.5-72.8)	N/A	N/A	N/A	N/A	N/A
†Mayulestidae	63.4 (60.4-67.0)	N/A	N/A	N/A	N/A	N/A
Marsupialia	56.2 (54.7-58.6)	75.5 (65.2-86.2)	81.8 (67.9-97.2)	87.0 (79.5-94.9)	78.6 (70.5-86.1)[f]	53.7 (49.3-58.9)
Didelphimorphia	27.1 (23.7-31.1)	32.5 (26.3-39.2)	31.4 (23.0-38.4)	38.3 (34.9-41.7)		38.2 (35.0-41.0)
Didelphis+ Philander	3.8 (3.3-5.2)	N/A	N/A	5.5 (4.3-6.9)	N/A	N/A
Paucituberculata+ Australidelphia	55.1 (54.6-56.6)	N/A	N/A	N/A	N/A	N/A
Paucituberculata	35.0 (28.2-44.2)	N/A	N/A	N/A	N/A	N/A
Peramelidae	8.8 (6.3-12.3)	10.0 (7.8-12.8)	12.3 (8.8-16.3)	14.3 (12.7-16.0)	14.8 (13.1-16.5)	20.7 (18.2-23.0)
Dasyuromorphia/ Dasyuroidea	31.2 (26.6-36.5)[g]	N/A	N/A	38.6 (35.0-42.4)[h]	N/A	N/A
Dasyurinae	13.9 (12.1-15.5)	11.9 (9.6-14.8)	N/A	18.5 (16.4-20.7)	14.7 (13.1-16.3)	19.2 (17.2-20.9)
Dasyurini	11.2 (9.5-12.4)[i]	N/A	N/A	13.4 (11.6-15.3)	N/A	13.9 (12.2-15.5)
†Thylacoleonidae	29.4 (21.0-37.7)	N/A	N/A	N/A	N/A	N/A
Phascolarctidae	25.3 (19.6-30.3)	N/A	N/A	N/A	N/A	N/A
Lasiorhinus+ Vombatus +†Warendja	11.4 (3.7-19.1)	N/A	N/A	N/A	N/A	N/A
†Diprotodontidae	24.4 (20.2-27.9)	N/A	N/A	N/A	N/A	N/A
Macropodi-formes/ Macropodoidea	27.7 (23.6-32.1)[j]	26.8 (22.0-32.3)[l]	32.1 (23.3-39.7)[k]	29.4 (26.6-32.2)[k]	31.9 (28.7-35.0)[k]	29.2 (27.9-30.3)

TABLE 6 *continued*

	This study[b]	Meredith et al. (2009)[c]	Meredith et al. (2011)[d]	Mitchell et al. (2014)[e]	Duchene et al. (2018)[e]	Álvarez-Carretero et al. (2021)[e]
Macropodidae+ Potoroidae	19.3 (18.0-22.0)	15.9 (12.7-19.7)	22.2 (13.5-26.6)	16.9 (16.0-18.4)	21.1 (19.0-23.2)	24.2 (22.9-25.0)
Macropodidae	18.2 (17.8-19.7)[l]	13.8 (10.9-17.5)[m]	N/A	14.7 (13.1-16.6)[m]	N/A	21.4 (20.0-22.6)
Macropodinae	9.1 (7.4-11.3)	7.6 (5.7-10.0)	N/A	8.3 (7.2-9.5)	11.6 (10.1-13.3)	16.1 (14.6-17.6)
Macropus sensu lato	4.7 (3.6-6.0)	5.4 (3.8-7.3)	N/A	5.3 (4.4-6.3)	N/A	11.3 (10.0-12.7)
Phalangeridae+ Burramyidae	29.9 (25.8-35.4)	42.8 (36.6-49.4)	43.5 (33.3-53.4)	43.5 (39.9-46.8)	47.1 (43.3-50.2)	32.9 (31.9-33.9)
Petauroidea	29.0 (26.4-32.7)	40.5 (34.5-46.8)	42.0 (31.5-53.1)	40.6 (37.3-43.7)	43.1 (39.8-46.1)	31.8 (30.5-33.0)
Petauridae+ Pseudocheiridae	24.4 (23.6-26.1)	34.7 (29.2-40.6)	34.8 (25.5-45.6)	32.3 (29.4-35.2)	N/A	28.1 (26.6-29.5)
Pseudocheiridae	15.8 (11.7-18.5)	24.9 (20.2-29.9)	N/A	24.1 (21.5-27.0)	28.9 (26.9-31.2)	23.0 (21.2-24.6)

[a] The results of this analysis, with estimated divergence dates for all nodes, are shown in figure 33.

[b] Values are median estimates, followed by the 95% highest posterior interval (HPD) in parentheses.

[c] Values are mean estimates, followed by the 95% credibility interval in parentheses, based on a molecular-clock analysis with multidivtime.

[d] Values are mean estimates, followed by a composite confidence interval, based on multiple molecular=clock analyses with MCMCTree.

[e] Values are mean estimates followed by the 95% HPD in parentheses, based on a molecular clock analysis with MCMCTree.

[f] Note that this analysis did not include paucituberculatans.

[g] Dasyuromorphia (total clade).

[h] Dasyuroidea (total clade).

[i] 95% HPD of the posterior does not overlap the 95% HPD of the effective prior.

[j] Macropodiformes (total clade).

[k] Macropodoidea (crown clade).

[l] Total clade.

[m] Crown clade.

approximately a quarter (97/406) of the total number of Recent species currently recognized; we therefore specified the fraction of extant species sampled to be 0.25. We used the MrBayes default priors for the speciation, extinction, and fossilization rate. Because the dated analysis already included topological constraints (corresponding to the age-calibrated nodes mentioned above), we did not specify starting topologies.

For both the dated and undated analysis, we again used four runs of four chains each—run for 50×10^6 generations and sampling trees every 5000 generations—with Tracer used to check for stationarity and convergence between chains, to determine the burnin for each chain, and to check that ESSs were greater than 200 for most parameters. The post-burnin trees were again concatenated into a single file using Burntrees and then summarized using 50% majority rule consensus in MrBayes. To determine how our specified priors on the ages of tips and selected nodes interacted with our other priors, we repeated our dated analysis without character data and then used the post-burnin trees from this analysis to calculate effective priors. The specified priors and effective priors for our calibrated nodes are given in appendix 2. Posterior age extimates for these calibrated nodes, as well as estimated ages for these same nodes (where available) taken from five recent molecular clock studies (Meredith et al., 2009a, 2011, 2014; Duchêne et al., 2018; Álvarez-Carretero et al., 2021), are given in table 6.

Nodal Support: As described in more detail above, nodal support was calculated using bootstrap values for our maximum parsimony analysis of morphological data and Bayesian posterior probabilities for all our Bayesian analyses. However, these two measures of nodal support are not equivalent, and they are difficult to compare directly (Suzuki et al., 2002; Douady et al., 2003; Erixon et al., 2003; Alfaro and Holder, 2006). Nevertheless, for the purposes of discussion, for our maximum parsimony analysis of morphological data, we refer to clades with <50% bootstrap support as "weakly supported," those with 50%–69% bootstrap support as "moderately supported," and those with ≥70% bootstrap support as "strongly supported" (Hillis and Bull, 1993). Likewise, for our Bayesian analyses, we refer to clades with posterior probabilities (BPP) of 0.5–0.74 as "weakly supported," those with BPPs of 0.74–0.94 as "moderately supported," and those with BPPs ≥0.95 as "strongly supported" (Erixon et al., 2003; Alfaro and Holder, 2006).

Visualization and Annotation of Phylogenetic Trees

We visualized our phylogenies (figs. 27–33) directly from the tree files output by TNT and MrBayes using the ggtree package (Yu et al., 2016; Yu, 2020) in R 4.0.3 (https://www.R-project.org/). We then used ggtree to annotate these with dots at nodes to indicate support values (bootstrap values for the maximum parsimony analysis of our morphological data, Bayesian posterior probabilities for the molecular and total-evidence analyses; see Nodal Support above) as follows: black dots for "strong support" (>70% bootstrap support or ≥0.95 Bayesian posterior probability); dark gray dots for "moderate support" (50%–69% bootstrap support or 0.75–0.94 Bayesian posterior probability); light gray dots for "weak support (<50% bootstrap support or 0.50–0.74 Bayesian posterior probability). For our dated total-evidence analysis (fig. 33), we used ggtree to add node bars representing 95% highest posterior density (HPD) intervals for the ages of nodes (for clarity, 95% HPD intervals were not included for the ages of fossil terminals), and we added a geological time scale using the R package MCMCtreeR (Puttick, 2019).

Identification of Craniodental Synapomorphies for Selected Clades

To identify craniodental synapomorphies of marsupial families and selected suprafamilial clades (see Taxonomic Accounts), we used the "DescribeTrees" command in PAUP* 4.0a169
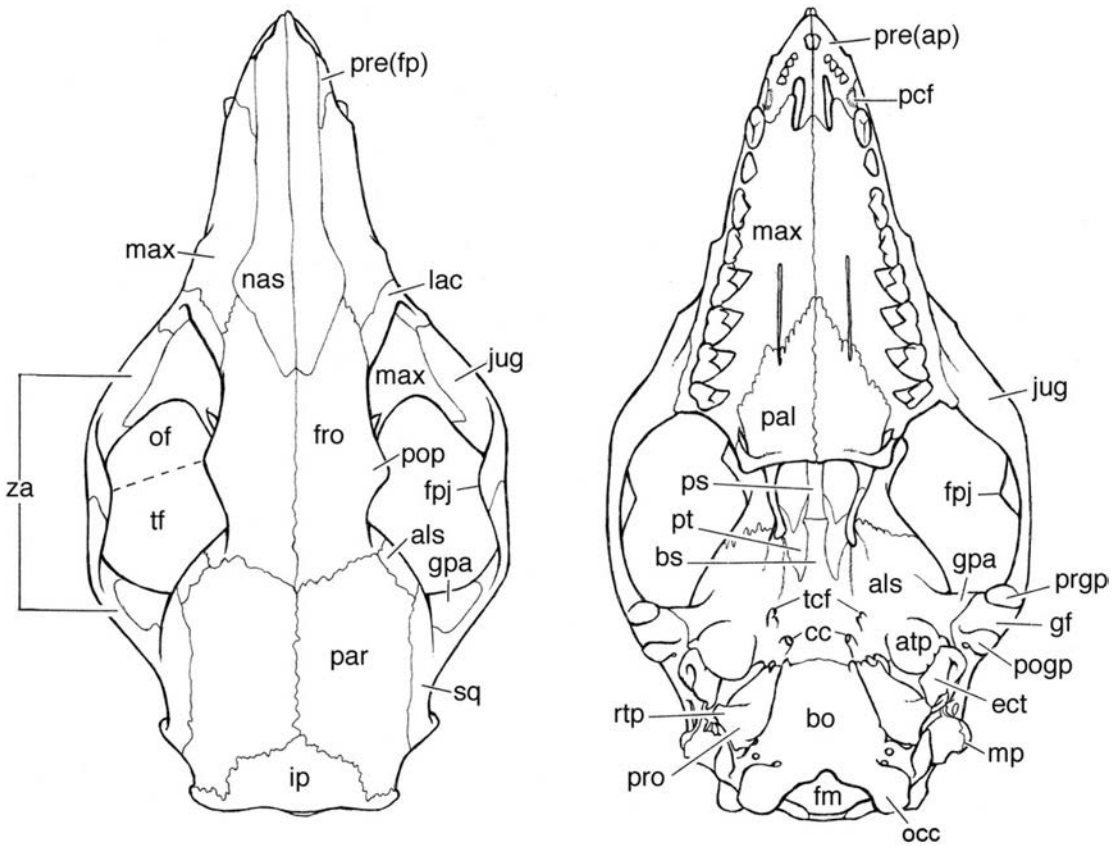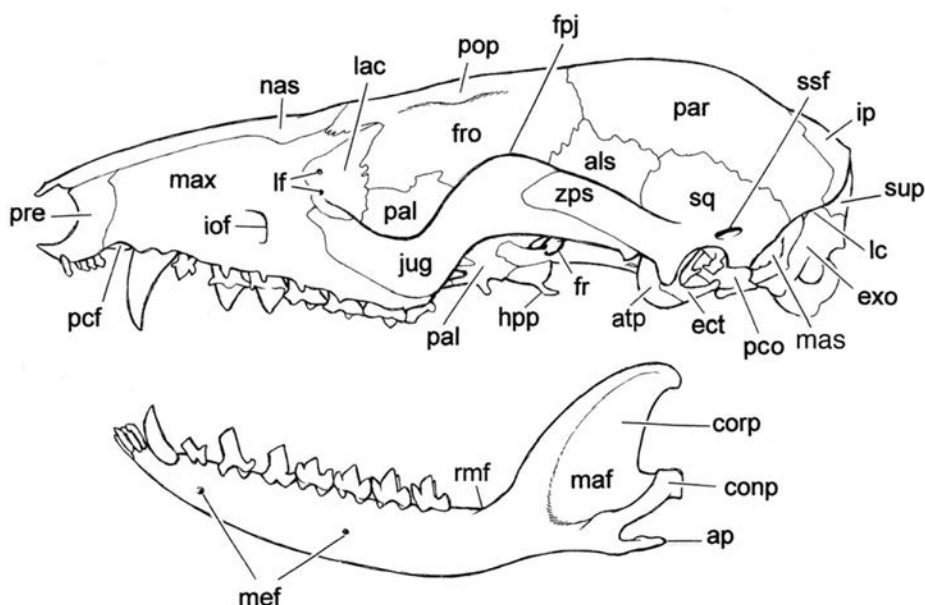
FIG. 1. Dorsal and ventral cranial views of *Marmosa murina* showing principal osteological features mentioned in the text. Abbreviations: **als,** alisphenoid (coossified with basisphenoid); **atp,** alisphenoid tympanic process; **bo,** basioccipital (coossified with exoccipitals); **bs,** basisphenoid (coossified with alisphenoid); **cc,** carotid canal; **ect,** ectotympanic; **fm,** foramen magnum; **fpj,** frontal process of jugal; **fro,** frontal; **gf,** glenoid fossa; **gpa,** glenoid process of alisphenoid; **ip,** interparietal; **jug,** jugal; **lac,** lacrimal; **max,** maxillary; **mp,** mastoid process (of petrosal); **nas,** nasal; **occ,** occipital condyle (of exoccipital); **of,** orbital fossa; **pal,** palatine; **par,** parietal; **pcf,** paracanine fossa; **pogp,** postglenoid process (of squamosal); **pop,** postorbital process; **pre(ap),** premaxillary (alveolar process); **pre(fp),** premaxillary (facial process); **prgp,** preglenoid process (of jugal); **pro,** promontorium (of petrosal); **ps,** presphenoid; **pt,** pterygoid; **rtp,** rostral tympanic process (of petrosal); **sq,** squamosal; **tcf,** transverse canal foramen; **tf,** temporal fossa; **za,** zygomatic arch.

(Swofford, 2003) to map craniodental characters onto our dated total-evidence topology (fig. 33). We only identify unambiguous synapomorphies (those that do not change between Accelerated and Delayed Transformation optimizations) together with their consistency indices (a consistency index less than 1 indicates some degree of homoplasy). A full list of unambiguous synapomorphies is given in file S3 in the online supplement (https://doi.org/10.5531/sd.sp.54).

CRANIAL AND MANDIBULAR CHARACTERS

Our survey of marsupial cranial morphology includes only taxonomically variable aspects of the cranium and mandible that do not require dissection, histology, or X-ray imaging for their study. Anatomical nomenclature in these accounts largely follows Wible (2003) and Voss and Jansa (2003, 2009), with exceptions as noted

FIG. 2. Left lateral cranial and mandibular views of *Marmosa murina* showing principal osteological features mentioned in the text. Abbreviations: **als,** alisphenoid; **ap,** angular process; **atp,** alisphenoid tympanic process; **conp,** condylar process; **corp,** coronoid process; **ect,** ectotympanic; **exo,** exoccipital; **fpj,** frontal process of jugal; **fr,** foramen rotundum; **fro,** frontal; **hpp,** hamular process of pterygoid; **iof,** infraorbital foramen; **ip,** interparietal (coossified with supraoccipital); **jug,** jugal; **lac,** lacrimal; **lc,** lambdoid crest; **lf,** lacrimal foramina; **maf,** masseteric fossa; **mas,** mastoid exposure of pars canalicularis (of petrosal); **max,** maxillary; **mef,** mental foramina; **nas,** nasal; **pal,** palatine; **par,** parietal; **pcf,** paracanine fossa; **pco,** pars cochlearis (of petrosal); **pop,** postorbital process; **pre,** premaxillary; **rmf,** retromolar fossa; **sq,** squamosal; **ssf,** subsquamosal foramen; **sup,** supraoccipital (coossified with interparietal); **zps,** zygomatic process of squamosal.

below. The principal cranial and mandibular features of *Marmosa murina*, a Recent didelphid that retains many plesiomorphic traits for Marsupialia, are illustrated in figures 1 and 2.

Dorsolateral Rostrum

The dorsolateral rostrum forms the roof and sides of the nasal cavity. It includes the nasal bones, together with facial processes of the premaxillary and maxillary bones. With the conspicuous exception of the infraorbital foramen, the bones of the dorsolateral rostrum are imperforate in marsupials and other metatherians. Therefore, taxonomic variation in this region primarily concerns the shape, relative positions, and patterns of contact among adjacent ele-

ments, presence/absence of sutural fusion, and the development of processes for muscle attachment. A (nonexhaustive) list of anatomical synonyms that have been applied to dorsolateral rostral structures in the marsupial-focused literature is given in table 7.

Character 1. *Nasals produced anteriorly beyond facial processes of premaxillae, concealing incisive foramina from dorsal view (0); or not produced beyond premaxillary facial processes, incisive foramina exposed in dorsal view (1).* The nasal bones of most metatherians (e.g., *Marmosa* [figs. 1, 2]) are produced anteriorly beyond the vertically oriented facial processes of the premaxillae that contribute to the lateral walls of the nasal cavity (state 0). Such nasals cover the anterior part of the nasal orifice and

TABLE 7

Selected Anatomical Synonyms for Structures of the Dorsolateral Rostrum[a]

This report	Synonyms
Anteorbital vacuity	antorbital vacuity (Sinclair, 1906); preorbital vacuity (Osgood, 1921)
Infraorbital foramen	anteorbital foramen (Tate, 1948); antorbital foramen (Owen, 1839); Foramen infraorbitale (NAV); opening of the antorbital canal (Tate, 1947)
Jugal	malar (Owen, 1839); zygomatic (Barbour, 1963); os zygomaticum (NAV)
Masseteric process	infrazygomatic process of the maxilla (Finlayson, 1932); maxillary zygomatic process (Owen, 1872); maxillary infrazygomatic process (Thomas, 1888); masseteric tuberosity (Stirton, 1967); malar tuberosity (Murray et al., 1987); maxillary boss (Abdala et al., 2001), maxillary tubercle (Forasiepi et al., 2009); superficial masseteric process (Louys et al., 2009)
Premaxilla	intermaxillary (Owen, 1939); os incisivum (NAV)

[a] References other than the *Nomina anatomica veterinaria* (6th ed., NAV) include the earliest relevant synonymic usage in the marsupial literature of which we are aware, but this list is not intended to be exhaustive.

effectively conceal the incisive foramina from dorsal view, with the undamaged tips of these bones typically also exhibiting a well-defined median apex. Relatively minor taxonomic variation in nasal length that was coded for phylogenetic analysis among Recent didelphids by Voss and Jansa (2003: char. 32; 2009: char. 41) is subsumed among the range of morphologies here assigned to state 0. The nasals extend anteriorly considerably beyond the alveolar processes of the premaxillae in a number of nondidelphid metatherians (e.g., *Notoryctes* [fig. 36], *Hypsiprymnodon moschatus* [fig. 52], and *Potorous* [fig. 54]), but a continuous range of intermediate morphologies prevents us from scoring this trait as a separate state.

A qualitatively distinct state, however, is seen in all examined dasyuromorphians that preserve intact nasal bones: the nasals are truncated anteriorly, terminating behind the anterior margins of the premaxillary facial processes, and the anterior floor of the nasal orifice (usually including the anterior part of the incisive foramina) is dorsally exposed (state 1; e.g., *Thylacinus* [fig. 40], *Myrmecobius* [fig. 41], and *Pseudantechinus* [fig. 42]). Typically, no median apex is developed; instead, the undamaged anterior nasal margins are prominently notched in the midline.

Character 2. *Nasals very broad posteriorly, contacting lacrimals on each side (0); or maxillae and frontals in contact (1); or premaxillae and frontals in contact (2).* Among the taxa included in this study, naso-lacrimal contact (state 0) only occurs consistently in †*Allqokirus* (see Muizon et al., 2018), †*Mayulestes* (see Muizon, 1998: figs. 5, 6), and *Tarsipes* ([fig. 49]), but this trait also occurs polymorphically in *Lasiorhinus*, *Phalanger*, *Spilocuscus*, and *Trichosurus*. In metatherians that lack naso-lacrimal contact, the maxillae usually contact the frontals (state 1; e.g., in *Marmosa* [figs. 1, 2, 34]. The relevant morphology of adult specimens of *Notoryctes* is obscured by sutural fusion, but CT-scans of a fluid-preserved juvenile (NMV C11082) reveal the presence of maxillo-frontal contact (Beck, in prep.). Although the nasals are very broad posteriorly in †*Ngapakaldia*, they do not prevent maxillo-frontal contact (based on SAM P13851, contra Stirton [1967: figs. 1, 2]). *Vombatus* also exhibits the widespread marsupial condition of maxillo-frontal contact, but the morphology of this taxon is distinctive: as the maxilla extends posterodorsally, it is reduced to a very thin strip interposed between the premaxilla and jugal, before widening again to contact the frontal (fig. 45). In *Dactylopsila* and *Dactylonax*, however, the premaxillae contact the frontals (and also the

lacrimals and jugals; Tate, 1948: 241); this latter morphology, which may be connected with the presence of greatly enlarged upper incisors (e.g., Gingerich, 1971), has been scored as an additional state ("2").

Because these states do not represent a clear morphocline, this character has not been ordered in any of our phylogenetic analyses.

Character 3. *Nasals extend posteriorly between lacrimals (0); or nasals truncated anterior to lacrimals (1).* The nasal bones extend posteriorly between the lacrimals in most metatherians (state 0; e.g., *Marmosa* [figs. 1, 2, 34]). In Recent peramelemorphians (e.g., *Chaeropus* [fig. 37], *Macrotis* [fig. 38], and *Perameles* [fig. 39]), however, the nasal bones are truncated anterior to the lacrimals (state 1; Filan, 1990: 618; Muirhead, 2000: 516; Travouillon et al., 2010: char. 31). This distinctive morphology does not occur in the fossil peramelemorphians †*Yarala*, †*Galadi*, or †*Bulungu* (Muirhead, 2000; Travouillon et al., 2010, 2013b; Gurovich et al., 2014), although it is present in the fossil †*Madju* (Travouillon et al., 2015b), which has not been included here. Among macropodiforms, it is seen in *Potorous* (fig. 54) as well as some specimens of *Aepyprymnus*, with the latter scored as polymorphic ("0+1") here. Adults of *Notoryctes* in which remnants of the naso-frontal suture can still be seen (e.g., AMNH 198651 [fig. 36]) demonstrate that the nasals did not extend between the orbits in this taxon, but the lacrimal cannot be identified as a discrete ossification due to extensive fusion of the bones making up the rostrum. However, CT-scans of a fluid-preserved juvenile (NMV C11082) suggest that the nasals do indeed terminate anterior to the lacrimals in this taxon (Beck, in prep.), so *Notoryctes* has also been scored as state 1.

Character 4. *Anteorbital vacuity between nasal, frontal, and maxillary bones on each side of rostrum absent (0); or present (1).* In most metatherians, the posterodorsal rostrum is essentially imperforate (state 0; e.g., in *Marmosa* [figures 1, 2, 34]). In Recent caenolestids (e.g., *Caenolestes* [fig. 35]), however, a prominent

unossified space—the anteorbital vacuity of Thomas (1895)—occurs between the nasal, frontal, and maxillary bones (state 1; Thomas, 1895; Osgood, 1921; 1924; Bublitz, 1987; Patterson and Gallardo, 1987; Goin et al., 2007b; Martin, 2013; Ojala-Barbour et al., 2013; González et al., 2020). Goin et al. (2003: 313; 2007b: 1272–1273) suggested that this feature might be connected with the elongate rostrum of these taxa. By contrast, the fossil paucituberculatans †*Acdestis* (Engelman and Croft, 2016: fig. 6) and †*Palaeothentes* (Forasiepi et al., 2014b) both unequivocally lack an anteorbital vacuity.

We note some discrepancies between our observations and those of previous authors regarding the presence or absence of anteorbital vacuities in other fossil paucituberculatans. In agreement with Marshall and Pascual (1977) but contra Goin et al. (2003; 2007b), we consider anteorbital vacuities to be present in †*Pichipilus*: in MLP-68-I-17-204 (a skull of †*P. centinelus*), the posteromedial margin of the right nasal has a distinctly ragged appearance (Marshall and Pascual, 1977: fig. 4) that does not appear to be the result of breakage and that is very similar in morphology to the equivalent region in living caenolestids (where the nasal forms the anteromedial margin of the anteorbital vacuity [fig. 35]; Patterson and Gallardo, 1987: fig. 1). We therefore scored †*Pichipilus* as state 1. Goin et al. (2007b) stated that anteorbital vacuities are absent in the dentally plesiomorphic late Oligocene paucituberculatan †*Evolestes hadrommatos*, but we consider the only known skull (MNHN Bol-V-004017, previously MNHN-Bol 96-400) to be insufficiently well preserved to score this character confidently, so we scored †*Evolestes* as unknown ("?"). Based on specimens available to us, it is unclear whether anteorbital vacuities are present in †*Stilotherium*, which has also been scored as unknown.

Character 5. *Infraorbital foramen enclosed by maxilla (0); or infraorbital foramen occupies maxillary-jugal suture (1).* In most metatherians, the infraorbital foramen—the anterior opening of the infraorbital canal, which transmits the infra-

orbital nerve and accompanying blood vessels (Sánchez-Villagra and Asher, 2002; Wible, 2003)—is contained entirely in the maxillary bone (state 0; e.g., as in *Marmosa* [fig. 2], *Monodelphis* [Wible, 2003: fig. 2], and *Macropus* [Wells and Tedford, 1995: fig. 9]). Although relevant sutures are not discernible in adult specimens of *Notoryctes*, CT-scans of a fluid-preserved juvenile (NMV C11082) demonstrate that the infraorbital foramen is, in fact, entirely enclosed by the maxilla in this taxon (Beck, in prep.). Although we observed minor taxonomic variation in the position of this foramen within the maxilla (for example, it is located close to the premaxilla in *Dactylopsila* and *Dactylonax*, but close to the jugal in most *Phascolarctos* specimens), a qualitatively distinct condition is seen in all examined specimens of *Thylacinus*, where the infraorbital foramen occupies the maxillary-jugal suture (fig. 40; see also Murray and Megirian, 2006a: appendix 1, figs. 1A, 2B; Warburton et al., 2019: fig. 4). This is an autapomorphy of *Thylacinus* in the current analysis, although we also observed it occasionally in *Phascolarctos* (e.g., AMNH 173404).

We observed additional variation in the morphology of the infraorbital foramen that we decided not to score in the current analysis but that merits brief discussion. The infraorbital foramen is occasionally subdivided into multiple, closely spaced foramina—usually arranged dorsoventrally—in older specimens of a few taxa (notably *Phalanger* [fig. 47], *Thylacinus*, and *Dactylopsila*). Uniquely among the taxa included in this study, most examined specimens of *Hypsiprymnodon moschatus* (fig. 52) have two similar-sized external openings of the infraorbital canal, with the two foramina arranged anteroposteriorly within the maxilla (see also Johnson and Strahan, 1982). By contrast, only a single foramen appears to be present in the only known cranium of *H.* †*bartholomaii* (QM F13051; see Flannery and Archer, 1987c: fig. 2A). A small accessory foramen posterior and slightly dorsal to the infraorbital foramen and adjacent to (or within) the maxillary-jugal suture is consistently present in *Potorous* (e.g., in AMNH 65332), whereas one or more small accessory foramina are usually present anterior to the infraorbital foramen in *Bettongia*.

Character 6. *Masseteric process absent or, if present, not projecting ventrally below plane of molar alveoli (0); or present and projecting ventrally below plane of molar alveoli (1).* Most examined metatherians have an indistinct-to-small rugose process at the base of the anterior root of the zygomatic arch, at or near the maxillary-jugal suture, which does not project ventrally below the level of the molar alveoli (state 0; e.g., in *Marmosa* [figs. 2, 34]). Dissections of *Didelphis* (e.g., Hiiemae and Jenkins, 1969; Turnbull, 1970) identify this structure as the attachment site for the tendon of origin of the superficial masseter. The attachment site for this tendon in most peramelemorphians (described by Filan, 1990) and a number of other metatherians (e.g., †*Herpetotherium*, *Dactylopsila*, *Dactylonax*, †*Nimbacinus*, and *Sarcophilus*) is difficult to distinguish osteologically. The degree of development of this process also appears to vary ontogenetically in other taxa, with older adults often having better-developed processes than younger individuals (e.g., as in *Potorous*). For these reasons, we do not distinguish here between presence of a small masseteric process and complete absence of such a process (subsuming both of these morphologies within state 0).

By contrast, a conspicuously different condition occurs in some metatherians, wherein the origin of the superficial masseter (dissected inter alia by Parsons, 1896: Abbie, 1939; Barbour, 1963; Sanson, 1980; and Warburton, 2009) extends along a large masseteric process that projects ventrally to, or below, the plane of the molar alveoli, as in the macropodids *Macropus* (Wells and Tedford, 1995: fig. 9) and *Osphranter* (Warburton, 2009: fig. 1). Among the taxa we examined, the latter condition (state 1) was observed in *Trichosurus* (but not in "*Trichosurus*" †*dicksoni*), †*Litokoala*, diprotodontids (e.g., †*Nimbadon* [Black and Hand, 2010: figs. 1, 2]), wynyardiids (e.g., †*Namilamadeta* [see Pledge,

TABLE 8

Selected Anatomical Synonyms for Structures of the Orbit and Zygoma

This report	Synonym
Ectoglenoid crest of the jugal	ectoglenoid process of the jugal (Murray, 1991); jugal flange (Murray, 1991); lateral glenoid crest (Murray, 1989); lateral glenoid eminence (Murray, 1989); lateral glenoid flange (Murray, 1989)
Glenoid process of the alisphenoid	articular process of the alisphenoid (Coues, 1872); entoglenoid process of the alisphenoid (Muizon, 1998)
Lacrimal crest	antorbital rim (Gregory, 1920); lacrimal rim (Muirhead, 2000), orbital crest (Gregory, 1920); orbital rim (Gregory, 1920)
Lacrimal foramen	foramen lacrimale (NAV); lachrymal canal (Thomas, 1895); lachrymal duct (Sinclair, 1906); opening of the lachrymal duct (Coues, 1872); perforation for the lachrymal duct (Sinclair, 1906)
Lacrimal tubercle	lacrimal tuberosity (Stirton, 1967)
Postorbital process of the frontal	orbital crest (Muirhead and Wroe, 1998); os frontale, processus zygomaticus (NAV); postorbital bar of frontal (Archer, 1984c); superior postorbital process (Hershkovitz, 1992); supraorbital process (Tate, 1931); supra-orbital prominence (Coues, 1872); supra-orbital protuberance (Coues, 1872); zygomatic process of the frontal (Scott et al., 1988)
Preglenoid process of the jugal	glenoid process of jugal (Rougier et al., 1998)
Sphenorbital fissure	foramen lacerum anterius (Owen, 1859); optic-orbital foramen (Marshall and Muizon, 1995); optic-sphenorbital fissure (Muizon et al., 2018); sphenoidal fissure (Osgood, 1921)

ᵃ References other than *Nomina anatomica veterinaria* (NAV, 6th ed.,) include the earliest relevant synonymic usage in the marsupial literature of which we are aware, but this list is not intended to be exhaustive.

2005: fig. 8A]), most Recent macropodids (e.g., *Lagostrophus* [fig. 53]), *Caloprymnus* (Finlayson, 1932), and *Myrmecobius* (fig. 41). Only one examined taxon, *Wyulda*, is polymorphic for this character. In some specimens of *Glironia*, the maxilla extends below the plane of the molar alevoli (Marshall, 1978: fig. 2; Voss and Jansa, 2009: fig. 37; Ardente et al., 2013: fig. 2; Arguero et al. 2017: fig. 2), but this is due to the large size of the orbit in this taxon; the masseteric process itself is weakly developed, so we scored *Glironia* as conforming to state 0.

Character 7. *Masseteric process formed at least partially by the maxilla (0); or maxillary process formed by the jugal alone (1).* The maxilla contributes to the masseteric process of most metatherians in which it occurs (state 0; e.g., in *Macropus* [Wells and Tedford, 1995: fig. 9]). However, †*Ngapakaldia* has a masseteric process that is formed entirely by the jugal (state 1). Tedford and Woodburne (1987: 404) reported that

the masseteric process is also formed entirely by the jugal in †*Ilaria*, but we observed that the maxilla does, in fact, make a clear contribution to this process.

This character was scored for all taxa in which a masseteric process is identifiable, whether or not the process extends ventrally below the plane of the molar alveoli (i.e., for some taxa scored as "0" for char. 6); only taxa in which no trace of a masseteric process could be identified (e.g., *Dactylopsila*, *Dactylonax*, *Tarsipes*, vombatids, most peramelemorphians, and †*Herpetotherium*; see char. 6) were scored as inapplicable ("-").

Orbit and Zygomatic Arch

The osteology of the orbit and zygomatic arch provide a rich source of characters for mammalian phylogenetics. In particular, the taxonomically variable morphology of the orbital mosaic—the patchwork of bones that

form the medial wall of the eye socket—has received much attention by systematists concerned with eutherian relationships (e.g., Muller, 1934; Cartmill, 1978; Cox, 2006), but this part of the skull has seldom been described in the metatherian literature (with some notable exceptions cited in the following accounts; see also Gregory, 1920: figs. 63–74). Unfortunately, certain elements of the marsupial orbital mosaic are misidentified in a number of published illustrations, including Dawson et al. (1989: fig. 17.3A), Hershkovitz (1992b: fig. 19; 1999: fig. 25), and Novacek (1993: fig. 9.4C), all of which mislabel the orbital process of the palatine as the "sphenoid" or orbitosphenoid.

The bones comprising this region include the lacrimal and jugal, together with orbital processes of the maxilla, palatine, frontal, and sphenoid complex. Anatomical nomenclature for this part of the skull is generally unproblematic, although multiple synonyms exist for several features (table 8). Whereas some structures in this part of the skull (notably those that resist mechanical forces associated with jaw movements) are robust and often well preserved in fossils, others are quite fragile; therefore, character information based on the latter is often missing for extinct taxa.

Character 8. *Lacrimal exposure on orbital rim smooth (0); or with one or more distinct tubercles (1); or forming a distinct crest (2).* The anterodorsal orbital exposure of the lacrimal is essentially smooth (state 0) in most metatherians, including †*Pucadelphys*, †*Allqokirus*, †*Mimoperadectes*, most didelphids (e.g., *Caluromysiops* [fig. 4A]), caenolestids, microbiotheriids, some peramelemorphians, some dasyurids, *Notoryctes*, acrobatids, petaurids, pseudocheirids, *Tarsipes*, and most phalangerids (e.g., *Ailurops* [fig. 3A]). However, distinct lacrimal tubercles (state 1) are present in †*Sparassocynus* (Beck and Taglioretti, 2020), all examined phascolarctids (e.g., *Phascolarctos* [fig. 3B]) and diprotodontids, all examined macropodiforms that preserve the lacrimal except *Hypsiprymnodon moschatus*, some phalangerids (*Trichosurus* [fig. 4B], *Wyulda*, and

some specimens of *Spilocuscus*), and Recent vombatids. Wells and Tedford (1995: fig. 9) distinguished dorsal (supralacrimal) from ventral (infralacrimal) tuberosities in *Macropus*, in which such structures are sometimes distinct, but the homology of either with the single tuberosity exhibited by other taxa is problematic. Because supra- and infralacrimal tuberosities appear to coalesce in some macropodid specimens—for example, in AMNH 107374, a specimen of *Osphranter robustus*—and in the absence of recognition criteria that can be applied unambiguously from taxon to taxon, we scored lacrimal tuberosities as present or absent regardless of number or position. Based on dissections of "*Halmaturus*" (probably a species of *Osphranter*; M.D.B. Eldridge, personal commun.) by Boas and Paulli (1908: plate 13), Gregory (1920: 143) stated that "the orbital tubercle, or rim, serves dorsally for the attachment of the fascia covering the temporal mass and ventrally for the attachment of the palpebral ligament."

A distinct crest extending along the lacrimal contribution to the orbital rim (state 2) is seen in †*Herpetotherium*, †*Acdestis*, *Hypsiprymnodon moschatus*, †*Wakaleo*, †*Thylacoleo*, †*Namilamadeta*, thylacinids, *Myrmecobius* (fig. 3C), many dasyurids (e.g., *Phascogale*, *Sarcophilus*, and *Sminthopsis*) and some peramelemorphians (e.g., *Chaeropus* [see Travouillon et al., 2019], *Macrotis*, and *Perameles*).

These states do not represent a clear morphocline, so this character has not been ordered here.

Character 9. *Distinct lacrimal foramen or foramina present (0); or absent (1) in adult specimens.* In the majority of metatherians examined for this study the lacrimal bone of adults is pierced by one or more distinct foramina that transmit the nasolacrimal ducts or canaliculi (state 0; figs. 3, 4). According to Archer (1976b: 221), the dasyurid lacrimal foramen transmits only the nasolacrimal duct, but Wible (2003: 79) stated that the two lacrimal foramina of *Monodelphis* each transmit a vein in addition to a nasolacrimal canaliculus. Adult specimens of *Lasiorhinus*

uniquely lack a discrete lacrimal foramen or foramina (state 1; Murray et al., 1987: table 2, 454), although a lacrimal foramen is reportedly visible in juveniles (J. Wible, personal commun.). Instead, the lacrimal of this taxon is pierced by many small perforations that resemble the (presumably nutrient) foramina observable on the adjacent surfaces of neighboring bones.

Character 10. *Two or more lacrimal foramina usually present (0); or one lacrimal foramen usually present (1).* Most metatherians have two lacrimal foramina on each side (state 0; e.g., as in *Phascolarctos* [fig. 3B], *Myrmecobius* [fig. 3C], and *Caluromysiops* [fig. 4A]). Although †*Nimbacinus* (based on the single known skull of †*N. dicksoni* [QMF 36357; Wroe and Musser, 2001: 495]) and some specimens of *Thylacinus* (e.g., SAM M922 and M95) appear to have three lacrimal foramina, we chose to score these taxa as state 0 rather than create an additional state for this condition. *Lestodelphys* has two distinct lacrimal foramina close to the orbital rim (Voss and Jansa, 2009: fig. 51), but one or two much smaller foramina are also present within the orbital fossa; the presence of dried blood within the lumina of the latter perforations in some specimens (e.g., BMNH 1928.12.11.206, 1928.12.11.207) suggests that these are vascular pores, possibly similar to the vascular foramen of the lacrimal observed in the bat *Pteropus* by Giannini et al. (2006), rather than true lacrimal foramina (see also Wible et al., 2004: 47–49). Beck and Taglioretti (2020: 9) also reported the presence of probable nutrient foramina within the orbital exposure of the lacrimal in †*Sparassocynus*. However, we have not scored presence or absence of these additional small foramina as an additional character here.

By contrast, only a single distinct lacrimal foramen (state 1) is present in some specimens of †*Pucadelphys*, a few didelphids (*Hyladelphys*, *Chironectes*, and some specimens of *Caluromysiops*), paucituberculatans (e.g., *Caenolestes* [fig. 35]), most peramelemorphians (with the exception of *Macrotis*), some dasyurids, *Notoryctes* (fig. 36), and many diprotodontians (e.g., *Ailurops* [fig. 3A] and *Trichosurus* [fig. 4B]). *Lasi-*

orhinus was scored as inapplicable ("-") for this character, based on the absence of any obvious lacrimal foramina in this taxon (see char. 9).

Character 11. *Lacrimal foramen (or foramina) contained entirely within lacrimal bone (0); or at least one lacrimal foramen located within suture between lacrimal and maxilla (1); or at least one lacrimal foramen located within suture between lacrimal and jugal (2).* The lacrimal foramen (or foramina) is (or are) usually entirely enclosed by the lacrimal bone in metatherians (state 0; e.g., as in figs. 2–4). However, at least one lacrimal foramen is consistently located within the suture between the lacrimal and maxilla (state 1) in *Petauroides*, *Cercartetus*, †*Thylacoleo*, †*Yarala* (Muirhead, 2000), *Macrotis* (fig. 38; see also Muirhead, 2000: 518), and *Peroryctes* (Aplin et al., 2010: 22). The latter morphology is also sometimes seen in *Chaeropus*, *Rhynchomeles*, *Pseudocheirus*, *Osphranter*, and *Petrogale*, all of which have been scored as polymorphic ("0+1"). *Rhyncholestes* is unique among the metatherians we surveyed in that the single lacrimal foramen is usually located within the lacrimal-jugal suture (state 2).

We scored *Notoryctes* as unknown ("?") for this character, due to the absence of relevant sutures in the specimens we examined (fig. 36; see char. 12), whereas we scored *Lasiorhinus* as inapplicable ("-") because it lacks lacrimal foramina (see char. 9). Although the lacrimal and maxillary bones are fused in all specimens of *Burramys* that we examined (see char. 12), the jugal suture is still identifiable and well separated from the lacrimal foramen (or foramina; fig. 46); therefore, *Burramys* has been scored using ambiguity coding (as "0/1").

Character 12. *Bones of orbital mosaic separate, unfused (0); or maxilla and lacrimal fused (1); or entire orbital mosaic fused (2).* In most metatherians, the bones comprising the orbital mosaic (i.e., frontal, lacrimal, maxilla, and palatine) are unfused, with sutures between them clearly identifiable (state 0; figs. 3, 4). In *Burramys*, however, the maxilla and lacrimal are fused, both within the orbital mosaic and, external to
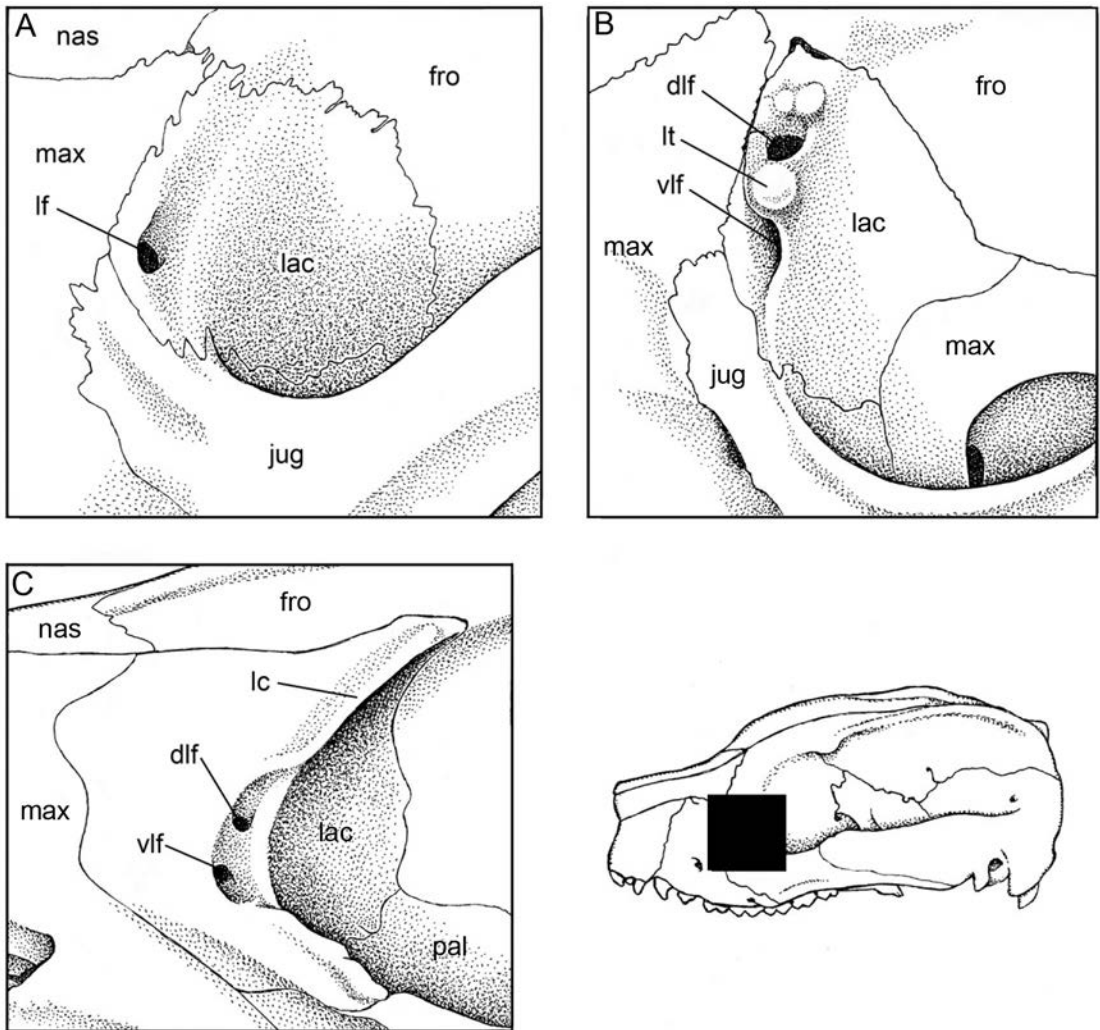
FIG. 3. Lacrimal region of *Ailurops ursinus* (**A,** AMNH 152884), *Phascolarctos cinereus* (**B,** AMNH 65612), and *Myrmecobius fasciatus* (**C,** AMNH 155328). Alternative states for characters 8 and 10 (see main text for descriptions of these characters and character states) are illustrated as follows: *Ailurops* 8(0), 10(1); *Phascolarctos* 8(1), 10(0); *Myrmecobius* 8(2), 10(0). Abbreviations: **dlf,** dorsal lacrimal foramen; **fro,** frontal; **jug,** jugal; **lac,** lacrimal; **lc,** lacrimal crest; **lf,** lacrimal foramen; **lt,** lacrimal tubercle; **max,** maxillary; **nas,** nasal; **pal,** palatine, **vlf,** ventral lacrimal foramen. Specimens are not drawn to the same scale.

the orbit, on the rostrum (state 1; fig. 46). In *Notoryctes*, the entire orbital mosaic is fused, with no sutures identifiable (state 2; fig. 36). As defined, these character states do not appear to represent an unequivocal morphocline (it is not obvious that the condition in *Notoryctes* must necessarily have evolved from a precursor mor-

phology in which only the maxillary-lacrimal suture was fused), so this character was not ordered in any of the analyses presented here.

Character 13. *Palatine and lacrimal bones in contact on medial wall of orbit (0); or maxillary and frontal bones in contact on medial orbital wall (1).* Two alternative patterns of contact
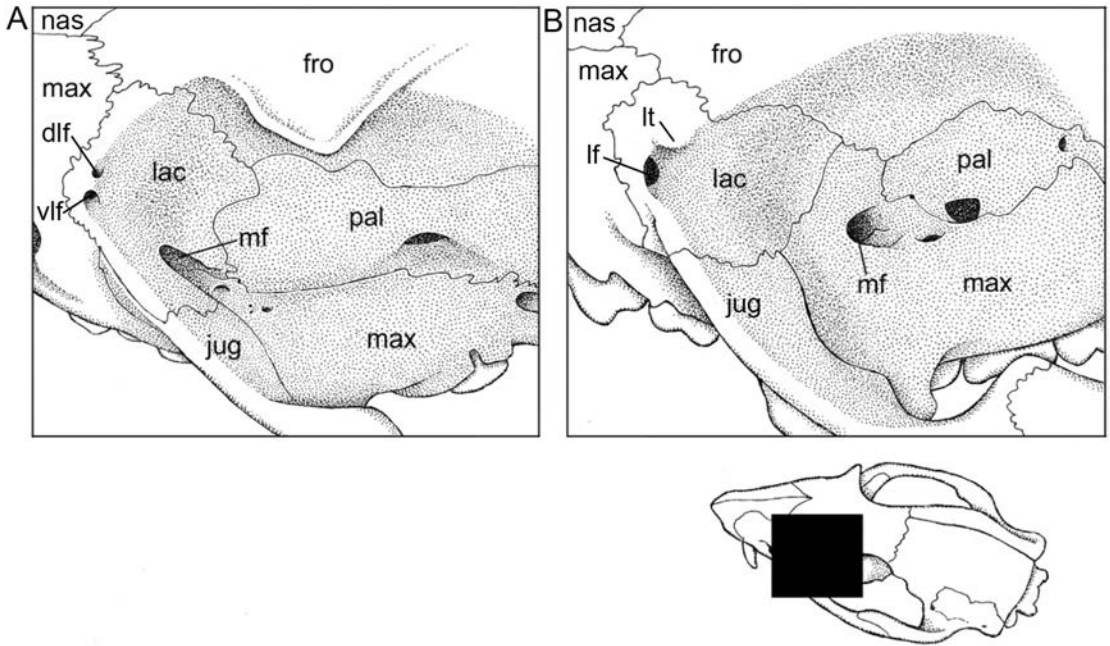
FIG. 4. Anterior orbital region of *Caluromysiops irrupta* (**A,** AMNH 208101) and *Trichosurus vulpecula* (**B,** AMNH 65543). Alternative states for characters 8, 10, 13, and 14 (see main text for descriptions of these characters and character states) are illustrated as follows: *Caluromysiops* 8(0) 10(0[but note that *C. irrupta* is polymorphic for this character]), 13(0), 14(0); *Trichosurus vulpecula* 8(1), 10(1), 13(1), 14(1). Abbreviations: **dlf,** dorsal lacrimal foramen; **fro,** frontal; **jug,** jugal; **lac,** lacrimal; **lf,** lacrimal foramen; **lt,** lacrimal tubercle; **max,** maxillary; **mf,** maxillary foramen; **nas,** nasal; **pal,** palatine; **vlf,** ventral lacrimal foramen. Specimens are not drawn to the same scale.

among the lacrimal, maxillary, palatine, and frontal bones in the anterior part of the orbit have been reported among metatherians. Most of the taxa we examined exhibit palatine-lacrimal contact (e.g., as in *Caluromysiops* [fig. 4A] and †*Pucadelphys* [Marshall and Muizon, 1995: fig. 15]). However frontal-maxillary contact (Gregory, 1920; Springer et al., 1997: char. 50) is consistently present in phalangerids (e.g., *Trichosurus* [fig. 4B]), *Dactylonax*, most macropodiforms (with the notable exceptions of *Potorous*, some specimens of *Dorcopsis* [e.g., the left side of AMNH 198088], and one specimen of †*Balbaroo* [QM F30456]), *Phascolarctos*, †*Nimiokoala*, †*Warendja,* and †*Namilamadeta*. *Ailurops* (Crosby, 2002b) and †*Nimbadon* are polymorphic for this character, with specimens of both taxa presenting different states on the

left and right sides (e.g., AMNH 196495 for *Ailurops*; QM F42677 for †*Nimbadon*). However, based on the specimens examined in this study, the modal condition in *Ailurops* appears to be frontal-maxillary contact (as in other phalangerids, contra Flannery et al., 1987; Crosby, 2002b), whereas in †*Nimbadon* it appears to be palatine-lacrimal contact. Other bones are occasionally exposed on the medial wall of the orbit, but we did not score these rare variants for phylogenetic analysis.

The orbital mosaic is not sufficiently well preserved to score this character in available specimens of †*Allqokirus*, †*Mayulestes*, †*Mimoperadectes*, and †*Herpetotherium*, all of which we coded as unknown ("?"). The lacrimal and maxilla appear to be fused within the orbital fossa in all specimens of *Burramys* that we examined, and
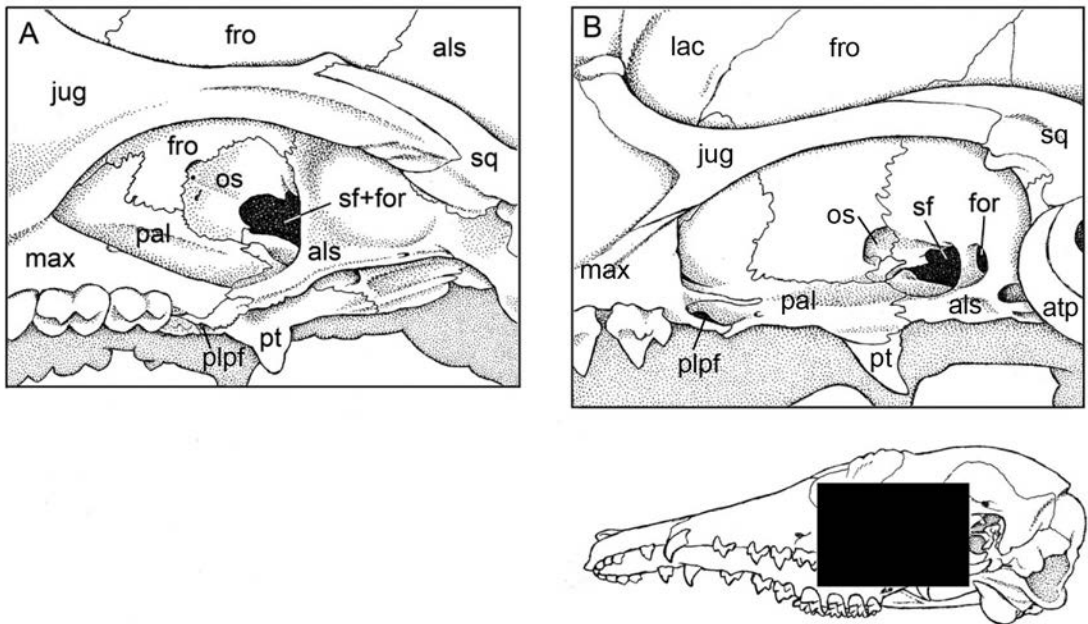
FIG. 5. Posterior orbital region of *Potorous tridactylus* (**A,** AMNH 65293) and *Perameles gunnii* (**B,** MVZ 127070). Alternative states for characters 15–17 (see main text for descriptions of these characters and character states) are illustrated as follows: *Potorous* 15(0), 16(1), 17(1); *Perameles* 15(1), 16(0), 17(0). Abbreviations: **als,** alisphenoid; **atp,** alisphenoid tympanic process; **for,** foramen rotundum; **fro,** frontal; **jug,** jugal; **lac,** lacrimal; **max,** maxillary; **os,** orbitosphenoid; **pal,** palatine; **plpf,** posterolateral palatal foramen; **pt,** pterygoid; **sf,** sphenorbital fissure; **sq,** squamosal. Specimens are not drawn to the same scale.

the entire orbital mosaic is fused in *Notoryctes* (see char. 12); therefore, we also scored both of these taxa as unknown pending examination of juvenile specimens that might preserve evidence of sutures in this region.

Character 14. *Maxillary foramen bordered by lacrimal (0); or contained entirely within the maxilla (1).* The maxillary foramen (the posterior opening of the infraorbital canal) is bordered dorsally by the lacrimal bone in most metatherians (state 0), and a small anterior process of the palatine occasionally forms part of the medial border as well. This widespread condition is seen in †*Pucadelphys*, †*Allqokirus*, †*Mayulestes*, †*Mimoperadectes*, didelphids (e.g., *Caluromysiops* [fig. 4A]), paucituberculatans, peramelemorphians, dasyuromorphians, microbiotheriids, and some diprotodontians (*Cercartetus*, acrobatids, pseudocheirids, *Tarsipes*,

Petaurus, *Gymnobelideus*, and *Potorous*). However, in other diprotodontians—namely, phalangerids (e.g., *Trichosurus* [fig. 4B]), phascolarctids, diprotodontids, thylacoleonids, †*Warendja*, †*Namilamadeta*, *Dactylonax*, most specimens of *Dactylopsila*, and all examined macropodiforms except *Potorous*—the maxillary foramen is contained entirely within the maxilla. *Lasiorhinus* and *Vombatus* are both polymorphic ("0+1") for this character. As for the preceding character, fusion of the lacrimal and maxilla in *Burramys* and of the entire orbital mosaic in *Notoryctes* (see char. 12) compelled us to score both taxa as unknown ("?").

This character is obviously at least partially correlated with character 13, because frontal-maxillary contact and full enclosure of the maxillary foramen by the maxilla both reflect a proportionally larger orbital exposure of the maxilla. How-

ever, some degree of independence between these characters is indicated by the observation that the maxillary foramen is entirely within the maxilla but the lacrimal and palatine remain in contact in some taxa (e.g., *Dactylopsila*, †*Silvabestius*, †*Litokoala*, †*Lekanoleo*, †*Thylacoleo*).

Character 15. *Orbitosphenoid exposed to lateral view in medial orbital wall (0); or orbitosphenoid laterally inapparent or absent (1).* Bilaterally paired orbitosphenoid ossifications, which always appear to be fused with the median presphenoid element, are prominently exposed to lateral view in the medial wall of the orbit in most metatherians (state 0; e.g., as in *Potorous* [fig. 5A]). Although the orbitosphenoid is fused to the frontal and alisphenoid in adult specimens of *Caenolestes*, it is identifiable as a separate ossification that is clearly exposed in lateral view in subadult specimens (e.g., FMNH 94948).

By contrast, in adult specimens of most Recent peramelemorphians (e.g., *Perameles* [fig. 5B]), the lateral exposure of the orbitosphenoid is much reduced or absent (state 1; Muirhead, 2000; Travouillon et al., 2010). In some specimens, this morphology appears to result from the orbitosphenoid being concealed behind outgrowths of the frontal and/or maxilla (as in AMNH 151939, a specimen of *Peroryctes raffrayana*), whereas in others the orbitosphenoid itself appears to be reduced in size (as in AMNH 190986, a specimen of *Echymipera kalubu*), but we have not distinguished between these apparently alternative conditions when scoring this character. However, the orbitosphenoid remains prominently exposed to lateral view in a few peramelemorphians, namely *Macrotis*, †*Yarala* (Muirhead, 2000), †*Galadi* (Travouillon et al., 2010), and †*Bulungu* (Gurovich et al., 2014), all of which have been scored as state 0. *Isoodon* and *Chaeropus* are both polymorphic ("0+1") for this character.

Character 16. *Maxillary and alisphenoid separate (0); or in contact on orbital floor (1).* Descriptions of character states and an account of their taxonomic distribution among Recent didelphids were provided by Voss and Jansa

(2003: char. 43; 2009: char. 51), who consistently observed maxillary-alisphenoid contact (state 1) only in *Lutreolina* and *Monodelphis* (Voss and Jansa, 2009: fig. 10B). We maintain Voss and Jansa's (2003, 2009) didelphid scoring here, except that we score *Tlacuatzin* as polymorphic ("0+1") for this character. We also observed broad maxillary-alisphenoid contact in †*Sparassocynus* (Beck and Taglioretti, 2020) and †*Thylatheridium*. The maxillary and alisphenoid are separated by the palatine (state 0) in most other metatherians (e.g., *Perameles* [fig. 5B]), but the maxilla and alisphenoid broadly contact one another in all examined macropodiforms (e.g., *Potorous* [fig. 5A] and *Macropus* [Wells and Tedford, 1995: fig. 9]). Narrower maxillary-alisphenoid contact is also consistently present in *Pseudochirops cupreus* (fig. 51), *Ps. archeri*, and *Petropseudes*, and it is sometimes also present in *Pseudochirulus* and *Burramys* (which have been scored as polymorphic).

Character 17. *Foramen rotundum laterally exposed and separate from sphenorbital fissure (0); or foramen rotundum concealed from lateral view, partly or wholly confluent with sphenorbital fissure in rear of orbit (1); or foramen rotundum ventral to sphenorbital fissure (2).* The foramen rotundum (by which the maxillary branch of the trigeminal nerve exits the skull) is separate from the sphenorbital fissure and exposed in lateral view (state 0) in †*Pucadelphys*, †*Allqokirus*, †*Mayulestes*, †*Herpetotherium*, didelphids (e.g., *Monodelphis* [Wible, 2003: fig. 4]), paucituberculatans (with the exception of some specimens of *Rhyncholestes*), †*Yalkaparidon*, peramelemorphians (e.g., *Perameles* [fig. 5B]), dasyuromorphians (with the exception of some specimens of *Neophascogale*, in which the medial wall of the foramen rotundum fails to ossify; see, e.g., right side of AMNH 109520), and many diprotodontians (e.g., diprotodontids, phalangerids, *Dactylopsila*, *Dactylonax*, and thylacoleonids), all of which are scored as state 0. Although Novacek (1993: 458) stated that the foramen rotundum and sphenorbital fissure are confluent in didel-

phids, both openings are distinct and clearly identifiable in all the Recent and fossil didelphid material we examined.

By contrast, the foramen rotundum is concealed from lateral view within a common vestibule that it shares with the sphenorbital fissure in the back of the orbit (state 1) in *Dromiciops*, most macropodiforms (e.g., *Potorous* [fig. 5A]), pseudocheirids, burramyids, and *Acrobates*. Several other taxa—including *Macropus*, *Phascolarctos*, *Distoechurus*, *Petaurus*, *Gymnobelideus*, and *Rhyncholestes*—are polymorphic ("0+1") for this character. A distinctive morphology is seen in *Notoryctes*, in which the foramen rotundum is ventral (rather than lateral) to the sphenorbital fissure (state 2), with the two openings sometimes appearing confluent (e.g., on the left and right sides of AMNH 202105; see also comments by Archer, 1976b: 270, 308). As noted by Voss and Jansa (2003: 27), the foramen rotundum has been misidentified in some published illustrations, notably in drawings of the skull of *Dromiciops* by Hershkovitz (1999: fig. 25), where the true foramen rotundum cannot be seen at all.

These states do not form a plausible morphocline, so this character has not been ordered in any analyses presented here.

Character 18. *Postorbital process of frontal absent or indistinct (0); or present (1).* The dorsal attachment point of the postorbital ligament (which delimits the orbital fossa from the temporal fossa; fig. 1) on the frontal lacks a distinct osteological marker in many metatherians (state 0), but in others (e.g., *Marmosa*, fig. 1) its position is indicated by a distinct, laterally directed postorbital process (state 1). Because the postorbital process (if present) often develops relatively late in postnatal ontogeny (see, e.g., Abdala et al., 2001; Flores et al., 2006, 2010), we scored this character only from adult specimens. Voss and Jansa (2003, 2009) reviewed the distribution of postorbital processes in Recent didelphids, and we largely followed their scoring criteria and decisions here. Following Voss and Jansa (2009), we do not distinguish between postorbital processes that are "flattened" from those that "not flattened" sensu

Voss and Jansa (2003). In addition, we scored Recent didelphids with supraorbital "beads" sensu Voss and Jansa (2009) but lacking distinct, laterally projecting processes as state 0.

Among other metatherians, postorbital processes are absent or indistinct in †*Pucadelphys* (Marshall and Muizon, 1995; Ladevèze et al., 2011: fig. 2), †*Mayulestes* (Muizon, 1994: fig. 1a; 1998), †*Allqokirus* (Muizon et al., 2018), caenolestids (e.g., *Caenolestes* [fig. 35]), *Notoryctes* (fig. 36), most dasyurids (e.g., *Pseudantechinus* [fig. 42]), peramelemorphians (e.g., *Perameles* [fig. 39]), *Dromiciops* (fig. 43), some †diprotodontids (e.g., †*Neohelos* [Murray et al., 2000]), burramyids (e.g., *Burramys* [fig. 46]), acrobatids, *Gymnobelideus*, *Tarsipes* (fig. 49), most pseudocheirids, most phalangerids, and some macropodiforms (e.g., *Lagostrophus* [fig. 53]). By contrast, distinct postorbital processes are present in †*Thylophorops* (Goin et al., 2009b: fig. 5A, B), †*Sparassocynus* (Reig and Simpson, 1972: fig. 2), a few dasyurids (e.g., *Sarcophilus*, *Myoictis*, *Dasyurus*, *Dasykaluta*), thylacinids (e.g., *Thylacinus* [fig. 40]), *Myrmecobius* (fig. 41), and various diprotodontians (e.g., thylacoleonids, phascolarctids, †*Namilamadeta*, *Lasiorhinus*, †*Silvabestius*, *Pseudochirulus*, most petaurids, and some macropodiforms). Specimens of *Macropus giganteus* have a distinct bulge in the lateral wall of the frontal approximately level with the frontal process of the jugal (Wells and Tedford, 1995: fig. 9C), but this convexity is due to an enlarged frontal sinus and is not a true postorbital process (it is distinctly ventral to the dorsolateral margin of the frontal), so we scored *Macropus* as lacking distinct postorbital processes.

Although not amenable to scoring as discrete character states, postorbital processes (where present) vary considerably in size and shape within Metatheria. They are particularly prominent in †*Mimoperadectes* (Horovitz et al., 2009), the Recent didelphids *Caluromys* and *Caluromysiops* (Voss and Jansa, 2009: figs. 38, 39), and †*Sparassocynus* (in which they are large and hornlike [Reig and Simpson, 1972: fig. 2]). In †*Thylacoleo*, they closely approach or meet the frontal

process of the jugal, forming a postorbital bar (see, e.g., Anderson, 1929). Nevertheless, these processes (where identifiable) are usually roughly triangular in outline when viewed dorsally, with the apex directed laterally. A notable exception is seen in *Myrmecobius* (fig. 41), where they form distinctly winglike outgrowths that extend along most of the dorsolateral margin of the frontal and almost contact the lacrimal crest anteriorly.

Character 19. *Postorbital process formed by frontal and parietal (0); or by frontal only (1); or by frontal and lacrimal (2).* The postorbital process is formed exclusively by the frontal (state 1) in most metatherians that possess such a structure (e.g., *Marmosa*, fig. 1), but the postorbital process (where identifiable) is formed by frontal and parietal moieties (state 0) in *Glironia* (Voss and Jansa, 2009: fig. 37), *Distoechurus* (fig. 48), *Petaurus* (fig. 50), *Hemibelideus*, *Petauroides*, *Pseudochirulus*, and some specimens of *Pseudochirops archeri* (e.g., AMNH 253664). Although postorbital processes are not always distinct in adult individuals of *Dactylopsila* and *Dactylonax*, where identifiable they are positioned far anteriorly, on the suture between the frontal and lacrimal, with both of these bones contributing (a remnant of the postorbital ligament is still attached to the right postorbital process of AMNH 194759, a specimen of *Dactylonax palpator*, confirming the identity of this structure); this unusual morphology has been assigned its own state here (state 2). The anterior position of the postorbital process in *Dactylopsila* and *Dactylonax* may be connected with their very dorsally directed orbits (Cartmill, 1974).

We scored this character as inapplicable ("-") only for those taxa in which a postorbital process was not identifiable in any specimen examined (as in, e.g., Recent caenolestids [e.g., *Caenolestes*; fig. 35], *Notoryctes* [fig. 36], *Dromiciops* [fig. 43], *Tarsipes* [fig. 49], and *Acrobates*). However, taxa in which at least one specimen exhibited a distinct postorbital process were scored for this character, even if the modal condition was absence. The states comprising this character have been arranged to form a plausible morphocline, corre-

sponding to a sequential anteroposterior shift in the position of the postorbital processes, and have been ordered in all our analyses.

Character 20. *Facial exposure of jugal variously developed but not deeply bifid (0); or facial exposure of jugal deeply bifid, with distinct anterodorsal and anteroventral processes (1).* The facial exposure of the jugal has a roughly crescentic, straight, or irregular suture with the maxilla in most metatherians (e.g., *Marmosa*; figs. 2, 34; state 0). However, in all peramelemorphians (including †*Yarala*, †*Galadi*, and †*Bulungu*; Muirhead, 2000; Travouillon et al., 2010; 2013b; Gurovich et al., 2014), the facial portion of the jugal is deeply bifid, with distinct anterodorsal and anteroventral processes, usually flanking a deep nasiolabial fossa (an excavation in the maxilla from which the maxillonasolabialis muscle originates) (state 1: figs. 37–39; Filan, 1990; Muirhead, 2000). Although the anteroventral jugal process is absent in one examined specimen of *Echymipera kalubu* (AMNH 190973), we coded the modal condition (bifid jugal with both processes present) for *Echymipera*. The facial exposure of the jugal is weakly bifid in †*Yalkaparidon* (Beck, 2009: fig. 3; Beck et al., 2014), *Dactylopsila*, and some specimens of *Dactylonax*, but the bifurcation is much weaker than in peramelemorphians, and there is no distinct nasiolabial fossa between the anteroventral and posteroventral processes; therefore, we scored these taxa as corresponding to state 0. The maxillo-jugal suture is fused in adult specimens of *Notoryctes*, but CT-scans of a fluid-preserved juvenile (NMV C11082) demonstrate that this suture is not bifid prior to fusion (Beck, in prep.).

Character 21. *Jugal extends posteriorly to glenoid region (0); or jugal terminates well anterior to glenoid region (1).* In all examined metatherians except *Tarsipes*, the jugal extends posteriorly to the glenoid fossa (state 0), a probable therian plesiomorphy (Wible et al., 2005). In *Tarsipes*, however, the jugal terminates well anterior to the glenoid region (fig. 49; Rosenberg and Richardson, 1995; fig. 1c), an autapomorphic morphology that we scored as a distinct state (state 1).

Character 22. *Jugal terminates posteriorly in a faceted preglenoid process (0); or in a ventrally expanded ectoglenoid crest (1); or jugal terminates posteriorly without a distinct process or crest (2).* The jugal produces a knoblike preglenoid process that bears a distinct, posteriorly oriented articular facet (state 0) in most metatherians (e.g., *Marmosa* [fig. 1], *Phascogale* [fig. 10A]). In *Myrmecobius*, however, the jugal terminates posteriorly in a ventrally expanded lateral (ectoglenoid) crest that sometimes bears an indistinct medial articular facet (state 1 [fig. 41]). A similar ventrally expanded crest is seen in *Phascolarctos* and some macropodiforms (e.g., †*Ekaltadeta* [Wroe et al., 1998], *Lagorchestes*, *Setonix*, *Wallabia*, *Lagostrophus*), all of which have also been scored as state 1. By contrast, neither a distinct preglenoid process nor an ectoglenoid crest is present in most diprotodontians (e.g., *Petaurus* [fig. 10B]); in these taxa, the posterior extremity of the jugal tapers dorsoventrally and does not appear to restrict the anterior excursion of the mandibular condyle (state 2). As noted above (char. 21), the jugal of *Tarsipes* terminates well anterior to the glenoid region, so we scored this taxon as inapplicable ("-").

In the absence of a clear transformational relationship among these three conditions, we treated this character as unordered (nonadditive) in all the phylogenetic analyses reported below.

Character 23. *Glenoid process of alisphenoid absent (0); or present (1).* In *Myrmecobius* and most diprotodontians—including diprotodontids, wynyardiids, vombatids (e.g., *Vombatus* [fig. 45]), thylacoleonids, burramyids (e.g., *Burramys* [fig. 46]), phalangerids (e.g., *Phalanger* [fig. 47]), and petaurids (e.g., *Petaurus* [figs. 9C, 10B, 50])—the posterior root of the zygomatic arch is formed exclusively by the squamosal with no contribution from the alisphenoid (state 0). By contrast, a distinct glenoid process ("entoglenoid process" sensu Muizon, 1998; 1999) of the alisphenoid, which may or may not actually participate in the temporomandibular joint, forms part of the posterior zygomatic root (state 1) in all the other metatherians we examined

that could be scored for this character. The latter include †*Allqokirus* (Muizon et al., 2018: fig. 21), †*Mayulestes* (Muizon, 1998: fig. 8), †*Pucadelphys* (Muizon, 1999: char. 5), didelphids (e.g., *Marmosa* [figs. 1, 9A, 34]), pauctituberculatans (e.g., *Caenolestes* [fig. 35]), thylacinids (e.g., *Thylacinus* [fig. 40]), dasyurids (e.g., *Phascogale* [figs. 9B, 10A], *Pseudantechinus* [fig. 42])), *Phascolarctos* (fig. 44), acrobatids (e.g., *Distoechurus* [fig. 48]), most macropodiforms (e.g., *Lagostrophus* [fig. 53]), and some specimens of the pseudocheirid *Hemibelideus*.

Dorsolateral Braincase

The dorsolateral braincase—including the parietals and the interparietal (if identifiable as a distinct ossification), together with parts of the frontals, alisphenoid, and squamosals—encloses and protects the brain and provides the surface of origin for the temporalis muscle. Taxonomically variable features of the dorsolateral braincase among Recent and extinct metatherians include the fusion or persistence of sutures, alternative patterns of contact among closely juxtaposed bones, the development of crests for muscle attachment, presence/absence of fenestrae, and pneumatization of braincase-roofing elements. For the most part, terminology for dorsolateral braincase features is not complicated by synonymous usage in the metatherian literature. Two exceptions that we note here are "postparietal," which has been used some authors (e.g., Marshall, 1976; see also Novacek, 1993: 472) to refer to the interparietal bone (= os interparietalis [International Committee on Veterinary Gross Anatomical Nomenclature, often cited as NAV]), and "temporal crest" (as in Macalister, 1872; Thomas, 1888) which is synonymous with the sagittal crest.

Character 24. *Median suture between left and right frontals unfused in subadults (0); or median frontal suture at least partially fused in subadults (1).* In most metatherians, the right and left frontals are separated by a median suture that persists throughout adult life (state 0). However,

Voss and Jansa (2009) noted that the frontals are coossified early in postnatal life in several Recent didelphids (*Chironectes*, *Didelphis*, *Lutreolina*, and *Philander*), such that the median suture between them is partly or completely fused in all examined subadult and young adult specimens (and in most juveniles as well; state 1). Partial or complete fusion of the median frontal suture is also consistently seen in subadult caenolestids, Recent vombatids, †*Sparassocynus*, *Thylacinus*, *Notoryctes*, and *Hemibelideus*, all of which have been scored as corresponding to state 1. Subadult frontal fusion is also variably present in *Ailurops*, which has been scored as polymorphic ("0+1").

Taxa in which the median frontal suture is unfused in subadults but fused in mid- to late-stage adults (e.g., †*Nimbadon*; Black et al., 2010: table 1) have been scored as state 0 because this fusion reflects the widespread mammalian trend of sutural obliteration during adulthood rather than the precocial fusion described above. Therefore, our scoring criteria are more restrictive than those employed by Voss and Jansa (2009), who scored the Recent didelphid *Caluromysiops* as exhibiting fusion of the median frontal suture based on the condition in most of the fully adult individuals they examined. Given that we were unable to examine any subadult specimens of *Caluromysiops*, and that one fully adult specimen retains an unfused median frontal suture (FMNH 84426; Voss and Jansa, 2009: 32), we prefer to score this taxon as unknown ("?"). Other taxa in which the median frontal suture is fused in adults but for which no subadult specimens could be examined (e.g., *Dactylonax*, and many fossil taxa) have also been scored as unknown. Taxa in which this suture remains completely unfused in most or all adult specimens could obviously be scored as state 0 regardless of the availability of younger individuals.

Character 25. *Median suture between left and right parietals unfused in subadults (0); or median parietal suture at least partially fused in subadults (1).* Resembling the widespread frontal morphology described above, the paired parietal bones are likewise separated by a median suture that per-

sists to adulthood in most metatherians (state 0). However, Osgood (1921: 103) noted the absence of a median parietal suture in *Caenolestes* (fig. 35) and implied that a similar condition is seen in peramelemorphians. We observed complete fusion of this suture (state 1) in subadult *Caenolestes* and *Rhyncholestes*, but we were unable to examine subadult specimens of *Lestoros*, which is here scored as unknown ("?"). The median parietal suture is at least partially fused in all examined subadult peramelemorphians except *Rhynchomeles*, which is polymorphic for this character (the median parietal suture is unfused in BMNH 1920.7.26.35, an adult male). Other taxa in which this suture is fused in subadults include †*Pucadelphys*, †*Allqokirus* (Muizon et al., 2018), several phalangerids (*Spilocuscus*, *Strigocuscus*, and some specimens of *Ailurops* and *Phalanger*), †*Nimbadon* (Black et al., 2010), Recent vombatids, *Thylacinus* (Warburton et al., 2019: fig. 3), and some specimens of *Myoictis* (e.g., AMNH 152010). As for the preceding character, we scored taxa as corresponding to state 1 only if this suture is at least partially fused in subadult specimens; taxa were scored as unknown ("?") if subadults were not examined. Taxa were also scored as unknown if the region of the median parietal suture is concealed by the sagittal crest in available specimens.

Character 26. *Parietal and alisphenoid in contact on lateral aspect of braincase (0); or frontal and squamosal in contact (1).* Descriptions of character states and an account of the distribution of this character among Recent didelphids were provided by Voss and Jansa (2003), whose character 36 is slightly rephrased above. As noted by Voss and Jansa (2003, 2009), most didelphids exhibit parietal-alisphenoid contact (state 0), with *Metachirus* uniquely exhibiting frontal-squamosal contact (state 1). Most non-didelphid metatherians also exhibit parietal-alisphenoid contact, notably including some fossil peramelemorphians (†*Yarala*, †*Galadi*, and †*Bulungu* [see Muirhead, 2000; Travouillon et al., 2010; Gurovich et al., 2014]) and the fossil vombatid †*Warendja*.

By contrast, frontal-squamosal contact occurs in Recent peramelemorphians (figs. 37–39), some dasyurids (*Sminthopsis* and *Antechinomys*; Archer, 1981), *Thylacinus* (fig. 40), *Dromiciops* (fig. 43; contra Hershkovitz, 1999: fig. 25), Recent vombatids, diprotodontids, †*Thylacoleo*, †*Namilamadeta*, *Petaurus* (fig. 50), *Gymnobelideus*, and many nonmacropodid macropodiforms (e.g., *Potorous* [fig. 54]). Frontal-squamosal contact is also occasionally seen in *Pseudantechinus* (e.g., AMNH 162569), but alisphenoid-parietal contact is the modal condition (fig. 42). *Phascolarctos*, *Neophascogale*, and *Phascolosorex* are polymorphic ("0+1") for this character. The sutural pattern of the lateral aspect of the braincase is not discernable in adult specimens of *Notoryctes*, but CT-scans of a fluid-preserved juvenile (NMV C11082) demonstrate that the frontal and squamosal are in contact (Beck, in prep.) contra Horovitz and Sánchez-Villagra (2003: char. 176) and subsequent studies that have used versions of their matrix (e.g., Sánchez-Villagra et al., 2007; Beck et al., 2008a; Horovitz et al., 2008, 2009).

In general, our observations are congruent with those of Wroe et al. (1998: 744), except that we score †*Yalkaparidon* as exhibiting parietal-alisphenoid contact: the squamosal and frontal are in contact in QMF13008 (the only known skull of *Y. coheni*), but much of the alisphenoid contribution to the lateral wall of the braincase appears to have flaked off; when intact, the alisphenoid would almost certainly have contacted the parietal in this specimen (Beck et al., 2014: fig. 7, 142).

Character 27. *Scars of M. temporalis origin on braincase not fused middorsally to form sagittal crest in adults (0); or sagittal crest short in adults, extending from nuchal crest onto parietals, but not extending onto frontals (1); or sagittal crest long in adults, extending onto frontals (2).* Voss and Jansa (2003: char. 35) summarized the morphology and taxonomic distribution of the sagittal crest among Recent didelphids, but we follow Voss and Jansa (2009: char. 57) in recognizing an intermediate state between absence of a sagittal

crest and presence of a large crest extending to the frontals, namely a small sagittal crest that is present on the parietals but that does not extend onto the frontals. Voss and Jansa (2009: 32–33) briefly discussed the distribution of sagittal crests in selected nondidelphid metatherians, and we extend their observations here. A sagittal crest is consistently absent (state 0) in adult caenolestids (e.g., *Caenolestes* [fig. 35]), *Notoryctes* (fig. 36), some peramelemorphians (e.g., *Chaeropus* [fig. 37] and *Perameles* [fig. 39]), *Myrmecobius* (fig. 41), some dasyurids (e.g., *Pseudantechinus* [fig. 42]), *Dromiciops* (fig. 43), Recent vombatids (e.g., *Vombatus* [fig. 45]), some macropodiforms, and most other diprotodontians.

In most of the remaining taxa we examined, a sagittal crest is present in at least some adult specimens, but it is usually small, present only on the parietals (state 1). However, a large sagittal crest extending to the frontals (state 2) is seen in †*Thylatheridium* (Reig, 1958a: figs. 5, 6), †*Thylophorops* (Goin et al., 2009b: fig. 5A), †*Yarala* (Muirhead, 2000), †*Galadi* (Travouillon et al., 2010), a few dasyurids (e.g., *Sarcophilus*, *Dasyurus*, and †*Barinya* [Wroe, 1999]), thylacinids (e.g., *Thylacinus* [fig. 40]), a few diprotodontians (e.g., †*Ekaltadeta* [Wroe et al., 1998], most specimens of *Dactylonax*, some specimens of *Dactylopsila*), and some specimens of *Macrotis* ([fig. 38]). Ontogenetically variable, the sagittal crest is often absent in juveniles but present in conspecific adults (e.g., Abdala et al., 2001; Flores et al., 2006; Black et al., 2010), so we scored this character only from specimens with fully erupted permanent dentitions. Because the states of this character form a plausible morphocline, we treated it as ordered in all our phylogenetic analyses.

Character 28. *Petrosal not exposed on posterolateral braincase (0); or exposed through a posterolateral fenestra (1).* In most metatherians, the petrosal is not exposed on the posterolateral braincase (state 0), but a distinct fenestra exposes the underlying pars canalicularis of the petrosal on the posterolateral surface of the braincase anterior to the lambdoid crest (state 1) in some Recent didelphids (Voss and Jansa, 2003: char.

37; 2009: char. 58). Interestingly, we observed a similar morphology in several macropodids, namely *Lagostrophus*, *Notomacropus*, *Osphranter*, *Onychogalea*, *Setonix*, *Wallabia*, and some specimens of *Macropus*, *Petrogale*, and *Thylogale*; in Wells and Tedford's (1995: fig. 9B) cranial illustration of *Macropus giganteus*, this fenestra is labelled as the postsquamosal fissure. In all the didelphids and in most of the macropodids in which it is present, this fenestra is contained within the squamosal-parietal suture (Voss and Jansa, 2009: fig. 12B), but it is surrounded by the squamosal in *Setonix* (see char. 29).

Character 29. *Fenestra exposing petrosal on posterolateral braincase within squamosal-parietal suture (0); entirely within squamosal (1).* As noted above, the fenestra that exposes the petrosal on the posterolateral braincase in some didelphids and macropodids is usually within the squamosal-parietal suture (state 0), but the fenestra is entirely within the squamosal (state 1) of *Setonix*. This character was scored as inapplicable ("-") in all taxa with an unfenestrated posterolateral braincase.

Character 30. *Interparietal absent, very small, or polymorphic (0); or large and consistently present (1).* There is significant disagreement in the literature concerning the occurrence of the interparietal (sometimes referred to as the postparietal) among metatherian mammals. Novacek (1993), for example, stated that marsupials lack an interparietal, whereas Rougier et al. (1998: char. 155) and subsequent studies that have used versions of this matrix (e.g., Wible et al., 2001; Rougier et al., 2015; Ni et al., 2016) scored an interparietal as absent in †*Mayulestes* but present in †borhyaenids, *Didelphis*, *Marmosa*, dasyurids, and *Dromiciops*. Because these authors did not explain the observational basis for their discrepant conclusions, the criteria by which an interparietal can be recognized as such clearly merit discussion. Our observations suggest that metatherians exhibit substantial parsimony-informative variation in interparietal morphology that has yet to be incorporated in any phylogenetic analysis. We also discuss Koyabu et

al.'s (2012: supplementary information, p. 4) observations regarding the presence or absence of this bone in metatherians.

A single, large, wedge-shaped or oblong interparietal bone is unequivocally present (state 1) in thylacinids, †*Barinya* (Wroe, 1999), *Myrmecobius* (fig. 41), *Dromiciops* (fig. 6A; fig. 43), and in all our diprotodontian terminals that could be scored for this character except vombatids. In these taxa, the sutures that separate the interparietal from adjacent bones (supraoccipital and parietals) are clearly visible in all of the juvenile skulls we examined—with the notable exception of *Dactylopsila* and *Dactylonax* (see char. 31)—and they remain obvious in adult specimens of *Myrmecobius*, *Dromiciops*, and most diprotodontians. In some adult diprotodontians (e.g., phalangerids and pseudocheirids), however, the interparietal is almost completely overgrown by parietal scars (from which the temporalis muscle originates), which meet in the midline to form a sagittal crest that conceals the median parietal suture (see comments under char. 27). This may explain Murray et al.'s (1987: table 2) statement that the interparietal is "very small" in *Trichosurus vulpecula*: the interparietal does indeed appear to be small in older adults due to overgrowth by the parietals, but it is a large and obvious element separated by distinct sutures from surrounding bones in all of the juvenile, subadult, and young adult specimens of *T. vulpecula* that we examined. Although large and distinctly sutured in juvenile *Thylacinus* (e.g., SAM M1958; see also Newton et al., 2018: supplemental material), the interparietal is indistinguishably fused with both the supraoccipital and the parietals in older specimens (fig. 40), whereas the interparietal fuses with the parietals (but not with the supraoccipital) in subadult and adult specimens of *Strigocuscus* (e.g., AMNH 196498, 196503).

Our observations regarding diprotodontians exhibit some apparent discrepancies with those of Black et al. (2012a: char. 63), who scored the interparietal as absent in †*Lekanoleo* and †*Nimbadon*. We consider the interparietal to be clearly present and large in both of these taxa: in

†*Lekanoleo*, the parietal-interparietal suture is identifiable in dorsal view on the left side of QM F23453 (contra Gillespie et al., 2020: 6), and the interparietal can be identified as a distinct ossification when viewed ventrally through the foramen magnum of this specimen. In †*Nimbadon*, the interparietal is clearly a large, distinct ossification in QM F53648 (a pouch young specimen; see Black et al., 2010: fig. 10A). Black et al. (2012a) also scored the interparietal as absent in †*Namilamadeta* and †*Ngapakaldia*, whereas we consider available specimens of both of these taxa to be insufficiently well preserved to determine whether or not this bone was present. However, Black et al. (2012a) used a slightly different scoring criterion to ours, namely whether or not a suturally distinct interparietal is visible in adult specimens (K.H. Black, personal commun.).

As discussed by Voss and Jansa (2009: 34–35), an interparietal is also unambiguously present in didelphids, all of which exhibit a large, unpaired element wedged between the right and left parietals anterior to the lambdoid crest (fig. 6B), in the same position as the sutured interparietals described above. The didelphid interparietal, however, is fused with the supraoccipital even in very young juveniles—including the youngest available postweaning juveniles (corresponding to age class 1 of Gardner [1973; see also Tyndale-Biscoe and MacKenzie, 1976; Tribe, 1990; van Nievelt and Smith, 2005a])—none of which show any trace of a suture (see also Koyabu et al., 2012: fig. S4A-D). Developmental studies of *Didelphis* (Nesslinger, 1956) and *Monodelphis* (Clark and Smith, 1993), however, demonstrate the presence of a distinct interparietal center of ossification that fuses to the supraorbital early in postpartum life (see char. 31). The didelphid interparietal does not, however, fuse with the parietals (as it does in *Thylacinus* and *Strigocuscus*), nor is it overgrown by them (as it is in some diprotodontians), the sutures between these bones persisting even in the largest adult specimens we examined (see also Koyabu et al., 2012: fig. 3A).

A large, wedge-shaped element that extends from the lambdoid crest between the left and right parietals and that is similar in size and position to the unequivocal interparietals discussed above is present in the only known skull of †*Yalkaparidon* (QM F13008; Beck et al., 2014). However, there is no clear suture separating this element from the supraoccipital in QM F13008, which is clearly a large adult (Beck et al., 2014). Nevertheless, given the large size of this element and its morphological resemblance to the undoubted interparietals of other metatherians in which these bones are present, we tentatively scored †*Yalkaparidon* as corresponding to state 1.

The interparietal is very small and polymorphic or absent (state 0) in all Recent dasyurids. Although at least some specimens of several dasyurids exhibit a minute sutured interparietal (e.g., *Pseudantechinus* [fig. 42]), we failed to identify a suturally distinct interparietal in dry skulls of comparably immature individuals of others (e.g., *Myoictis*), and it does not seem useful to distinguish these conditions (vestigial versus absent) in the context of this analysis. Frigo and Woolley (1996: figs. 2, 3) labeled a middorsal ossification center on the occiput of cleared-and-stained pouch young of *Sminthopsis* as the interparietal, but the absence of any other mineralized element between the foramen magnum and the parietals in their material strongly suggests that the structure in question is the supraoccipital. This supposition is supported by images of cleared and stained *Sminthopsis* pouch young provided to us by D. Koyabu (see also Koyabu et al., 2012), in which the large single middorsal ossification on the occiput is clearly the supraoccipital. The same images reveal the presence of several (probably three) much smaller ossifications between the supraoccipital and paired parietals, and we agree with Koyabu et al. (2012) that these are likely homologous with the interparietal. However, these ossifications are very small, and our failure to identify a distinct interparietal in dry skulls of immature *Sminthopsis* specimens (e.g., SAM M11536) suggests that they are variably present or absent; therefore, we scored *Sminthopsis* as state 0 for this study.

The interparietal is also very small or not identifiable as a suturally distinct ossification in *Vombatus* and *Lasiorhinus*. We were not able to ascertain the morphology of the interparietal in †*Warendja* based on specimens we examined. However, Brewer (2007: 164) described additional material of †*Warendja*, and stated that "there is no evidence of an interparietal process [sic] of the occipital," implying that an interparietal was absent in this taxon as well; therefore, we score it as absent here. The interparietal of *Dactylopsila* and *Dactylonax* is apparently fused to the supraoccipital in even the youngest juvenile specimens that we examined, resembling didelphids in this respect (see char. 31).

Based on our observations of dry skulls, a distinct interparietal appears to be entirely absent in peramelemorphians, which show no trace of any bony element wedged between the parietals anterior to the lambdoid crest; instead, the median parietal suture extends all the way to the supraoccipital in juvenile specimens (e.g., *Echymipera* [fig. 6C]). Unfortunately, the neonatal specimens of *Isoodon obesula* and *Perameles nasuta* examined by Esdaile (1916) were too young to show any ossification centers behind the parietals, and Koyabu et al. (2012) were unable to find conclusive evidence for either the presence or absence of the interparietal in *Perameles* (D. Koyabu, personal commun.). Peramelemorphia may therefore represent an exception to Koyabu et al.'s (2012) general conclusion that the interparietal is present (at least embryologically) in all extant mammalian orders.

As discussed by Voss and Jansa (2009: 88), a specimen of †*Herpetotherium* (AMNH 127684) preserves the dorsal skull roof and reveals the presence of a median parietal suture that extends posteriorly as far as the supraoccipital, without any other intervening bony element. Thus, †*Herpetotherium* resembles peramelemorphians in lacking an obvious interparietal. Selva and Ladevèze (2016) identified a fragment of bone on the left side of a specimen of another herpetotheriid, †*Peratherium cuvieri* (MNHN GY679), as representing part of the interparietal, but this fragment appears to be located well lateral to the median parietal suture (Selva and Ladevèze, 2016: fig. 3), in which case it is more likely to be part of the squamosal.

We scored as missing ("?") taxa in which all available specimens show partial or complete fusion of the median parietal suture. In such taxa, which include Recent caenolestids (e.g., *Caenolestes* [fig. 35]) and *Notoryctes* (fig. 36), it is impossible to distinguish between absence of the interparietal (as in peramelemorphians) versus fusion of the interparietal with the parietals (as in *Thylacinus*). In this context, we note some important discrepancies between our observations and published accounts of certain key fossil taxa. We examined multiple individuals of †*Pucadelphys*, including several subadults (MHNC 8265, 8384, 8388, 8391 [see Ladevèze et al., 2011]), but all of these specimens exhibit fusion of the sutures of the dorsal braincase. We therefore scored †*Pucadelphys* as unknown ("?") contra Marshall and Muizon (1995: 50, fig. 12), who identified paired "postparietals" in this taxon. Although the interparietal of mammals apparently develops from four ossification centers—homologous with the paired postparietals and tabulars of plesiomorphic amniotes (Koyabu et al., 2012)—the interparietal is almost always a single ossification in the taxa we examined (exceptions include two specimens each of *Myrmecobius* [AM 3102, SAM M20184] and *Vombatus* [AM 7937, SAM M840]). Hence, the alleged presence of paired interparietals in †*Pucadelphys* (which our observations failed to confirm) would be highly unusual within Metatheria. Similarly, we could not identify the median parietal suture in the holotype (and only known) skull of †*Mayulestes* (MHNC 1249), which we also scored as unknown (contra Muizon 1998: fig. 6, which implies that an interparietal is absent in this taxon). Muizon et al. (2018: 399) inferred that †*Allqokirus* has an interparietal because "this bone is apparently universal for mammals (Koyabu et al., 2012)" (but note our comments regarding peramelemorphians and some dasyurids, above). However, fusion of the
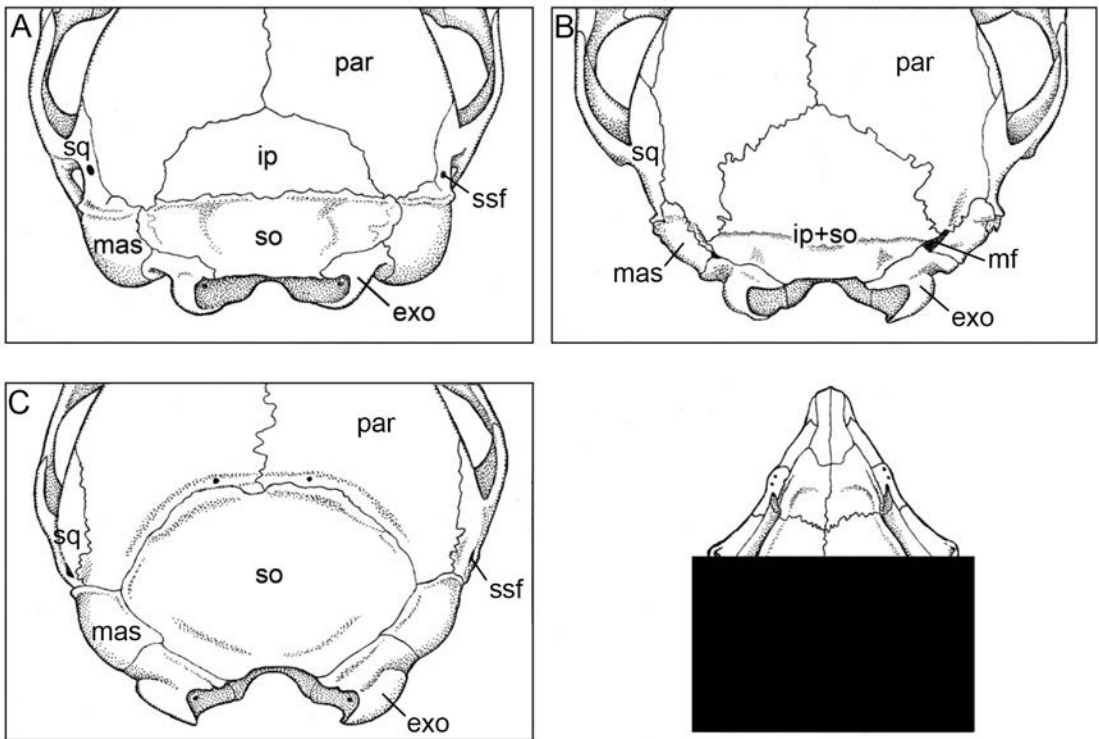
FIG. 6. Posterior braincase of *Dromiciops gliroides* (**A,** UWBM 78641), *Marmosa murina* (**B,** AMNH 266418), and *Echymipera kalubu* (**C,** AMNH 190977). Alternative states for characters 30 and 31 (see main text for descriptions of these characters and character states) are illustrated as follows: *Dromiciops* 30(1), 31(0); *Marmosa* 30(1), 31(1); *Echymipera* 30(0), 31(-). Note that the incompletely mineralized lambdoid sesamoids (see Character 89) have fallen away in this juvenile specimen of *Echymipera* (the mature morphology is illustrated in fig. 11), fully exposing the parietal-supraoccipital suture. Abbreviations: **exo,** exoccipital; **ip,** interparietal; **mas,** mastoid; **mf,** mastoid fenestra; **par,** parietal; **so,** supraocciptal; **sq,** squamosal; **ssf,** subsquamosal foramen. Specimens are not drawn to the same scale.

median parietal suture in the holotype and only known specimen of †*Allqokirus* (MHNC 8267) means that the interparietal cannot be identified as a suturally distinct ossification, so we also scored this taxon as unknown.

Muizon and Ladevèze (2020) described the cranial anatomy of another Tiupampan metatherian, †*Andinodelphys cochabambensis* (which has not been included here, but which appears to be a close relative of †*Pucadelphys*) and concluded that a large interparietal was probably present in this taxon. This inference was based on the presence of a thickened ridge on the left side of the dorsal skull roof of †*A. cochabambensis* (MHNC

8370) that Muizon and Ladevèze (2020) identified as a probable fused parietal-interparietal suture. If so, then the interparietal is anteriorly more extensive in †*Andinodelphys* than in any other metatherian we have examined (Muizon and Ladevèze, 2020: fig. 17A). However, this ridge is present on only one side of MHNC 8370, and it is not apparent on another specimen of †*A. cochabambensis* in which the dorsal skull roof is similarly well preserved (MHNC 8264), so we are not convinced that it is a fused parietal-interparietal suture; it may instead be a raised area of muscle attachment (temporal line) for the temporalis muscle. Frustratingly, it there-

fore remains unclear whether an interparietal was present or absent in any of the Tiupampan metatherians due to fusion of the sutures of the bones making up the posterior part of the dorsal skull roof in all available specimens that preserve this region.

Character 31. *Interparietal separated from supraoccipital by an open suture, at least in juvenile specimens (0); or interparietal-supraoccipital suture fused in juveniles and adults alike (1).* In most taxa in which an interparietal is identifiable, this bone is separated from the supraoccipital by an obvious suture in juveniles (state 0), although this suture sometimes fuses in adult specimens (e.g., *Thylacinus*). However, as discussed above (see char. 30), the large interparietal of didelphids is fused with the supraoccipital (state 1; e.g., in *Marmosa* [fig. 6B]) in even the smallest examined juvenile skulls. Although Voss and Jansa (2009: 39) stated that this morphology "appears to be unique among marsupials," we additionally note its presence in *Dactylopsila* and *Dactylonax*: examination of very young juveniles of *Dactylopsila* (e.g., AMNH 154417, 101988) and *Dactylonax* (e.g., AMNH 109415, 221611) reveals no evidence of a suture separating the interparietal from the supraoccipital in these specimens. This suture is also fused in some juvenile specimens of *Vombatus* (e.g., MVZ 135036), which has been scored as polymorphic ("0+1") here.

The suture separating the interparietal from the supraoccipital cannot be unequivocally identified in the only known cranium of †*Yalkaparidon* (QM F13008, the holotype of †*Y. coheni*). However, based on its large size compared with cranial fragments and isolated mandibles of other †*Yalkaparidon* specimens, QM F13008 appears to represent an old adult individual (Beck et al., 2014), and it is possible that the interparietal-supraoccipital suture fused relatively late in ontogeny, as occurs in *Thylacinus*; in the absence of cranial material of younger †*Yalkaparidon* individuals, we scored this taxon as unknown ("?").

We scored this character as inapplicable ("-") for peramelemorphians, in which a distinct interparietal appears to be absent (e.g., *Echymipera*; fig. 6C), and as unknown ("?") in †*Pucadelphys*, †*Allqokirus*, †*Mayulestes*, caenolestids, *Notoryctes*, and other taxa in which the presence or absence of an interparietal cannot be determined with confidence (see char. 30).

Character 32. *Parietal and mastoid in contact (0); or squamosal prevents parietal-mastoid contact (1).* The parietal extends posteriorly to the lambdoid crest and contacts the mastoid exposure of the pars canalicularis of the petrosal in most didelphids (state 0; fig. 6B; Voss and Jansa, 2009: fig. 13A, B). In other didelphids, however, parietal-mastoid contact is prevented by contact between the squamosal and the interparietal (state 1; Voss and Jansa, 2009: fig. 13C, D). The parietal and mastoid are in contact in most other metatherians (e.g., *Dromiciops* [fig. 6A] and *Echymipera* [figs. 6C, 11]). However, parietal-mastoid contact is prevented in some taxa, either by contact between the squamosal and interparietal or between the squamosal and the supraoccipital; the latter morphology is seen in some taxa that entirely lack an interparietal, such as *Lasiorhinus*. Thus, we do not distinguish between the alternative ways that the squamosal prevents parietal-mastoid contact, but subsume them within state 1 and have modified the character description of Voss and Jansa (2009: char. 61) accordingly.

In *Setonix*, there is a large unossified vacuity dorsal to the mastoid exposure (the mastoid fenestra; see char. 91), so neither parietal-mastoid nor squamosal-supraoccipital contact is present; we therefore scored *Setonix* as inapplicable ("-"). Because parietal-mastoid contact is possible only when the mastoid is extensively exposed on the lateral occiput, we also scored this character as inapplicable for taxa in which the occipital exposure of the mastoid is restricted ventrally, namely phalangerids (fig. 12C; see char. 90). This character was scored as unknown ("?") in acrobatids because the squamosal and mastoid of *Acrobates* and *Distoechurus* are seamlessly fused and cannot be distinguished as separate elements (see char. 88). Although this region is

fused in adult specimens of *Notoryctes*, CT-scans of a fluid-preserved juvenile (NMV C11082) demonstrate that the parietal and mastoid are in contact in this taxon (Beck, in prep.).

Character 33. *Extensive pneumatized endocranial sinuses within parietal absent (0); or present (1).* Enlarged frontal sinuses are present in many marsupials (e.g., *Spilocuscus* [Helgen and Flannery, 2004], †*Ekaltadeta* [Wroe et al., 1998], and *Thylacinus* [Warburton et al., 2019: fig. 5]), but the parietal usually lacks extensive pneumatization (state 0). Although damaged and sectioned skulls reveal that the parietal is greatly thickened in *Lasiorhinus* and *Vombatus* (the "thickhead" condition sensu Murray, 1992), we did not score this condition as a distinct state. A qualitatively distinct morphology, however, is observable in damaged skulls of †*Nimbadon* (Black et al., 2010: fig. 11), †*Neohelos* (Murray et al., 2000a: fig. 38), †*Silvabestius*, and †*Thylacoleo*. In these taxa, extensive air-filled endocranial sinuses separate the inner table of the endocranial cavity from the outer table of the external skull surface throughout the parietal contribution to the dorsolateral braincase (the "airhead" condition sensu Murray, 1992), a morphology that we scored as state 1.

<center>Palate</center>

The bony palate separates the nasal cavity from the oral cavity, and it includes parts of only three bones—premaxillaries, maxillaries, and palatines. Despite this simplicity of function and composition, the palate exhibits remarkable taxonomic variation in several mammalian clades, notably Metatheria and Rodentia. Among metatherians, most noteworthy palatal variation involves foramina (which transmit nerves and blood vessels) and fenestrae. The latter term is used here for openings that are not known to transmit anything, as well as those that are much larger than the vessels or nerves that pass through them (thus resembling windows—fenestrae—rather than conduits). Unhappily, much terminological inconsistency is associated with
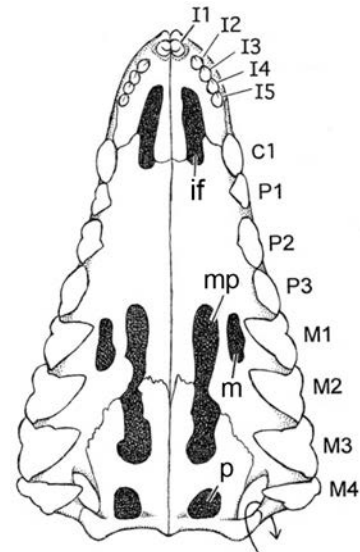
FIG. 7. Palatal morphology of *Thylamys venustus* (AMNH 261254) illustrating nomenclature for fenestrae, foramina, and other features described in the text (reproduced from Voss and Jansa, 2003: fig. 5; 2009: fig. 14). Dental loci (I1–M4) provide convenient landmarks for defining the size and position of palatal structures. Abbreviations: **if**, incisive foramen; **m**, maxillary fenestra; **mp**, maxillopalatine fenestra; **p**, palatine fenestra; **plpf**, posterolateral palatal foramen.

metatherian palatal foramina and fenestrae; the nomenclature adopted in these accounts follows that of Voss and Jansa (2009) and is illustrated in figure 7; it is compared with synonymous usage in table 9.

Character 34. *Paracanine fossa present (0); or absent (1).* A distinct paracanine fossa occupies the diastema between the posteriormost upper incisor and C1, where it accommodates the apex of the lower canine (state 0) in fully adult specimens of †*Pucadelphys* (Marshall and Muizon, 1995: fig. 12; Muizon et al., 2018: fig. 4D), †*Allqokirus* (Muizon et al., 2018: fig. 4A), †*Mayulestes* (Muizon, 1998: fig. 6; Muizon et al., 2018: fig. 4B), most Recent didelphids (e.g., *Marmosa* [figs. 1, 2, 34]), †*Thylatheridum,* †*Thylophorops*, most dasyuromorphians, and †*Microbiotherium*. A paracanine fossa is also present in †*Sparas-*

TABLE 9

Selected Anatomical Synonyms for Structures of the Palate

This report	Synonym
Accessory palatal fenestra	anterior palatal foramen (Helgen and Flannery, 2004); accessory vacuity (Lynne and Mort, 1981)
Incisive foramen	anterior palatal fenestra (Murray, 1992); anterior palatal fissure (Ride et al., 1997); anterior palatal foramen (Osgood, 1924); anterior palatal vacuity (Ride, 1956); anterior palatine foramen (Thomas, 1888); anterior palatine vacuity (Dederer, 1909); fissura palatina (NAV); incisive fenestra (Goin et al., 2007; Martin, 2007); incisive palatal foramen (Owen, 1839); incisive vacuity (Goin and Candela, 1998; Muirhead and Wroe, 1998); interincisive foramen (Black, 2010; Black and Hand, 2010); palatal fissure (Ride et al., 1997); palatine fissure (Rowe et al., 2005); palatine foramen (Thomas, 1888); premaxillary foramen (Hershkovitz, 1992); premaxillary palatal vacuity (Van Dyck, 1980); premaxillary vacuity (Archer, 1975)
Maxillary fenestra	lateral vacuity (Hershkovitz, 1992); maxillary vacuity (Hershkovitz, 1992); mesolateral fenestra (Creighton, 1984)
Maxillopalatine fenestra	greater palatine fenestra (Murray, 1989); greater palatine vacuity (Murray, 1989); major palatine foramen (Wible, 2003); maxillary fenestra (Archer, 1976c); maxillary palatal vacuity (Archer, 1975); maxillary-palatine vacuity (Wroe et al., 1998); maxillary vacuity (Archer, 1975); maxillopalatine vacuity (Hershkovitz, 1992); mesolateral vacuity (Hershkovitz, 1992); palatal vacuity (Gregory, 1910); palatine fenestra (Clemens et al., 1989); palatine foramen (Novacek, 1993); palatine vacuity (Marshall, 1977); posterior palatal fenestra (Tate and Archbold, 1941); posterior palatal foramen (Tate, 1933); posterior palatal vacuity (Owen, 1839); posterior palatine fenestra (Goodwin, 1961); posterior palatine foramen (Esdaile, 1916); posterior palatine vacuity (Thomas, 1888)
Palatine fenestra	accessory post-palatal vacuity (Tate, 1933); palatine palatal vacuity (Van Dyck, 1980); palatine vacuity (Archer, 1975); posterior palatal foramen (Owen, 1839); posterior palatine vacuity (Thomas, 1888); posteromedial fenestra (Creighton, 1984); posteromedial vacuity (Hershkovitz, 1992); postpalatal foramen (Owen, 1873); postpalatine foramen (Owen, 1877)
Posterolateral palatal foramen	foramen palatinum caudale (NAV); lateral posterior palatal foramen (Tate, 1933); minor palatine foramen (Horovitz and Sánchez-Villagra, 2003; Wible, 2003); palatine canal (Clemens, 1989); posterior palatal foramen (Kirsch and Archer, 1982); posterior palatine foramen (Wells and Tedford, 1995); posteroexternal palatine foramen (Gregory, 1910); posterolateral fenestra (Creighton, 1984); posterolateral foramen (Dederer, 1909); posterolateral palatine foramen (Dederer, 1909); posterolateral vacuity (Hershkovitz, 1992); postpalatine foramen (Marshall and Muizon, 1995)

[a] References other than *Nomina anatomica veterinaria* (NAV, 6th ed.) include the earliest relevant synonymic usage in the marsupial literature of which we are aware, but this list is not intended to be exhaustive.

socynus, although it takes the form of an open notch rather than an enclosed fossa (Reig and Simpson, 1972). By contrast, a distinct paracanine fossa is absent (state 1) in *Dromiciops*, most peramelemorphians (†*Galadi* is a notable exception; Travouillon et al., 2010: fig. 3), a few dasyurids (*Ningaui*, *Phascogale*, and *Antechinomys*), *Notoryctes*, †*Yalkaparidon*, and all known paucituberculatans and diprotodontians.

Character 35. *Accessory palatal fenestrae absent (0); or present (1).* The bony palate of most metatherians is unperforated between the incisive foramina and the maxillopalatine fenestrae (state 0), but some peramelemorphians (e.g., †*Yarala* [Muirhead, 2000: fig. 1.1], †*Bulungu* [Gurovich et al., 2014: fig. 3], *Chaeropus* [fig. 37], *Microperoryctes*, *Perameles* [fig. 39], some specimens of *Peroryctes*) exhibit one or more pairs of nonvascular openings in the maxillary palate at the level of P1 and/or P2 (state 1). These appear to have first been named by Lyne and Mort (1981: 124), who called them

"accessory vacuities." They appear to lack obvious homologs in other examined taxa. By contrast, Osgood (1921: 107) implied that the long incisive foramina of Recent caenolestids (e.g., *Caenolestes* [fig. 35]) correspond to both the incisive foramina and the anteriormost palatal fenestrae of peramelemorphians. Although we have not dissected the soft tissues of any peramelemorphian palates, this equivalence seems implausible. Except in length, the well-formed incisive foramina of peramelemorphians and Recent caenolestids are structurally indistinguishable from each other and from the incisive foramina of didelphids, which are thought to transmit both the nasopalatine duct, blood vessels, and nerves (Wible, 2003: 175). By contrast, the accessory palatal fenestrae of peramelemorphians have the irregular aspect of nonvascular openings that result from osseous resorption; on incompletely cleaned crania they are covered by a thin membrane (presumably connective tissue) unperforated by ducts, and no trace of emerging vessels or nerves can be seen on surrounding bony margins (as in, e.g., AMNH 151937, a specimen of *Peroryctes raffrayana*). Pending histological examination, we conclude that these openings are analogous to the more posteriorly located palatal fenestrations long familiar to comparative anatomists and are not remnants (or precursors) of longer incisive foramina.

The incisive foramina of both *Burramys* (fig. 46) and *Tarsipes* (fig. 49) are also anteroposteriorly elongate (extending nearly as far back as P3), resembling caenolestids in this respect; in *Burramys* they are also markedly expanded posteriorly. As in caenolestids, the margins of these foramina are well formed, and there is no compelling evidence that any part of these openings is homologous with the accessory palatal fenestrae of peramelemorphians. Therefore, we score both *Burramys* and *Tarsipes* as state 0 for this character.

Character 36. *Maxillopalatine fenestrae consistently absent (0); or present (1).* Descriptions of character states and an account of their taxonomic distribution among Recent didelphids were provided by Voss and Jansa (2003: char. 38; 2009), who noted that maxillopalatine fenestrae are absent (state 0) only in *Caluromys* and *Caluromysiops*. Obvious fenestrae between the maxilla and palatine are present in most other metatherians (state 1), but they are absent in †*Pucadelphys*, †*Allqokirus*, †*Mayulestes*, *Myrmecobius* (fig. 41), diprotodontids (e.g., †*Nimbadon* [Black and Hand, 2010: figs. 1B, 2B]), *Phascolarctos* (fig. 44; see also char. 38), vombatids (e.g., *Vombatus* [fig. 45]), *Dactylopsila*, *Dactylonax*, *Potorous* (fig. 54), *Osphranter*, *Macropus* (Wells and Tedford, 1995: fig. 9E), some specimens of *Notoryctes* (e.g., AMNH 198651 [fig. 36]), and some specimens of *Aepyprymnus*. However, small foramina (probably homologous with the major palatine foramina of placental mammals; see Voss and Jansa, 2009: 36) are often present within the maxillopalatine suture of these taxa. Several authors (e.g., Reig and Simpson, 1972; Simpson, 1972; Engelman and Croft, 2014) have stated that †*Sparassocynus* lacks maxillopalatine fenestrae, but short, slotlike openings similar in size to the maxillopalatine fenestrae of some *Monodelphis* species (e.g., *M. dimidiata*; Pine et al., 1985: fig. 4; Chemisquy, 2015: fig. 1c) are present in at least one adult specimen (MMP 339-S) of †*S. derivatus* (see Beck and Taglioretti, 2020); thus, †*Sparassocynus* has been scored as state 1 for this character.

At least some palatal fenestrae are ontogenetically variable in didelphids, resulting from bone resorption in postweaning juveniles (Abdala et al., 2001), and a similar pattern has been observed in the dasyurids *Dasyurus geoffroii* (see Archer, 1984b: fig. 5) and *D. albopunctatus* (see Flores et al., 2006). Therefore, we scored this and subsequent fenestral characters from fully adult specimens only.

Character 37. *Left and right maxillopalatine fenestrae separated by a median septum (0); or confluent, septum absent (1).* Where present, the left and right maxillopalatine fenestrae are always separated by a median septum in didelphids (state 0; figs. 1, 7, 34). A dividing septum

is present in most other metatherians that possess such vacuities, although the septum is very narrow in some taxa (e.g., *Pseudochirops cupreus*). However, this septum appears to be naturally incomplete or entirely absent, such that the maxillopalatine fenestrae are confluent (state 1), in *Rhyncholestes* (Patterson and Gallardo, 1987: fig. 1), some peramelemorphians (e.g., *Macrotis* [fig. 38]), some macropodiforms (e.g., *Lagostrophus* [fig. 53]), most Recent phalangerids (except *Wyulda*), acrobatids (e.g., *Distoechurus* [fig. 48]), †*Thylacoleo*, and *Petropseudes*. We scored this character based on adult specimens only, because a complete septum is sometimes present in juveniles or subadults but subsequently lost during ontogeny.

We noted a few discrepancies between our own observations and those of other authors. Wroe and Musser (2001: 493) stated that "the maxillary vacuities [= maxillopalatine fenestrae here] appear to have been large and conjoined" in †*Barinya*, but a complete median septum is clearly present in QM F31408 (Wroe, 1999: figs. 1.1, 2.1). Murray et al. (1987: 444) stated that the median septum that partially divides the maxillopalatine fenestrae of the only known skull of †*Wakaleo vanderleuri* (NTM P85553-4; CPC26604) is "naturally discontinuous," but we do not consider this specimen to be sufficiently well preserved to score this character with confidence, so we scored †*Wakaleo* as unknown ("?"). Similarly, we scored this character as unknown for fossil taxa in which the palate of available specimens was damaged or incomplete.

This character was scored as inapplicable ("-") for all taxa lacking maxillopalatine fenestrae (see char. 36).

Character 38. *Palatine fenestrae absent (0); or present (1).* Descriptions of character states and an account of their taxonomic distribution among Recent didelphids (which exhibit either state 0 or state 1) were provided by Voss and Jansa (2003: char. 39; 2009). Palatine fenestrae are absent in most other metatherians, including †*Pucadelphys*, †*Allqokirus*, †*Mayulestes*, †*Herpetotherium*, †*Sparassocynus*, †*Thylatheridium*,

Caenolestes (fig. 35), †*Pichipilus*, microbiotheriids, some peramelemorphians, *Notoryctes* (fig. 36), most dasyuromorphians, and most diprotodontians. However, distinct palatine fenestrae (vacuities fully enclosed by the palatines) are present in some peramelemorphians (*Chaeropus* [fig. 37], *Macrotis* [fig. 38], *Perameles* [fig. 39], some specimens of *Isoodon* [Lyne and Mort, 1981]), some dasyurids (e.g., *Antechinomys* [Archer, 1977], *Dasycercus*, *Dasyuroides*, *Ningaui* [Archer, 1975; Kitchener et al., 1983: fig. 2], *Sminthopsis* [Archer, 1981: fig. 60]) and some diprotodontians (e.g., *Phascolarctos* [fig. 44], *Vombatus* [fig. 45], *Lasiorhinus*, *Hypsiprymnodon moschatus* [fig. 52], *Potorous* [fig. 54], *Hemibelideus*, and some specimens of *Cercartetus*). Multiple tiny openings pierce the palatine of the pseudocheirid *Pseudochirulus*, but large vacuities are absent, so we scored this taxon as state 0. As for the preceding character, this character was scored from adult specimens only.

The palatal vacuities of phascolarctids warrants further discussion. The posterior region of the palate of †*Litokoala* is perforated by a single pair of fenestrae that are within the maxillary-palatine suture (Louys et al., 2009), and so are identified here as maxillopalatine fenestrae, following the nomenclature proposed by Voss and Jansa (2003, 2009; fig. 7). However, the single pair of palatal vacuities in *Phascolarctos* lie entirely within the palatine bone (fig. 44), and so represent palatine fenestrae following Voss and Jansa's (2003, 2009) nomenclature, and yet they are otherwise similar in relative position and size to the paired openings in †*Litokoala* (compare figs. 1A and 4 of Louys et al., 2009). Therefore, it is possible that the palatine fenestrae of *Phascolarctos* are, in fact, homologous with the maxillopalatine fenestrae of †*Litokoala*—differing only with respect to their position relative to the maxillopalatine suture—and not homologous with the palatine fenestrae of taxa in which both maxillopalatine and palatine openings are present (such as *Thylamys* [fig. 7], *Chaeropus* [fig. 37], and *Perameles* [fig. 39]). The same logic may apply to other taxa in which maxillopalatine

fenestrae are absent but palatine fenestrae are present, such as *Vombatus* (fig. 45) and *Potorous* (fig. 54). Despite such perplexities, we follow Voss and Jansa's (2003, 2009) operational nomenclature to maximize consistency and repeatability of scoring for this study.

We have scored this character as inapplicable ("-") in taxa where maxillopalatine fenestrae are present and extend posteriorly as far as the postpalatine torus—as in, for example, *Rhyncholestes* (Patterson and Gallardo, 1987: fig. 1), phalangerids (e.g., *Phalanger* [fig. 47]), and some macropodiforms (e.g., *Lagostrophus* [fig. 53]). In such cases, it is unclear whether or not these very large openings represent fused maxillopalatine and palatine fenestrae; indeed, young juveniles of *Phalanger* (AMNH 198728) and *Spilocuscus* (AMNH 157173) have separate maxillopalatine and palatine fenestrae, whereas these openings are confluent in all older specimens.

Character 39. *Maxillary fenestrae absent (0); or present (1).* As discussed by Voss and Jansa 2003, 2009), some Recent didelphids have an additional pair of nonvascular openings that are located entirely within the maxillary bone lateral to the maxillopalatine fenestrae, approximately level with M1 and/or M2 (state 1; fig.7). No nondidelphid metatherian that we examined has similar fenestrae, with the exception of some specimens of *Chaeropus* (e.g., AM 422, BMNH 1848.1.27.40, and BMNH 1848.1.27.41; see Travouillon et al., 2019: figs. 3c, 6c, j, k), which we scored as polymorphic ("0+1").[6] In *Tarsipes* an unossified space is present on each side between the anterior root of the zygomatic arch and the maxillopalatine fenestra, but close examination suggests that this opening represents an enlarged and highly modified maxillary foramen (i.e., the posterior opening of the infraorbital canal). However, the general palatal morphology of *Tar-*

sipes is difficult to decipher owing to weak ossification, so we scored this taxon as unknown ("?"). As for the preceding character, we scored this character based on adult specimens only.

Character 40. *Posterolateral palatal foramina present, with complete posterior margins (0); or absent, posterior margins incomplete (1).* Most metatherians have a foramen that transmits the minor palatine artery (Archer, 1976), and presumably also the minor palatine nerve (Evans, 1993; Wible, 2003), through the maxillo-palatine suture near the posterolateral corner of the palate (state 0; fig. 7). However, the posterolateral palatal margins are only notched (not perforated) by this artery (state 1) in †*Allqokirus* (Muizon et al., 2018), †*Sparassocynus*, †*Nimbacinus*, †*Barinya*, and most Recent dasyurids (Wroe, 1997b; Wroe et al., 2000) except *Neophascogale* (in which the posterolateral palatal foramen is consistently complete) and *Myoictis* (which is polymorphic ["0+1"] for this character). *Thylacinus* is also polymorphic for this character (with some individuals exhibiting different states on the left and right sides; e.g., SAM M922), as are *Monodelphis* (Voss and Jansa, 2009: fig. 42) and †*Thylatheridium*. Murray and Megirian (2006a: 252) argued that the posterolateral palatal foramen was incomplete in †*Mutpuracinus*, but the posterior palate is poorly preserved in the only known skull of this taxon (NTM P91168-5), which we scored as unknown ("?") for this character.

Character 41. *Posterolateral palatal foramina (or equivalent notches) small, posterior to M4 on each side (0); or very large, extending lingual to M4 protocones (1).* We scored this character regardless of whether a complete posterolateral palatal foramen or an incomplete notch is present (see char. 40). Scoring criteria and information about the distribution of this character among Recent didelphids were provided by Voss and Jansa (2003: char. 41; 2009), who reported that very large posterolateral palatal foramina extend lingual to the protocone of M4 only in *Lestodelphys* and *Thylamys*. Of the nondidelphid taxa we examined in this study, only

---

[6] Presence or absence of maxillary fenestrae serves to distinguish *Chaeropus ecaudatus* (in which they are present) from the recently described *C. yirratji* (in which they are absent; Travouillon et al., 2019); both species have been used for scoring purposes here (see Materials and Methods and appendices 1 and 5).

†*Herpetotherium* (based on AMNH 22304) has similarly enlarged posterolateral palatal foramina (see also Horovitz et al., 2008: plate 2H). The posterolateral palatal foramen opens level with the M4 protocone in †*Ngapakaldia* (Stirton, 1967: fig. 3), but it is very small, so we scored this taxon as exhibiting state 0. Although *Acrobates*, *Distoechurus* (fig. 48), and †*Wakaleo* all lack M4, we scored these taxa as state 0 because the posterolateral palatal foramen is small and located well posterior to M3. However, the absence of M2–4 in †*Thylacoleo* precludes meaningful scoring of this character, which is clearly inapplicable ("-") for that taxon.

Character 42. *Posterior palatal margin is anterior to presphenoid-basisphenoid suture (0); or palate extends posterior to presphenoid-basisphenoid suture (1).* The bony palate terminates anterior to the presphenoid-basisphenoid suture (state 0) in most metatherians examined here (e.g., *Caluromys*; fig. 8A), but in *Myrmecobius* the palate is very long and extends posteriorly well behind the presphenoid-basisphenoid suture (state 1; fig. 41).

Nasopharyngeal and Postpalatal Regions

The nasopharyngeal and postpalatal regions (including the internal nares and the interpterygoid fossa) have been peculiarly neglected by systematists (but see Wible et al., 2018: for a recent exception). Five bones—the pterygoids, palatines, vomer, presphenoid, and basisphenoid—are closely juxtaposed in this part of the skull, and their alternative patterns of contact provide several characters of interest for metatherian researchers. A sixth bone, the parasphenoid, can also occur in this region, but in most metatherians it is a minor ossification that is variably present or absent and has been overlooked by most researchers (Wible et al., 2018); an apparent exception is the condition in *Dromiciops*, with Wible et al. (2018) reporting that in this taxon the parasphenoid is present and fused to the basisphenoid, where it forms part of an unusual midline crest that is continued anteriorly by what we identify as the pterygoids and vomer (char. 48), but which Wible et al. (2018: fig. 13, 128–129) identified as the presphenoid and vomer.

Immediately adjacent to the interpterygoid (or mesopterygoid) fossa are other postpalatal structures—sites of muscle attachment and vascular foramina—that we also treat in this section. We note in passing that, although the basisphenoid and the alisphenoid are invariably discussed as though they were separate bones, these elements are indistinguishably fused in all metatherians, including the youngest postweaning juveniles we examined (in *Monodelphis domestica*, they are fused by postnatal day 25; Wible, 2003: 151). Ontogenetic evidence provides an indication of the approximate boundary between basisphenoid and the alisphenoid, as the transverse canal foramen and carotid canal develop within the basisphenoid, whereas the primary foramen ovale and foramen rotundum develop within the alisphenoid (Maier, 1987; Clark and Smith, 1993; Wible, 2003: 151–153; Sánchez-Villagra and Forasiepi, 2017).

FIG. 8. Postpalatal region of *Caluromys philander* (**A,** AMNH 267002), *Dromiciops gliroides* (**B,** UWBM 78641), *Dactylonax palpator* (**C,** AMNH 191042), and *Potorous tridactylus* (**D,** AMNH 66168). Alternative states for characters 43 and 45–50 (see main text for descriptions of these characters and character states) are illustrated as follows: *Caluromys* 43(0), 45(0), 46(0), 47(1; but note that *C. philander* is polymorphic for this character), 48(0), 49(0), 50(0); *Dromiciops* 43(1), 45(1), 46(3), 47(0), 48(1), 49(0), 50(0); *Dactylonax* 43(1), 45(1), 46(2), 47(1), 48(0), 49(0), 50(1); *Potorous* 43(-), 45(2), 46(1; but note that the modal condition for *P. tridactylus* is 0), 47(1), 48(0), 49(1), 50(0). Abbreviations: **als,** alisphenoid (purple, coossified with basisphenoid); **apf,** anterior pterygoid foramen; **atp,** alisphenoid tympanic process; **bk,** basisphenoid keel; **bs,** basisphenoid (purple, coossified with alisphenoid); **cc,** carotid canals; **ecr,** ectopterygoid crest; **fo,** foramen ovale; **pal,** palatine (green); **plfp,** posterolateral palatal foramen; **ps,** presphenoid (blue); **pt,** pterygoid (yellow); **ptf,** pterygoid fossa; **tcf,** transverse canal foramen; **v,** vomer (orange). Specimens are not drawn to the same scale.
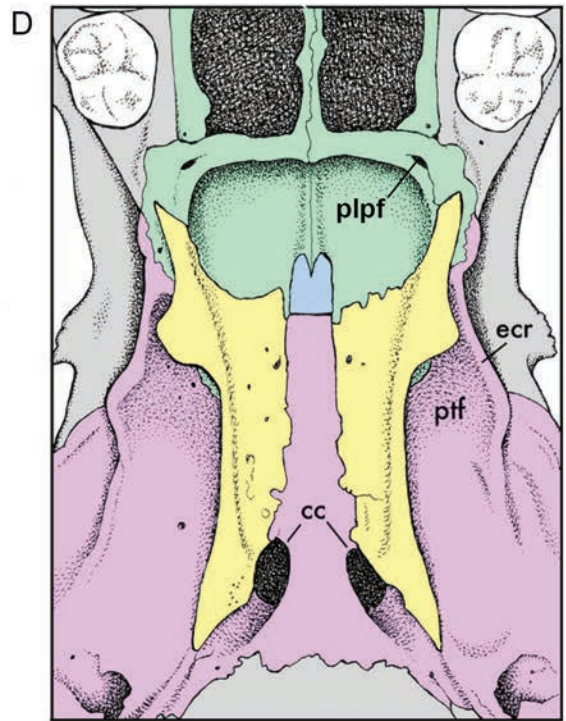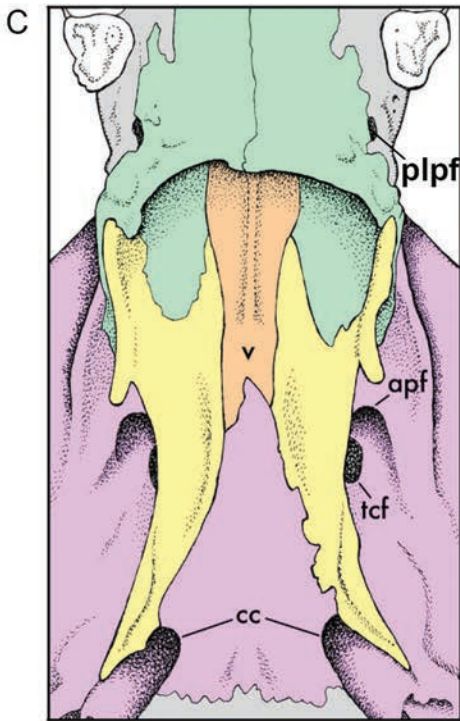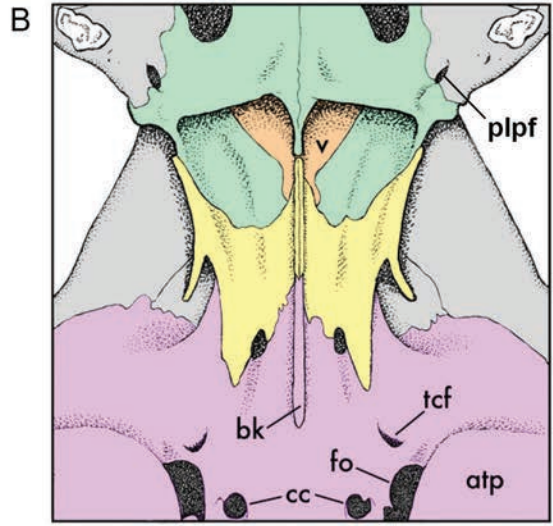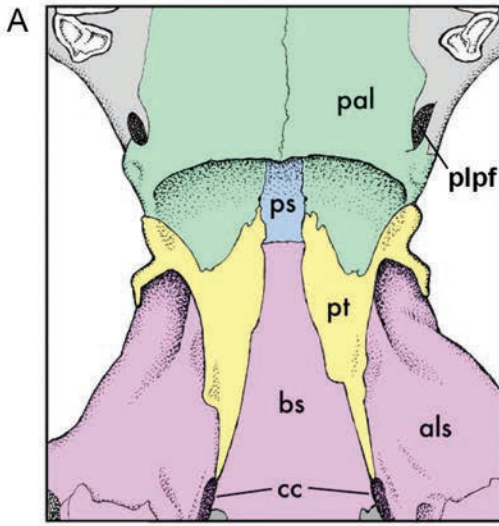
Two cases of synonymous usage for structures in this region are worth noting. The carotid canal (= canalis caroticus [NAV]) has been referred to as the "anterior entocarotid foramen" (e.g., Black and Hand, 2010), "carotid foramen" (e.g., Dederer, 1909), "entocarotid canal" (e.g., Owen, 1859), "entocarotid foramen" (e.g., Coues, 1872), "foramen carotidus" (e.g., Reig et al., 1987), "internal carotid foramen" (e.g., Murray, 1986), and "foramen lacerum medium" (e.g., Marshall 1976), although the last of these terms is usually applied to the foramen for the greater petrosal nerve, or to the confluence of the latter foramen and the primary foramen ovale (see Marshall and Muizon, 1995; Muizon, 1998, 1999; Wroe et al., 1998, 2000: char. 69; Forasiepi, 2009: 37). The transverse canal foramen is sometimes known as the "transverse canal" (e.g., Dederer, 1909), "transverse foramen" (e.g., Archer, 1976b), or the "foramen for transverse sinus canal" (e.g., Aplin et al., 2010).

Character 43. *Presphenoid exposed in roof of nasopharyngeal fossa above posterior palate (0); or presphenoid concealed by vomer above posterior palate (1).* In most metatherians, the nasopharyngeal fossa above the posterior palate is at least partially roofed by unpaired median bones. The presphenoid is typically the exposed median element in didelphids (e.g., *Marmosa* [figs. 1, 34], *Caluromys* [fig. 8A], *Monodelphis* [Wible, 2003: fig. 5]), thylacinids, burramyids, thylacoleonids, some macropodiforms (e.g., *Caloprymnus, Dendrolagus, Dorcopsulus, Lagostrophus, Notamacropus, Setonix, Thylogale*), *Petaurus, Gymnobelideus*, and *Acrobates*. In these taxa, the vomer (if visible) is represented by flanking lateral processes, one on either side of the presphenoid.

By contrast, in caenolestids, many diprotodontians (e.g., *Dactylonax* [fig. 8C], *Phascolarctos, Tarsipes,* †*Nimbadon, Vombatus, Lasiorhinus*, most pseudocheirids, some macropodiforms), most peramelemorphians, and most dasyurids, the presphenoid is typically concealed by the vomer, which extends posteriorly as an undivided element at least as far as the posterior palatal margin (state 1). We consider this morphology to be also present in

Dromiciops (fig. 8B), based on examination of multiple specimens (e.g., FMNH 22675, 127445, 127453, 127465 and 129804; UWBM 78631, 78633 and 78640), all of which appear to us to demonstrate that the vomer conceals the presphenoid, so we have scored this taxon as state 1. However, Wible et al. (2018: fig. 13, 128–129) instead identified the presphenoid as an exposed element contributing to the midline crest of *Dromiciops*. These discrepant observations warrant further investigation. In *Wallabia* (e.g., AMNH 100112) and *Macropus* (e.g., AMNH 66173), the vomer extends beyond the level of the posterior palatal margin as an undivided element, but it is transversely narrow and spinelike (see also Wible et al., 2018: 128, fig. 15), such that the presphenoid remains clearly visible on either side; we also scored these taxa as exhibiting state 1. Several taxa are polymorphic ("0+1") for this character, including *Neophascogale, Chaeropus, Microperoryctes, Notoryctes, Distoechurus, Lagorchestes, Onychogalea, Osphranter, Petrogale* and *Aepyprymnus*.

We scored this character as inapplicable ("-") for taxa in which the palatines and/or the pterygoids are in midline contact, completely concealing the presphenoid above the posterior palate (e.g., *Potorous* [fig. 8D]; see chars. 45, 46). *Myrmecobius* has also been scored inapplicable ("-"), because the posterior margin of the palate extends posteriorly beyond the presphenoidbasisphenoid suture in this taxon (char. 42).

Character 44. *Right and left choanae confluent posteriorly (0); or partially or completely divided by a bony septum (1).* The internal choanae are confluent in most metatherians (state 0), but a bony septum formed by the palatines and the vomer partially or completely separates the left and right choanae (state 1) in several diprotodontians, including *Vombatus, Lasiorhinus,* †*Nimbadon, Phascolarctos, Dendrolagus,* and †*Bohra*. A few taxa—*Aepyprymnus, Dactylonax,* and *Notoryctes*—are polymorphic ("0+1") for this character.

Character 45. *Palatines in lateral contact with presphenoid (0); or separated from presphenoid by*

vomerine-pterygoid contact (1); or right and left palatines in midline contact ventral to presphenoid (2). Several different patterns of contact among the palatines, vomer, and pterygoids are present in the roof of the nasopharyngeal and interpterygoid (mesopterygoid) fossae. In some taxa (e.g., *Acrobates*, *Tarsipes*, burramyids, most macropodids, thylacoleonids, thylacinids, *Myrmecobius*, most caenolestids, and most didelphids [e.g., *Marmosa* [fig. 1]; *Caluromys* [fig. 8A]; *Monodelphis* [Wible, 2003: fig. 5]), the left and right palatines are in lateral contact with, and at least partially separated by, the presphenoid (state 0). In other taxa, the palatines are separated by vomerine-pterygoid contact (state 1) as in, for example petaurids (e.g., *Dactylonax* [fig. 8C]), pseudocheirids, phalangerids, most dasyurids, and most peramelemorphians. We also consider the vomer and pterygoids to be in contact in *Dromiciops* (fig. 8B), although we note that Wible et al. (2018: fig. 13, 128–129) interpreted the morphology of this region differently.

A third, qualitatively distinct morphology is seen in *Bettongia*, *Caloprymnus*, *Potorous* (fig. 8D), *Hypsiprymnodon moschatus* and *H.* †*bartholomaii*, in which the left and right palatines are in midline contact (state 2). This distinctive morphology was remarked by Archer (1984c: fig. 216) as supporting the monophyly of Potoroidae sensu lato (i.e., including *Hypsiprymnodon*). However, we note (as did Ride, 1956) that it is absent in *Aepyprymnus*, and it is also present in the probable stem-macropodid †*Ganguroo* (Travouillon et al., 2014b: fig. 1).

The pterygoids are commonly lost or broken in skulls of fossil and extant taxa alike. When the pterygoids are missing or damaged, the presence of ridges on adjacent bones can sometimes give an indication as to their extent. However, we scored this and the following character only for those taxa in which at least one pterygoid bone appeared to be fully intact.

Character 46. *Pterygoids in lateral contact with presphenoid (0); or separated from presphenoid by palatine-basisphenoid contact (1); or separated from presphenoid by vomerine-basisphenoid*

contact (2); or left and right pterygoids in midline contact ventral to presphenoid (3). In most metatherians—including most didelphids (e.g., *Marmosa* [fig. 1]; *Caluromys* [fig. 8A]; *Monodelphis* [Wible, 2003: fig. 5]), caenolestids, most dasyurids, most peramelemorphians, *Petaurus*, *Gymnobelideus*, and most macropodiforms—the pterygoids are in lateral contact with, and separated by, the presphenoid. However, we observed several alternative conditions among the taxa scored for this study.

In *Acrobates*, *Burramys*, several macropodiforms, *Lasiorhinus*, †*Wakaleo*, *Myrmecobius*, and *Chironectes* (Voss and Jansa, 2009: fig. 45), for example, pterygoid-presphenoid contact is prevented by palatine-basisphenoid contact (state 1; note that this morphology is illustrated by a specimen of *Potorous* in figure 8D, although the modal condition for this terminal is, in fact, pterygoid-presphenoid contact [state 0]). By contrast, in *Pseudocheirus*, *Dactylonax* (fig. 8C), and some specimens of *Pseudochirops*, *Pseudochirulus*, *Ailurops*, and various dasyurids (e.g., *Dasycercus*, *Dasyurus*, *Murexia*, *Phascogale*, and *Sminthopsis*), the vomer and basisphenoid are in contact (state 2). In yet other taxa, the right and left pterygoids contact one another under the presphenoid, which they conceal from ventral view (state 3); this is the condition seen in †*Pucadelphys*, *Macrotis*, *Isoodon*, †*Yarala* (Muirhead, 2000: fig. 1), and various diprotodontians (e.g., †*Nimbadon*, †*Namilamadeta*, *Dactylopsila*, most phalangerids, and some pseudocheirids). We also interpret the left and right pterygoids as contacting one another in *Dromiciops* (fig. 8B) based on several specimens that preserve a midline suture between these elements (e.g., FMNH 22675 and 127445; UWBM 78633 and 78640), as well as one in which the suture is located to the left of the midline (UWBM 78644); however, Wible et al. (2018: fig. 13) interpreted the pterygoids as separated by the presphenoid in this taxon.

Based on our observations, the pterygoids contribute to a sagittal keel in *Dromiciops* (fig. 8B) and certain other taxa (including †*Microbiotherium*), but pterygoid keels range from

distinct to indistinct; therefore, we did not score such variation for phylogenetic analysis. The pterygoid keel in *Dromiciops* and †*Microbiotherium* is part of a continuous carina that is formed by the vomer anteriorly and by the basisphenoid posteriorly (see char. 48). Although Hershkovitz (1999), Giannini et al. (2004), and Wible et al. (2018) all stated that the postpalatal carina of *Dromiciops* is formed by the presphenoid and the basisphenoid, the presphenoid is not ventrally exposed in any of the specimens we examined (e.g., FMNH 22675, 127445, 127453, 127465, and 129804; UWBM 78631, 78633, and 78640). We have not, however, examined the specimen described and illustrated by Wible et al. (2018) and acknowledge that our discrepant interpretations warrant further investigation.

As for the previous character, we scored this character only for taxa preserving at least one fully intact pterygoid.

Character 47. *Pterygoids short, not extending posteriorly to the carotid canal on each side (0); or long, extending posteriorly to sheath the ventral margin of the carotid canal (1); or very long, extending beyond the carotid canal to contact the petrosal (2).* In most metatherians, the pterygoids do not extend posteriorly to the external opening of the carotid canal (state 0), which is entirely enclosed by the basisphenoid (Wible, 2003) (e.g., in *Dromiciops* [fig. 8B]). However, in nearly all diprotodontians (with the exception of *Petropseudes*, some specimens of *Pseudochirops cupreus*, and some specimens of †*Thylacoleo*) the pterygoids contribute to the ventral border of the external opening of the carotid canal (state 1; e.g., in *Dactylonax* [fig. 8C] and *Potorous* [fig. 8D]; note that the left pterygoid is missing from the specimen of *Petaurus* illustrated in fig. 9C). This morphology is uncommon among nondiprotodontian metatherians, but we also observed it in *Caluromysiops*, *Myrmecobius* (fig. 41), and in all examined peramelemorphians with intact pterygoids (e.g., *Perameles* [fig. 39]; unfortunately, †*Yarala* and †*Galadi* could not be scored for this character). It is also present in some, but not all, speci-

mens of *Caluromys* (including the specimen illustrated in fig. 8A), which we scored as polymorphic ("0+1"). In *Onychogalea*, the pterygoid extends posteriorly beyond the external opening of the carotid canal to contact the petrosal, a distinctive morphology that we did not observe in any other examined taxon (state 2).

As defined, these states represent a plausible morphocline, reflecting progressive posterior extension of the pterygoid, so we ordered this character in all our analyses. As for characters 45 and 46, we scored this character only for taxa represented by specimens with at least one intact pterygoid bone.

Character 48. *Basisphenoid unkeeled (0); or with a distinct sagittal keel (1).* In most metatherians, the basisphenoid forms a relatively flat plate in ventral view (state 0). However, the basisphenoid of *Dromiciops* (fig. 8B) and †*Microbiotherium* (based on MACN A 8505) develops a distinct midline keel (state 1), which we identify as being continued anteriorly by the pterygoids (see char. 46). According to Wible et al. (2018), the posterior part of the keel in *Dromiciops* is formed by a coossified parasphenoid (which in other metatherians is present only as a very minor element, if at all) fused to the basisphenoid; if so, then the same presumably applies to †*Microbiotherium*.

Character 49. *Fossa of origin for internal pterygoid muscle absent or small and indistinct (0); or pterygoid fossa large, deeply excavated (1).* In most marsupials, the origin of the internal pterygoid muscle (dissected inter alia by Coues, 1872; Barbour, 1963; Hiiemae and Jenkins, 1969; Turnbull, 1970; Filan, 1990) is not marked by conspicuous osteological features (state 0). However, in *Burramys* and in all examined macropodiforms (e.g., *Potorous* [fig. 8D]) this muscle originates from a distinct fossa (state 1) that is deeply excavated anteriorly and bounded anterolaterally by a well-developed ectopterygoid crest of the alisphenoid (Winge, 1941: 92; Aplin, 1990; Tomo et al., 2007; Warburton, 2009). Curiously, as far as we are aware this distinctive feature has not previously been scored for phylogenetic analysis,

and it is not included in any recent list of macropodiform synapomorphies that we have encountered. A well-excavated pterygoid fossa bound laterally by an ectopterygoid crest is also present in the fossil phascolarctids †*Litokoala* and †*Nimiokoala* (but not *Phascolarctos*; Louys et al., 2009), the wynyardiids †*Muramura* and †*Namilamadeta*, and the vombatid *Lasiorhinus*, all of which have been scored as state 1; however, in these taxa (and also *Burramys*) the ectopterygoid crest does not extend as far ventrally, nor is it as posteriorly extensive, as it is in macropodiforms. Although the ectopterygoid crest is well developed in *Dactylopsila* and *Dactylonax* (fig. 8C), the pterygoid fossa itself is not deeply excavated, so these two taxa have been scored as state 0 for this character.

Character 50. *Anterior pterygoid foramen absent (0); or present (1).* The anterior surface of the pterygoid fossa of *Dactylopsila* is perforated by a large venous foramen that communicates with the foramen rotundum within the alisphenoid bone (state 1). Aplin (1990: 327) suggested that this foramen may transmit "an aberrant venous connection, perhaps linking the orbital sinus and the pterygoid plexus." We observed an apparently identical perforation in *Dactylonax* (fig. 8C) and *Gymnobelideus*, both of which have been scored as state 1, but it is absent in *Petaurus*. The anterior pterygoid region of other metatherians is usually imperforate, but is sometimes pierced by tiny foramina that are highly variable in both position and number. These minute foramina differ qualitatively from the large and conspicuous anterior pterygoid foramen seen in *Dactylopsila*, *Dactylonax*, and *Gymnobelideus*, so we scored taxa in which they are sometimes present (such as many macropodiforms) as corresponding to state 0.

Character 51. *Transverse canal foramen absent (0); or present (1).* When present, the transverse canal foramen (figs. 1, 8B, 8C) "transmits a vein communicating with the cavernous sinus and that [sometimes] communicates across the midline with its antimere" (Wible, 2003: 184; see also Wortman, 1902: 440; Gregory, 1910: 223; Archer,

1976b; Aplin, 1990; Sánchez-Villagra, 1998; Sánchez-Villagra and Wible, 2002). Descriptions of character states and an account of their taxonomic distribution among Recent didelphids were provided by Voss and Jansa (2003: char. 44; 2009), whereas Sánchez-Villagra and Wible (2002) provided information (partly based on Aplin, 1990) about the presence or absence of the transverse canal foramen in both Recent didelphids and nondidelphid metatherians.

Among the taxa scored for this study, an identifiable transverse canal foramen is absent (state 0) in †*Allqokirus* (Muizon et al., 2018)¸ †*Mayulestes* (Muizon, 1998), *Caluromys* (fig. 8A), *Caluromysiops*, *Planigale* (see below), †*Lekanoleo*, and *Tarsipes*. The transverse canal foramen has been reported as absent in †*Pucadelphys* (e.g., by Marshall and Muizon, 1995; Sánchez-Villagra and Wible, 2002), but examination of a large number of recently collected skulls reveals that the transverse canal foramen is clearly present in some specimens (e.g., MHNC 8377; MHNC 8380; Ladevèze et al., 2011), so we scored this taxon as polymorphic ("0+1"). Similarly, a transverse canal foramen is absent in some, but not all, specimens of *Myoictis*, *Gymnobelideus*, and *Pseudochirops archeri*—all of which we also scored as polymorphic. Rougier et al. (1998) coded the transverse canal foramen as absent in *Dromiciops*, whereas Sánchez-Villagra and Wible (2002: 30) identified this foramen in all but one of the *Dromiciops gliroides* specimens that they examined. We found the transverse canal foramen to be consistently present in the *D. gliroides* specimens we examined (e.g., UWBM 78641 [fig. 8B]), so we scored this taxon as corresponding to state 1.

The condition in *Dactyopsila* and *Dactylonax* warrants further discussion. Sánchez-Villagra and Wible (2002: 30) implied that the anterior pterygoid foramen present in *Dactylopsila* (see char. 50) is homologous with the transverse canal foramen, whereas Aplin (1990: 326) stated that *Dactylopsila trivirgata* has a "very reduced transverse canal foramen" distinct from, and in addition to, the anterior pterygoid foramen. Based on our own observations, a transverse canal fora-

men that is clearly distinct from the anterior pterygoid foramen appears to be present in some, but not all, adult specimens of *D. trivirgata*, although it often occurs on only one side of the skull (e.g., in AMNH 157142, 159480, 198710). Therefore, we scored *Dactylopsila* as polymorphic ("0+1") for this character. Where present, this foramen is posterior to the pterygoid fossa in *Dactylopsila*, in a similar position to that seen in *Petaurus*. In *Dactylonax*, by contrast, the transverse canal foramen appears to be consistently present but shares a common opening with the anterior pterygoid foramen (fig. 8C).

Although *Planigale maculata* exhibits a transverse canal foramen (Archer, 1976b: fig. 3A, 3B), we could not identify this foramen in examined specimens of *P. ingrami* (our generic exemplar). Archer (1976b: 307) stated that "in some *Planigale*…the venous sinus passes transversely via the anterior edges of the enormous foramina pseudovale [= primary foramen ovale; see table 10 and char. 52] which are so large that they incise the alisphenoid in the normal position of the transverse canal." Therefore, it is possible that a transverse canal is present in *P. ingrami* but is externally confluent with the foramen ovale. Despite this, and in the absence of serially sectioned specimens or vascular casts of *P. ingrami*, we scored *Planigale* as corresponding to state 0.

Where present, the transverse canal foramen is usually enclosed by the basisphenoid in metatherians (e.g., *Marmosa* [fig. 1]; *Dromiciops* [fig. 8B]; *Dactylonax* [fig. 8C]; *Monodelphis* [Wible, 2003: 151]). In acrobatids, however, a deep sulcus that houses the transverse canal vein extends laterally from the carotid canal and is floored ventrally either by the posterior part of the pterygoid (in *Distoechurus*) or a strut of the alisphenoid (in *Acrobates*; see Aplin, 1990: 326; Sánchez-Villagra and Wible, 2002: 30).

In some metatherians the connection between the left and right transverse canal foramina is roofed dorsally by a continuous sheet of bone that separates the transverse canal from the endocranium, whereas in others the transverse canal foramen opens directly into the endocra-

nial cavity (Sánchez-Villagra and Wible, 2002 [char. 2]; see also Horovitz and Sánchez-Villagra, 2003 [char. 197], and subsequent studies that used modified versions of their matrix). However, we observed an apparently continuous range of intermediate morphologies (sometimes within a single taxon), in which a partial dorsal roof is present but fenestrae of varying sizes open within it. Thus, we were unable to consistently score presence or absence of an intramural transverse canal, and so have not included this character in our analyses.

Ear Region

No part of the skull has contributed more characters to marsupial phylogenetic studies than the ear region. Although little is known with any certainty about the adaptive significance of relevant character transformations, it is reasonable to suppose that auditory specializations are largely responsible for most observed taxonomic differences. However, closely juxtaposed structures—including the jaw joint and various processes for muscle attachment—participate in other (nonauditory) functions and must resist large forces. These mechanically important features, together with several nerves and blood vessels that are also crowded into this part of the skull, may constrain the evolution of auditory phenotypes and account for some of the apparent homoplasy noted by various authors. This region includes four small bones in their entirety (ectotympanic, malleus, incus, and stapes) as well as parts of another four (alisphenoid, exoccipital, petrosal, and squamosal) that help form auditory sinuses, contain the internal organs of hearing and balance, or impinge so closely on auditory structures that they are more conveniently discussed here than elsewhere. Many anatomical features of the ear region are known by multiple synonyms; a nonexhaustive list of these is given in table 10.

Character 52. *Extracranial course of mandibular nerve not fully enclosed by bone (0); or extracranial course of mandibular nerve fully enclosed by*

TABLE 10

Selected Anatomical Synonyms for Structures of the Ear Region[a]

This report	Synonym
Alisphenoid tympanic process	alisphenoid bulla (Owen, 1859); alisphenoid hypotympanic wing (Cooper, 2000); alisphenoid tympanic wing (Archer, 1975); posteroventral wing of alisphenoid (Prideaux and Warburton, 2008); sphenoid bulla (Owen, 1839); tympanic wing of the alisphenoid (Reig and Simpson, 1972)
Anterior process of the malleus[b]	follian process of malleus (Archer, 1976b); processus rostralis (NAV); processus gracilis (Doran, 1877)
Caudal tympanic process of the petrosal	caudal tympanic process of pars mastoidea of petromastoid (Marshall and Muizon, 1995); caudal tympanic process of the petromastoid (Marshall and Muizon, 1995); mastoid wing of periotic (Archer, 1976b); mastoid tympanic process (Archer, 1976b); mastoid tympanic wing (Archer, 1975); tympanic process of the mastoid part (pars mastoidea) of the periotic (Wroe, 1999); wing of the pars mastoidea (Reig and Simpson, 1972)
Ectotympanic	os temporale, pars tympanica, anulus tympanicus (NAV); tympanic (Coues, 1872)
Hypotympanic sinus	alisphenoid hypotympanic sinus (Archer, 1976b); alisphenoid tympanic sinus (Muirhead and Wroe, 1998); anterior epitympanic sinus (Marshall, 1976); anterior tympanic chamber (Aplin, 1987); rostral paratympanic space (Forasiepi et al., 2019); tympanic sinus (Muizon, 1999)
Obturator foramen of the stapes	foramen intercrurale (Schmelzle et al., 2005); foramen intracrurale (Fleischer, 1973); intracrural foramen of stapes (Wible, 2003); stapedial foramen (Archer, 1976b)
Pars canalicularis of the petrosal	mastoid part of the periotic (Archer, 1976b); mastoid portion of the periotic (MacCormick, 1886); pars mastoidea of periotic (Patterson, 1965); pars mastoidea of petromastoid (Marshall and Muizon, 1995)
Pars cochlearis of the petrosal	pars petrosa of the periotic (Patterson, 1965); pars petrosa of petromastoid (Marshall and Muizon, 1995); petrosal part of the periotic (Archer, 1976c); petrosal wing of periotic (Norris, 1993); petrous part of the periotic (Osgood, 1921); petrous periotic (Osgood, 1921)
Petrosal	os temporale, pars petrosa (NAV); periotic (MacCormick, 1886)
Posterior epitympanic sinus	posterior epitympanic fossa (Stirton, 1967); lateral paratympanic space (Forasiepi et al., 2019)
Postglenoid foramen	foramen retroarticulare (NAV)
Primary foramen ovale	anterior lacerate foramen[c] (Hershkovitz, 1992); foramen lacerum medium (Marshall and Muizon, 1995); foramen ovale (Dederer, 1909); foramen pseudovale (Archer, 1975); petrotympanic fissure (Hershkovitz, 1992); piriform fenestra[d] (Gabbert, 1998); pyriform fenestra[d] (Murray, 1991)
Promontorium of the petrosal	promentorium (Murray et al., 1987); promontory of cochlea (Aplin, 1987)
Rostral tympanic process of the petrosal	anterior process of the periotic (Reig and Simpson, 1972); ectotympanic process of the petrosal (Norris, 1994); ectotympanic process of the promontory (Aplin, 1987); "medial crest" of the pars cochlearis of petrosal (Aplin, 1987); periotic tympanic wing (Archer, 1975); petrosal tympanic crest (Murray and Megirian, 2006a); petrosal tympanic wing (Archer, 1976c); petrosal tympanic wing of periotic (Archer, 1975); ridge of promontorium (Muirhead, 2000); rostral hypotympanic wing of the petrosal (Cooper et al., 2000); tympanic process of the pars petrosa (Reig and Simpson, 1972); tympanic process of the pars petrosa of the perioticum (Reig et al., 1987); tympanic process of the periotic (Segall, 1969); tympanic process of the perioticum (Reig et al., 1987); tympanic wing of the pars petrosa (Reig et al., 1987); tympanic wing of the periotic (Archer, 1976c) tympanic wing of the perioticum (Reig et al., 1987); wing of the pars petrosa (Reig and Simpson, 1972)

TABLE 10 *continued*

Secondary facial foramen	facial foramen (Murray, 1986)
Secondary foramen ovale	foramen ovale (Owen, 1859); lateral opening of foramen ovale canal (Aplin et al., 2010)
Squamosal tympanic process	squamosal tympanic wing (Archer 1978)
Subsquamosal foramen	postsquamosal foramen (Marshall, 1976); suprameatal foramen (Groves and Flannery (1990)
Zygomatic epitympanic sinus of the squamosal	postglenoid cavity (Louys et al., 2009); postzygomatic foramen (Flannery and Archer, 1987c)

[a] References other than *Nomina anatomica veterinaria* (NAV, 6th ed.) include the earliest relevant synonymic usage in the marsupial literature of which we are aware, but this list is not intended to be exhaustive.

[b] Additional synonyms for this process that have been used in the mammalian literature are listed in Wible and Spaulding (2012: table 1), who referred to it as the "Rostral Process of Malleus."

[c] Hershkovitz's (1992) use of "anterior lacerate foramen" for the foramen we call the primary foramen ovale is anomalous; in marsupials (and other mammals), the name "foramen lacerum anterius" has typically been applied to the opening we refer to as the sphenorbital fissure (Table 9; see e.g., Owen, 1859; Coues, 1872; Novacek, 1993: 458).

[d] This term was used by Gabbert (1998) in cases where the primary foramen ovale and foramen for the greater petrosal nerve are at least partially confluent, rather than forming separate openings (see also Murray, 1991; Forasiepi et al., 2019; Wible et al., 2021).

FIG. 9. Ventral view of left ear region of *Marmosa murina* (**A,** AMNH 267368), *Phascogale tapoatafa* (**B,** AMNH 160267), and *Petaurus breviceps* (**C,** AMNH 154468; note that the pterygoid bone, which when intact extends posteriorly as far as the carotid canal in *P. breviceps* [char. 47], is missing in this specimen). Alternative states for characters 23, 55, 60, 68, 79, 84, and 87 (see main text for descriptions of these characters and character states) are illustrated as follows: *Marmosa* 23(1), 55(1), 60(0), 68(0), 79(0), 84(0), 87(0); *Phascogale* 23(1), 55(2), 60(0), 68(2), 79(3), 84(1), 87(0); *Petaurus* 23(0), 55(3), 60(2), 68(1[not visible on intact skulls]), 79(4), 84(1[not visible on intact skulls], 87(1; not visible on intact skulls). Abbreviations: **als,** alisphenoid; **atp,** alisphenoid tympanic process; **bo,** basioccipital; **bs,** basisphenoid; **cc,** carotid canal; **cf,** condyloid foramen; **ctp,** caudal tympanic process (of pars canalicularis of petrosal); **ect,** ectotympanic; **fgpn,** foramen for greater petrosal nerve; **fips,** foramen for inferior petrosal sinus; **gf,** glenoid fossa; **gpa,** glenoid process of alisphenoid; **hf,** hypoglossal foramen; **jf,** jugular foramen; **jug,** jugal; **mas,** mastoid exposure of pars canalicularis of petrosal); **mf,** mastoid fenestra; **oc,** occipital condyle; **pes,** posterior epitympanic sinus (of squamosal); **pfo,** primary foramen ovale; **pgf,** postglenoid foramen; **pogp,** postglenoid process (of squamosal); **pp,** paroccipital process (of exoccipital); **pro,** promontorium (of pars cochlearis of petrosal); **pt,** pterygoid; **ptps,** postympanic process (of squamosal); **rtp,** rostral tympanic process (of pars cochlearis of petrosal); **smf,** stylomastoid foramen; **smn,** stylomastoid notch; **sq,** squamosal; **ssf,** subsquamosal foramen; **tcf,** transverse canal foramen. Specimens are not drawn to the same scale.
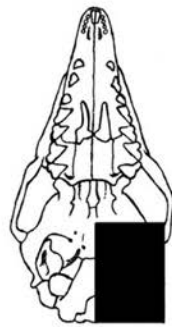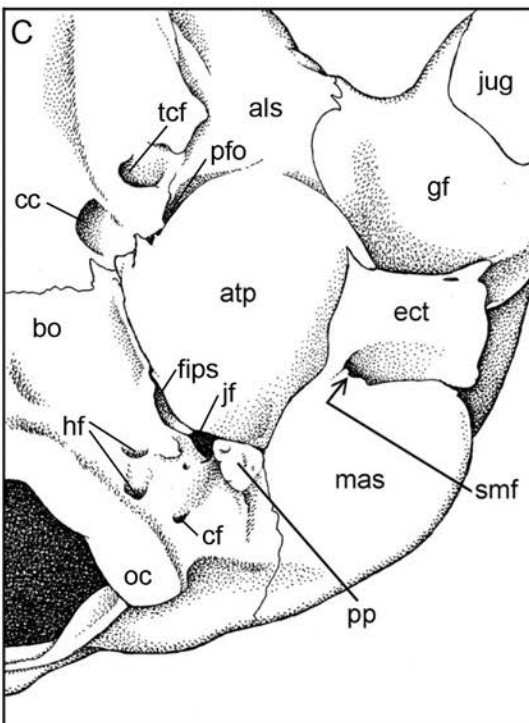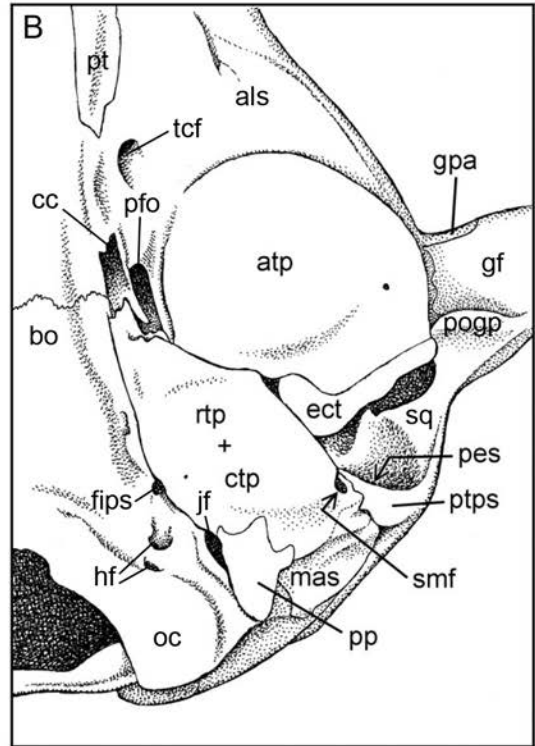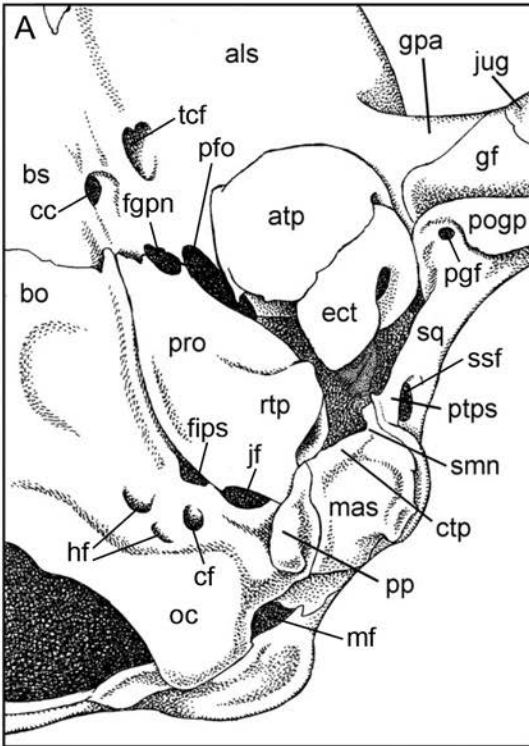
medial outgrowths of the ossified hypotympanic sinus floor (1) or extracranial course of mandibular nerve traverses a bony canal in the roof of the hypotympanic sinus (2); or extracranial course of mandibular nerve traverses a bony canal in the medial wall of the hypotympanic sinus (3). Following Gaudin et al. (1996) and Voss and Jansa (2003, 2009; see also Wroe, 1997b; Wroe et al., 1998; Muirhead, 2000), we use the general term foramen ovale to refer to all bony enclosures of the mandibular division of the trigeminal nerve, regardless of which bones participate. By contrast, MacIntyre (1967) proposed the term "foramen pseudovale" for cases in which the primary orifice by which the mandibular nerve exits the skull is not fully enclosed by the alisphenoid, and his usage was followed, inter alia, by Archer (1976b; 1981) and Marshall (1977; 1979). We refer to the ventrally directed foramen by which the mandibular nerve exits the braincase as the primary foramen ovale, following most recent works on metatherian cranial anatomy (e.g., Wroe, 1997b, 1999; Wroe et al., 1998; Muirhead, 2000; Voss and Jansa, 2003, 2009; Murray and Megirian, 2006a; Travouillon et al., 2010, 2014b, 2015b; Black et al., 2014c; Gurovich et al., 2014; Butler et al., 2016); however, Gaudin et al. (1996) used the term "true foramen ovale" for this orifice.

In most metatherians in which the primary foramen ovale is clearly externally identifiable, this opening appears to be between the petrosal and the alisphenoid (e.g., in the Recent didelphids *Marmosa* [fig. 9A], *Marmosops* [Voss and Jansa, 2003: fig. 8B], and *Monodelphis* [Voss and Jansa, 2003: fig. 8c; Wible, 2003: fig. 6]), but it is between the petrosal, alisphenoid, and squamosal in *Vombatus* and *Lasiorhinus*. In all these taxa, the endocranial exit of the greater petrosal nerve (the "foramen lacerum medium" sensu Marshall and Muizon, 1995; Muizon, 1998; 1999; see Forasiepi, 2009: 37) is confluent with the primary foramen ovale, although the two openings are sometimes partially separated by a posterolaterally directed process of the alisphenoid (fig. 9A; see also right side [anatomical left side] of fig. 6 of Gaudin et al., 1996; Wible, 2003: fig. 6).

Forasiepi (2009: 37) proposed the term "sphenopetrosal fissure" for the shared opening by which V3 and the greater petrosal nerve exit the endrocranium (following Maier, 1987), whereas Gabbert (1998) referred to it as the "piriform fenestra" (see also Murray, 1991; Forasiepi et al., 2019; Wible et al., 2021). In a few metatherians, however, the primary foramen ovale is entirely enclosed by alisphenoid, with the greater petrosal nerve exiting via a separate foramen (see left side [anatomical right side] of fig. 6 of Gaudin et al., 1996). As noted by Voss and Jansa (2003: 28–30, 2009: 39), the location of the primary foramen ovale—between the petrosal and alisphenoid; between the petrosal, alisphenoid, and squamosal; or fully enclosed by the alisphenoid—is often ambiguous or difficult to interpret by external inspection. This difficulty may explain some discrepancies between our observations and those reported by previous authors, which we briefly discuss here.

The primary foramen ovale of *Dromiciops* appears to be between the alisphenoid and petrosal (based on FMNH 129804 and UWBM 78644), and not entirely within the alisphenoid (as stated by Wroe, 1997: 27), nor is it between the alisphenoid and squamosal (as stated by Rougier et al., 1998: char. 111; Wible et al., 2001: char. 111; and Ladevèze, 2004: char. 30). Marshall and Muizon (1995) and Muizon et al. (1997: fig. 2A) suggested that the squamosal contributes to the posterolateral rim of the primary foramen ovale in †*Pucadelphys* (see also Muizon et al., 2018; Muizon and Ladevèze, 2020). However, none of the †*Pucadelphys* specimens we examined provide unambiguous evidence of this (this region is poorly preserved in most available specimens), and in YPFB Pal 6105 (the holotype) a narrow connection between the alisphenoid and petrosal posterolateral to the primary foramen ovale clearly excludes the squamosal from the rim of this foramen (R.M.D.B., personal obs.). Horovitz et al. (2008: 117) stated that "a foramen just anterior to the large alisphenoid bulla…may be the foramen ovale" in a specimen of †*Herpetotherium* cf. *H. fugax* (MB.Ma.50672) from the early Oligocene

White River Formation in Wyoming. However, we examined their material and additional well-preserved specimens of †*Herpetotherium* (notably AMNH FM 22304; see Gabbert, 1998) and conclude that the structure referred to by Horovitz et al. (2008) is probably the foramen rotundum. Instead, the primary foramen ovale of †*Herpetotherium* is medial (rather than anterior) to the alisphenoid tympanic process and appears to lie between the alisphenoid and the petrosal (see Gabbert, 1998: fig. 1).

In several metatherians—including *Caluromysiops*, *Philander* (Voss and Jansa, 2009: fig. 48; Wible et al., 2021: fig. 2), *Isoodon*, many macropodiforms (e.g., *Lagostrophus* [fig. 52]), and some *Sarcophilus* individuals (Wroe, 1997: 33–34, figs. 4D, 5C)—the primary foramen ovale is largely or entirely concealed from ventral view in intact crania, due to the presence of an extensive lamina of bone that forms a secondary foramen ovale. In these taxa, the bone(s) that form the primary foramen ovale cannot always be determined by external inspection. We have, therefore, followed Voss and Jansa (2003, 2009) in not scoring the bony composition of the primary foramen ovale as a character. Instead, we scored the morphology of the course of the mandibular nerve after it leaves the endocranium.

In many metatherians—such as †*Herpetotherium* (Gabbert, 1998), some Recent didelphids (e.g., *Marmosa* [fig. 9A]), caenolestids, *Dromiciops*, most dasyurids (e.g., *Phascogale* [fig. 9B]), *Myrmecobius*, *Aepyprymnus*, acrobatids, *Cercartetus*, and most petaurids—the mandibular nerve is usually not fully enclosed by bone after exiting the endocranium via the primary foramen ovale. Although bony outgrowths from the ossified tympanic sinus floor sometimes partially enclose the nerve in some of these taxa, a complete secondary foramen ovale sensu Gaudin et al. (1996) and Wroe (1997b) is usually absent (state 0). In the only known skull of †*Yalkaparidon* (QMF13008) the alisphenoid tympanic process is damaged on both sides, but it does not appear that a strut or lamina forming a complete secondary foramen ovale was ever present (Beck et

al., 2014: 143), so we scored this taxon as corresponding to state 0.

In other metatherians (e.g., many didelphids, *Notoryctes*, peramelemorphians, thylacinids, and most diprotodontians), bony outgrowths from the medial side of the ossified hypotympanic sinus floor form a complete secondary foramen ovale that encloses the extracranial course of the mandibular nerve after it exits the primary foramen ovale (state 1). Although Voss and Jansa (2003, 2009) identified two distinct patterns of secondary foramen ovale formation in didelphids, and Wroe et al. (2000: chars. 51–53; see also Wroe, 1997) distinguished three patterns of secondary foramen ovale formation in dasyuromorphians, the alternative conditions described by those authors cannot be consistently distinguished among the wider range of metatherian taxa examined in this study. Therefore, we simply scored a secondary foramen ovale as present or absent, regardless of its apparent osteological origin.

In some taxa in which a secondary foramen ovale is present (e.g., *Chironectes*, *Gracilinanus*, most peramelemorphians, *Thylacinus*, some diprotodontians), the enclosure is a relatively narrow strut, and the primary foramen ovale remains clearly visible dorsal to the secondary enclosure (Voss and Jansa, 2003: fig. 8B). However, as already noted, in some taxa (e.g., *Caluromysiops*, *Philander*, *Isoodon*, many macropodiforms, some *Sarcophilus* individuals), the bone secondarily enclosing the mandibular nerve is more extensive and forms a lamina that conceals the primary foramen ovale from external view. In such cases, the secondary foramen ovale might be confused for the (concealed) primary foramen ovale. However, the primary foramen ovale is not formed by outgrowths of the ossified hypotympanic sinus floor, is immediately adjacent to the anterior pole of the petrosal, opens ventrally, and is usually in approximately the same horizontal plane as the basisphenoid and basioccipital. By contrast, the secondary foramen ovale (if present) is formed by outgrowths of the ossified hypotympanic sinus floor, and, as a result, is more distant from the anterior

pole of the petrosal, opens anterolaterally, and is usually clearly ventral to the basisphenoid and basioccipital.

Both †*Yarala* and †*Galadi* have been described as lacking a secondary foramen ovale (Muirhead, 2000; Travouillon et al., 2010), but Wroe et al. (2000: char. 52; see also Wroe and Musser, 2001) scored †*Yarala* as having a complete secondary foramen ovale formed by a "mesial fold in [the] alisphenoid tympanic wing." In both †*Yarala* and †*Galadi* an outgrowth of the alisphenoid tympanic process (labelled as "arch of alisphenoid" in †*Yarala* by Muirhead, 2000: fig. 3) forms a complete foramen anterolateral to the primary foramen ovale; the small size of this foramen and its relatively lateral position suggests that it probably enclosed only the masseteric branch of the mandibular nerve, in which case it arguably does not represent a secondary foramen ovale sensu stricto. However, in the absence of soft-tissue evidence regarding foraminal contents for the vast majority of taxa included in the current analysis, we scored †*Yarala* and †*Galadi* as possessing a secondary foramen ovale (contra Muirhead, 2000; Travouillon et al., 2010, 2013b).

In *Phascolarctos*, the mandibular nerve takes an unusual course after leaving the endocranial cavity: it passes through (rather than anteromedial to) the hypotympanic sinus, enclosed within a bony canal in the sinus roof, and then emerges onto the external surface of the cranium via an anterolaterally facing foramen on the anterolateral side of the ossified hypotympanic sinus floor (Aplin, 1987, 1990). Damaged cranial material of †*Litokoala* and †*Nimiokoala* reveals the presence of a similar canal in the hypotympanic sinus roof (see Louys et al., 2009). Because the mandibular nerve is enclosed *within* the hypotympanic sinus (rather than by bony outgrowths that extend *from* the ossified hypotympanic sinus floor) in *Phascolarctos*, †*Litokoala*, and †*Nimiokoala*, we scored this morphology as a distinct alternative condition (state 2). We observed a somewhat similar morphology in the sparassocynin didelphids †*Sparassocynus* and †*Hesperocynus*, in which the mandibular nerve passes within a

bony tube in the medial wall (not the dorsal roof, as seen in phascolarctids) of the hypotympanic sinus (Beck and Taglioretti, 2020); nevertheless, given the distinctly different (medial) path of the mandibular nerve compared to the (dorsal) phascolarctid condition, we scored †*Sparassocynus* and †*Hesperocynus* as corresponding to an additional state (state 3). Both †*Pucadelphys* and †*Mayulestes* lack an ossified hypotympanic sinus floor (Muizon, 1994, 1998; Marshall and Muizon, 1995; Muizon et al., 1997), as do †*Allqokirus* (Muizon et al., 2018) and †*Mimoperadectes* (see Horovitz et al., 2009: fig. S3), so we scored these four taxa as inapplicable for this character. As defined here, our states do not form a clear morphocline, so we left this character as unordered in all our analyses.

We observed additional taxonomic variation in the extracranial course of the mandibular nerve that we did not score for phylogenetic analysis, but which merits brief discussion. In some taxa, the masseteric nerve, the buccinator (or buccal) nerve, or both nerves, sometimes emerge from foramina that are separate from the secondary foramen ovale—as in some macropodiforms (e.g., †*Balbaroo*, †*Ganawamaya*, *Lagostrophus*, *Onychogalea*, and *Wallabia*; see Aplin, 1990: 182–183), some peramelemorphians (e.g., *Chaeropus* and *Peroryctes*; see Aplin et al., 2010: fig. 8; Travouillon et al., 2019: 15), and *Pseudochirops cupreus*. However, presence or absence of these additional foramina often appears to be highly variable within species. In the peramelemorphian *Macrotis*, a small foramen in the alisphenoid anteromedial to the glenoid fossa suggests that the masseteric nerve exits the skull far lateral to the secondary foramen ovale. A similar foramen is also present in *Notoryctes* (Archer, 1976b: 270) and likewise appears to transmit the masseteric nerve. However, *Acrobates* and *Distoechurus* are apparently unique in having a distinct foramen at the anteromedial end of the glenoid fossa that opens directly into the endocranium and which transmits the masseteric nerve, a morphology that we have scored as an additional character (see char. 53).

Character 53. *Single endocranial exit for mandibular nerve (0); or separate foramen for ramus lateralis present at anteromedial end of the glenoid fossa (1).* In most marsupials for which relevant information is available (see, e.g., Aplin, 1990; Tomo et al., 2007), the mandibular nerve branches after exiting the endocranium via the primary foramen ovale (state 0). In taxa with a secondary foramen ovale, the nerve either branches after exiting the secondary foramen ovale (as in *Macropus giganteus*; Tomo et al., 2007: fig. 2) or immediately before; in the latter case, additional foramina for individual branches of the mandibular nerve may be present, as described above (see char. 52).

By contrast, Aplin (1990: 315) examined sectioned and stained specimens and discovered that the mandibular nerve branches endocranially in the acrobatid *Acrobates*, with the "ramus lateralis" (= the common trunk of the masseteric and posterior temporal nerves) arising "direct[ly] from the mandibular lobe of the trigeminal ganglion…." This nerve then exits the endocranium via a separate foramen at the anteromedial end of the glenoid fossa—between the alisphenoid and squamosal—rather than via the foramen ovale (state 1). An identical foramen is present in our other acrobatid terminal, *Distoechurus*, which has also been scored as state 1. A superficially similar foramen that appears to transmit the masseteric nerve is also identifiable within the alisphenoid, anteromedial to the glenoid fossa, in *Notoryctes* and the peramelemorphian *Macrotis* (see char. 52). However, careful examination of damaged cranial material of both taxa indicates that the masseteric nerve originates *after* the mandibular nerve has exited the endocranium, unlike the acrobatid condition (which appears to be unique among the metatherians we surveyed). Direct evidence regarding the branching pattern of the mandibular nerve is, of course, unavailable for fossil metatherians, as it is for most Recent taxa. Therefore, this character has been scored purely on the basis of the presence or absence of a separate foramen (in addition to the foramen ovale) anteromedial to the glenoid fossa—either within or immediately adjacent to the alisphenoid-squamosal suture—that opens directly into the endocranium. Such a foramen is present only in *Acrobates* and *Distoechurus*.

Character 54. *Hypotympanic sinus roof formed by alisphenoid and petrosal only (0); or by alisphenoid, squamosal, and petrosal (1); or by squamosal and petrosal only (2).* A distinct concavity in the ventral surface(s) of one or more bones anterior to the epitympanic recess defines the roof of the hypotympanic sinus (within the middle ear; van der Klaauw, 1931: 19). It has been reported that no such distinct concavity exists in †*Pucadelphys*, and hence that a true hypotympanic sinus was absent (e.g., Muizon, 1994, 1998; Marshall and Muizon, 1995; Muizon et al., 1997). However, we observed a shallow concavity that appears to correspond to the roof of the hypotympanic sinus in several recently prepared specimens (MHNC 8376, 8377, and 8380; Ladevèze et al., 2011: fig. 1). What we interpret to be a hypotympanic sinus roof is therefore present in all metatherians included in the current analysis for which specimens exposing this region were available.

The roof of the hypotympanic sinus is variously formed in metatherians. Most nondiprotodontians have a sinus roof formed by the alisphenoid with a small (often negligible) petrosal component (state 0), as in most didelphids, *Caenolestes*, *Dromiciops*, †*Yalkaparidon* (see Beck et al., 2014: fig. 8), dasyuromorphians (e.g., *Mutpuracinus*; Murray and Megirian, 2006a: fig. 8), and most peramelemorphians. However, the squamosal sends a medial process into the hypotympanic sinus of †*Mayulestes* (Muizon, 1994, 1998; Muizon et al., 1997), †*Pucadelphys* (Muizon, 1994, 1998; Muizon et al., 1997), †*Allqokirus* (Muizon et al., 2018), and †*Mimoperadectes* (see Horovitz et al., 2009: fig. S3A) (state 1). The hypotympanic sinus roof also has both alisphenoid and squamosal components in *Lutreolina*, *Philander*, *Rhyncholestes*, and several diprotodontians (Aplin, 1987; 1990; Gillespie, 1997; Louys et al., 2009), including †*Lekanoleo*, *Phascolarctos*, †*Nimiokoala*, †*Litokoala*, †*Bulungamaya*, *Calo-*

prymnus, *Potorous*, *Burramys*, and *Cercartetus*. Both the alisphenoid and squamosal contribute to the hypotympanic sinus roof in some specimens of *Echymipera*, *Microperoryctes*, and *Peroryctes*, but the squamosal is excluded from this region in others, so we scored these taxa as polymorphic ("0+1"). Only the squamosal and petrosal roof the hypotympanic sinus of most diprotodontians (Aplin, 1987; 1990; Gillespie, 1997; Black, 2008; Louys et al., 2009; Black and Hand, 2010), including petaurids, pseudocheirids, phalangerids, diprotodontids, vombatids, wynyardiids, †*Thylacoleo*, and †*Ilaria* (state 2). We were unable to determine the composition of the hypotympanic sinus roof of *Notoryctes*, *Acrobates*, and *Distoechurus*, which we scored as unknown ("?"). As defined, the states comprising this character represent a plausible morphocline, so this character was ordered in all our analyses.

Although the presence/absence of a medial process of the squamosal and the composition of the hypotympanic sinus were coded as separate characters by Rougier et al. (1998: chars. 140, 141; see also Wible et al., 2001), these are clearly nonindependent aspects of auditory morphology that seem better treated as part of the same transformation series. Springer and Woodburne (1989: char. 1) and Springer et al. (1997: char. 61) coded the medial wall of the "mandibular" (glenoid) fossa as formed by either the alisphenoid or the squamosal, but the medial wall of the mandibular fossa is typically formed by the squamosal whenever the squamosal contributes to the hypotympanic sinus roof, and so these would also appear to be nonindependent characters.

Character 55. *Hypotympanic sinus floor unossified (0); or hypotympanic sinus floor ossified but does not contact rostral tympanic process of petrosal (1); or hypotympanic sinus floor ossified and contacts rostral tympanic process of petrosal (2); or hypotympanic sinus floor ossified and extends posteriorly across the petrosal to contact the exoccipital (3).* The hypotympanic sinus of †*Allqokirus*, †*Mayulestes*, and †*Pucadelphys* is not enclosed anteriorly or ventrally by any kind of ossified tympanic process (state 0; Muizon, 1994, 1998; Marshall and Muizon, 1995; Muizon et al., 1997, 2018), although an unossified fibrous membrane of the tympanic cavity sensu MacPhee (1981) was presumably present. Horovitz et al. (2009: 3) reported that a "poorly developed tympanic wing of the alisphenoid" is present in †*Mimoperadectes* (see also Muizon et al. 2018: 402), but we examined their material (USNM 482355) and did not find any trace of an alisphenoid tympanic process. We therefore also scored †*Mimoperadectes* as state 0 (see also Horovitz et al., 2009: fig. S3A).

By contrast, the hypotympanic sinus of all other metatherian taxa examined here is at least partially floored by bone. We assume here that, where present, the bony floor of the hypotympanic sinus exhibits primary homology (sensu de Pinna, 1991) across Metatheria, regardless of exactly which bones form it. This assumption seems justified by reports that, in specimens of *Phalanger orientalis* from the Solomon Islands, the hypotympanic sinus floor is alternatively composed of the alisphenoid only, of alisphenoid and squamosal components, or of the squamosal only (Aplin, 1990; Norris, 1993). These morphologies appear otherwise identical; indeed, a number of examples are known in which the hypotympanic sinus floor is entirely alisphenoid on one side and entirely squamosal on the other (Aplin, 1990; Norris, 1993). Similarly, although Aplin (1990) identified the the bony hypotympanic sinus floor of acrobatids (e.g., *Distoechurus* [fig. 48]) as being formed by the petrosal and an "entotympanic-like" intramembraneous ossification, it otherwise resembles the condition in other diprotodontians, in which the sinus floor is formed by the alisphenoid or the squamosal (figs. 44–47, 49–54), so we assume that these structures are homologous regardless of bony composition (see also Aplin, 1990: 344–345)[7].

When present, the ossified hypotympanic sinus floor exhibits striking taxonomic variation in size and in its contact with adjacent bones. The ossified hypotympanic sinus floor does not

---

[7] See Wible (2009) for an analogous case regarding the bony composition and homology of the intrabullar septa and spaces in tupaiids.

extend far enough posteriorly to contact the rostral tympanic process of the petrosal (state 1) in most Recent didelphids (e.g., *Marmosa* [fig. 9A], *Didelphis* [Wible, 1990: fig. 1A], *Monodelphis* [Wible, 2003], *Philander* (Wible et al., 2021: figs. 2, 4), †*Sparassocynus*, caenolestids, thylacinids, most peramelemorphians, diprotodontids, wynyardiids, phascolarctids, †*Lekanoleo*, and †*Wakaleo*, although the hypotympanic sinus floor itself varies markedly in size and shape among these taxa (it is particularly large in †*Sparassocynus*, *Phascolarctos*, the dasyurids *Dasycercus* and *Dasyuroides*, and the peramelemorphians *Isoodon* and *Macrotis*). By contrast, the ossified hypotympanic sinus floor clearly contacts the rostral tympanic process of the petrosal (state 2) in dasyurids (e.g., *Phascogale*; fig. 9B), *Chaeropus*, microbiotheriids, burramyids, *Tarsipes*, *Dactylonax*, and in some specimens of *Caluromys* (e.g., AMNH 267002), *Dactylopsila*, *Pseudochirops*, and *Ailurops*. The ossified hypotympanic sinus floor of *Myrmecobius* resembles that of dasyurids, except that it extends somewhat farther posteriorly, contacting the caudal tympanic process of the petrosal, as well as the rostral tympanic process (Archer, 1976b: 244; Murray and Megirian, 2006a: fig. 16H), a condition we subsume in state 2. The ossified hypotympanic sinus floor is still larger, extending posteriorly across the petrosal to contact the base of the paroccipital process of the exoccipital (state 3) in macropodiforms and most petaurids (e.g., *Petaurus*; fig. 9C), phalangerids, and pseudocheirids (as previously described by Springer and Woodburne, 1989: char. 3).

In several taxa—mostly fossil forms represented by damaged cranial material—an ossified hypotympanic sinus floor is clearly present, but its posterior extent cannot be determined based on available specimens. Such taxa have been scored using ambiguity ("either/or") coding, with plausible alternative character states represented. For example, we scored †*Yalkaparidon*, †*Yarala*, †*Galadi*, and †*Litokoala* (in which the hypotympanic sinus floor is ossified but clearly did not contact the exoccipital) as "1/2." Because of sutural fusion, the precise extent of the ossified hypotympanic sinus floor is also unclear in *Notoryctes*, but it extends posteriorly either as far as the rostral tympanic process of the petrosal, or further posteriorly to contact the exoccipital, so we scored this taxon as "2/3." Because these conditions appear to represent a successive series of tympanic expansions, we treated this character as ordered (additive) in all our analyses.

Character 56. *Ossified hypotympanic sinus floor formed at least partially by alisphenoid (0); or by squamosal only (1); or by petrosal and an "entotympanic-like" ossification (2).* There is considerable taxonomic variation in the composition of the ossified hypotympanic sinus floor within Metatheria, where such a structure is present. In most nondiprotodontian metatherians, it appears to be formed exclusively by a tympanic process—referred to as a "wing" by some authors (e.g., Archer, 1975, 1976; Cooper et al., 2000; see table 10), although MacPhee (1981: 26) restricted "wing" to components of the auditory roof only—of the alisphenoid. This morphology is seen in didelphids (e.g., *Marmosa*: fig. 9A; *Philander* [Wible et al., 2021: fig. 4), caenolestids, *Dromiciops*, †*Yalkaparidon* (Beck et al., 2014), peramelemorphians. and dasyuromorphians (e.g., *Phascogale*; fig. 9B). In many diprotodontians, by contrast, damaged or sectioned skulls reveal the presence of a squamosal contribution to the floor of the hypotympanic sinus, in addition to an alisphenoid tympanic process (Aplin, 1990; Beck et al., 2008a: char. 244; Sánchez-Villagra and Forasiepi, 2017: 26, fig. 23). However, this squamosal tympanic process is often largely covered by the alisphenoid tympanic process, so its presence is not readily apparent based on external examination of intact skulls (Murray et al., 1987; Sánchez-Villagra, 1998: 184–185; Sánchez-Villagra and Forasiepi, 2017: 26, fig. 23). Indeed, in some diprotodontians, the ossified hypotympanic sinus floor is largely or entirely bilaminar, comprising an internal squamosal tympanic process and an external alisphenoid tympanic process—as in †*Wakaleo* (Murray et

al., 1987), †*Namilamadeta*, †*Muramura*, and †*Ngapakaldia* (based on SAM P13851, the holotype of †*N. tedfordi*; contra Murray et al., 2000: 98). Because it is difficult to verify the presence and extent of the squamosal tympanic process in taxa that also have an alisphenoid tympanic process (unless broken skulls are available), we scored all taxa in which the alisphenoid contributes to the ossified hypotympanic sinus floor as corresponding to state 0, regardless of whether the squamosal also contributes.

A qualitatively distinct morphology is seen in *Vombatus*, *Lasiorhinus*, †*Warendja*, and †*Thylacoleo*. In these taxa the ossified hypotympanic floor is formed exclusively by a tympanic process (again, referred to as a "wing" by some authors [e.g., Archer, 1978; Murray et al., 1987; Springer and Woodburne, 1989; see table 10], contra MacPhee, 1981: 26) of the squamosal, without any contribution by the alisphenoid (state 1; Aplin, 1987, 1990; Murray et al., 1987; Murray, 1998). A third type of middle ear enclosure is seen in acrobatids, but the osseous composition of the hypotympanic sinus floor of adult acrobatids is difficult to determine due to seamless fusion of the squamosal, ectotympanic, and petrosal. However, developmental studies by Aplin (1990) suggest that the acrobatid hypotympanic sinus floor is formed by three distinct elements that correspond (from posterior to anterior) to the caudal tympanic process of the petrosal, the rostral tympanic process of the petrosal, and an "entotympanic-like" intramembraneous ossification (state 2). We scored *Notoryctes* as unknown ("?"), because fusion of the basicranial sutures obscures the homology of bones contributing to the hypotympanic sinus floor (Aplin, 1990: 370). By contrast, both Archer (1976b) and Ladevèze et al. (2008) considered the hypotympanic sinus to be formed by the alisphenoid in this taxon. We scored †*Pucadelphys*, †*Allqokirus*, †*Mayulestes*, and †*Mimoperadectes* as inapplicable ("-") for this character because they lack an ossified hypotympanic sinus floor (see char. 55).

As defined, the states of this character do not represent a plausible morphocline, so we treated it as unordered in all our analyses.

Character 57. *Ectotympanic laterally exposed (0); or concealed from lateral view by ossified hypotympanic sinus floor (1).* In lateral view the ectoympanic is an externally obvious element of the ear region in most metatherians (state 0; e.g., *Didelphis* [Wible, 1990: fig. 1], *Monodelphis* [Wible, 2003], *Philander* [Wible et al., 2021: fig. 4], *Phascogale* [fig. 10A], and *Petaurus* [fig. 10B]), but the ectotympanic is concealed by the ossified hypotympanic sinus floor in *Dromiciops* (state 1; Segall, 1969b; Springer and Woodburne, 1989: char. 2). Aplin (1990: 370) stated that "the ectotympanic in *Notoryctes* is…phaneric or 'intrabullar' in location…and is hidden from external view by other, major elements of the tympanic floor," implying that the ectotympanic of *Notoryctes* is concealed in a manner similar to that seen in *Dromiciops*. Our own examination of *N. typhlops* specimens in which the ossified hypotympanic sinus floor is broken or damaged (e.g., AMNH 16717 and 198651) confirms Aplin's (1990: 370) observation, so we also scored *Notoryctes* as corresponding to state 1. The ectotympanic of some dasyurids (e.g., *Dasykaluta* and *Pseudantechinus*; fig. 42) is largely concealed by the ossified hypotympanic sinus floor in ventral view, with only the ends of the anterior and posterior limbs visible, but (unlike the condition in *Dromiciops* and *Notoryctes*) it remains clearly exposed in lateral view, so we scored these taxa as state 0.

Character 58. *Lateral margin of ectotympanic with posterodorsal incisura (0); or ectotympanic forms a closed tube that completely encircles the ear canal (1).* The ectotympanic of most metatherians (e.g., *Didelphis* [Wible, 1990: fig. 1], *Monodelphis* [Wible, 2003], *Philander* [Wible et al., 2021: fig. 4], *Phascogale* [fig. 10A], and *Petaurus* [fig. 10B]) does not completely encircle the ear canal, leaving a more or less prominent posterodorsal opening (the incisura tympanica; Segall, 1969a) between the anterior and posterior limbs (state 0); such ectotympan-
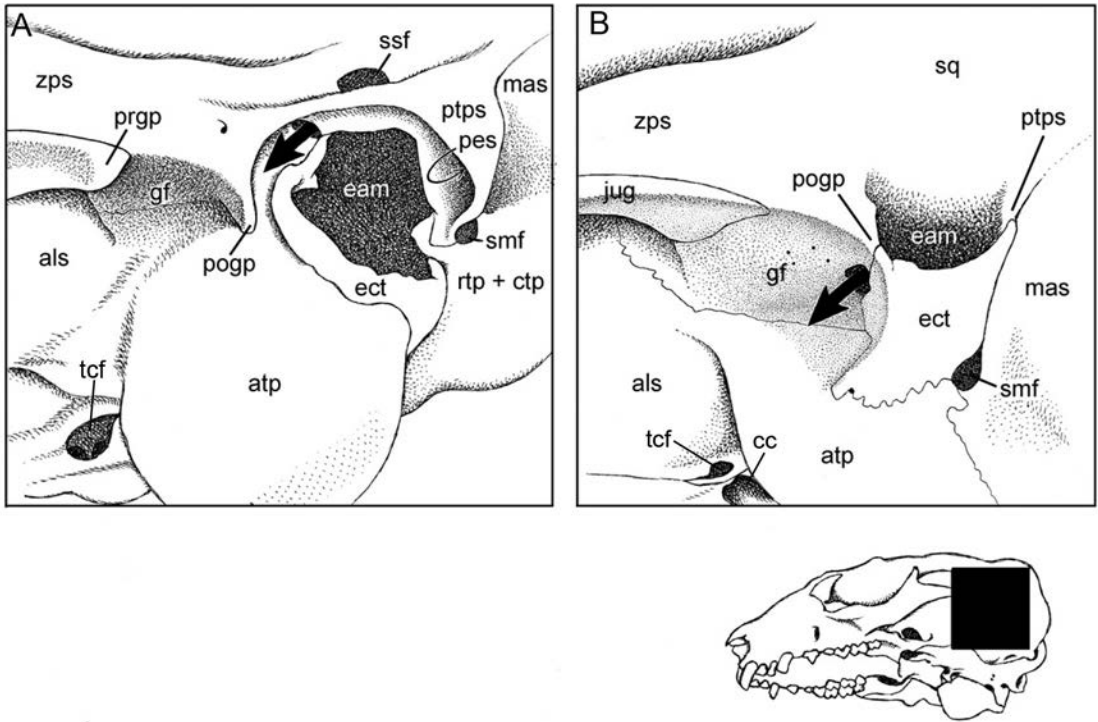
FIG. 10. Anteroventrolateral views of left ear region of *Phascogale tapoatafa* (**A,** AMNH 160267) and *Petaurus breviceps* (**B,** AMNH 154468) with reconstructed course of postglenoid vein shown by heavy arrow in each panel. Alternative states for characters 22, 23, 59, 60, 77, 79 and 87 (see main text for descriptions of these characters and character states) are illustrated as follows: *Phascogale* 22(0), 23(1), 59(1), 60(0), 77(0), 79(3), 87(0); *Petaurus* 22(1), 23(0), 59(2), 60(2), 77(1), 79(4), 87(1[not visible on intact skulls]). Abbreviations: **als,** alisphenoid; **atp,** alisphenoid tympanic process; **cc,** carotid canal; **eam,** external auditory meatus; **ect,** ectotympanic; **gf,** glenoid fossa; **jug,** jugal; **mas,** mastoid exposure of petrosal pars canalicularis (pneumatized in *Petaurus*); **pes,** posterior epitympanic sinus (not externally visible in *Petaurus*); **pogp,** postglenoid process (of squamosal); **prgp,** preglenoid process (of squamosal); **ptps,** posttympanic process of squamosal; **rtp + ctp,** rostral and caudal tympanic processes of petrosal (fused to form petrosal plate); **sq,** squamosal (pneumatized in *Petaurus*); **smf,** stylomastoid foramen; **ssf,** subsquamosal fenestra (out of view, between squamosal and parietal, in *Petaurus*); **tcf;** transverse canal foramen; **zps,** zygomatic process of squamosal. Specimens are not drawn to the same scale.

ics were referred to as U-shaped by Wroe et al. (1998). Although the incisura exhibits obvious taxonomic variation in size and position among metatherians—tending to be widely open and more posteriorly oriented in taxa with mediolaterally unexpanded (ringlike) ectotympanics, but narrower and more dorsally oriented in taxa with mediolaterally expanded (tubelike) ectotympanics—we were unable to code observed differences in relative closure or location as discrete states due to an almost continuous range of intermediate conditions (contra Springer et al., 1997: chars. 74, 75; Horovitz and Sánchez-Villagra, 2003: chars. 192, 193).

In a few diprotodontians, however, the ectotympanic forms a fully enclosed tube that completely encircles the ear canal (state 1), as in *Tarsipes* (Aplin, 1990: 290), *Cercartetus* (contra Wroe et al., 1998: 743), *Vombatus*, *Lasiorhinus*, *Macropus*, *Notamacropus*, *Osphranter*, *Petrogale*,

and *Wallabia*. Although the ectotympanic forms a complete tube in a few specimens of *Dendrolagus lumholtzi*, it is incomplete in most individuals that we examined, so we scored *Dendrolagus* as state 0 based on the modal condition. In some diprotodontians with mediolaterally expanded (tubelike) ectotympanics, the anterior and posterior limbs do not contact each other at the lateral edge of the ectotympanic but are in contact further medially—within the ear canal—as in *Hemibelideus* (e.g., AMNH 65510) and *Petauroides* (AMNH 65378); thus, the lateral margin of the ectotympanic has an incisura tympanica whereas the medial margin does not. Determining whether there is medial contact between the anterior and posterior limbs usually requires broken skulls or CT-scans, so we scored this character based on contact between the externally obvious lateral edges of the anterior and posterior limbs. In consequence, *Hemibelideus* and *Petauroides* correspond to state 0.

Character 59. *Anterior limb of ectotympanic suspended from anterior process of the malleus, not contacting squamosal or petrosal dorsally (0); or loosely attached to the petrosal or squamosal behind postglenoid process (1); or attached firmly to postglenoid process of squamosal (2); or tightly articulated with suspensory process of petrosal (3).* The ectotympanic exhibits a wide range of taxonomic variation in its attachments to adjacent bones of the marsupial skull. As described and illustrated by Voss and Jansa (2003: char. 46, fig. 9; 2009), the anterior limb of the ectotympanic is only indirectly attached to the skull via the anterior process of the malleus (state 0) in some didelphids (e.g., *Caluromys*, *Didelphis*, and *Philander* [see also Wible et al., 2021: fig. 4]). However, in most metatherians—including other didelphids, caenolestids, dasyuromorphians (e.g., *Phascogale* [fig. 10A]), some peramelemorphians, and *Dromiciops*—the anterior limb of the ectotympanic is loosely attached to either the petrosal or to the squamosal behind the postglenoid process, from which it is usually separated by a distinct gap (state 1). This condition likewise characterizes some diprotodontians, including

Tarsipes, *Phascolarctos*, †*Thylacoleo*, †*Wakaleo*, †*Neohelos*, and many macropodiforms (Aplin, 1990). In most diprotodontians, however, the ectotympanic is firmly sutured to or seamlessly fused with the postglenoid process of the squamosal (state 2; see Springer and Woodburne, 1989; Aplin, 1990; Wroe et al., 1998: 743), as in petaurids (e.g., *Petaurus* [fig. 10B]), pseudocheirids, burramyids, phalangerids, Recent vombatids, and a few macropodiforms (e.g., *Caloprymnus*, *Dendrolagus*, *Petrogale*, †*Balbaroo*, †*Ekaltadeta*, and †*Ganawamaya*). The ectotympanic is similarly fused to the postglenoid process in *Notoryctes*. We are unable to meaningfully distinguish the ectotympanic attachment in *Burramys*—which Wroe et al. (1998: 743) described as showing "less intimate association with the alisphenoid tympanic wing or the postglenoid process of the squamosal"—from that observed in *Cercartetus*, petaurids, pseudocheirids, or phalangerids (the postglenoid process and ectotympanic of which are said to be fused; Springer and Woodburne, 1989; Marshall et al., 1990: fig. 2, node 71; Wroe et al., 1998: 743).

A qualitatively different morphology is seen in some peramelemorphians (*Isoodon*, *Macrotis*, and *Perameles*) in which the anterior limb of the ectotympanic articulates with a distinct suspensory process of the petrosal (state 3; Archer, 1976b: 310). Taxa in which the ectotympanic is missing in available specimens (as for many fossil taxa in this analysis) have been scored as unknown ("?") for this character, which (in the absence of any obvious morphological sequence among these conditions) we treated as unordered (nonadditive) in all our phylogenetic analyses.

Character 60. *Posterior limb of ectotympanic does not contact pars canalicularis of the petrosal or posttympanic process of squamosal (0); or in contact with but suturally distinct from pars canalicularis of the petrosal and/or posttympanic process of the squamosal (1); or seamlessly fused with pars canalicularis of the petrosal and/or posttympanic process of the squamosal (2).* In didelphids (e.g., *Didelphis* [Wible, 1990: fig. 1], *Monodelphis* [Wible, 2003], *Philander* [Wible et al., 2021: fig.

4], *Marmosa* [fig. 9A]), caenolestids, peramelemorphians, *Thylacinus*, and *Myrmecobius* (see Archer, 1976), the posterior limb of the ectotympanic does not directly contact any adjacent bony structure except (sometimes) the rostral tympanic process of the petrosal (state 0). In Recent dasyurids (e.g., *Phascogale* [figs. 9B, 10A]) the posterior limb of the ectotympanic contacts the petrosal plate (the fused rostral and caudal tympanic processes of the petrosal; see char. 68) anterior to the stylomastoid foramen. In adult dasyurids there is no suture between the rostral tympanic process (an outgrowth of the pars cochlearis) and the caudal tympanic process (an outgrowth of the pars canalicularis; Wible, 1990, 2003), but examination of juveniles indicates that the boundary between these processes coincides with the stylomastoid foramen (the caudal tympanic process is posterior to the foramen). Therefore, the ectotympanic does not contact the pars canalicularis in dasyurids, which we also scored as state 0.

By contrast, in some diprotodontians (e.g., *Phascolarctos*, †*Neohelos*, †*Wakaleo*, †*Thylacoleo*, vombatids, and most macropodiforms) the posterior limb of the ectotympanic clearly contacts the pars canalicularis of the petrosal, the posttympanic process of the squamosal, or both with a suture clearly marking the point of contact (Murray et al., 1987; Aplin, 1990; Wroe et al., 1998: 743). In other diprotodontians—namely phalangerids, burramyids, petaurids (e.g., *Petaurus*; figs. 9C, 10B), pseudocheirids, acrobatids, *Tarsipes*, and †*Ekaltadeta*—and also in *Dromiciops* the posterior limb of the ectotympanic is seamlessly fused to the pars canalicularis of the petrosal and/or to the posttympanic process of the squamosal (Segall, 1969b; Murray et al., 1987; Springer and Woodburne, 1989; Aplin, 1990; Marshall et al., 1990: fig. 2, node 71; Wroe et al., 1998: 743). In *Notoryctes* the posterior limb of the ectotympanic appears to contact the pars canalicularis without fusion in some specimens (e.g., AMNH 16717), but these structures appear fused in others (e.g., AMNH 198651), so we scored this taxon as polymorphic ("1+2").

Available specimens of many fossil taxa lack ectotympanics, but if the ectotympanic is missing and the pars canalicularis of the petrosal and the posttympanic process of the squamosal are intact, we considered this sufficient evidence that the posterior limb of the ectotympanic could not have been fused to either of these structures, and we scored such taxa using ambiguity coding as "0/1."

Because these states form a plausible morphocline (reflecting increasingly intimate contact between the posterior limb of the ectotympanic and adjacent bones), we ordered this character in all our analyses.

Character 61. *Ectotympanic and pars cochlearis of petrosal are separate bones distinguishable by gaps or open sutures (0); or ectotympanic and pars cochlearis seamlessly coossified (1).* The ectotympanic and the pars cochlearis of the petrosal are separated by gaps (as in *Marmosa* [fig. 9A]) or open sutures (as in *Phascogale* [fig. 9B]) in most metatherians (state 0), but the ectotympanic is seamlessly fused to the acrobatid bulla, a structure that is partly formed by the rostral tympanic process of the pars cochlearis (state 1; see Aplin, 1990: 292). In *Tarsipes*, the posterior part of the ectotympanic is seamlessly fused to the petrosal plate, which appears to represent conjoined rostral and caudal tympanic processes of the petrosal (originating from the pars cochlearis and pars canalicularis respectively; Aplin, 1990: 290; see char. 68); hence, we also scored this taxon as corresponding to state 1. The ectotympanic might be fused to the rostral tympanic process in *Notoryctes* (e.g., AMNH 15015; see also Archer, 1976b: 269), but we are not certain which bone(s) form(s) the hypotympanic sinus floor in this taxon, so we scored it as unknown ("?"). We scored fossil taxa in which the ectotympanic is missing, but the petrosal appears undamaged as "0" because loss of the ectotympanic without damage to the petrosal indicates that these elements were not coossified.

Character 62. *Ear canal not occluded by ossifications (0); or ear canal largely occluded by a bony disk (1).* The external auditory meatus is not

occluded in most metatherians (state 0), but this aperture is nearly filled by a bony disk that is attached by a stalk to the ventral wall of the ear canal in *Acrobates* and *Distoechurus* (state 1; see Segall, 1971: fig. 5B; Aitkin and Nelson, 1989: fig. 1B-C; Aplin, 1990: plate 5.10c). This extraordinary structure is reported to attenuate all but a narrow range of low-frequency sounds (Aitkin and Nelson, 1989; Aplin, 1990). According to Aplin (1990: 308; see also Aitkin and Nelson, 1989), "detailed calculations based on the physical parameters of the disk and associated tympanic membrane in *Acrobates pygmaeus* indicate that the cut-off frequency above which transmission is impaired is probably around 4 kHz. Interestingly enough, this is about the frequency generated by the wing beats of owls (Webster and Webster, 1975); coincidentally, owls probably represent the major predator of *Acrobates pygmaeus*. Comparable calculations have not yet been made for *Distoechurus pennatus*." Unfortunately, a fuller exposition of this hypothesis remains to be published (see also Ward and Woodside, 2008; Ashwell, 2010: 184; Harris, 2015: 35). More recently, Archer et al. (2019) proposed that the presence of the disk helps create Helmholtz resonance (which can amplify a particular frequency; Griffiths, 1978) but, again, no detailed explanation of the underlying basis for this conclusion nor for its potential biological significance has yet been published.

Archer (1984) inferred that this "obstructing process" is ectotympanic in origin, presumably based on its attachment to the ventral surface of the ear canal, but the ectotympanic is fused with the petrosal bulla in even the youngest acrobatids we examined, with no trace of sutures that might confirm or refute this conjecture (see char. 61). Despite extensive ontogenetic studies, Aplin (1990: 293–294) similarly could not distinguish whether the occluding disk is ectotympanic in origin or represents an independent ossification.

Character 63. *Malleo-incudal and stapedio-incudal articulations unfused in adult specimens, with clearly identifiable sutures (0); or fused, without sutures (1).* In most metatherians in which we were able to examine the ossicles, the articulations between the malleus, incus, and stapes are unfused (state 0; see also Doran, 1878; Segall, 1969b; 1969a; 1970; 1971; Sánchez-Villagra et al., 2002; Schmelzle et al., 2005; Czerny, 2015). However, Aplin (1990: 301) reported that both the malleo-incudal and stapedio-incudal articulations are fused in *Acrobates* and *Distoechurus* (state 1), with the common body of the malleo-incudal joint perforated by the chorda tympani nerve.

Character 64. *Anterior process of the malleus well developed (0); or weakly developed and spine-like (1); or entirely absent (2).* The anterior process of the metatherian malleus is usually well developed (state 0). Segall (1969b: 494) stated that the anterior process "is very small and simplified in *Dromiciops*," but an elongate process was clearly identifiable in all of the *D. gliroides* specimens we examined; additionally, a well-developed anterior process is labelled in figure 3 of Segall (1969b), whereas it appears to have broken off the malleus illustrated in his figure 4. The anterior process of the malleus of *Dromiciops* is unusual, however, in lacking a well-developed lamina (Voss and Jansa, 2009: 44); nevertheless, we scored *Dromiciops* as corresponding to state 0 because the process is still elongate. Aplin (1990) observed that the anterior process of the malleus is extremely weakly developed in *Acrobates* and *Distoechurus*, "reduced to a delicate spine" (Aplin, 1990: 301, fig. 5.10d), an apparently distinct condition (state 1). The anterior process of the malleus is similarly vestigial in *Tarsipes* (Parker, 1890), which we also scored as state 1. The anterior process is entirely absent in *Notoryctes* (see Segall, 1970: fig. 3; Mason, 2001: fig. 11D; Czerny, 2015: abb. 19), another distinctive malleolar condition (state 2). As defined, these states comprise a plausible morphocline reflecting gradual reduction in the size of the anterior process of the malleus, so we ordered this character in all our analyses.

We observed additional variation in the morphology of the anterior process of the malleus (as did Doran, 1878; Segall, 1969b; 1969a; 1970; 1971; Sánchez-Villagra et al., 2002; Schmelzle et

al., 2005) that we did not score for phylogenetic analysis, but which merits brief discussion. The anterior process is notably elongate (over twice as long as the manubrium) in some diprotodontians, such as *Vombatus* and *Macropus* (Doran, 1878), but a continuous range of intermediate lengths among other metatherians precludes defining additional character states for these outliers. In a number of macropodiforms—for example, *Dorcopsulus* (e.g., AMNH 151854)—the tip of the anterior process is visible on the external surface of the auditory bulla, where it protrudes between the ectotympanic and the alisphenoid tympanic process (Aplin, 1990: 158). The tip of the anterior process is also visible externally in *Vombatus* and *Lasiorhinus*, projecting ventrally from the anteromedial border of the ectotympanic within a distinct sulcus on the squamosal tympanic wing; Aplin (1990: 219) reported that the chorda tympani exits the middle ear via this sulcus in *Vombatus*. This condition is also seen in some didelphids, including some species of *Monodelphis* (e.g., *M. brevicaudata*; Wible, 2003: fig. 6; Pavan and Voss, 2016: fig. 10A).

Character 65. *Stapes triangular, perforated by a large obturator foramen (0); or stapes columelliform and microperforate or imperforate (1).* The morphological diversity of the marsupial stapes was reviewed by Gaudin et al. (1996; see also Czerny, 2015; Gaillard et al., 2021), whose character-state definitions we followed for scoring foraminal size: the maximum width of a large obturator (stapedial or intercrural) foramen—characteristic of triangular or bicrurate stapedes—is equal to or greater than the width of a surrounding crus (Novacek and Wyss, 1986: fig. 5D–G), whereas the maximum width of the opening in a microperforate stapes is less than the width of a surrounding crus (Novacek and Wyss, 1986: fig. 5C, H–J). However, unlike Gaudin et al. (1996), we do not distinguish between the microperforate and imperforate conditions, because these are often very difficult to tell apart (see, e.g., comments by Segall [1970: 177] and Gaudin et al. [1996: 41] regarding *Notoryctes* and *Thylacinus*); both morphologies are

subsumed by state 1 here. We found other aspects of stapedial morphology incorporated by Gaudin et al. (1996: 38) into their scoring scheme, as well as other features that have been scored in previous analyses—for example, the relative sizes of the openings of the obturator foramen on either side of the stapes (Schmelzle et al., 2005: char. 12), and the stapedial ratio (e.g., Springer et al., 1997: char. 79; Rougier et al., 1998, char. 127; Horovitz and Sánchez-Villagra, 2003: char. 211; Schmelzle et al., 2005: char. 11; Gaillard et al., 2021: char. 3)—to be too subjective or too difficult to score consistently due to the presence of intermediate morphologies.

A large obturator foramen is present (state 0) in the stapedes of most Recent didelphids (e.g., *Caluromys* [Czerny, 2015: abb. 31–33]; *Philander* [Czerny, 2015: abb. 34–45]), *Dromiciops* (Gaillard et al., 2021: fig. 4), and most diprotodontians (e.g., *Trichosurus* [Czerny, 2015: abb. 38]; *Bettongia* [Czerny, 2015: abb. 40]). Schmelzle et al. (2005: table 1) coded *Didelphis* as possessing a collumeliform stapes, but most specimens examined by us exhibit a large obturator foramen (see also Voss and Jansa, 2009: char. 81; Gaillard et al., 2021: fig. 5). In *Dactylonax* (based on AMNH 221601), there is asymmetry in the size of the obturator foramen: the opening is large on one side of the stapes but much smaller on the other side of the same bone (Schmelzle et al., 2005, reported that connective tissue covers most of the obturator foramen in *Dactylonax*, and also in *Dendrolagus*). However, the overall morphology of the stapes of *Dactylonax* most closely resembles state 0.

By contrast, the stapes is columelliform and either imperforate or microperforate on both sides of the same bone in a few didelphids (*Caluromysiops*, *Lestodelphys*, and some specimens of *Tlacuatzin*; Voss and Jansa, 2009), all Recent caenolestids (e.g., *Caenolestes*; Gaillard et al., 2021), *Notoryctes* (Czerny, 2015: abb. 36), all peramelemorphians (e.g., *Echymipera* [Czerny, 2015: abb. 37]) and dasyuromorphians for which we were able to examine the ossicles (see also Gaillard et al., 2021), and a few diprotodontians

(*Vombatus*, *Lasiorhinus*, *Phascolarctos*, *Burramys*, and *Dactylopsila*).

Character 66. *Stapedial footplate concave (0); or flat or weakly convex (1); or strongly convex (2).* Most mammals, including the majority of metatherians, have a more or less flat stapedial footplate (state 1; see Doran, 1878; Czerny, 2015; Gaillard et al., 2021), but the stapes of some diprotodontians are bullate (Wilkins et al., 1999), with a strongly convex footplate that protrudes into the vestibule of the middle ear (state 2; see Sánchez-Villagra and Nummela, 2001: fig. 1; Schmelzle et al., 2005: fig. 6; Czerny, 2015: abb. 38). This obviously derived morphology has previously been reported for *Acrobates* and phalangerids (Hyrtl, 1845; Segall, 1971; Sánchez-Villagra and Nummela, 2001; Schmelzle et al., 2005; Czerny, 2015)[8]. Our observations confirm that the stapes is strongly bullate in acrobatids and Recent phalangerids (the stapedial morphology of the fossil phalangerids †*Onirocuscus* and "*Trichosurus*" †*dicksoni* is unknown), but not in other examined metatherians. Although Schmelzle et al. (2005: char. 13) scored taxa with a weakly convex stapedial footplate (e.g., *Petauroides*) as exhibiting the same character state as those with a strongly bullate footplate, we consider these morphologies to be qualitatively distinct: in the weakly convex condition, the footplate protrudes only slightly, in contrast to the strongly convex condition, in which the footplate is enormously

expanded and almost hemispherical (Sánchez-Villagra and Nummela, 2001: fig. 1; Schmelzle et al., 2005: fig. 6; Czerny, 2015: abb. 38). For this reason, we scored taxa with weakly convex stapedial footplates (e.g., pseudocheirids, petaurids, and *Cercartetus*) as corresponding to state 1.

Schmelze et al. (2005) observed concave stapedial footplates (state 0) in all the dasyurid taxa included in their study (e.g., *Dasycercus byrnei*, *Dasyurus viverrinus* [Schmelzle et al., 2005: fig. 5]), and the footplate also appeared distinctly concave in all dasyurid stapedes that we examined. Direct inspection of the stapes of one specimen of *Myrmecobius* (BMNH 1843.8.12.46) and CT-scans of another (AMNH 155328) indicate that the footplate is also concave in this taxon, but we were unable to score this character for *Thylacinus* or for any fossil dasyuromorphians. Among nondasyuromorphians, we observed a distinctly concave stapedial footplate only in *Isoodon* and *Potorous* (the latter based on AMNH 65330). For a number of taxa (e.g., *Lasiorhinus*, *Chaeropus*, *Rhyncholestes*) the stapedial footplate was sufficiently exposed in available specimens to determine that it is clearly not bullate but not to distinguish between the flat and concave morphologies; we scored such taxa using ambiguity coding (as "0/1") Because these states represent a plausible morphocline, we ordered this character in all of our analyses.

Character 67. *Rostral tympanic process of petrosal absent or indistinct (0); or present and well developed (1).* A distinct rostral tympanic process (sensu MacPhee, 1981) is present on the promontorium of the petrosal of most of the metatherian taxa included in the current analysis (e.g., *Marmosa*; fig. 9A; state 1). However, a distinct rostral tympanic process is absent (state 0) in †*Pucadelphys* (Marshall and Muizon, 1995: fig. 19; Ladevèze and Muizon, 2007: text-fig. 1), †*Badjcinus* (Muirhead and Wroe, 1998: figs. 3–4), vombatids, †*Neohelos*, †*Namilamadeta*, *Phalanger*, and some specimens of †*Nimbadon* and †*Onirocuscus*.

In Muizon's (1998) detailed description of the holotype and only known skull of †*Mayulestes*

---

[8] Hyrtl (1845: tab. V fig. 3) illustrated the stapes of a specimen of "*Phalangista cookii*" that clearly shows a strongly convex footplate (state 2). "*Phalangista cookii*" is a synonym of *Pseudocheirus peregrinus* (see Groves and Jackson, 2015), and Sánchez-Villagra and Nummela (2001) specifically identified Hyrtl's (1845) specimen as *P. peregrinus* (see also Aplin, 1990: 301). However, the degree of convexity illustrated by Hyrtl (1845: tab. V fig. 3) is far greater than in any *P. peregrinus* specimen we have examined, in which the stapedial footplate is only weakly convex (state 1), and we are confident that Hyrtl's (1845) figure does not pertain to this taxon. "*Phalangista cookii*" is also a synonym of *Trichosurus vulpecula* (see Groves and Jackson, 2015), which does have a strongly convex footplate (Sánchez-Villagra and Nummela, 2001 fig. 1; Schmelzle et al., 2005: fig. 6). Although we have not examined Hyrtl's (1845) material, and he did not provide specimen numbers, it seems more likely to us, based on available evidence, that the "*Phalangista cookii*" specimen he described and illustrated is *T. vulpecula* and not *P. peregrinus*.

(MHNC 1249) he discussed the presence of a small tubercle on the promontorium, just ventral to the fenestra cochleae. Based on this, Wroe et al. (2000: char. 65; see also Wroe and Musser; 2001), Sánchez-Villagra and Wible (2002: char. 7), Horovitz and Sánchez-Villagra (2003: char. 215), and several subsequent studies that have employed versions of Horovitz and Sánchez-Villagra's (2003) matrix (e.g., Sánchez-Villagra et al., 2007; Beck et al., 2008a; Horovitz et al., 2008, 2009; Beck, 2012) have all coded the rostral tympanic process as present in †*Mayulestes*. By contrast, Ladevèze and Muizon (2007: char. 133; 2010: char. 17) scored †*Mayulestes* as lacking a rostral tympanic process, and commented that "the presence of a low and tiny ridge or tubercle, anterolateral to the fenestra vestibuli is not regarded as equivalent to the development of a tympanic process, since it is not a process, i.e., a raised shelf of bone" (Ladevèze and Muizon, 2007: 1150). Rougier et al. (1998: char. 130; see also Wible et al., 2001) employed a different coding convention, distinguishing between a rostral tympanic process that is "absent or [a] low ridge" (state 0) and one that is a "tall ridge, occasionally contacting ectotympanic" (state 1), with †*Mayulestes* scored as state 0. We examined MHNC 1249 and confirmed that a small tubercle is indeed present on the promontorium (see also Muizon, 1994: fig. 2A, 1998: fig. 8B; Muizon et al., 1997: fig. 2C; 2018: supplementary data), in the same position occupied by the rostral tympanic process of didelphids. However, this minute protuberance is so weakly developed that it is not comparable to the macroscopically distinct structure coded as state 1 in our matrix; we therefore scored †*Mayulestes* as state 0. †*Allqokirus* appears to exhibit a similar morphology to †*Mayulestes* (see Muizon et al., 2018) and so has also been scored as state 0.

Following Sánchez-Villagra (1998), Sánchez-Villagra and Wible (2002: fig. 11), and Sánchez-Villagra and Forasiepi (2017), we interpret the bulla of *Dromiciops* as principally formed by (1) an alisphenoid tympanic process and (2) fused rostral and caudal tympanic processes of the petrosal (with smaller contributions by the ectotympanic, basioccipital, and exoccipital; see also Giannini et al., 2004), so we scored the rostral tympanic process as present in this taxon. By contrast, Segall (1969b) and Hershkovitz (1992b; 1999) interpreted the structure we identify as the rostral tympanic process of *Dromiciops* as an "entotympanic" (i.e., an independent ossification within the tympanic floor). Unequivocal entotympanics do not appear to occur in metatherians (Archer, 1976b; MacPhee, 1979; Aplin, 1990; Sánchez-Villagra, 1998; Sánchez-Villagra and Forasiepi, 2017; but see Norris, 1993), with the possible exception of acrobatids (see char. 56; Aplin, 1990).

In *Thylacinus*, a distinct crest extends along the medial edge of the promontorium, immediately adjacent to the contact between the petrosal and the basioccipital; we agree with Archer (1976b) and Muirhead and Wroe (1998) that this crest is homologous with the rostral tympanic process of the petrosal. By contrast, Murray and Megirian (2006a) interpreted this crest as a nonhomologous structure—a "ventromedial crest of the petrosal"—that they alleged is present in "derived Thylacinidae" (†*Nimbacinus*, †*Badjcinus*, and *Thylacinus*; Murray and Megirian, 2006a: fig. 16F, G, I), "derived Dasyuridae" (*Antechinus* and *Dasyurus*; Murray and Megirian, 2006: fig. 16C, D), and *Myrmecobius* (Murray and Megirian, 2006a: fig. 16H). They further argued that the apparent rostral tympanic process of the petrosal in *Myrmecobius* is in fact a "neomorphic structure developed from the ventromedial crest" (Murray and Megirian, 2006a: 258). Based on our own observations of these taxa, we consider the "ventromedial crest of the petrosal" sensu Murray and Megirian (2006a) to be simply the ventromedial edge of the rostral tympanic process, rather than a distinctly different structure. Thus, a rostral tympanic process of the petrosal appears to be present in all dasyuromorphians that we examined (including *Thylacinus* and *Myrmecobius*).

The rostral tympanic process is clearly present and very large in acrobatids and *Tarsipes*, in

which it is seamlessly fused with the caudal tympanic process, forming a petrosal plate (see char. 68; Aplin, 1990; Sánchez-Villagra and Forasiepi, 2017: 27). Sánchez-Villagra and Wible (2002: 34) stated that the rostral tympanic process of the petrosal is "lacking entirely" in *Vombatus* and *Phascolarctos* (see also Wible, 1990: 198). We agree that a rostral tympanic process is absent in *Vombatus* (and also *Lasiorhinus*), but comparisons between the petrosal of *Phascolarctos* and those of †*Litokoala* and †*Nimiokoala*—both of which possess unambiguous rostral tympanic processes (Louys et al., 2009: figs. 4, 9)—convinces us that the rugose, crestlike structure along the ventromedial border of the promontorium of *Phascolarctos* corresponds to the rostral tympanic process. Aplin (1987: fig. 4) referred to this structure as the "medial crest of the pars cochlearis of petrosal" and stated that it represents the zone of attachment of the fibrous membrane of the tympanic cavity (Aplin, 1987: 380; 1990: 221), further supporting its identification as the rostral tympanic process (MacPhee [1981: 16] noted that tympanic processes typically originate "adjacent to the intratympanic surface of the fibrous membrane"). Interestingly, Aplin (1990: 221) found that the fibrous membrane of the tympanic cavity does not attach to the petrosal in *Vombatus*, but rather to the lateral rim of the basioccipital, which may explain why this taxon lacks any obvious homolog of the rostral tympanic process.

In all macropodiform specimens for which we were able to examine the ventral surface of the pars cochlearis, we observed a distinct promontorial process that contacts the ectotympanic (when the latter element is also present). Aplin (1990: 148) referred to this structure as the "ectotympanic process of the petrosal," but we tentatively identify it as homologous with the rostral tympanic process (which contacts the posterior limb of the ectotympanic in many didelphids [Wible, 2003; Voss and Jansa, 2009: 42] and dasyuromorphians [Archer, 1976b]). We observed a similar raised process where the ectotympanic contacts the promontorium in petau-

rids, pseudocheirids, and most phalangerids—with the exceptions of *Phalanger* (in which no raised process was identifiable in the specimens we examined), and †*Onirocuscus* (in which it is only variably present [scored as "0+1"]). By contrast, Norris (1994) and Crosby and Norris (2003) identified a rostral tympanic ("ectotympanic") process on isolated petrosals of *Phalanger* (e.g., Norris, 1994: fig. 5B, C); we suspect that this feature may show polymorphism in these and other phalangerids, given sufficiently large sample sizes. It should be noted that we identify the rostral tympanic process of phalangerids (where present) as the discrete structure immediately anteromedial to the fenestra cochleae (the "ectotympanic process" of Norris, 1994), and we do not consider the crest extending anteriorly from the promontorium (or "cupula cochleae") to represent a continuation of this process, contra Norris (1994) and Crosby and Norris (2003; see also comments by Beck et al., 2008a: char. 221).

In some taxa the rostral tympanic process appears as a more or less conical or knoblike structure located anteroventral to the fenestra cochleae—as in some didelphids (e.g., *Marmosa*: fig. 9A; *Philander* [Wible et al., 2021: fig. 5A–C), caenolestids (e.g., *Caenolestes*; Sánchez-Villagra and Wible, 2002: fig. 4a), and some peramelemorphians. In others, however, it forms an elongate crest that extends the entire length of the promontorium to the anterior pole—as in *Caluromys* (see Sánchez-Villagra and Wible, 2002: fig. 3f), †*Acdestis* (Goin et al., 2003: text-fig. 3), *Notoryctes* (Ladevèze et al., 2008: fig. 4), †*Yalkaparidon* (Beck, 2009: fig. 7; Beck et al., 2014), some peramelemorphians (e.g., †*Yarala*; Muirhead, 2000: figs. 1, 3), and dasyurids (e.g., *Antechinus*; Sánchez-Villagra and Wible, 2002: fig. 4c). In a number of these taxa, the rostral tympanic process partially encloses a prominent sinus (the "periotic hypotympanic sinus" of Archer, 1976b), most obviously in dasyurids and the peramelemorphians *Isoodon* and *Macrotis* (Archer, 1976b; Muirhead, 1994; Wroe, 1997b; Muirhead, 2000; Travouillon et al., 2010: char. 47).

Several previous studies have distinguished between these conical or knoblike and elongate and crestlike morphologies of the rostral tympanic process of the petrosal as described above (e.g., Sánchez-Villagra and Wible, 2002: char. 7; Horovitz and Sánchez-Villagra, 2003: char. 215; Ladevèze and Muizon, 2007: char. 134). However, within the larger taxonomic context of the current study, we observed an apparently continuous range of intermediate morphologies, particularly in diprotodontian groups such as pseudocheirids. It is also noteworthy that Wible (2003: 157) described a low ridge that extends anteromedially from the main "finger-like" rostral tympanic process for the entire length of the promontorium to the basioccipital in the didelphid *Monodelphis*, whereas Sánchez-Villagra and Wible (2002: char. 7) and Horovitz and Sánchez-Villagra (2003: char. 215) both scored *Monodelphis* as having a process that "does not reach the anterior pole of the promontorium." This apparent discrepancy emphasises the difficulty in consistently distinguishing between "conical" and "crestlike" morphologies of the rostral tympanic process. The presence of intermediate morphologies also prevents us from scoring presence or absence of a sinus formed by the rostral tympanic process (contra Travouillon et al., 2010: char. 47). Instead, we simply distinguish between presence and absence of the rostral tympanic process here.

Character 68. *Caudal tympanic process of petrosal separated from pars cochlearis by a distinct gap (0); or caudal tympanic process of petrosal contacts but is not fused with pars cochlearis (1); or caudal and rostral tympanic processes of petrosal seamlessly fused, forming a petrosal plate (2).* The caudal tympanic process of the petrosal is separated from the pars cochlearis by a distinct gap in most didelphids (e.g., *Marmosa* [fig. 9A]; *Didelphis* [Wible, 1990]; *Monodelphis* [Wible, 2003]; *Philander* [Wible et al., 2021: fig. 5A-C]), caenolestids (Ladevèze, 2005: fig. 11), †*Yalkaparidon* (Beck, 2009: fig. 7; Beck et al., 2014), peramelemorphians (contra Voss and Jansa, 2009: 42), thylacinids, thylacoleonids, vombatids, *Phascolarctos*, †*Litokoala*, †*Muramura*, and most

diprotodontids. By contrast, the caudal tympanic process either contacts the rostral tympanic process or it contacts the promontorium posterodorsal to the rostral tympanic process in many other taxa. As described by Voss and Jansa (2009: char. 76), the rostral and caudal tympanic processes of the petrosal are in contact in some didelphids (e.g., *Caluromysiops*, *Lestodelphys*, and also †*Sparassocynus*; see Beck and Taglioretti, 2020), but in others the caudal tympanic process contacts the promontorium dorsal to the rostral tympanic process—as in *Hyladelphys* (e.g., AMNH 267339). Contra Voss and Jansa (2009: char. 76), we do not distinguish between these two morphologies, both of which are subsumed in our state 1. This revised description has the advantage of enabling meaningful scoring of taxa in which the rostral tympanic process of the petrosal is absent, such as our outgroup taxa †*Mayulestes* and †*Allqokirus*, and also vombatids (see char. 67).

In most taxa in which the caudal tympanic process contacts the pars cochlearis, the point of contact is unfused, as in †*Sparassocynus*, *Caluromysiops*, *Lestodelphys*, *Thylamys*, macropodiforms, phalangerids, burramyids, petaurids, and pseudocheirids (contact between the rostral and caudal tympanic processes of the petrosal can be determined for most diprotodontian taxa only by examining isolated petrosals or crania with broken auditory bullae).

Only one specimen of †*Herpetotherium* that we examined (AMNH FM 22304) preserves an intact caudal tympanic process; comparisons between this structure (on the left side of AMNH FM 22304) and the left petrosal of MB.Ma.50672 illustrated by Sánchez-Villagra et al. (2007: fig. 1i) and Horovitz et al. (2008: plate 3) suggest that the caudal tympanic process is damaged in the latter specimen. On the left side of AMNH FM 22304, the caudal tympanic process of the petrosal is clearly in contact with, but nevertheless suturally distinct from, the rostral tympanic process; however, this morphology may be the result of taphonomic crushing of this specimen, and hence we score †*Herpetotherium* as "0/1" here.

In adult specimens of *Notoryctes* (see Ladevèze et al., 2008: fig. 4), *Tarsipes*, acrobatids, and dasyurids (e.g., *Phascogale*; fig. 9B), no suture between the rostral and caudal tympanic processes is identifiable; instead, these processes are seamlessly fused to form a petrosal plate sensu Klaauw (1931), a morphology we score as a distinct state. Giannini et al. (2004) correctly observed that a sutureless petrosal plate is present in juvenile specimens of *Dromiciops*, but they implied that a suture develops within the petrosal plate such that distinct rostral and caudal tympanic processes can be identified in adult individuals. However, the apparent suture identified by these authors is, in fact, simply an abrupt change of curvature of the external bullar surface that coincides with an internal septum; the absence of any osteological discontinuity within the petrosal plate can be confirmed by microscopic comparison of the sutureless septal junction with the actual suture between the petrosal plate and the alisphenoid tympanic process. We therefore scored *Dromiciops* (and also †*Microbiotherium*; Segall, 1969b: fig. 5) as corresponding to state 2 (see also Sánchez-Villagra, 1998; Sánchez-Villagra and Wible, 2002; Sánchez-Villagra and Forasiepi, 2017).

Character 69. *Prootic canal foramen on tympanic face of petrosal present (0); or absent (1).* Presence of the prootic canal, through which the prootic sinus communicates with the lateral head vein in the middle ear, is thought to be a mammalian plesiomorphy (Wible, 1990; Wible and Hopson, 1995; Wible et al., 2001, 2009; Ekdale et al., 2004; Rougier and Wible, 2006). In metatherians that retain an unambiguous prootic canal (state 0), it is short, roughly horizontal, and fully enclosed by the petrosal, connecting a foramen within the sulcus for the prootic sinus on the squamosal side of the petrosal to a foramen adjacent to the secondary facial foramen on the tympanic side (Wible, 1990; 2003; Ladevèze, 2005; Wible et al., 2021).

Sánchez-Villagra and Wible (2002: chars. 9, 10) scored presence or absence of a foramen for the prootic canal on the squamosal face of the petrosal and presence or absence of a foramen on the tympanic face as two separate characters. However, we scored the presence or absence of a foramen only on the tympanic face of the petrosal because: (1) the two characters scored by Sánchez-Villagra and Wible (2002) are at least partially dependent (assuming that the prootic canal usually transmits a vessel), and (2) scoring the presence or absence of the prootic canal on the squamosal side of the petrosal usually requires access to isolated petrosals. By contrast, it is relatively easy to score presence or absence of a foramen on the tympanic side of the petrosal of taxa in which the middle ear is incompletely enclosed by bone (such as many didelphids). For taxa in which the auditory bulla is more extensive (such as most diprotodontians), however, isolated petrosals are still required to score this character.

A foramen for the prootic canal on the tympanic face of the petrosal is clearly present in †*Pucadelphys* (Ladevèze and Muizon, 2007: text-fig. 1), †*Mayulestes* (contra Muizon, 1998; see Muizon et al., 2018: 412), †*Allqokirus* (Muizon et al., 2018), all Recent didelphids that could be scored for this character (e.g., *Didelphis* [Wible, 1990: fig. 4] and *Monodelphis* [Wible, 2003: fig. 7]), *Caenolestes* (Ladevèze, 2005), †*Yalkaparidon* (Beck et al., 2014: fig. 9), some peramelemorphians (e.g., *Perameles* [Sánchez-Villagra and Forasiepi, 2017: fig. 12] and *Peroryctes*), some dasyurids (e.g., *Antechinus*, *Phascolosorex*), the few macropodiforms that could be assessed for this character (e.g., *Notamacropus* [Sánchez-Villagra and Forasiepi, 2017: fig. 14b]), *Pseudochirops cupreus*, *Ailurops* (see Norris, 1994), †*Nimbadon*, †*Lekanoleo*, and some specimens of *Thylacinus* and *Petaurus*.

Isolated petrosals of *Phascolarctos* exhibit an enclosed canal that closely resembles the prootic canal in both location and morphology, with a foramen present on both the tympanic and squamosal faces of the petrosal. However, based on sectioned specimens, Aplin (1990: 233) identified the occupant of this canal in *Phascolarctos* to be a cutaneous branch of the auricular ramus of

the vagus nerve, rather than a venous connection. Although this observation raises obvious questions concerning the homology of petrosal canals in the absence of direct observation of their contents, we scored a prootic canal as present in *Phascolarctos*, given its structural and topographical similarities to the definitive prootic canal of, for example, didelphids.

A foramen that may be the tympanic foramen for the prootic canal is located between the squamosal and petrosal in †*Sparassocynus* (based on MLP-88-V-25-2), suggesting that at least part of this canal may lie between these two bones (rather than fully enclosed by the petrosal) in this taxon. If so, this morphology would be unique among all known metatherians. The position of this foramen in †*Sparassocynus* is also unusual because it is lateral to the fossa incudis rather than medial to the epitympanic recess (as in, for example, *Monodelphis*; Wible, 2003: fig. 7D). Because we are not certain of the identity of this foramen, we scored †*Sparassocynus* as unknown ("?").

A tympanic foramen for the prootic canal appears to be absent (state 1) in *Notoryctes* (Ladevèze et al., 2008), some peramelemorphians (e.g., *Chaeropus*, *Isoodon*, *Macrotis*), some dasyurids (e.g., *Dasyurus*, *Sminthopsis*), †*Namilamadeta*, *Lasiorhinus*, *Strigocuscus celebensis*, most pseudocheirids that could be scored for this trait (i.e., *Petauroides*, *Pseudocheirus*, *Pseudochirops archeri*), and *Dactylopsila*.

Overall, our observations are in close agreement with those of Sánchez-Villagra and Wible (2002), but a few discrepancies are noteworthy. In particular, Sánchez-Villagra and Wible (2002: 35, table 2) coded a foramen for the prootic canal on the tympanic surface of the petrosal as absent in †*Mayulestes* based on Muizon's (1998) description of the holotype and only known skull of this taxon (MHNC 1249). However, our own examination of MHNC 1249 revealed what appears to be a foramen for the prootic canal dorsomedial to the epitympanic recess, in a similar position to that seen in *Didelphis* (Wible, 1990: fig. 4) and *Monodelphis* (Wible, 2003: fig. 7), with the epi-

tympanic recess forming its ventral floor, a finding apparently confirmed by Muizon et al. (2018: 412). Similarly, whereas Sánchez-Villagra and Wible (2002) scored this foramen as absent in *Echymipera kalubu* and *Perameles gunnii*, we identified a foramen on the tympanic surface of the petrosal in specimens of both these taxa (e.g., *E. kalubu* specimens AMNH 190982 and 198708; *P. gunnii* specimens MVZ 127060 and 127072); Sánchez-Villagra and Forasiepi (2017: fig. 12) subsequently identified the lateral head vein within the prootic canal in a *Perameles* specimen that was not identified to species. Sánchez-Villagra and Wible (2002) also scored this foramen as absent in the macropodoids *Aepyprymnus rufescens* and *Setonix brachyurus*, but it is present in specimens that we examined of both species (e.g., *A. rufescens* specimen AMNH 160121; *S. brachyurus* specimens AMNH 160044 and 160258). Sánchez-Villagra and Wible (2002) and Ladevèze (2005) both reported the prootic canal as absent in adult *Dromiciops* specimens, but it is present in a sectioned late juvenile (Sánchez-Villagra and Wible, 2002: fig. 9); we have not examined isolated petrosals of *Dromiciops*, and prefer to score it as unknown ("?").

Character 70. *Tensor tympani muscle unenclosed ventrally (0); or enclosed ventrally by a bridge of bone derived from petrosal (1)*. In most metatherians, the tensor tympani muscle, which originates from the anterolateral face of the promontorium, is not enclosed ventrally (state 0). However, Aplin (1990: 302) identified a "narrow bridge of bone derived from the petrosal" that ventrally encloses the tensor tympani of *Tarsipes*; he also suggested that the "small oval nodule of bone" that Parker (1890: 81) observed in the tensor tympani tendon of *Tarsipes* was, in fact, a remnant of this bridge. Examination of the left ear region of *T. rostratus* (e.g., AMNH 119716, the bulla of which has been removed) confirms Aplin's (1990) observations: the ventral bridge of bone can be identified anterior to the stapes, anteromedial to the epitympanic recess, and medial to a dorsally extensive accessory airspace within the petrosal. Dried remnants of the

tensor tympani muscle can be seen emerging dorsal to the margins of the bridge in AMNH 119716. Sánchez-Villagra and Wible (2002: fig. 10) illustrated the ear region of AMNH 119716 (probably the left side, although the figure is reversed as if it were the right side), but the structures they identified as the "hiatus fallopii (hF)" and "secondary facial foramen (sff)" in their figure actually represent the anteromedial and posterolateral margins of the bony bridge respectively (*Tarsipes* entirely lacks a secondary facial foramen; see char. 72). Ventral enclosure of the tensor tympani by bone (state 1) is an autapomorphy of *Tarsipes* in the current analysis.

Character 71. *Cavum supracochleare roofed by petrosal (0); or not roofed by petrosal (1).* In most metatherians, the cavum supracochleare is completely roofed by the petrosal (state 0; e.g., in *Didelphis*; Wible, 1990: fig. 4D). However, Wible (1990: 195) noted that the petrosal roof is incomplete—and, hence, that the cavum supracochleare and cavum epiptericum are connected by a fenestra semilunaris sensu Rougier et al. (1992)—in caenolestids and "some marmosine didelphids." In taxa in which the cavum supracochleare lacks a complete roof, a prominent depression that houses the geniculate ganglion is visible in isolated petrosals (e.g., Ladevèze, 2004: fig. 2; 2005: fig. 11).

Of the taxa examined in this study for which isolated petrosals were available, the cavum supracochleare lacks a complete roof only in *Caenolestes* (see Ladevèze, 2005: fig. 11; Wible, 1990: 195; we were unable to score other Recent canolestids or fossil paucituberculatans), *Hyladelphys*, *Marmosa* (see Wible, 1990: 195), and †*Thylacoleo*. Although not included in this analysis, some isolated "Type II" metatherian petrosals from the Eocene Itaborai fossil fauna of Brazil also lack a complete roof (Ladevèze, 2004); Beck (2017a) argued that these petrosals probably belong to the polydolopimorphian *Epidolops ameghinoi* (but see criticism of this by Muizon et al., 2018: 422–423).

Character 72. *Facial nerve exits the substance of the petrosal within the middle ear (0); or is* enclosed within a bony tube formed by the petrosal until it exits the skull via the stylomastoid foramen (1). In most metatherians, the facial nerve exits the substance of the petrosal within the middle ear and extends posteriorly within an open facial sulcus of the petrosal before leaving the middle ear via the stylomastoid notch or foramen (state 0). Usually, the facial nerve exits the petrosal via the secondary facial foramen, while the greater petrosal nerve exits via a separate foramen (the hiatus fallopii), as in, for example, *Didelphis* (Wible, 1990: fig. 4C), *Monodelphis* (Wible, 2003: fig. 8A), and *Philander* (Wible et al., 2021). We observed minor taxonomic differences in the relative positions of the hiatus fallopii and secondary facial foramen but, contra previous studies (e.g., Sánchez-Villagra and Wible, 2002: char. 12; Horovitz and Sánchez-Villagra, 2003: char. 218), we were unable to partition this variation into unambiguously distinct states (see also Wible [2003: 174] regarding polymorphism in the position of the hiatus fallopii in *Monodelphis*).

In some specimens of *Lasiorhinus* and *Vombatus*, the floor of the cavum supracochleare (the petrosal chamber that houses the geniculate ganglion, from which arise the facial and greater petrosal nerves) is unossified (as previously noted by Wible, 1990: 188; Sánchez-Villagra and Wible, 2002: 35). In such specimens, the hiatus fallopii and secondary facial foramen are not present as separate openings; instead, a single foramen (the primary facial foramen) opens into the pars cochlearis. However, we observed considerable polymorphism in the degree of ossification of the floor of the cavum supracochleare in *Lasiorhinus* and *Vombatus* (Wible, [2010: 11–12] discussed similar polymorphism of this feature in the xenarthran *Dasypus novemcinctus*), and so we scored both of these taxa as state 0.

A qualitatively distinct morphology is seen in acrobatids and *Tarsipes*, the facial nerve of which is fully enclosed by a bony petrosal tube that extends all the way to the stylomastoid foramen; hence, there is no exit for the facial nerve anywhere within the middle ear space (state 1; see also Aplin, 1990: 304).

Character 73. *Subarcuate fossa deeply excavated (0); or a shallow depression (1).* The subarcuate (or floccular) fossa of the petrosal, which houses the petrosal lobule of the paraflocculus of the cerebellum, is a deep cavity (state 0) in most metatherians (e.g., Archer, 1976b; Wible, 1990, 2003; Rougier et al., 1998; Sánchez-Villagra, 2002; Ladevèze, 2004; 2005; Ladevèze and Muizon, 2007, 2010; Sánchez-Villagra et al., 2007; Horovitz et al., 2008, 2009; Muizon et al., 2018). Minor taxonomic variation in subarcuate fossa size and shape has sometimes been partitioned into discrete traits in previous phylogenetic studies (e.g., Ladevèze, 2004: char. 2), but we are unable to distinguish these consistently. However, the subarcuate fossa is just a shallow depression on the cerebellar side of the petrosal in *Vombatus* and *Lasiorhinus*, a qualitatively distinct condition (state 1; see Sánchez-Villagra, 2002). The subarcuate fossa is similarly shallow in †*Neohelos* (Murray et al., 2000a), †*Ngapakaldia*, †*Nimbadon* (Black and Hand, 2010: fig. 5B), †*Muramura*, †*Namilamadeta*, and some specimens of †*Thylacoleo*. Although the subarcuate fossa of *Sarcophilus* is somewhat shallower than that of most other metatherians (Archer, 1976b: 259), it is not comparable to the vombatid condition (Sánchez-Villagra, 2002), so we scored *Sarcophilus* as state 0.

Character 74. *Glenoid fossa essentially flat or slightly concave, sometimes with a raised articular eminence (0); or convex and mediolaterally very broad (1).* In most metatherians, the glenoid fossa is flat or slightly concave (state 0), but in most diprotodontians (e.g., phalangerids, pseudocheirids, macropodiforms, diprotodontids, phascolarctids) the glenoid region includes a raised articular eminence anteriorly and a shallow, transversely oriented mandibular fossa posteriorly (Aplin, 1987; 1990). This widespread diprotodontian morphology appears to reflect the spatial displacement of the mandibular condyle for different dental functions: the condyle rests within the mandibular fossa during molar occlusion, but it slides forward onto the articular eminence to bring the upper and lower incisors

into occlusion (Aplin, 1987; 1990). Although Aplin (1987: 387) suggested that this feature may be a "key innovation in the origin of Diprotodontia as a whole," we observed continuous variation in glenoid morphology among most of the diprototodontian taxa we examined (see also comments by Aplin, 1990: 310), so we did not code this trait as a separate character state.

By contrast, the glenoid morphology of Recent vombatids (e.g., *Vombatus*: fig. 45) is qualitatively distinct (Aplin, 1987; 1990; Murray, 1998), being convex and narrow anteroposteriorly (with no evidence of a mandibular fossa), but very broad mediolaterally (state 1). *Lasiorhinus* and *Vombatus* are also unusual in entirely lacking a postglenoid process (see char. 75).

Character 75. *Postglenoid process of squamosal well developed (0); or weakly developed or absent (1).* The glenoid fossa of most metatherians is buttressed posteriorly by a well-developed postglenoid process of the squamosal (state 0; e.g., in *Phascogale* [fig. 10A] and *Petaurus* [fig. 10B]). By contrast, this process is entirely absent in *Hypsiprymnodon moschatus* (fig. 52), *Potorous* (fig. 54), *Tarsipes* (fig. 49), *Vombatus* (fig. 45), and *Lasiorhinus* (state 1). Although still identifiable as a distinct structure, the postglenoid process is very weakly developed in †*Yalkaparidon* (Beck, 2009: fig. 7A; Beck et al., 2014), so we also scored this taxon as state 1.

Character 76. *Postglenoid foramen present (0); or absent (1).* A postglenoid foramen (which transmits the postglenoid vein) is consistently present in most metatherians (state 0; e.g., *Didelphis* [Wible, 1990: fig. 1], *Monodelphis* [Wible, 2003: fig. 6], *Philander* [Wible et al., 2021: figs. 2, 4], *Phascogale* [fig. 10A], and *Petaurus* [fig. 10B]), although its position is taxonomically variable (see char. 77). Aplin (1990: 240) stated that vombatids "lack a conventional postglenoid foramen [but] a variable number of foramina usually perforate the posterior surface of the condylar process/anterior wall of the squamosal epitympanic sinus" and reported that these foramina "typically convey a small branch of the postglenoid artery, and sometimes, a small satel-

lite vein." We found that a bristle inserted into the largest of the multiple subsquamosal foramina that are present in *Vombatus* and *Lasiorhinus* (see chars. 81, 82) exits via a distinct foramen within the zygomatic epitympanic sinus of the squamosal, so we interpret the latter foramen as homologous with the postglenoid foramen. We observed a similar foramen within the zygomatic epitympanic sinus in †*Warendja*. Therefore, *Vombatus*, *Lasiorhinus*, and †*Warendja* have all been scored as state 0.

By contrast, †*Neohelos* and †*Nimbadon* both appear to lack an identifiable postglenoid foramen (state 1). Black and Hand (2010: 37) referred to a "deep, recessed pocket" in the posterior wall of the postglenoid process of the squamosal in some †*Nimbadon* specimens (e.g., QM F53642) as a "postglenoid foramen," but this structure is a blind sinus (possibly homologous with the laterally open zygomatic epitympanic sinus seen in vombatids; see chars. 85, 86), rather than a foramen.

Character 77. *Postglenoid vein exits skull via the postglenoid foramen above the ear region, posterior or posteromedial to the glenoid fossa and the postglenoid process (if present) (0); or postgenoid vein emerges from the postglenoid foramen in the posteromedial corner of the glenoid fossa, medial or anteromedial to the postglenoid process (if present) (1).* In most metatherians in which the postglenoid foramen is present (see char. 76), this foramen opens above the ear region and behind the postglenoid process (state 0), as in, for example, *Phascogale* (fig. 10A), *Didelphis* (Wible, 1990: fig. 1), *Philander* (Wible et al., 2021: figs. 2, 4), and *Monodelphis* (Wible, 2003: fig. 6). Among these taxa, there is minor variation in the position of this foramen that we have not scored here: for example, it is located in a more medial position (but still slightly posterior to the glenoid fossa and postglenoid process) in *Thylacinus* than in most other dasyuromorphians (Murray and Megirian, 2006a: appendix 1, fig. 1C; Warburton et al., 2019: fig. 7).

A qualitatively distinct state, however, is observed in most examined diprotodontians: the postglenoid vein passes anteroventrally in a bony canal that is primarily formed by the squamosal (although an ectotympanic component is often also present; Wroe et al., 1998: 744) and emerges medial (or anteromedial) to the postglenoid process, in the posteromedial corner of the glenoid fossa (state 1; e.g., *Petaurus*, fig. 10B). Springer and Woodburne (1989: table 2, char. 11) described the latter condition as "sheathing of the ventral postglenoid foramen" and reported that it does not occur in phascolarctids or macropodoids (see also Marshall et al., 1990: fig. 2, node 71). Our observations, by contrast, are more consistent with those of Wroe et al. (1998) who reported enclosure ("sheathing") of the postglenoid vein (or foramen) in macropodiforms, and the same morphology is clearly expressed in the phascolarctids *Phascolarctos*, †*Litokoala*, and †*Nimiokoala* (Louys et al., 2009). Although *Hypsiprymnodon moschatus* and *Potorous* both lack a postglenoid process of the squamosal (see char. 75), the enclosure of the postglenoid vein in these taxa and its opening in the posteromedial corner of the glenoid fossa more closely resembles the widespread diprotodontian condition than it does the morphology seen in other metatherians; we therefore scored these taxa as conforming to state 1.

However, this condition is not universal among diprotodontians. In *Tarsipes*, the postglenoid foramen is at the lateral end of the deep groove posterior to the glenoid fossa (Aplin, 1990: 311); this morphology most closely corresponds to state 0. In *Vombatus*, *Lasiorhinus*, and †*Warendja*, a foramen that appears to be homologous to the postglenoid foramen opens within the zygomatic epitympanic sinus of the squamosal (see char. 76); although these taxa all lack a postglenoid process of the squamosal (see char. 75), this foramen clearly does not open within the glenoid fossa, but rather posteromedial to it, so we also score them as state 0 (contra Springer and Woodburne, 1989: table 2, char. 11, who scored "sheathing of ventral postglenoid foramen" as present in Vombatidae). Similarly, the postglenoid foramen of †*Silvabestius*, †*Mura-*

mura, †*Namilamadeta*, and thylacoleonids opens within the zygomatic epitympanic sinus of the squamosal, posteromedial to the glenoid fossa and postglenoid process, rather than within the glenoid fossa (see comments by Aplin, 1987: 383); because this morphology resembles the vombatid condition, we scored these taxa as state 0.

The morphology of this region in *Notoryctes* is difficult to interpret, in part because the postglenoid process of the squamosal appears to be fused to the pars canalicularis of the petrosal (with the external auditory meatus below, rather than behind, the postglenoid process; see char. 78). However, the postglenoid vein does appear to emerge medial to the postglenoid process in *Notoryctes*, in the posteromedial corner of the glenoid fossa. Nevertheless, CT-scans indicate that, unlike the condition in most diprotodontians, it is not enclosed proximally within an elongate bony canal (Beck, in prep.); despite this difference, we tentatively scored *Notoryctes* as state 1. This character is inapplicable ("-") for †*Neohelos* and †*Nimbadon*, both of which lack a distinct postglenoid foramen (see char. 76).

Character 78. *External auditory meatus dorsal to the glenoid fossa (0); posterior to the glenoid fossa (1); or ventral to the glenoid fossa (2).* In most metatherians, the external auditory meatus is posterior to the glenoid fossa, behind the postglenoid process of the squamosal (if present) and anterior to the posttympanic process of the squamosal and the mastoid exposure of the petrosal (state 1; e.g., in *Phascogale* [fig. 10A] and *Petaurus* [fig. 10B]). However, in *Dactylopsila* and *Dactylonax*, the postglenoid process is in direct contact with the mastoid, and the external auditory meatus is located dorsal (rather than posterior) to the glenoid fossa (state 0). As a result, the external auditory meatus appears to lie within the posterior root of the zygomatic arch (Aplin, 1990: plate 5.2a; Beck, 2009: fig. 3). Interestingly, Aplin (1990: 311) reported that *Dactylopsila* juveniles resemble other metatherians in the position of the external auditory meatus, suggesting that the unique adult morphology develops relatively late in ontogeny. The position of

the external auditory meatus is also unusual in *Notoryctes*, directly ventral to the glenoid fossa (fig. 36); this morphology has been scored as an additional state (state 2). Because the states comprising this character represent a plausible morphocline, reflecting a progressive shift in the position of the external auditory meatus along a dorsoventral axis, we ordered them in all our analyses.

Character 79. *Facial nerve exits middle ear via a stylomastoid notch (0); or via a stylomastoid foramen formed by the squamosal and caudal tympanic process of the petrosal (1); or via a stylomastoid foramen formed by the caudal tympanic process of the petrosal only (2); or via a stylomastoid foramen formed by the rostral and caudal tympanic processes of the petrosal (3); or via a stylomastoid foramen formed by the ectotympanic, posttympanic process of the squamosal, and pars canalicularis of the petrosal (4); or via a stylomastoid foramen formed by the ectotympanic and pars canalicularis of the petrosal (5).* The facial nerve exits the middle ear via a notch (the stylomastoid notch) in the petrosal, posterior to the tympanohyal, in most Recent didelphids (e.g., *Marmosa* [fig. 9A]), *Caenolestes*, *Rhyncholestes*, all examined peramelemorphians, thylacinids, *Myrmecobius*, †*Barinya*, †*Thylacoleo*, †*Wakaleo*, *Phascolarctos*, and some specimens of *Vombatus* (state 0). In other marsupials for which specimens with an intact basicranium were available, the exit of the facial nerve is entirely enclosed by bone, forming a complete stylomastoid foramen. However, the position and bony composition of this foramen vary markedly within Marsupialia, and we consider that the five different types of stylomastoid foramen we identify here fail the test of primary homology (sensu de Pinna, 1991). We therefore score the different foraminal types as alternative states within a single character that also includes absence of a stylomastoid foramen (state 0).

In *Caluromysiops* (see comments by Gabbert, 1998: 7) and †*Sparassocynus*, the stylomastoid foramen is formed by the squamosal and caudal

tympanic process of the petrosal (state 1), whereas in *Lestoros* (based on BMNH 1922.1.1.129) this foramen appears to be entirely within the caudal tympanic process of the petrosal (state 2). In Recent dasyurids (e.g., *Phascogale* [figs. 9B, 10A]), the stylomastoid foramen is within the petrosal plate formed by the rostral and caudal tympanic processes of the petrosal, which are seamlessly fused in adult specimens; however, juvenile specimens, in which the rostral and caudal tympanic processes are not fused, indicate that the stylomastoid foramen probably lies on the boundary between them (state 3; Archer, 1976b: 255; see also comments by Wroe, 1999: 513). The stylomastoid foramen of Recent dasyurids is sometimes also bordered anterodorsally by the squamosal (Archer, 1976b; Wroe, 1999; Wroe et al., 2000: char. 54). Another form of enclosure is seen in *Dromiciops*, in which the stylomastoid foramen is between the posterior limb of the ectotympanic and the posttympanic process of the squamosal (which are fused; see char. 60) anteriorly and the caudal tympanic process of the petrosal posteriorly (state 4). In phalangeridan diprotodontians (e.g., *Petaurus* [figs. 9C, 10B]), the stylomastoid foramen is between the squamosal, the mastoid exposure of the petrosal, and the ectotympanic (Aplin, 1990; Wroe et al., 1998); because these are the same bones that enclose the stylomastoid foramen in *Dromiciops*, we also scored phalangeridan diprotodontians as state 4. Isolated petrosals reveal the presence of an additional, internal foramen for the facial nerve formed by the caudal tympanic process in macropodoids (Aplin, 1990: 148, plate 3.8e), whereas this internal foramen is absent in other phalangeridans. Nevertheless, lacking isolated petrosals for most taxa, we scored this character based on the external aspect of the stylomastoid orifice only.

In †*Neohelos* (based on NTMP 87108-1), *Lasiorhinus*, and some specimens of *Vombatus* (e.g., AMNH 66197), the stylomastoid foramen is formed by the ectotympanic and the pars canalicularis of the petrosal (state 5). Presence or absence of a stylomastoid foramen appears to be age related in *Vombatus* because it is more commonly present in older and larger individuals (reflecting increasing ossification of the ear region with advancing age).

It is unclear exactly which bones enclose the stylomastoid foramen in *Notoryctes*, but the morphology of this region most closely corresponds to state 4 based on the position of the foramen and the fact that the ectotympanic appears to contribute to its ventral border (e.g., in AMNH 15015; see also Archer, 1976b: 313). Thus, we tentatively scored *Notoryctes* as state 4.

Character 80. *Process of the exoccipital does not extend as far as the exit of the facial nerve (stylomastoid notch or foramen) (0); or extends laterally or anterolaterally as far as the stylomastoid notch or foramen (1).* In most metatherians, the exoccipital ends laterally at a suture with the pars canalicularis of the petrosal immediately lateral to the paroccipital process (state 0), as in *Marmosa*, *Phascogale*, and *Petaurus* (fig. 9). In acrobatids, however, a process of the exoccipital extends laterally as far as the stylomastoid foramen, covering the posterior part of the auditory bulla in ventral view (state 1), as in *Distoechurus* (fig. 48; see also Aplin and Archer [1987: lviii]; Aplin [1990: 332]). A somewhat similar morphology is seen in †*Thylacoleo*, in which the exoccipital is sufficiently laterally extensive to contribute to the external opening of the stylomastoid notch, so we also scored this taxon as state 1.

Character 81. *Subsquamosal foramen present (0); or absent (1).* In many metatherians, the squamosal is pierced immediately dorsal to the external auditory meatus by a prominent foramen (state 0), as in *Marmosa* (fig. 2), *Caenolestes* (Osgood, 1921: plate XX fig. 2), *Phascogale* (fig. 10A), and *Thylacinus* (Murray and Megirian, 2006a: appendix 1, fig. 1). This foramen connects to the postglenoid foramen through the squamosal and has been shown to transmit a temporal branch of the postglenoid artery and an accompanying vein in didelphids (Wible, 2003) and dasyurids (Archer, 1976b). It was named the subsquamosal foramen by Cope (1880),

and this terminology has been followed by most subsequent authors (e.g., Gregory, 1910; Archer, 1976b; Voss and Jansa, 2009; Pavan and Voss, 2016). By contrast, Wible (2003) referred to this orifice as the "suprameatal foramen" and used "subsquamosal foramen" for one or more small foramina that are variably present within the squamosal dorsal to the suprameatal bridge (the horizontal squamosal crest that extends posteriorly from the dorsal margin of the zygomatic process to the occiput) in *Monodelphis*. We follow Cope's (1880) terminology here to maintain consistency with most of the metatherian literature.

In some diprotodontians there is no foramen immediately above the external auditory meatus, but a smaller foramen occurs farther dorsally, often close to (or even within) the squamosal suture with the parietal (see char. 83). This foramen can be seen in dorsal view in (for example) some specimens of *Phalanger* (in which it is enclosed by the squamosal [fig. 47]; Springer and Woodburne, 1989: fig. 2B) and *Petaurus* (in which it is contained within the squamosal-parietal suture [fig. 50]). Despite its position—dorsal to the suprameatal bridge—this foramen appears to be homologous with the subsquamosal foramen: a bristle introduced into this foramen emerges from the postglenoid foramen. Multiple foramina piercing the dorsal surface of the squamosal in *Vombatus* (fig. 45) and *Lasiorhinus* also appear to be homologous with the subsquamosal foramen because they are connected internally to the foramen within the zygomatic epitympanic sinus that we identify as the homologue of the postglenoid foramen (see char. 76); additionally, Aplin (1990: 240) reported that they transmit branches of the postglenoid artery. CT-scans demonstrate that the small foramen posterior to the glenoid fossa and dorsal to the external auditory meatus in *Notoryctes* connects to the postglenoid foramen, and therefore can also be identified as the subsquamosal foramen (Beck, in prep.).

By contrast, we observed complete absence of the subsquamosal foramen (state 1) in *Hemibelideus*, *Petauroides*, *Pseudochirops cupreus* (but not *P. archeri*), *Acrobates*, *Distoechurus* (fig. 48), and

Tarsipes (fig. 49), none of which exhibits any trace of a squamosal perforation above the ear region. The subsquamosal foramen is also only variably present in *Phalanger* (often being present on only one side of an individual), so we scored this taxon polymorphic ("0+1").

Character 82. *Subsquamosal foramen single (0); or multiple (1).* In most metatherians in which the subsquamosal foramen is present (see char. 81), it is marked by a single opening (state 0). However, as discussed above, there are multiple apparently homologous perforations of the squamosal (state 1) in *Vombatus* (fig. 45) and *Lasiorhinus*. Two or three subsquamosal foramina are present in †*Namilamadeta*, which we also scored as state 1. Pledge (1992: 111) reported that the squamosal of †*Warendja* is "not perforated by foramina as in modern wombats," based on a partial skull of †*W. wakefieldi* (SAM P21405), implying that only a single subsquamosal foramen is present. However, we consider the squamosal of SAM P21405 to be too incomplete to determine this with any confidence, and Brewer (2007) described a cranial fragment of †*W. wakefieldi* (AM F129857) that preserves multiple subsquamosal foramina; although we have not examined the latter specimen, we scored †*Warendja* as state 1 here.

Character 83. *Subsquamosal foramen entirely within squamosal (0); or within squamosal-parietal suture (1).* In most metatherians that retain a subsquamosal foramen (see char. 81), this foramen opens entirely within the squamosal (state 0). In the pseudocheirids *Pseudocheirus* and *Pseudochirulus*, however, it opens within the squamosal-parietal suture (state 1). The subsquamosal foramen is also within the squamosal-parietal suture in some specimens of *Petaurus* (fig. 50), so we scored this taxon as polymorphic ("0+1") for this character.

Character 84. *Posterior squamosal epitympanic sinus absent or indistinct, without any lateral enclosure (0); or distinct and at least partially enclosed laterally (1).* Epitympanic sinuses are pneumatic (air-filled) cavities that communicate with the epitympanic recess dorsal to the tym-

panic membrane (van der Klaauw, 1931; Beck and Taglioretti, 2020: 5). The presence of a distinct pneumatic cavity within the squamosal posterolateral to the epitympanic recess was proposed as a synapomorphy of Australian marsupials to the exclusion of South American forms by Marshall et al. (1990), so the distribution of this feature within Metatheria warrants careful assessment. Archer (1976a) simply referred to this cavity as the squamosal epitympanic sinus, but we follow Wroe et al. (1998) in distinguishing a posterior epitympanic sinus (which is posterolateral to the epitympanic recess, as in, e.g., *Phascogale* [figs. 9B, 10A) from a zygomatic epitympanic sinus (which is anterior to the epitympanic recess and invades the zygomatic process of the squamosal; char. 85). In addition to these two sinuses, Wroe et al. (1998: 743) also referred to a third, the dorsal epitympanic sinus present in some diprotodontians (e.g., *Burramys*). However, we were unable to consistently determine the presence or absence of a dorsal epitympanic sinus among our terminals.

A posterior squamosal epitympanic sinus is absent or indistinct (state 0) in †*Pucadelphys* (Marshall and Muizon, 1995), †*Allqokirus* (Muizon et al., 2018), most Recent didelphids (e.g., *Marmosa* [fig. 9A]; *Didelphis* [Wible, 1990: fig. 1]; *Monodelphis* [Wible, 2003]; *Philander* [Wible et al., 2021: fig. 4]), Recent caenolestids, *Dromiciops*, †*Yalkaparidon* (Archer et al., 1988; Beck et al., 2014), †*Badjcinus* (Muirhead and Wroe, 1998), wynyardiids (Aplin, 1987; Pledge, 2005), and some macropodiforms (e.g., *Dorcopsis*, *Setonix*, *Thylogale*, and †*Ganawamaya*). A shallow depression that is ventral or posteroventral to the subsquamosal foramen in †*Galadi*, *Echymipera*, *Peroryctes*, and some didelphids (e.g., *Lestodelphys* [Voss and Jansa, 2009: fig. 13B]) might be homologous with the posterior epitympanic sinus (see comments by Archer, 1976b: 304; 1982a: 461; Beck and Taglioretti, 2020: 19), but these indistinct concavities are difficult to distinguish from absence, so we scored them all as state 0.

By our definition, a distinct posterior squamosal epitympanic sinus (state 1) is at least par-

tially enclosed laterally by bone; such sinuses occur in †*Mimoperadectes* (Horovitz et al., 2009), *Caluromysiops* (Reig et al., 1987: fig. 44C; see also Wible, 1990: 200, who implied that a "suprameatal fossa" is present in this taxon), †*Sparassocynus* (Beck and Taglioretti, 2020), all examined dasyuromorphians except †*Badjcinus* (e.g., *Phascogale* [figs. 9B, 10A]), some peramelemorphians (e.g., *Chaeropus* [fig. 37]), and most diprotodontians, with the exception of wynyardiids, some macropodiforms (discussed above), and some specimens of †*Neohelos*. In many diprotodontians (e.g., *Petaurus* [fig. 10B]), this sinus is fully enclosed by the squamosal such that it is not externally visible (Springer and Woodburne, 1989; Wroe et al., 1998); therefore, we determined sinus morphology in these taxa by examination of broken or damaged skulls. Although *Notoryctes* lacks external evidence of a posterior squamosal epitympanic sinus, broken skulls reveal the presence of what appear to be auditory sinuses dorsolateral and posterolateral to the epitympanic recess (see also Archer, 1976b: 269); fusion of cranial bones in this region, however, makes it impossible to determine conclusively whether or not these auditory sinuses are within the squamosal, so we scored *Notoryctes* as unknown ("?").

Examination of incompletely cleaned crania suggests that, where present, this sinus is covered by the pars flaccida of the tympanic membrane in dasyuromorphians and peramelemorphians (van der Klaauw, 1931; Archer, 1976b; Marshall, 1977; Aplin, 1990). The apparently homologous shallow depression seen in some Recent didelphids also appears to be covered by the pars flaccida, as in *Chironectes* (e.g., AMNH 212909) and *Lutreolina* (e.g., BMNH 1939.4221]). However, this does not appear to be the case in diprotodontians (Aplin, 1990: 367). Thus, the homology of the posterior epitympanic sinus in all the taxa scored as possessing this trait is open to reasonable doubt.

Character 85. *Zygomatic epitympanic sinus absent (0); or present (1).* Most metatherians have, at most, a single squamosal epitympanic

sinus, namely the posterior sinus described above (see char. 84). However, an additional epitympanic sinus that invades the squamosal zygomatic process is present (state 1) in all examined diprotodontians for which suitable specimens were available, with the notable exception of *Tarsipes.* We follow Wroe et al. (1998) in referring to the latter cavity as the zygomatic epitympanic sinus. There is considerable variation in zygomatic epitympanic sinus morphology within Diprotodontia, which we coded as an additional character below (char. 86).

Character 86. *Zygomatic epitympanic sinus fully enclosed by squamosal without external opening (0); or enclosed laterally by squamosal but with prominent external opening on posterior surface of squamosal zygomatic process (1); or shallow and largely open laterally (2).* The zygomatic epitympanic sinus is fully enclosed by the squamosal and lacks an obvious external opening (state 1) in acrobatids, phalangerids, pseudocheirids, petaurids (e.g., *Petaurus* [fig. 10B]), and *Cercartetus;* broken or damaged skulls reveal that the zygomatic epitympanic sinus of these taxa is extensive and usually filled with cancellous bone. By contrast, a prominent external opening is visible on the posterior surface of the squamosal zygomatic process (state 1) in *Burramys,* †*Wakaleo,* phascolarctids (see Murray et al., 1987. and Louys et al., 2009: figs. 3, 4, who referred to this orifice as the "postglenoid cavity"), and most macropodiforms (see Springer and Woodburne, 1989 [fig. 2A], where it is the more anterior of the two "openings in squamosal," and Wells and Tedford, 1995 [fig. 9D], where it is labelled as the "postzygomatic foramen"). In *Petrogale,* the region of the squamosal posterodorsal to the external auditory meatus is strongly pneumatized and contacts the posterior part of the zygomatic process of the squamosal (Prideaux and Warburton, 2010: char. 12). As a result, there is no large, posteriorly facing external opening leading into the zygomatic epitympanic sinus in *Petrogale;* at most, there is a tiny, laterally oriented, slitlike opening within the point of contact between the two squamosal processes. Thus, we scored *Petrogale* as state 0. Although we agree with Prideaux

and Warburton (2010: char. 12) that the region of the squamosal posterodorsal to the external auditory meatus is also inflated and contacts the posterior part of the zygomatic process of the squamosal in *Dendrolagus* and †*Bohra,* a large, posterior-facing opening into the zygomatic epitympanic sinus remains visible in both of these taxa, which we scored as state 1.

A third distinct morphology is seen in *Vombatus* (fig. 45), *Lasiorhinus,* and †*Warendja* (Aplin, 1987: 381; 1990; Pledge, 1992), in which the zygomatic epitympanic sinus does not deeply invade the zygomatic process of the squamosal but is largely open laterally (state 2). We observed a similarly shallow, laterally open zygomatic epitympanic sinus in †*Muramura,* †*Namilamadeta,* †*Ngapakaldia,* and †*Lekanoleo.*

In †*Neohelos* (Murray et al., 2000a: fig. 40), †*Nimbadon* (Black and Hand, 2010: figs. 4, 17, 18), †*Silvabestius* (Black, 2008: fig. 5.2A), and †*Thylacoleo,* an enclosed epitympanic sinus extends deep into the squamosal zygomatic process and communicates with the external surface of the skull via a large "epitympanic fenestra" (sensu Murray, 1992); this morphology most closely resembles state 1. In all four of these taxa, however, another shallow concavity—the "postglenoid sinus" of Black (2008: fig. 5.2A) and Black and Hand (2010: fig. 18A)—also invades the posterior face of the postglenoid process, a trait similar to that seen in taxa that we scored as state 2. The apparent presence of two zygomatic epitympanic sinuses in these taxa raises obvious questions about the homology of such structures among diprotodontians, but in the current study we scored †*Neohelos,* †*Nimbadon,* †*Silvabestius,* and †*Thylacoleo* using ambiguity coding (as "1/2").

This character was scored as inapplicable ("-") for all taxa lacking a distinct zygomatic epitympanic sinus (i.e., all taxa scored as state 0 for char. 85). Because the states of this character form a plausible morphocline reflecting the degree of enclosure of the zygomatic epitympanic sinus, we treated this character as ordered in all our analyses.

Character 87. *Squamosal and pars canalicularis of the petrosal not extensively pneumatized posterior and dorsal to external auditory meatus (0); or extensively pneumatized and cancellous (1).* In most metatherians (e.g., *Marmosa* [fig. 1]), the squamosal and pars canalicularis of the petrosal are not greatly pneumatized posterior and dorsal to the external auditory meatus (state 0), apart from the presence of a posterior epitympanic sinus of the squamosal in some taxa (char. 84). By contrast, the squamosal and pars canalicularis are both extensively pneumatized and are composed of cancellous bone in this region (state 1) in all examined petaurids (e.g., *Petaurus* [fig. 10B]), pseudocheirids, acrobatids, phalangerids, and *Petrogale* (Aplin, 1987: 384; Aplin, 1990). Notably, this region is not strongly pneumatized in *Tarsipes*, *Burramys*, or *Cercartetus* (Aplin, 1987: 384; Aplin, 1990). Our observations with regard to this feature largely agree with those of Springer and Woodburne (1989: char. 14), except that this region also appears to be extensively pneumatized in *Ailurops* (e.g., in AMNH 152884), albeit to a slightly lesser extent than in other phalangerids (Flannery et al., 1987: 482); thus, we scored *Ailurops* as state 1.

Character 88. *Squamosal and the pars canalicularis of the petrosal unfused (0); or seamlessly fused, with no evidence of a suture between the two bones even in juveniles (1).* In most metatherians, the squamosal and the pars canalicularis of the petrosal are clearly distinguishable throughout ontogeny, with an obvious suture between the two bones (state 0). In phalangerids, the suture between the mastoid exposure of the pars canalicularis of the petrosal (which is restricted to a small ventral strip on the occiput; fig. 12C) and the squamosal is sometimes difficult to identify in adult individuals but is obvious in juvenile and subadult specimens (see char. 90), so we scored phalangerids as state 0. By contrast, the squamosal and the pars canalicularis of *Acrobates* and *Distoechurus* are seamlessly fused (state 1), even in the youngest juvenile specimens we examined (contra Voss and Jansa, 2009: 36); indeed, Aplin (1990: 291) specifically compared the acrobatid morphology to the human temporal bone.

Occipital Region

The occipital region includes the basi-, exo-, and supraoccipital bones as well as the mastoid exposure of the pars canalicularis of the petrosal. Broadly speaking, this part of the skull provides surfaces for the cervical articulation, for the insertion of nuchal muscles, and for the origin of the digastric and various hyoid muscles. Occipital bones are also pierced by foramina that transmit cranial nerves and blood vessels, and they form a protective ring around the medula oblongata. Characters of the occipital region have not played a major historical role in debates about metatherian phylogeny, but there is more anatomical variation here than might be expected from this traditional neglect. A nonexhaustive list of synonyms for anatomical features in this region is given in table 11.

Character 89. *Lambdoid sesamoids absent (0); or present (1).* Sesamoids for the insertion of the dorsal neck musculature are absent (state 0) in most metatherians, but they are present (state 1) in all examined peramelemorphians (including †*Yarala* and †*Galadi*; Muirhead, 2000; Travouillon et al., 2010) as bilaterally paired, suturally distinct ossifications on the lambdoid crest between the parietals and the supraoccipital (e.g., in *Echymipera* [fig. 11]). These sesamoids are markedly smaller, but still identifiable, in *Chaeropus* (fig. 37) than in other peramelemorphians we examined (e.g., *Macrotis* [fig. 38] and *Perameles* [fig. 39]). Although often illustrated by authors (e.g., Freedman, 1967), these distinctive structures were first described explicitly by Filan (1990), who hypothesized their role as force-multipliers for M. rectus capitis dorsalis and other head extensors. Although bilateral thickenings of the lambdoid crest are present in several other marsupials (for example, many dasyurids), they lack obvious, suturally distinct sesamoids; therefore, we scored such taxa as state 0.

Character 90. *Mastoid exposure of petrosal extensively exposed on occiput, contacting supraoccipital on each side (0); or restricted to ventralmost part of occiput, not contacting supraoccipital*

TABLE 11

Selected Anatomical Synonyms for Structures of the Occipital Region[a]

This report	Synonym
Hypoglossal foramen	canalis nervus hypoglossi (NAV); condylar foramen (Dederer, 1909); condyloid foramen (Sinclair, 1906)
Lambdoid crest	crista nuchae (NAV); nuchal crest (Osgood, 1921); occipital crest (Owen, 1859)
Mastoid fenestra	mastoid foramen (Osgood, 1921)
Mastoid process	mastoid tympanic process (Ladevèze and Muizon, 2007[b]; Sánchez-Villagra et al., 2007); paroccipital process (Rougier et al., 1998); processus mastoideus (NAV)
Paroccipital process	paracondylar process (Rougier et al., 1998); processus paracondylaris (NAV)

[a] References other than *Nomina anatomica veterinaria* (6th ed., NAV) include the earliest relevant synonymic usage in the marsupial literature of which we are aware, but this list is not intended to be exhaustive.
[b] Ladevèze and Muizon (2007: 1130) stated that their usage of "mastoid tympanic process" follows that of Archer (1976b) and Wible (1990). However, Archer (1976b) used "mastoid tympanic process" or "mastoid tympanic wing" to refer to the structure we call here the caudal tympanic process of the petrosal (see table 11), and Wible (1990) did not use the term "mastoid tympanic process" (only "mastoid process"). Archer's (1976b) and Wible's (1990) usage of "mastoid process" is the same as ours, referring to the process of the petrosal from which the sternocleidomastoid muscle originates (see char. 93).

(1). In most metatherians the pars canalicularis of the petrosal is extensively exposed on the occiput, where it is commonly known as the mastoid (or as the mastoid exposure of the petrosal). In this taxonomically widespread morphology the mastoid extends dorsally to contact the supraoccipital (state 0), as in †*Mayulestes* (Muizon, 1998: fig. 9), didelphids (e.g., *Lestodelphys* [fig. 12A] and *Metachirus* [fig. 12B]), *Dromiciops* (Giannini et al., 2004: fig. 3), and most diprotodontians (e.g., *Macropus*; Wells and Tedford, 1995: fig. 9). Although Wroe et al. (2000: char. 68) and Wroe and Musser (2001: char. 68) scored †*Pucadelphys* as lacking a mastoid contribution to the occiput, a large mastoid exposure is, in fact, clearly present on the occiput of this taxon (Marshall and Muizon, 1995; personal obs.). The bones comprising the occiput are fused in adult specimens of *Notoryctes*, but CT-scans of a fluid-preserved juvenile (NMV C11082) indicate the presence of a large mastoid exposure on the occiput of this taxon as well (Beck, in prep.).

By contrast, in all examined phalangerids (e.g., *Trichosurus* [fig. 12C]) the mastoid exposure is reduced to a narrow strip on the ventrolateral aspect of the occiput (Flannery et al., 1987), where it does not contact the supraoccipital (state 1). Instead, phalangerids exhibit squamosal-exoccipital contact. The transverse suture between the squamosal and mastoid is hard to see on adult skulls of some phalangerids, with the result that the mastoid is sometimes incorrectly illustrated as extending between the squamosal and the exoccipital (e.g., as by Springer and Woodburne, 1989: fig. 2B). However, the squamosal-mastoid suture is ontogenetically persistent in other taxa, notably *Trichosurus* (fig. 12C). The mastoid exposure is slightly more extensive dorsally in *Ailurops* than it is in other phalangerids (Flannery et al., 1987: fig. 4D), but it does not contact the supraoccipital in any examined specimen, so we scored this taxon as corresponding to state 1.

As noted above (char. 88), the pars canalicularis of the petrosal is seamlessly fused to the squamosal in *Acrobates* and *Distoechurus*, so the relative contribution of the mastoid to the occiput is unclear in these taxa, both of which we scored as unknown ("?").

Character 91. *Mastoid fenestra absent (0); or present dorsal and medial to the mastoid exposure of petrosal (1).* In most metatherians the occiput is imperforate (state 0), with the obvious excep-
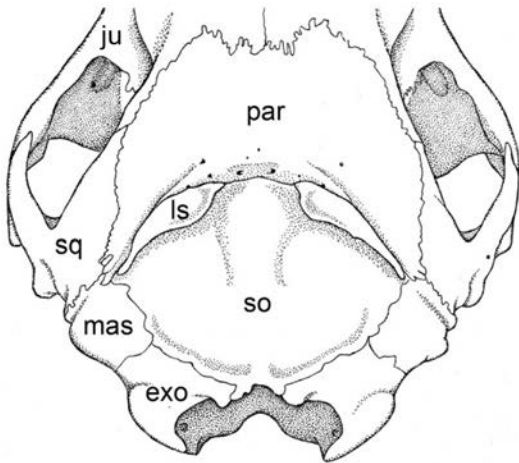
FIG. 11. Occiput of *Echymipera kalubu* (AMNH 192168) illustrating the mature peramelemorphian morphology (a conspecific juvenile is shown in fig. 6C). States for characters 25 and 89 (see main text for descriptions of these characters and character states) are illustrated as follows: 25(1), 89(1). Abbreviations: **exo,** exoccipital; **ju,** jugal; **ls,** lambdoid sesamoid; **mas,** mastoid; **par,** parietal; **so,** supraoccipital; **sq,** squamosal.

tion of the foramen magnum (e.g., in *Metachirus* [fig. 12B] and *Trichosurus* [fig. 12C]). Although a foramen is sometimes present within the mastoid, this trait is often polymorphic, and we did not code it as a character. However, a qualitatively distinct condition is seen in Recent caenolestids (but not †*Acdestis*) and some didelphids (e.g., *Marmosa* [fig. 6B]; *Lestodelphys* [fig. 12A]), which exhibit a large unossified vacuity between the dorsal margin of the mastoid and the supraoccipital (state 1). Osgood (1921: 150–151) referred to this vacuity as a "large persistent mastoid foramen," but we prefer the term mastoid fenestra, based on the previously explained distinction between foramina and fenestrae (see Palate, above). The same name has been applied to topologically similar vacuities (albeit entirely within the mastoid) in rodents (e.g., by Carleton and Musser, 1989). Most macropodiforms (e.g., *Macropus* [Wells and Tedford, 1995: fig. 9D]) have a foramen within the mastoid but not a mastoid fenestra, so we scored them as state 0.

The sole exception is *Setonix*, in which a large unossified vacuity is present dorsal to the mastoid (e.g., in AMNH 196398, 196399); therefore, we scored *Setonix* as state 1.

Character 92. *Two hypoglossal foramina (0); or only one hypoglossal foramen opening on the extracranial surface (1).* Most metatherians have two hypoglossal foramina opening on the extracranial surface (e.g., *Didelphis* [Wible, 2003: fig. 1]; *Monodelphis* [Wible, 2003: fig. 6]; *Philander* [Wible et al., 2021]), which Forasiepi et al. (2019) referred to as rostral and caudal hypoglossal foramina and which transmit branches of the hypoglossal nerve and accompanying arteries and veins (state 0). Marshall and Muizon (1995: fig. 19) identified three hypoglossal foramina (but called them "condyloid foramina") in a specimen of †*Pucadelphys* (YPFB Pal 6110), but our examination of YPFB Pal 6110 suggests that only the medial two foramina would have transmitted branches of the hypoglossal nerve in life; the lateralmost of the three foramina appears to be a venous foramen for the condyloid canal, and we refer to it as a condyloid foramen here (see also Forasiepi et al., 2019: 45–47). The presence of one or more condyloid foramina lateral to the hypoglossal foramen or foramina and the paroccipital process is common in metatherians (e.g., *Marmosa* [fig. 9A]; *Petaurus* [fig. 9C]; *Didelphis* [Wible, 1990: fig. 1]; *Monodelphis* [Wible, 2003: 171]). Based on the specimens examined for this study, †*Pucadelphys* appears to consistently exhibit two hypoglossal foramina, and so has been scored as state 0. Three hypoglossal foramina are occasionally present in *Phascolarctos* (e.g., the left side of AM M6805), but we have not scored such rare variants. However, both *Tarsipes* and *Notoryctes* consistently have only a single hypoglossal foramen opening on the extracranial surface (state 1; contra Sánchez-Villagra and Forasiepi [2017: 18]). *Thylacinus* is polymorphic ("0+1") for this character.

Our observations conflict with those of Horovitz and Sánchez-Villagra (2003: char. 205), who scored *Caenolestes*, *Cercartetus*, *Dasyuroides*,
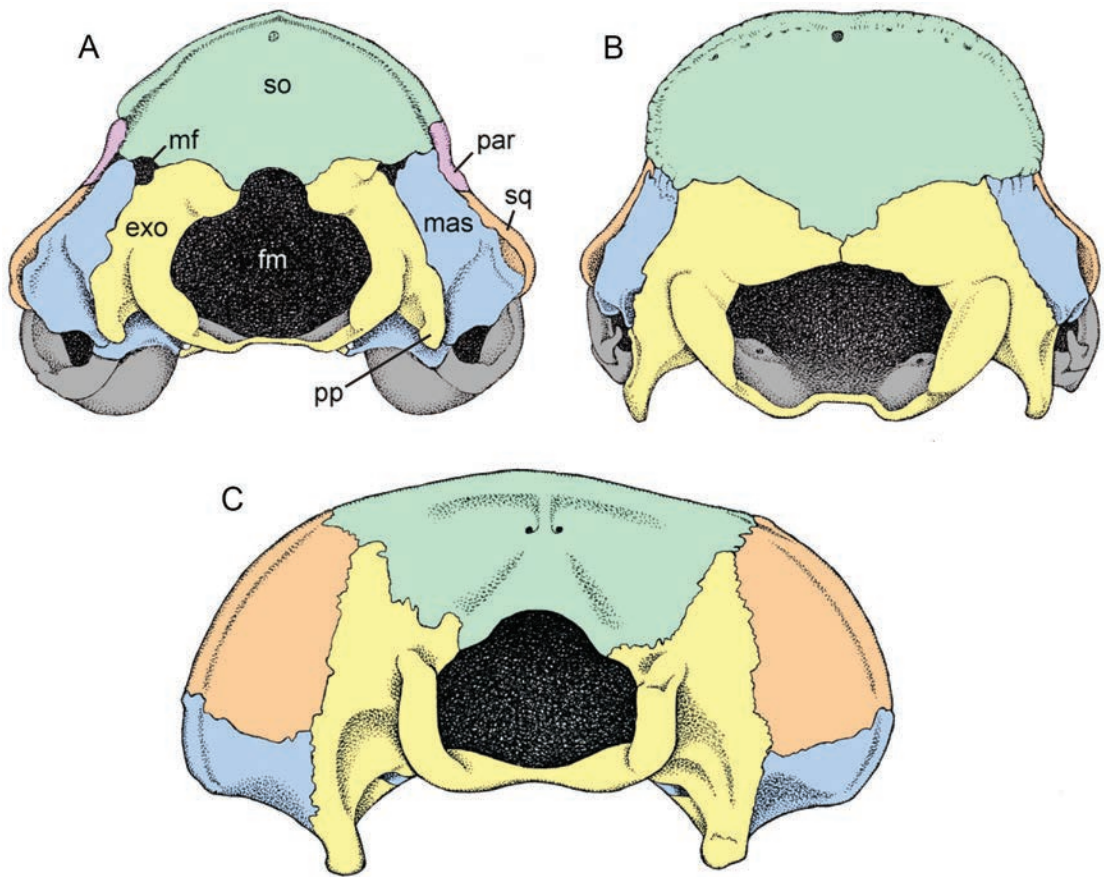
FIG. 12. Occipital views of *Lestodelphys halli* (**A,** UWZM 22422), *Metachirus nudicaudatus* (**B,** AMNH 267009), and *Trichosurus vulpecula* (**C,** AMNH 65557). Alternative states of characters 32, 90, 91, 93, and 95 (see main text for descriptions of these characters and character states) are illustrated as follows: *Lestodelphys*: 32(0), 90(0), 91(1), 93(1), 95(0); *Metachirus*: 32(1[but note that the modal condition for *M. nudicaudatus* is 0]), 90(0), 91(0), 93(2), 95(1); *Trichosurus vulpecula*: 32(-), 90(1), 91(0), 93(2), 95(0). Abbreviations: **exo,** exoccipital (yellow, coossified with basioccipital); **fm,** foramen magnum; **mas,** mastoid exposure of pars canalicularis of petrosal (blue, coossified with pars cochlearis); **mf,** mastoid fenestra; **par,** parietal (purple); **pp,** paroccipital process (of exoccipital); **so,** supraoccipital; **sq,** squamosal (orange). Specimens are not drawn to the same scale.

Echymipera, and *Vombatus* as having only a single hypoglossal foramen, and *Didelphis* and *Thylogale* as polymorphic. Based on the specimens examined for this study, all these taxa consistently have two hypoglossal foramina opening on the extracranial surface.

Character 93. *Paroccipital process of exoccipital absent (0); or small and broadly adnate to the petrosal (1); or a large erect process usually directed ventrally (2).* There is some debate in the mammalian literature regarding the use of the term "paroccipital process." Rougier et al. (1998: char. 131; following Wible and Hopson, 1993) and several subsequent works (e.g., Wible and Gaudin, 2004; Wible et al., 2004, 2009; Giannini et al., 2006; Wible, 2008; Wible and Spaulding, 2013) have applied this term to a process of the petrosal from which the sternocleidomastoid muscle originates, a structure that we (and most other morphologists) refer to as the mastoid process. Instead, we follow traditional usage (e.g., Coues, 1872; Muizon et al., 2015) by employing

paroccipital process for the bony site of attachment of the posterior belly of the digastric on the exoccipital; by contrast, Wible and coworkers have referred to this process as the "paracondylar process" (following Evans, 1993).

Descriptions of character states and an account of their taxonomic distribution among Recent didelphids were provided by Voss and Jansa (2003: char. 48). In most didelphids (e.g., *Marmosa* [fig. 9A], *Lestodelphys* [fig. 12A]) the paroccipital process is small and adnate to the petrosal, but in others (e.g., *Metachirus* [fig. 12B]) this process is much larger, erect, and directed ventrally. Among other metatherians, a paroccipital process appears to be entirely absent (state 0) in †*Herpetotherium* (Gabbert, 1998: 4), *Dromiciops* (fig. 43), *Notoryctes* (fig. 36), *Tarsipes*, and *Acrobates*. This process is also absent in *Microperoryctes* (which we likewise scored as state 0), but *Microperoryctes* has a sesamoid attached to the region of the exoccipital where the paroccipital process occurs in other peramelemorphians (see also Voss and Jansa, 2009: 45). The paroccipital process is absent or indistinct in some specimens of †*Pucadelphys* (e.g., YPFB Pal 6105), and was said to be absent by Marshall and Muizon (1995); however, a small but distinct process is present in other specimens (e.g., MHNC 8376, MHNC 8379, MHNC 8381), so we scored †*Pucadelphys* as polymorphic ("0+1"). *Distoechurus* is also polymorphic, with the specimen illustrated here (AMNH 227121 [fig. 48]) lacking a distinct process.

The paroccipital process is large and erect in †*Thylophorops*, †*Galadi* (Travouillon et al., 2010: fig. 7B), *Thylacinus* (Murray and Megirian, 2006a: appendix 1, fig. 1), †*Badjcinus* (Muirhead and Wroe, 1998: fig. 3A), †*Nimbacinus* (Wroe and Musser, 2001: figs. 1b, 7), †*Barinya*, and many diprotodontians. The last includes pseudocheirids, Recent macropodids (e.g., *Macropus* [Wells and Tedford, 1995: fig. 9]), *Vombatus* (but not *Lasiorhinus*), diprotodontids (e.g., †*Nimbadon* [Black and Hand, 2010: fig. 6]), wynyardiids, and most phalangerids (e.g., *Trichosurus* [fig. 12C]). We scored *Macrotis* as state 2 based on its large and erect paroccipital process, even though this process remains in contact with the petrosal due to the proportionally enormous size of the rostral tympanic process. Most remaining taxa that we examined have small paroccipital processes (state 1), such as *Phascogale* (fig. 9B), *Petaurus* (fig. 9C), and †*Sparassocynus* (Beck and Taglioretti, 2020).

We observed additional variation in the morphology of this region that we did not code for phylogenetic analysis but that we discuss here for completeness (see also char. 94). In *Echymipera*, *Peroryctes*, and *Perameles* the paroccipital process is capped with a sesamoid that is suturally distinct in juveniles and subadults but is often partially or completely fused with the paroccipital process—and hence unrecognizable as a discrete structure—in adults (Voss and Jansa, 2009: 45). As already noted, a digastric sesamoid is also present in *Microperoryctes*, but there is no distinct paroccipital process. There does not, however, appear to be a sesamoid capping the paroccipital process in *Isoodon*. In *Macrotis*, the paroccipital process and mastoid process are in contact ventrally, enclosing a distinct fenestra or foramen (we cannot tell whether this orifice transmits any soft-tissue structure; fig. 38). The ventral surface of the paroccipital process is distinctly concave in *Cercartetus*. In *Phascolarctos* a long, vertically directed notch or groove is present in the base of paroccipital process just medial to the medialmost part of the pars canalicularis of the petrosal; although we are uncertain as to the functional significance of this feature, it may be connected with the unusual hyo-laryngeal morphology of koalas (Aplin, 1990; Louys et al., 2009).

Character 94. *Paroccipital process of exoccipital not greatly pneumatized (0); or greatly pneumatized, enclosing a large sinus (1).* In most metatherians, the paroccipital process is not greatly pneumatized (state 0), but in *Dasycercus*, *Dasyuroides*, and *Dasykaluta* it encloses a large pneumatic sinus that is continuous with the middle ear cavity (state 1; see Jones, 1949; Ride, 1964b; Archer, 1976b). This character was scored as inapplicable ("-") for all taxa lacking a distinct paroccipital process.

Character 95. *Dorsal margin of adult foramen magnum formed by exoccipitals and supraoccipital (0); or by exoccipitals only (1).* Descriptions of character states and an account of their taxonomic distribution among Recent didelphids were provided by Voss and Jansa (2003: char. 49), who reported that the supraoccipital is excluded from the dorsal margin of the foramen magnum (state 1) in *Didelphis*, *Lutreolina*, *Metachirus* (fig. 12B), and *Philander*. By contrast, the dorsal margin of the foramen magnum is formed by both the supraoccipital and exoccipitals (state 0) in other Recent didelphids (e.g., *Lestodelphys* [fig. 12A]) and in most other metatherians (e.g., *Trichosurus* [fig. 12C]; see Sánchez-Villagra and Wible, 2002: char. 3). Although the supraoccipital is excluded from the foramen magnum in a few older individuals of *Isoodon* (e.g., AMNH 108890), the modal condition for this taxon is state 0. However, the supraoccipital does not contribute to the dorsal margin of the foramen magnum in †*Thylophorops*, *Dasyurus*, *Sarcophilus*, *Thylacinus*, or †*Barinya*, all of which have been scored as state 1. *Notamacropus* is polymorphic ("0+1") for this character. In general, our observations match those of Sánchez-Villagra and Wible (2002: char. 3), except that we score *Phascolarctos* as state 0 here.

As noted by Abdala et al. (2001: 195), Flores et al. (2003: 4), and Giannini et al. (2004: 6), the supraoccipital contributes to the dorsal rim of the foramen magnum in juveniles of *Didelphis* and *Lutreolina* but is excluded from the foramen magnum in subadults and adults due to medial growth of the exoccipitals, and the same may apply more generally within Metatheria. Due to the potentially confounding effect of such ontogenetic variation, we scored this character based on subadult and adult specimens only. However, the occipital sutures were fused in all available specimens of some taxa, which we scored as unknown ("?") because the osseous composition of the dorsal rim of the foramen magnum could not be determined.

Prideaux and Warburton (2010: char. 11) noted that the foramen magnum is markedly larger in some macropodids (e.g., *Dendrolagus*) than others; although we concur with this observation, variation in foramen magnum size was not amenable to partitioning into discrete states in the context of the taxonomically broader sample of metatherians used here.

Mandible

The mandible is a much simpler structure than the syncranium and provides correspondingly fewer phylogenetic characters. Most mandibular characters are presumably related, directly or indirectly, to the key mechanical role of the dentary as a supporting platform for the lower dentition and as the site of insertion for masticatory muscles, but a few (e.g., the size and position of mental foramina) likely reflect the development and distribution of tactile organs (vibrissae) on the mandibular integument. Terminology for metatherian mandibular traits is generally not problematic.

Character 96. *Mandible large and well developed, with distinct coronoid and angular processes (0); or much reduced and splintlike, lacking coronoid and angular processes (1).* In most metatherians, the mandible is a robust bone, with prominent coronoid and angular processes (state 0); this morphology is seen even in *Myrmecobius*, despite its weakly developed dentition (fig. 41). However, the mandible of *Tarsipes* (fig. 49) is reduced to little more than a splint of bone that lacks distinct coronoid or angular processes (state 1), an obviously autapomorphic condition.

Character 97. *Mandibular symphysis unfused (0); or fused (1).* Most metatherians have an unfused mandibular (or mental) symphysis (state 0), such that the two hemimandibles are capable of some degree of independent movement. By contrast, the symphysis is completely fused, or "synostosed" sensu Scapino (1981; see also Prideaux, 2004: 214)—with the hemimandibles consequently immobile relative to one another and no symphyseal suture identifiable between them—in adult specimens of Recent vombatids (but not †*Warendja*; Hope and Wilkinson, 1982) and

Phascolarctos (see Archer, 1984c; Springer et al., 1997: char. 48). Because the symphysis is unfused in juveniles of these taxa, we scored this character based only on fully adult specimens. Although we also observed symphyseal fusion in some adult specimens of †*Nimbadon*, fusion in this taxon occurs only after the permanent dentition is fully erupted and has undergone some wear (in "Stage VI" adults sensu Black et al., 2010), so we scored †*Nimbadon* as polymorphic ("0+1") for this character. Our definition of symphyseal fusion corresponds to "state 4" of Scott et al. (2012: 662), who described it as "completely ossified"; however, those authors recorded the symphysis of *Sarcophilus* as completely ossified, whereas we scored *Sarcophilus* as state 0 based on the modal morphology (absence of complete fusion) in our examined material.

Character 98. *Mandible usually with one mental foramen (0); or usually with two or more mental foramina (1).* We distinguish true mental foramina—which transmit branches of the inferior alveolar nerve and accompanying vessels (Wible, 2003: 178), and which are relatively large and usually consistent in number and position among conspecific specimens—from nutrient foramina (which are often also present on the lateral surface of the mandible but are considerably smaller and highly variable in number and position, even between left and right sides of the same individual). When only a single mental foramen is present, it is invariably a large opening in the position of the anterior foramen of individuals or taxa with two or more foramina.

Descriptions of character states and an account of their taxonomic distribution among Recent didelphids were provided by Voss and Jansa (2003: char. 50; 2009: char. 85). Although Voss and Jansa (2009: char. 85) subsequently included an additional state to account for the presence of three mental foramina, which they observed in specimens of *Perameles gunnii*, we observed considerable polymorphism in our sample of *P. gunnii* (with roughly equal numbers of individuals with two and three mental foramina). In other metatherians we examined that

sometimes have three mental foramina, we always observed multiple individuals with two foramina when large sample sizes were available (e.g., *Chaeropus*, *Isoodon*, *Peroryctes*, *Myrmecobius*, *Dasyurus*, *Murexia*, *Phascolosorex*, and *Sarcophilus*). We therefore decided not to include an additional state for presence of three mental foramina, but simply distinguish between presence of a single foramen (state 0) and presence of two or more foramina (state 1).

We confirmed Voss and Jansa's (2003, 2009) observations regarding the number of mental foramina in Recent didelphids, except that one and two mental foramina appear to be equally common in *Philander*, which we scored as polymorphic ("0+1"). Two or more mental foramina are usually present in other metatherians, including †*Pucadelphys* (see Marshall and Muizon, 1995: fig. 8A), †*Mayulestes* (see Muizon, 1998: fig. 3A), †*Allqokirus* (see Muizon et al., 2018: fig. 28A), and †*Herpetotherium*. However, only a single mental foramen is typically present in petaurids (e.g., *Petaurus* [fig. 50]), acrobatids (e.g., *Distoechurus* [fig. 48]), *Tarsipes* (fig. 49), *Cercartetus*, some phalangerids (*Strigocuscus*, *Wyulda*, †*Onirocuscus*), most macropodiforms (†*Balbaroo* and †*Ganawamaya* are noteworthy exceptions; Kear et al., 2007: fig. 4.3), †*Ngapakaldia* (see Black, 2010), vombatids (e.g., *Vombatus* [fig. 45]), wynyardiids, †*Thylacoleo*, *Antechinomys*, *Planigale*, †*Yalkaparidon* (see Beck et al., 2014), and *Dromiciops* (fig. 43). We observed polymorphism in this feature in *Notoryctes*, *Ningaui*, *Bettongia*, *Spilocuscus*, and *Petauroides*.

Character 99. *Masseteric fossa imperforate (0); or perforated by a distinct masseteric foramen (1); or by a masseteric canal (2); or by a large unossified vacuity (3).* The masseteric fossa is a prominent concavity for the insertion of the deep masseter on the posterolateral aspect of the mandible (Turnbull, 1970). This fossa is imperforate (with the occasional exception of tiny nutrient foramina) in †*Pucadelphys* (see Marshall and Muizon, 1995: fig. 8A), †*Allqokirus* (see Muizon et al., 2018: fig. 28A), †*Herpetotherium* (see Horovitz et al., 2008: plate 2A), didelphids,

microbiotheriids, peramelemorphians, and all dasyuromorphians except *Myrmecobius* (state 0). Among diprotodontians, the masseteric fossa is consistently imperforate in most phalangerids, the burramyid *Cercartetus*, and the ilariid †*Ilaria*. In most other examined nonmacropodiform diprotodontians, the fossa is penetrated by a distinct masseteric foramen (state 1). However, *Dactylopsila*, *Dactylonax*, *Pseudochirops archeri*, *Phalanger*, *Trichosurus*, and †*Nimbadon* (Black and Hand, 2010: 41; Murray et al., 2000: 81) are all polymorphic for the presence or absence of the masseteric foramen ("0+1"). Abbie (1939) showed that, at least in diprotodontians, this foramen transmits a branch of the inferior alveolar artery ("inferior dental artery" of Abbie, 1939) and always communicates internally with the lumen of the mandibular foramen from the opposite (medial) side of the dentary (as illustrated for *Vombatus* by Owen, 1866: fig. 220). Voss and Jansa (2009: 46) noted that one or more small foramina within the masseteric fossa of *Caenolestes* also appear to communicate internally with the mandibular foramen. We observed a similar foramen or foramina within the masseteric fossae of *Lestoros*, †*Stilotherium*, *Myrmecobius*, *Notoryctes*, and †*Yalkaparidon*, all of which have been scored as state 1. *Rhyncholestes* and †*Palaeothentes* are polymorphic ("0+1") for the presence of this foramen or foramina.

All examined macropodiforms uniquely exhibit a distinctly different morphology, in which the masseteric fossa is penetrated by a masseteric canal sensu Abbie (1939; state 2; figs. 52–54). In contrast with the masseteric foramen described above, the macropodiform masseteric canal is much larger, is bounded laterally by the masseteric crest, provides a clear view into the mandibular canal (= "inferior dental canal" of Abbie, 1939), and is the site of insertion for a slip of the deep masseter (Abbie, 1939; Warburton, 2009). Because we could not consistently recognize Abbie's (1939) distinction between a masseteric canal that is only partially confluent with the mandibular canal (supposedly diagnostic of macropodids; but see comments by Woodburne,

1984a: 1071; Archer and Flannery, 1985: 1344; Cooke, 1999: 249; Kear et al., 2007: 1164) and a masseteric canal that is fully confluent with the mandibular canal (apparently seen in *Hypsiprymnodon moschatus*, potoroids, and most fossil macropodiforms; Woods, 1960; Flannery et al., 1983, 1984; Case, 1984; Archer and Flannery, 1985; Kear et al., 2007: char. 15), we did not code these as separate conditions. Instead, both are combined among the range of morphologies that we assign to state 2. Uniquely, the masseteric fossa of *Tarsipes* is pierced by a large, unossified vacuity or fenestra (fig. 49), the homology of which is unclear; we therefore scored this as an additional, autapomorphic condition (state 3). Abbie (1939) argued persuasively that states 0, 1, and 2 form an ordered transformation series (0 ↔ 1 ↔ 2), but *Tarsipes* (state 3) is difficult to accommodate in this sequence, so we treated this character as unordered in all of our analyses.

Character 100. *Retromolar fossa imperforate (0); or pierced by large retrodental canal (1).* The retromolar fossa—a shallow concavity between the last mandibular molar and the base of the coronoid process—is essentially imperforate in most metatherians (state 0), although tiny nutrient foramina are often present in this region. However, a distinct foramen is consistently present behind m4 in *Caenolestes*, *Lestoros*, †*Palaeothentes*, and †*Stilotherium* (state 1). This foramen is the opening for a vertical canal that, in *Caenolestes* at least, connects to the mandibular canal (Beck, 2017a: fig. 13c, 405). We refer to this vertical canal as the retrodental canal, following Hoffstetter and Villarroel. (1974: 1950) and subsequent authors (e.g., Sánchez-Villagra et al., 2000; Voss and Jansa, 2009; Goin and Abello, 2013). A similar foramen is also seen in some specimens of *Rhyncholestes*, which has been scored as polymorphic ("0+1") contra Voss and Jansa (2009), who scored *Rhyncholestes* as lacking a foramen for the retrodental canal.

Character 101. *Condylar process variously formed but articular surface more or less oblong and dorsoventrally flattened (0); or transversely elongate and medially extensive (1).* The condy-

lar process of the mandible exhibits modest taxonomic variation within Metatheria, but in most taxa it can be described as mediolaterally directed and irregularly oblong, with a flattened dorsal surface; in dorsal view, the condylar process extends much farther laterally than it does medially, relative to the coronoid process. By contrast, the condyle is transversely elongate, such that it extends as far or farther medial to the coronoid process as it does lateral to this process in the Recent vombatids *Vombatus* and *Lasiorhinus* (but not †*Warendja*; Hope and Wilkinson, 1982), †*Neohelos* (Murray et al., 2000a: fig. 43B), †*Nimbadon* (Black and Hand, 2010: fig. 7), and †*Muramura* (Pledge, 2003: fig. 19.4).

The only known mandibular material of †*Silvabestius* is from a juvenile (QM F30504), in which the condylar process is neither transversely elongate nor medially extensive (Black and Archer, 1997a: fig. 3). However, in their ontogenetic study of †*Nimbadon*, Black et al. (2010: 997) noted that the condylar process "becomes longer, wider, more laterally expansive, and more heavily ossified" with increasing age. Allowing for the possibility that similar ontogenetic changes may also have occurred in †*Silvabestius*, we scored this taxon as unknown ("?") pending description of adult mandibular specimens.

Although we have scored *Lagostrophus* as state 0 here, the morphology of its condylar process is distinctive: a nonarticular outgrowth (medial to the coronoid process) projects anteromedially, such that the medial and lateral parts of the process form an obtuse angle in dorsal view (see also comments by Warburton, 2009).

Character 102. *Angular process strongly medially inflected (0); or weakly or not inflected (1).* The morphology of the metatherian angular process has been reviewed by Sánchez-Villagra and Smith (1997), Sánchez-Villagra and Wible (2002: char. 4), and Voss and Jansa (2003: char. 51; 2009: 46). Most metatherians, including †*Pucadelphys* (Marshall and Muizon, 1995), †*Allqokirus* (Muizon et al., 2018), and †*Herpe-*

totherium (Horovitz et al., 2008), have a strongly medially inflected mandibular angle (state 0). However, we agree with previous authors that *Caluromys*, *Caluromysiops*, *Myrmecobius*, *Phascolarctos*, *Dactylopsila*, and *Dactylonax* all possess a weakly inflected or uninflected angle (state 1). We coded this character as inapplicable ("-") for *Tarsipes*, which does not possess a distinct angular process.

DENTAL CHARACTERS

Didelphids and microbiotheriids have a total of 50 teeth, as did many nonmarsupial metatherians (Kielan-Jaworowska et al., 2004). We refer to this unreduced marsupial complement as comprising five incisors (I1–5), one canine (C1), three premolars (P1–3), and four molars (M1–4) in the upper dentition, and four incisors (i1–4), one canine (c1), three premolars (p1–3), and four molars (m1–4) in the lower dentition, as in the majority of the metatherian literature. However, a number of alternative schemes have been proposed based on different hypotheses of dental homology (table 12). In particular, recent attempts to homologize dental loci across Mammaliaformes have led to novel hypotheses of homology between the teeth of metatherians and those of other mammals (e.g., Averianov et al., 2010; O'Leary et al., 2013).

Most other marsupial taxa scored for this study have fewer than 50 teeth. In some taxa the suppressed dental loci can be identified with confidence, but dental homologies in other taxa are obscure for lack of relevant evidence. As described by multiple authors (e.g., Flower, 1867; Luckett, 1993b; Luo et al., 2004; van Nievelt and Smith, 2005a; 2005b; Forasiepi and Sánchez-Villagra, 2014), dental replacement in marsupials is known to occur only at the posteriormost premolar locus in both the upper and the lower jaw, where a single first-generation tooth (dP3/dp3) is usually replaced by a permanent successor (P3/p3). Further discussions of dental homologies are provided in the relevant character descriptions below.

TABLE 12

Alternative Hypotheses of Marsupial Tooth Homologies

(modified from Voss and Jansa, 2009: table 7)[a]

This study[b]	Thomas (1887)[c]	Archer (1984)[d]	Hershkovitz (1992b)[e]	Luckett (1993b)[f]	Goin (1997)[g]	Averianov et al. (2010)[h]	O'Leary et al. (2013)[h]
P1	P1	P1	P1	dP1	P1	P2	P1
P2	P3	P2	P2	dP2	P2	P3	P2
dP3	dP4	M1	M1	dP3	M0	dP4	dP4
P3	P4	P3	P3	P3	P3	P4	P4
M1	M1	M2	M2	M1	M1	dP5	dP5
M2	M2	M3	M3	M2	M2	M1	M1
M3	M3	M4	M4	M3	M3	M2	M2
M4	M4	M5	M5	M4	M4	M3	M3
i1	i1	i1	i2	i1	i2	i1	i1
i2	i2	i2	i3	i2	i3	i2	i2
i3	i3	i3	i4	i3	i4	i3	i3
i4	—	—	i5	i4	i5	i4	i4
p1	p1	p1	p1	dp1	p1	p2	p1
p2	p3	p2	p2	dp2	p2	p3	p2
dp3	dp4	m1	m1	dp3	m0	dp4	dp4
p3	p4	p3	p3	p3	p3	p4	p4
m1	m1	m2	m2	m1	m1	dp5	dp5
m2	m2	m3	m3	m2	m2	m1	m1
m3	m3	m4	m4	m3	m3	m2	m2
m4	m4	m5	m5	m4	m4	m3	m3

[a] All of these schemes refer to the upper incisors as I1–5. See van Nievelt (2002) for a more detailed discussion of these and other hypotheses of dental homology.

[b] The system adopted here was used by Tate (1933) and is currently followed by most metatherian researchers (e.g., Marshall and Muizon, 1995; Rougier et al., 1998; Wroe et al., 2000; Voss and Jansa, 2003). Note that there is no substantive inconsistency in the literature regarding the identification of I1–I5, C1, or c1. In order to focus these comparisons on real differences in assumptions about dental homologies, semantically equivalent notations used by authors (e.g., I_2 for i2, pm³ for P3) have been modified as necessary to conform to our usage.

[c] Also Thomas (1888), who assumed that marsupials primitively had four premolars, of which the second was lost.

[d] Based on the assumption that the replaced teeth are M1/m1 (Archer, 1978), this was the nomenclature followed throughout most of the marsupial literature for the next 10 years (e.g., Marshall, 1987; Reig et al., 1987).

[e] Based on the assumption that marsupials primitively had five lower incisors, of which the first was lost (Hershkovitz, 1982). Note that whereas Hershkovitz (1992b) accepted Archer's (1984) system of postcanine homologies, Hershkovitz (1997, 1999) did not.

[f] The only difference between Luckett's (1993) notation and ours concerns his designation of the anterior premolars as first-generation (formerly deciduous) teeth. Although we do not dispute his interpretation of the developmental data at hand, we think it confusing to use deciduous notation for unreplaced teeth.

[g] Goin's (1997) system was based on Hershkovitz's (1982) theory that the ancestral first lower incisor of marsupials is missing in living taxa, and on Archer's (1978) conjecture that replaced teeth in the upper and lower dentition are molars; by designating these as M0/m0, Goin intended to preserve traditional notation for the permanent molariform teeth.

[h] Based on the assumption that the ancestral postcanine dental formula for Theria comprises four or five premolars and three molars, and that the marsupial formula arose by loss of one premolar—either the ancestral first premolar as concluded by Averianov et al. (2010: 323) or the ancestral third as argued by O'Leary et al. (2013)—and suppression of dental replacement at the fifth premolar locus.

Upper Incisors

Five upper incisors are present in didelphids, microbiotheriids, and many nonmarsupial metatherians, but other metatherians have four or fewer upper incisors. In order to meaningfully score taxonomic variation in tooth number for phylogenetic analysis, it is necessary to make assumptions about the homologies of these teeth. Although a seemingly agnostic alternative is to code the total number of upper incisors without reference to specific loci (e.g., as by Kirsch and Archer, 1982: char. 1; Springer et al., 1997: char. 1; Rougier et al., 1998: char. 8; Wroe et al., 2000: char. 1; Horovitz and Sánchez-Villagra, 2003: char. 150), such coding may be problematic because it implicitly assumes that homologous teeth were gained or lost to account for similarities in number. If, for example, there is compelling evidence that one taxon with three upper incisors lacks I1 and I2, whereas another with the same total lacks I4 and I5, then it is obviously inappropriate to score both with the same state. Where possible, we prefer to code the presence or absence of specific dental loci rather than simply counting teeth, on the methodological principle that it is better to make explicit rather than implicit assumptions.

Following Thomas (1887a), and in the absence of information to the contrary, we assume that upper teeth are lost from (or added to) the posterior (distal) end of the incisor row (see also Ziegler, 1971; Wible, 2008: 324–326; 2011: 151).[9] Although there appears to be no developmental data to support this notion, we observed that I5

is small and occupies a separate alveolus from I2–I4 (the alveoli of which are usually at least partially confluent) in some taxa with five upper incisors (e.g., *Glironia* [Voss and Jansa, 2009: fig. 37], *Isoodon*, *Peroryctes*, and *Perameles* [fig. 39]) and that the loss of such a tooth would simply enlarge an already existing diastema between the incisors and C1 rather than opening a fresh gap in the dental arcade. Ziegler (1971: 233) also reported the occasional, unilateral presence of a supernumerary upper incisor in the peramelemorphian *Echymipera* (which normally has only four upper incisors) in the same position that I5 occupies in peramelemorphians that retain this tooth. Conversely, it would seem less difficult to add teeth at one end of the incisor row than to insert them between occupied loci. Because the anteriormost upper incisor is a conspicuously differentiated (styliform or chisellike) tooth in most metatherians (see char. 104), this locus does not appear to be a plausible site for dental additions or subtractions.

Character 103. *Five upper incisors present (0); or I5 absent (1); or I4 and I5 absent (2); or I2–I5 absent (3).* The fifth upper incisor (I5) is present (state 0) in †*Mayulestes*, †*Allqokirus*, †*Pucadelphys*, †*Herpetotherium*, didelphids (e.g., *Marmosa* [fig. 1], *Thylamys* [fig. 7]), most peramelemorphians (figs. 37–39), *Dromiciops* (fig. 43), and †*Microbiotherium*. A single upper incisor (assumed to be I5 for the reasons discussed above) has been lost (state 1) in caenolestids (e.g., *Caenolestes* [fig. 35]), *Rhynchomeles*, *Echymipera*, and dasyuromorphians (figs. 40–42). Of the other taxa included in this analysis, †*Acdestis* (Goin et al., 2003), †*Palaeothentes* (Marshall, 1980: 69; Forasiepi et al., 2014b), *Notoryctes* (fig. 36), †*Yalkaparidon* (Archer et al., 1988; Beck et al., 2014), and most diprotodontians have three upper incisors (I4 and I5 assumed to be missing teeth; state 2). Recent vombatids (e.g., *Vombatus* [fig. 45]) have only a single upper incisor (state 3); the number of incisors in the fossil vombatid †*Warendja* is unknown based on available material. Following the argument outlined

---

[9] Information to the contrary does exist for at least one metatherian clade not represented in this study. Specifically, the second upper incisor of the sparassodont †*Paraborhyaena boliviana* is distinctly smaller than I1, I3, and I4 (based on the size of the alveoli in the only known skull, MNHN SAL 51), and it is also "staggered" (shifted anteriorly) such that the alveoli of I1 and I3 are almost in contact (Hoffstetter and Petter, 1983: fig. 1). An apparently similar upper incisor array, with staggering of I2, also occurs in another sparassodont †*Callistoe vincei* (Babot et al., 2002: 622, fig. 2c). Plausibly, sparassodonts with three incisors might therefore retain I1, I3, and I4, having lost I2 from the middle of the incisor row. Forasiepi (2009: char. 108), however, argued that three-incisored sparassodonts had lost I1 and I5.

above (that upper incisors are lost sequentially from posterior to anterior), we treated this character as ordered (additive) in all the analyses reported below.

Character 104. *First upper incisor styliform or chisellike, conspicuously unlike I2 and I3 (0); or mesiodistally expanded and flat crowned, resembling I2 and I3 (1).* In most metatherians, I1 differs from the more posterior incisors (if present) in being styliform or chisellike, somewhat hypsodont, and often slightly procumbent (state 0; see Voss and Jansa, 2009: 46, fig. 18). Although *Vombatus* (fig. 45) and *Lasiorhinus* retain only a single upper incisor, this tooth is large and chisellike, so we scored both taxa as state 0. In all Recent peramelemorphians, by contrast, I1 is mesiodistally expanded and flat crowned, such that I1–3 form a single morphologically continuous series (state 1; figs. 37–39). In *Thylacinus*, I1–3 also form a morphologically continuous series (fig. 40), so we also scored this taxon as state 1. We scored *Tarsipes* as inapplicable ("-") for this character as its upper incisors are greatly reduced (fig. 49).

A number of previous studies have distinguished between hypsodonty and nonhypsodonty of the first upper incisor (e.g., Takahashi, 1974; Archer, 1976c: char. 2; Reig et al., 1987; Wroe, 1999; Wroe et al., 2000: char. 3; Wroe and Musser, 2001: char. 3), and between "spatulate" and "peglike" upper incisors (e.g., Archer, 1976c: char. 3; Wroe et al., 2000: char. 2; Wroe and Musser, 2001: char. 2). However, we were unable to consistently score either of these characters for our taxon sample and have not included them in the current study.

Character 105. *Second and third upper incisors with enamel present (0); or entirely lacking enamel (1).* In all but one of the metatherians we examined that retain I2 and I3, these teeth are enamelled (state 0). By contrast, †*Yalkaparidon* uniquely lacks enamel on its second and third upper incisors (Beck, 2009; Beck et al., 2014), an obvious autapomorphy. This character was scored as inapplicable ("-") for *Vombatus* and *Lasiorhinus*, both of which lack I2 and I3.

Character 106. *Occlusal surface of I3 variously formed, but without a well-developed anterolabial crest separated from the main crest by a mesiodistally elongate groove or basin (0); or occlusal surface of I3 bifid, with a well-developed anterolabial crest separated from the main crest by a mesiodistally elongate groove or basin (1).* The occlusal morphology of newly erupted, unworn second and third upper incisors varies considerably within Marsupialia. Of particular note is the complex morphology seen in unworn I2 and I3 of many diprotodontians (e.g., *Cercartetus* [e.g., AMNH 222711], *Dactylopsila* [e.g., AMNH 101988, 192155, 157140], *Dactylonax* [e.g., AMNH 221611], *Ailurops* [e.g., AMNH 108799], and *Pseudochirops cupreus* [e.g., AMNH 191142, 191155]). Although this variation is striking, most of the variants we observed are difficult to code as discrete character states. The sole exception is the presence or absence of a distinct anterolabial crest on the occlusal surface of I3. This crest is present (state 1) in several macropodids, where it is separated from the main (posterolingual) crest by a distinct, mesiodistally elongate and posteriorly open groove or (as in *Dendrolagus*) a posteriorly enclosed basin (Prideaux, 2004: 237–239, figs. 16, 17; Prideaux and Warburton, 2010: char. 15). The major posterolingual crest appears to be homologous with the single blade present on I3 of most nondiprotodontian metatherians, whereas the anterolabial crest appears to be a neomorph (Prideaux and Warburton, 2010). The groove can be lost through wear, so we scored this character based on lightly worn specimens (preferably juveniles) where possible. Our observations are in general agreement with those of Prideaux and Warburton (2010), but we scored *Lagostrophus* as corresponding to state 1 because a distinct anterolabial crest appears to be present in this taxon (e.g., on WAM M6791; see also Prideaux, 2004: figs. 16B, 17A). We scored *Tarsipes* as inapplicable ("-") for this character as its upper incisors are greatly reduced (fig. 49).

Character 107. *Fourth upper incisor (I4) similar in size to I1–I3 (0); or I4 markedly larger*

than I1–I3 (1). In most metatherians, I4 (if present) is similar in size to I1–I3. However, in *Thylacinus* I4 is markedly larger than more anterior teeth (fig. 40). This character was scored as inapplicable ("-") for all taxa lacking I4, and as unknown ("?") for all taxa in which I4 is not preserved in available specimens. Wroe and Musser (2001: 499) stated that the alveolus for I4 in †*Nimbacinus* is the largest of the upper incisor arcade, as it is in *Thylacinus*. However, our examination of QM F36357, the well-preserved skull of †*N. dicksoni* described by Wroe and Musser (2001), suggests otherwise: although the left I4 alveolus is, indeed, markedly larger than the adjacent I3 alveolus, this is due to damage to the anterior margin of the former; the right I4 alveolus, which appears to be intact, is not noticeably larger than that for I3 (see Wroe and Musser, 2001: fig. 1B). Because no specimen of †*Nimbacinus* preserves the crown of I4 itself, we prefer to score this taxon as unknown ("?"). In effect, state 1 is an autapomorphy of *Thylacinus* in the current analysis.

Upper Canine

The upper canine (C1), which in most therian mammals is a single-rooted unicuspid tooth that occupies the premaxillary-maxillary suture (Kielan-Jaworowska et al., 2004), is absent in some marsupials and exhibits noteworthy morphological variation in others. Remarkably, marsupial canines are sometimes bi- or tricuspid, sometimes double-rooted, and sometimes wholly contained in the maxilla, as briefly discussed by Voss and Jansa (2009: 48–49). Additionally, C1 is sexually dimorphic in shape and root number in certain clades. Few of these unusual traits have been represented in previous phylogenetic datasets.

Character 108. *Upper canine (C1) present (0); or absent (1).* The upper canine is present in most metatherians, but some diprotodontians usually lack C1, including some macropodids (e.g., *Lagostrophus* [fig. 53]), †*Nimbadon*, †*Neohelos*, and Recent vombatids (e.g., *Vombatus* [fig. 45]). Other macropodids exhibit morphologies that are intermediate between simple presence and absence of C1. In *Onychogalea*, for example, C1 is present in juveniles, subadults, and young adults, but it is lost in old adults (e.g., AMNH 197525); we scored this taxon as state 0 because C1 is present throughout most of its ontogeny. By contrast, C1 is present only in the youngest juveniles we examined of *Osphranter* (e.g., AMNH 154509), *Notamacropus* (e.g., AMNH 154504), and *Macropus* (e.g., AMNH 65017); we scored these taxa as state 1 because C1 is absent throughout most of their ontogeny. In yet other macropodids (e.g., *Thylogale*, *Wallabia*) what may be a remnant of the C1 alveolus is sometimes identifiable within the premaxillary-maxillary suture, but this cavity is not occupied by a tooth even in young juveniles; we scored such taxa as state 1. Although most specimens of †*Nimbadon* lack C1, this tooth is present in a few individuals (e.g., QM F50470 [Black and Hand, 2010]); we scored this taxon as state 1 based on the observed modal condition.

Character 109. *Upper canine (C1) single-rooted (0); or double-rooted (1).* Where present, C1 is single-rooted (state 0) in most metatherians. However, this tooth is consistently double-rooted in *Lestoros* (state 1; Martin, 2013). Osgood (1924: 171) and Travouillon et al. (2019: 15) stated that C1 is double-rooted in the peramelemorphian *Chaeropus*, whereas Thomas (1888: 250) reported that this tooth is "sometimes double-rooted" in this taxon. A shallow, vertically directed sulcus or sulcus is sometimes visible on the lateral face of the root of C1 in *Chaeropus* (Travouillon et al., 2019: figs. 3b, i, 6b), but in none of the specimens we examined did the root itself appear to bifurcate, and the C1 alveolus is apparently single in crania in which this tooth is missing (Travouillon et al., 2019: figs. 6i, j); therefore, we scored this taxon as state 0. Among fossil paucituberculatans, C1 is single-rooted in known specimens of †*Palaeothentes* (Marshall, 1980; Forasiepi et al., 2014), †*Acdestis* (Goin et al., 2003), and †*Stilotherium* (Marshall, 1980 [fig. 4]), all of which we scored as state 0. However, C1 is single-rooted in males but dou-

ble-rooted in females of *Caenolestes* (fig. 35; Bublitz, 1987: abb. 8) and *Rhyncholestes* (Osgood, 1924; Patterson and Gallardo, 1987; Voss and Jansa, 2009), so we scored these taxa as polymorphic ("0+1"). By contrast, Horovitz and Sánchez-Villagra (2003 [char. 171]), Sánchez-Villagra et al. (2007 [char. 156]), and most subsequent studies that have employed versions of their matrices (e.g., Sánchez-Villagra et al., 2007; Beck et al., 2008a; Horovitz et al., 2008, 2009; Abello and Candela, 2010) scored *Caenolestes* as having a single-rooted C1.

We acknowledge that coding sexual dimorphism as polymorphism conflates sex-specific differences with variability due to other phenomena (e.g., alleles segregating in a population, geographic variation). An alternative approach would be to explicitly recognize sexual dimorphism in canine root number (or crown morphology; see below) as a distinct state within in an ordered transformation series. Unfortunately, reliable indications of sex are seldom available for fossil taxa, so this suboptimal expedient seems preferable to scoring all fossils as missing ("?"). This character was scored as inapplicable ("-") for taxa lacking C1 (see char. 108).

Character 110. *Upper canine (C1) separated from posteriormost upper incisor by a distinct diastema (0); or diastema between C1 and upper incisor row absent (1).* In most metatherians, a conspicuous diastema separates C1 from the posteriormost upper incisor, and these teeth have clearly separate alveoli (e.g., in *Marmosa* [figs. 1, 34]; state 0). By contrast, in acrobatids (e.g., *Distoechurus* [fig. 48]), *Dactylopsila* (Aplin, 1990: plate 5.2a), *Dactylonax*, *Pseudochirops cupreus*, some phalangerids (e.g., *Phalanger* [fig. 47]), *Bettongia* (but not ?*Bettongia* †*moyesi*; Flannery and Archer, 1987b), and †*Thylacoleo* (Anderson, 1929: plate XXI), no diastema is consistently present between C1 and I3 (state 1), the alveoli of which are often confluent. *Pseudochirops archeri* and *Notoryctes* are both polymorphic ("0+1") for this character, which we scored as inapplicable ("-") for taxa lacking C1 (see char. 108).

Character 111. *Upper canine (C1) alveolus occupies premaxillary-maxillary suture (0); or C1 alveolus contained entirely in maxillary bone (1).* Descriptions of character states and an account of their taxonomic distribution among Recent didelphids were provided by Voss and Jansa (2003: char. 30; 2009: 48), who misleadingly described taxa exhibiting state 1 as lacking a premaxillary palatal process. Among didelphids, only *Caluromys* and *Caluromysiops* have the C1 alveolus entirely enclosed by the maxilla (state 1). Engelman and Croft (2014: 675) stated that the C1 alveolus is within the maxilla in †*Sparassocynus*, presumably based on the line drawing shown in figure 4 of Reig and Simpson (1972), but in several †*Sparassocynus* specimens that we examined the alveolus is in the premaxillary-maxillary suture, as it is in most Recent didelphids (Beck and Taglioretti, 2020); thus, this taxon has been scored as state 0 here.

Among other metatherians, the upper canine is typically within the premaxillary-maxillary suture (state 0), but this tooth is entirely within the maxilla in †*Pucadelphys*, microbiotheriids (e.g., *Dromiciops* [fig. 43]), *Myrmecobius* (fig. 41), dasyurids (e.g., *Pseudantechinus* [fig. 42]), †*Yalkaparidon* (Beck et al., 2014: fig. 5), and several peramelemorphians (†*Galadi*, *Macrotis*, *Echymipera*, and *Isoodon*). *Lestoros*, *Chaeropus*, *Microperoryctes*, *Perameles*, and *Rhynchomeles* are all polymorphic ("0+1") for this character. We scored taxa lacking C1 (see char. 108) as inapplicable ("-").

Character 112. *Upper canine simple, without distinct accessory cusps (0); or with distinct posterior accessory cusp only (1); or with distinct anterior and posterior accessory cusps (2); or with distinct anterior accessory cusp only (3).* As described by Voss and Jansa (2003: char. 53; 2009: 48), didelphid upper canines are either simple unicuspids (state 0), or they have only a posterior accessory cusp (state 1), or they have both anterior and posterior accessory cusps (state 2). Some previous authors (e.g., Osgood, 1924; Archer, 1976c: char. 5; 1981; Patterson and

Gallardo, 1987; Wroe et al., 2000: char. 4) have described variation in this trait using the modifier "premolariform" for canines with accessory cusps and "caniniform" for simple teeth. Most nondidelphid metatherians—including all diprotodontians that retain C1—have simple, unicuspid upper canines that exhibit only minor variation in morphology, so we scored them as state 0. However, a distinct posterior accessory cusp (state 1) occurs in several dasyurids (e.g., *Planigale*, *Pseudantechinus*, *Phascogale*, *Sminthopsis*), and an anterior accessory cusp is present (state 3) in some peramelemorphians (e.g., *Chaeropus* [fig. 37]; Travouillon et al., 2019).

The upper canine is sexually dimorphic in Recent caenolestids (Osgood, 1924: 169, 171; Bublitz, 1987; Patterson and Gallardo, 1987: 1; Voss and Jansa, 2009: 48–49). Whereas C1 is consistently unicuspid in the male caenolestids we examined, this tooth has an anterior accessory cusp (state 3) in female *Caenolestes* and *Lestoros* (but see Martin, 2013: 610, who reported nonsexually dimorphic polymorphism in the presence or absence of anterior and posterior cusps in *Lestoros*). In female *Rhyncholestes*, C1 has both anterior and posterior accessory cusps (state 2). As for canine root number (see char. 109), we scored these traits as polymorphisms, with *Caenolestes* and *Lestoros* scored as "0+3" and *Rhyncholestes* scored as "0+2" (after Voss and Jansa, 2009: char. 94).

Polymorphism in C1 crown morphology is also seen in some dasyurids. *Dasyuroides* and *Ningaui* either lack accessory cusps or exhibit a posterior accessory cusp ("0+1"), whereas *Antechinomys* has either a posterior accessory cusp or both anterior and posterior accessory cusps ("1+2"). Canine morphology appears to be particularly variable in *Micromurexia*, for which some specimens lack accessory cusps (e.g., AMNH 190909), others have a distinct anterior cusp only (e.g., AMNH 190914), some have both anterior and posterior accessory cusps (e.g., AMNH 190912), and some have only a posterior accessory cusp (e.g., AMNH 190906); we scored this apparently hypervariable taxon as "0+1+2+3."

The peramelemorphian *Rhynchomeles* is also polymorphic: specimens either lack accessory cusps or have only an anterior accessory cusp ("0+3"). Unlike the pattern of C1 variation we observed among Recent caenolestids, the polymorphic traits seen in *Rhynchomeles* and some dasyurids do not appear to be sexual dimorphic.

Although Voss and Jansa (2003) regarded state 1 as intermediate to states 0 and 2 among their terminal taxa and treated this character as an ordered transformation series, the observation of a different bicuspid condition (state 3) in some nondidelphids makes their ordering scheme problematic. We therefore treated this character as unordered in all our analyses following Voss and Jansa (2009: char. 94). This character was scored as inapplicable ("-") for taxa lacking C1 (see char. 108).

Postcanine Dentition

Character 113. *Postcanine dentition with identifiable cusps (0); or postcanine teeth are featureless spicules (1).* The postcanine teeth of most metatherians exhibit one or more well-defined and presumably functional cusps (state 0), but in *Tarsipes* the upper and lower postcanine dentition is uniquely reduced to tiny, featureless, apparently nonfunctional spicules of enamel (Parker, 1890; Bensley, 1903; Archer, 1984c; Russell and Renfree, 1989), an obvious autapomorphy (state 1). In addition, none of the postcanine teeth of *Tarsipes* can be confidently homologized with specific loci in other metatherians (Bensley, 1903; Archer, 1984c; Russell and Renfree, 1989). We therefore scored this taxon as inapplicable ("-") for characters relating to the presence or absence of particular structures (e.g., cusps and crests) in the postcanine dentition, and unknown ("?") for characters relating to the presence or absence of specific postcanine loci.

Upper Premolars

Three upper premolars, the maximum number normally seen in any metatherian (Kielan-

Jaworowska et al., 2004), are present in †*Mayulestes*, †*Allqokirus*, †*Pucadelphys*, †*Herpetotherium*, microbiotheriids, most didelphids, paucituberculatans, peramelemorphians, most dasyuromorphians, †*Lekanoleo*, †*Thylacoleo*, pseudocheirids, petaurids, *Cercartetus*, acrobatids, and some phalangerids. By contrast, other marsupials have fewer upper premolars, with the result that tooth-locus homologies in this series are sometimes problematic. In the accounts that follow, we base decisions about premolar homologies on tooth size and morphology, the presence and position of diastemata, the presence or absence of deciduous precursors, supernumerary teeth, and other relevant evidence.

Apart from variation in tooth number, the marsupial upper premolar dentition seems remarkably conservative except among diprotodontians, which exhibit extraordinary modifications of these teeth. Indeed, it is doubtful whether any other mammalian order exhibits such exuberant variation in premolar morphology as that seen among members of Diprotodontia, which include the only living mammals with plagiaulacoid dentitions (sensu Simpson, 1933). Further studies on diprotodontian premolar function would be a welcome addition to the mammalian dental literature.

Character 114. *First upper premolar (P1) present (0); or absent (1).* Only two upper premolars are consistently present in *Notoryctes* (fig. 36), *Burramys* (fig. 46), most phalangerids (i.e., *Ailurops, Spilocuscus, Strigocuscus, Trichosurus* [the fossil "*Trichosurus*" †*dicksoni* could not be scored for this character], *Wyulda*), juvenile macropodiforms, and some dasyurids (*Dasyurus, Dasykaluta*, and *Sarcophilus*). Specimens of *Caluromysiops, Dasycercus*, and *Pseudantechinus* exhibit either two or three upper premolars. Phascolarctids (e.g., *Phascolarctos* [fig. 44]), vombatids (e.g., *Vombatus* [fig. 45]), diprotodontids, wynyardiids, and †*Yalkaparidon* have only a single upper premolar. Although some authors have scored number of premolars as a phylogenetic character without reference to tooth homologies (e.g., Archer, 1976c: char. 7; Rougier

et al., 1998: char. 1), plausible premolar homologies can be determined for most of our terminal taxa with fewer than three premolars based on a combination of ontogenetic, positional, and other morphological criteria.

Comparison of three-premolared and two-premolared specimens of *Caluromysiops* clearly indicates that it is P1 that is sometimes absent in this taxon, which we scored as polymorphic ("0+1"). When present, P1 of *Caluromysiops* is vestigial and single-rooted (see char. 115).

The dasyurids *Dasyurus, Dasykaluta*, and *Sarcophilus* consistently have only two premolars (as does *Planigale gilesi*, although we used three-premolared *P. ingrami* to represent the genus in this study). Examination of juvenile specimens of *Dasyurus* and *Sarcophilus* indicates that neither tooth seems to have a deciduous precursor in these taxa (we were unable to examine juveniles of *Dasykaluta*). Because P3 is a replacement tooth in all other metatherians with rooted cheekteeth, we agree with the traditional view that the missing tooth in two-premolared dasyurids is P3 (e.g., Thomas, 1887a; Woodward, 1896; Bensley, 1903; Tate, 1947; Bartholomai, 1971a; Archer, 1976c; 1982b; 1984c; Wroe and Mackness, 2000a; 2000b). This inference is additionally supported by the presence of a small but distinct diastema between the posteriormost premolar and M1 in both *Dasyurus* and *Dasykaluta*, whereas no diastema is present between P3 and M1 in dasyurids with three premolars. A diastema is absent in *Sarcophilus* (see Archer, 1984c: figs. 14–15; Rose et al., 2017: fig. 2), but this may be due to autapomorphic rostral shortening. An obviously vestigial tooth that may represent dP3 is sometimes present within the diastema between the fully erupted posteriormost premolar and M1 in specimens of *Dasyurus* (e.g., AM 35911; see also Woodward, 1896).

Although not in itself direct evidence that *Dasykaluta, Dasyurus*, and *Sarcophilus* have lost P3, it is also noteworthy that P3 is only variably present in *Dasycercus* and *Pseudantechinus* and that this tooth is small and single-rooted in *Dasyuroides* and in three-premolared speci-

mens of *Dasycercus*. Similarly, comparison between the two-premolared *Planigale gilesi* with other *Planigale* species indicates that the missing upper premolar in the former is P3 (Archer, 1976a: 356–357). By contrast, P1 and P2 are always well developed, double-rooted, premolariform teeth in three-premolared dasyurids. We therefore scored all dasyurids as retaining P1 (state 0). We acknowledge that our interpretation conflicts with the hypothesis of Luckett (1993b; see also Luckett and Woolley, 1996; Luckett et al., 2019) that the missing tooth in *Dasyurus* is P2; a fresh appraisal of the ontogenetic basis for inferring premolar homologies in this taxon would be welcome.

The posterior macropodiform premolar—a large sectorial tooth that replaces a molariform deciduous precursor—is clearly P3, and so the missing tooth in this group is either P1 or P2. We favor the hypothesis that P1 is the missing tooth in macropodiforms because a prominent diastema is present immediately behind C1 in those macropodiforms that retain this tooth (see char. 108), but not between the anterior and posterior premolars; thus, we scored all of our macropodiform terminal taxa as corresponding to state 1. Although data from taxa unrepresented in our study cannot be taken as evidence for a priori homology, we note that the hypothesis that macropodiforms have lost P1 is consistent with observations of a suppressed tooth bud at this locus in sectioned pouch young of several Recent macropodoid species (Woodward, 1893; Berkovitz, 1966; Kirkpatrick, 1969; 1978).

In *Burramys* (fig. 46), the more posterior of the two upper premolars is very large, sectorial, and in direct contact with M1; we identify it as P3 (after, e.g., Ride, 1956; Brammall and Archer, 1997). The more anterior upper premolar is tiny, single-rooted, and in direct contact with the base of P3 but separated from C1 by a large diastema; based primarily on the presence of this diastema, we identify the anterior premolar of *Burramys* as P2 (again, as in, e.g., Ride, 1956; Brammall and Archer, 1997), and therefore score P1 as absent in this taxon.

Two of the thylacoleonids included in our study—†*Lekanoleo* and †*Thylacoleo*—retain three premolars; in these taxa P1 is separated from C1 and P2 by flanking diastemata, but P2 is in contact with the hypertrophied, sectorial P3 (Gillespie, 2007). By contrast, the species used to score our †*Wakaleo* terminal (†*W. vanderleuri*) has only two premolars (Murray et al., 1987; Gillespie, 2007; Gillespie et al., 2017), the more posterior of which is hypertrophied, sectorial, and in direct contact with M1, and so can be confidently identified as P3 based on its resemblance in morphology and position to the unequivocal P3 of †*Lekanoleo* and †*Thylacoleo*. As discussed by Gillespie (2007: 75) and Gillespie et al. (2017: 26–27), the anterior premolar of †*Wakaleo* is well separated from both P3 and C1 by diastemata, suggesting that it is homologous with P1 of †*Lekanoleo* and †*Thylacoleo*, rather than P2 (contra Murray et al., 1987); therefore, we scored all three thylacoleonids as retaining P1.

The single upper premolar of *Phascolarctos* is a large sectorial tooth that replaces a vestigial milk precursor that may or may not erupt (Thomas, 1887b; Blanshard, 1990), so the missing premolars in this taxon are clearly P1 and P2. A single upper premolar is also present in †*Nimiokoala* and †*Litokoala*; this tooth is similar in morphology and position to the P3 of *Phascolarctos* (i.e., large, sectorial, and in contact with M1 but separated from C1 by a large diastema; Black and Archer, 1997b; Louys et al., 2007, 2009; Black et al., 2014a), so we identify it also as P3 and score all three phascolarctids as lacking P1. †*Muramura* (see Pledge, 1987c; 2003) and †*Namilamadeta* (see Rich and Archer, 1979; Pledge, 2005) also have a single large sectorial premolar in contact with M1 but widely separated from C1, suggesting that it is P3, and this inference is further supported by a juvenile specimen of †*Namilamadeta* (QM F51348; Pledge, 2005: fig. 11D), which indicates that the sectorial premolar of this taxon has a deciduous precursor. We therefore scored both wynyardiids as lacking P1.

In the diprotodontids †*Neohelos*, †*Ngapakaldia*, †*Nimbadon*, and †*Silvabestius* the single upper premolar is molariform rather than sectorial, but, as in phascolarctids and wynyardiids, this tooth is in direct contact with M1 and there is a large diastema between it and C1 in those taxa that retain the latter tooth (see char. 108); therefore, we scored these diprotodontids as corresponding to state 1. Juveniles of †*Nimbadon* (see Black and Hand, 2010) and †*Ngapakaldia* (e.g., SAM P35313, a specimen of †*N. bonythoni*) demonstrate that the single premolar of both taxa had a deciduous precursor, confirming its identity as P3.

The enigmatic †*Yalkaparidon* also retains a single upper premolar, which is nearly in contact with M1 but separated from C1 by a large diastema (Beck, 2009; Beck et al., 2014). Although juvenile specimens that might reveal the presence or absence of a deciduous precursor are unknown, we tentatively identified this tooth as P3 (following Beck, 2009; Beck et al., 2014) and scored this taxon as lacking P1 and P2.

Premolar homologies in phalangerids also merit discussion. *Phalanger* has three premolars, all of which are morphologically distinctive (fig. 47): P1 is large, single-rooted, and caniniform; P2 is a tiny, single-rooted, and occlusally featureless button flanked by diastemata; and P3 is a large sectorial replacement tooth (see, e.g., Flannery et al., 1987; Norris and Musser, 2001: fig. 5). A similar premolar complement was apparently present in †*Onirocuscus*, but P1 is double-rooted in this taxon, and there is no diastema between P2 and P3 (Crosby, 2007; Case et al., 2008). By contrast, *Spilocuscus*, *Strigocuscus*, *Trichosurus*, *Wyulda*, and *Ailurops* each have only two premolars, of which the posterior one (a large, sectorial, replacement tooth closely appressed to M1) is unambiguously identifiable as P3 (Flannery et al., 1987). Following previous authors (Bensley, 1903; Archer, 1984c; Flannery et al., 1987), we hypothesize that the anterior premolar of *Trichosurus* and *Wyulda*—a single-rooted, more or less caniniform tooth—is P1 on the basis of its morphology, proximity to the canine, and the presence of a large diastema between it and P3 in juvenile specimens (e.g., AMNH 65547 [*Trichosurus vulpecula*] and WAM 21625 [*Wyulda squamicaudata*]). This inference is also consistent with Berkovitz's (1968) report of a nonfunctional enamel organ at the second upper premolar locus in *Trichosurus vulpecula* pouch young. Therefore, we scored both *Trichosurus* and *Wyulda* as retaining P1 (state 0).

Although *Spilocuscus maculatus* (the generic exemplar used for scoring purposes in this study) has only two premolars (Archer, 1984c: fig. 166; Flannery et al., 1987: fig. 15; Flannery and Calaby, 1987), several congeners retain three premolars in at least some specimens (Flannery and Calaby, 1987; Helgen and Flannery, 2004). In the latter taxa (e.g., *S. papuensis*, *S. rufoniger*, *S. wilsoni*), P2 is very small (when present) and is clearly the polymorphically absent tooth. Based on the size, position, and morphological similarity of the two premolars in *S. maculatus* with the teeth of congeneric species that sometimes retain three, we identify the missing tooth in *S. maculatus* as P2.

We examined two juvenile specimens of *Ailurops* (BMNH 1950.1011 and 1950.1012) in which a distinct diastema separates the erupted anterior premolar from dP3, but no diastema separates the anterior premolar from C1 (with which it shares a partially confluent alveolus). We consider this a plausible indication that P2 has been lost in *Ailurops* (Flannery et al., 1987). In *Strigocuscus*, however, the anterior premolar is equally separated from C1 and P3 by diastemata (Flannery et al., 1987: fig. 9; Groves, 1987), rendering its homology uncertain. Although multiple tiny foramina in the diastema between P3 and the anterior premolar of *Strigocuscus* may represent vestiges of a dental alveolus (in which case it is P2 that has been lost in this taxon), based on the evidence at hand we prefer to code *Strigocuscus* as unknown ("?") for this character (and for other characters based on P1 and/or P2; see below).

The single, open-rooted upper premolar of *Vombatus* (fig. 45), *Lasiorhinus*, and †*Warendja*

(see Pledge, 1992: fig. 1) lacks any diastema between it and M1, consistent with the traditional identification of this tooth as P3. However, the evidence that this is a replacement tooth rather than a retained dP3 is somewhat less compelling. Thomas (1887b) argued that this tooth is P3 rather than dP3 based, in part, on the observation that the open-rooted premolars of placentals (e.g., *Cavia*) are known to be replacement teeth (see also Adloff, 1904; Harman and Smith, 1936; Berkovitz, 1972a; Luckett, 1985). Thomas (1887b) also noted that *Phascolarctos* (the presumed closest extant relative of vombatids) has vestigial milk premolars, which he suggested may represent an intermediate condition between the large and persistent deciduous teeth of other diprotodontians and their apparent absence in vombatids. Brewer et al. (2018: 2–3) also noted that the premolars of *Vombatus* erupt at about the same time as the replacement premolars of *Phascolarctos* (Green and Rainbird, 1987; Blanshard, 1990; Triggs, 2009), suggesting that they are also replacement teeth in *Vombatus*. Nevertheless, because replacement of dP3 by P3 has not (to our knowledge) been directly observed in vombatids, and that dP3 is often a well-developed molariform tooth in other marsupials (including diprotodontids and wynyardiids; see below), it is possible that the large open-rooted tooth in the third premolar position of vombatids is a retained dP3.

The only study of dental development directly bearing on this question seems to be that of Röse (1893), who serially sectioned a single pouch young (1.9 cm body length) of "*Phascolomys wombat*" (= *Vombatus ursinus*). Röse (1893) identified dP3 in this specimen, but concluded that this tooth is subsequently replaced by another that develops from the successional lamina ("Ersatzleiste"; Röse, 1893: fig. 3). However, the sectioned specimen examined by Röse (1893) does not, in fact, preserve any evidence of a developing P3 because the successional lamina he illustrated shows no indication of the localized thickening that is characteristic of the earliest visible (= early bud) stage of

dental development (Luckett, 1993a). Despite such equivocal evidence for the homology of the vombatid premolar, we treat this tooth as P3, in agreement with most previous studies (see also char. 120), but contra Brewer et al. (2018: 2–3), who treated the identity of this tooth in vombatids as unknown.

Notoryctes typically has two upper premolars (Gadow, 1892; Archer, 1984c: 657), the more posterior of which is well developed and occludes with the paracristid of m1, suggesting that it is P3. However, the anterior upper premolar is of less certain homology. As noted by Archer et al. (2011), P1 is tiny compared with P2 and P3 in the Miocene notoryctid †*Naraboryctes philcreaseri*, which is evidently closely related and potentially ancestral to *Notoryctes* (see Beck et al., 2016). Further, in specimens of *Notoryctes* that appear to retain three upper premolars, the first of these is the smallest (Thomas, 1920: 112), suggesting that it is indeed P1 absent in specimens with only two upper premolars. Based on this collective evidence, we assume here that it is P1 has been lost in *Notoryctes*.

The upper postcanine dentition of *Tarsipes* (fig. 49) comprises between three and four undifferentiated spicules of enamel that cannot be homologized to specific dental loci (see char. 113), so we scored this taxon as unknown ("?") for this and for most other characters of the upper dentition.

Character 115. *First upper premolar (P1) conventionally premolariform (0); or single-rooted (1).* When present, the first upper premolar of most metatherians is conventionally premolariform, having two subequal roots (one anterior and one posterior) and a more or less laterally compressed crown bearing a single dominant median cusp that may or may not be flanked by much smaller anterior and/or posterior accessory cusps (state 0); in these respects it resembles the widespread and presumably primitive therian condition (Kielan-Jaworowska et al., 2004). By contrast, pseudocheirids (with the exception of some *Pseudocheirus* specimens, in which P1 is double-rooted; Archer, 1984c: figs. 185–186),

phalangerids (except †*Onirocuscus* and some specimens of *Ailurops*, in which this tooth is also double-rooted; Flannery et al., 1987; Crosby, 2007), thylacoleonids (Gillespie, 2007), *Dactylopsila* (Archer, 1984c: fig. 208), *Dactylonax, Gymnobelideus* (Archer, 1984c: fig. 192), and *Caluromysiops* have a single-rooted, subconical P1 (state 1). *Pseudocheirus, Cercartetus, Ailurops,* and *Lestoros* are polymorphic ("0+1") for this character, which we scored as inapplicable ("-") for taxa lacking P1 and as unknown ("?") for taxa with indeterminate anterior upper premolar homologies (see char. 114).

Character 116. *Second upper premolar (P2) present (0); or absent (1).* Scoring for this character is based on previously discussed assumptions about upper premolar homologies (char. 114). However, we note that P2 is present in juvenile macropodiforms but is lost in adult specimens of most taxa, in which it is displaced by the eruption of P3 (the only known exception is †*Ekaltadeta*; see char. 117). Therefore, metatherians that unambiguously lack P2 as adults were scored for this character only if juvenile specimens were available for examination. In the absence of juvenile material, we scored such taxa (namely †*Bohra,* †*Hadronomas,* †*Rhizosthenurus,* ?*Bettongia* †*moyesi,* †*Balbaroo,* †*Ganawamaya, Hypsiprymnodon* †*bartholomaii,* †*Neohelos,* †*Ngapakaldia,* †*Warendja,* †*Muramura,* †*Nimiokoala,* †*Litokoala,* †*Wakeleo,* and †*Yalkaparidon*) as unknown ("?").

Based on examination of juvenile material, P2 is unequivocally absent in some phalangerids (*Ailurops, Spilocuscus, Trichosurus,* and *Wyulda*), †*Silvabestius,* †*Nimbadon, Vombatus* (fig. 45), *Lasiorhinus,* †*Namilamadeta,* and *Phascolarctos* (fig. 44). Taxa in which anterior upper premolar homologies are unrecognizable (i.e., *Strigocuscus* and *Tarsipes;* see above) were scored as unknown ("?") for this character.

Character 117. *Second upper premolar (P2) ontogenetically persistent (0); or P2 retained briefly and then shed after dP3 is replaced by P3 (1); or P2 and dP3 simultaneously replaced by P3 (2).* When present, the metatherian second upper premolar usually persists into adulthood (state 0). In most macropodiforms, however, the erupting third premolar (P3) simultaneously displaces P2 and dP3 (state 2), a remarkable phenomenon admirably described and illustrated by Thomas (1888: figs. 1, 2; see also Flower, 1867: plate XXIX fig. 4; Archer, 1984c: fig. 214). An obviously intermediate condition occurs in *Hypsiprymnodon,* where P2 is retained for a brief period after dP3 has been replaced by P3 (state 1). In this taxon, both P2 and P3 are present in younger individuals (Ride, 1961: fig. 1b) whereas older specimens have only P3 (fig. 52; see also Woods, 1960; Ride, 1961; Johnson and Strahan, 1982). Uniquely, the fossil macropodiform †*Ekaltadeta ima* retained P2 into adulthood (Wroe, 1996b; Wroe et al., 1998). Because dental replacement patterns in the macropodiform upper dentition are paralleled by those in the mandibular teeth, we did not code the latter as a separate character.

Interestingly, although a tiny, single-rooted P2 is consistently present in juvenile and subadult specimens of *Dactylonax* and *Dactylopsila,* this tooth is sometimes absent from one or both sides of adults, particularly older individuals (e.g., AMNH 194760, a specimen of *Dactylonax palpator*). However, this occasional, apparently ontogeny-related loss of P2 in *Dactylopsila* and *Dactylonax* is unconnected with the eruption of P3, and so we scored both taxa as state 0.

As for the preceding character, taxa that unequivocally lack P2 were scored as inapplicable ("-"), whereas those that lack P2 as adults but for which juvenile material is unavailable (including †*Yalkaparidon* and many fossil diprotodontians) were scored as unknown ("?"), because it is unclear in these taxa whether P2 is absent throughout ontogeny or, alternatively, present in juveniles but subsequently evicted by P3. Taxa in which P2 cannot be unequivocally identified (see above) were also coded as unknown.

This character was treated as ordered (additive) in all the analyses reported below.

Character 118. *Second upper premolar conventionally premolariform (0); or P2 "pseudocheiri-*

form" (1); or P2 sectorial (2); or P2 bicuspid (3); or P2 single-rooted and caniniform or vestigial and occlusally featureless (4). The second upper premolar of most metatherians (when present) is conventionally premolariform (as defined above; see char. 115), as it is in †*Mayulestes*, †*Allqokirus*, †*Pucadelphys*, †*Herpetotherium*, didelphids, paucituberculatans, *Dromiciops*, dasyuromorphians, peramelemorphians, acrobatids, *Cercartetus*, and *Petaurus* (state 0). By contrast, the unworn P2 of pseudocheirids is a distinctively bulbous tooth about as wide as it is long; the occlusal surface of this tooth usually consists of two subequal labial cusps connected by a sharp crest, and there is a prominent lingual heel that is not present in other taxa (state 1; see Archer, 1984c: figs. 180, 185, 186). As in the widespread therian condition, the pseudocheiriform premolar has just two roots, but the posterior root is substantially larger than the anterior root.

The second upper premolar crown of all macropodiforms except *Onychogalea* and *Macropus* consists of a single large shearing crest (state 2), a morphology that has traditionally been described in the literature as "sectorial" (e.g., by Bensley, 1903) or "secant" (e.g., by Tate, 1948). As far as can be determined from the material at hand, macropodiform P2s always have three roots, one anterior and two posterior. Although there is substantial taxonomic variation in the morphology of P2 among macropodiform genera, this variation seems to correspond closely with that observed for P3 (also a sectorial tooth) as described below (see chars. 125–127); therefore, we did not code these simultaneous transformations as separate characters. The crown morphology of P2 in *Onychogalea* (e.g., AMNH 183443) and *Macropus* (e.g., AMNH 65017) differs from that of other examined macropodiforms (state 3): in both taxa, two large, laterally compressed cusps (of which the anterior is larger) are arranged anteroposteriorly along the labial edge of the tooth and are not connected by a crest (Thomas, 1888: 17; Tate, 1948: 277–276, 331–332; Bartholomai, 1971b: fig. 1). A prominent posterolingual cusp and somewhat smaller

anterolingual cusp are also present in *Macropus* (Tate, 1948: 331–332; Bartholomai, 1971b: 2–3, fig. 1).

The second upper premolar is single-rooted and caniniform or occlusally featureless (state 4) in *Dactylopsila* (Archer, 1984c: fig. 208), *Dactylonax*, *Gymnobelideus* (Archer, 1984c: fig. 192), *Burramys* (fig. 46), the phalangerids *Phalanger* (fig. 47) and †*Onirocuscus* (see discussion under char. 114), the †thylacoleonids †*Lekanoleo* and †*Thylacoleo* (Woods, 1956; Archer, 1984c; Gillespie, 1997, 2007), and *Notoryctes* (Gadow, 1892: 367).

In the absence of any clear sequence of transformations among these alternative conditions, we treated this character as unordered (nonadditive) in all the analyses reported below. This character was coded as inapplicable ("-") for taxa in which P2 is unambiguously missing and as unknown ("?") for taxa in which P2 could not be identified with certainty (see above).

Character 119. *Premolariform second upper premolar (P2) distinctly taller than premolariform P3 (0); or premolariform P2 and premolariform P3 subequal in height (1); or premolariform P3 distinctly taller than premolariform P2 (2).* Descriptions of character states and an account of their taxonomic distribution among Recent didelphids were provided by Voss and Jansa (2003: char. 55; 2009), who observed considerable variation in the relative heights of P2 and P3 within Didelphidae; however, only in *Caluromys*, *Caluromysiops*, and *Hyladelphys* is P2 distinctly taller than P3.

The second and third upper premolars are always present and always premolariform in didelphids (Voss and Jansa, 2003; 2009). However, one or the other of these loci is absent in many other metatherians (see chars. 116, 122) and, when both teeth are present, there is considerable variation in their crown morphology (see chars. 118, 123). To minimize character nonindependence (for example, in cases where P2 or P3 is vestigial), we scored this character only for taxa in which P2 and P3 are both present and premolariform (i.e., taxa scored as state 0 for
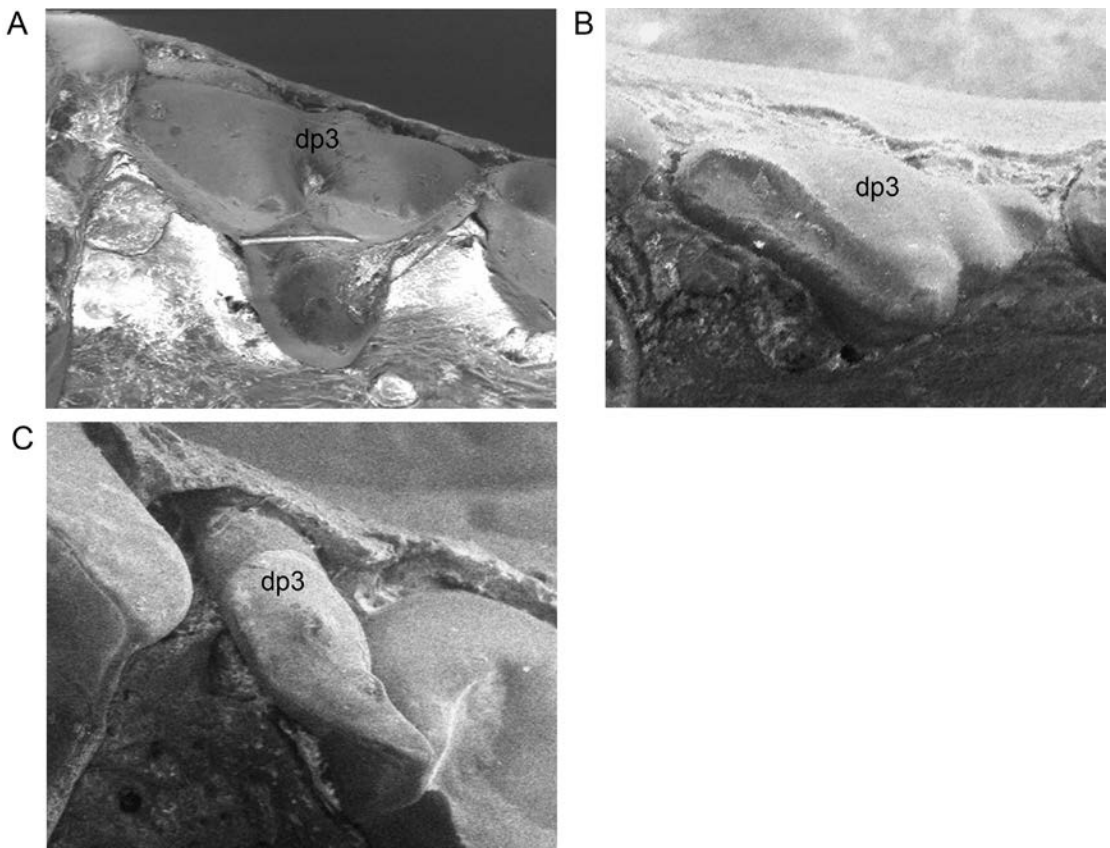
FIG. 13. Occlusal views of right deciduous third upper premolars (dP3) of *Dromiciops gliroides* (**A,** FMNH 127415), *Sminthopsis crassicaudata* (**B,** AMNH 196686), and *Echymipera kalubu* (**C,** AMNH 221654). Alternative states of character 120 (see main text for description of this character and character states) are illustrated as follows: *Dromiciops* 120(0); *Sminthopsis* 120(1); *Echymipera*: 120(2). Note the obvious wear facet on the postmetacrista of dP3 in *S. crassicaudata*, indicating that this tooth is occlusally functional.

chars. 118, 123). We scored taxa in which one or both teeth are missing or exhibit other (nonpremolariform) crown morphologies as inapplicable ("-"). Among nondidelphid taxa with premolariform teeth at both loci, P3 is taller than P2 in †*Pucadelphys*, †*Allqokirus*, †*Mayulestes*, †*Herpetotherium*, paucituberculatans (e.g., *Caenolestes* [fig. 35]), thylacinids (e.g., *Thylacinus* [fig. 40]), several dasyurids (e.g., *Antechinomys*, *Murexia*, *Ningaui*), most peramelemorphians (e.g., †*Galadi*, *Echymipera*, *Isoodon*), and *Petaurus* (fig. 50). By contrast, these teeth are subequal in height in some dasyurids (e.g., *Antechinus*, *Pseudantechinus* [fig. 42], some specimens of *Phasco-*

gale) and a few peramelemorphians (*Macrotis* [fig. 38], some specimens of *Microperoryctes* and *Peroryctes*). Finally, premolariform P2 is distinctly taller than premolariform P3 in acrobatids (e.g., *Distoechurus* [fig. 48]), *Myrmecobius* (fig. 41), and several dasyurids (*Myoictis*, *Neophascogale*, and some specimens of *Phascogale*). This character was treated as ordered (additive) in all the analyses reported below.

Character 120. *Deciduous upper premolar (dP3) large and molariform, occluding with both dp3 and m1 (0); or dP3 smaller and occluding only with m1 (1); or dP3 very small, nonoccluding, and structurally simplified, or absent (2).* The

deciduous upper premolar is a large, molariform tooth that occludes with both the deciduous lower premolar (dp3) and with m1 (state 0) in most Recent didelphids (Voss and Jansa, 2009). We scored †*Herpetotherium* as state 0 based on Rothecker and Storer's (1996) description of dP3 in the taxon they identified as †*Herpetotherium* cf. *marsupium*, but this tooth is currently unknown for many other nonmarsupial metatherians, including †*Pucadelphys*, †*Mayulestes*, and †*Mimoperadectes*. Among marsupials, dP3 is also a large molariform tooth in †*Sparassocynus* (Beck and Taglioretti, 2020), †*Thylophorops*, *Dromiciops* (fig. 13A; see also Hershkovitz, 1999: fig. 30), macropodiforms, phalangerids, †*Namilamadeta* (Pledge, 2005: 150–152, fig. 11; but note that this author referred to dP3 as "DP2," an obvious lapsus), †*Nimbadon* (Black and Hand, 2010), and †*Ngapakaldia* (based on SAM P35313, a juvenile †*N. bonythoni*).

Among other marsupials for which we were able to examine juvenile material, dP3 is variously reduced in size, functional relationships, and occlusal complexity. This tooth is small, does not occlude with dp3, but maintains occlusal contact with m1 (state 1) in some dasyurids (e.g., *Antechinomys*, *Murexia*, and *Sminthopsis* [fig. 13B]), *Macrotis*, and *Chaeropus*. By contrast, dP3 is very small, does not occlude with any element of the lower dentition, and retains few (if any) distinct occlusal features (state 2) in *Hyladelphys* (Voss et al., 2001), *Caenolestes* (Luckett and Hong, 2000), some dasyurids (e.g., *Dasyuroides*, *Myoictis*, *Planigale*), *Thylacinus* (Flower, 1866; 1867; Luckett et al., 2019), some peramelemorphians (*Echymipera* [fig. 13C], *Isoodon*, *Microperoryctes*, *Perameles*, *Peroryctes*, *Rhynchomeles*), *Distoechurus*, petaurids, and pseudocheirids. As noted above, *Dasyurus* lacks P3 but we observed a vestigial tooth that appears to represent dP3 in some specimens (e.g., AM 35911; see also Woodward, 1896), so we also scored *Dasyurus* as state 2.

In *Phascolarctos*, dP3 is vestigial and appears to be resorbed early in development (Thomas, 1887b), and so we scored this taxon as state 2. The condition in vombatids is more equivocal.

As already discussed (see char. 114), we assume that the tooth immediately anterior to M1 in vombatids is P3 rather than a retained dP3. Röse (1893: fig. 3) illustrated a developing dP3 in *Vombatus*, but the ultimate fate of this tooth is uncertain. However, the youngest juvenile specimens of *Vombatus* and *Lasiorhinus* we examined have P3 already erupting, with no evidence of dP3, which we interpret as indicating that dP3 was either absent or vestigial and lost very early in development. We therefore scored *Vombatus* and *Lasiorhinus* as state 2. However, we scored †*Warendja* as unknown ("?") due to an absence of juvenile specimens for this taxon.

The dP3 of *Myrmecobius*—which is retained into adulthood and positioned behind P3 (see char. 121)—varies considerably in morphology between individuals and on opposite sides of the same skull, being a small, essentially featureless unicuspid in some cases (e.g., on the right side of UMZC A6.41/3) but bicuspid (on the left side of UMZC A6.41/6) or tricuspid and distinctly premolariform (on the right side of UMZC A6.41/6) in others. In addition to this variability, the difficulty of meaningful scoring of *Myrmecobius* for this character is further complicated by the fact that the entire postcanine dentition of this taxon is structurally simplified compared with those of most other metatherians, and there is minimal occlusal contact between the upper and lower postcanines as a whole; therefore, *Myrmecobius* has been scored as inapplicable ("-") for this character.

Because these states appear to represent successive stages of reduction and loss, we treated this character as ordered (additive) in all our analyses.

Character 121. *Deciduous upper premolar (dP3) absent in adults (0); or retained in adults (1).* There has been considerable debate in the literature about whether the large number of postcanine teeth in *Myrmecobius* (eight or nine depending on the specimen, versus a maximum of seven in all other metatherians included in our analysis; char. 130) is in part due to retention of the deciduous pre-

molars (Winge, 1882; Dependorf, 1898; Tate, 1951; Forasiepi and Sánchez-Villagra, 2014) or whether dP3 and dp3 are replaced by P3 and p3 respectively (Thomas, 1887a; Leche, 1891; Bensley, 1903). Part of this controversy stems from the fact that dP3 and dp3 appear to be more variable in morphology and size in *Myrmecobius* than in other marsupials (see chars. 120, 157), leading to these teeth sometimes being misidentified as molars.

On the assumption that dP3 develops and erupts before M1 in *Myrmecobius* (as in other marsupials; Wilson and Hill, 1897; Fosse, 1969; Fosse and Risnes, 1972; Archer, 1974a, 1974b; Berkovitz, 1978; Kirkpatrick, 1978; Luckett and Woolley, 1996; van Nievelt and Smith, 2005a; Black et al., 2010; Luckett et al., 2019), we were able to confidently identify dP3 in very young juvenile specimens of this taxon (e.g., BMNH 1844.9.2.18, 1844.9.2.19 and 1844.1.22). None of the older *Myrmecobius* specimens that we examined (which included juveniles, subadults, and adults) show any evidence of dP3 being evicted by P3, whereas a tooth that closely resembles the unequivocal dP3 of juveniles is consistently present in adults of this taxon (contra Bensley, 1903). Thus, we conclude that dP3 is retained in *Myrmecobius*.

In the lower dentition, Thomas (1887a: plate 27 fig. 9) and Bensley (1903: fig. 3) illustrated juvenile BMNH specimens that they interpreted as indicating replacement of dp3 by p3. Neither Thomas (1887a) nor Bensley (1903) gave catalog numbers, but it is clear from our reexamination of BMNH material that the specimen illustrated by Thomas (1887a: plate 27 fig. 9) and Bensley (1903: fig. 3c) is BMNH 44.1.22.21,[10] whereas the second specimen illustrated by Bensley (1903: fig. 3a, b) is BMNH 44.9.2.18. Unfortunately, the teeth from the left side of BMNH 44.9.2.18 that Bensley (1903: fig. 3a) identified as dp3 and m1 are now missing from this specimen, but the equivalent teeth remain in place on

the right side, and we concur with Bensley's (1903: fig. 3a, b) proposed homologies. As for the second specimen illustrated by Thomas (1887a: plate 27 fig. 9) and Bensley (1903: fig. 3c)—namely BMNH 1844.1.22.21—we believe that both of these authors wrongly identified dp3 as m1 and that the true m1 is the more posterior tooth that Thomas (1887a: plate 27 fig. 9) labelled as m2. As a result, we interpret the so-called sixth lower molar seen in some *Myrmecobius* specimens (Thomas, 1887a; Thomas, 1888; Bensley, 1903; Archer and Kirsch, 1977; Archer, 1984c) as m5.

Our examination of a large sample of *Myrmecobius* individuals of various ages suggests that (as in the upper dentition) the sizes of dp3 and of the lower molars vary considerably in this taxon. Although the tooth we identify as dp3 in BMNH 1844.1.22.21 is somewhat larger than the corresponding tooth of BMNH 1844.9.2.18, they share a similar crown morphology (namely three cusps arranged anteroposteriorly), and we are confident that they are homologous. By contrast, m1 of both specimens exhibits a distinctly triangulated trigonid and talonid. In other, older specimens, however, the protoconid and hypoconid are often lost as the result of wear, resulting in an apparently linear tricuspid morphology. We therefore agree with Winge (1882; see also Dependorf, 1898; Tate, 1951; Forasiepi and Sánchez-Villagra, 2014) that *Myrmecobius* retains both dP3 and dp3 into adulthood (state 1), presumably because elongation of its jaws means that this tooth is no longer evicted by the erupting third premolar, which, instead, erupts anterior to it. Retention of dP3 and dp3 do not appear to vary independently, so we scored presence/absence of these teeth within the context of a single character. In other metatherians known to have dP3/dp3 as juveniles (i.e., those not scored as unknown ["?"] for char. 120), these teeth are replaced by P3/p3 in adulthood (state 0), so state 1 is an autapomorphy of *Myrmecobius*.

Character 122. *Third upper premolar (P3) present (0); or absent (1).* As already discussed (see char. 114), P3 is present (state 0) in most metatherians, but this tooth is consistently absent

---

[10] Although Thomas (1887a: plate 27 fig. 9) depicted a left mandible, both his figure and Bensley's are evidently based on the right mandible of this specimen.

(state 1) in *Dasyurus*, *Dasykaluta*, and *Sarcophilus* (Thomas, 1887a; Woodward, 1896; Bensley, 1903; Tate, 1947; Bartholomai, 1971a; Archer, 1976c, 1982b, 1984c; Wroe and Mackness, 2000a, 2000b). Two other dasyurids, namely *Dasycercus* (Woolley et al., 2013) and *Pseudantechinus* (Spencer, 1896; Ride, 1964b; Woolley, 2011), are polymorphic ("0+1") for this character (the specimen of *Pseudantechinus* illustrated here [fig. 42] retains this tooth).

Character 123. *Third upper premolar (P3) conventionally premolariform (0); or P3 semisectorial (1); or P3 fully sectorial (2); or P3 open-rooted (3); or P3 molariform (4); or P3 reduced and single-rooted (5).* After the molars, the third premolar position is arguably the most variable dental locus in terms of occlusal morphology within Metatheria. When present (see char. 122), P3 is conventionally premolariform (state 0) in most metatherians, including †*Mayulestes*, †*Allqokirus*, †*Pucadelphys*, †*Mimoperadectes*, †*Herpetotherium*, didelphids, paucituberculatans, microbiotheriids, *Notoryctes*, most dasyuromorphians (except *Dasycercus*, *Dasyuroides*, and some specimens of *Pseudantechinus*), peramelemorphians, acrobatids, *Petaurus*, *Gymnobelideus*, and some specimens of †*Yalkaparidon* (Beck et al., 2014). By contrast, some diprotodontians exhibit very different P3 morphologies that can be partitioned into qualitatively distinct states.

The pseudocheirid P3 is a bulbous tooth, usually bearing three subequal labial cusps connected by tall, sharp, anteroposteriorly oriented crests; a prominent lingual heel gives this tooth a broad, subtriangular outline in occlusal view (state 1; Archer, 1984c: figs. 180, 185, 186). Because the pseudocheirid condition is neither conventionally premolariform nor unambiguously sectorial, we refer to it as semisectorial. Other diprotodontians have semisectorial P3s in which distinct cusps can be recognized but which are connected by tall, sharp, anteroposteriorly oriented crests; in this respect, they somewhat resemble those of pseudocheirids, although the overall morphology of the teeth varies considerably among taxa. Non-

pseudocheirid taxa with semisectorial P3s include *Dactylopsila* (Archer, 1984c: fig. 208), *Dactylonax*, the wynardiids †*Muramura* (Pledge, 1987c; 2003: fig. 19.2) and †*Namilamadeta* (Rich and Archer, 1979), †*Lekanoleo* (Gillespie, 1997), †*Nimiokoala* (Black and Archer, 1997b), †*Litokoala* (Louys et al., 2007; Pledge, 2010: fig. 5), and *Macropus* (Bartholomai, 1971b), all of which we scored as state 1.

Many other diprotodontians (including phalangerids, burramyids, *Phascolarctos*, †*Thylacoleo*, and all macropodiforms except *Macropus*) have a fully sectorial P3, the dominant crest of which lacks clearly distinguishable cusps (state 2). In available specimens of the species of †*Wakaleo* used for scoring purposes here, namely †*W. vanderleuri*, P3 is too worn to determine whether it exhibits a semisectorial or fully sectorial morphology, so we scored this taxon using ambiguity coding (as "1/2"); however, P3 of †*W. schouteni* is semisectorial (Gillespie et al., 2017).

In vombatids (including †*Warendja*; Hope and Wilkinson, 1982; Flannery and Pledge, 1987), the tooth we identify as P3 (see char. 114) is evergrowing and open-rooted (state 3), similar in overall morphology to M1–4, but smaller in occlusal area. The P3 of the four diprotodontid taxa included here (†*Nimbadon*, †*Ngapkaldia*, †*Silvabestius*, and †*Neohelos*) lacks distinct crests, but each has a well-developed cusp in the protocone position, and a cusp in the hypocone (posterolingual) position is sometimes also present (Stirton, 1967; Stirton et al., 1967a; Hand et al., 1993; Murray et al., 2000; Black, 2010; Black and Hand, 2010; Black et al., 2013); we refer to this morphology as molariform (state 4). In *Dasycercus* and *Dasyuroides*, P3 is vestigial and single-rooted (state 5; Archer, 1982b: table 2; 1984c: fig. 7; Woolley et al., 2013). Both †*Yalkaparidon* (Beck et al., 2014) and *Pseudantechinus* are polymorphic for this character, because P3 is double-rooted and premolariform in some specimens but reduced and single-rooted in others ("0+5").

Although the transition from premolariform (state 0) to semisectorial (state 1) to fully sectorial (state 2) represents a plausible morphocline, the

other states we code for this character cannot be incorporated into a linear transformation sequence. Therefore, we treated this character as unordered (nonadditive) in all the analyses reported below. We scored this character as inapplicable ("-") for *Dasyurus*, *Dasykaluta*, and *Sarcophilus* (all of which lack P3; see char. 122), and also for *Tarsipes*, whose entire postcanine dentition is reduced to vestigial elements (see char. 113), none of which can be homologized with P3.

Character 124. *Premolariform P3 with well-developed anterior and posterior cutting edges (0); or only posterior cutting edge well developed (1); or neither anterior nor posterior cutting edges well developed (2).* Descriptions of character states and an account of their taxonomic distribution among Recent didelphids were provided by Voss and Jansa (2003: char. 56; 2009), who observed that a well-developed anterior cutting edge on P3 (state 0) consistently occurs only in *Caluromys*, *Caluromysiops*, *Glironia*, and *Hyladelphys*. Among other metatherians with a premolariform P3 (see char. 123), only the posterior cutting edge is well developed (state 1) in most taxa examined here. However, P3 lacks both anterior and posterior cutting edges (state 2) in †*Barinya* (Wroe, 1999; Archer et al., 2016a: 8) and *Myrmecobius*. Because the states of this character form a plausible morphocline, they have been ordered in all our analyses. We scored this character as inapplicable ("-") for taxa in which P3 is nonpremolariform or absent (see chars. 122, 123).

Character 125. *Distinct posterolingual cusp on semisectorial or fully sectorial P3 absent (0); or present (1).* Among the metatherians included in our study that possess a semisectorial or fully sectorial P3 (i.e., those taxa scored as states 1 or 2 for char. 123), a distinct posterolingual cusp is absent (state 0) in thylacoleonids, a few macropodiforms (e.g., †*Ekaltadeta* [see Wroe, 1996], *Hypsiprymnodon* †*bartholomaii* and *H. moschatus* [Woods, 1960; Ride, 1961; Flannery and Archer, 1987b; Bates, et al., 2014], *Potorous*, and some specimens of *Aepyprymnus*), most phalangerids (with the exception of *Ailurops*), burramy-

ids (fig. 46; Ride, 1956; Archer, 1984b: figs. 145, 154), pseudocheirids (Archer, 1984b: figs. 180, 185, 186), *Dactylopsila* (Archer, 1984b: fig. 208), and *Dactylonax* (whose teeth may differ in other details of occlusal structure but are similar in this respect). By contrast, a prominent cusp is consistently present lingual to the posterior terminus of the P3 blade (state 1) in *Ailurops*, wynyardiids (Rich and Archer, 1979; Pledge, 1987c; 2003; 2005), phascolarctids (this cusp is anteroposteriorly elongate and crestlike in *Phascolarctos* but more cusplike in †*Litokoala* and †*Nimiokoala*; Black and Archer, 1997b; Louys et al., 2007; Pledge, 2010: fig. 5; Black et al., 2014a), and most macropodiforms. Rich and Archer (1979) and Pledge (1987c; 2003; 2005) referred to this cusp as a hypocone in the wynyardiids †*Namilamadeta* and †*Muramura*. This character was scored as inapplicable ("-") for taxa in which P3 is either nonsectorial or absent (see chars. 122, 123).

Character 126. *Sectorial P3 smooth sided, without enamel ridges (0); or with weakly developed ridges (1); or with well-developed ridges extending from apex to base of crown (2).* The sectorial or semisectorial third upper premolars of *Dactyopsila* (Archer, 1984b: fig. 208), *Dactylonax*, thylacoleonids, *Cercartetus* (Archer, 1984b: fig. 154), *Phascolarctos* (Black et al., 2014a), and many macropodiforms (e.g., *Dendrolagus*, *Macropus*, *Notomacropus*, *Osphranter*, *Onychogalea*, *Petrogale*, and *Caloprymnus*) are smooth-sided teeth that may be dimpled or creased but lack distinct ridging (state 0). The unworn sectorial P3s of all examined phalangerids, however, have incipient (or vestigial) ridges that are often distinct near the apex of the tooth but do not extend to the base of the crown (state 1), a morphology also seen in some macropodiforms (e.g., *Lagostrophus*, *Setonix*, *Thylogale*, and *Potorous*). By contrast, the third upper premolars of *Burramys* (Ride, 1956; Archer, 1984b: fig. 145) and many other macropodiforms (e.g., *Dorcopsis*, *Dorcopsulus*, *Lagorchestes*, †*Hadronomas*, *Aepyprymnus*, *Bettongia* and ?*Bettongia* †*moyesi*, *Hypsiprymnodon* †*bartholomaii* and *H. moschatus*, †*Balbaroo*, †*Ganawamaya*, and †*Ekaltadeta*;

Woods, 1960; Ride, 1961; Woodburne, 1967: fig. 15; Flannery and Archer, 1987a, 1987b; Wroe, 1996; Cooke, 2000; Prideaux, 2004; Kear et al., 2007; Bates et al., 2014) are distinctly ridged from the dental apex to the base of the crown (state 2). Taxa exhibiting the latter condition are sometimes described in the literature as "plagiaulacoid" (after Simpson, 1933).

The lingual and labial faces of P3 in pseudocheirids are characterized by a single broad "rib" that extends vertically from the large central cusp; because it is unclear whether this rib is homologous or not with the multiple, much narrower ridges seen in phalangerids, *Burramys*, and some macropodiforms, we scored pseudocheirids as unknown ("?") for this character. Between two and four broad ribs descend vertically from the major cusps of P3 in †*Namilamadeta* (Rich and Archer, 1979: fig. 1A; Pledge, 2005: fig. 1), †*Muramura* (Pledge, 1987c: fig. 2; 2003: fig. 19.2), †*Nimiokoala* (Black and Archer, 1997b), and †*Litokoala* (Louys et al., 2007: fig. 1; Pledge, 2010: fig. 5); again, because the homology of these structures with the much narrower ridges seen in other diprotodontians is not obvious, we also scored these taxa as unknown. This character was scored as inapplicable ("-") for taxa in which P3 is neither semisectorial nor fully sectorial or is absent (see chars. 122, 123).

Character 127. *Major crest of semisectorial or fully sectorial P3 oriented posterolingual to anterolabial (0); or major crest of semisectorial or fully sectorial P3 parallel to molar row (1); or major crest of semisectorial or fully sectorial P3 oriented posterolabial to anterolingual (2).* The cutting edge of the semisectorial or fully sectorial P3 is oriented obliquely to the molar row, slanting from posterolingual to anterolabial in occlusal view ("flexed buccally" sensu Flannery, 1989; state 0) in most phalangerids that we examined, with the exception of *Spilocuscus* and some specimens of *Ailurops*. Flannery et al. (1987: table 2, char. 15) did not score *Phalanger* as having an obliquely oriented P3, but all the *Phalanger* material that we examined is indistinguishable from most other phalangerids in this respect

(see, e.g., Norris and Musser, 2001: fig. 5). The same posterolingual-to-anterolabial orientation is seen in several macropodiforms, namely *Hypsiprymnodon moschatus* (fig. 52; Woods, 1960; Ride, 1961) and *H.* †*bartholomaii* (see Flannery and Archer, 1987c: fig. 1b), †*Balbaroo* (Cooke, 2000: fig. 2), †*Ganawamaya* (Kear et al., 2007: figs. 1, 3.1), and †*Ekaltadeta* (Wroe, 1996b: fig. 1.1; Wroe et al., 1998: fig. 1.3).

By contrast, the major crest of the semi- or fully sectorial P3 is more or less in line with the long axis of the cheektooth row (state 1), in pseudocheirids, burramyids, wynyardiids, phascolarctids, thylacoleonids, most macropodiforms, and *Spilocuscus* (Flannery et al., 1987: fig. 15). *Ailurops* is variable for this character, with P3 oriented posterolingual to anterolabial in some specimens (e.g., AMNH 196495; see also Flannery et al., 1987: fig. 2A) but in line with the molar row in others (e.g., AMNH 153361), so we scored it as polymorphic ("0+1").

A third, qualitatively distinct morphology is seen in *Dactylopsila* (Archer, 1984c: fig. 208) and *Dactylonax*: the semisectorial P3 of these taxa is oriented obliquely but in the opposite direction (i.e., posterolabial to anterolingual; state 2) to that seen in phalangerids and some macropodiforms. These differing orientations of sectorial or semisectorial P3 among diprotodontians were well illustrated by Ride (1956: fig. 3); because they form a plausible transformation series, we ordered this character in all of our analyses. The orientation of the occluding mandibular tooth (p3) is an obviously nonindependent trait that we did not code separately for phylogenetic analysis. This character was scored as inapplicable ("-") for taxa in which P3 is neither semisectorial nor fully sectorial or is absent (see chars. 122, 123).

Upper Molars

Available evidence (see, e.g., Kielan-Jaworowska et al., 2004) supports the hypothesis that the last common therian ancestor was characterized by a tribosphenic molar dentition (sensu Simpson, 1936) in which each upper
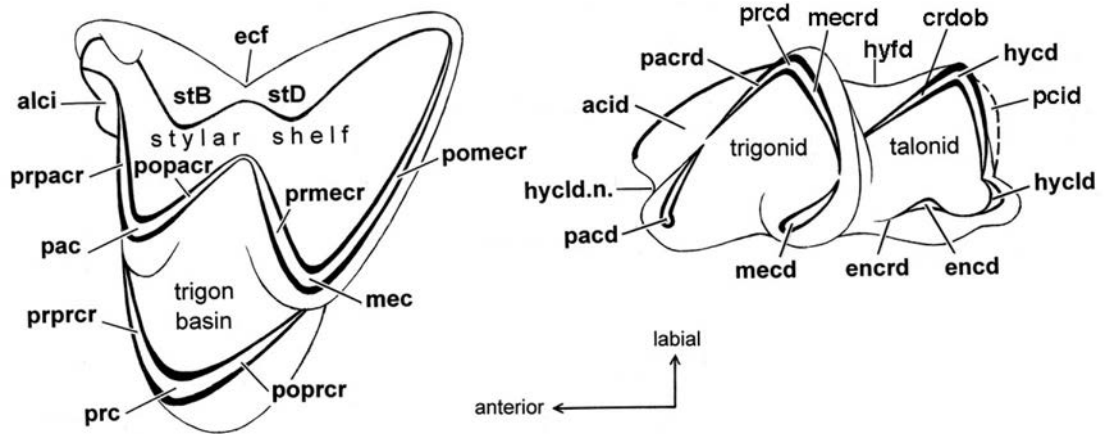
FIG. 14. Occlusal views of left upper and right lower didelphid molars illustrating features of tribosphenic upper molar crown morphology discussed in the text. Abbreviations: **acid,** anterior cingulid; **alci,** anterolabial cingulum; **crdob,** cristid obliqua; **ecf,** ectoflexus; **encd,** entoconid; **encrd,** entocristid; **hycd,** hypoconid; **hycld,** hypoconulid; **hycld.n.,** hypoconulid notch; **hyfd,** hypoflexid; **mec,** metacone; **mecd,** metaconid; **mecrd,** metacristid; **pac,** paracone; **pacd,** paraconid; **pacrd,** paracristid; **pcid,** posterior cingulid (not present in most didelphids); **pomecr,** postmetacrista; **popacr,** postparacrista; **poprcr,** postprotocrista; **prc,** protocone; **prcd,** protoconid; **prmecr,** premetacrista; **prpacr,** preparacrista; **prprcr,** preprotocrista; **stB,** stylar cusp B; **stD,** stylar cusp D.

molar had three well-developed cusps (paracone, metacone, and protocone) forming a triangular array with the protocone at its lingual apex (figs. 14, 15A). The upper molar dentition of nonmarsupial metatherians, didelphids, microbiotheriids, and many dasyuromorphians closely approximates this ancestral morphology, in which the principal cusps are interconnected by crests (cristae) that are named following widely accepted conventions (figs. 14, 15A; see, e.g., Bown and Kraus, 1979: fig. 9-1; Reig et al., 1987: fig. 1; Wroe, 1999: text-fig. 1A; Goin and Candela, 2004: fig. 2A; Kielan-Jaworowska et al., 2004: fig. 11.1; Williamson et al., 2014: fig. 3). Some nonmarsupial metatherians and tribosphenic marsupials also have additional small cusps (known as conules) that occupy the pre- and postprotocristae; of these, the paraconule (on the preprotocrista) is usually absent or vestigial, but the metaconule (on the postprotocrista) is sometimes distinct. In all the taxa properly considered tribosphenic in this report, the postparacrista is connected with the premetacrista, forming the so-called centrocrista (figs. 14, 15A).

The upper molars of most tribosphenic metatherians are also characterized by several more or less distinct cusps on the stylar shelf, a (usually broad) platform labial to the paracone and metacone (figs. 14, 15A). Most recent studies have employed some version of Clemens' (1966) terminology for these structures, recognizing five more or less distinct positions: (1) stylar cusp A (stA, sometimes referred to as the parastyle) is anterolabial to the paracone and is often indistinct or soon reduced by wear; (2) stylar cusp B (stB), almost always larger than stA, is more or less labial to the paracone (to which it is often connected via the preparacrista), and appears to be homologous with the stylocone (or cusp "B") of various Mesozoic mammals (Patterson, 1956; Kielan-Jaworowska et al., 2004); (3) stylar cusp C (stC, sometimes referred to as the mesostyle), when present, is posterolabial to the paracone and anterolabial to the metacone; (4) stylar cusp D (stD) is labial to the metacone; and stylar cusp E (stE, sometimes referred to as the metastyle), often indistinct or absent, is posterolabial to the metacone. Although this strictly topological
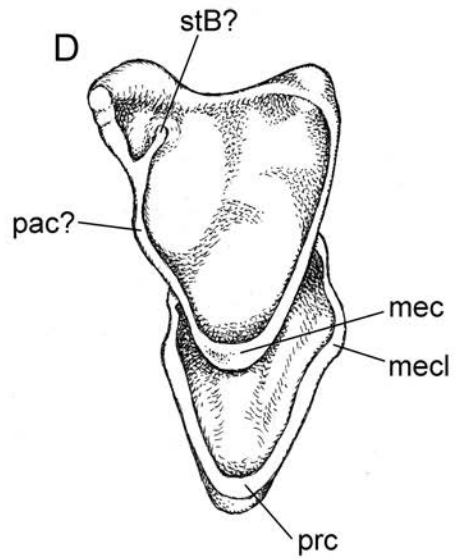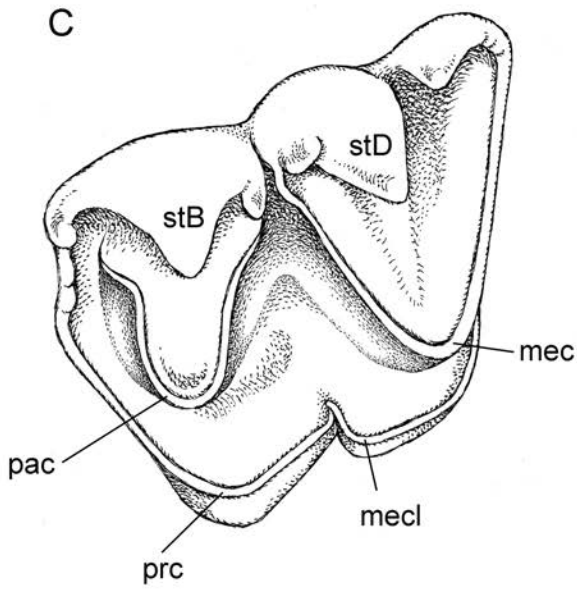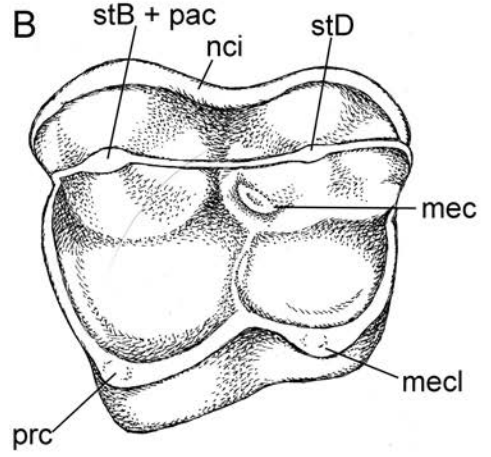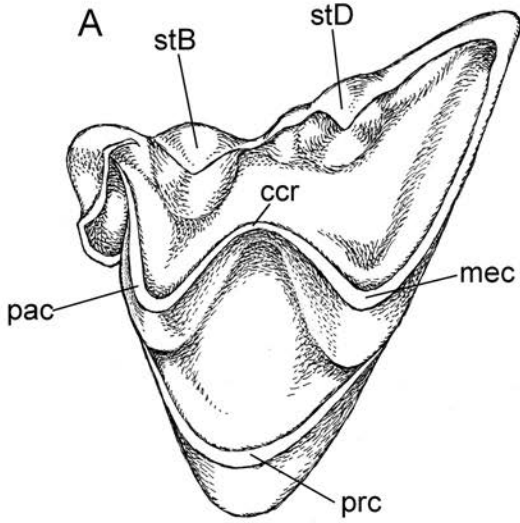
scheme has the advantage of consistency, other authors have modified it somewhat to maintain assumed homologies between stylar cusps that appear to have shifted position.[11]

There are, in addition to the tribosphenic morphotype just described, several nontribosphenic molar bauplans represented among the marsupial taxa included in this study. Fortunately, intermediate phenotypes link most nontribosphenic designs to their tribosphenic precursors, allowing cusp homologies to be identified in many otherwise problematic cases (Archer, 1976e; Ride, 1993; Abello, 2013). The details by which relevant cusp homologies have been inferred are discussed in the following accounts, but it is useful to give a brief description here of each of the major upper molar variants, illustrating examples and providing our terminology for trenchant occlusal features.

The upper molars of caenolestids (fig. 15B; Abello, 2013: fig. 2B) differ from the tribosphenic morphotype by having hypertrophied stylar elements (stB and stD) as the main labial cusps, the paracone having been lost by fusion with stB (a remnant of the paracone may be identifiable in the unworn teeth of some caenolestid specimens;

---

[11] For example, the largest stylar cusp on dasyurid upper molars is often somewhat anterior to the metacone (particularly on M3) and was referred to as stC by Clemens (1966: 23), but it is now generally regarded as homologous with stD of didelphids (e.g., by Archer, 1976c; 1982b; Wroe, 1996a; 1997b), and we agree. Similarly, the major stylar cusp on the upper molars of *Thylacinus cynocephalus* is in the E position (as defined by Clemens, 1966), but some authors (e.g., Muirhead and Archer, 1990; Wroe, 1996a; 1997b) consider it to be homologous with stD of dasyurids; we follow the latter interpretation here.

see char. 136), and the metacone being much reduced in size and partially fused to stD. In addition, the dental outline is quadrangular rather than triangular because an enlarged metaconule occupies the posterolingual ("hypocone") position. Other caenolestid departures from the tribosphenic plan include loss of the centrocrista (postparacrista + premetacrista)—the result of fusion of the paracone to stB—and the presence, in some taxa, of a neomorphic labial cingulum. This molar bauplan lacks a name, although some of its distinctive features are shared among other paucituberculatans and a few diprotodontians.

Recent peramelemorphian molars do not depart quite so markedly from the tribosphenic design, but two differences are noteworthy (fig. 15C). The first is that the centrocrista is usually interrupted by a gap between the postparacrista and the premetacrista (both of which terminate at or near the labial margin of the tooth), effectively dividing the stylar shelf into separate V-shaped segments. The second is the typically quadrangular occlusal outline that, as in caenolestids, is usually the consequence of a hypertrophied metaconule in the "hypocone" position. Other unusual features of peramelemorphian upper molars are restricted to single teeth (e.g., M1) or to single taxa (e.g., *Macrotis*) as described below.

The molars of *Notoryctes* (fig. 15D; Murray and Megirian, 2006b: fig. 6I) and †*Yalkaparidon* (Archer et al., 1988; Beck, 2009; Beck et al., 2014) are zalambdodont, a distinctive morphotype that is also seen among several groups of placental mammals (e.g., chrysochlorids, tenrecids, and

---

FIG. 15. Occlusal views of left upper second molars (M2) of *Metachirus nudicaudatus* (**A,** AMNH 266453), *Caenolestes fuliginosus* (**B,** UMMZ 155575), *Echimipera kalubu* (**C,** AMNH 221654), and *Notoryctes typhlops* (**D,** AMNH 198651). General features of upper molar crown morphology discussed in the text are illustrated, as are characters 132, 133, 136, 137, 140, 141, 143, and 144 (see main text for description of these characters and character states), as follows: *Metachirus* 132(1), 133(0), 136(0), 137(1), 140(3), 141(0), 143(0), 144(0); *Caenolestes* 132(-), 133(1), 136(2), 137(-), 140(-), 141(0), 143(1), 144(0); *Echimipera* 132(1), 133(0), 136(0), 137(1), 140(4), 141(0), 143(1), 144(0); *Notoryctes* 132(1), 133(0), 136(0), 137(2), 140(-), 141(0), 143(0), 144(0). Note, however, that some *C. fuliginosus* specimens retain a paracone and can be scored as 137(1). Abbreviations: **alci,** anterolabial cingulum; **ccr,** centrocrista; **mec,** metacone; **mecl,** metaconule; **nci,** neomorphic cingulum; **pac,** paracone; **prc,** protocone; **stB,** stylar cusp B; **stD,** stylar cusp D. Teeth are not drawn to the same scale.
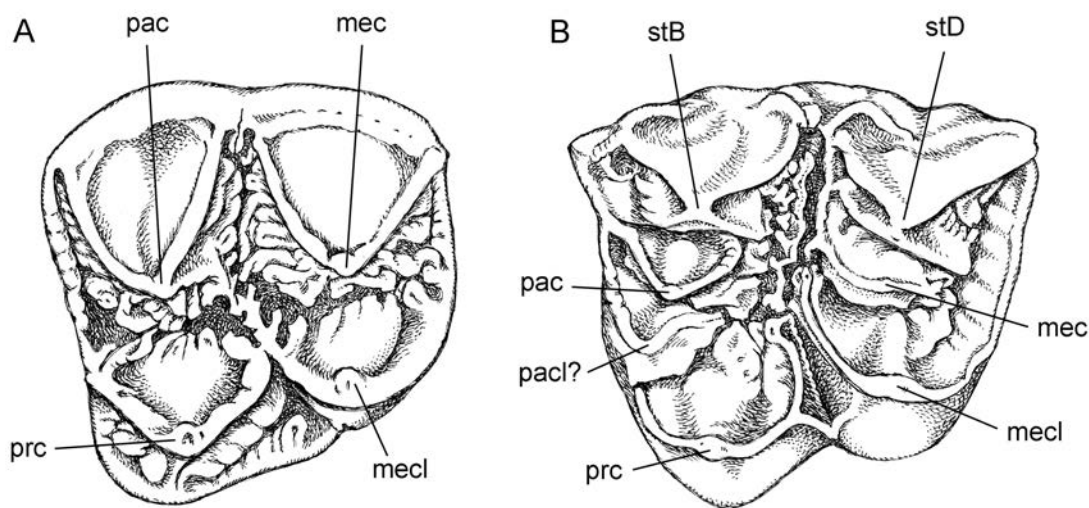
FIG. 16. Occlusal views of left upper second molars (M2) of *Phascolarctos cinereus* (**A,** AMNH 173504) and *Pseudochirops cupreus* (**B,** AMNH 109633). General features of upper molar crown morphology discussed in the text are illustrated, as are characters 132, 133, 136, 137, 140, 141, 143, and 144 (see main text for description of these characters and character states), as follows: *Phascolarctos* 132(0), 133(0), 136(0), 137(0), 140(4), 141(0), 143(1), 144(0); *Pseudochirops cupreus* 132(0), 133(0), 136(0), 137(0), 140(5), 141(0), 143(1), 144(0). Abbreviations: **mec,** metacone; **mecl,** metaconule; **pac,** paracone; **pacl,** paraconule; **prc,** protocone; **stB,** stylar cusp B; **stD,** stylar cusp D. Teeth are not drawn to the same scale.

solenodontids; Asher and Sánchez-Villagra, 2005). Zalambdodont molars are characterized by suppression of either the paracone or the metacone and by the hypertrophy of the remaining cusp, which becomes the dominant upper molar feature; there is little or no occlusion between the protocone and the talonid basin of the lower molars, and the talonid itself is usually reduced or entirely absent (Asher and Sánchez-Villagra, 2005). The dominant upper molar cusp in *Notoryctes* is the metacone, but this taxon also retains a protocone, and the unworn teeth of some specimens retain what may be an anterolabial vestige of the paracone (fig. 15D; Asher and Sánchez-Villagra, 2005; Murray and Megirian, 2006b: fig. 6I; Archer et al., 2011). Based on occlusal relationships, the dominant upper-molar cusp of †*Yalkaparidon* seems likely to be the metacone (Beck et al., 2014), but this homology remains open to question in the absence of annectant taxa (see char. 137).

Several molar morphotypes among diprotodontians have traditionally been recognized (e.g., by Bensley, 1903; Archer, 1976e; Archer, 1984c). In the so-called selenodont condition the dominant molar cusps and their associated crests somewhat resemble crescent moons, as they do in the selenodont teeth of various placental clades (e.g., numerous artiodactyl groups; Loomis, 1925; Fortelius, 1985; Prothero and Foss, 2007). Among Recent marsupials, the selenodont condition is exemplified by *Phascolarctos* (fig. 16A) and pseudocheirids (fig. 16B; see also Archer, 1976e; Archer, 1984c), but this superficial resemblance masks underlying differences in cusp homologies. Whereas the dominant labial cusps of phascolarctids are the paracone and metacone (as in tribosphenic marsupials), the dominant labial and lingual cusps of pseudocheirids appear to be hypertrophied stylar elements (nominally stB and stD), with the paracone and metacone reduced to smaller anterointernal and posterointernal elements, respectively (see discussion under char. 136).

Other diprotodontians—except *Tarsipes*, whose postcanine dentition is vestigial (fig. 49;

char. 113)—have nonselenodont upper molars that have variously been described as bunodont, bunolophodont, or lophodont (fig. 17). These distinctions, which are not always consistently recognized in the literature, refer to the presence or absence of transverse crests or lophs that (when fully developed) connect the principal labial cusps—which we identify as hypertrophied stylar elements in the B and D positions (Ride, 1971; see also Archer, 1976e, 1984c: 683; Tedford et al., 1977; Woodburne and Clemens, 1986a: 96–97, 1986b: 20–21, Tedford and Woodburne, 1987: 416; Woodburne et al., 1987a: 600; Ride, 1993; Crosby and Archer, 2000: 331; Beck et al., 2020)—with their lingual counterparts (protocone and metaconule). Such lophs are altogether absent in some taxa (e.g., *Acrobates, Dactylopsila,* and †*Thylacoleo*) that might properly be called bunodont, but they are increasingly distinct in others (e.g., *Distoechurus* [fig. 17A], *Hypsiprymnodon* [fig. 17B], and phalangerids [fig. 17C]) that we refer to as bunolophodont (after, e.g., Case, 1984; Flannery et al., 1984; Woodburne, 1984a). In fully lophodont taxa (such as diprotodontids and Recent macropodids; fig. 17D), the cusps are fully incorporated into tall transverse crests and no longer appear as distinct structures. In bunolophodont and fully lophodont forms, the anterior crest (connecting stB with the protocone) is commonly referred to as the protoloph, and the posterior crest (connecting stD with the metaconule) as the metaloph (fig. 17). A median crest that sometimes connects the protoloph and metaloph and that appears to be homologous with the postprotocrista in macropodiforms (e.g., Cooke, 2000; Kear et al., 2007; Prideaux and Warburton, 2010: char. 25; Travouillon et al., 2015a; Butler et al., 2016) has been referred to as the "midlink" by some authors (e.g., Stirton, 1955; Tedford, 1966; Woodburne, 1967; Bartholomai, 1971b; Sanson, 1980). Another that projects posteriorly from the metaloph has been alternatively referred to as the "postlink" (e.g., Flannery, 1983; Flannery and Rich, 1986), the "neometaconule crista" (Travouillon et al., 2014b, 2015a, 2016; Butler et al.,

2016), or the "urocrista" (e.g., Prideaux, 2004; see char. 146). Among the taxa we examined, the midlink (formed by the postprotocrista) and postlink/neometaconule crista/urocrista occur only in some macropodiforms (fig. 17D).

Character 128. *Molars with closed roots and static crowns (0); or molars with open roots, the crowns growing throughout adulthood (1).* Most adult metatherians have molars with closed roots and static crowns (state 0), but vombatids—including †*Warendja* (see Hope and Wilkinson, 1982; Flannery and Pledge, 1987; Brewer, 2007)—have open-rooted, evergrowing cheekteeth (state 1) corresponding to the "hypselodont" condition of Simpson (1970) and the "euhypsodont" condition of Mones (1982). The molar roots of *Isoodon* and *Macrotis* appear to close late in ontogeny (e.g., the molar roots of AMNH 35717, a young adult specimen of *Macrotis lagotis*, are still partially open), but differ from those of vombatids, which remain widely open even in the oldest examined individuals. Therefore, we scored *Isoodon* and *Macrotis* as state 0.

Character 129. *M1–4 present (0); or M4 absent (1); or M2–4 absent (2).* Most metatherians with clearly differentiated cheek teeth have four upper molars (state 0). By contrast, M4 is absent (state 1) in acrobatids (e.g., *Distoechurus* [fig. 49]) and †*Wakaleo* (see Gillespie et al., 2017). We scored *Cercartetus* as state 0 based on *C. caudatus,* which retains a small M4, but this tooth is absent in *C. concinnus* and *C. nanus* (see Archer, 1984c: figs. 154–156). †*Thylacoleo* retains only a single upper molar, which, based on its position and morphology in comparison to teeth of other thylacoleonids, represents M1 (state 2). Postcanine homologies are not resolvable in *Tarsipes* (char. 113), so the precise number of molars cannot be determined for this taxon (Bensley, 1903; Archer, 1984c; Russell and Renfree, 1989), which we scored as unknown ("?").

All examined taxa with four upper molars also have four lower molars, with the unique exception of *Myrmecobius,* in which some specimens exhibit a supernumerary fifth lower molar (referred to by
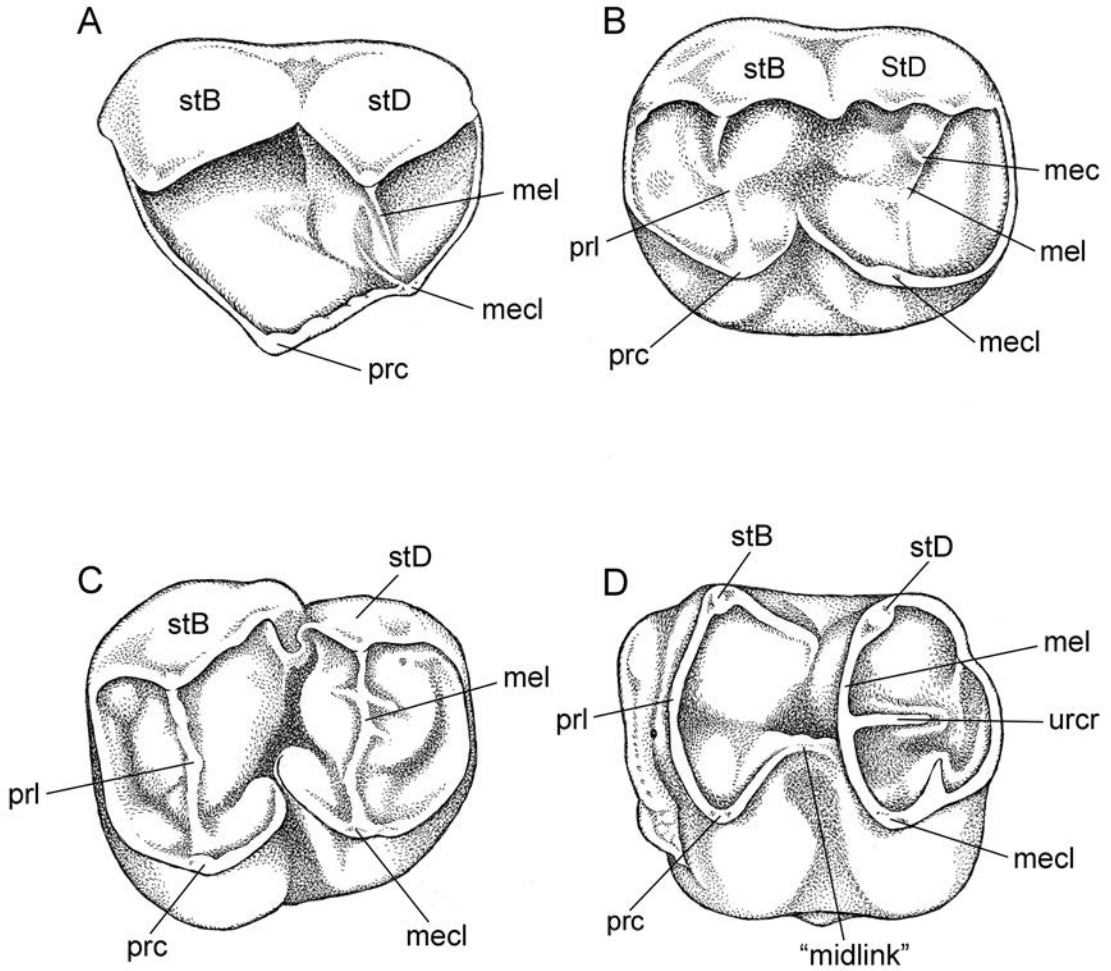
FIG. 17. Occlusal views of left upper molars of *Distoechurus pennatus* (**A,** AMNH 104058 [M1]), *Hypsiprym-nodon moschatus* (**B,** AMNH 160120 [M2]), *Trichosurus vulpecula* (**C,** AMNH 65547 [M2]), and *Lagostrophus fasciatus* (**D,** AMNH 155105 [M2]). General features of upper molar crown morphology discussed in the text are illustrated, as are characters 132, 133, 136, 137, 140, 141, 143, 144, 145, and 146 (see main text for descrip-tion of these characters and character states), as follows: *Distoechurus* 132(-), 133(1), 136(2), 137(-), 140(-), 141(0), 143(1), 144(1), 145(0), 146(0); *Hypsiprymnodon moschatus* 132(-), 133(0), 136(2), 137(-[but note that this can be scored in lightly worn specimens of *H. moschatus*; see fig. 18A]), (140(-), 141(0), 143(1), 144(1), 145(-), 146(-); *Trichosurus vulpecula* 132(-), 133(0), 136(2), 137(-), 140(-), 141(0), 143(1), 144(1), 145(0), 146(0); *Lagostrophus* 132(-), 133(0), 136(2), 137(-), 140(-), 141(0), 143(1), 144(2), 145(1), 146(1). Note that in the illustrated specimen of *D. pennatus* the neomorphic labial cingulum is restricted to the region between the major labial cusps, but in other specimens it extends along the entire labial margin of the upper molars. Abbreviations: **mec,** metacone; **mecl,** metaconule; **mel,** metaloph; **prc,** protocone; **prl,** protoloph; **stB,** stylar cusp B; **stD,** stylar cusp D; **urcr,** urocrista. Teeth are not drawn to the same scale.

some previous authors, e.g., Thomas, 1887a; Thomas, 1888; Bensley, 1903; Archer and Kirsch, 1977; Archer, 1984c as a "sixth" molar; see discussion under char. 121). Similarly, all taxa with three upper molars also have three lower molars. Although †*Thylacoleo* has one upper molar and two lower molars (Archer and Dawson, 1982; Archer and Rich, 1982; Archer, 1984c: fig. 128; Rauscher, 1987; Gillespie, 1997, 2007; Gillespie et al., 2016), it seems probable that the numbers of upper and lower molars are evolutionarily correlated, and on this assumption we did not score them as separate characters. Although not included here as a terminal, *Petrogale* (= "*Peradorcas*") *concinna* is unique among known metatherians in exhibiting continuous molar replacement (Thomas, 1904; Tate, 1948; Sanson, 1989; Rodrigues et al., 2017). Recognizing the progressive loss of more posterior molars as steps in an ordered transformation series, we ordered this character in all our analyses.

Character 130. *P3 erupts after M4 (0); or P3 and M4 erupt simultaneously (1); or P3 erupts before M4 but after M3 (2); or P3 and M3 erupt simultaneously (3); or P3 erupts before M3 (4).* The timing of the eruption of P3 relative to the upper molars has been shown to encompass potentially useful phylogenetic information among didelphids (Tribe, 1990; Voss and Jansa, 2003: char. 61; 2009), and additional phylogenetically informative variation occurs among other metatherians. In most examined taxa (including all didelphids), P3 erupts after M3, but P3 can erupt after M4 (state 0), simultaneously with M4 (state 1) or before M4 (state 2; Tribe, 1990; Hershkovitz, 1999; Voss and Jansa, 2003: char. 61; 2009). By contrast, P3 erupts earlier, either simultaneously with (state 3) or before M3 (state 4), in petaurids, pseudocheirids (with the possible exceptions of *Petauroides* and *Pseudochirops archeri*, for which we were unable to examine appropriate juvenile or subadult material), burramyids, *Acrobates* (but not *Distoechurus*, in which P3 erupts after M3; e.g., in AMNH 191045), vombatids, *Phascolarctos*, *Thylacinus*, and *Myrmecobius* (Flower, 1867).

We are unaware of intact maxillary specimens of juveniles or subadults of †*Herpetotherium*, which we scored as unknown ("?"). We examined several subadult specimens of †*Pucadelphys* in which M3 is fully erupted and P3 is incompletely erupted, but none preserve M4 (e.g., MNHC 8265; see Cifelli and Muizon, 1998a: fig. 1B; Muizon et al., 2018: 373–375); on the assumption that M4 was not fully mineralized or was still within its crypt in these subadult individuals, we scored †*Pucadelphys* as state 2. Cifelli and Muizon (1998a) discussed a supposed subadult specimen of †*Mayulestes* (MNHC 8267), but this specimen was subsequently referred to †*Allqokirus* (see Muizon et al., 2018), so the eruption pattern of †*Mayulestes* is currently unknown; however, based on MNHC 8267 (in which M3 is fully erupted, P3 is nearly fully erupted, and M4 is partially erupted; Cifelli and Muizon, 1998a; Muizon et al., 2018), †*Allqokirus* can be scored as state 2. Several taxa that could not be assigned a unique character state based on available specimens (e.g., *Petauroides*, *Pseudochirops archeri*, *Distoechurus*, *Strigocuscus celebensis*, *Wyulda*, †*Ekaltadeta*, †*Neohelos*) were scored using appropriate ambiguity codings. Because these states form a plausible transformation series, we ordered this character in all our phylogenetic analyses.

Character 131. *Molar progression leading to eviction of P3 absent (0); or present (1).* In most metatherians, there is no major change in the position of the molars within the maxilla and dentary over ontogeny (state 0). However, in some macropodids there is a gradual anterior or mesial movement by the upper and lower molars with age, a phenomenon known as molar progression (Tate, 1948; Ride, 1957; Sanson, 1980, 1989; Lentle and Hume, 2010; Prideaux and Warburton, 2010: char. 22). The degree of molar progression is often slight and can be hard to recognize in the absence of convenient landmarks, but molar progression in several taxa leads to the eviction of P3 and p3 from the upper and lower jaws (state 1). In older individuals of *Macropus* and *Osphranter*, the anterior molars are also

evicted (see, e.g., Kido et al., 2018: fig. 2d), and Sanson (1980) reported that some very old individuals retain only a single molar as a result of this process.

Character 132. *Upper molars without a distinct ectoflexus on any tooth (0); or distinct ectoflexus present on one or more teeth (1).* Descriptions of character states and an account of their taxonomic distribution among Recent didelphids were provided by Voss and Jansa (2003: char. 59; 2009), who defined the ectoflexus as a "V-shaped labial indentation of the stylar shelf" (see fig. 14). *Caluromys* and *Caluromysiops* are the only Recent didelphids that lack a distinct ectoflexus on all their upper molars (Voss and Jansa, 2009: fig. 21).

Among other metatherians, an ectoflexus is present on at least one molar in †*Pucadelphys* (Marshall and Muizon, 1995: figs. 6B, 7B; Ladevèze et al., 2011: fig. 4d-f), †*Allqokirus* (Muizon et al., 2018: figs. 7–9), †*Mayulestes* (Muizon, 1998: fig. 2), †*Mimoperadectes* (Horovitz et al., 2009: fig. 1), †*Herpetotherium* (Horovitz et al., 2008: plate 1A), †*Hesperocynus* (Forasiepi et al., 2009), †*Sparassocynus* (Reig and Simpson, 1972: fig. 8; Beck and Taglioretti, 2020: fig. 3a), †*Thylophorops* (Reig et al., 1987: fig. 28), †*Thylatheridium* (Reig, 1952: fig. 11A; Reig et al., 1987: fig. 25A), †*Evolestes* (Goin et al., 2007b: figs. 2, 3), *Dromiciops* (Marshall, 1982: fig. 16), †*Microbiotherium* (Marshall, 1982: fig. 9), †*Yalkaparidon* (Beck, 2009: fig. 6B; Beck et al., 2014), *Notoryctes* (Figure 15D; Asher and Sánchez-Villagra, 2005: fig. 6A; Murray and Megirian, 2006b: fig. 6I; Archer et al., 2011: fig. 1), peramelemorphians (but note that the weak ectoflexus seen in unworn molars of *Macrotis* is lost with slight wear), dasyurids, thylacinids, †*Muramura* (Pledge, 2005: fig. 19.2), and young individuals of *Lasiorhinus* (Brewer et al., 2018: fig. 13.1). By contrast, the ectoflexus is absent among other diprotodontians that retain a distinct stylar shelf, namely pseudocheirids and phascolarctids (fig. 16).

We scored this character as inapplicable ("-") in taxa that lack a distinct stylar shelf, as evidenced by fusion between the paracone and stB and between the metacone and stD on all upper molars (see char. 136); such taxa include all examined paucituberculatans except †*Evolestes* (Goin et al., 2007b; Abello, 2013) and all examined diprotodontians with the exception of phascolarctids (fig. 16A), pseudocheirids (fig. 16B), †*Muramura*, and *Lasiorhinus*. In addition, we scored this character as inapplicable in all taxa in which a neomorphic cingulum is present labial to the stylar region (see char. 133), because this cingulum fills the region normally occupied by the ectoflexus (if present). Finally, we also scored *Myrmecobius* as inapplicable, because its highly modified upper molar morphology makes it unclear as to whether a true stylar shelf is present (Archer, 1984c: fig. 23), and *Tarsipes*, because its vestigial postcanine dentition (Parker, 1890; Bensley, 1903; Archer, 1984c; Russell and Renfree, 1989) precludes meaningful scoring of this character (see char. 113).

Character 133. *Neomorphic labial cingulum absent (0); or present on M1–3 (1).* As discussed by Voss and Jansa (2009: 54), an apparently neomorphic cingulum that extends along the entire labial margin of each upper molar (state 1) is present in *Caenolestes* (fig. 15B and 18B) and *Rhyncholestes*. The identification of this ridge as an evolutionary novelty rather than as a remnant of the stylar shelf follows from the interpretation of caenolestid cusp homologies suggested by Osgood (1921) and subsequently accepted by Marshall (1987) and most other recent authors (e.g., Goin and Candela, 1996, 2004; Goin et al., 2007b, 2009a; Abello, 2013; Rincón et al., 2015; Engelman et al., 2016), namely that the major labial cusps in living caenolestids are stylar in origin, rather than representing the paracone and metacone (see char. 136). Among other paucituberculatans, a well-developed cingulum extending along the entire labial margin of the upper molars appears to be absent (state 0) in *Lestoros* (Martin, 2013), †*Evolestes* (Goin et al., 2007b: figs. 2–3), †*Acdestis* (Engelman and Croft, 2016: fig. 4), and †*Pichipilus* (Abello, 2007: lámina 6I), but it is identifiable in †*Stilotherium*

(Marshall, 1980: fig. 5). This structure is only variably present in †*Palaeothentes*, which we scored as polymorphic ("0+1").

A cingulum is also present labial to stB and stD (the "paracone" and "metacone," respectively, of previous authors; see char. 136) on the first upper molar of †*Lekanoleo* (see Gillespie, 1997, and Gillespie et al., 2020, who referred to it as a "stylar basin") and †*Wakaleo* (Murray et al., 1987: fig. 8A), both of which we scored as state 1. The occlusal morphology of M1 (the only remaining upper molar) in †*Thylacoleo* is too heavily modified (Archer and Rich, 1982; Archer, 1984c: fig. 128) to score this character with any confidence, so we scored this taxon as inapplicable ("-").

A cingulum that extends along the entire labial margin of the upper molars is also present in some specimens of *Cercartetus* (e.g., AMNH 222711), *Acrobates* (e.g., AMNH 37185; fig. 18C), and *Distoechurus* (e.g., AMNH 157169); in other specimens of these three taxa, however, the cingulum does not extend along the entire labial margin of the teeth, but is instead restricted to the region immediately labial to the space between the major labial cusps (stB and stD; see char. 136). Nevertheless, based on the presence of this cingulum, we scored *Cercartetus*, *Acrobates*, and *Distoechurus* as state 1 for this character (see also comments regarding *Cercartetus* by Turnbull and Schram, 1973: 443).

Character 134. *Stylar cusp B (stB) taller than or subequal in height to stD on M2 (0); or stD taller than stB on M2 (1).* The number, position, and size of the stylar cusps are commonly cited as characters in metatherian systematics, particularly for fossil taxa known primarily from teeth (e.g., by Wroe et al., 2000; Wroe and Musser, 2001; Goin et al., 2006; Davis, 2007; Ladevèze and Muizon, 2007; 2010; Carneiro and Oliveira, 2017b). However, examination of multiple conspecific individuals of both Recent and fossil taxa often reveals polymorphism in stylar cusp number and morphology (e.g., Bensley, 1906; Korth, 1994; Hershkovitz, 1997: fig. 19; Flores and Abdala, 2001; Hayes, 2005; Martin, 2005; Ladevèze et al., 2011, 2012; Korth, 2018). Despite

such variability, the stylar cusp in the B position is consistently taller than or subequal in height to the stylar cusp in the D position (state 0) in most tribosphenic metatherians (Godthelp et al., 1999: 302). This morphology is observed in †*Pucadelphys*, †*Allqokirus*, †*Mayulestes*, †*Mimoperadectes*, didelphids, and all peramelemorphians with the exception of †*Yarala* (Muirhead and Filan, 1995).

By contrast, stD is taller than stB (state 1) in most dasyuromorphians (Wroe, 1997b). This trait is most obvious on M2, where stD is usually greatly enlarged relative to stB (fig. 19A). However, stB and stD are subequal in height on the M2 of some specimens of *Thylacinus*, *Micromurexia*, *Murexia*, *Phascolosorex*, and *Phascomurexia*, all of which we scored as polymorphic ("0+1").[12] Stylar cusp D is also taller than stB in †*Herpetotherium* (Korth, 1994; Horovitz et al., 2008), †*Stilotherium* (Marshall, 1980: fig. 5), and †*Yarala* (Muirhead and Filan, 1995). We scored *Dromiciops* and †*Microbiotherium* as inapplicable ("-"), because the stylar cusps are not identifiable as discrete structures in these taxa but instead form a continuous, low crest along the labial margin of M2 and M3 (see also Goin et al., 2007b: 600). We scored *Myrmecobius* as unknown ("?") because upper molar cusp homologies cannot be identified with confidence in this taxon.

Among metatherians with more derived upper molar morphologies, stB is taller than or subequal in height to stD on M2 in †*Evolestes* (which retains a clearly tribosphenic bauplan) and in all other paucituberculatans we examined (e.g., *Caenolestes*; fig. 19B)—in which the major labial cusps are enlarged stB and stD—

---

[12] It should be noted that the cusp we identify as stD in *Thylacinus cynocephalus* is posterolabial (rather than labial) to the metacone, and it has been suggested by some authors that this cusp might instead be stE (Archer, 1982a; Muirhead and Archer, 1990; Warburton et al., 2019). The inferred posterior shift in the position of stD in *T. cynocephalus* (what appears to be the same cusp is more conventionally positioned in *T.* †*potens*; Woodburne, 1967) has been hypothesized to be connected with enlargement of the posterior region of the tooth (Muirhead and Archer, 1990: 215) or with the evolution of a dolichocephalic skull (Wroe, 1997b: 40).

with the exception of †*Stilotherium*, in which stD is taller (Marshall, 1980: fig. 5). Although *Notoryctes* is zalambdodont rather than tribosphenic, the cusps that we identify as stB and stD are still present on the labial margin of the tooth crown (Murray and Megirian, 2006b: fig. 6I), where stB is either slightly taller than or subequal in height to StD.

Small but distinct stylar cusps are identifiable labial to the paracone and metacone of M2 in *Phascolarctos* and †*Litokoala* (Black et al., 2014a), with stB slightly taller than or subequal in height to stD (state 0); however, stylar elements are indistinct in †*Nimiokoala*, which we scored as inapplicable ("-"). Among other diprotodontians, scoring this character is somewhat less straightforward. As discussed in greater detail below (char. 136), the cusps conventionally identified as the paracone and metacone in pseudocheirids appear to correspond to stB and stD, respectively. In all pseudocheirids included in this analysis, stB (the "paracone" of previous authors) is taller than or subequal in height to stD (the "metacone" of previous authors). We also consider the labial ends of the protoloph and metaloph of lophodont and bunolophodont diprotodontians to be homologous with stylar cusps B and D, respectively (see char. 136; see also Ride, 1971; Archer, 1976e, 1984c: 683; Tedford et al., 1977; Woodburne and Clemens, 1986a: 96–97, 1986b: 20–21; Tedford and Woodburne, 1987: 416; Woodburne et al., 1987a: 600; Ride, 1993; Crosby and Archer, 2000: 331; Beck et al., 2020), so this character can be scored for such taxa based on the relative heights of the structures that most previous authors have identified as the paracone and metacone. Stylar cusp B (by our interpretation) is taller than or subequal in height to stD in all of the lophodont and bunolophodont diprotodontians we examined, with the exception of some specimens of *Dorcopsulus* and *Lagorchestes* (in which stD is taller than stB); we scored both of the latter taxa as polymorphic ("0+1").

Character 135. *Stylar cusp D (stD) shorter than or subequal in height to the metacone on M2 (0); or stD markedly taller than the metacone on*

M2 (1). In most metatherians in which stD and the metacone can both be identified as distinct cusps on M2, stD is shorter than or subequal in height to the metacone (state 0). This trait is seen in †*Pucadelphys*, †*Allqokirus*, †*Mayulestes*, †*Mimoperadectes*, †*Herpetotherium*, didelphids, dasyurids (e.g., *Pseudantechinus*; fig. 19A), thylacinids, peramelemorphians (except *Macrotis*, which is inapplicable for this character), and †*Evolestes*. In other paucituberculatans (e.g, *Caenolestes*; fig. 19B), however, the metacone is markedly shorter than stD (state 1) and is partially fused to the lingual face of that cusp (figs. 18B, 19B; see also Marshall, 1980: fig. 5c; Abello, 2007, 2013; Goin et al., 2009a).

We scored this character as inapplicable ("-") for most lophodont and bunolophodont diprotodontians, because the metacone is no longer identifiable as a distinct cusp in such taxa (having been incorporated into the metaloph; see char. 136). The exceptions are *Hypsiprymnodon moschatus* and *H.* †*bartholomaii*, in both of which a cusp that we consider to be homologous with the metacone—but identified as a "neometaconule" by Flannery and Archer (1987c)—is identifiable lingual to stD (figs. 17B, 18A; see also Ride, 1993). In both *H. moschatus* and *H.* †*bartholomaii*, the metacone is subequal in height to stD, so we scored these taxa as "0." Among other diprotodontians, stD is shorter than or subequal in height to the metacone in *Phascolarctos*, †*Litokoala*, †*Muramura*, †*Namilamadeta*, and (based on unworn molars of juvenile specimens) *Lasiorhinus*. By contrast, stD (the "metacone" of previous authors; see char. 136) is clearly taller than the metacone (the "neometaconule" of previous authors) in all examined pseudocheirids. Because stylar cusps are indistinct in †*Nimiokoala*, we scored this taxon as inapplicable ("-"). We also scored *Macrotis* as inapplicable because the metacone has been displaced lingually in this taxon (see char. 143) and is no longer in close proximity to StD.

Character 136. *Paracone not completely fused with any stylar elements (0); or paracone completely fused with stB on M1 but not on more pos-*

terior teeth (1); or paracone completely fused with stB on all upper molars (2); or paracone unfused with stB on M1 and M2 but completely fused with stB on M3 and M4 (3). The paracone is remote from the labial margin on all the upper molars and is not fused with any stylar element (state 0) in most tribosphenic metatherians (e.g., †*Puca-delphys*, †*Allqokirus*, †*Mayulestes*, †*Mimopera-dectes*, †*Herpetotherium*, didelphids [figs. 14, 15A], peramelemorphians [fig. 15C], most dasy-urids [fig. 19A], and most thylacinids). By contrast, the paracone lies on the labial margin of M1 and appears to have completely fused with stB on that tooth, but not on more posterior molars (state 1), in some dasyurids (including *Dasycercus*, *Dasyuroides*, *Dasyurus*, and *Sarcoph-ilus*; Archer, 1976c, 1982b, 1984c; Wroe, 1996a, 1998; Wroe and Mackness, 2000a) and in †*Bad-jcinus* (Muirhead and Wroe, 1998: 613). The same morphology is seen in some, but not all, specimens of *Phascolosorex* and *Pseudantechinus*, which we scored as polymorphic ("0+1").

A single cusp close to the anterolabial margin of M1 in *Dromiciops* (see Marshall, 1982: fig. 15) and †*Microbiotherium* superficially resembles the structure that results from fusion of the paracone with stB in some dasyuromorphians (the taxa we scored as state 1, above). However, in both microbiotheriids the stylar shelf of M1 is narrowly continuous along the entire labial margin of the tooth, whereas the stylar shelf is discontinuous anteriorly in dasyuromorphians with fused paracone + stB. This observation, together with the fact that stB is not identifiable as a clearly distinct structure on M2–4 of *Dromiciops* and †*Microbiotherium*, suggests that the antero-labial cusp on M1 in these taxa is nothing more than a labially displaced paracone. Therefore, we scored them both as state 0.

We agree with Osgood (1921: 122–126) and Marshall (1987: 140) that the paracone is fused with stB on all of the upper molars of most pau-cituberculatans (state 2; see also Goin and Can-dela, 1996, 2004; Goin et al., 2007b; Abello, 2013; Rincón et al., 2015; Engelman et al., 2016). This conclusion is principally based on the identifi-

cation of the postero-internal cusp on unworn M1–3 as the metacone (figs. 15B, 18B, 19B), from which it follows that the large posterolabial cusp is stD, and that the enamel ridge along the labial margin of the tooth crown is a neomorph (see char. 133). This hypothesis of cusp homologies is further supported by the presence of a small but distinct paracone on the lingual flank of stB in †*Pichipilus* (Abello, 2007: lámina 6H, I), †*Palaeo-thentes* (Engelman et al., 2016), and several other fossil paucituberculatans not included here, such as †*Phonocdromus*, †*Palaepanorthus*, †*Pitheca-lites*, and †*Perulestes* (Goin and Candela, 2004; Abello, 2013). We have also examined a subadult specimen of *Caenolestes fuliginosus* (BMNH 1954.295) and another of *C. caniventer* (BMNH 1954.302) in which the paracone is identifiable as a small but distinct structure on M3, where it is closely appressed to the lingual face of stB, and Martin (2013: fig. 1A, 611) reported a similar morphology in *Lestoros*. An alternative—but to us less convincing—interpretation of caenolestid crown homologies was expounded by Marshall (1980: fig. 5b) and was apparently followed by Springer et al. (1997: chars. 6, 7), Sánchez-Villa-gra (2001), Horovitz and Sánchez-Villagra (2003: chars. 154, 155), and a number of subsequent studies that used versions of their craniodental matrix (e.g., Sánchez-Villagra et al., 2007; Beck et al., 2008a; Horovitz et al., 2008, 2009); however, this was revised by Abello and Candela (2010: 1516; see also Beck, 2012, 2017a; Beck et al., 2014, 2016; Maga and Beck, 2017).

Among the paucituberculatans included in the current analysis, specimens of *Lestoros*, *Rhyncholestes*, †*Acdestis*, †*Palaeothentes*, and †*Stilotherium* that we examined appear to exhibit complete fusion between the paracone and stylar cusp B on all upper molars (but see Martin, 2013: fig. 1A, 611; Engelman, et al., 2016), so these taxa have been scored as state 2. Although we observed a vestigial paracone on M3 of two *Caenolestes* specimens (see above), most individuals lack any trace of the paracone, so we also scored *Caenolestes* as state 2. How-ever, because †*Pichipilus* retains a distinct para-

cone on M1–3 (see Abello, 2007), we scored this taxon as state 0.

Although the major upper molar cusp of †*Yalkaparidon* is presumably either the paracone or (perhaps more likely) the metacone (Beck et al., 2014), its homology is uncertain in the absence of annectant, dentally more plesiomorphic relatives, so we scored †*Yalkiparidon* as unknown ("?"). *Notoryctes* is also zalambdodont, with the major upper molar cusp homologous with the metacone (Archer et al., 2011), but a tiny remnant of the paracone, distinct from stylar cusp B, appears to be present on the premetacrista of some specimens (fig. 15D; Murray and Megirian, 2006b: fig. 6I), and the fossil notoryctid †*Naraboryctes* retained a paracone that is distinct from stB on M1–4 (Archer et al., 2011). Collectively, these observations suggest that the paracone has not fused with stB in *Notoryctes*, so we scored this taxon as state 0.

The paracone is clearly distinguishable in phascolarctids, †*Muramura* (Pledge, 2003: fig. 19.2), and on the unworn molars of *Lasiorhinus* (in which it is removed from the labial margin of the teeth and connected to stylar cusp B by an obvious preparacrista; Brewer et al., 2018: fig. 13.1). In bunodont, bunolophodont, and lophodont diprotodontians (figs. 17, 18A, 18C), however, the principal anterolabial cusp appears to be stB and the paracone is only weakly distinct (as in unworn molars of *Hypsiprymnodon moschatus*; fig. 18A; Ride, 1993: fig. 8) or is entirely absent, having largely or completely fused to stB or (equivalently) having been incorporated into the labial terminus of the protoloph (Ride, 1971; Archer, 1976e, 1984c: 683; Tedford et al., 1977; Woodburne and Clemens, 1986a: 96–97, 1986b: 20–21; Tedford and Woodburne, 1987: 416; Woodburne et al., 1987a: 600; Ride, 1993; Crosby and Archer, 2000: 331; Beck et al., 2020), so we scored these taxa as state 2. In †*Namilamadeta*, the paracone is basally fused with stB but is still clearly identifiable as a discrete structure on M1 and M2, whereas this cusp appears to have completely fused with stylar cusp B on M3 and M4 (Rich

and Archer, 1979; Archer, 1984b: 682–683; Pledge, 2005), an apparently autapomorphic trait (state 3).

Living pseudocheirids are selenodont, but Roberts (2008) and Roberts et al. (2008: 843) noted that the upper molars of the oldest known members of the family (the early Oligocene †*Pildra antiquus* and †*P. secundus*; Woodburne et al., 1987b) are only weakly selenodont, being dentally similar to Recent (bunolophodont) petaurids and, most strikingly, to the "bunoselenodont" petauroid †*Djaludjangi yadjana* (see Brammall, 1998 and Roberts, 2008: figs. 4.1.12A, 4.1.12B, 4.1.15). The existence of such structurally intermediate forms supports the conclusions of Roberts (2008) and Roberts et al. (2008: 843) that the fully selenodont molars of Recent pseudocheirids are derived from bunolophodont precursors, in which the principal labial cusps are stB and stD (as discussed above). On this assumption, the antero-internal pseudocheirid cusp previously identified by authors as the paraconule is probably the paracone, and the postero-internal pseudocheirid cusp previously identified as the "neometaconule" is the metacone (see also Black et al., 2012a: 132). Another consequence of this hypothesis is that the structure conventionally identified as the "centrocrista" in pseudocheirids is, in fact, a nonhomologous stylar crest linking stB (the "paracone" of authors) and stD (the "metacone").[13] Therefore, all pseudocheirids

---

[13] Support for this hypothesis of pseudocheirid cusp homologies is provided by the fact that in †*Priscakoala* (the dentally most plesiomorphic known phascolarctid; Black et al., 2012a), †*Muramura* (see Pledge, 1987c; 2003), and †*Namilamadeta* (see Rich and Archer, 1979; Pledge, 2005) the paracone and metacone are centrally placed on the tooth crown; prominent stylar cusps are present labial to the paracone and metacone, but there is no paraconule between the paracone and protocone nor any "neometaconule" between the metacone and metaconule. By contrast, in †*Djaludjangi* and the earliest known pseudocheirids (e.g., †*Pildra* spp.), the cusps referred to by previous authors (e.g., Woodburne et al., 1987b; Brammall, 1998; Roberts, 2008; Roberts et al., 2008) as the paracone and metacone (here identified as stB and stD, respectively) are located close to the labial margin of the tooth, and the "paraconule" and "neometaconule" (here identified here as
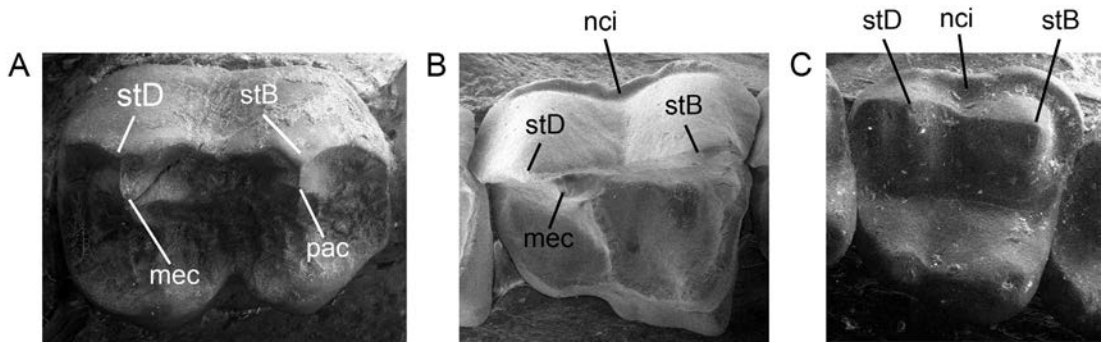
FIG. 18. Occlusal views of upper molars of *Hypsiprymnodon moschatus* (**A,** AMNH 160120 [right M1]), *Caenolestes fuliginosus* (**B,** BMNH 1954.295 [left M2, reversed]), and *Acrobates pygmaeus* (**C,** AMNH 37185 [right M2]). General features of upper molar crown morphology discussed in the text are illustrated, as are characters 132, 133, 136, 137, 140, 141, 143, 144, 145, and 146 (see main text for description of these characters and character states), as follows: *Hypsiprymnodon moschatus* 132(-), 133(0), 136(2), 137(1), 140(-), 141(0), 143(1), 144(1), 145(-), 146(-); *Caenolestes* 132(-), 133(1), 136(2), 137(-[but note that some *Caenolestes* specimens retain a paracone and can be scored as 1]), 140(-), 141(0), 143(1), 144(0), 145(-), 146(-); *Acrobates* 132(-), 133(1), 136(2), 137(-), 140(-), 141(0), 143(1), 144(0), 145(-), 146(-). Abbreviations: **mec,** metacone; **nci,** neomorphic cingulum; **pac,** paracone; **stB,** stylar cusp B; **stD,** stylar cusp D. Teeth are not shown to the same scale.

included in the current analysis have been scored as state 0.

Although states 0, 1, and 2 form a plausible morphocline, state 3 cannot be incorporated into a linear transformation series, so this character has not been ordered in any of our analyses.

Character 137. *Paracone and metacone subequal in height (0); or metacone much taller than paracone (1); or paracone absent or vestigial, only metacone present (2).* Among the tribosphenic metatherians we examined, the paracone and metacone are subequal in height (state 0) only in the didelphid *Caluromys* (Reig et al., 1987: fig. 12B), microbiotheriids (Marshall, 1982: figs. 9, 15; Szalay, 1993: fig. 15.3), and the peramelemorphian

the paracone and metacone, respectively) are smaller but still prominent, centrally located cusps with obvious crests (here identified as homologous with the centrocrista) emanating from them. This latter arrangment closely resembles the condition in *Hypsiprymnodon moschatus*, in which the large labial cusps appear to be stylar in origin and are connected by a prominent stylar crest, whereas the paracone and metacone are located more lingually and retain remnants of the centrocrista when unworn (fig. 18A; Ride, 1993: fig. 8). We note that enlargement of stB and stD, often in combination with reduction of the paracone and metacone, is a recurrent trend within Metatheria as a whole, and is likewise seen in several taxa not included in the current analysis (such as caroloameghiniids and polydolopimorphians; Beck et al., 2008b).
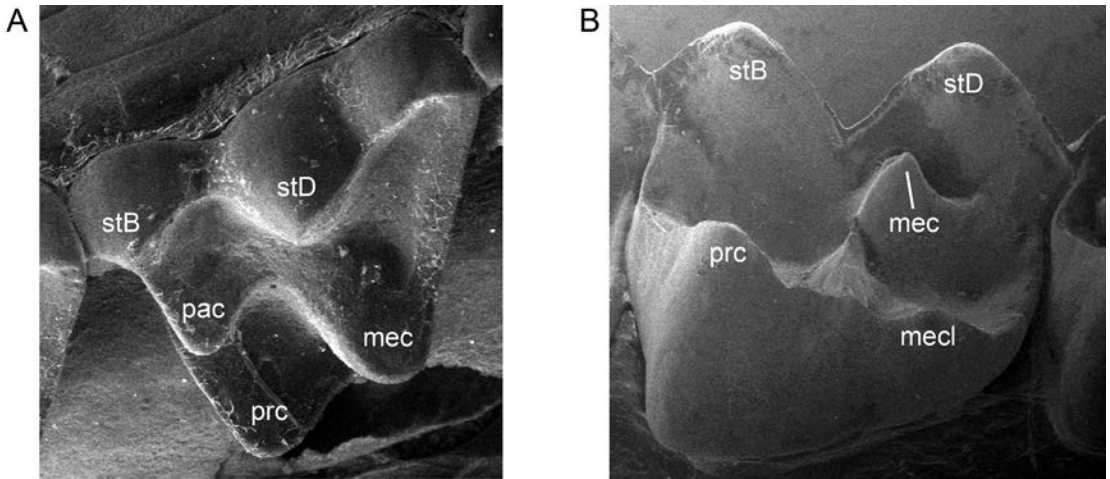
Chaeropus (Wright et al., 1991: plate 1A). By contrast, the metacone is clearly taller (state 1) in †*Pucadelphys,* †*Allqokirus,* †*Mayulestes,* †*Mimoperadectes,* †*Herpetotherium,* all didelphids except *Caluromys,* thylacinids, dasyurids, and all peramelemorphians except *Chaeropus.* Wroe et al. (2000: char. 8) and Wroe and Musser (2001: char. 8) coded *Didelphis* as exhibiting state 0, an obvious *lapsus.* The relative heights of the paracone and metacone vary along the molar row in some taxa, (e.g., †*Microbiotherium,* in which the metacone is taller than the paracone on M1 and M2 but subequal in height on M3; Marshall, 1982: fig. 9; Szalay, 1993: fig. 15.3); in such cases, we scored this character based on M3 only.

Among the paucituberculatans included in the current analysis, an obvious paracone is present and clearly shorter than the metacone in †*Evolestes* (Goin et al., 2007b) and †*Pichipilus* (Abello, 2007). Although the paracone is not identifiable in most specimens of *Caenolestes,* it is present on M3 of two subadult specimens (BMNH 1954.295 [= *C. fuliginosus*] and 1954.302 [= *C. caniventer*]) and is clearly shorter than the metacone. All examined specimens of other paucituberculatans (i.e., *Rhyncholestes, Lestoros,*

FIG. 19. Upper second molars (M2) of *Pseudantechinus macdonnellensis* (**A,** AMNH 196786 [left M2 in labio-occlusal view]) and *Caenolestes caniventer* (**B,** BMNH1954.302 [right M2 in lingual view and reversed]). General features of upper molar crown morphology discussed in the text are illustrated, as are characters 134, 135, 140, 141, 143, and 144 (see main text for description of these characters and character states), as follows: *Pseudantechinus* 134(1), 135(0), 140(3), 141(0), 143(0), 144(0); *Caenolestes* 134(0), 135(1), 140(-), 141(0), 143(1), 144(0). Abbreviations: **mec,** metacone; **mecl,** metaconule; **pac,** paracone; **prc,** protocone; **stB,** stylar cusp B; **stD,** stylar cusp D. Teeth are not shown to the same scale.

†*Acdestis*, †*Palaeothentes*, and †*Stilotherium*) lack an identifiable paracone and have been scored as inapplicable ("-"; but see Martin, 2013: fig. 1A, 611; Engelman, et al., 2016).

In most selenodont diprotodontians that retain a paracone and metacone distinct from the stylar cusps, namely phascolarctids, wynyardiids and pseudocheirids (note that in pseudocheirids, we assume that the "paraconule" and "neometaconule" of previous authors [e.g., Archer, 1984b; Woodburne et al., 1987; Roberts, 2008; Roberts et al., 2008] actually represent the paracone and metacone; see char. 136), the paracone and metacone are usually subequal in height, although the paracone is sometimes slightly taller, particularly on M1 and M2. However, *Ilaria* is an exception, with the metacone distinctly taller than the paracone on M1–3 (Tedford and Woodburne, 1987). A distinct paracone and metacone are also present and subequal in height on the unworn molars of *Lasiorhinus* (Brewer et al., 2018: fig. 13.1). In most bunodont, bunolophodont, and lophodont diprotodontians the paracone and metacone are not identifiable as distinct cusps due to fusion with stylar elements and/or incorporation into the protoloph and metaloph respectively (see char. 136), so we scored these taxa as inapplicable ("-"). The exceptions are *Hypsiprymnodon moschatus* and *H.* †*bartholomaii*, in which the paracone and metacone (identified as the "protoconule" and "neometaconule" respectively by Flannery and Archer, 1987c) are identifiable as distinct cusps (see char. 136; fig. 18A, see also Ride, 1993: fig. 8); in both taxa the paracone appears only slightly taller than the metacone, so we scored both as state 0.

The zalambdodont morphology of *Notoryctes* resulted from extreme reduction of the paracone (Archer et al., 2011), a distinct condition we coded as an additional state (state 2). This hypothesis is supported by the presence of what may be a tiny remnant of the paracone in some *Notoryctes* specimens (fig. 15D; Murray and Megirian, 2006b: fig. 6I), and the presence of a greatly reduced (but still identifiable) paracone in the fossil notoryctid (not included here) †*Naraboryctes* (Archer et al., 2011). Although

Beck et al. (2014) concluded that the major cusp of the upper molars of †*Yalkaparidon* probably represents the metacone based on occlusal relations (following Asher et al., 2007: 7), this identification remains tentative in the absence of taxa exhibiting intermediate morphologies. Indeed, occlusal relations are evidently not an infallible guide to cusp homologies, as they led Asher et al. (2007: 7) to identify the major upper molar cusp of the meridiolestidan "dryolestoid" †*Necrolestes* as probably representing the metacone, whereas subsequent evidence strongly suggests that it is in fact the paracone (Rougier et al., 2012; O'Meara and Thompson, 2014). Even if the major cusp were shown to be the metacone in †*Yalkaparidon*, it would still be unclear whether the paracone had been suppressed (as in *Notoryctes*) or lost via another mechanism (e.g., by fusion with stylar cusp B; see char. 136); we therefore scored †*Yalkaparidon* as unknown ("?") for this character.

We score this character as inapplicable ("-") for *Myrmecobius*, in which homologs of the paracone and/or metacone cannot be distinguished with certainty (Archer, 1984b: 641–642), and *Tarsipes*, in which the entire postcanine dentition is reduced to tiny spicules of enamel (see char. 113).

Character 138. *M1 preparacrista present (0); or absent or indistinct (1).* The preparacrista of conventionally tribosphenic metatherians is a low crest that extends anterolabially or labially from the apex of the paracone to terminate on the stylar shelf at or near stA or stB (figs. 14, 15A, 19A, 20A). By contrast, several authors (e.g., Archer, 1976c; Muirhead, 1994, 2000; Muirhead and Filan, 1995; Travouillon et al., 2010) have remarked on the unusual morphology of the M1 "preparacrista" of peramelemorphians, in which a tall crest passes *posterolabially* from the paracone to connect with a large stylar cusp at or near the stC position (but usually identified as stB), with which it forms a prominent crescentic or bladelike structure (fig. 20B; see also Turnbull et al., 2003: fig. 18.1). However, in *Chaeropus* it can be seen that two crests extend from the paracone of M1; this morphology is most obvious in

young *Chaeropus* specimens with unworn molars (e.g., AM PA422; Travouillon et al., 2019: fig. 4A), but can still be observed in some specimens with worn teeth (Travouillon et al., 2019: figs. 7c, 12a). One of these crests extends anterolabially and diminishes rapidly in height, terminating at stA near the anterolabial corner of the tooth (Wright et al., 1991: fig. 3); in height and orientation, this crest closely resembles the preparacrista of conventionally tribosphenic metatherians (such as didelphids). The second crest, however, is much taller and extends posterolabially to a cusp at the stC position (but usually referred to as "stB"; Archer, 1976c; Muirhead, 1994, 2000; Muirhead and Filan, 1995; Travouillon, et al., 2010), resembling the "preparacrista" previously described from M1 of other peramelemorphians. Because two homologous structures cannot (by definition) coexist in the same taxon (Patterson, 1982), we infer that the tall, posterolabially directed crest connecting the paracone to stB on the M1 of peramelemorphians is not the preparacrista, but a neomorph that we here designate the "pseudopreparacrista" (see char. 139). On this hypothesis, we scored the preparacrista as absent (state 1) in all peramelemorphians except *Chaeropus* (which we scored as "0").

In *Neophascogale* (e.g., AMNH 156343 and 109516), there appear to be two separate crests extending from the paracone: one reduces in height as it extends anterolabially from the apex of the paracone, terminating at a stylar cusp (?StA) at the anterolabial corner of the tooth, and we identify it here as the preparacrista; the second, taller crest, extends posterolabially, terminating at StB, and we refer to it as the pseudopreparacrista, based on its overall topological similarity to the crest to which we assign that name in peramelemorphians. The condition seen in *Neophascogale* may explain Archer's (1982: 429) enigmatic comment that "some of the unusual stylar shelf morphology [of the molars, and particularly M1, of *Neophascogale* and *Phascolosorex*] is reminiscent of that found in bandicoots." However, the condition in the *Phascolosorex* species we have used for scoring
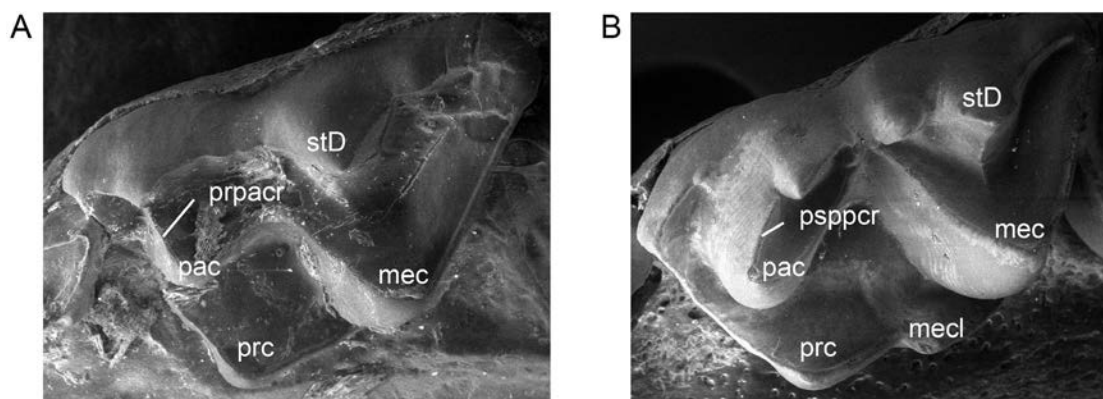
FIG. 20. Left first upper molars (M1) of *Murexia longicaudata* (**A,** AMNH 101970) and *Echymipera kalubu* (**B,** AMNH 221654). General features of upper molar crown morphology discussed in the text are illustrated, as are characters 132, 133, 136, 137, 138, 139, 140, 141, 143, and 144 (see main text for description of these characters and character states), as follows: *Murexia* 132(1), 133(0), 136(0), 137(1), 138(0), 139(0), 140(3), 141(0), 143(0), 144(0); *Echymipera* 132(1), 133(0), (136(0), 137(1), 138(1), 139(1), 140(4), 141(0), 143(1), 144(0). Abbreviations: **mec,** metacone; **mecl,** metaconule; **pac,** paracone; **prc,** protocone; **prpacr,** preparacrista; **psppcr,** pseudopreparacrista; **stD,** stylar cusp D. Teeth are not shown to the same scale.

purposes here, *P. dorsalis*, resembles most other dasyurids in having a preparacrista only, rather than preparacrista and pseudopreparacrista as in *Neophascogale*.

We scored dasyuromorphians in which the paracone and stB are consistently fused on M1 (char. 136) as inapplicable ("-"). We also scored this character as inapplicable for *Myrmecobius*, *Notoryctes*, †*Yalkaparidon*, and most examined paucituberculatans, because examined specimens of these taxa lack unambiguously identifiable paracones (a necessary landmark for identifying presence or absence of the paracrista; see char. 136). However, the M1 preparacrista is absent in †*Evolestes* (Goin et al., 2010: fig. 6.1G-H), and present (albeit very short) in †*Pichipilus* (Abello, 2007: lámina 6H-I).

Among diprotodontians, the preparacrista is unambiguously present on M1 of pseudocheirids, wynyardiids, and phascolarctids. In these taxa, all of which we scored as state 0, the preparacrista is anterolabially or labially directed. By contrast, in lophodont and bunolophodont diprotodontians a low crest usually extends anteriorly from the labial end of the protoloph toward the anterolabial corner of the tooth. Although

this crest has been called the preparacrista by numerous authors (e.g., Flannery and Rich, 1986; Cooke, 1997c; Prideaux, 2004; Kear et al., 2007; Prideaux and Warburton, 2008, 2009; Bates et al., 2014; Black et al., 2014c; Travouillon et al., 2014b, 2015a, 2016; Butler et al., 2016, 2018), we believe it to be a remnant of a stylar crest (on the hypothesis that the labial terminus of the protoloph is stB rather than the paracone; see char. 136). Instead, the preparacristae of lophodont and bunolophodont diprotodontians may have been incorporated into the labial portion of the protoloph (see chars. 136, 144). Therefore, we scored these taxa as inapplicable ("-").

Character 139. *M1 pseudopreparacrista absent (0); or present (1).* As discussed above (char. 138), the tall crest that extends posterolabially from the paracone to stB (or stC) on M1 of most peramelemorphians (fig. 20B) does not appear to be homologous with the preparacrista but, instead, appears to be a neomorph—the pseudopreparacrista. This crest is present (state 1) on the M1 of all extant and fossil peramelemorphians that we examined, with the exception of *Macrotis* (in which the preparacrista and pseudopreparacrista are both consistently

absent, even on minimally worn specimens; state 0), some specimens of *Isoodon* (e.g., AMNH 154499), and *Microperoryctes* (e.g., left side of AMNH 108546), with the latter two taxa scored as polymorphic ("0+1"). As already discussed (see char. 138), a topologically and morphologically similar (although presumably independently derived) crest is seen in the dasyurid *Neophascogale* (e.g., AMNH 156343 and 109516), which has also been scored as state 1 here.

As for the preceding character, we coded this character as inapplicable ("-") in *Myrmecobius*, *Notoryctes*, †*Yalkaparidon*, and all examined paucituberculatans except †*Evolestes* and †*Pichipilus* (in both of which the pseudopreparacrista is undoubtedly absent; see Goin, et al., 2010: fig. 6.1G-H; Abello, 2007: lámina 6H-I) because the absence of an identifiable homolog of the paracone in these taxa precludes meaningful scoring of this character.

Among diprotodontians, an M1 pseudopreparacrista is unequivocally absent in pseudocheirids, wynyardiids and phascolarctids, all of which we scored as state 0. As explained above in the context of scoring the preparacrista character, the probable incorporation of the paracone into the protoloph of lophodont and bunolophodont diprotodontians precludes meaningful observations from these taxa, which were all scored as inapplicable ("-").

Character 140. *Centrocrista straight, midpoint almost level with the floor of the trigon basin (0); or straight, midpoint high above floor of trigon basin (1); or weakly Λ-shaped, midpoint distinctly elevated above floor of trigon basin (2); or strongly Λ-shaped, midpoint high above floor of trigon basin (3); or centrocrista discontinuous, postparacrista and premetacrista extending to labial margin of tooth and forming a narrowly open embrasure (4); or centrocrista discontinuous, with postparacrista and premetacrista terminating in stylar region, not extending to labial margin of tooth (5).* Tribosphenic metatherian molars exhibit considerable variation in the shape of the centrocrista (postparacrista + premetacrista), which is associated with a traditional and some-

times confusing descriptive nomenclature (see discussion by Voss and Jansa, 2003: char. 58; 2009: 51–52). Taxa with a Λ-shaped (labially inflected) centrocrista are traditionally described as "dilambdodont" because the ectoloph (preparacrista + centrocrista + postmetacrista) then resembles two inverted capital Greek lambdas, whereas taxa with a straight centrocrista have often been called "predilambdodont" (e.g., by Reig et al., 1987) or rectilinear.

In some taxa with a straight centrocrista (e.g., †*Mimoperadectes*, *Caluromysiops*, and microbiotheriids) the midpoint is almost level with the floor of the trigon basin (state 0; see discussion by Johanson, 1996a), but †*Mayulestes* (Muizon, 1998: fig. 2; Muizon et al., 2018: fig. 18B), †*Allqokirus* (Muizon et al., 2018: figs. 7B, 8B, 9, 10A) and *Thylacinus* (Muizon and Lange-Badré, 1997: fig. 4A) have a straight centrocrista that is elevated above the trigon basin (state 1).

In taxa with a labially inflected centrocrista, the apex of this crest is always raised above the trigon basin, but in some it is only weakly Λ-shaped (state 2), as in †*Pucadelphys* (Marshall and Muizon, 1995: figs. 6B, 7B; Ladevèze et al., 2011: fig. 4d-f), †*Sparassocynus* (Reig et al., 1987: fig. 29B; Beck and Taglioretti, 2020: fig. 3a), †*Thylophorops* (Reig et al., 1987: fig. 28B), many Recent didelphids, †*Badjcinus* (Muirhead and Wroe, 1998: fig. 2B), and †*Nimbacinus* (Muirhead and Archer, 1990: fig. 1B).

By contrast, in †*Herpetotherium* (Fox, 1983: figs. 1A, 2A; ; Horovitz et al., 2008: plate 1A; Korth, 2018: fig. 6a), †*Thylatheridium* (Reig, 1952: fig. 11A; Reig et al., 1987: fig. 25A), many Recent didelphids (e.g., *Marmosa* [fig. 14]), †*Barinya*, †*Mutpuracinus* (Murray and Megirian, 2000: fig. 3), all Recent dasyurids (e.g., *Dasyurus* [Smits and Evans, 2012: fig. 1A]; *Pseudantechinus* [fig. 19A]; *Murexia* [fig. 20A]), and †*Yarala* (Muirhead and Filan, 1995: figs. 1.2, 2.2), the centrocrista is strongly Λ-shaped, with the postparacrista and premetacrista of unworn molars forming a lingual angle of 90 degrees or less in occlusal view (state 3). Wroe et al. (2000: char. 10) scored *Sarcophilus* as having a rectilinear centrocrista, but we con-

sider the centocrista of this taxon to be strongly dilambdodont, resembling that of other dasyurids (see, e.g., Sakai and Yamada, 1992: fig. 2), so we scored it as state 3.

Recent peramelemorphian molars are also strongly dilambdodont, but the centrocrista is usually discontinuous (state 4; figs. 15C, 20B), because the postparacrista and premetacrista extend through the stylar region to terminate on the labial margin of the tooth, where they are separated by a gap (Archer, 1976c, 1976e, 1984c; Muirhead, 1994; Muirhead and Filan, 1995; Kear et al., 2016; Warburton and Travouillon, 2016; Travouillon and Phillips, 2018); Muirhead and Filan (1995: 131) described this condition as resulting from the centrocrista "breaching" the ectoloph, whereas other authors have referred to it as an "incomplete" centrocrista (e.g., Travouillon et al., 2010, 2013b, 2014a; Kear et al., 2016). Although such a discontinuous centrocrista is characteristic of most Recent peramelemorphians, we observed a few specimens of *Peroryctes* in which the centrocrista is strongly dilambdodont but continuous (e.g., AMNH 151958; see also comments by Aplin et al., 2010: 20, fig. 10)[14]; nevertheless, we scored *Peroryctes* as state 4 based on the modal condition. In †*Galadi*, the centrocrista is strongly dilambdodont but continuous on M1 and M2, whereas it is discontinuous on M3 (Travouillon et al., 2010); we therefore scored †*Galadi* as polymorphic ("3+4").

Among diprotodontians, the centrocrista of phascolarctids (see, e.g., Archer, 1976e, 1984c: fig. 62; Woodburne et al., 1987c; Black et al., 2014a) and wynyardiids (see, e.g., Pledge, 2003: fig. 19.2) is discontinuous, with the postparacrista and premetacrista extending to the labial margin of the tooth and forming an open embrasure, resembling in this respect the morphology seen in most peramelemorphians; thus, we scored representatives of both taxa as state 4.

Based on our hypothesis of pseudocheirid cusp homologies (in which the cusps referred to by most recent authors as the paraconule and "neometaconule" are identified as the paracone and metacone respectively; see char. 136), the centrocrista of pseudocheirids is also discontinuous, because the labial ends of the postparacrista (the "postparaconulecrista" of previous authors) and premetacrista (the "preneometaconulecrista" of previous authors) are separated by a distinct gap (Archer, 1984c: fig. 178A-C; Roberts, 2008; Roberts et al., 2008). However, these crests do not extend to the labial margin of the upper molars, but instead terminate lingual to the major labial cusps (identified here as stB and stD), a morphology we score as state 5.

In many lophodont and bunolophodont diprotodontians (e.g., acrobatids, burramyids, petaurids), an anteroposteriorly directed crest connects the labial ends of the protoloph and metaloph. Although this crest has been homologized with the centrocrista by previous authors (e.g., Springer et al., 1997: char. 8; Horovitz and Sánchez-Villagra, 2003: char. 156), this crest cannot be the centrocrista if the labial termini of the protoloph and metaloph are, in fact, stylar cusps (see chars. 134–136). In fact, what appears to be a vestigial centrocrista is present lingual to the crest connecting stB and stD on the unworn molars of *Hypsiprymnodon moschatus* (fig. 18A; see also Ride, 1993: 451, fig. 8). Although this vestige appears to be approximately linear in *H. moschatus*, the postparacrista and premetacrista are weakly developed and do not form an obviously continuous crest, making interpretation difficult. We therefore scored *H. moschatus* and all other lophodont and bunolophodont diprotodontians as inapplicable ("-").

In †*Evolestes* the centrocrista of M2 is discontinuous: the postparacrista terminates at the base of the lingual face of stB, the premetacrista terminates at the base of the lingual face of stD, and the labial ends of these crests are separated by a narrow gap (Goin et al., 2007b; Abello, 2013: fig. 2A). Although this morphology most closely resembles state 5 as defined above, the M3 cen-

---

[14] Travouillon and Phillips (2018: 241) also observed that the centrocrista becomes continuous with wear in species of the Recent peramelemorphian genera *Peroryctes*, *Echymipera*, *Rhynchomeles*, and *Microperoryctes*.

trocrista of this taxon is strongly dilambdodont but complete (Goin et al., 2007b). We have therefore scored †*Evolestes* as polymorphic ("3+5").

Specimens of most of the other paucituberculatans we examined for this study lack an unambiguous homolog of the centrocrista because the paracone is fused with stB and a distinct postparacrista is not present (see char. 136). Thus, we scored *Caenolestes*, *Lestoros*, *Rhyncholestes*, †*Acdestis*, †*Palaeothentes*, and †*Stilotherium* as inapplicable ("-") for this character. By contrast, Goin et al. (2007b: char. 31; 2009a: char. 33) scored *Caenolestes*, *Rhyncholestes*, and †*Stilotherium* as having a discontinuous centrocrista. However, the centrocrista is identifiable in †*Pichipilus*, in which the paracone and metacone are both distinct on M1–3 (Abello, 2007; 2013: fig. 2F, I); the centrocrista is discontinuous in this taxon, with the postparacrista and premetacrista terminating against the enlarged stylar cusps (as on M2 of †*Evolestes*), so we scored it as state 5.

This character was also scored as inapplicable for *Tarsipes*, *Notoryctes*, †*Yalkaparidon*, and *Myrmecobius*, all of which lack an unambiguously identifiable centrocrista. Because the states we define do not form an obvious morphocline, we did not order this character in any of our analyses. As discussed by Beck et al. (2008b), the shape of the centrocrista can change due to wear by the hypoconid (with the centrocrista becoming increasingly strongly inflected in more heavily worn molars), so we scored this character based on specimens with unworn or lightly worn teeth (see also comments by Travouillon and Phillips, 2018: 241, on the impact of wear on centrocrista shape in peramelemorphians).

Character 141. *Protocone present (0); or absent (1).* Among the metatherians included in this study, the zalambdodont taxon †*Yalkaparidon* uniquely lacks the protocone and other related structures—preprotocrista and postprotocrista—lingual to the metacone (Archer et al., 1988; Beck, 2009; Beck et al., 2014). Although *Notoryctes* is also zalambdodont, it resembles nonzalambdodont metatherians in retaining a distinct protocone (fig. 15D; Asher and Sánchez-

Villagra, 2005: fig. 6A; Murray and Megirian, 2006b: fig. 6I; Archer et al., 2011: fig. 1).

Character 142. *Preprotocrista and anterolabial cingulum joined to form a continuous shelf along anterior margin of M3 (0); or preprotocrista and anterolabial cingulum separate on M3, not forming a continuous shelf (1).* The preprotocrista of many metatherians passes anterolabially around the base of the paracone and merges with the anterolabial cingulum (or paracingulum; see Van Valen, 1966: fig 1A; Marshall, 1987: fig. 2; Reig et al., 1987: fig. 1), forming a continuous shelf along the anterior margin of one or more upper molars (Voss and Jansa, 2003: fig. 13, left); such taxa include †*Mimoperadectes* (Horovitz et al., 2009: fig. 1), †*Allqokirus* (Muizon et al., 2018: figs. 7B, 8B, 10A), †*Herpetotherium* (Horovitz et al., 2008: plate 1A), many Recent didelphids (e.g., *Caluromys*, *Glironia*, *Hyladelphys*, *Marmosa*; Voss and Jansa, 2003; 2009), microbiotheriids (Marshall, 1982: fig. 9 and 16), †*Galadi* (Travouillon et al., 2010), *Echymipera*, *Isoodon*, *Macrotis*, many Recent dasyurids (e.g., *Antechinus*, *Murexia*, *Phascogale*, *Planigale*), phascolarctids, wynyardiids, and pseudocheirids. By contrast, the preprotocrista terminates at or near the base of the paracone, without contacting the anterolabial cingulum (Voss and Jansa, 2003: fig. 13, right), in other Recent didelphids (e.g., *Didelphis*, *Chacodelphys*, *Chironectes*, *Lestodelphys*, *Lutreolina*, *Metachirus*, *Monodelphis*, *Philander*, *Thylamys*; Voss and Jansa, 2003, 2009), fossil didelphids (e.g., †*Sparassocynus*, †*Thylophorops*, †*Thylatheridium*), and many nondidelphimorphian metatherians, including †*Pucadelphys* (Marshall and Muizon, 1995: figs. 6B, 7B; Ladevèze et al., 2011: fig. 4d–f), †*Mayulestes* (Muizon, 1998: fig. 2), †*Evolestes* (Goin et al., 2007b: text figs. 2, 3), *Notoryctes* (fig. 15D; Asher and Sánchez-Villagra, 2005: fig. 6A; Murray and Megirian, 2006b: fig. 6I; Archer et al., 2011: fig. 1), †*Yarala* (Muirhead and Filan, 1995: figs. 1.2, 2.2), *Rhynchomeles*, *Perorytes* (Aplin et al., 2010: fig. 10C, D), *Microperorytes*, and some dasyuromorphians (e.g., thylacinids, †*Barinya*, and several Recent dasyurids).

We scored this character as inapplicable ("-") in all taxa in which an anterolabial cingulum is absent on M3 or cannot be certainly identified as such: this includes most paucituberculatans (except †*Evolestes*; see above), †*Yalkaparidon*, *Notoryctes*, *Perameles*, *Chaeropus*, *Myrmecobius*, and all diprotodontians except †*Ilaria*, phascolarctids, and wynyardiids.

Character 143. *Upper molar posterolingual cusp absent (0); or posterolingual cusp formed by metaconule (1), or posterolingual cusp is the metacone (2).* A distinct posterolingual cusp is consistently absent from the upper molars of †*Mayulestes* (Muizon, 1998: fig. 2; Muizon et al., 2018: fig. 10B), †*Allqokirus* (Muizon et al., 2018: figs. 7B, 8B, 9, 10A), †*Pucadelphys* (Marshall and Muizon, 1995: figs. 6B, 7B; Ladevèze et al., 2011: fig. 4d–f), †*Mimoperadectes* (Horovitz et al., 2009: fig. 1), †*Herpetotherium* (Horovitz et al., 2008: plate 1A), didelphids, most dasyuromorphians, microbiotheriids, *Notoryctes* (fig. 15D; Asher and Sánchez-Villagra, 2005: fig. 6A; Murray and Megirian, 2006b: fig. 6I; Archer et al., 2011: fig. 1), and †*Yarala* (Muirhead and Filan, 1995: figs. 1.2, 2.2), all of which have triangular or subtriangular teeth (state 0).

By contrast, a distinct posterolingual cusp (or "hypocone") is present in many other taxa (figs. 15B, 15C, 16, 17, 18, 20B), giving their upper molars a more quadrilateral occlusal outline (see, e.g., Springer et al., 1997: char. 5; Horovitz and Sánchez-Villagra, 2003: char. 153). The homology of this structure has been disputed by several authors (e.g., Tedford and Woodburne, 1987; Sánchez-Villagra and Kay, 1996; Tedford and Woodburne, 1998). In peramelemorphians (with the notable exception of *Macrotis*), and several diprotodontian groups (e.g., acrobatids, burramyids, and petaurids), this cusp occupies the postprotocrista, and we agree with Tedford and Woodburne (1987; 1998) that it probably corresponds to the metaconule of the tribosphenic bauplan; for this reason, Beck et al. (2008b) referred to it as a "metaconular hypocone." However, other authors (e.g., Ladevèze et al., 2010; Gheerbrant et al., 2016) have used the term "pseudohypocone" for this cusp to distinguish it from a "true" hypocone (= "cingular hypocone" sensu Beck et al., 2008b), which is a neomorphic outgrowth of the talon or postprotocingulum. A virtually continuous array of intermediate forms (e.g., the macropodiform †*Jackmahoneya*; Ride, 1993) plausibly establishes the metaconular origin of the posterolingual cusp (state 1) in other diprotodontians. Among thylacoleonids, the upper molars of †*Lekanoleo* are relatively quadrilateral in outline, due to the presence of a well-developed, posterolingual metaconule (state 1; see Gillespie, 1997: figs. 2, 3; Gillespie et al., 2020: fig. 4), but this cusp is less well developed and more labially positioned in †*Wakaleo*, resulting in a more triangular outline (state 0; see Murray et al., 1987: fig. 8); the sole upper molar (M1) of †*Thylacoleo*, meanwhile is highly modified, with uncertain cusp homologies (Archer and Rich, 1982; Archer, 1984c: fig. 128), and so we score it as unknown ("?") here.

By contrast, the posterolingual cusp of *Macrotis* appears to be the metacone (state 2), the large posterolabial cusp in that taxon corresponding to a hypertrophied stylar element (usually interpreted as stylar cusp D; Bensley, 1903: fig. 52; Archer and Kirsch, 1977; Archer, 1984c). Presence or absence of an enlarged posterolingual cusp appears to be constant within most of our terminal taxa, with the notable exception of *Microperoyctes ornata*, in some specimens of which the metaconule is large (giving the upper molars a somewhat quadrilateral appearance; e.g., AMNH 108546), whereas in others the metaconule is distinctly smaller (and the upper molars correspondingly more triangular in occlusal outline; e.g., AMNH 190939). We therefore scored *Microperoryctes* as polymorphic ("0+1").

The large posterolingual cusp on M1–3 of paucituberculatans has been interpreted as the metaconule by most recent authors (e.g., Marshall, 1987; Goin and Candela, 2004; Abello, 2007, 2013; Goin et al., 2007b; Rincón et al., 2015; Engelman et al., 2016), but as a "true" hypocone ("cingular hypocone" sensu Beck et al., 2008b) by Hunter

and Jernvall (1995: table 1). The reasoning behind the latter authors' interpretation was not made explicit, but it is seemingly supported by the existence of a crest on the unworn molars of *Caenolestes* (figs. 15B, 18B, 19B) and *Rhyncholestes* that extends labially from a point on the lingual margin of the tooth about midway between the protocone and the posterolingual cusp and terminates at the base of the metacone (which is partially fused to the lingual face of stylar cusp D). If this crest is assumed to be the postprotocrista, then the posterolingual cusp in these taxa would appear not to be the metaconule, which (when present in tribosphenic metatherians) always lies on the postprotocrista (Tedford and Woodburne, 1998), not posterolingual to it. However, evidence from fossil taxa (e.g., †*Evolestes*, †*Palaeothentes*, †*Palaepanorthus*, †*Perulestes*, †*Pitheculites*, †*Parabderites*, †*Acdestis*) that provide a graded series of morphological intermediates from tribosphenic molars to the nontribosphenic teeth of Recent caenolestids suggests that the crest in question is, in fact, the premetaconulecrista or "pre-metaconular crest" (Goin and Candela, 2004; Abello, 2007, 2013; Goin et al., 2007b; Rincón et al., 2015). We therefore scored the posterolingual cusp of Recent caenolestids and other paucituberculatans as representing the metaconule, in agreement with most recent authors (Goin and Candela, 2004; Abello, 2007, 2013; Goin et al., 2007b; Rincón et al., 2015; Engelman et al., 2016).

In *Notoryctes* (fig. 15D; Asher and Sánchez-Villagra, 2005: fig. 6A; Murray and Megirian, 2006b: fig. 6I; see Archer et al., 2011: fig. 1), both the protocone and postprotocrista are identifiable and there is no enlarged metaconule on the postprotocrista, so we scored this taxon as state 0. However, †*Yalkaparidon* (in which the entire region of the tooth crown lingual to the metacone is absent; see char. 141), *Tarsipes* (in which the molars are so reduced that individual cusps can no longer be identified; char. 113), and *Myrmecobius* (whose teeth are too derived for this character to be scored confidently) were all scored as inapplicable ("-"). In the absence of any clear sequence of transformations among these

alternative conditions, we treated this character as unordered (nonadditive) in all the phylogenetic analyses reported below.

Character 144. *Principal labial and lingual cusps of upper molars not connected by transverse lophs (0); or connected by incipient lophs (1); or connected by well-developed lophs (2).* The principal labial and lingual cusps of tribosphenic metatherian molars are not connected by transverse lophs (state 0), nor are transverse lophs present in such nontribosphenic taxa as paucituberculatans, peramelemorphians, phascolarctids, pseudocheirids, and *Acrobates*. By contrast, in fully lophodont (or "bilophodont") diprotodontians, each tooth is provided with two tall transverse crests (state 2) that are relatively constant in height throughout their length. On lophodont upper molars, the more anterior protoloph extends labially from the protocone to terminate labially at what we identify as stylar cusp B, whereas the metaloph connects the metaconule (or "hypocone"; see char. 143) to what we interpret as stylar cusp D (fig. 17D). On lophodont lower molars, the protolophid connects the protoconid with the metaconid, and the hypolophid connects the hypoconid with the entoconid. Among the taxa included in this study, only †diprotodontids, Recent macropodids and some fossil macropodiforms (e.g., †*Hadronomas*, †*Rhizosthenurus*, †*Balbaroo*, †*Bulungamaya*, †*Ganguroo*, and †*Ganawamaya*) are fully lophodont.

An apparently annectant condition (state 1) is exhibited by many other diprotodontian taxa that are sometimes referred to as "incipiently lophoid" (by Bensley, 1903: 143) or "bunolophodont" (e.g., by Case, 1984; Flannery et al., 1984; Woodburne, 1984a; Springer et al., 1997: char. 42; Kear and Cooke, 2001; Horovitz and Sánchez-Villagra, 2003: char. 173; Prideaux, 2004; Kear et al., 2007; Prideaux and Warburton, 2010: char. 23). In this morphotype the protoloph and metaloph are less distinct and lower (particularly toward their midpoints) than in fully lophodont taxa, and the cusps at the ends of each loph are identifiable as distinct structures rather than

seamlessly incorporated into the lophs (figs. 17A–C, 18A). Additionally, remnants of the paracone and metacone can sometimes be distinguished on the unworn teeth of some bunolophodont taxa (chars. 134–136; figs. 17B, 18A).

Within Diprotodontia, we observed an almost continuous range of intermediate morphologies between the nonlophodont condition (state 0) and bunolophodonty (state 1). We scored taxa in which lophs are identifiable on unworn upper molars as state 1, even if such lophs were only weakly developed; only taxa lacking any trace of lophodonty were scored as state 0. Under this scoring criterion, bunolophodont taxa (scored as state 1) include phalangerids, *Petaurus*, *Gymnobelideus*, burramyids, *Distoechurus*, several nonmacropodid macropodiforms (*Aepyprymnus*, *Bettongia* and ?*Bettongia* †*moyesi*, *Caloprymnus*, *Potorous*, *Hypsiprymnodon moschatus* [figs. 17B, 18A], *H.* †*bartholomaii*, and †*Ekaltadeta*), wynyardiids, and Recent vombatids (the molars of †*Warendja* are too worn to score for occlusal characters). In fact, with the exception of pseudocheirids and phascolarctids (both of which are selenodont), most diprotodontians included in this study are either incipiently or fully lophodont. Strikingly, the upper molars of †*Muramura* and †*Namilamadeta* are both selenodont and incipiently lophodont (Rich and Archer, 1979; Pledge, 1987c; 2003; 2005; Beck et al., 2020), as is another fossil taxon not included here, the petauroid †*Djaludjangi* (Brammall, 1998).

Noteworthy nonlophodont exceptions among diprotodontians include *Acrobates* (fig. 18C), *Dactylopsila*, *Dactylonax*, and †*Thylacoleo* (the molars of †*Lekanoleo*, however, exhibit weakly developed lophs; Gillespie, 1997: fig. 2; Gillespie et al., 2020: fig. 4); all these bunodont taxa have been scored as state 0. †*Ilaria* lacks any trace of lophs on its (strongly selenodont) upper molars, and so has also been scored as state 0, but we note that its lower molars have weakly developed transverse lophids (Tedford and Woodburne, 1987). We scored †*Yalkaparidon* (in which the entire region of the crown lingual to the metacone is absent; char. 141) and *Tarsipes* (in which

the upper molars are spicules lacking any identifiable structures; char. 113) as inapplicable ("-").

Character 145. *Protoloph and metaloph not connected by a median enamel crest (0); or protoloph and metaloph connected by a midlink (1).* The protoloph and metaloph are entirely separate structures in most incipiently and fully lophodont diprotodontians (e.g., *Trichosurus* [fig. 17C]), but a median enamel crest—the so-called midlink (e.g., Stirton, 1955; Tedford, 1966; Woodburne, 1967; Bartholomai, 1971b; Sanson, 1980)—connects the protoloph and metaloph in all examined Recent macropodids (e.g., *Lagostrophus* [fig. 17D]) and several fossil macropodiforms (e.g., †*Hadronomas*, †*Rhizosthenurus*, †*Balbaroo*, †*Ganawamaya*). Within Macropodiformes, this crest appears to be formed at least partially by the postprotocrista: in unworn specimens of at least some taxa (e.g., *Lagostrophus* [fig. 17D]), the anterior part of the midlink extends from the apex of the protocone. The postprotocrista is also present, extending from the protocone apex at the anterolingual margin of the tooth, in macropodiforms that lack a midlink (Woodburne, 1967; Cooke, 1999; 2000; Prideaux and Warburton, 2010: char. 25, fig. 5). By contrast, the midlink of palorchestid diprotodontoids (not included in this analysis) appears to have a different evolutionary origin (Murray, 1990; Black, 2006).

This character was scored as inapplicable ("-") for nonlophodont taxa and for incipiently lophodont taxa (see char. 144) in which the lophs are so weakly developed that it cannot be meaningfully scored (e.g., *Hypsiprymnodon moschatus* [figs. 17B, 18A]).

Character 146. *Metaloph without a posteriorly projecting median crest (0); or urocrista ("postlink") present (1).* A distinct enamel crest projecting posteriorly from the middle of the metaloph is observed in some macropodiforms (e.g., *Lagostrophus* [fig. 17D]). This crest has been called the postlink by some authors (Flannery, 1983: fig. 4; Flannery and Rich, 1986), but other researchers have applied that term to a different occlusal structure, namely the postmetaconule-

crista or posthypocrista (e.g., Tedford, 1966: fig. 3; Woodburne, 1967); we therefore follow Prideaux (2004) in referring to the crest in question as the urocrista.[15] Travouillon et al. (2014b; 2015a; 2016) and Butler et al. (2016), however, called this crest the neometaconule crista.

Among the Recent macropodoids included in this study, only *Lagostrophus* exhibits a distinct urocrista (fig. 17D). Contra Prideaux (2004: 209), we did not observe this crest in any examined specimens of *Dorcopsulus*, *Dendrolagus*, *Thylogale*, or *Wallabia*. However, an obvious urocrista is present in some specimens of †*Ganguroo* (see Travouillon et al., 2014b; Cooke et al., 2015) and †*Rhizosthenurus* (Kirkham, 2004: plate 9), both of which have been scored as polymorphic ("0+1"). This character was scored as inapplicable ("-") for nonlophodont taxa and for incipiently lophodont taxa (see char. 144) in which the lophs are so weakly developed that it cannot be meaningfully scored (e.g., *Hypsiprymnodon moschatus* [figs. 17B, 18A]).

Lower Incisors

Didelphids, microbiotheriids, and some nonmarsupial metatherians have four lower incisors, but many other living and extinct metatherians have three or fewer lower incisors, and the identity of the missing tooth (or teeth) in clades with fewer than four lower incisors has vexed researchers for many years. Although embryological studies (cited below) have sometimes been cited to support alternative theories about lower incisor homologies, we expect that

---

[15] As discussed above, we consider that the metacone of at least some lophodont diprotodontians has been incorporated into the middle of the metaloph, rather than forming its labial terminus (see also Ride, 1971; Archer, 1976d, 1984b: 683; Tedford et al., 1977; Tedford and Woodburne, 1987: 416; Woodburne et al., 1987b: 600; Ride, 1993; Crosby and Archer, 2000: 331; Beck et al., 2020). Thus, the "neometaconule" present within the metaloph of several plesiomorphic macropodiforms, such as †*Balbaroo* (see Cooke, 2000) and *Hypsiprymnodon* †*bartholomaii* (Flannery and Archer, 1987a) may, in fact, be a remnant of the metacone (see chars. 135, 137). If so, the urocrista (which, where present, extends posteriorly from the "neometaconule") may, in turn, be homologous with the postmetacrista of tribosphenic metatherians.

only the discovery of fossil intermediates between the unreduced dentitions exemplified by didelphids and the derived morphologies of other groups is likely to convincingly resolve these issues. In addition to taxonomic variation in number, metatherian lower incisors exhibit striking differences in morphology, most notably by the presence of an enlarged gliriform tooth of notoriously uncertain homology at the first erupted mandibular locus in paucituberculatans and diprotodontians.

Character 147. *Anteriormost lower incisor small and short crowned (0); or large, long crowned, and conspicuously procumbent (1).* Most metatherians have a small, short-crowned incisor at the anteriormost (mesialmost) mandibular dental locus (state 0). By contrast, the anteriormost lower incisor of paucituberculatans (e.g., *Caenolestes* [fig. 35]) and diprotodontians (figs. 44–54) is a large, long-crowned, procumbent tooth (state 1) that is sometimes described as "gliriform" by analogy with the corresponding mandibular teeth of rodents and lagomorphs. Many previous students of marsupial dental morphology (e.g., Luckett, 1994: char. 12; Springer et al., 1997: char. 33; Sánchez-Villagra, 2001: char. 33; Horovitz and Sánchez-Villagra, 2003: char. 167) have regarded these teeth as nonhomologous in paucituberculatans and diprotodontians (but see Beck et al., 2014; Beck, 2017a: char. 163; Maga and Beck, 2017: char. 163). This is based on evidence from serially sectioned developmental series of a few macropodids and phalangerids—(which have been used to conclude that the gliriform tooth in diprotodontians is i2, i3, or i4; e.g., Woodward, 1893; Dependorf, 1898; Hopewell-Smith and Marett Tims, 1911; Bolk, 1929; Engelhardt, 1932; Ride, 1962; Berkovitz, 1972b; Kirkpatrick, 1978)—and tooth-counts from fossil paucituberculatans (which have been used to argue that the gliriform tooth in Recent caenolestids is i1 or i2; Sinclair, 1906; Ride, 1962; Marshall, 1980). However, coding the gliriform lower incisor of unsectioned diprotodontians as i2 (for example) and that of Recent caenolestids as i1 cannot be

justified unless it is assumed a priori that Diprotodontia and Paucituberculata are separate clades. Analyses of character data based on such a priori assumptions—which are seldom stated explicitly—cannot then be validly interpreted as supporting either diprotodontian or paucituberculatan monophyly (contra Luckett, 1994; Springer et al., 1997; Sánchez-Villagra, 2001; Horovitz and Sánchez-Villagra, 2003). In addition, using this approach it is unclear how to score taxa that have a gliriform lower incisor but do not appear to be members of either Paucituberculata or Diprotodontia (as in the case of †*Yalkaparidon*; Archer et al., 1988; Beck et al., 2014). Rather than perpetuate such circular inference, we prefer to code the presence/ absence of a gliriform tooth at the anteriormost mandibular position (i.e., an assumption of primary homology sensu de Pinna, 1991), an option that permits global parsimony (or other phylogenetic optimality criterion, such as maximum likelihood) to distinguish between the alternative interpretations of the diprotodontian, paucituberculatan, and yalkaparidontian conditions as homologous or homoplastic (see also Beck et al., 2014; Beck, 2017a: char. 163; Maga and Beck, 2017: char. 163).

Although it may seem perverse to reject evidence that so many other morphologists have considered sufficient to code these teeth as nonhomologous, we note that there is still no consensus about their hypothesized positional identity (Ride, 1962; Marshall, 1980; Murray et al., 1987; Luckett, 1994; Springer et al., 1997; Luckett and Hong, 2000; Sánchez-Villagra, 2001; Horovitz and Sánchez-Villagra, 2003). In fact, a careful review of available evidence suggests that the gliriform incisors of paucituberculatans and diprotodontians plausibly occupy the same dental locus—which we refer to as i1 (see Materials and Methods and table 12), but which several other researchers have referred to as i2 (following Hershkovitz, 1982). In several fossil paucituberculatans (see, e.g., Sinclair, 1906; Hershkovitz, 1982; Abello, 2007; 2013; Engelman et al., 2016) the alveolus immediately behind the gliriform

tooth is "staggered" (sensu Hershkovitz, 1982; 1995; see char. 150), and hence presumably homologous with the staggered alveolus seen in didelphids (i2); if so, then the gliriform paucituberculatan tooth occupies the same locus as the anteriormost lower incisor of didelphids (i1). The i2 alveolus is also staggered in dasyurids, thylacinids, and peramelemorphians (see char. 149), suggesting that the missing lower incisor (relative to the four seen in didelphids) in these taxa has been lost from the rear of the incisor series, in which case they retain i1–3 (see char. 148). Woodward (1896) reported an unerupting incisor anterior to the erupting i1 in sectioned pouch young of the dasyurid *Dasyurus*, as did Wilson and Hill (1897) in young specimens of *Perameles*. Additionally, Kirkpatrick (1978) examined dental development in *Macropus giganteus* and found evidence of an unerupting deciduous and successor incisor at a locus anterior to the gliriform tooth, which itself has an unerupting deciduous predecessor.[16] As noted by Kirkpatrick (1978), if the anterior, nonerupting lower incisor locus in *Macropus* is homologous with the nonerupting locus reported in *Dasyurus* and *Perameles* by Woodward (1896) and Wilson and Hill (1897) respectively, then the gliriform tooth of the former is plausibly homologous with the anteriormost erupting lower incisor of dasyurids, thylacinids, and peramelemorphians, which in turn appears to be (for reasons discussed above) homologous with the anteriormost erupting lower incisor of paucituberculatans and didelphids (the tooth we refer to as i1). Ultimately, however, confident resolution of this question will probably require further ontogenetic studies of living taxa (most informative in this regard would be caenolestid pouch young, which have so far proven impossible to collect) using more modern techniques (such as Diffus-

---

[16] Kirkpatrick (1978) ascribed the conflicting interpretations of the homology of the diprotodontian gliriform incisor by previous authors (e.g., Woodward, 1893; Dependorf, 1898; Hopewell-Smith and Marett Tims, 1911; Bolk, 1929; Engelhardt, 1932; Ride, 1962; Berkovitz, 1972b) to the use of inadequate material.
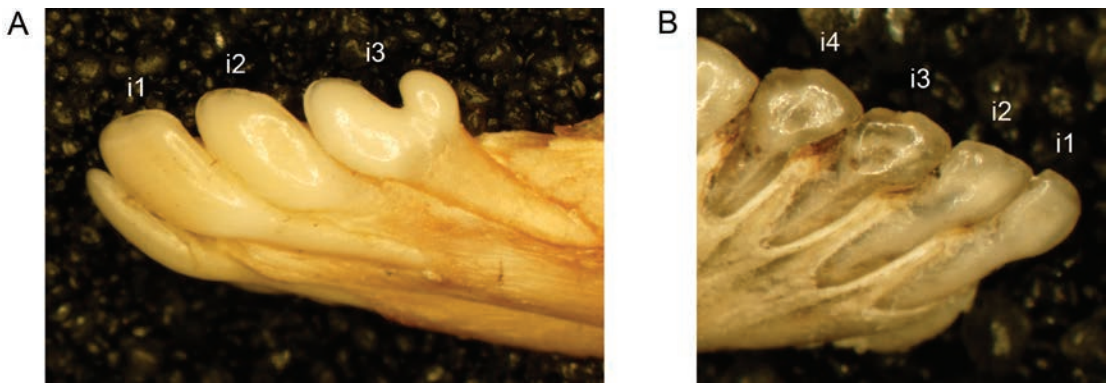
FIG 21. Lateral views of anterior mandible of *Perameles gunnii* (**A,** MVZ 127060 [left mandible]) and *Dromiciops gliroides* (**B,** FMNH 127445 [right mandible]). Alternative states of characters 148, 149, and 150 (see main text for descriptions of these characters and character states) are illustrated as follows: *Perameles* 148(1; note that the anteriormost visible incisor is the i1 of the right mandible), 149(0), 150(1); *Dromiciops* 148(0), 149(1), 150(0). Abbreviations: **i1,** first lower incisor; **i2,** second lower incisor; **i3,** third lower incisor; **i4,** fourth lower incisor. Specimens are not shown to the same scale.

ible Iodine-based Contrast-Enhanced CT; Nasrullah et al., 2018), and discovery of fossil taxa that unambiguously demonstrate which locus (or loci) has been lost in particular clades.

Character 148. *Four lower incisors present (0); or i4 missing (1); or i3 and i4 missing (2); or i2–4 missing (3).* Four lower incisors, the complete metatherian complement, are present in †*Mayulestes*, †*Allqokirus*, †*Pucadelphys*, †*Herpetotherium*, and didelphids (e.g., *Marmosa* [fig. 34]). In all these taxa, the numerical second incisor (i2) is unambiguously recognizable by its staggered alveolus (see char. 149). Both *Dromiciops* (figs. 21B, 43) and †*Microbiotherium* also have four lower incisors, although the alveolus of i2 is not staggered in either taxon (see char. 149; Hershkovitz, 1982, 1995, 1999).

In most metatherians with three lower incisors (dasyuromorphians and peramelemorphians; see fig. 21A) the identity of the middle tooth as i2 is suggested by its staggered alveolus (see char. 149). This, together with the assumption that reductions in incisor number result from losses of the posteriormost teeth in ancestral dentitions (see char. 103), leads us to identify the missing element in these taxa as i4 (state 1). The presence of a distinct posterior lobe on the

numerical third incisor of peramelemorphians and some dasyuromorphians (char. 150) may be further evidence that i4 was lost if, as Muirhead (1994: 60) suggested, this lobe evolved as a functional replacement.

Myrmecobius also has only three lower incisors (fig. 41), but none of these teeth are staggered. Thomas (1887b: 311) noted two BMNH specimens of *Myrmecobius* that have four rather than three lower incisors unilaterally and concluded, based on this material, that the missing tooth is i4. However, it should be noted that *Myrmecobius* exhibits numerous other dental anomalies, such as retention of dP3 and dp3 into adulthood (see char. 121), presence of a supernumerary lower fifth molar in many specimens, and the occasional presence of a supernumerary tooth (usually a largely featureless unicuspid) between P3 and dP3 (as in BMNH 1906.8.1.357) or between p3 and dp3 (as in BMNH 1906.8.1.361). Nevertheless, given our general assumption that incisors are lost from the posterior end of the series, and in the absence of compelling evidence for alternative interpretations, we also assume that *Myrmecobius* has lost i4.

Scoring this character is more difficult in metatherian taxa with problematic lower antemo-

lar homologies, such as paucituberculatans, most diprotodontians, †*Yalkaparidon*, and *Notoryctes*. In paucituberculatan terminals that exhibit an unambiguously identifiable double-rooted p2, and in which the anterior part of the dentary is intact in at least one specimen—namely *Caenolestes* (fig. 35), *Rhyncholestes*, *Lestoros*, and †*Stilotherium*—there are typically four unicuspids between i1 and p2 (Marshall, 1980; Abello, 2007, 2013; Martin, 2007, 2013). Assuming that the ancestral metatherian lower antemolar formula is i1–4, c1, p1–3, a minimum of two and a maximum of three of these unicuspids could be incisors. Hence, the total lower incisor count of these taxa, including the gliriform i1 (see char. 147), is either three (i1–3) or four (i1–4); therefore, we scored these taxa using ambiguity coding ("0/1") to account for this uncertainty.

Diprotodontians can have anywhere from zero to three unicuspids between i1 and p2 (in the case of macropodiforms) or p3 (in all others). In those that consistently lack uncuspids in this interval—namely diprotodontids, phascolarctids (e.g., *Phascolarctos* [fig. 44]), vombatids (e.g., *Vombatus* [fig. 45]), wynyardiids, and most macropodiforms (e.g., *Potorous* [fig. 54])—three incisors (i2–4) are obviously absent (state 3). *Tarsipes* also lacks any teeth between i1 and its undifferentiated lower postcanine dentition (see fig. 49), so we also scored it as state 3. In diprotodontians that consistently have only a single tooth in this interval—namely †*Wakaleo* (Megirian, 1986; Murray, et al., 1987; Murray and Megirian, 1990; Gillespie, 2007; Yates, 2015b; Gillespie et al., 2017), *Pseudochirops archeri* (see Archer, 1984c: fig. 186), *P. cupreus* (fig. 51), *Pseudochirulus*, †*Balbaroo* (Cooke, 2000), ?*Bettongia* †*moyesi* (see Flannery and Archer, 1987b), †*Bulungamaya* (Travouillon et al., 2014b), †*Ganguroo* (Cooke, 1997b; Travouillon et al., 2014b; Cooke et al., 2015), †*Ganawamaya* (Kear et al., 2007), †*Ekaltadeta* (Wroe, 1996b), and *Hypsiprymnodon moschatus* (fig. 52)—at least two (i3–4) and potentially three (i2–4) of the lower incisors have been lost, so we scored these taxa as "2/3." Diprotodontians with two unicuspids between i1 and

p3 (†*Thylacoleo*, *Petropseudes*, acrobatids [fig. 48], and some phalangerids) must have lost at least one and potentially two or three lower incisors; we scored such taxa using ambiguity coding (as "1/2/3"). Finally, taxa with three unicuspids between i1 and p3 (e.g., †*Lekanoleo* [Gillespie et al., 2020: fig. 5]; petaurids, burramyids [fig. 46], some pseudocheirids, and some phalangerids [fig. 47]) could feasibly retain i2–4 or, alternatively, might have lost between one and three of these teeth; these alternatives are not distinguishable based on available evidence, so we scored such taxa as unknown ("?").

The number of unicuspids present between i1 and m1 varies between one and four among specimens of †*Yalkaparidon coheni*, so we scored this taxon as unknown (by contrast, †*Y. jonesi* lacks any teeth between i1 and m1; Archer et al., 1988; Beck et al., 2014). Because *Notoryctes* has four or five teeth anterior to p3, it is possible that this taxon retains four lower incisors; however, based on our own observations and those of previous authors (e.g., Gadow, 1892; Archer, 1984c; Archer et al., 2011), *Notoryctes* appears to have two or three lower incisors, and has therefore been scored using ambiguity coding as "1/2."

This character was ordered (0 ↔ 1 ↔ 2 ↔ 3) based on the hypothesized pattern of sequential loss.

Character 149. *Second lower incisor (i2) with "staggered" alveolus (0); or i2 alveolus like those of i1 and i3 (1).* The alveolus of i2 is "staggered"—displaced lingually and dorsally relative to the alveoli of adjacent incisors (i1 and i3) and with a prominent labial buttress of alveolar bone (fig. 21A)—in all examined metatherians with unambiguously distinguishable antemolar tooth homologies with the exception of *Myrmecobius*, *Dromiciops* (fig. 21B), and †*Microbiotherium* (Hershkovitz, 1982, 1995, 1999).[17] A single specimen of †*Pucadelphys* was originally reported to have an unstaggered i2 (Marshall and Muizon,

[17] Staggering has also been reported to be absent in some Mesozoic metatherians not included in the current study (Cifelli and Muizon, 1997, 1998; Kielan-Jaworowska et al., 2004).

1995: 68), but subsequently studied material clearly shows that i2 was staggered in this taxon (Muizon, 1998: 81; R.M.D.B., personal obs.).

Conflicting opinions have been expressed regarding the presence or absence of a staggered i2 in paucituberculatans (Hershkovitz, 1982, 1995; Abello, 2007, 2013; Voss and Jansa, 2009). A crucial preliminary issue is whether i2 can be unambiguously identified in these taxa. All of the caenolestids included in our analysis (namely *Caenolestes*, *Rhyncholestes*, *Lestoros*, and †*Stilotherium*; table 2) are represented by at least one specimen preserving an unambiguously identifiable double-rooted p2 and an intact anterior part of the dentary; in these, four unicuspids are typically present between p2 and i1, of which at least two must be incisors. Assuming that incisors are lost from the end of the series (char. 103), then the unicuspid immediately posterior to i1 can be identified as i2 (see also Voss and Jansa, 2009: 55). Among our other pauctuberculatan terminals, it is unclear whether p2 is present or not in †*Acdestis* and †*Palaeothentes* (char. 154), although p3 can be unambiguously identified in both taxa. However, four unicuspids are present between i1 and p3 in both †*Acdestis* (Rae et al., 1996: fig. 9; Engelman et al., 2016) and †*Palaeothentes* (e.g., MACN A 5671), of which one must be an incisor for the same reasons outlined above (at most, the remaining three could potentially represent c1, p1, and p2); again assuming that incisors are lost from the end of the series, the unicuspid immediately following i1 in †*Palaeothentes* can also be identified as i2. Thus, *Caenolestes*, *Rhyncholestes*, *Lestoros*, †*Stilotherium*, †*Acdestis*, and †*Palaeothentes* can all be scored for this character.

In no specimen of *Caenolestes*, *Rhyncholestes*, or *Lestoros* that we examined is the alveolus of putative i2 staggered (contra Hershkovitz, 1995): there is no evidence of a buttress of alveolar bone displacing the alveolus of i2 dorsally relative to those of the more posterior unicuspids, nor does i2 appear to be lingually displaced (Voss and Jansa, 2009: 55; Abello, 2013). Therefore, we scored these taxa as state 1. Abello (2007: 249–250; 2013) considered i2 (her "i3") to be staggered in †*Palaeothentes* and †*Stilotherium*. We agree that i2 is indeed staggered (state 0) in †*Stilotherium dissimile*, based on specimens MACN A 8466 (see Abello, 2013: fig. 5A) and 8467. However, whereas two specimens of †*Palaeothentes minutus* (MACN A 8347-8354b and 8331) also appear to preserve a staggered i2, two others that we examined (MACN A 5671 and 8376) do not show clear evidence of staggering at this locus: the labial margin of the i2 alveolus is not dorsally raised, and this alveolus appears to be approximately in line (rather than lingually displaced) with those of the following three uncuispids when viewed dorsally. Thus, we scored †*Palaeothentes* as polymorphic ("0+1"). Engelman et al. (2016: 6, 8) reported that i2 (their "u1") is "slightly staggered" in †*Acdestis maddeni*, but in UF 99687 this tooth appears to be approximately in line with the succeeding unicuspids in dorsal view (based on Morphobank media number M406548), so we scored †*Acdestis* as state 1. Staggering of i2 has been reported in several other fossil paucituberculatans not included in the current analysis (Sinclair, 1906: 420, fig. 7; Abello, 2007; 2013).

Some diprotodontians (phascolarctids, wynyardiids, vombatids, diprotodontids, and most macropodiforms) lack any teeth between i1 and p2 (in the case of macropodiforms) or p3 (the others); these taxa were therefore scored as inapplicable ("-") for this character. In *Tarsipes* too, there are no teeth between i1 and the undifferentiated postcanine dentition, so we also scored this taxon as inapplicable. In other diprotodontians, however, between one and three unicuspids are typically present between i1 and p3; although one of these unicuspids might be i2, there is no way to be sure, so we scored all such taxa as unknown ("?"). Similarly, in known mandibular specimens of †*Yalkaparidon* there are alveoli for between one and four unicuspids between i1 and a tooth that we identify as m1 ("p3" of Archer et al., 1988; see Beck et al., 2014); because it is unclear whether i2 is present, we also scored †*Yalkaparidon* as unknown.

In *Notoryctes*, there are a maximum of five lower teeth anterior to the large premolariform tooth that we identify as p3. Of these, the fifth (immediately anterior to p3) is a tiny spicule when it is present at all (e.g., on the right side of AMNH 198651). Again, on the assumption that there can be at most seven teeth anterior to p3 (i1–4, c1, p1–2), at least two incisors must be present in *Notoryctes* specimens with five. We therefore tentatively identify the two anteriormost lower teeth as i1 and i2. Because the alveolus of the putative i2 does not appear to be staggered in this taxon, we scored it as state 1.

Character 150. *Third lower incisor (i3) not bilobed (0); or bilobed (1).* The third lower incisor of most metatherians that possess this tooth has a simple, undivided cutting edge (state 0; e.g., *Dromiciops* [fig. 21B]), but the cutting edge of i3 is conspicuously bilobed in peramelemorphians (state 1; e.g., *Echymipera* [fig. 21A]), a potential synapomorphy that has been remarked by several authors (e.g., Muirhead and Filan, 1995). However, this trait also occurs in dasyurids, among which it is most commonly observed on unworn teeth (Bensley, 1903; Archer, 1976c; Voss and Jansa, 2009). We therefore scored i3 as bilobed if this morphology was distinct in examined juvenile or subadult specimens. Besides peramelemorphians (in which this trait is consistently expressed), we observed a bilobed i3 in most dasyurids (albeit with the posterior lobe sometimes very weakly developed, as in *Planigale*), with the exception of *Dasyuroides*, *Dasyurus*, *Myoictis*, *Parantechinus*, *Phascogale*, and *Sarcophilus*; a bilobed i3 is variably present in *Dasycercus*, which we scored as polymorphic ("0+1"). A distinctly bilobed i3 is also present in juvenile specimens of *Thylacinus* (e.g., UMZC A6.7/10, and SAM M1956 and M1957), but it is absent in all examined specimens of *Myrmecobius*, including juveniles. Our scoring of this feature in dasyuromorphians differs from that of Archer (1976c: S39)—who stated that only *Phascolosorex*, *Neophascogale*, and *Sminthopsis granulipes* have a bilobed i3—and that of Wroe et al.

(2000: char. 27) and Wroe and Musser (2001: char. 27)—who stated that *Murexia*, *Antechinus*, and *Thylacinus* lack a bilobed i3—perhaps because we were able to examine a greater range of juvenile and subadult material.

Taxa in which i3 is absent (those scored as state 2 for char. 148) were scored as inapplicable ("-") for this character, whereas those in which the presence or absence of i3 cannot be unequivocally determined were scored as unknown ("?").

Character 151. *Tall lingual cusp of lower incisors (subequal in height to labial cusp) absent (0); or present (1).* Voss and Jansa (2003: char. 62, fig. 14; 2009) identified the presence or absence of a small but distinct lingual cusp or heel on unworn lower incisors as distinguishing members of the tribe Didelphini (*Chironectes*, *Didelphis*, *Lutreolina*, *Philander*)—in which this structure is absent—from other didelphids, in which it is present. However, we were unable to consistently score this character in other metatherians, for three reasons. First, we observed a continuous range of intermediate morphologies, sometimes including variation along the toothrow of a single individual (for example, a distinct lingual cusp is absent on i1 and i2 but present on i3 in AMNH 109536, a juvenile specimen of *Neophascogale lorentzii*). Second, this cusp is often lost with minimal wear (Voss and Jansa [2009: 55] reported a lingual cusp or heel to be absent in *Dasyurus*, but it is present in a number of juvenile and subadult specimens that we examined [e.g., AM M35911]). Third, we encountered various scoring ambiguities among taxa with gliriform teeth (e.g., the distinctively "bulbous" [sensu Roberts, 2008: 377] morphology of the first lower incisor in *Pseudochirops archeri* [see Archer, 1984c: fig. 186c] and *P. cupreus* [fig. 51]).

A qualitatively distinct morphology that we scored for this analysis, however, is seen in *Thylacinus*, in which a lingual cusp that is as tall as the major, labial cusp (from which it is separated by a distinct fissure) is present on all three lower incisors. State 1 is therefore an autapomorphy of *Thylacinus* in the current analysis.

Lower Canine

The lower canine (c1) is a nonproblematic tooth in most polyprotodont taxa, easily recognized by virtue of its position between the incisor and premolar series and by its occlusion with a similarly shaped tooth that usually occupies the premaxillary-maxillary suture in the upper dentition. Unlike C1 (see char. 109), c1 is always single-rooted in metatherians. Although c1 exhibits noteworthy taxonomic variation in crown morphology in some clades (e.g., didelphids; Voss and Jansa, 2009: fig. 23), such variation is correlated with similar modifications of C1 such that occlusal transformations of these teeth seem to be nonindependent. By contrast, c1 is absent in some marsupial taxa that consistently retain C1, clear evidence of independent dental expression at the upper and lower canine loci.

Character 152. *Lower canine present (0); or absent (1).* The lower canine is present (state 0) in most metatherians, but it is unambiguously absent (state 1) in *Phascolarctos* (fig. 44), †*Nimiokoala*, vombatids (including †*Warendja*; Hope and Wilkinson, 1982), diprotodontids, wynyardiids, and most macropodiforms (e.g., *Lagostrophus* [fig. 53]), all of which lack teeth between the gliriform lower incisor and large multirooted teeth at the second or third premolar locus (see below). *Tarsipes* (fig. 49) also lacks any teeth between its gliriform i1 and its vestigial postcanine dentition. We scored other diprotodontians (i.e., thylacoleonids, burramyids, phalangerids, pseudocheirids, petaurids, acrobatids, and macropodiforms that retain a unicuspid posterior to i1), paucituberculatans, and †*Yalkaparidon* as unknown ("?") because the homologies of single-rooted unicuspids that occur behind the gliriform lower incisor are uncertain in these taxa (see char. 148). Based on examined specimens it is unclear whether *Notoryctes* retains a lower canine or not (Gadow, 1892, reported that presence of the lower canine is variable in marsupial moles), so we also scored this taxon as unknown.

Lower Premolars

The number of lower premolars in metatherian taxa examined for this study ranges from one to three. Complete complements are present in the nonmarsupial metatherians included here, didelphids, microbiotheriids, peramelemorphians, and most dasyuromorphians, but one or more lower premolars are clearly missing or are assumed to be missing in other marsupial taxa. Because assumptions made in previous studies about which lower premolar loci are present and which are absent in different taxa are often not clearly justified, we discuss the basis for our scoring decisions in substantive detail. The two or three lower postcanine teeth present in *Tarsipes* are vestigial and of uncertain homology (see char. 113; Parker, 1890; Archer, 1984c: 690, fig. 133; Russell and Renfree, 1989; Rosenberg and Richardson, 1995), so we scored characters relating to the lower premolars as unknown ("?") or inapplicable ("-") in this taxon.

Character 153. *First lower premolar present (0); or absent (1).* We scored the first lower premolar (p1) as present (state 0) in all metatherians with three unambiguously recognizable premolars; these taxa include †*Mayulestes*, †*Allqokirus*, †*Pucadelphys*, †*Mimoperadectes*, †*Herpetotherium*, didelphids, microbiotheriids, peramelemorphians, thylacinids, *Myrmecobius*, and most dasyurids. In the didelphid *Caluromysiops*, P1 is only variably present (see char. 114), whereas p1 (although small; Voss and Jansa, 2009: 57) is consistently present in the specimens we examined, indicating that presence or absence of of one of these teeth is at least partially independent of the other.

We coded p1 as present in dasyurids that typically retain only two lower premolars (*Dasycercus*, *Dasykaluta*, *Dasyuroides*, *Dasyurus*, *Pseudantechinus*, and *Sarcophilus*), because none of these exhibit any evidence of dental replacement at the more posterior locus (suggesting that p3 has been lost). In effect, the same dental locus appears to have been suppressed in both the upper and lower dentitions of these taxa (see

accounts for chars. 114, 122, above). *Myoictis* is polymorphic for presence of p3 (char. 155; as noted by Tate, 1947; Woolley, 2005a), and this tooth is also occasionally present as a single-rooted vestigial element in *Pseudantechinus* (e.g., AMNH 196786; see also Spencer, 1896: 28; Ride, 1964: 62; Woolley, 2011: 58, appendix 3). By contrast, p1 and p2 are well-developed, double-rooted premolariform teeth in all examined dasyurids. Although not conclusive, we consider this additional supportive evidence that it is p3 that has been lost in two-premolared dasyurids.

In the fossil phalangerid †*Onirocuscus*, there are alveoli for two double-rooted teeth (inferred from two narrowly separated pairs of alveoli) anterior to p3 (Flannery and Archer, 1987a; Crosby, 2007); to our knowledge, lower incisors and lower canines are consistently single-rooted in metatherians, so we interpret these alveoli in †*Onirocuscus* as housing p1 and p2 and score this taxon as state 0 here. We coded p1 as absent (state 1) in macropodiforms that lack teeth between the gliriform i1 and the tooth that we interpret as p2 (see chars. 148, 154). We also coded p1 as absent in phascolarctids, diprotodontids, wynyardiids, and vombatids, all of which lack teeth between the gliriform lower incisor and a large tooth appressed to the molar series that we interpret as p3 (see char. 155).

We coded this character as unknown ("?") in other diprotodontians and in all paucituberculatans, because the homologies of the single-rooted, unicuspid teeth that occur between the gliriform lower incisor and p2 and/or p3 in these taxa are unclear (char. 148). By contrast, Martin (2007: 400, fig. 4) tentatively identified the presence of p1 (which he referred to as "dp1," following Luckett [1993b] and Luckett and Hong [2000]) in *Rhyncholestes*, based on the presence of a "slightly developed talonid" on a tooth immediately anterior to p2 in young specimens with unworn dentitions. We also observed a talonidlike structure on the tooth immediately anterior to p2 in a specimen of *Rhyncholestes* (BMNH 1975.1723), but the tooth anterior to

that has an almost identical crown morphology (likewise with a "talonid"); therefore, this structure does not seem sufficient to identify p1 in *Rhyncholestes*, which we scored as unknown ("?"). We also scored †*Yalkaparidon* and *Notoryctes* as unknown due to the uncertain homologies of the antemolar dentition in both taxa (see chars. 148, 152).

Character 154. *Second lower premolar present (0); or absent (1).* We coded the second lower premolar (p2) as present in all examined taxa with three lower premolars and in dasyurids with two lower premolars for the reasons previously discussed (see char. 153). We also identify as p2 the double-rooted tooth immediately anterior to p3 in most paucituberculatans, including *Caenolestes*, *Rhyncholestes*, and *Lestoros*; however, we scored †*Acdestis* and †*Palaeothentes* as unknown because the tooth immediately anterior to p3 in these taxa is single-rooted and hence of uncertain homology (see chars. 148, 149, and 152).

The acrobatids *Acrobates* and *Distoechurus* (fig. 48) exhibit a conventionally premolariform p2, the tallest tooth in the lower jaws of these taxa (Archer, 1984c: fig. 143). We also identify as p2 the double-rooted tooth (inferred from a narrowly separated pair of alveoli) immediately anterior to p3 in †*Onirocuscus* (see char. 153 and Flannery and Archer, 1987a). Available juvenile specimens of macropodiforms have a large two-rooted sectorial tooth appressed to a deciduous tooth that is clearly dp3; we interpret this sectorial tooth as p2, in agreement with previous authors (e.g., Thomas, 1888; Tate, 1948; Ride, 1961; Bartholomai, 1971b; Kirkpatrick, 1978; Archer, 1984c; Flannery, 1987; Kear and Cooke, 2001; but note that some of these authors followed Thomas's (1888) hypothesis of dental homologies and referred to this tooth as "p3"; see table 12). As described above (char. 117), both the macropodiform p2 and its occluding partner in the maxillary dentition (P2) are shed when the permanent third premolars erupt (or shortly thereafter), except in †*Ekaltadeta* (see Wroe and Archer, 1995).

To avoid a priori assumptions of macropodiform monophyly, we coded all macropodiform and nonmacropodiform taxa in which adult specimens lack p2 but for which juvenile specimens (which would reveal whether p2 is present earlier in ontogeny) are unavailable as unknown ("?"); such taxa include †*Rhizosthenurus*, †*Balbaroo*, †*Ganawamaya*, †*Neohelos*, †*Silvabestius*, †*Ilaria*, †*Muramura*, †*Warendja*, and †*Nimiokoala*. By contrast, p2 is unequivocally absent in adult and juvenile specimens of †*Ngapakaldia* and †*Nimbadon* (Black et al., 2010), †*Namilamadeta* (Pledge, 2005), *Phascolarctos*, *Vombatus*, and *Lasiorhinus*. We scored all remaining diprotodontians (thylacoleonids, pseudocheirids, burramyids, petaurids, *Tarsipes*, and all phalangerids except †*Onirocuscus*) as well as *Notoryctes* and †*Yalkaparidon* as unknown due to uncertain dental homologies.

Character 155. *Third lower premolar present (0); or absent (1).* Although p3 is present (state 0) in all metatherians that unambiguously exhibit three lower premolars (including examined nonmarsupial metatherians, didelphids, peramelemorphians, and most dasyuromorphians), we scored p3 as absent (state 1) in two-premolared dasyurids (*Dasycercus*, *Dasykaluta*, *Dasyuroides*, *Dasyurus*, *Pseudantechinus*, and *Sarcophilus*; see discussion under char. 153). As noted earlier, *Myoictis* is polymorphic ("0+1") for the presence of p3 (Tate, 1947; Woolley, 2005a). All other metatherians in which premolar homologies are uncontroversial consistently retain p3, with the exception of *Distoechurus*, in which this tooth is only variably present (Archer, 1984b: 695), and which we also scored as polymorphic (the specimen illustrated in fig. 48 lacks p3).

Obviously, presence or absence of p3 could be expected to show some degree of covariation with presence or absence of P3 (char. 122). However, both *Distoechurus* and *Myoictis* consistently retain P3 but sometimes lack p3, whereas *Dasyuroides* retains P3 and lacks p3. Some specimens of *Pseudantechinus* (e.g., AMNH 196786; see also Spencer, 1896: 28; Ride, 1964b: 62; Woolley, 2011: 58, appendix 3) and *Dasycercus* (Archer,

1976c: table 1; 1982b: table 2; Woolley, 2005b; Woolley et al., 2013) also retain P3 and lack p3. Collectively, this implies some degree of character independence. Thus, we scored the presence or absence of these loci as separate characters.

Character 156. *Second lower premolar (p2) distinctly taller than p3 (0); or p2 and p3 subequal in height (1); or p3 distinctly taller than p2 (2).* The relative heights of the second and third premolars (as indicated by the tips of fully erupted but unworn or lightly worn teeth when the alveolar plane of the mandible is oriented horizontally) exhibit consistent taxonomic variation in Marsupialia. Descriptions of character states and an account of their distribution among Recent didelphids were provided by Voss and Jansa (2003: char. 63). Among other metatherians, p2 is taller than p3 (state 0) in †*Thylophorops*, many dasyurids (including †*Barinya*; Wroe, 1999: textfig. 3), †*Badjcinus* (Muirhead and Wroe, 1998: fig. 1D), some peramelemorphians (e.g., *Chaeropus* [fig. 37]), and *Acrobates*. Most specimens of *Pseudantechinus* and *Distoechurus* lack p3, and this tooth is only variably present in *Myoictis* (char. 155); where present, however, p3 is smaller than p2 in these three taxa, so we scored them all as state 0. By contrast, these teeth are subequal in height (state 1) in †*Sparassocynus*, several peramelemorphians (e.g., *Macrotis* [fig. 38]), some dasyurids (e.g., *Antechinomys*, *Murexia*), and *Myrmecobius* (fig. 41). Lastly, p3 is taller than p2 (state 2) in †*Pucadelphys* (Marshall and Muizon, 1995: fig. 6D), †*Herpetotherium*, all paucituberculatans in which p2 can be unambiguously identified (e.g., *Caenolestes* [fig. 35]), microbiotheriids (e.g., *Dromiciops* [fig. 43]), *Thylacinus* (fig. 40), †*Nimbacinus*, †*Ekaltadeta* (Wroe and Archer, 1995), and *Hypsiprymnodon moschatus* (Ride, 1961: plate I, fig. 3).

We scored this character as inapplicable ("-") in taxa that entirely lack p2 and/or p3, and in those where p2 and p3 do not cooccur (i.e., those macropodiforms in which p3 simultaneously evicts p2 and dp3). Taxa in which the presence or absence of p2 cannot be determined with certainty (char. 154) were scored as unknown ("?").
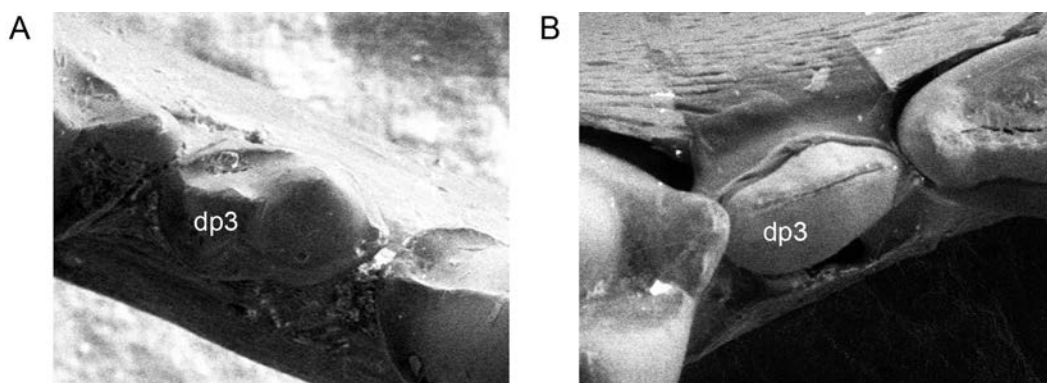
FIG. 22. Occlusal views of right deciduous third lower premolars (dp3) of *Sminthopsis crassicaudata* (**A,** AMNH 196686) and *Isoodon macrourus* (**B,** AMNH 160085). Alternative states of character 157 (see main text for description of this character and character states) are illustrated as follows: *Sminthopsis* 157(0); *Isoodon* 157(1). Teeth are not shown to the same scale.

Character 157. *Deciduous lower third premolar (dp3) with distinct trigonid and talonid (0); or without distinct trigonid and talonid (1).* The deciduous third lower premolar is a large and more or less molariform tooth (state 0) in most metatherians, but it has been reduced to a functionless vestige (state 1) in several groups. This character is modified from Voss and Jansa (2003: char. 64), because we were unable to consistently distinguish between a complete (tricuspid) and incomplete (bicuspid or unicuspid) trigonid of dp3 among the taxa in this study. Instead, we simply distinguish between taxa in which dp3 comprises an obviously distinct trigonid (regardless of the number of cusps) and talonid, and those in which a distinct trigonid and talonid cannot be identified.

Juvenile specimens retaining dp3 were not available for all the terminals included in our analysis. However, dp3 is large and exhibits distinct trigonid and talonid moieties in most Recent didelphids (except *Hyladelphys*; Voss et al., 2001), †*Sparassocynus* (Beck and Taglioretti, 2020), *Dromiciops* (Hershkovitz [1999: fig. 30B, 30C], but note that dp3 is incorrectly labelled as p3 in fig. 30C), the dasyurids *Sminthopsis* (fig. 22A) and *Antechinomys*, †*Namilamadeta*, †*Nimbadon* (Black and Hand, 2010), †*Ngapakaldia*, and all macropodiforms and phalangerids for which specimens preserving dp3 were available for examination.

As noted above (char. 121), *Myrmecobius* appears to retain dp3 into adulthood. The morphology and size of this tooth varies considerably among examined specimens, but it is typically tricuspid, with the cusps arranged anteroposteriorly (as in, e.g., BMNH 1844.1.22.21 and 1844.9.2.18); we tentatively identify these cusps as representing (from anterior to posterior) the paraconid, either the metaconid or the fused metaconid + protoconid, and the entoconid. We consider this morphology to correspond most closely to state 0 and scored *Myrmecobius* accordingly.

By contrast, dp3 is vestigial and occlusally featureless in *Caenolestes* (Luckett and Hong, 2000), the only paucituberculatan for which we were able to examine juvenile material. This tooth is also small and lacks a distinct trigonid and talonid in peramelemorphians (e.g., *Isoodon*; fig. 22B), most three-premolared dasyurids (with the notable exceptions of *Sminthopsis* and *Antechinomys*; see above), *Thylacinus* (Flower, 1867; Luckett et al., 2019), and several diprotodontians (including *Phascolarctos* [Thomas, 1887a], *Distoechurus*, *Petaurus*, *Dactylopsila*, *Dactylonax*, *Pseudochirops cupreus*, and *Petropseudes*).

As previously discussed (see chars. 120, 155), we assume that the tooth at the third premolar locus in adult vombatids is a successor tooth (P3 in the upper dentition, p3 in the lower denti-

tion). Examination of young juvenile specimens of *Vombatus* and *Lasiorhinus* did not reveal the presence of an obvious dp3, and indicated that p3 erupts very early in ontogeny (Thomas, 1887b). As for the upper dentition (see char. 120), we consider this evidence that dp3 was either absent or vestigial and lost very early in development, and score both *Vombatus* and *Lasiorhinus* as state 1. However, in the absence of juvenile material, we score †*Warendja* as unknown ("?"). The deciduous dentition of thylacoleonids has never been identified, and the permanent third premolar erupts at a very early stage (before m1) in †*Thylacoleo carnifex* (see Finch, 1971; Pledge, 1975). These facts have been interpreted as evidence that this taxon may have lacked deciduous premolars (Finch, 1971; Pledge, 1975). We therefore scored †*Thylacoleo* as state 1. Juvenile specimens are unavailable for †*Lekanoleo* and †*Wakaleo*, however, which have therefore been scored as unknown ("?").

Lower Molars

Tribosphenic lower molars include three anterior cuspids (paraconid, protoconid, and metaconid) that form an elevated wedge-shaped array (the trigonid) with the protoconid at its labial apex, and three posterior cuspids (hypoconid, hypoconulid, and entoconid) that surround the talonid basin (figs. 14, 23A–C; see also Bown and Kraus, 1979: fig. 9-1; Reig et al., 1987: fig. 1; Wroe, 1999: text-fig. 1A; Goin and Candela, 2004: fig. 2A; Kielan-Jaworowska et al., 2004: fig. 11.1; Williamson et al., 2014: fig. 3). Typically (but not invariably), these cusps are linked by enamelled crests, notably the paracristid (connecting the paraconid and protoconid), the metacristid (connecting the protoconid and metaconid),[18] and the cristid obliqua (connect-

ing the hypoconid with the metacristid). In many (but not all) tribosphenic taxa, the paracristid and the metacristid are prominently notched. Other lower-molar structures common to many tribosphenic taxa include shelflike anterior and posterior cingulids.

In general, lower-molar cuspid homologies among nontribosphenic metatherians are less controversial than the upper-molar cusp homologies discussed in the preceding accounts. The anterior lower molars (m1–3) of caenolestids (fig. 23B) and other paucituberculatans (Abello, 2013: figs. 2–4), for example, include all the usual six tribosphenic cuspids, although the paraconid is not always clearly identifiable when the paracristid is unnotched. The lower molars of peramelemorphians (fig. 23C) preserve all of the usual tribosphenic cuspids, differing in only minor details from the plesiomorphic condition (e.g., by the absence of a hypoconulid notch in the anterior cingulid and by the presence in some forms of a neomorphic labial cuspid in the hypoflexid region).

By contrast, zalambdodont taxa have radically modified lower molars. Correlated with reduction or loss of the occluding protocone on the upper molars, the talonid is greatly reduced in both *Notoryctes* (fig. 23D; Asher and Sánchez-Villagra, 2005: fig. 6A; Archer et al., 2011: fig. 1) and †*Yalkaparidon* (Archer et al., 1988; Beck, 2009; Beck et al., 2014). As a consequence, only the trigonid moiety—complete with paraconid, protoconid, metaconid, and the usual connecting cristids—remains as a fully functional component of zalambdodont metatherian lower molars.[19]

Selenodont lower molars appear strikingly different from the tribosphenic condition

---

[18] This crest is commonly referred to as the metacristid in the metatherian literature (e.g., Archer, 1976c, 1982a, 1982b; Muirhead and Filan, 1995; Wroe, 1996, 1999; Godthelp et al., 1999; Murray and Megirian, 2000, 2006a; Beck et al., 2008; Voss and Jansa, 2009), which we follow here, but it is also referred to as the protocristid (e.g., Van Valen 1966; Bown and Kraus 1979; Marshall, 1987; Reig et al. 1987; Marshall and

Muizon, 1995; Kielan-Jaworowska et al., 2004). Note that the distal metacristid is an entirely distinct, non-homologous structure (Bown and Kraus, 1979; Kielan-Jaworowska et al., 2004; Davis, 2011).

[19] However, Beck et al. (2014: 155) noted the possibility that the posterolingual part of the lower molars of *Yalkaparidon* may in fact be a vestigial talonid, rather than homologous with the metaconid, as it clearly is in *Notoryctes* (Asher and Sánchez-Villagra, 2005: fig. 6A; Archer, et al., 2011: fig. 1)
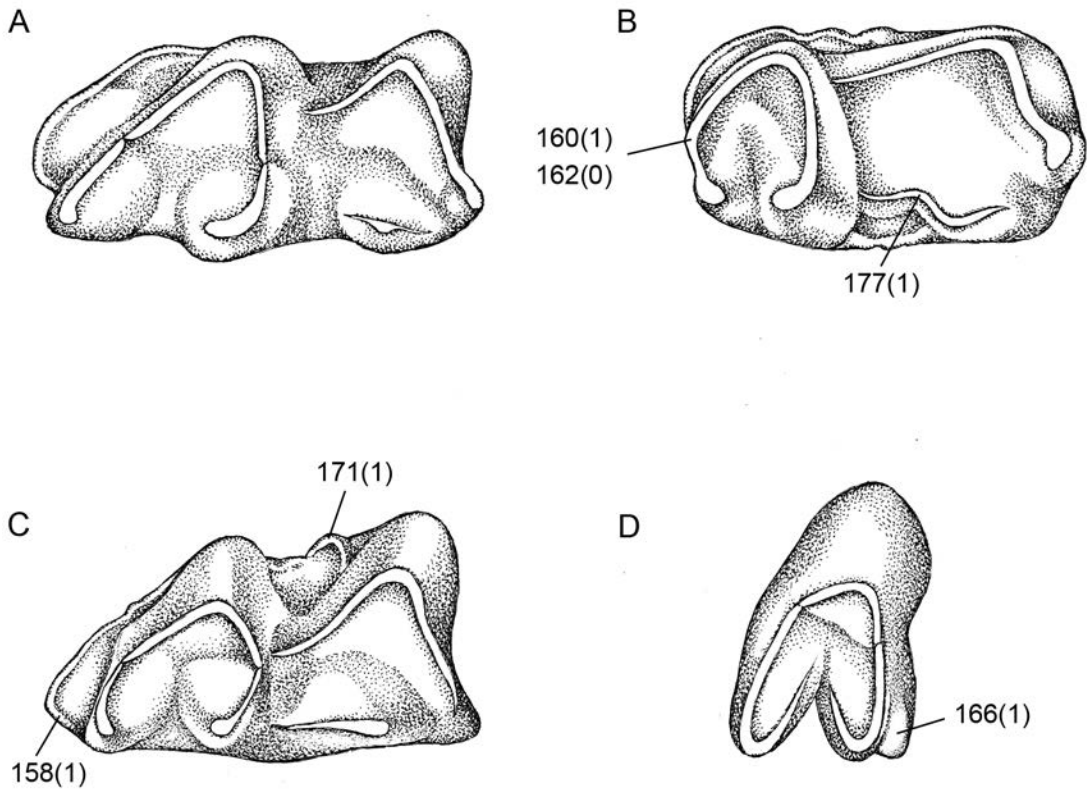
FIG. 23. Occlusal views of right lower molars of *Metachirus nudicaudatus* (**A,** AMNH 266453 [m2]), *Caenolestes fuliginosus* (**B,** UMMZ 155575 [m3]), *Echimipera kalubu* (**C,** AMNH 221654 [m2]), and *Notoryctes typhlops* (**D,** AMNH 198651 [m2]). General features of lower molar crown morphology discussed in the text are illustrated, as are characters 158, 161, 162, 163, 166, 167, 168, 170, 171, 172, 174, 175, 176, 177, 178, 179, and 180 (see main text for descriptions of these characters and character states), as follows: *Metachirus* 158(0), 161(0), 162(1), 163(0), 166(0), 167(0), 168(0), 170(0), 171(0), 172(0), 174(0), 175(0), 176(0), 177(0), 178(0), 179(0), 180(0); *Caenolestes* 158(0), 161(0), 162(0), 163(0), 166(0), 167(0), 168(0), 170(0), 171(0), 172(0), 174(0), 175(0), 176(0), 177(1), 178(0), 179(0), 180(0); *Echimipera* 158(1), 161(0), 162(1), 163(0), 166(0), 167(0), 168(0), 170(0), 171(1), 172(0), 174(0), 175(0), 176(0), 177(0), 178(0), 179(0), 180(0); *Notoryctes* 158(-), 161(0), 162(-), 163(0), 166(1), 167(-), 168(-), 170(-), 171(-), 172(-), 174(-), 175(-), 176(-), 177(-), 178(-), 179(-), 180(-). Numerical labels refer to character states defined in the text. Teeth are not drawn to the same scale.

because the cuspids and cristids are modified as crescentic blades ("selenes"), but four of the six main cuspids of the tribosphenic bauplan remain, at least on the posterior molars (m2–4), in both phascolarctids (fig. 24A) and pseudocheirids (fig. 24B). Only the paraconid is consistently missing in both selenodont groups, although the hypoconulid is also indistinct or absent in phascolarctids (compare Archer, 1984b: figs. 62, 178D-I). In both groups, however, the

m1 trigonid exhibits additional nontribosphenic features (see below).

Most nonselenodont diprotodontians consistently have only four well-developed lower-molar cusps, the paraconid and the hypoconulid having atrophied or disappeared completely. Although the lower molars of bunodont, bunolophodont, and fully lophodont taxa differ in many other occlusal details, the principal contrast among these dentitions concerns the development of
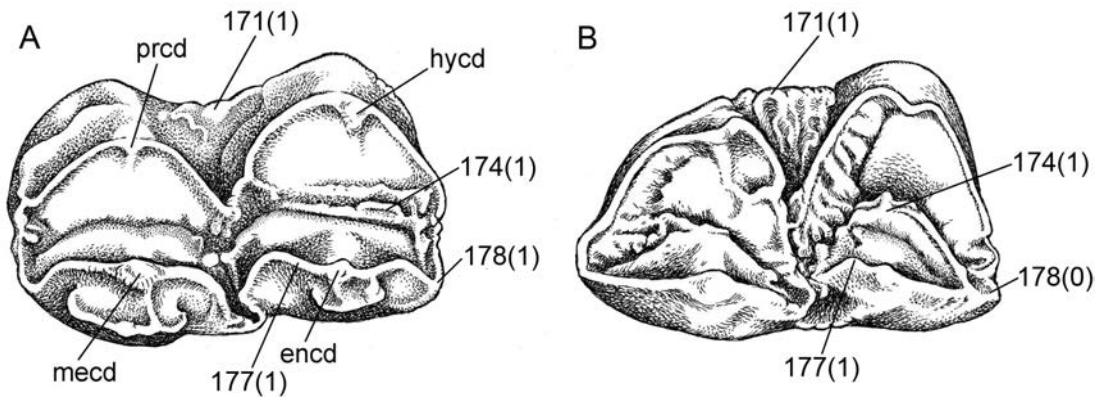
FIG. 24. Occlusal views of right second lower molars (m2) of *Phascolarctos cinereus* (**A,** USNM 534818) and *Pseudochirops cupreus* (**B,** AMNH 109633). General features of lower molar crown morphology discussed in the text are illustrated, as are characters 158, 161, 162, 166, 167, 168, 170, 171, 172, 174, 175, 176, 177, 178, 179, and 180 (see main text for descriptions of these characters and character states), as follows: *Phascolarctos* 158(-), 161(0), 162(-), 166(0), 167(0), 168(0), 170(0), 171(1), 172(0), 174(1), 175(0), 176(0), 177(1), 178(1), 179(-), 180(0); *Pseudochirops cupreus* 158(-), 161(0), 162(2), 166(0), 167(0), 168(0), 170(0), 171(1), 172(0), 174(1), 175(0), 176(0), 177(1), 178(0), 179(0), 180(0). Abbreviations: **encd,** entoconid; **hycd,** hypoconid; **mecd,** metaconid; **prcd,** protoconid. Numerical labels refer to character states defined in the text. Teeth are not drawn to the same scale.

transverse lophids, of which the anteriormost is called the protolophid and the posteriormost the hypolophid (fig. 25A–D). However, because these lophids occlude with the transverse lophs of upper molars, we did not score incipient or fully developed lophodonty in the lower dentition as a separate character. Similar to characters relating to the lower premolars (see above), we scored lower molar characters as or unknown ("?") or inapplicable ("-") in *Tarsipes*, due to the uncertain homology of its two or three vestigial lower postcanine teeth (char. 113; Parker, 1890; Archer, 1984c: 690, fig. 133; Russell and Renfree, 1989; Rosenberg and Richardson, 1995).

Character 158. *Hypoconulid notch in anterior cingulid of m2–4 present (0); or absent (1).* The anterior cingulid of m2–4 in most tribosphenic metatherians has a distinct notch that receives the hypoconulid of the preceding molar (state 0; figs. 14, 23A, B). However, the hypoconulid notch is absent (state 1) in peramelemorphians, in which the hypoconulid is directly posterior to the entoconid, and the anterior cingulid of the following tooth extends without interruption to

the lingual margin of the tooth (fig. 23C). Absence of a hypoconulid notch has been interpreted as a peramelemorphian synapomorphy (Wroe, 1997b; Muirhead, 2000), but this indentation is also absent in *Sarcophilus* (see Wroe, 1997b; 1997a; 1999; Wroe et al., 2000: char. 30; Wroe and Musser, 2001: char. 30).

We note some discrepancies between our own observations and those previously reported in the literature about this character. Wroe (1997b, 1997a, 1999) and Muirhead and Wroe (1998) stated that a hypoconulid notch is absent in *Thylacinus*, and Wroe (1997b, 1999) also claimed that it is absent in microbiotheriids; nevertheless, Wroe et al. (2000: char. 30) and Wroe and Musser (2001: char. 30) scored the hypoconulid notch as present in both *Thylacinus* and *Dromiciops*. We observed a distinct hypoconulid notch on m2–4 of all examined specimens of *Thylacinus cynocephalus* (see also Warburton et al., 2019: figs. 11–13), *Dromiciops gliroides*, and †*Microbiotherium tehuelchum*, so we scored these three taxa as state 0. Wroe (1997b) also stated that the hypoconulid notch is absent in *Myrmecobius*, but
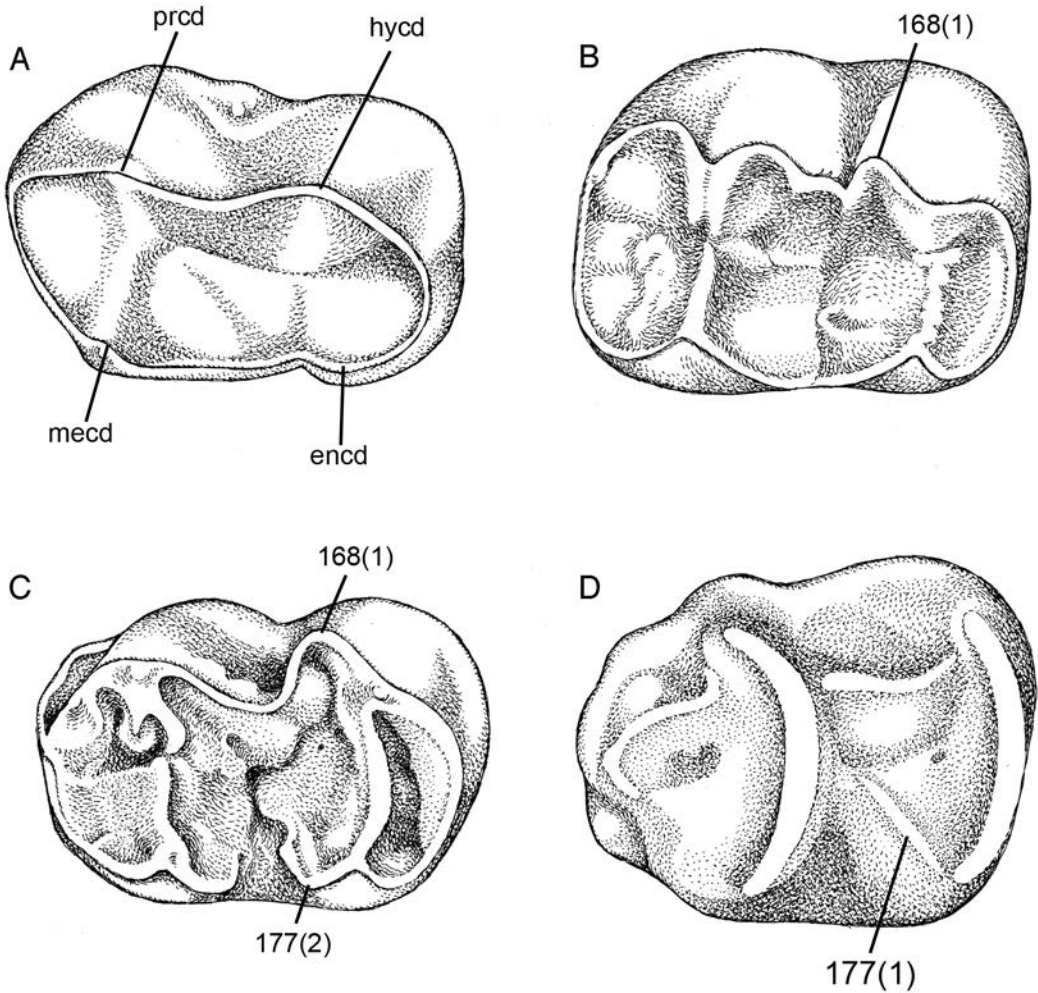
FIG. 25. Occlusal views of right lower molars of *Distoechurus pennatus* (**A,** AMNH 104058 [m2]), *Hypsiprymnodon moschatus* (**B,** AMNH 160120 [m2]), *Trichosurus vulpecula* (**C,** AMNH 65547 [m1]), and *Lagostrophus fasciatus* (**D,** AMNH 155105 [m1]). General features of lower molar crown morphology discussed in the text are illustrated, as are characters 158, 161, 162, 163, 166, 167, 168, 170, 171, 172, 174, 175, 176, 177, 178, 179, and 180 (see main text for descriptions of these characters and character states), as follows: *Distoechurus* 158(-), 161(0), 162(-), 163(0), 166(0), 167(0), 168(0), 170(0), 171(0), 172(0), 174(0), 175(1), 176(0), 177(0), 178(1), 179(-), 180(0); *Hypsiprymnodon moschatus* 158(-), 161(0), 162(-), 163(0), 166(0), 167(0), 168(1), 170(0), 171(0), 172(0), 174(0), 175(0), 176(0), 177(0), 178(1), 179(-), 180(0); *Trichosurus vulpecula* 158(-), 161(0), 162(-), 163(0), 166(0), 167(0), 168(1), 170(0), 171(0), 172(0), 174(-), 175(0), 176(0), 177(2), 178(1), 179(-), 180(0); *Lagostrophus* 158(-), 161(0), 162(-), 163(0), 166(0), 167(0), 168(0), 170(0), 171(0), 172(0), 174(-), 175(0), 176(0), 177(1), 178(1), 179(-), 180(0). Abbreviations: **encd,** entoconid; **hycd,** hypoconid; **mecd,** metaconid; **prcd,** protoconid. Numerical labels refer to character states defined in the text. Teeth are not drawn to the same scale.

because we could not identify an anterior cingulid in this taxon, we scored it as inapplicable ("-"). Other taxa that we scored as inapplicable—because they lack an anterior cingulid, a hypoconulid (see char. 178), or both—include most examined diprotodontians, †*Acdestis*, *Notoryctes*, and †*Yalkaparidon*.

Character 159. *Lower first molar (m1) paracristid present and distinct (0); or both paracristid and paraconid indistinct or absent (1); or paraconid well developed but paracristid indistinct or absent (2).* Both the paracristid and paraconid are distinct occlusal features (state 0) in most tribosphenic metatherians, including †*Pucadelphys*, †*Allqokirus*, †*Mayulestes*, †*Herpetotherium*, †*Mimoperadectes*, didelphids (figs. 14, 23A), microbiotheriids, peramelemorphians (fig. 23C), and most dasyuromorphians (Wroe, 1996a). They are also distinct in some nontribosphenic taxa, including *Notoryctes* (fig. 23D), †*Yalkaparidon*, phascolarctids (fig. 24A), wynyardiids, and most pseudocheirids. However, in many diprotodontians (e.g., petaurids, diprotodontids, thylacoleonids, some macropodiforms) the paracristid is clearly identifiable as a distinct crest extending anterolingually or anteriorly from the protoconid (the major trigonid cusp), but it does not always terminate in a distinct, cusplike paraconid. Examined specimens of *Vombatus* were too worn to score for this character, but Brewer et al. (2018: fig. 13.2) illustrated a juvenile specimen that suggests that a short, but distinct paracristid is present in this taxon, which we therefore scored as state 0. The paracristid is also clearly present on m1 in paucituberculatans, although this crest does not always end in a distinct, cusplike paraconid (Abello, 2013: char. 15). Similarly, in several dasyurids (*Dasycercus*, *Dasyuroides*, *Dasyurus*, *Myoictis*, *Sarcophilus*, and some specimens of *Murexechinus* and *Pseudantechinus*) the paracristid is clearly present, but the paraconid is either vestigial or absent; in at least some of these taxa (e.g., *Pseudantechinus*, *Murexechinus*), the paraconid appears to have fused with the anterior cingulid. Because the degree of development of the para-

conid appears to vary continuously among these taxa and is noticeably affected by even slight wear, we scored all examined metatherians with a distinct paracristid as state 0 whether or not this crest terminates in a distinct paraconid. Taxa without a distinct paraconid typically lack a paracristid notch, a trait that we score separately (see char. 160).

By contrast, both the paraconid and paracristid appear to be entirely absent from m1 (state 1) in *Burramys* (Archer, 1984b: fig. 147E), *Acrobates* (Archer, 1984b: fig. 143), and in all specimens of *Macrotis* that we examined (but see Bensley, 1903: 115; Ride, 1964b: 112, fig. 9; and Archer and Kirsch, 1977: 22 for conflicting reports regarding the distribution of this character in *Macrotis*). In *Macrotis* at least, absence of a distinct paraconid and paracristid appears to be the result of fusion of the paraconid with the anterior flank of the metaconid (e.g., on WAM M632). *Distoechurus* is polymorphic for this character, with the m1 paracristid present in some specimens (e.g., AMNH 191045) but absent in others (e.g., AMNH 104058), so we scored this taxon as polymorphic ("0+1"). We observed a third distinct morphology (state 2) in *Myrmecobius*, which has a well-developed paraconid in the usual tribosphenic position (anterolingual to the protoconid and anterior to the metaconid), but which lacks a crest linking this cuspid to the protoconid. Although all specimens of *Lasiorhinus* we examined were too worn to score this character, a juvenile specimen of *L. latifrons* illustrated by Brewer et al. (2018: fig. 13) demonstrates that both the paraconid and paracristid are also absent in this taxon, which we scored as state 1.

We scored this character as inapplicable ("-") in *Tarsipes* (due to its vestigial postcanine dentition) and as unknown ("?") in the fossil vombatid †*Warendja*, because all available specimens of this taxon were too worn to allow confident scoring. As defined, the states of this character do not represent an obvious morphocline, so we did not order them in any of our analyses.

Character 160. *Lower first molar (m1) paracristid notched (0); or m1 paracristid unnotched*

(1). In tribosphenic metatherians that retain a distinct paracristid terminating in a well-developed paraconid on m1, this crest is usually notched (state 0). This morphology characterizes †*Herpetotherium*, †*Pucadelphys*, †*Allqokirus*, †*Mayulestes*, fossil and Recent didelphids (Voss and Jansa, 2009: figs. 24, 25), microbiotheriids, peramelemorphians, and most dasyuromorphians. The m1 paracristid is also notched in zalambdodont marsupials (*Notoryctes* and †*Yalkaparidon*). By contrast, in all examined paucituberculatan lower dentitions (i.e., of Recent caenolestids, †*Acdestis*, †*Palaeothentes*, †*Pichipilus*, and †*Stilotherium*) the m1 paracristid is unnotched, sloping gently without interruption from the protoconid to the anterolingual corner of the tooth (state 1; see Marshall, 1980: fig. 6; Rae et al., 1996: fig. 9; Goin et al., 2007a: char. 11; 2009a; char. 11; Abello, 2007: char. 15; 2013: char. 14, fig. 3K–L). The paracristid of m1 is similarly unnotched in dasyurids that lack a distinct paraconid on that tooth (namely, *Dasyuroides*, *Dasyurus*, *Myoictis*, *Sarcophilus*, *Murexechinus*, and *Pseudantechinus*), whereas more posterior teeth have notched paracristids; we also scored these taxa as state 1. In two other dasyurids (*Dasycercus* and *Phascolosorex*) the m1 paracristid is unnotched in some specimens but not others, so we scored them as polymorphic ("0+1").

The m1 paracristid is consistently notched in some pseudocheirids (*Pseudochirops archeri*, *Pseudochirulus*, and *Petropseudes*), but this notch is only variably present in other pseudocheirids (*Hemibelideus*, *Petauroides*, and *Pseudochirops cupreus*), *Phalanger*, *Ailurops*, and *Trichosurus*, which we scored as polymorphic ("0+1"). In all other diprotodontians in which the m1 paracristid is identifiable, this crest is unnotched. We scored this character as inapplicable ("-") in *Burramys*, *Acrobates*, *Myrmecobius*, *Lasiorhinus* and *Tarsipes*, none of which exhibit a distinct paracristid (char. 159), and we scored it as unknown ("?") in †*Warendja* because the first lower molars of available specimens were too worn to score confidently.

Character 161. *Second and third lower molars (m2, m3) with distinct paracristids (0); or both paraconids and paracristids indistinct or absent from m2 and m3 (1); or paraconid well developed but paracristid indistinct or absent on m2 and m3 (2).* As on m1 (see char. 159), the presence of distinct paracristids and paraconids on m2 and m3 appears to be plesiomorphic for metatherians, as seen (for example) in †*Herpetotherium*, †*Pucadelphys*, †*Allqokirus*, †*Mayulestes*, †*Mimoperadectes*, didelphids, microbiotheriids, dasyuromorphians, *Notoryctes*, †*Yalkaparidon*, and most peramelemorphians and paucituberculatans. In *Macrotis*, the pauctituberculatans †*Acdestis* and †*Palaeothentes* (see Marshall, 1980: 124; Marshall et al., 1990: fig. 2, node 33; Abello, 2007: char. 24, 2013: char. 23), and many diprotodontians (e.g., petaurids, pseudocheirids, burramyids, most macropodiforms), the paracristid is clearly identifiable on m2 and m3, but it does not terminate in a distinct, cusplike paraconid. However, because the degree of development of the paraconid on these teeth appears to vary continuously among examined taxa, we scored all of these as state 0 based on the presence or absence of the paracristid only, regardless of whether a distinct paraconid is present.

By contrast, both the paraconid and paracristid are absent from m2 and m3 in *Acrobates* and diprotodontids (state 1). In *Myrmecobius*, m2 and m3 resemble m1 (see char. 159) in possessing a well-developed paraconid anterolingual to the protoconid and anterior to the metaconid, but these teeth lack a paracristid linking the paraconid to the protoconid (state 2). As defined, the states of this character do not represent an obvious morphocline, so we did not order them in any of our analyses.

Character 162. *Paracristids of m2 and m3 deflected posterolingually by hypoconulid of preceding tooth (0); or paracristids of m2 and m3 undeflected (1); or paracristids of m2 and m3 terminate labial to the hypoconulid (2).* In most tribosphenic metatherians, the paracristid extends anterolingually in a more or less straight line from the protoconid to the paraconid (state 1), as in

†*Herpetotherium*, †*Pucadelphys*, †*Allqokirus*, †*Mayulestes*, didelphids (fig. 23A), microbiotheriids, peramelemorphians (fig. 23C), and most dasyuromorphians. However, in all examined paucituberculatan lower dentitions, the paracristids of m2 and m3 are abruptly deflected posterolingually by the hypoconulids of m1 and m2, respectively (fig. 23B; state 0).[20] Lower dental material referable to †*Evolestes hadrommatos* has not been described, but Goin et al. (2010: 75) reported that in †*Evolestes* sp. "the paracristid is not straight: there is a ~90° angle at the meeting of the postparacristid [their term for the lingual segment of the paracristid] and the preprotocristid [their term for the labial segment of the paracristid]," indicating that the paracristid is deflected as we observed in other paucituberculatans, so we also scored †*Evolestes* as state 0.

In pseudocheirids the paracristid extends anterolingually from the protoconid to terminate near the midpoint of the anterior margin of m2–4, well labial to the hypoconulids of the preceding teeth (Archer, 1984a [fig. 178D-H]; Roberts et al., 2008 [fig. 2B], 2009 [text-fig. 1B]), an apparently distinctive morphology (state 2).

We scored this character as inapplicable in taxa that lack an identifiable paracristid on m2 and m3 (*Myrmecobius*; see char. 161), or that lack an identifiable hypoconulid (†*Yalkaparidon*, *Notoryctes* (fig. 23D), most diprotodontians; see char. 178), or that lack both structures (diprotodontids, *Acrobates*).

Character 163. *Metaconid present on all lower molars (0); or absent on m1 only (1); or absent on all lower molars (2).* The metaconid is consistently present on m1–4 of most tribosphenic metatherians, including †*Pucadelphys*, †*Allqokirus*, †*Mayulestes*, †*Herpetotherium*,

†*Mimoperadectes*, didelphids (figs. 14, 23A), paucituberculatans (fig. 23B), microbiotheriids, peramelemorphians (fig. 23C), *Notoryctes* (fig. 23D), and most dasyuromorphians (state 0). However, the metaconid is absent on all four lower molars of *Thylacinus* (state 2; see, e.g., Ride, 1964a: fig. 7; Archer, 1984c: fig. 29; Muizon and Lange-Badré, 1997: fig. 4C, D; Archer et al., 2016b: fig. 9F; Solé and Ladevèze, 2017: fig. 4). An apparently intermediate morphology is seen in †*Badjcinus* (Muirhead and Wroe, 1998) and *Sarcophilus* (Ride, 1964a: fig. 7; Archer, 1984c: fig. 15B; Archer et al., 2016b: fig. 9E), in which the metaconid is absent on m1 but present on m2–4 (state 1). The metaconid is absent from m1 in some specimens of *Pseudantechinus* but present in others, whereas it is consistently present on m2–4; therefore, we scored this taxon as polymorphic (0+1). Although m2–4 of †*Mutpuracinus* clearly possess metaconids (Murray and Megirian, 2006a), m1 is unknown for this taxon, which we scored using ambiguity coding (as 0/1).

A distinct metaconid is present on all four lower molars of *Gymnobelideus*, most pseudocheirids (with the exception of *Hemibelideus* and some specimens of *Pseudochirops cupreus*), burramyids, some phalangerids (e.g., †*Onirocuscus*, *Phalanger*, *Spilocuscus*, *Trichosurus*, "*Trichosurus*" †*dicksoni*, and *Wyulda*), all modern and fossil macropodiforms, wynyardiids, diprotodontids, and phascolarctids. Among lophodont and bunolophodont diprotodontians, the metaconid forms the lingual end of the protolophid. Acrobatids have only three upper and lower molars (see char. 130), but a distinct metaconid is present on all three lower molars, so these terminals were scored as 0. Examined specimens of the vombatids *Vombatus* and *Lasiorhinus* were too worn to confidently score this character, but juvenile specimens illustrated by Brewer et al. (2018: fig. 13) suggest that the metaconid is present on m1–4 of both taxa, which have been scored as state 0.

The m1 trigonid of thylacoleonids comprises a single cuspid, which we consider to be homologous with the protoconid following Gillespie

---

[20] Both *Acdestis* and *Palaeothentes* lack a distinct paracristid on m2 and m3; it is probably fused with the metaconid, given the closely twinned morphology of the paraconid and metaconid seen in †*Phonocdromus*, †*Pichipilus*, and †*Pliolestes* (see Marshall, 1980: fig. 7; Goin et al., 1994, 2007a: char. 23, 2009a: char. 23; Ortiz Jaureguizar, 1997: char. 13; Abello, 2007: char. 26, 2013: char. 25). However, the paracristid (which forms the anterior margin of m2 and m3 in these taxa, the anterior cingulid being essentially absent) appears sharply deflected, so we scored them as state 0.

(2007), but contra Woods (1956), Clemens and Plane (1974), and Megirian (1986), all of whom identified it as the metaconid. In †*Lekanoleo* (which has four lower molars; Gillespie, 2007: fig. 8.8) and †*Wakaleo* (which has only three lower molars; Gillespie et al., 2014: fig. 5C), a distinct metaconid is present on m2. The morphology of the more posterior lower molars (m3–4) is currently unknown in †*Lekanoleo* (Gillespie, 2007; Gillespie et al., 2020), and the m3 of †*Wakaleo* is occlusally simplified (Gillespie et al., 2014); nevertheless, we scored both terminals as state 1 based on the condition in m1–2. The m2 of †*Thylacoleo* is very small and occlusally simple, so it is unclear whether a metaconid is present on this tooth; given that the metaconid is unequivocally absent from m1 in this taxon (see above), we scored †*Thylacoleo* as ambiguous (1/2) for this character. A distinct metaconid is also absent from m1 in *Dactylopsila* (Archer, 1984c: fig. 208), *Dactylonax*, *Hemibelideus*, and *Strigocuscus*, but the metaconid is clearly identifiable on at least one more posterior molar in all these taxa, which we therefore scored as state 1. A metaconid is variably present on m1 in *Petaurus*, *Pseudochirops cupreus*, and *Ailurops*, all of which we scored as polymorphic ("0+1"). The homology of the posterolingual cusp on the lower molars of †*Yalkaparidon* is unclear: it might either be the metaconid (as in *Notoryctes*) or a remnant of the talonid (Beck et al., 2014: 155). We therefore scored †*Yalkaparidon* as unknown ("?").

The states of this character represent a plausible morphocline and have been so ordered in all of our phylogenetic analyses.

Character 164. *Trigonid of m4 resembles that of m3 (0); or m4 trigonid structurally simplified, only the metaconid distinct (1); or m4 trigonid structurally simplified, only the protoconid distinct (2).* In most metatherians the trigonid of m4 resembles that of m3 (state 0). However, in living caenolestids and †*Acdestis* only a single cuspid is distinct on the m4 trigonid; based on its position and comparisons with m1–3, this cuspid appears to be the metaconid (state 1; Voss and Jansa,

2009: 59–60). In *Burramys*, the trigonid of m4 is also reduced to a single distinct cuspid, but comparison with more anterior molars suggest that in this case it is the protoconid (state 2). We scored this character as inapplicable ("-") in taxa lacking m4 (acrobatids, †*Wakaleo*, and †*Thylacoleo*). As defined, these states do not form a plausible morphocline, so we left this character as unordered in all our phylogenetic analyses.

Character 165. *Additional cuspid labial to m1 protoconid absent (0); or present, forming a cusplike protostylid (1); or present, forming a vertically directed crest (2).* In most metatherians, the protoconid is the labialmost trigonid cuspid (state 0). However, in a number of diprotodontians the m1 trigonid is strongly compressed labiolingually and a neomorphic cuspid—the protostylid sensu Flannery and Rich (1986)—is present labial to the protoconid (state 1). This obviously derived morphology is seen in pseudocheirids (in which the protostylid is particularly large; Archer, 1984c: figs. 178E–H, 180B, F), phascolarctids (Black et al., 2012a), *Phalanger* (Flannery and Rich, 1986: fig. 13. 1), *Hypisprymnodon moschatus* (Cooke, 1997a: fig. 6F), †*Ganawamaya* (Kear et al., 2007; Butler et al., 2018), and †*Ekaltadeta* (Archer and Flannery, 1985). Some specimens of *Spilocuscus* exhibit a distinct cusplike protostylid on m1, but in others this cusp is absent (Cooke, 1997b: 278), and it is only variably present in †*Ilaria* spp. (present in †*I. illumidens*, absent in †*I. lawsoni*; Tedford and Woodburne, 1987: 410), so we scored both of these taxa as polymorphic ("0+1"). Archer (1984c: fig. 143) and Aplin and Archer (1987: lviii) suggested that the major labial cuspid of the trigonid in the acrobatids *Acrobates* and *Distoechurus* might represent a protostylid, but unpublished fossil acrobatid material from late Oligocene to middle Miocene sites at Riversleigh World Heritage Area convincingly demonstrate that it is the protoconid (Fabian, 2012).

In the thylacoleonids †*Lekanoleo* (Gillespie, 2007: fig. 8.8), †*Wakaleo* (Gillespie et al., 2014: fig. 5A, C), and †*Thylacoleo* there is a well-developed vertical crest (rather than a cuspid) but-

tressing the labial face of m1 (state 2). Because these states do not form a plausible transformation series, we did not order this character in any of our phylogenetic analyses.

Character 166. *Talonid present (0); or greatly reduced or absent (1).* A distinct talonid is present posterior to the trigonid (state 0) in most metatherians, but in *Notoryctes* the talonid is absent or reduced to a tiny, cingulidlike remnant posterior to the metaconid (state 1; Archer, 1984c: fig. 57F, G; Asher and Sánchez-Villagra, 2005: fig. 6A; Archer et al., 2011: fig. 1). As discussed earlier (see char. 163), the homology of the part of the lower molars posterior to the protoconid in †*Yalkaparidon* is unclear, representing either the metaconid or a remnant of the talonid (Beck et al., 2014: 155); whichever it is, the talonid is clearly reduced to a vestige in this taxon (Archer et al., 1988; Beck, 2009; Beck et al., 2014), which we also scored as state 1. Due to the absence of a distinct talonid in both *Notoryctes* and †*Yalkaparidon*, we scored all subsequent characters relating to talonid structures (i.e., chars. 167–180) as inapplicable ("-") for these two taxa. We also scored this character as inapplicable in *Tarsipes* due to the vestigial nature of its postcanine dentition (see char. 113).

Character 167. *Cristid obliqua present (0); or absent or indistinct (1).* The cristid obliqua is present (state 0) in most tribosphenic metatherians as a prominent crest that extends anterolingually from the hypoconid (figs. 14, 23A–C). The cristid obliqua is also present in most fully and incipiently lophodont diprotodontians (fig. 25); in many of these forms, the cristid obliqua connects the protolophid and hypolophid, and hence is often referred to as the "midlink." In phalangerids, a crest that is probably homologous with the cristid obliqua is strongly kinked (see char. 168). However, the cristid obliqua is entirely absent from the lower molars of †*Neohelos* (Murray et al., 2000a; Black et al., 2013: fig. 6C), †*Silvabestius* (Black and Archer, 1997a: fig. 3), and †*Nimbadon* (Hand et al., 1993: fig. 3; Black et al., 2010: figs. 7, 10M, N; Black and Hand, 2010: fig. 8); in these taxa the protolophid

(homologous with the metacristid of tribosphenic molars) and hypolophid are separated by a crestless valley. In †*Ngapakaldia*, however, the cristid obliqua is variably present (Black, 2010, referred to this crest as the "midlink"), so we scored this taxon as polymorphic ("0+1"). The cristid obliqua is consistently absent in *Myrmecobius*, which we also scored as state 1.

We scored this character as inapplicable ("-") in *Notoryctes*, †*Yalkaparidon*, and *Tarsipes* for reasons previously discussed (see char. 166). We also scored it as inapplicable in †*Thylacoleo*, in which the occlusal structures of the talonid are extremely simplified.

Character 168. *Cristid obliqua not strongly kinked (0); or with strongly developed buccal kink (1).* Flannery et al. (1987: 482–483) identified the presence of a buccal kink in the cristid obliqua— a morphology referred to as an "angulate cristid obliqua" by Woodburne (1984b: 65) and several other authors (e.g., Woodburne and Clemens, 1986a, 1986b; Black and Archer, 1997b; Crosby and Archer, 2000)—as a distinctive feature of Recent phalangerids, some fossil phalangeroids, and the fossil macropodoid *Hypsiprymnodon* †*bartholomaii* (see also Flannery and Archer, 1987c). Despite its potential phylogenetic significance, most authors have not provided a clear description of this trait, although it was well illustrated by Flannery and Rich (1986: fig. 2-2). Here we employ a modified version of the definition provided by Crosby (2002a: 337), namely, that this crest is kinked when it extends for a short distance anteriorly from the hypoconid before changing direction sharply lingually, resulting in a distinctly angled deflection in occlusal view (fig. 25B-C).

This kinked crest has been universally identified as the cristid obliqua by previous authors (e.g., Woodburne, 1984b; Woodburne and Clemens, 1986a, 1986b; Archer et al., 1987; Flannery and Archer, 1987a, 1987c; Flannery et al., 1987; Woodburne et al., 1987a; Marshall et al., 1990; Black and Archer, 1997b; Brammall, 1998; Crosby and Archer, 2000; Crosby, 2002a, 2002b; Helgen and Flannery, 2004; Schwartz, 2006a).

However, we observed two separate, well-developed crests extending anteriorly from the hypoconid on the unworn m2 and m3 of young specimens of *Burramys* (e.g., NMV C26919). The more labial of these two crests is slightly kinked, somewhat resembling the morphology seen in phalangerids, whereas the more lingual crest resembles the uninflected cristid obliqua of, for example, *Cercartetus* (Archer, 1984c: figs. 154–156), petaurids, and acrobatids. Two crests, resembling those we observed in *Burramys*, can also be seen on an unworn m2 of "*Trichosurus*" †*dicksoni* (QM F13061), but on this tooth the more lingual, unkinked crest (referred to as an "accessory ridge" by Flannery and Archer, 1987b: 534) is vestigial and extends only a short distance from the hypoconid, whereas the kinked crest is well developed (see Flannery and Archer, 1987b: fig. 3F). The presence of two crests extending from the hypoconid in *Burramys* and "*T.*" †*dicksoni* raises the possibility that the kinked crest is not homologous with the cristid obliqua, but instead represents a neomorph. Alternatively, it could be that the unkinked crest seen in these two taxa is neomorphic. However, in the absence of more compelling data, we follow traditional usage here and refer to the kinked crest as the cristid obliqua.

The cristid obliqua is strongly kinked (state 1) in phalangerids, *Dactylopsila* (e.g., AMNH 157140), *Hypsiprymnodon* †*bartholomaii* (based on QM F13053, an unworn left m3; Flannery and Archer, 1987c: fig. 4B), and *H. moschatus* (e.g., AMNH 160120). Because we are uncertain which of the two crests extending from the hypoconid in *Burramys* is the homolog of the cristid obliqua (see above), we scored this taxon as unknown ("?"). Some pseudocheirids (e.g., *Pseudochirulus*) exhibit a distinctly kinked crest extending from the hypoconid on m4, but not on more anterior molars, so we scored these taxa as state 0. This character is inapplicable for *Myrmecobius* (in which the cristid obliqua is absent; char. 167) and †*Thylacoleo* (in which the occlusal structures of the talonid are greatly reduced; char. 167). We scored all other examined taxa

with nonvestigial talonids as state 0. (Note, however, that a kinked cristid obliqua has also been reported in a number of fossil diprotodontians not included here; Crosby and Archer [2000].)

Character 169. *Cristid obliqua of m1 contacts metaconid (0); or contacts metacristid labial to metaconid (1); or terminates labial to protoconid (at protostylid) (2).* In most metatherians in which the cristid obliqua is present (see char. 167), this crest extends anterolingually from the hypoconid to contact the metacristid (or protolophid), at a point labial to the metaconid (state 1). Minor positional differences in the point of contact between the cristid obliqua and metacristid (specifically, whether it is labial or lingual to the "carnassial notch" of the metacristid) have been coded in several previous analyses of metatherian phylogeny (e.g., Springer et al., 1997 [char. 23]; Horovitz and Sánchez-Villagra, 2003 [char. 160]), but we observed continuous variation in this trait among the taxa examined for the present study. However, a qualitatively distinct morphology (state 0) is seen in most pseudocheirids, where the m1 cristid obliqua extend lingually past the metacristid to connect directly with the metaconid (Archer, 1984c: fig. 178E–H; Roberts et al., 2008: fig. 2A). An m1 cristid obliqua that contacts the metaconid has been identified as a potential synapomorphy of Pseudocheiridae (e.g., Archer, 1984c; Archer et al., 1987; Woodburne et al., 1987b), but the cristid obliqua consistently terminates at the metacristid (anterolabial to the metaconid) in *Pseudochirulus*; *Pseudochirops archeri* is polymorphic ("0+1") for these traits; and *Hemibelideus* cannot be meaningfully scored for this character because it lacks a distinct m1 metaconid (see char. 163). Additionally, we observed state 0 in a number of other metatherians, namely *Burramys* (Archer, 1984c: fig. 147E), acrobatids (Archer, 1984c: fig. 143), †*Acdestis* (Bown and Fleagle, 1993: figs. 14, 15.5; Abello, 2007: lámina 11; Abello, 2013: fig. 3I), †*Palaeothentes* (Bown and Fleagle, 1993: fig. 11; Abello, 2007: lámina 9F–L; Abello, 2013: fig. 3G–H), and *Chaeropus* (Travouillon, 2016: fig. 2i, j).

In *Hypsiprymnodon moschatus* (see Cooke, 1997a: fig. 6F) and †*Ekaltadeta* (Archer and Flannery, 1985: fig. 7.4), the m1 cristid obliqua terminates at the protostylid, labial to the protoconid, a distinctive morphology that we scored as an additional state (state 2; see char. 165).

We scored this character as inapplicable ("-") in taxa that lack an identifiable m1 metaconid (e.g., *Hemibelideus*, thylacoleonids, some dasyuromorphians; char. 163) or that lack an m1 cristid obliqua (i.e., *Myrmecobius*, †*Neohelos*, †*Nimbadon*, †*Silvabestius*; char. 167). We also scored this character as inapplicable ("-") in *Notoryctes*, †*Yalkaparidon*, and *Tarsipes* for reasons previously discussed (see char. 166). As arranged here, the states comprising this character comprise a plausible morphocline, reflecting a progressive labial shift in the point of termination of the m1 cristid obliqua. Thus, we ordered this character in all our phylogenetic analyses.

Character 170. *Anterior terminus of cristid obliqua of m2–4 contacts protoconid or metacristid (0); or bypasses metacristid to terminate at entoconid or entocristid (1); or terminates at distinct fissure (2).* In the vast majority of metatherians in which the cristid obliqua of m2–4 is present, this crest terminates at the protoconid, or slightly lingual to this, at the metacristid or protolophid (figs. 23A–C, 24; state 0). However, the cristid obliqua of m2–4 bypasses the metacristid to terminate at the entoconid or entocristid (state 1) in *Chaeropus* (Travouillon, 2016: fig. 2i, j)[21] and †*Nimiokoala*. The bandicoot *Isoodon* is polymorphic for this character ("0+1"). A qualitatively distinct morphology is observed in some phalangerids (*Ailurops*, *Phalanger*, *Spilocuscus*, *Strigocuscus* [Flannery and Rich, 1986: fig. 2.2], and †*Onirocuscus*), in which a distinct fissure separates the anterior terminus of the cristid obliqua from other structures on the occlusal surface of m2–4 (state 2). The morphology of the cristid obliqua can be obscured by wear, so we only scored it from specimens with unworn or

lightly worn teeth. We scored diprotodontids (with the exception of †*Ngapakaladia*) and *Myrmecobius* as inapplicable ("-") due to the consistent absence of a cristid obliqua on m2–4 in these taxa (see char. 167). We also scored †*Thylacoleo* as inapplicable (due to its highly reduced m2), and we scored *Notoryctes*, †*Yalkaparidon*, and *Tarsipes* as inapplicable for reasons previously discussed (see char. 166). As defined, these states do not represent an obvious morphocline, so we left this character as unordered in all our phylogenetic analyses.

Character 171. *Neomorphic cuspid(s) in hypoflexid region absent (0); or present (1).* Where present, the hypoflexid of metatherians is a shallow labial indentation of the tooth crown adjacent to the cristid obliqua, between the protoconid and hypoconid (fig. 14). In most metatherians in which it is identifiable, this region is essentially featureless (state 0), although a small cingulid is sometimes present (fig. 23A-B). However, one or more distinct, neomorphic cuspids (ectostylids sensu Van Valen, 1966: fig. 1B) are present within the hypoflexid region (state 1) of the peramelemorphians *Echymipera*, *Isoodon*, and *Macrotis* (see Travouillon et al., 2010 [char. 23] and subsequent papers that used versions of their matrix for the distribution of this character in peramelemorphians), as well as the diprotodontians *Phascolarctos*, *Hemibelideus*, *Pseudochirops cupreus*, and *Petropseudes*. Hypoflexid cuspids are also variably present in *Ailurops*, *Lestoros*, and *Lestodelphys* (e.g., MMNH 17171), all of which we scored as polymorphic ("0+1"). We scored this character as inapplicable ("-") in *Notoryctes*, †*Yalkaparidon*, and *Tarsipes* for reasons previously discussed (see char. 166).

Character 172. *Hypoconid large and distinct (0); or small and indistinct (1).* The hypoconid is the prominent posterolabial cuspid of the lower molars in most metatherians that retain a talonid (figs. 14, 23A–C, 24; state 0). However, as described by Bensley (1903: 103; see also Waterhouse, 1841: 150; Tate, 1951: 4; Archer and Kirsch, 1977: 20), both of the labial cusps (protoconid and hypoconid) are reduced relative to

---

[21] This distinctive morphology was also illustrated by Wright et al. (1991: fig. 2) who, however, labelled the cristid obliqua as the prehypocristid.

the lingual cusps (paraconid, metaconid, and entoconid) on the lower molars of *Myrmecobius*, with the reduction of the hypoconid particularly striking (state 1). The hypoconid is also small and indistinct on m1 and m2 of †*Wakaleo* (Gillespie et al., 2014: fig. 5) and †*Thylacoleo*, and on all lower molars of †*Sparassocynus* (Beck and Taglioretti, 2020); we therefore also scored these three terminals as state 1. We scored this character as inapplicable ("-") in *Notoryctes*, †*Yalkaparidon*, and *Tarsipes* for reasons previously discussed (see char. 166).

Character 173. *Lower third molar hypoconid labially salient, projecting beyond the protoconid or level with it (0); or m3 hypoconid lingual to salient protoconid (1).* Descriptions of character states and an account of their taxonomic distribution among Recent didelphids were provided by Voss and Jansa (2003: char. 65). This character is equivalent to characters in other studies that considered the relative widths of the trigonid and talonid (e.g., Springer et al., 1997: char. 13; Rougier et al., 1998: char. 50; Horovitz and Sánchez-Villagra, 2003: char. 158). We corroborated the scoring of Voss and Jansa (2003, 2009), except that we observed the m3 hypoconid to be approximately level with the protoconid in *Lutreolina* (e.g., on AMNH 133255, 210421; see also Martinez-Lanfranco et al., 2014: fig. 7D), which we therefore scored as state 0. In effect, the only Recent didelphids in which the m3 hypoconid is lingual to the protoconid are *Chacodelphys*, *Lestodelphys*, and *Monodelphis*.

Among other metatherians, the m3 hypoconid is labially salient in †*Herpetotherium* (Korth, 2018: fig. 6b), paucituberculatans, microbiotheriids, some peramelemorphians (e.g., *Echymipera*, *Perameles*, *Peroryctes*, *Rynchomeles*, and †*Galadi* [Travouillon et al., 2010: fig. 11]), †*Litokoala* (Black and Archer, 1997b: fig. 6A, C), *Phascolarctos* (Black et al., 2014a: figs. 2C, D, 11), †*Namilamadeta* (Pledge, 2005), Recent vombatids, several macropodiforms (including most macropodids), most phalangerids (with the exception of *Wyulda* and "*Trichosurus*" †*dick-*

soni), pseudocheirids, petaurids, and *Burramys* (Archer, 1984c: fig. 147E).

By contrast, the m3 hypoconid is consistently lingual to the protoconid in †*Pucadelphys* (Marshall and Muizon, 1995: fig. 7E; Ladevèze et al., 2011: fig. 4), †*Mayulestes* (Muizon, 1998: figs. 3B, E, 4C), †*Allqokirus* (Muizon et al., 2018: figs. 11–13), †*Mimoperadectes* (Bown and Rose, 1979: text-fig. 1A), †*Sparassocynus* (Abello et al., 2015: fig. 3A; Beck and Taglioretti, 2020: fig. 3b), †*Hesperocynus* (Forasiepi et al., 2009: fig. 7C), †*Thylophorops* (Goin et al., 2009b: fig. 4A), †*Thylatheridium* (Reig, 1952: fig. 11B), *Macrotis*, †*Yarala*, most examined dasyuromorphians, †*Nimiokoala* (Black and Archer, 1997b: figs. 2C, 3B), †*Muramura* (Pledge, 1987c: fig. 4D), diprotodontids, several macropodiforms (including *Aepyprymnus*, *Caloprymnus*, *Potorous*, *Bettongia*, and ?*Bettongia* †*moyesi* [Flannery and Archer, 1987a: figs. 1B, 3), *Wyulda*, "*Trichosurus*" †*dicksoni* (Flannery and Archer, 1987a: fig. 3F, K), acrobatids (Archer, 1984c: fig. 143), and *Cercartetus* (Archer, 1984c: figs. 154–156). We observed polymorphisms in several taxa—including *Chaeropus*, *Isoodon*, *Microperoryctes*, *Micromurexia*, *Myrmecobius*, *Osphranter*, and †*Warendja*—all of which we scored as "0+1." We scored this character as inapplicable ("-") in *Notoryctes*, †*Yalkaparidon*, and *Tarsipes* for reasons previously discussed (see char. 166). The m3 of †*Wakaleo* is so reduced as to preclude meaningful scoring (Gillespie et al., 2014: figs. 5, 6A), so this taxon has also been scored as inapplicable ("-").

Character 174. *Entostylid labial to the entoconid absent (0); or present (1).* In most nonlophodont metatherians that possess a distinct entoconid there is no structure immediately labial to this cuspid (state 0). However, a distinct cusplike structure that we refer to as an entostylid (after Archer, 1984c: figs. 178E–H, 185, 186D, 187; Roberts et al., 2008: fig. 2A) is present labial and slightly posterior to the entoconid (state 1) on the lower molars of *Pseudochirops cupreus* and *P. archeri* (see Archer, 1984c: fig. 178D–G, 186D, 187). A cusplike entostylid is

also present in †*Litokoala* (Springer, 1987; Black and Archer, 1997b) and †*Nimiokoala* (Black and Archer, 1997b). An entostylid is clearly identifiable on the unworn m1 posterolabial to the entoconid in *Phascolarctos* (see Black et al. [2014a:], who referred to it as an "entostylid ridge"), but it is less obvious on more posterior molars; however, we also scored *Phascolarctos* as state 1. Following Tedford and Woodburne's (1987) homologies for the lower molar cuspids of †*Ilaria*, a neomorphic "central" cuspid is present between the entoconid and hypoconid; we tentatively identify this as an entostylid, and score †*Ilaria* as state 1.

We scored most incipiently or fully lophodont diprotodontians (i.e., those scored as state 1 or state 2 for char. 144) as inapplicable ("-") for this character, because it is unclear whether an entostylid is genuinely absent or has been incorporated into the hypolophid of such taxa. However, this character can be meaningfully scored in a few incipiently lophodont diprotodontians—including *Petaurus*, *Gymnobelideus*, *Distoechurus*, *Cercartetus*, and *Hypispymnodon moschatus*—all of which have been scored as state 0. By contrast, a cusplike entostylid is clearly identifiable on the unworn lower molars of †*Namilamadeta* (e.g., QM F51342; Pledge, 2005: fig. 7B), although this structure has been partially incorporated into the hypolophid.

This character was scored as inapplicable in †*Thylacoleo* (due to the extremely simplified morphology of its m1, the only lower molar in this taxon) and in *Notoryctes*, †*Yalkaparidon*, and *Tarsipes* for reasons previously discussed (see char. 166). As defined, these states do not comprise a plausible morphocline, and hence this character has been left unordered in all analyses presented here.

Character 175. *Entoconid large and well developed on m1–3 (0); or very small or indistinct (1).* Among metatherians that retain a fully developed talonid, the entoconid is usually a large lingual cuspid (state 0). However, this cusp is very small or indistinct (state 1) in a number of metatherians. Descriptions of character states

and an account of their taxonomic distribution among Recent didelphids were provided by Voss and Jansa (2003: char. 66, fig. 16; 2009), who observed that the entoconid is very small (subequal to or smaller than the hypoconulid) in *Chacodelphys* and *Monodelphis*.

Among our other terminals, we observed an entoconid that is subequal to or smaller than the hypoconulid in †*Mayulestes* (Muizon, 1998: figs. 3C, D, 4B), †*Allqokirus* (Muizon et al., 2018: figs. 11–13), †*Mimoperadectes* (Bown and Rose, 1979: text-fig. 1A), †*Sparassocynus* (Beck and Taglioretti, 2020), †*Hesperocynus* (Forasiepi et al., 2009: fig. 7D), †*Thylatheridium* (Reig, 1952: fig. 10B), *Thylacinus* (Muizon and Lange-Badré, 1997: fig. 4C; Archer et al., 2016b: fig. 9F; Warburton et al., 2019: figs. 10–13), and several dasyurids (*Antechinomys*, *Dasycercus*, *Dasykaluta*, *Dasyuroides*, *Ningaui*, *Parantechinus*, *Planigale*, and *Pseudantechinus*). In *Sarcophilus*, the entoconid appears to have been lost entirely (Archer et al., 2016b), as also seems to be the case in some sparassodonts (Forasiepi et al., 2014a). Archer (1981) observed that the degree of development of the entoconid in dasyurids appears to be correlated with habitat, with arid-adapted taxa typically exhibiting smaller entoconids than those living in areas of higher rainfall. Although *Distoechurus*, †*Wakaleo* (Gillespie et al., 2014: fig. 5), and †*Thylacoleo* lack identifiable hypoconulids for relative size comparisons, the entoconid is clearly very small in these taxa, which we also scored as state 1. We scored this character as inapplicable ("-") in *Notoryctes*, †*Yalkaparidon*, and *Tarsipes* for reasons previously discussed (see char. 166).

Character 176. *Entocristid present (0); or indistinct or absent (1).* In most metatherians, the entocristid is a well-developed crest that extends anteriorly or anterolabially (see char. 177) from the entoconid (state 0). However, the entocristid is indistinct or absent (state 1) in *Myrmecobius*, some peramelemorphians (*Chaeropus*, *Macrotis*, *Perameles* [fig. 26A], †*Yarala* [Muirhead and Filan, 1995: fig. 1.3], some specimens of *Isoodon*), *Sminthopsis*, and some diprotodontians (e.g.,
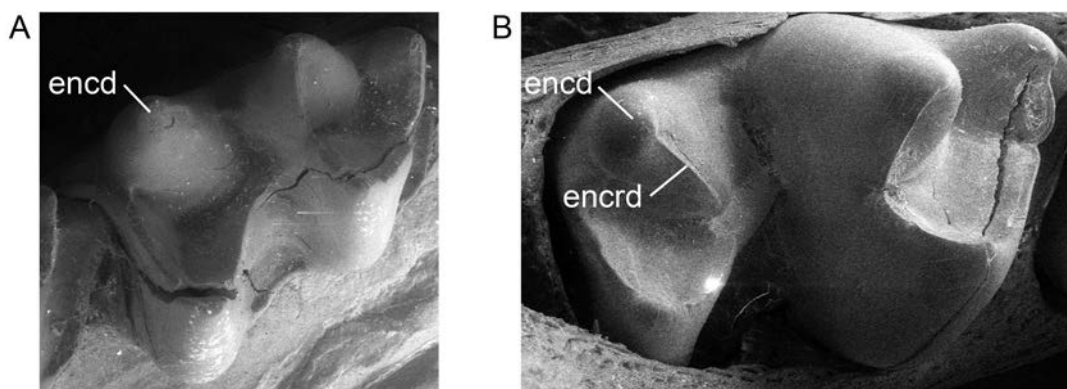
FIG. 26. Occlusal views of lower molars of *Perameles gunnii* (**A,** MVZ 127060[left m2]) and *Isoodon macrourus* (**B,** AMNH 160085[right m3, not fully erupted]). General features of lower molar crown morphology discussed in the text are illustrated, as are characters 176 and 177 (see main text for descriptions of these characters and character states), as follows: *Perameles* 176(1), 177(-); *Isoodon* 176(0), 177(1). Abbreviations: **encd,** entoconid; **encrd,** entocristid. Teeth are not shown to the same scale.

†diprotodontids, most Recent macropodids). In other diprotodontians—for example, *Dactylopsila* (in which an additional, presumably neomorphic cuspid [= entoconulid sensu Van Valen, 1966: fig. 1B] is present between the metaconid and entoconid on m2–4), †*Namilamadeta* (Pledge, 2005: fig. 1), †*Nimbadon* Hand, et al., 1993: 201), †*Bulungamaya* (Travouillon et al., 2014b: fig. 4.7), †*Ganguroo* (Travouillon et al., 2014b: figs. 2.5, 2.7, 4.8), and *Dorcopsulus*—a distinct entocristid is present on m1 but absent from m2–4; we scored these taxa as state 1 based on the condition observed for m2–4. Because the entocristid extends from the entoconid, we scored this character as inapplicable ("-") for taxa in which the entoconid is unidentifiable, absent, or so indistinct as to preclude meaningful scoring (i.e., *Tarsipes*, †*Thylacoleo*, *Thylacinus*, *Dasykaluta*, *Ningaui*, *Planigale*, *Sarcophilus*, *Notoryctes*, and †*Yalkaparidon*; see char. 175).

Character 177. *Entocristid extends along the lingual margin of the tooth (0); or entocristid well labial of the lingual margin (1); or entocristid with distinct anterolabial kink (2).* When present, the entocristid is usually a short, straight crest that extends anteriorly from the entoconid along the lingual edge of the talonid (figs. 14, 23A, C). However, as discussed by Voss and Jansa (2009:

60; see also Abello, 2007: char. 38; Goin et al., 2007b: char. 19; Goin et al., 2009a: char. 19; Abello, 2013: char. 37), the entocristid of *Caenolestes* and *Rhyncholestes* is long and deflected labially, terminating within the talonid basin (state 0; fig. 23B). Among other paucituberculatans, the same (labially deflected) entocristid morphology occurs in *Lestoros* and †*Pichipilus*, whereas †*Acdestis*, †*Palaeothentes*, and †*Stilotherium* are polymorphic ("0+1") for this character. The entocristid also extends somewhat labially, away from the lingual margin of the tooth, on unworn molars of *Isoodon* (e.g., AMNH 160085; fig. 26B) and in several diprotodontians—including phascolarctids (e.g., *Phascolarctos*; fig. 24A), pseudocheirids (fig. 24B; Archer, 1984c: figs. 178E–H, 185, 186D; Roberts et al., 2008: fig. 2, 2009: text-fig. 1A, B), *Cercartetus*, *Dorcopsis* (e.g., AMNH 109396), and *Lagostrophus* (e.g., WAM M2432)—and the same trait occurs on m1 (only) of *Dorcopsulus* (e.g., AMNH 158998), and †*Nimbadon* (e.g., QM F53648b, F30784; see also Hand et al., 1993: 201). Although the entocristid in these taxa is usually not as long nor as strongly deflected as it is in paucituberculatans, we also scored them as state 1.

On unworn molars of all examined Recent and fossil phalangerids the entocristid is short

and distinctly kinked, somewhat resembling the kinked cristid obliqua of these taxa (see char. 168): the entocristid extends anteriorly and slightly lingually from the apex of the entoconid before changing direction sharply and extending anterolabially for a short distance toward the center of the tooth (state 2). We scored this character as inapplicable ("-") in all taxa entirely lacking an entocristid (see char. 176), and we scored it as inapplicable in *Notoryctes*, †*Yalkaparidon*, and *Tarsipes* for reasons previously discussed (see char. 166). As defined, these states do not represent an obvious morphocline, so we left this character as unordered in all our phylogenetic analyses.

Character 178. *Hypoconulid present (0); or absent or indistinct (1).* A distinct hypoconulid is present (state 0) in most metatherians with an identifiable talonid, including †*Pucadelphys*, †*Mayulestes*, †*Allqokirus*, †*Mimoperadectes*, †*Herpetotherium*, didelphids (fig. 14, 23A), paucituberculatans (fig. 23B), microbiotheriids, dasyuromorphians, and peramelemorphians (fig. 23C). By contrast, the hypoconulid is absent (state 1) from most examined diprotodontians that could be scored for this character. However, we observed a distinct hypoconulid in pseudocheirids, in which this cusp is clearly identifiable immediately posterior to the entoconid on m1 and m2 (fig. 24B). Springer (1993: fig. 1) referred to this cusp in pseudocheirids as the "entostylid," but we follow Archer (1984b [fig. 178F–I]), Bassarova et al. (2001 [fig. 1b]), and Roberts et al. (2007 [fig. 1], 2008 [fig. 2]), who identified it as the hypoconulid and referred to the cusp labial to the entoconid as the entostylid (see char. 174).

In juvenile specimens of *Vombatus* (e.g., AMNH 65623; Brewer et al., 2018: fig. 13.2) two cuspids visible on the unworn m3 might represent the hypoconulid. The first of these is immediately posterior to and basally confluent with the entoconid, whereas the second is smaller and located in the middle of a low cristid that connects the hypoconid with the entoconid and defines the posterior margin of the talonid. Although it is unclear which of these two cuspids is homologous

with the hypoconulid, it seems probable that one of them is, so we scored *Vombatus* as state 0. By contrast, there is no trace of a hypoconulid on any of the unworn lower molars of *Lasiorhinus* (Brewer et al., 2018: fig. 13.2).

We scored this character as inapplicable ("-") in *Notoryctes*, †*Yalkaparidon*, and *Tarsipes* for reasons previously discussed (see char. 166).

Character 179. *Hypoconulid at or near posterolingual margin of talonid, twinned with entoconid on m1–3 (0); or at midline of tooth, approximately equidistant to hypoconid and entoconid, not "twinned" with the latter cusp (1).* Descriptions of character states and an account of their taxonomic distribution among Recent didelphids were provided by Voss and Jansa (2003: char. 67; 2009). In most didelphids (including all the fossil didelphids included here, namely, †*Hesperocynus*, †*Sparassocynus*, †*Thylatheridium*, and †*Thylophorops*), the hypoconulid is positioned near the posterolingual margin of the talonid and is said to be twinned with the entoconid (state 0), but in *Caluromysiops* the hypoconulid is about equidistant to the entoconid and hypoconid, near the midline of the tooth (state 1). When present, the hypoconulid is also twinned with the entoconid in most examined nondidelphid metatherians, with the exceptions of *Thylacinus* and †*Acdestis*. In *Thylacinus*, the hypoconulid is distinctly cusplike but approximately on the dental midline (Muizon and Lange-Badré, 1997: fig. 4D; Archer et al., 2016b: fig. 9F; Solé and Ladevèze, 2017: fig. 4; Warburton et al., 2019: figs. 11–13). In †*Acdestis*, the hypoconulid forms a cingulidlike structure (Abello, 2007: char. 46, 2013: char. 45; Goin et al., 2007b: char. 16, 2009a: char. 16), which is approximately equidistant between the entoconid and hypoconid (Bown and Fleagle, 1993: fig. 13; Abello, 2007: lámina 11; 2013: fig. 3I),[22] Both of these taxa have been scored as state 1 here.

As remarked by several authors (e.g., Muirhead, 1994, 2000; Muirhead and Filan, 1995;

---

[22] The hypoconulid is also cingulidlike in †*Palaeothentes*, but it is closer to the entoconid than to the hypoconid.

Woodburne and Case, 1996; Wroe, 1996a, 1997b, 2003; Beck et al., 2008b), the hypoconulid is in a very lingual position in all Recent and fossil peramelemorphians, immediately posterior (rather than posterolabial) to the entoconid. We did not score this morphology as a distinct state (contra, e.g., Wroe et al., 2000: char. 28; Wroe and Musser, 2001: char. 28; Travouillon et al., 2010: char. 20) because we observed a continuous range of variation in the position of the hypoconulid (from posterolingual to lingual) among the taxa included in this study, and because the position of the hypoconulid in peramelemorphians appears to be at least partially connected with the absence of a hypoconulid notch, which we have already coded as a separate character (see char. 158).

We scored this character as inapplicable ("-") in all taxa lacking an unambiguously identifiable hypoconulid (see char. 178). Although the hypoconulid is clearly present in *Sarcophilus*, the absence of an unambiguously identifiable entoconid (see Archer et al., 2016b) likewise precludes meaningful scoring of this character for this taxon. We also scored this character as inapplicable ("-") in *Notoryctes*, †*Yalkaparidon*, and *Tarsipes* for reasons previously discussed (see char. 166).

Character 180. *Lower molars without a posterior cingulid (0); or distinct posterior cingulid present (1).* Many tribosphenic metatherians have a posterior cingulid (or postcingulid), a narrow but distinct basal shelf of enamel that extends along the posterolabial margin of each lower molar from the hypoconid to the hypoconulid (state 1). This is the morphology seen in †*Allqokirus*, †*Mayulestes*, †*Pucadelphys* (Ladevèze et al., 2011: fig. 4a, b), †*Herpetotherium* (Fox, 1983: figs. 1b, 2b; Korth, 2018), †*Mimoperadectes* (at least on m2–3; see Bown and Rose, 1979: plate 1 fig. 2), thylacinids, and most dasyurids. By contrast, posterior cingulids are absent (state 0) in all the Recent and fossil didelphids included in this study[23] as well as in paucituberculatans,

peramelemorphians (Muirhead, 2000: 513), and microbiotheriids (state 0). *Sarcophilus* is polymorphic ("0+1") for this character (Archer, 1976c). We observed some discrepancies between our scoring and that of Wroe et al. (2000: char. 36) and Wroe and Musser (2001: char. 36), both of whom scored the posterior cingulid as present but reduced in *Metachirus* and absent in *Dasyurus* and *Sarcophilus*. In fact, none of the *Metachirus* specimens we examined exhibits any trace of a posterior cingulid and, although the posterior cingulid is absent in some (but not all) *Sarcophilus* specimens we examined (e.g., AMNH 65674), it is consistently present in *Dasyurus* (although vestigial on m1).

A posterior cingulid is unequivocally absent in selenodont diprotodontians (pseudocheirids and phascolarctids; fig. 24), in which there is no structure posterior to the elongate, labially directed posthypocristid (or postcristid) that forms the posterior margin of the tooth. It is also clearly absent in some lophodont diprotodontians (such as Recent macropodids), because there is no structure posterior to the hypolophid (which forms the posterior margin of the tooth). In other lophodont and bunolophodont forms, a cingulidlike structure is present posterior to the hypolophid, but in most cases it is clear that this structure corresponds to the posthypocristid (or posthypocristid + postentocristid)—as in *Burramys*, †*Ekaltadeta*, †*Namilamadeta* (Pledge, 2005: fig. 1), and phalangerids. The sole exception among the taxa we examined is †*Balbaroo*, in which a distinct posterior cingulid is identifiable posterior to the posthypocristid (Cooke, 1997a; Black et al., 2014c). In diprotodontids, a cingulidlike structure is present posterior to the hypolophid (e.g., in *Nimbadon* [Hand, et al., 1993: fig. 3; Black and Hand, 2010: fig. 10M, N], *Ngapakaldia* [Black, 2010: fig. 3A, D], and *Neohelos* [Black, et al., 2014: fig. 6C_1]), but it is unclear whether this is a true posterior cingulid or whether it is formed by the posthypocristid

---

[23] Posterior cingulids were formerly believed to be altogether absent in didelphids (Voss and Jansa, 2009), but they have subsequently been discovered in a few didelphines,

including *Philander pebas* (see Voss et al., 2018: fig. 20) and *Marmosa rapposa* (see Voss et al., 2020: fig. 11).

and postentocristid; we therefore scored diprotodontids as unknown ("?"). The lower molars of *Myrmecobius* are too derived to score this character confidently, so we also scored it as unknown. We scored this character as inapplicable ("-") in *Notoryctes*, †*Yalkaparidon*, and *Tarsipes* for reasons previously discussed (see char. 166).

RESULTS

Molecular Analyses

Analyses of sequence data from the combined nuclear loci (fig. 27) and from whole mitochondrial genomes (fig. 28) result in broadly similar topologies, with only a few noteworthy examples of phylogenetic conflict. Both analyses place Paucituberculata as sister to the remaining marsupial orders, with strong support for the sister-group relationship between Didelphimorphia and Australidelphia. Within Australidelphia, both analyses also recover a sister relationship between Diprotodontia and Microbiotheria with moderate to strong support.

At the interordinal level, the greatest difference between our analyses of the nuclear and mitochondrial datasets concerns the position of Peramelemorphia: in the nuclear analysis (fig. 27) it is strongly supported as sister to Dasyuromorphia within the clade Agreodontia (which also includes Notoryctemorphia), whereas in the mitochondrial analysis (fig. 28) it is sister to a strongly supported clade comprising the other australidelphian orders (Notoryctemorphia, Dasyuromorphia, Microbiotheria, and Diprotodontia).

Monophyly of the only extant paucitubeculatan family, Caenolestidae, is strongly supported by analyses of both datasets. Monophyly of the didelphimorphian crown clade (Didelphidae) is also strongly supported by both the nuclear and mitochondrial analyses, and both analyses likewise strongly support Caluromyinae as sister to the remaining didelphids. However, the nuclear analysis places Hyladelphinae (= *Hyladelphys*) and Glironiinae (= *Glironia*) as successive sister taxa to Didelphinae with strong support, whereas the mitochondrial analysis weakly supports Hyladelphinae and Glironiinae as sister to Metachirini (= *Metachirus*) + Didelphini. Within Didelphinae, both analyses recover monophyly of the tribes Didelphini and Thylamyini, but support values for relationships within Didelphinae are much lower in the mitochondrial analysis than in the nuclear analysis.

Monophyly of Peramelemorphia is strongly supported by both the nuclear and the mitochondrial analyses. Within Peramelemorphia, the mitochondrial analysis places Chaeropodidae (*Chaeropus*) as the sister to the remaining terminals, but nuclear sequences are unavailable for *Chaeropus*.[24] Both analyses agree in placing Thylacomyidae (*Macrotis*) as the next taxon to diverge. The nuclear analysis supports the monophyly of Peramelinae (*Isoodon* and *Perameles*), Echymiperinae (*Echymipera* and *Microperoryctes*), and Echymiperinae + Peroryctinae (the latter represented by the sole modern genus *Peroryctes*), but the mitochondrial analysis does not.

Monophyly of Dasyuromorphia is strongly supported by both the nuclear and mitochondrial analyses. Within Dasyuromorphia, only mitochondrial sequences are available for *Thylacinus*, and the mitochondrial analysis weakly supports Myrmecobiidae + Thylacinidae to the exclusion of Dasyuridae. Within Dasyuridae, nuclear and mitochondrial analyses both strongly support the reciprocal monophyly of Sminthopsinae (*Antechinomys*, *Ningaui*, *Planigale,* and *Sminthopsis*) and Dasyurinae (containing the remaining modern genera). Analyses of both datasets also strongly support monophyly of Sminthopsini (*Antechinomys*, *Ningaui*, and *Sminthopsis*), Phascogalini (*Antechinus*, *Micromurexia*, *Murexechinus*, *Murexia*, *Paramurexia*, *Phascogale*, and *Phascomurexia*), and Dasyurini (comprising the remaining dasyurine genera).

---

[24] Although a *RAG1* sequence is available for *Chaeropus* (EU369367), Travouillon and Phillips (2018: 226) noted that it shows some unusual, potentially anomalous characteristics, so we have not used it here.
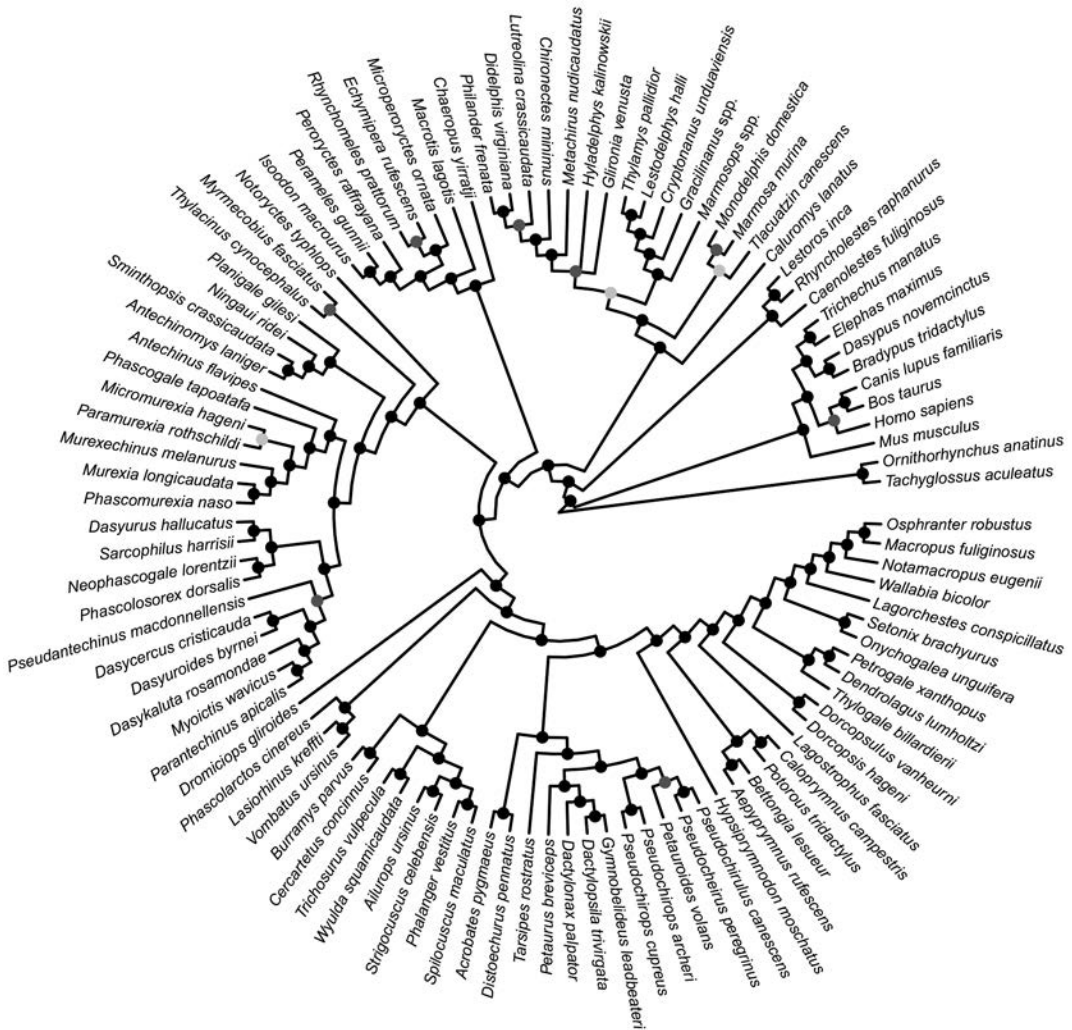
FIG. 27. Fifty-percent majority rule consensus of post-burn-in trees that results from Bayesian analysis of our nuclear sequence-only dataset. Black dots at nodes indicate ≥0.95 Bayesian posterior probability ("strong support"); dark gray dots indicate 0.75–0.94 Bayesian posterior probability ("moderate support"); light gray dots indicate 0.50–0.74 Bayesian posterior probability ("weak support").

Monophyly of Diprotodontia is strongly supported by analyses of the nuclear and mitochondrial datasets, both of which also support a basal divergence between Vombatiformes (*Lasiorhinus*, *Phascolarctos*, and *Vombatus*) and Phalangerida (the remaining diprotodontian genera). The nuclear and mitochondrial datasets both strongly support monophyly of Vombatiformes and Vombatidae, but monophyly of Phalangerida

receives strong support only from the nuclear dataset. Analyses of both datasets strongly support the existence of three major clades within Phalangerida: Phalangeridae + Burramyidae, Macropodoidea (*Hypsiprymnodon,* Potoroidae, and Macropodidae), and Petauroidea (Acrobatidae, *Tarsipes*, Petauridae, and Pseudocheiridae). Nuclear and mitochondrial analyses also place Macropodoidea and Petauroidea as sister taxa, to

FIG. 28. Fifty-percent majority rule consensus of post-burn-in trees that results from undated Bayesian analysis of our mitochondrial sequence-only dataset. Black dots at nodes indicate ≥0.95 Bayesian posterior probability ("strong support"); dark gray dots indicate 0.75–0.94 Bayesian posterior probability ("moderate support"); light gray dots indicate 0.50–0.74 Bayesian posterior probability ("weak support").

the exclusion of Phalangeridae + Burramyidae, but support for this arrangement is weak.

Within Phalangeridae, analyses of both datasets strongly support a basal divergence between *Trichosurus* +*Wyulda* (= Trichosurinae) and the remaining genera, with strong support for monophyly of Trichosurinae, *Phalanger* + *Spilocuscus* (= Phalangerinae) and *Ailurops* + *Strigocuscus* (= Ailuropinae). Within Petauroidea,

both analyses strongly support Acrobatidae as sister to the remaining families, as well as a Petauridae + Pseudocheiridae clade. Within Petauridae, the nuclear analysis strongly supports *Gymnobelideus* as sister to Dactylopsilinae (*Dactylopsila* and *Dactylonax*), whereas the mitochondrial analysis strongly supports a *Gymnobelideus* + *Dactylopsila* clade to the exclusion of *Dactylonax*. Within Pseudocheiridae, the

nuclear and mitochondrial analyses strongly support the same overall topology, with three subclades—Pseudocheirinae (*Pseudocheirus* + *Pseudochirulus*), Hemibelidinae (*Hemibelideus* + *Petauroides*; represented by *Petauroides* only in the mitochondrial analysis) and Pseudochiropsinae (*Pseudochirops* + *Petropseudes*)—of which Pseudocheirinae and Hemibelidinae are recovered as sister taxa.

Monophyly of Macropodiformes is strongly supported by both the nuclear and the mitochondrial analyses, which also agree that Hypsiprymnodontidae (*Hypsiprymnodon*) is sister to Macropodidae + Potoroidae. Reciprocal monophyly of Macropodidae and Potoroidae is strongly supported by both datasets, which likewise agree that *Lagostrophus* (the only extant lagostrophine) is sister to the remaining modern macropodid genera (= Macropodinae).

Unsurprisingly, analyses of the combined-molecular (nuclear + mitochondrial) dataset recover nearly all of those relationships common to the separate analyses described above (fig. 29). For example, at the interordinal level, Paucituberculata is again placed as sister to the other orders, and there is again strong support for Didelphimorphia + Australidelphia, and for Microbiotheria + Diprotodontia. Where our nuclear and mitochondrial results differ, the combined-molecular topology is usually more similar to the nuclear results; for example, in providing strong support for monophyly of Agreodontia (with Notoryctemorphia sister to Dasyuromorphia + Peramelemorphia) and in recovering similar relationships within Didelphidae (with Caluromyinae sister to Glironiinae + Didelphinae).

Morphological Analyses

Maximum parsimony analysis (fig. 30) and the undated Bayesian analysis (fig. 31) of our craniodental dataset both place †*Mimoperadectes* outside Marsupialia. However, both analyses recover a polytomy at the base of Marsupialia that includes †*Herpetotherium*, and in which

Didelphimorphia is not recovered as monophyletic. Dasyuromorphia, Diprotodontia, Microbiotheria, and Peramelemorphia are monophyletic in both analyses, but support for these clades is generally higher in the Bayesian analysis. In both analyses, the caenolestids *Caenolestes*, *Rhyncholestes*, and *Lestoros* form a clade with the fossil paucituberculatans †*Acdestis*, †*Palaeothentes*, †*Pichipilus*, and †*Stilotherium* with weak to moderate support, but †*Evolestes* is not recovered as a member of this clade.

Few relationships above the ordinal level are recovered in either the maximum parsimony or Bayesian analyses of these phenotypic data. However, both analyses weakly support the notoryctemorphian *Notoryctes* as sister to Microbiotheria. The Bayesian analysis weakly supports a clade that includes all our terminals known to have gliriform lower incisors (diprotodontians, paucituberculatans, †*Yalkaparidon*) plus †*Evolestes* (for which lower incisor morphology is currently unknown), and there is similarly weak support for a sister-taxon relationship between Paucituberculata (excluding †*Evolestes*) and Diprotodontia. The maximum parsimony analysis recovers a weakly supported superordinal clade that comprises †*Yalkaparidon*, †*Evolestes*, Dasyuromorphia, Peramelemorphia, Paucituberculata (excluding †*Evolestes*), and Diprotodontia, within which Paucituberculata (excluding †*Evolestes*) and Diprotodontia are sister taxa, but other interordinal relationships are unresolved.

Neither morphology-only analysis recovers monophyly of Didelphimorphia, but among the didelphimorphian clades found in both analyses are Caluromyinae, Thylamyini, and Didelphini (including †*Thylophorops*), although these clades are only weakly supported in the maximum parsimony analysis. The Bayesian analysis also places †*Hesperocynus*, †*Sparassocynus*, and †*Thylatheridium* in a clade with *Monodelphis* with moderate support, but this clade is not found in the maximum parsimony analysis.

Within Peramelemorphia, †*Galadi*, †*Bulungu*, and †*Yarala* are recovered outside the crown clade,

FIG. 29. Fifty-percent majority rule consensus of post-burn-in trees that results from undated Bayesian analysis of our combined nuclear and mitochondrial sequence dataset. Black dots at nodes indicate ≥0.95 Bayesian posterior probability ("strong support"); dark gray dots indicate 0.75–0.94 Bayesian posterior probability ("moderate support"); light gray dots indicate 0.50–0.74 Bayesian posterior probability ("weak support").

but monophyly of the clade excluding these fossil taxa receives strong support only in the Bayesian analysis. Both analyses recover a clade comprising *Chaeropus*, *Perameles*, *Isoodon,* and *Macrotis*, with the last two taxa also forming a clade.

Within Dasyuromorphia, the Bayesian analysis strongly supports a monophyletic Dasyuridae, sister to a weakly supported clade comprising *Myrmecobius*, Thylacinidae, and the fossil dasyuromorphians †*Barinya* and †*Mupuracinus*. Thy-

lacinidae (here comprising *Thylacinus*, †*Badjcinus*, and †*Nimbacinus*) is also strongly supported as monophyletic. The maximum parsimony analysis recovers a broadly similar topology (albeit with weak support), except that Dasyuridae is not monophyletic.

Within Paucituberculata (excluding †*Evolestes*), both analyses support a clade comprising †*Pichipilus*, *Lestoros*, *Caenolestes*, and *Rhyncholestes*.

FIG. 30. Strict consensus of 99,999 most parsimonious trees (each of 949 steps, consistency index =0.269, retention index = 0.815) that result from maximum parsimony analysis of our morphological dataset. Black dots at nodes indicate ≥70% bootstrap support ("strong support"); dark gray dots indicate 50%–69% bootstrap support ("moderate support"); light gray dots indicate <50 bootstrap support ("weak support").

Within Diprotodontia, the maximum parsimony analysis recovers a basal split between Vombatiformes (†Thylacoleonidae, Phascolarctidae, Vombatidae, †Diprotodontidae, and †Wynyardiidae) and Phalangerida, although both of these clades receive weak support. The Bayesian analysis, meanwhile, places †Thylacoleonidae as sister to the remaining diprotodontians and fails to recover a monophyletic Phalangerida. Both analyses place Phascolarctidae as sister to a clade (= Vombatomorphia sensu Beck et al., 2020: table 1) that includes vombatids, diprotodontids, wynyardiids, and the ilariid †*Ilaria*. Both analyses strongly sup-

port monophyly of Dactylopsilinae, Acrobatidae, Pseudocheiridae, and Phalangeridae, and they weakly support monophyly of Macrodiformes, but they do not recover a monophyletic Petauridae, Petauroidea, Burramyidae, or Burramyidae + Phalangeridae.

Undated Total-Evidence Analysis

Undated Bayesian analysis of our total-evidence dataset (fig. 32) strongly supports a clade comprising our definitive marsupial terminals plus †*Herpetotherium*, to the exclusion of †*Mimoperadectes* and our outgroup taxa (†*Pucadelphys*, †*Mayulestes*, and †*Allqokirus*). However, similar to our morphology-only analyses (figs. 30, 31), Didelphimorphia is not recovered as monophyletic. Our remaining marsupial terminals form a strongly supported clade, within which there is a weakly supported monophyletic grouping comprising a trichotomy of †*Evolestes*, the remaining paucituberculatans, and †*Yalkaparidon*. There is weak support for a clade comprising the living paucituberculatans (the caenolestids *Caenolestes*, *Rhyncholestes*, and *Lestoros*) and †*Pichipilus*.

Our remaining terminals comprise a moderately supported clade that corresponds to Australidelphia. Within Australidelphia, the first divergence is between a strongly supported Microbiotheria + Diprotodontia clade and a moderately supported clade (= Agreodontia) comprising the remaining three orders, namely Dasyuromorphia, Notoryctemorphia, and Peramelemorphia. Within Diprotodontia, there is moderate support for monophyly of Vombatiformes, with †Thylacoleonidae the first family to diverge, followed by Phascolarctidae, and then a weakly supported clade comprising †Diprotodontidae, †Ilariidae (†*Ilaria*), Vombatidae, and †Wynyardiidae; within the last, †Wynyardiidae and †Ilariidae are weakly supported as sister taxa, with †Diprotodontidae sister to this clade. Monophyly of Phalangerida is also strongly supported. Relationships among our modern pha-

langeridan terminals are essentially identical to those recovered by our combined nuclear and mitochondrial sequence analyses, but placement of our fossil terminals in Phalangerida merits comment: within Phalangeridae, "*Trichosurus*" †*dicksoni* and †*Onirocuscus* are sister to *Wyulda* and *Strigocuscus*, respectively; within Hypsiprymnodontidae, *Hypsiprymnodon* †*bartholomaii* is sister to *H. moschatus*, and †*Ekaltadeta* is sister to this clade; within Potoroidae, ?*Bettongia* †*moyesi* is sister to *Bettongia* + *Aepyprymnus*; within Macropodidae, †*Balbaroo*, †*Ganawamaya*, †*Gangaroo*, †*Hadronomas*, and †*Rhizosthenurus* form a clade with *Dorcopsulus*, and within that clade, †*Balbaroo* and †*Ganawamaya* are sister taxa (=†Balbaridae).

Within Agreodontia, Dasyuromorphia and Peramelemorphia are strongly supported as sister taxa to the exclusion of Notoryctemorphia. Similar to the situation within Phalangerida, the relationships of extant dasyuromorphians and peramelemorphians are essentially identical to the results of our combined nuclear and mitochondrial sequence analyses. Monophyly of Dasyuromorphia is strongly supported and all our fossil taxa are placed within the crown clade (= Dasyuroidea). Within Dasyuroidea, Myrmecobiidae (*Myrmecobius*) and Dasyuridae are strongly supported as sister taxa to the exclusion of Thylacinidae. †*Barinya*, †*Badjcinus*, †*Mutpuracinus*, and †*Nimbacinus* are all placed within Thylacinidae, with †*Badjcinus* sister to *Thylacinus* and †*Nimbacinus* sister to †*Badjcinus* + *Thylacinus*. Monophyly of Peramelemorphia is also strongly supported and there is weak support for a clade comprising all our Recent peramelemorphian terminals (= Perameloidea), to the exclusion of †*Galadi* (which is sister to Perameloidea), and †*Yarala* + †*Bulungu*, which form a clade that is sister to all other peramelemorphians. Within Perameloidea, Chaeropodidae (*Chaeropus*) is the first family to diverge, followed by Thylacomyidae (*Macrotis*); although Peramelinae and Echymiperinae + Peroryctinae are recovered as sister taxa, this clade is only moderately supported.
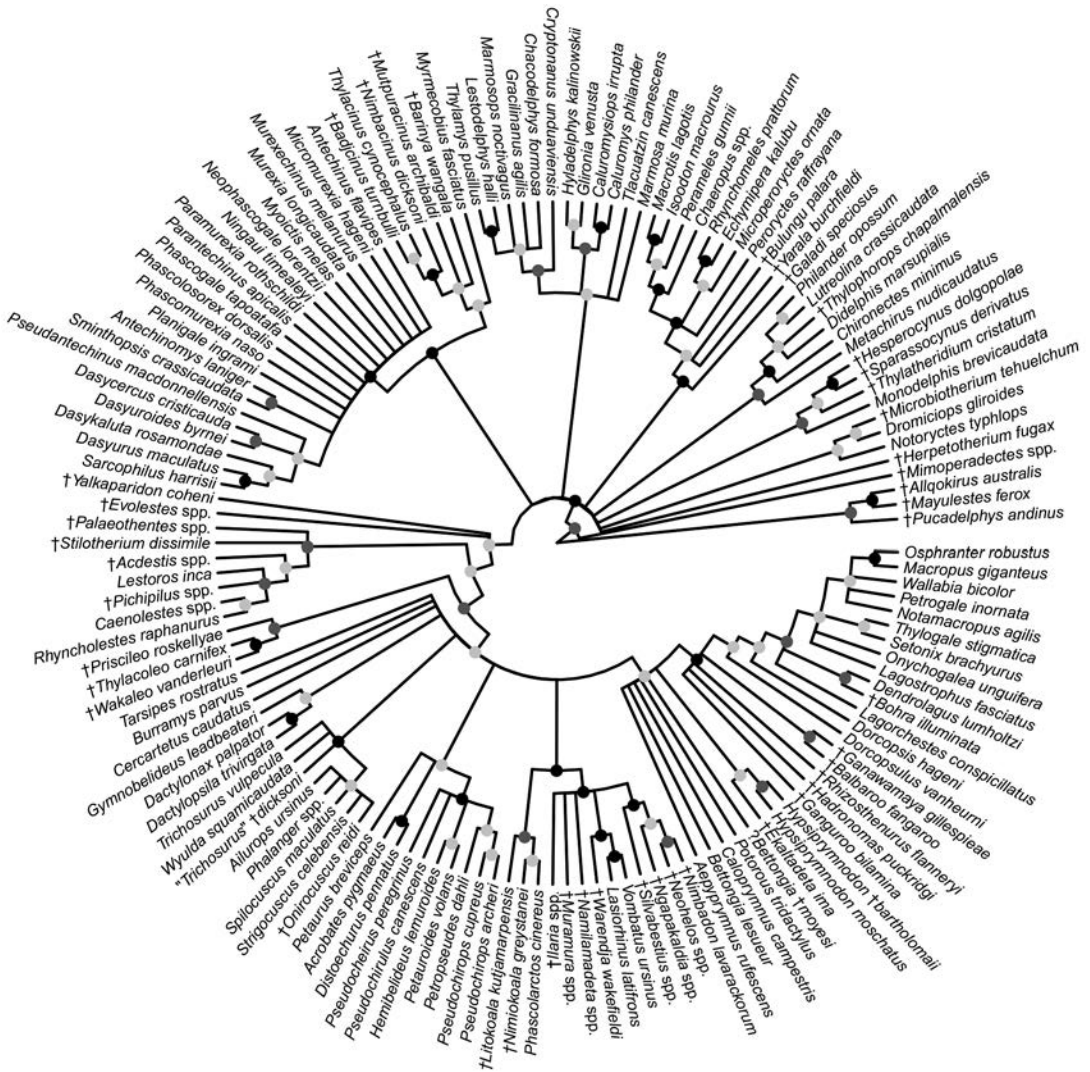
FIG. 31. Fifty-percent majority rule consensus of post-burn-in trees that results from undated Bayesian analysis of our morphological dataset. Black dots at nodes indicate ≥0.95 Bayesian posterior probability ("strong support"); dark gray dots indicate 0.75–0.94 Bayesian posterior probability ("moderate support"); light gray dots indicate 0.50–0.74 Bayesian posterior probability ("weak support").

Dated Total-Evidence Analysis

Incorporating temporal information in the form of calibrating the ages of our terminals and selected nodes and then carrying out a Bayesian total-evidence dating analysis (fig. 33) has little impact on the relationships of our extant terminals compared to the equivalent undated analysis

(fig. 32). There is, however, a major difference in the position of the root of Marsupialia, but we emphasize that this is due largely to the topological and temporal constraints we enforced in our dated analysis. In the undated analysis (fig. 32), the root of Marsupialia was positioned on a polytomy comprising †*Herpetotherium*, a nonmonophyletic Didelphimorphia, and a clade comprising
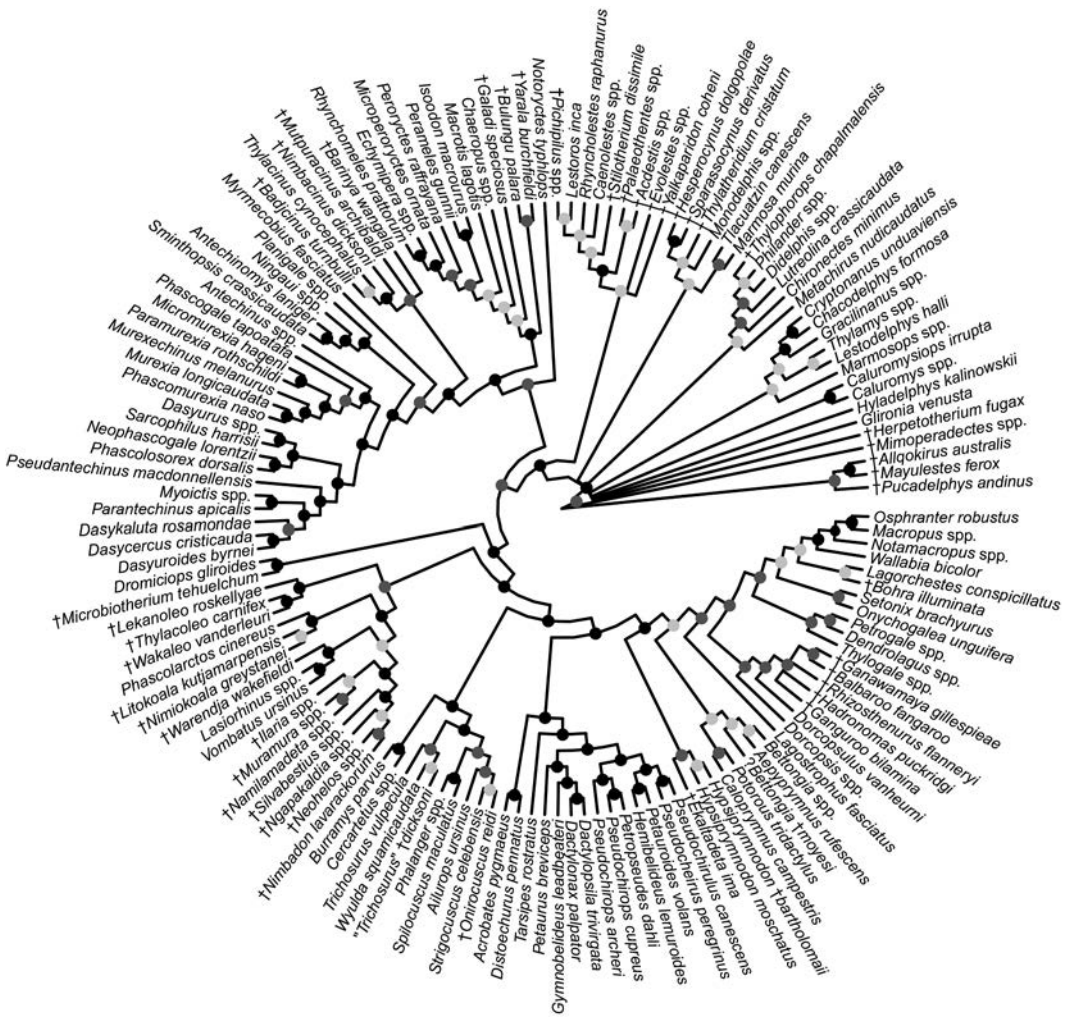
FIG. 32. Fifty-percent majority rule consensus of post-burn-in trees that results from undated Bayesian analysis of our total evidence dataset. Black dots at nodes indicate ≥0.95 Bayesian posterior probability ("strong support"); dark gray dots indicate 0.75–0.94 Bayesian posterior probability ("moderate support"); light gray dots indicate 0.50–0.74 Bayesian posterior probability ("weak support").

our remaining ingroup terminals. By contrast, in the dated analysis (fig. 33), we constrained †*Herpetotherium* to fall outside crown-clade Marsupialia, congruent with most recent published phylogenetic analyses (e.g., Sánchez-Villagra et al., 2007; Horovitz et al., 2008; Horovitz et al., 2009; Ladevèze et al., 2020). We also constrained Didelphimorphia to be the sister to the remaining marsupial orders, given the statistically significant support for this topology provided by retrotrans-

poson insertions (Gallus et al., 2015a), whereas our molecular analyses consistently place the marsupial root between Paucituberculata and Didelphimorphia + Australidelphia (figs. 27–29).

Many of our fossil taxa take up very different positions in the dated total-evidence analysis (fig. 33) compared to the equivalent undated analysis (fig. 32), in most cases occupying deeper positions in the tree. This might be expected given that they predate (often by tens of millions
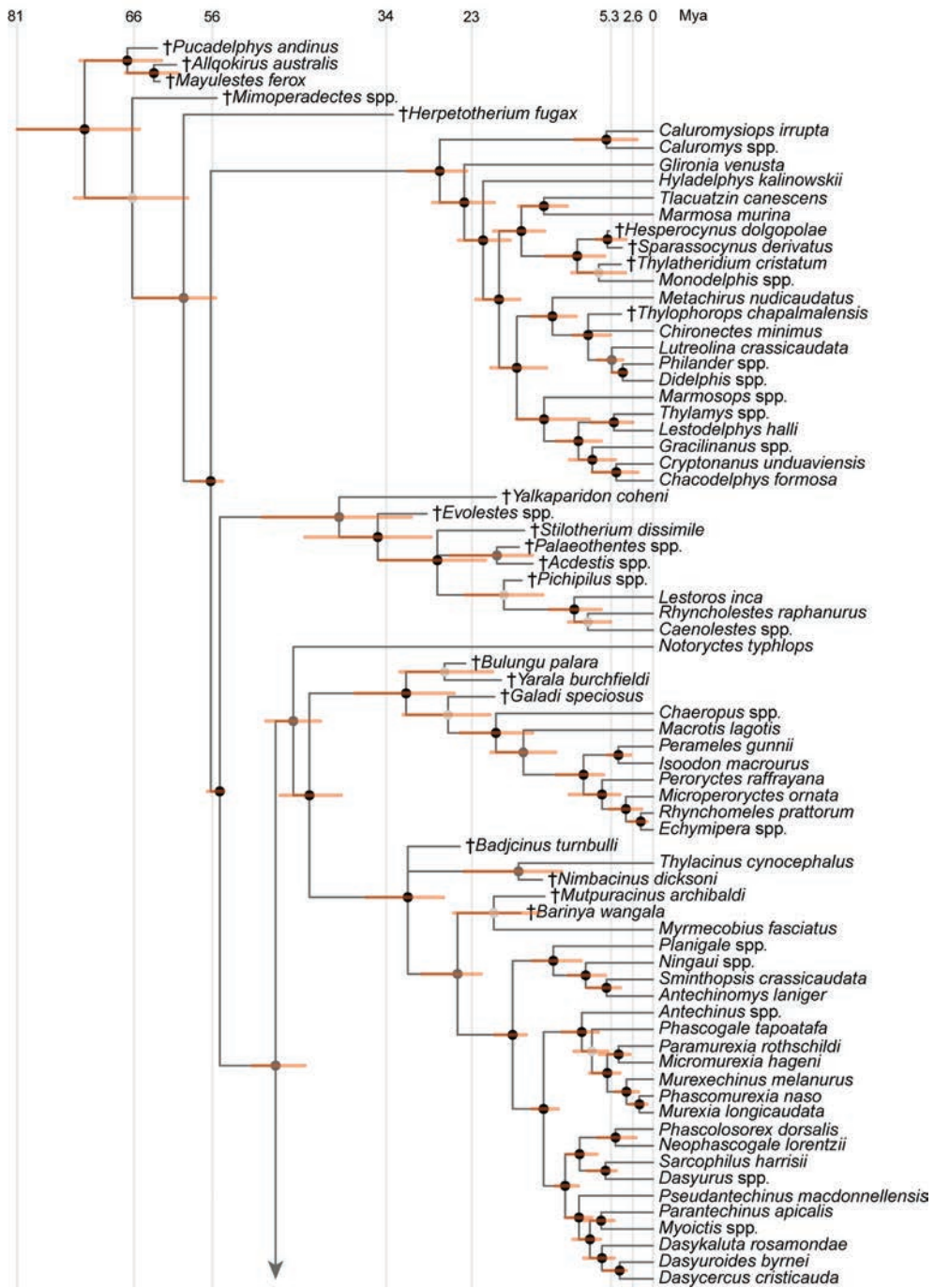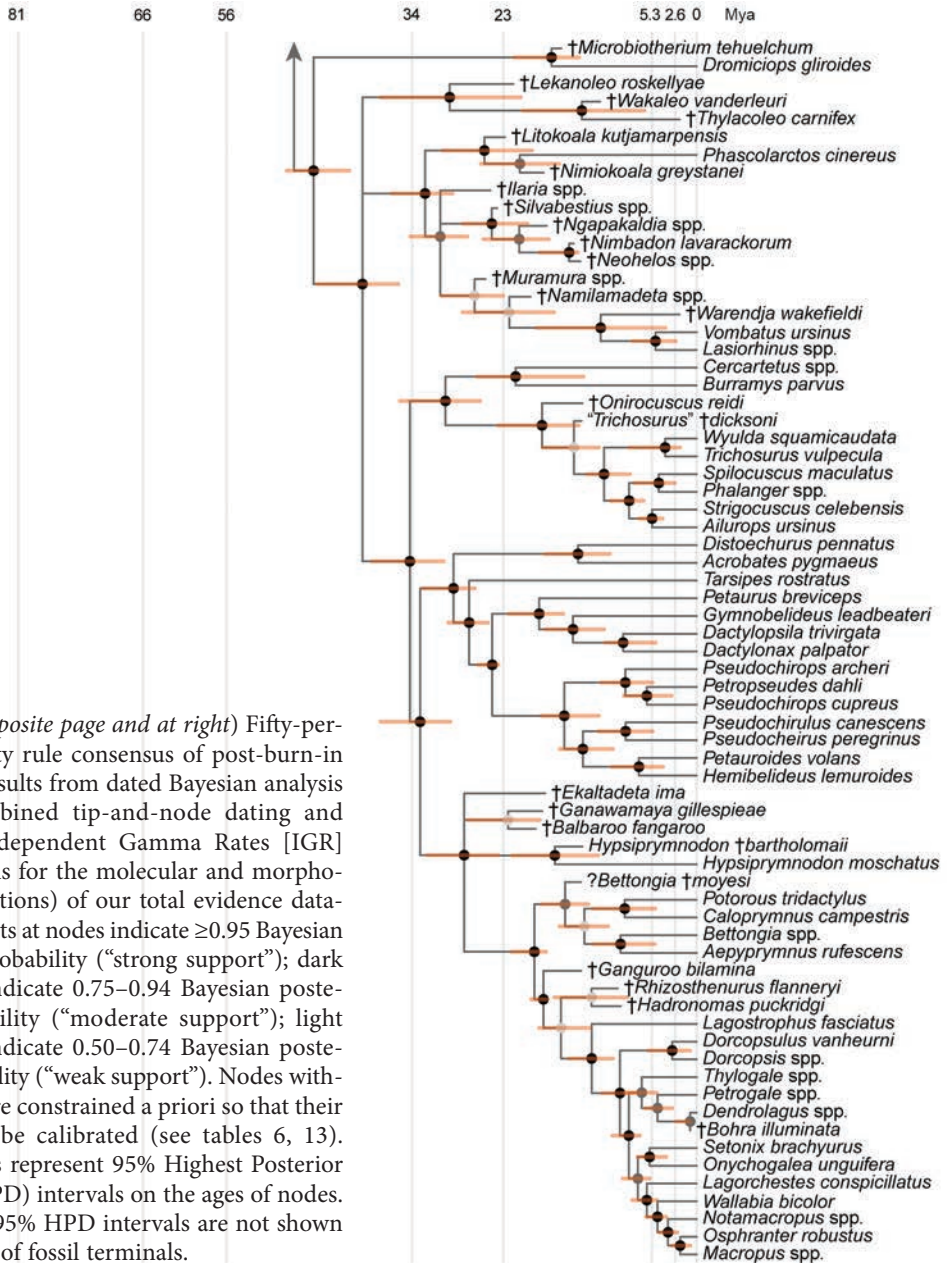
FIG. 33. (*opposite page and at right*) Fifty-percent majority rule consensus of post-burn-in trees that results from dated Bayesian analysis (using combined tip-and-node dating and separate Independent Gamma Rates [IGR] clock models for the molecular and morphological partitions) of our total evidence dataset. Black dots at nodes indicate ≥0.95 Bayesian posterior probability ("strong support"); dark gray dots indicate 0.75–0.94 Bayesian posterior probability ("moderate support"); light gray dots indicate 0.50–0.74 Bayesian posterior probability ("weak support"). Nodes without dots were constrained a priori so that their ages could be calibrated (see tables 6, 13). Orange bars represent 95% Highest Posterior Density (HPD) intervals on the ages of nodes. For clarity, 95% HPD intervals are not shown for the ages of fossil terminals.

of years) our Recent terminals (see, e.g., Lee and Yates, 2018; Beck and Taglioretti, 2020; King and Beck, 2020). Within Didelphimorphia, †*Thyloph-orops* moves from forming a weakly supported clade with *Didelphis* and *Philander* to forming a trichotomy with *Chironectes* and a clade comprising *Didelphis*, *Philander*, and *Lutreolina*. Within Paucituberculata, †*Pichipilus* moves from a weakly supported position as sister to the extant *Lestoros*, to a position outside a strongly supported clade comprising all three extant caenolestid genera. Within Dasyuromorphia, †*Barinya*, †*Badjcinus*, and †*Mutpuracinus* are no longer placed within Thylacinidae. Instead, †*Badjcinus* is placed in a trichotomy at the base of Dasyuromorphia, together with a moderately supported clade comprising *Thylacinus* and †*Nimbacinus* (= Thylacinidae) and a moderately supported clade comprising remaining dasyuromorphian terminals, whereas †*Barinya* and †*Mutpuracinus* form a weakly supported clade with *Myrmecobius*, which is in turn sister to a strongly supported Dasyuridae.

The biggest topological changes are seen within Diprotodontia. Perhaps most notably, thylacoleonids are not unambiguously supported as members of Vombatiformes in our dated total-evidence analysis, Instead, the first divergence within Diprotodontia in this analysis is a trichotomy comprising Phalangerida, †Thylacoleonidae, and a clade comprising the remaining terminals currently classified as members of Vombatiformes (diprotodontids, the ilariid †*Ilaria*, phascolarctids, wynyardiids, and vombatids). Within this last clade, Phascolarctidae is the sister to the remaining terminals and there is strong support for monophyly of Diprotodontidae and Vombatidae. The wynyardiids †*Namilamadeta* and †*Muramura* no longer form a clade; instead †*Namilamadeta* is sister to Vombatidae, with †*Muramura* sister to this clade, although support values for these relationships are weak.

Within Phalangeridae, †*Onirocuscus* and "*Trichosurus*" †*dicksoni* are now placed outside the phalangerid crown clade, the monophyly of which receives strong support. At the base of

Macropodiformes, there is now a polytomy comprising †*Ekaltadeta* (which no longer forms a clade with *Hypsiprymnodon moschatus* and *H.* †*bartholomaii*), Hypsiprymnodontinae (= *Hypsiprymnodon moschatus* + *H.* †*bartholomaii*), †Balbaridae (= †*Balbaroo* + †*Ganawamaya*), and Macropodidae + Potoroidae. Within Potoroidae, ?*Bettongia* †*moyesi* moves outside the crown-clade, monophyly of which is weakly supported. Within Macropodidae, †*Ganguroo*, †*Hadronomas*, and †*Rhizosthenurus* are likewise placed outside the crown clade, with †*Hadronomas* and †*Rhizosthenurus* forming a weakly supported clade (equivalent to the subfamily †Sthenurinae; Kear, 2002; Kirkham, 2004; Prideaux, 2004). However, it should be noted that some of these macropodiform relationships are the result of topological constraints that were required to calibrate selected nodes within Macropodoidea (see Methods and appendix 2).

Our dated total-evidence analysis places the first divergence within Marsupialia (between Didelphimorphia and the remaining marsupial taxa, a relationship that was constrained and calibrated a priori; see above, table 6, and appendix 2) in the late Paleocene or earliest Eocene (median estimate: 56.2 Mya; 95% HPD: 54.7–58.6 Mya). The divergence between Paucituberculata and Australidelphia (another constrained and calibrated node) is estimated as close to the Paleocene-Eocene boundary (median estimate: 55.1 Mya; 95% HPD: 54.6–56.6 Mya), whereas the first split within Australidelphia (between Agreodontia and Microbiotheria + Diprotodontia) is ~7 Myr later (median estimate: 48.0 Mya; 95% HPD: 44.3–50.9 Mya). The estimated divergence times between Notoryctemorphia and Dasyuromorphia + Peramelemorphia (median estimate: 45.7 Mya; 95% HPD: 42.3–49.2 Mya) and between Dasyuromorphia and Peramelemorphia (median estimate: 43.7 Mya; 95% HPD: 39.6–47.4 Mya) fall entirely within the Eocene, as does the divergence between Microbiotheria and Diprotodontia (median estimate: 45.6 Mya; 95% HPD: 41.4–48.8 Mya). The divergence between †*Yalkaparidon* and Paucitubercu-

lata (with monophyly of the latter clade enforced a priori), meanwhile, is estimated as Eocene or earliest Oligocene (median estimate: 39.9 Mya; 95% HPD: 30.7–49.7 Mya). Estimated divergence times of selected intraordinal clades are summarized in table 6 and discussed in the individual taxonomic accounts below.

DISCUSSION

Molecular Analyses

Our results document the presence of strong phylogenetic signal in the molecular data analyzed here. Phylogenetic congruence between the results of analyzing the nuclear (fig. 27) and mitochondrial (fig. 28) datasets separately seems particularly impressive despite discrepancies at a few problematic nodes. The results of our separate (figs. 27, 28) and combined analyses (fig. 29) of these molecular data are also broadly consistent with those reported by other recent, large-scale sequence-based analyses of marsupial phylogeny (Meredith et al., 2009a, 2011; Mitchell et al., 2014; May-Collado et al., 2015; Duchêne et al., 2018; Álvarez-Carretero et al., 2021), but there remain several noteworthy areas of conflict and uncertainty together with some incongruence with the results of retrotransposon-based analyses (Nilsson et al., 2010; Gallus et al., 2015a).

One conspicuous point of uncertainty concerns the position of the marsupial root node. Whereas all our molecular analyses and several previous studies (e.g., Meredith et al., 2009a, 2011; Mitchell et al., 2014; May-Collado et al., 2015; Álvarez-Carretero et al., 2021) place the root between Paucituberculata and the remaining Recent marsupial orders, sequence-based analyses reported by other researchers (e.g., Nilsson et al., 2003, 2004; Beck, 2008a; Meredith et al., 2008b, 2009c; reviewed by Eldridge et al., 2019: 806) have placed the marsupial root node on the branch leading to Didelphimorphia. The latter position also receives statistically significant support from retrotransposon insertions

(five uncontradicted insertions, p = 0.001; Gallus et al., 2015a), so this was the root position we enforced to calibrate this node in our dated total-evidence analysis despite the conflicting signal in our own results.

Within Didelphimorphia, our mitochondrial analysis shows some conflict with other recent molecular studies (Jansa and Voss, 2000; Voss and Jansa, 2003, 2009; Jansa and Voss, 2005; Jansa et al., 2006, 2014; Gruber et al., 2007; May-Collado et al., 2015; Vilela et al., 2015; Álvarez-Carretero et al., 2021) by, for example, placing Hyladelphinae (*Hyladelphys*) and Glironiinae (*Glironia*) in a trichotomy with Didelphini + Metachirini, albeit with relatively weak support. However, our nuclear and combined-molecular analyses are in strong agreement with the current consensus view of subfamilial and tribal relationships within Didelphidae (Voss and Jansa, 2009; Amador and Giannini, 2016; Eldridge et al., 2019), as we discuss in more detail in the annotated classification that follows.

A major difference between the results of our mitochondrial and nuclear analyses concerns the position of Peramelemorphia. Whereas our mitochondrial analysis strongly supports Peramelemorphia as sister to a clade comprising the remaining four australidelphian orders (Dasyuromorphia, Diprotodontia, Microbiotheria, and Notoryctemorphia), our nuclear and combined-molecular analyses strongly support Peramelemorphia as sister to Dasyuromorphia, with which (together with Notoryctemorphia) it forms the clade Agreodontia. Several early studies based on mitochondrial genes (e.g., Krajewski et al., 1997; Burk et al., 1999; Palma and Spotorno, 1999) as well as some based on combined nuclear and mitochondrial data (e.g., Springer et al., 1998; Asher et al., 2004) have found Peramelemorphia in a relatively basal position within Marsupialia, often quite distant from the other Australian orders (but see Nilsson et al., 2004).[25] However, Phillips et al. (2006; see also Beck,

---

[25] A similarly basal position for Peramelemorphia has also been consistently found in DNA-DNA hybridization studies (Kirsch et al., 1991, 1997).

2008a) showed convincingly that this position for Peramelemorphia is due to base-compositional bias in mitochondrial protein-coding and ribosomal genes; when this bias is corrected (e.g., by RY-coding or deleting a particularly biased partition, such as the third codon positions of protein-coding genes), Peramelemorphia forms a clade (= Agreodontia) with Dasyuromorphia and (when included) Notoryctemorphia, in agreement with the results of nuclear-sequence data analyses (Phillips et al., 2006; Beck, 2008a). However, only one retrotransposon insertion has been found that supports monophyly of Agreodontia (Nilsson et al., 2010; Gallus et al., 2015a).

Within Agreodontia, our nuclear and combined-molecular analyses provide moderate to strong support for Dasyuromorphia + Peramelemorphia to the exclusion of Notoryctemorphia. By contrast, the phylogenomic study of Duchêne et al. (2018), which used 867 kb of DNA sequence data from 1550 nuclear loci, found strong support for Peramelemorphia + Notoryctemorphia. Nevertheless, the short branches separating these divergences and the lack of retrotransposon insertion data supporting any specific branching pattern between Dasyuromorphia, Notoryctemorphia, and Peramelemorphia (Nilsson et al., 2010; Gallus et al., 2015a) suggest a rapid radiation at the base of Agreodontia that may approximate a "hard" polytomy (see also Duchêne et al., 2018: 408).

Within Dasyuromorphia, *Thylacinus* (for which only mitochondrial sequence data were used) is sister to *Myrmecobius* in the mitochondrial analysis, but sister to *Mymecobius* + Dasyuridae in the combined-molecular analyses; the latter topology is congruent with other recent molecular and total-evidence analyses (Miller et al., 2009; May-Collado et al., 2015; Westerman et al., 2016; Kealy and Beck, 2017). Feigin et al. (2018) found 11 retrotransposon insertions supporting a sister relationship between *Myrmecobius* and Dasyuridae, to the exclusion of *Thylacinus*, which represents statistically significant support for this clade, but the presence of a

few conflicting insertion patterns suggests incomplete lineage sorting at the base of Dasyuromorphia. The relationships we recover within Dasyuridae are largely congruent between our mitochondrial and nuclear analyses and in agreement with recent molecular and total-evidence analyses (Miller et al., 2009; May-Collado et al., 2015; Westerman et al., 2016; Kealy and Beck, 2017; García-Navas et al., 2020; Álvarez-Carretero et al., 2021), all of which strongly support monophyly of the subfamilies Dasyurinae and Sminthopsinae and of the tribes Dasyurini, Phascogalini, and Sminthopsini.

Our molecular results for relationships within Peramelemorphia are congruent with those reported from several recently published molecular analyses (Westerman et al., 2012; Kear et al., 2016; Travouillon and Phillips, 2018) in supporting *Chaeropus* (represented by mitochondrial sequence data only) as sister to other Recent taxa, and in supporting *Macrotis* as sister to Peramelidae. However, we note that other molecular and total-evidence studies have found alternative resolutions for the position of *Chaeropus*, including as sister to *Macrotis* (Travouillon and Phillips, 2018: figs. 1E, 2) and within a paraphyletic Peramelidae (May-Collado et al., 2015; Travouillon et al., 2019). The results of our molecular analyses agree with those of most recent molecular and total-evidence studies (Meredith et al., 2008a; Westerman et al., 2012; Mitchell et al., 2014; May-Collado et al., 2015; Kear et al., 2016; Travouillon and Phillips, 2018; Álvarez-Carretero et al., 2021) in supporting the monophyly of Peramelinae (*Isoodon* + *Perameles*) and Echymiperinae (*Echymipera* + *Rhynchomeles* + *Microperoryctes*). Most of these studies also support a Peroryctinae + Echymiperinae clade (Meredith et al., 2008a; Mitchell et al., 2014; May-Collado et al., 2015; Kear et al., 2016; Travouillon and Phillips, 2018; Álvarez-Carretero et al., 2021), and some authors have recognized this clade as the family Peroryctidae, restricting Peramelidae to *Isoodon* and *Perameles* only (e.g., Travouillon and Phillips, 2018: see also Groves and Flannery, 1990; Eldridge et al., 2019). However, only our

nuclear and and combined-molecular analyses support Peroryctinae + Echymiperinae. Given the inconsistent results found here and in other published molecular and total-evidence analyses (see especially Travouillon et al., 2019), it is clear that further research with even larger sequence datasets will be required to robustly resolve relationships among extant peramelemorpians, with retrotransposon insertion data also likely to prove useful.

A conspicuous result of our nuclear and combined-molecular analyses is consistently strong support for a sister-group relationship between Microbiotheria and Diprotodontia. This biogeographically anomalous clade has also been found in DNA-DNA hybridization studies (Kirsch et al., 1991, 1997) and the combined nuclear and mitochondrial sequence analysis of May-Collado et al. (2015). However, most other phylogenetic analyses that have included nuclear sequence data (Phillips et al., 2006; Beck, 2008a; Meredith et al., 2008b, 2009a, 2009c, 2011; Mitchell et al., 2014; Duchêne et al., 2018; Álvarez-Carretero et al., 2021) have found Microbiotheria to fall outside a clade comprising the four Australian orders (= Eomarsupialia sensu Beck et al., 2014), and mitochondrial data appear to favor the latter topology when corrected for compositional heterogeneity (Phillips et al., 2006). Some of these studies found only weak support for monophyly of Eomarsupialia over alternative topologies, but the phylogenomic study of Duchêne et al. (2018) strongly supported this clade, and four uncontradicted retrotransposon insertions also provide statistically significant support (p = 0.0123) for Eomarsupialia (Nilsson et al., 2010; Gallus et al., 2015a). Although this collective evidence persuades us that Eomarsupialia is probably monophyletic, we did not enforce monophyly of this clade in our dated total-evidence analysis to avoid a priori constraints on taxa with uncertain relationships—in particular †*Yalkaparidon*, which fell within Eomarsupialia in the total-evidence analysis of Beck et al. (2016), but not in other published analyses (Beck et al., 2014; Abello and Candela, 2019; Zimicz and Goin, 2020).

Within Diprotodontia, our nuclear, mitochondrial, and combined-molecular analyses are congruent with recent molecular studies in supporting a basal split between Vombatiformes and Phalangerida, and in strongly supporting monophyly of Petauroidea, Macropodoidea, Phalangeridae + Burramyidae, and all the families, subfamilies, and tribes recognized in table 13 (Beck, 2008a; Meredith et al., 2008b, 2009a, 2009c; Phillips and Pratt, 2008; Mitchell et al., 2014; May-Collado et al., 2015; Duchêne et al., 2018; Álvarez-Carretero et al., 2021). Within Phalangerida, our molecular analyses consistently recover Macropodoidea + Petauroidea and Phalangeridae + Burramyidae as reciprocally monophyletic clades, each with strong support. This topology agrees with some other recent molecular analyses (e.g., Meredith et al., 2011; Mitchell et al., 2014; May-Collado et al., 2015; Álvarez-Carretero et al., 2021). However, others (e.g., Beck, 2008a; Meredith et al., 2008b, 2009a, 2009c; Phillips and Pratt, 2008) have instead supported a Macropodoidea + (Phalangeridae + Burramyidae) clade, with Meredith et al. (2009a) going so far as to formally recognizing this clade with the name Australoplagiaulacoidea. The phylogenomic study of Duchêne et al. (2018) found that some individual gene trees for their 1550 nuclear loci supported Macropodoidea + Petauroidea whereas others supported Macropodoidea + (Phalangeridae + Burramyidae), suggesting that divergences among these three clades occurred close together in time, or involved large population sizes, or both. However, Duchêne et al. (2018) found that the clear majority (approximately two-thirds) of the gene trees for their individual loci supported Macropodoidea + Petauroidea, which was the topology that was consistently found here.

Morphological Analyses

In contrast to the strong and generally consistent phylogenetic signal observed in the preceding molecular analyses, the results of our morphological analyses are characterized by

TABLE 13

Comparisons of Clade Support Values among Different Analyses

Dataset abbreviations: CM, combined molecular; Mo, morphological; Mt, mitochondrial; Nu, nuclear; TE, total evidence. Analytic abbreviations: DB; dated Bayesian; MP, maximum parsimony; UB, undated Bayesian. Bootstrap support values are tabulated for the Mo/MP analysis and Bayesian posterior probabilities for all others; bootstrap values and posterior probabilities interpreted as strong support are boldfaced. Other table entries: n/a, not applicable; no, actively contradicted; calibrated, constrained to be monophyletic; unresolved, clade not recovered but not contradicted.

	Mo/MP	Mo/UB	Mt/UB	Nu/UB	CM/UB	TE/UB	TE/DB
Marsupialia (excl. †*Herpetotherium*)	unresolved	unresolved	1.00	1.00	1.00	unresolved	calibrated
Didelphidae	unresolved	unresolved	1.00	1.00	1.00	unresolved	calibrated
Caluromyinae	70%	1.00	n/a	1.00	1.00	1.00	1.00
Didelphinae	no	no	no	1.00	1.00	unresolved	1.00
Didelphini	<50%	0.99	1.00	1.00	1.00	0.91	1.00
Marmosini	unresolved	unresolved	no	1.00	1.00	0.89	1.00
Monodelphini	unresolved	no	n/a	n/a	n/a	unresolved	0.52
†Sparassocynini	<50%	0.99	n/a	n/a	n/a	0.99	1.00
Thylamyini	<50%	0.77	0.96	1.00	1.00	0.64	1.00
Paucituberculata	no	no	n/a	n/a	n/a	unresolved	calibrated
Caenolestidae	no[a]	no[a]	1.00[b]	1.00[b]	1.00[b]	no[a]	no[a]
†Palaeothentoidea	no	no	n/a	n/a	n/a	no	no
†Palaeothentidae	unresolved	no	n/a	n/a	n/a	0.60	0.76
Australidelphia	no	no	1.00	1.00	1.00	0.76	0.83
Microbiotheriidae	62%	0.74	n/a	n/a	n/a	1.00	1.00
Agreodontia	no	no	no	1.00	1.00	0.76	0.86
Dasyuromorphia/Dasyuroidea	<50%[g]	0.98[g]	1.00[h]	1.00[h]	1.00[h]	1.00[g]	calibrated[g]
Dasyuridae	unresolved	0.98	1.00	1.00	1.00	1.00	1.00
Dasyurinae	unresolved	unresolved	1.00	1.00	1.00	1.00	calibrated
Dasyurini	unresolved	unresolved	1.00	1.00	1.00	1.00	calibrated
Phascogalini	unresolved	unresolved	1.00	1.00	1.00	1.00	1.00
Sminthopsinae	unresolved	unresolved	1.00	1.00	1.00	1.00	1.00
Sminthopsini	unresolved	unresolved	1.00	1.00	1.00	1.00	1.00
Thylacinidae	<50%[i]	0.83[i]	n/a	n/a	n/a	0.98[i]	0.92[j]
Peramelemorphia/Perameloidea	58%[k]	1.00[k]	1.00[l]	1.00[l]	1.00[l]	1.00[k]	1.00[k]
Peramelidae	no	no	1.00	1.00	1.00	0.92	1.00
Peramelinae	no	no	1.00	1.00	1.00	1.00	1.00
Echymiperinae	unresolved	0.70	1.00	1.00	1.00	1.00	1.00
Diprotodontia	<50%	0.91	1.00	1.00	1.00	1.00	1.00
Vombatiformes	<50%	no	1.00	1.00	1.00	0.93	unresolved

TABLE 13 *continued*

Phascolarctidae	<50%	0.80	n/a	n/a	n/a	0.97	calibrated
Vombatidae	53%	1.00	1.00	1.00	1.00	1.00	calibrated
†Diprotodontidae	76%	1.00	n/a	n/a	n/a	1.00	calibrated
†Thylacoleonidae	<50%	0.84	n/a	n/a	n/a	1.00	calibrated
†Wynyardiidae	<50%	unresolved	n/a	n/a	n/a	0.76	no
Burramyidae	no	unresolved	1.00	1.00	1.00	1.00	1.00
Phalangeridae	81%	1.00	1.00	1.00	1.00	1.00	calibrated
Ailuropinae	unresolved	unresolved	1.00	1.00	1.00	0.82[c]	1.00[d]
Phalangerinae	unresolved	unresolved	1.00	1.00	1.00	0.97	1.00
Trichosurinae	unresolved	unresolved	1.00	1.00	1.00	0.86	1.00
Petauroidea	no	unresolved	1.00	1.00	1.00	1.00	calibrated
Pseudocheiridae	88%	1.00	1.00	1.00	1.00	1.00	calibrated
Pseudocheirinae	<50%	unresolved	1.00	1.00	1.00	1.00	1.00
Pseudochiropsinae	<50%	0.74	1.00	1.00	1.00	1.00	1.00
Hemibelideinae	<50%	0.65	n/a	1.00	1.00	1.00	1.00
Petauridae	no	no	1.00	1.00	1.00	1.00	1.00
Dactylopsilinae	99%	1.00	no	1.00	1.00	1.00	1.00
Acrobatidae	99%	1.00	1.00	1.00	1.00	1.00	1.00
Macropodiformes/ Macropodoidea	<50%[e]	0.72[e]	1.00[f]	1.00[f]	1.00[f]	1.00[e]	calibrated[e]
Macropodidae	unresolved	unresolved	1.00	1.00	1.00	no	calibrated
Macropodinae	no	no	1.00	1.00	1.00	no	calibrated
Dendrolagini	no	no	1.00	1.00	1.00	no	0.90
Dorcopsini	no	no	1.00	1.00	1.00	no	1.00
Macropodini	no	no	1.00	0.69	1.00	no	0.96
†Sthenurinae	no	unresolved	n/a	n/a	n/a	unresolved	0.66
Potoroidae	no	unresolved	1.00	1.00	1.00	0.53	0.87
†Balbaridae	<50%	0.95	n/a	n/a	n/a	0.94	0.74

[a] Assuming †*Stilotherium* is a caenolestid (see table 2).
[b] Crown-clade only.
[c] Includes †*Onirocuscus*.
[d] Excludes †*Onirocuscus*.
[e] Macropodiformes (total clade).
[f] Macropodoidea (crown clade).
[g] Dasyuromorphia (total clade).
[h] Dasyuroidea (crown clade).
[i] Includes †*Badjcinus*.
[j] Excludes †*Badjcinus*.
[k] Peramelemorphia (total clade).
[l] Perameloidea (crown clade).

much less resolution and generally lower support values (figs. 30, 31). Of the 44 clades at the tribe level or above that receive strong support in the undated Bayesian analyses of our combined-molecular data (table 13), only 16 (36.4%) are recovered in the MP analysis of our craniodental data and, of those, only five (Caluromyinae, Phalangeridae, Pseudocheiridae, Dactylopsilinae, and Acrobatidae) are strongly supported; the remainder are either unresolved (14/44 = 31.8%) or actively contradicted (14/44 = 31.8%). Undated Bayesian analysis of our craniodental data performs only marginally better: of the same 44 clades strongly supported by our combined-molecular analyses, 16 (36.4%) are recovered (the same proportion as in the MP analysis), of which 10 are strongly supported, whereas 16 (36.4%) are unresolved, and 12 (27.3%) are actively contradicted.

Although the lack of strong morphological support for many clades that are strongly supported by our analyses of molecular data seem disappointing, this result is not unexpected for several reasons. First, our morphological analyses are based on many fewer characters but include more taxa, so even in the absence of character conflict there are fewer state changes to apportion among more nodes. Second, including extinct taxa that are sister to crown groups with strong molecular support has the result of breaking up the long branches along which crown-group synapomorphies accumulated (Horovitz, 1999; Wilkinson, 2003; Cobbett et al., 2007; Bapst, 2013). And third, fossil taxa are almost always incompletely preserved, introducing abundant missing data to the morphological matrix.

There is considerable debate in the literature as to whether Bayesian analyses of discrete morphological data using Lewis's (2001) Mk model and its variants are likely to result in more accurate phylogenies than are parsimony-based approaches (Wright and Hillis, 2014; O'Reilly et al., 2016, 2018; Brown et al., 2017; Goloboff et al., 2018a, 2018b, 2019; Puttick et al., 2017a, 2017b; Sansom et al., 2018; Schrago et al., 2018; Golo-

boff and Arias, 2019; Smith, 2019). Here, we found no difference in the number of clades strongly supported by molecular data that are recovered by the two methods used to analyze our morphological data (table 13). However, we note that some molecular clades are recovered by one morphological analysis only and not by the other; for example, our undated Bayesian analysis of morphology strongly supports monophyly of Dasyuridae, whereas maximum parsimony analysis of the same morphological data fails to resolve dasyurids as monophyletic. Interestingly, of the clades that are strongly supported by our molecular data and that are recovered in both of our morphological analyses, more receive strong support in the undated Bayesian analysis than in the maximum parsimony analysis (table 13). Nevertheless, we recognize that meaningful comparisons of Bayesian posterior probabilities with bootstrap frequencies are difficult (Suzuki et al., 2002; Wilcox, 2002; Erixon et al., 2003; García-Sandoval, 2014), so the significance of this observation is unclear.

Maximum parsimony and undated Bayesian analyses of our morphological data recover monophyly of most marsupial orders represented by more than one terminal, namely Dasyuromorphia, Diprotodontia, Peramelemorphia, and Microbiotheria. Both analyses of our morphological dataset also recover a clade comprising all our paucituberculatan terminals except †*Evolestes*. However, Didelphimorphia is not resolved as a clade in either morphological analysis due to a lack of resolution at the base of Marsupialia. This is not surprising given that didelphids are morphologically plesiomorphic by comparison with other marsupials (Wible, 1990, 2003; Voss and Jansa, 2009, 2021; Williamson et al., 2014). Although didelphids are characterized by apomorphic fusion between the interparietal and supraoccipital early in postnatal life (char. 31; Nesslinger, 1956; Clark and Smith, 1993; Voss and Jansa, 2009), this feature could not be assessed in any of our outgroup terminals (†*Pucadelphys*, †*Andinodelphys*, †*Allqokirus*, and †*Mimoperadectes*) or in paucituberculatans (see

chars. 25, 30), and it is inapplicable in †*Herpetotherium* (due to apparent absence of the interparietal in this taxon; chars. 30, 31), so precocious interparietal-supraoccipital fusion does not optimize as a didelphimorphian synapomorphy in these analyses. The apomorphic absence of a posterior cingulid on the lower molars (char. 180) is a dental feature that distinguishes most didelphids[26] from otherwise dentally similar outgroup terminals, but, based on its distribution within Marsupialia and nonmarsupial metatherians, it is likely a synapomorphy of Marsupialia as a whole rather than of Didelphimorphia (Voss and Jansa, 2009).

More problematically, our craniodental analyses recover some higher-level relationships that are incongruent with our current understanding of marsupial phylogeny (Eldridge et al., 2019). In particular, Australidelphia is not supported in our craniodental results, which instead group all of our ingroup terminals characterized by gliriform lower anterior incisors (diprotodontians, paucituberculatans, and †*Yalkaparidon*) into a single clade despite compelling molecular evidence that gliriform lower anterior incisors originated independently in diprotodontians and paucituberculatans (Weisbecker and Beck, 2015). Our failure to recover Australidelphia from analyses of craniodental characters is not surprising, however, because morphological support for this clade seems to consist only of the tarsal characters described by Szalay (1982a). In fact, all studies of marsupial phylogeny based on the cranium and dentition previous to Szalay (1982a) consistently failed to link microbiotherians with Australian marsupials (reviewed by Archer, 1984c: 760–785). Although some analyses of craniodental data that postdate Szalay (1982a) have recovered Australidelphia (e.g., Sánchez-Villagra, 2001; Ladevèze and Muizon, 2007; Carneiro and Oliveira, 2017b; Carneiro, 2018; Engelman et al., 2020; Muizon et al., 2018), only those by Car-

neiro and coworkers have included both paucituberculatan and diprotodontian terminals (Carneiro and Oliveira, 2017a; Carneiro et al., 2018; Carneiro, 2019; Rangel et al., 2019). Similar to our results, several other analyses that have focused on craniodental characters have likewise failed to support australidelphian monophyly (Springer et al., 1997; Ladevèze and Muizon, 2010; Wilson et al., 2016).

Although our craniodental analyses fail to recover monophyly of Didelphimorphia (see above), they do recover several didelphid subclades that are well corroborated by previous molecular, morphological, and total-evidence studies (e.g., Steiner et al., 2005; Flores, 2009; Voss and Jansa, 2009; Jansa et al., 2014; Mitchell et al., 2014; May-Collado et al., 2015; Vilela et al., 2015; Amador and Giannini, 2016; Beck and Taglioretti, 2020; Álvarez-Carretero et al., 2021), including Didelphini, *Metachirus* + Didelphini, and Caluromyinae. Interestingly, they also recover monophyly of Thylamyini sensu Voss and Jansa (2009), whereas Voss and Jansa's (2009) own analysis of 129 nonmolecular (external morphology, craniodental, and karyotype) characters did not. Our craniodental analyses agree with recent studies of fossil didelphimorphians in consistently placing †*Thylophorops* within Didelphini, and in supporting the monophyly of †Sparassocynini (Forasiepi et al., 2009; Goin et al., 2009b; Voss and Jansa, 2009; Suárez Gómez, 2019; Beck and Taglioretti, 2020). However, only our Bayesian analysis supports a close relationship between †Sparassocynini, *Monodelphis*, and †*Thylatheridium* (in agreement with Beck and Taglioretti, 2020), whereas the relationships among these taxa is unresolved in our maximum parsimony analysis.

Within Peramelemorphia, our craniodental grouping of *Perameles* and *Isoodon* with *Macrotis* and *Chaeropus* agrees with Groves and Flannery's (1990) classification as well as with recent craniodental analyses by Travouillon and coauthors (Travouillon et al., 2010, 2013a, 2013b, 2015b, 2017, 2019, 2021; Gurovich et al., 2014; Chamberlain et al., 2015; Travouillon and Phil-

---

[26] This trait was formerly thought to characterize all didelphids (Voss and Jansa, 2009), but recent studies have revealed the presence of small posterior cingulids in a few species (Voss et al., 2018, 2020).

lips, 2018). However, this result is notably incongruent with the results of most molecular analyses, including our own, which consistently support peramelid monophyly. As noted by several authors (Travouillon et al., 2010; Chamberlain et al., 2015; Kear et al., 2016; Warburton and Travouillon, 2016; Travouillon and Phillips, 2018), morphological support for grouping *Perameles*, *Isoodon*, *Macrotis*, and *Chaeropus* may reflect convergent adaptations to open, xeric habitats. By contrast, our analyses agree with all published morphological and total-evidence analyses of Peramelemorphia (Travouillon et al., 2010, 2013a, 2013b; 2015b, 2017, 2019, 2021; Gurovich et al., 2014; Chamberlain et al., 2015; Kear et al., 2016; Travouillon and Phillips, 2018) in placing the fossil taxa †*Bulungu*, †*Galadi*, and †*Yarala* outside the crown clade.

Within Dasyuromorphia, our craniodental analyses place *Myrmecobius* closer to *Thylacinus* than to Dasyuridae, whereas most recent molecular and total-evidence analyses have instead placed *Myrmecobius* closer to Dasyuridae (Miller et al., 2009; Mitchell et al., 2014; May-Collado et al., 2015; Kealy and Beck, 2017; Feigin et al., 2018). However, an undated Bayesian analysis of craniodental and postcranial characters by Kealy and Beck (2017: fig. 1b) also recovered *Myrmecobius* + Thylacinidae, and a maximum parsimony analysis of the same dataset did not resolve this relationship (Kealy and Beck, 2017: fig. 1a). Our analyses also place †*Badjcinus*, †*Mutpuracinus*, †*Barinya*, and †*Nimbacinus* in a clade with *Thylacinus*, whereas the relationships of these fossil taxa have varied in other analyses. †*Nimbacinus* has been consistently recovered as a thylacinid in recently published phylogenetic analyses (Murray and Megirian, 2006a; Kealy and Beck, 2017; Rovinsky et al., 2019), and †*Badjcinus* was also recovered as a thylacinid by Rovinsky et al. (2019) and by the morphological and undated total-evidence analyses of Kealy and Beck (2017), but a dated total-evidence analysis by the latter authors placed †*Badjcinus* as a stem-dasyuromorphian (Kealy and Beck, 2017: fig. 3). The positions of †*Mutpuracinus* and †*Barinya*

within Dasyuromorphia were unresolved in the morphological analyses of Kealy and Beck (2017), but their undated total-evidence analysis placed †*Barinya* as sister to *Myrmecobius*, and their dated total-evidence analysis placed both †*Mutpuracinus* and †*Barinya* in a clade with *Myrmecobius*. However, most of the morphological analyses of Rovinsky et al. (2019) instead placed †*Mutpuracinus* and †*Barinya* together with crown-clade dasyurids.

Wroe (1999) identified four cranial features as synapomorphies of crown-clade Dasyuridae: "presence of a fully enclosed stylomastoid foramen that includes a periotic component; contact between the pars petrosa and a paroccipital tympanic process[27] that fully encloses the paroccipital hypotympanic sinus ventrally; extensive dorsal enclosure of the internal jugular canal; and contact between the mastoid tympanic process [= caudal tympanic process of the petrosal here] and the pars petrosa" (Wroe, 1999: 501). We incorporated versions of the first and last of these features into our craniodental character set by scoring presence/absence and composition of the stylomastoid foramen (char. 79) and contact between the caudal tympanic process and the pars cochlearis of the petrosal (char. 68). Despite this, our maximum parsimony analysis fails to resolve monophyly of crown-clade Dasyuridae. In contrast, our undated Bayesian analysis of our craniodental characters does strongly support monophyly of crown-clade Dasyuridae.

---

[27] Wroe (1999: 56) defined the paroccipital tympanic process as a process that "projects anteriorly from the base of the paroccipital process and floors a…paroccipital hypotympanic sinus." Wroe (1999: 56) reported that this process is partially fused to the "posteroventral portion of the pars petrosa anteromesially" in all crown-clade dasyurids, but not in other fossil or extant dasyuromorphians or non-dasyuromorphian metatherian taxa examined (*Pucadelphys*, sparassodonts, didelphids, *Dromiciops*, peramalemorphians, *Myrmecobius*, thylacinids). We were unable to consistently and unambiguously score presence or absence of this feature as it was defined by Wroe (1999; see also Wroe et al., 2000: char. 66; Wroe and Musser, 2001: char. 66). However, we did score presence or absence of a greatly pneumatized paroccipital process (presence of which is a distinctive feature found in a few dasyurids) as a distinct character (see char. 94).

Both of our craniodental analyses recover relationships within Paucituberculata that conflict with recent studies of paucituberculatan phylogeny (Abello, 2007, 2013; Goin et al., 2007b, 2009a; Forasiepi et al., 2013; Rincón et al., 2015; Engelman et al., 2016; Abello et al., 2020, 2021). In particular, neither of our analyses groups †*Evolestes* with other paucituberculatans, whereas this important fossil has been consistently recovered as a plesiomorphic paucituberculatan in other published analyses (Goin et al., 2007b; Abello, 2013; Rincón et al., 2015; Engelman et al., 2016; Abello et al., 2020, 2021). Our analyses also conflict with those studies in failing to group the fossil caenolestid †*Stilotherium* with extant caenolestids, instead placing †*Pichipilus* (a pichipilid palaeothentoid) within crown-clade Caenolestidae, and in failing to recover monophyly of †Palaeothentoidea (= †*Acdestis* + †*Palaeothentes* + †*Pichipilus*) or †Palaeothentidae (= †*Acdestis* + †*Palaeothentes*). The grouping of †*Pichipilus* with extant caenolestids may be due to the shared presence of an anteorbital vacuity, which is absent in †*Acdestis* and †*Palaeothentes* (the condition in †*Stilotherium* is unknown; char. 4). In addition, we included only the best-preserved fossil paucituberculatan taxa as terminals here, whereas other studies (Abello, 2007, 2013; Goin et al., 2007b, 2009a; Forasiepi et al., 2013; Rincón et al., 2015; Engelman et al., 2016; Abello et al., 2020, 2021) included a much denser sampling of fossil paucituberculatans (including taxa only known from fragmentary dental remains), and they used a wider range of paucituberculatan-specific morphological characters that could not be included here due to the difficulty of scoring them consistently across our broader taxonomic sampling.

To our knowledge, ours is the first published study using discrete morphological characters to include a dense sampling of modern and fossil terminals across all major subclades within Diprotodontia. Other published studies have included only a few diprotodontian terminals within the context of broader marsupial relationships—e.g., Horovitz and Sánchez-Villagra

(2003), Carneiro et al. (2018), Carneiro (2019), and Rangel et al. (2019)—or have focused on specific subclades within Diprotodontia, such as Macropodiformes (Kear et al., 2007; Kear and Pledge, 2008; Prideaux and Warburton, 2010; Black et al., 2014c; Travouillon et al., 2014b, 2015a, 2016; Cooke et al., 2015; Butler et al., 2016, 2018; den Boer and Kear, 2018) and Vombatiformes (Munson, 1992; Black et al., 2012a; Gillespie et al., 2016; Beck et al., 2020). In particular, sampling of "possums" (non-macropodiform phalangeridans) has been limited in previous studies.

Maximum parsimony and undated Bayesian analyses of our craniodental characters both recover monophyly of Diprotodontia, albeit with only weak support. Our maximum parsimony analysis recovers monophyly of Vombatiformes, with †Thylacoleonidae as the sister to the remaining vombatiforms, in agreement with Gillespie et al. (2016) and Beck et al. (2020). By contrast, our undated Bayesian analysis places †Thylacoleonidae as sister to the rest of Diprotodontia, a novel result that has not (to our knowledge) been proposed previously (see the taxonomic account for †Thylacoleonidae, below). Phascolarctidae is sister to the remaining vombatiform taxa (= Vombatomorphia sensu Beck et al., 2020: table 1) in both of our morphological analyses, a result that is congruent with those of other recent morphological studies (Black et al., 2012a; Gillespie et al., 2016; Beck et al., 2020). Neither of our morphological analyses robustly resolves the branching pattern between the vombatomorphian families †Diprotodontidae, Vombatidae, †Ilariidae, and †Wynyardiidae, but we note that there is no current consensus regarding their interrelationships based on previous studies (Archer, 1984c; Woodburne, 1984b; Aplin and Archer, 1987; Marshall et al., 1990; Munson, 1992; Murray, 1998; Gillespie, 2007; Black, 2008; Black et al., 2012a; Gillespie et al., 2016; Beck et al., 2020).

Although monophyly of Phalangerida is strongly corroborated by molecular sequence data (e.g., Meredith et al., 2009a, 2011; Mitchell et al.,

2014; May-Collado et al., 2015; Duchêne et al., 2018; Álvarez-Carretero et al., 2021), only our maximum parsimony analysis recovers this clade; our undated Bayesian analysis instead finds a major polytomy at the base of Diprotodontia. Both our craniodental analyses recover monophyly of some widely accepted clades such as Macropodiformes, Pseudocheiridae, Acrobatidae, Phalangeridae and Dactylopsilinae, but not of others such as Burramyidae, Potoroidae, or a Phalangeridae + Burramyidae clade. Interestingly, our undated Bayesian analysis recovers a clade that comprises pseudocheirids, acrobatids, and *Petaurus*, a grouping that somewhat resembles the well-corroborated clade Petauroidea (e.g., Aplin and Archer, 1987; Phillips and Pratt, 2008; Meredith et al., 2009a, 2011; Mitchell et al., 2014; May-Collado et al., 2015; Duchêne et al., 2018; Álvarez-Carretero et al., 2021) but that lacks *Tarsipes*, *Gymnobelideus*, and dactylopsilines.

Within Macropodiformes, maximum parsimony and undated Bayesian analyses of our craniodental characters both place †Balbaridae in a clade with macropodids and potoroids, whereas other published analyses have placed balbarids outside Macropodidae + Potoridae (Kear et al., 2007; Kear and Pledge, 2008; Black et al., 2014c; Travouillon et al., 2014b, 2015a, 2016; Cooke et al., 2015; Butler et al., 2016, 2018; den Boer and Kear, 2018). Our two craniodental analyses differ in the position of †*Ekaltadeta*: whereas our maximum parsimony analysis places this taxon as sister to all other macropodiforms, our undated Bayesian analysis places it as sister to *Hypsiprymnodon*. †*Ekaltadeta* and the two other genera currently recognized within the subfamily †Propleopinae (†*Propleopus* and †*Jackmahoneya*, not included here) have been placed in Hypsiprymnodontidae by some authors (Ride, 1993; Ride et al., 1997; Kear and Cooke, 2001), but Wroe et al. (1998) proposed that propleopines and balbarids form a clade to the exclusion of *Hypsiprymnodon*. The position of †*Ekaltadeta* has also varied in other published analyses (Kear et al., 2007; Kear and Pledge, 2008; Bates et al., 2014; Black et al., 2014c; Travouillon et al., 2014b, 2015a, 2016,

2022; Cooke et al., 2015; Butler et al., 2016, 2018; den Boer and Kear, 2018).

Undated Total-Evidence Analysis

Our undated total-evidence analysis (fig. 32) fails to unequivocally place †*Herpetotherium* outside Marsupialia; instead, †*Herpetotherium* forms a polytomy with various didelphid terminals (which do not form a clade) and a clade comprising our remaining marsupial terminals. Based on previous studies (e.g., Sánchez-Villagra et al., 2007; Horovitz et al., 2008, 2009; Ladevèze et al., 2020), it seems probable that †*Herpetotherium* does indeed fall outside Marsupialia, and we enforced this topology in our dated total-evidence analysis to enable us to calibrate the age of Marsupialia; however, we note that a few analyses have placed †*Herpetotherium* within the crown clade (Wilson et al., 2016; Maga and Beck, 2017: fig. 39).

Our failure to recover a didelphid clade in the undated total-evidence analysis is probably related to the overall plesiomorphic morphology of opossums as discussed above. Although our undated total-evidence analysis fails to recover didelphid monophyly, a position for our didelphid terminals outside a Paucituberculata + Australidelphia clade is in agreement with retroposon evidence (Gallus et al., 2015a) and contrasts with our molecular results, wherein the marsupial root node is consistently placed between Paucituberculata and Didephimorphia + Australidelphia (see above).

With the exception of didelphid nonmonophyly and the shifted position of the marsupial root node, relationships among Recent terminals in our undated total-evidence analysis (fig. 32) closely resemble those recovered by our combined-molecular analysis (fig. 29), suggesting that the addition of craniodental characters had little impact on the resultant topology. This is perhaps unsurprising given the relative sizes of the molecular and craniodental partitions—24.5 kb of molecular sequence data (representing 16,116 variable sites, of which 13,794 are parsi-

mony informative) versus 180 morphological characters (all of which are variable, and 163 are parsimony informative)—and (as discussed above) the evidently much stronger phylogenetic signal in the molecular data (Scarpetta, 2020; but see Neumann et al., 2021).

The positions of fossil terminals in this analysis are generally similar to those recovered in the craniodental analyses. For fossil didelphids, the positions of †*Thylophorops* within Didelphini and of †*Thylatheridium* and the sparassocynins †*Hesperocynus* and †*Sparassocynus* in a clade with *Monodelphis* agree with the results of previous studies (Reig, 1958b; Goin and Rey, 1997; Voss and Jansa, 2009; Beck and Taglioretti, 2020). Within Paucituberculata, †*Evolestes* groups with the other paucituberculatan terminals, †*Acdestis* and †*Palaeothentes* form a clade (†Palaeothentidae), and †*Stilotherium* is sister to crown caenolestids, all of which are in closer agreement with other published studies (Abello, 2007, 2013; Goin et al., 2007b, 2009a; Forasiepi et al., 2013; Rincón et al., 2015; Engelman et al., 2016; Abello et al., 2020, 2021) than are our craniodental results. However, as in our craniodental analyses (see above), the presence of †*Pichipilus* within the paucituberculatan crown clade conflicts with several published studies that place †*Pichipilus* closer to †Palaeothentidae (represented here by †*Acdestis* and †*Palaeothentes*) within the superfamily †Palaeothentoidea. As in our craniodental analyses, this result is probably at least partly due to the presence of an anteorbital vacuity in †*Pichipilus*, a derived feature shared with extant caenolestids (the condition in †*Stilotherium* is unknown) but absent in †*Acdestis* and †*Palaeothentes* (see char. 4).

The presence of †*Yalkaparidon* in a trichotomy with †*Evolestes* and our remaining paucituberculatan terminals conflicts with the phylogenetic analyses of Beck et al. (2014, 2016), which suggest that †*Yalkaparidon* is probably an australidelphian (isolated tarsals referred to †*Yalkaparidon* by Beck et al. [2014] exhibit apparently australidelphian apomorphies). However, subsequent analyses by Beck (2017) and

Zimicz and Goin (2020), which also included data from the putative †*Yalkaparidon* tarsals described by Beck et al. (2014), placed *Yalkaparidon* in a clade with the caenolestids *Caenolestes* and †*Palaeothentes* (and with argyrolagid terminals not included in this study), a result similar to that obtained in this analysis.

As in our craniodental analyses, †*Bulungu*, †*Galadi*, and †*Yarala* all fall outside crown-clade Peramelemorphia, in agreement with many recent studies (Travouillon et al., 2010, 2013a, 2013b, 2014a, 2015b, 2017, 2019, 2021; Gurovich et al., 2014; Chamberlain et al., 2015; Kear et al., 2016; Travouillon and Phillips, 2018). Our undated total-evidence analysis also resembles our craniodental analyses in placing the fossil dasyuromorphians †*Barinya*, †*Mutpuracinus*, †*Badjcinus*, and †*Nimbacinus* in a clade with *Thylacinus*; as already discussed (see above), the positions of †*Barinya*, †*Mutpuracinus*, and †*Badjcinus* has varied considerably in published phylogenetic analyses, and there is no current consensus regarding their affinities (Wroe et al., 2000; Wroe and Musser, 2001; Murray and Megirian, 2006a; Kealy and Beck, 2017; Rovinsky et al., 2019).

Within Diprotodontia, relationships within Vombatiformes (here including †Thylacoleonidae) are better resolved than in our craniodental analyses. As already discussed, the position of †Thylacoleonidae as sister to the remaining vombatiforms is congruent with some recent studies (Black et al., 2012a; Gillespie et al., 2016; Beck et al., 2020), as is the position of Phascolarctidae as the next family to diverge (Black et al., 2012a; Gillespie et al., 2016; Beck et al., 2020). The relationships among vombatomorphians—a †Wynyardiidae + †*Ilaria* clade sister to †Diprotodontidae, with Vombatidae outside this— found in our undated total-evidence analysis have not been recovered in any other published analysis of vombatiform relationships, but other studies are characterized by conflicting topologies (Archer, 1984c; Woodburne, 1984b; Aplin and Archer, 1987; Marshall et al., 1990; Munson, 1992; Murray, 1998; Gillespie, 2007; Black, 2008;

Black et al., 2012a; Gillespie et al., 2016; Beck et al., 2020).

Within Phalangeridae, the position of "*Trichosurus*" †*dicksoni* within Trichosurinae and †*Onirocuscus* within Ailuropinae is broadly congruent with the original description of these fossil taxa by Flannery and Archer (1987a), who referred "*T.*" †*dicksoni* to the modern genus and identified †*O. reidi* as a fossil member of the ailuropine genus *Strigocuscus*. However, in an unpublished Ph.D. dissertation, Crosby (2002b) concluded that "*T.*" †*dicksoni* should be assigned to a different genus, and she subsequently (Crosby, 2007: fig. 7) presented an informal phylogeny in which "*T.*" †*dicksoni* and †*Onirocuscus* were placed in a clade separate from Recent phalangerids.

Within Macropodiformes, the position of †*Ekaltadeta* as sister to Hypsiprymnodontinae is (as already discussed above) congruent with some of the phylogenetic analyses of den Boer and Kear (2018), but most published analyses instead place †*Ekaltadeta* in a clade with balbarids (Kear et al., 2007; Kear and Pledge, 2008; Bates et al., 2014; Black et al., 2014c; Travouillon et al., 2014b, 2015a, 2016; Cooke et al., 2015; Butler et al., 2016, 2018; den Boer and Kear, 2018; see also Wroe et al., 1998). ?*Bettongia* †*moyesi* does not form a clade with our extant *Bettongia* terminal, contra Flannery and Archer (1987b), but nevertheless is recovered as a bettongin; the position of ?*Bettongia* †*moyesi* in other published analyses has varied and does not always fall within Potoroidae (Kear et al., 2007; Kear and Pledge, 2008; Bates et al., 2014; Black et al., 2014c; Travouillon et al., 2014b, 2015a, 2016; Cooke et al., 2015; Butler et al., 2016, 2018; den Boer and Kear, 2018).

The balbarids †*Balbaroo* and †*Ganawamaya* form a clade with three fossil macropodids (†*Gangaroo*, †*Hadronomas*, and *Rhizosthenurus*) that is sister to the living macropodid *Dorcopsulus*, with *Dorcopsis* outside this. This arrangement is strongly incongruent with currently accepted relationships, as †Balbaridae is consistently supported as falling outside Mac-

ropodidae + Potoroidae, whereas †*Gangaroo*, †*Hadronomas*, and *Rhizosthenurus* (the last two placed together in †Sthenurinae) are likely stem macropodids (Kear and Cooke, 2001; Cooke, 2006; Kear et al., 2007; Kear and Pledge, 2008; Bates et al., 2014; Black et al., 2014c; Travouillon et al., 2014b, 2015a, 2016; Cooke et al., 2015; Butler et al., 2016, 2018; den Boer and Kear, 2018). The anomalous topology found in our undated total-evidence analysis may be due to (1) the fact that *Dorcopsis* and *Dorcopsis* are generally accepted to be the most plesiomorphic living macropodids (Prideaux and Warburton, 2010), and (2) our omission of several fragmentary fossil macropodiforms that Cooke (1997a, 1997b, 1997c, 2006) interpreted as evidence that the fully lophodont dentitions of balbarids and macropodids evolved convergently.

Dated Total-Evidence Analysis

Comparing the results of our undated (fig. 32) and dated total-evidence (fig. 33) analyses, the only major topological change among our Recent terminals concerns the position of the root—the direct result of imposing topological constraints so that the ages of Marsupialia and Didelphimorphia could be calibrated (see appendix 3). Our decision to enforce †*Herpetotherium* as falling outside Marsupialia is congruent with most recent published phylogenies (e.g., Sánchez-Villagra et al., 2007; Horovitz et al., 2008, 2009; Ladevèze et al., 2020). Similarly, our decision to enforce Didelphimorphia as sister to the remaining marsupial orders is congruent with statistically significant retrotransposon insertion evidence for this rooting position (Gallus et al., 2015a).

However, the incorporation of temporal information had a major effect on the positions of many fossil terminals, which moved to nodes deeper within the tree (a phenomenon previously reported in other studies; see, e.g., Lee and Yates, 2018; Beck and Taglioretti, 2020; King and Beck, 2020). This is presumably due to two inter-

related factors. All else being equal, dated analyses using a Fossilized Birth-Death model are expected to reconstruct fossil terminals as originating from deeper nodes than modern terminals, particularly when phylogenetic signal in the character data that might otherwise overwhelm the temporal signal is weak (Lee and Yates, 2018; King, 2021). In addition, most current implementations of Fossilized Birth-Death models (including our own) assume constant rates of speciation, extinction, and fossilization/sampling through time and between lineages. This assumption means that long, unsampled branches will be disfavored, such that fossil terminals are shifted to deeper positions if fossil sampling is not consistent throughout the tree (Turner et al., 2017; King, 2021). Fossil sampling is undoubtedly not consistent through time or between lineages in this study. Most obviously, we did not include any crown-clade (marsupial) terminals older than the late Oligocene, because older taxa tend to be highly incomplete, typically known only from fragmentary dental remains. Indeed, for some clades we did not include any fossil representatives, either because fossil members described to date are highly incomplete (e.g., Pseudocheiridae, Petauridae, Burramyidae), or because no fossil members are currently known (e.g., Tarsipedidae, Myrmecobiidae; Long et al., 2002; Archer and Hand, 2006; Eldridge et al., 2019). Thus, the phylogenetic affinities of taxa that shift position between our undated and dated total-evidence analyses (e.g., †*Onirocuscus* and "*Trichosurus*" †*dicksoni*, which are within crown-clade Phalangeridae in the undated analysis, but outside it in the dated analysis) require further study.

In general, the divergence dates found in our dated total-evidence analysis are younger than those reported by most other molecular-clock studies of pan-marsupial relationships (table 6). In particular, several such studies estimated the first divergence within Marsupialia to have occurred during the Cretaceous, whereas we date this divergence to the late Paleocene or earliest Eocene. However, a recent species-level phylogenomic analysis of mammalian divergence times by Álvarez-Carretero et al. (2021) also recovered a late Paleocene to early Eocene age (58.9–49.3 Ma) for the first divergence within Marsupialia. There are several plausible, nonexclusive explanations for such discrepancies.

Although we have not undertaken a detailed reassessment of the fossil calibrations used by previous molecular-clock studies, we note that some calibrations appear to be problematic in the light of current evidence. For example, Meredith et al. (2009a) assigned a mean prior distribution of 75 Mya on the age of Marsupialia, whereas Meredith et al. (2011: table S3) specified a minimum of 65.18 Mya for the split between Didelphimorphia and Australidelphia. Both dates were predicated on the assumption that peradectids are stem didelphimorphians as proposed by Horovitz et al. (2009); however, most subsequently published analyses suggest that peradectids fall outside Marsupialia, as we also found in our morphological and undated total-evidence analyses. As summarized by Eldridge et al. (2019), the oldest definitive marsupials are from the early Eocene Tingamarra Local Fauna, and so have a minimum age of only 54.55 million years old (Godthelp et al., 1992; Beck et al., 2008). Álvarez-Carretero et al. (2021: supplementary information) did use these Tingamarran fossils to provide a minimum bound on the first divergence within Marsupialia, but they specified a date of 48.07 Mya (the minimum age of the Ypresian; Speijer et al. 2020) following Benton et al. (2015: 60) rather than the actual radiometric date reported for the Tingamarra site by Godthelp et al. (1992). Kealy and Beck (2017: 16, 17) provided evidence that some of the calibrations used by Mitchell et al. (2014)—and subsequently by Duchêne et al. (2018)—are also inappropriate. Lastly, different dating programs, including MrBayes (used here) and MCMCTree (used by Meredith et al. 2011, Mitchell et al., 2014, Duchêne et al., 2018, and Álvarez-Carretero et al., 2021), are known to give different posterior estimates of divergence times even when provided with the same data and fossil calibrations (Barba-Montoya et al., 2017).

A relevant methodological difference between our study and previous molecular-dating studies based on Recent taxa (which necessarily used only node calibrations) is that we used a total-evidence dataset that included both extant and fossil terminals (allowing the use of tip calibrations), which we analyzed using the Fossilised Birth-Death model. Total-evidence dating arguably makes the best use of paleontological data for constructing evolutionary timescales (O'Reilly and Donoghue, 2016), and combining both tip and node calibrations (as done here) appears to resolve the issue of tip-dating-only analyses recovering unrealistically ancient dates (O'Reilly et al., 2015; O'Reilly and Donoghue, 2016; Ronquist et al., 2016). In particular, tip calibrations can interact with node calibrations to more objectively define maximum bounds on the ages of calibrated nodes (O'Reilly and Donoghue, 2016), whereas molecular-clock studies that use only node calibrations often specify highly conservative maximum bounds (or no maximum bound at all on some calibrated nodes), which tend to favor older divergence dates.

However, the use of morphological data (either alone or in the context of a total-evidence analysis) to directly estimate divergence times has been criticized (O'Reilly et al., 2015; Ronquist et al., 2016; Parins-Fukuchi and Brown, 2017). Much of this criticism surrounds the realism (or lack thereof) of the Lewis (2001) Mk model for discrete morphological character data (but see Klopfstein et al., 2019). Simulation studies also suggest that accurate estimates of divergence times using the Fossilized Birth-Death model require the inclusion of as much fossil occurrence data as possible, including highly incomplete taxa (Klopfstein et al., 2019; Luo et al., 2020; O'Reilly and Donoghue, 2020), whereas we included only well-preserved taxa among our terminals. Nevertheless, molecular-clock analyses are also sensitive to several assumptions (Warnock et al., 2012, 2015; Condamine et al., 2015; Bromham, 2019; Budd and Mann, 2020; Klopfstein, 2020) that have seldom been convincingly addressed in the marsupial literature.

In summary, although there is reason to believe that our date estimates are based on more appropriate calibration points and improved estimation methods than those employed in previous molecular-clock studies, all phylogenetic date estimates should be viewed with caution, and ours are no exception. In particular, we are concerned that our estimates for the the split between Didelphimorphia and our remaining terminals (median age: 56.2 Mya; 95% HPD: 54.7–58.6 Mya) and the split between Paucituberculata + *Yalkaparidon* and Australidelphia (median age: 55.1 Mya; 95% HPD: 54.6–56.6 Mya) are close to the minimum bound of the calibration applied to these nodes (54.55 Mya), suggesting that there may be some incongruence between this calibration and the overall clock model (which would presumably favor younger dates for these nodes if they were not calibrated). Additionally, this 54.55 Mya calibration is based on a K-Ar date for the Tingamarra Local Fauna that needs to be confirmed with improved geochronological methods (e.g., Ar-Ar dating). If the currently accepted age for Tingamarra is too old, then the crown age of Marsupialia may be even younger than estimated here. However, if the Tingamarran fossils are discounted, then the oldest definitive marsupials are probably australidelphian-type tarsals from the La Barda locality in Argentina, which have a minimum age of 43 Mya (Tejedor et al., 2009; Lorente et al., 2016).

Ultimately, however, the highly incomplete nature of the marsupial geological record—especially the very limited Australian record prior to the late Oligocene (Black et al., 2012b; Woodhead et al., 2014; Beck, 2017b; Bennett et al., 2018; Eldridge et al., 2019)—means that a wide range of potential divergence dates are congruent with the available fossil evidence. In the taxonomic accounts that follow, we consider the plausibility of our estimated divergence times given the known fossil record of the taxon in question and note any instances of obvious incongruence.

TAXONOMIC ACCOUNTS

The following classification of Marsupialia formalizes clade membership at the Linnaean rank of family and above and summarizes our conclusions regarding what appear to be well-corroborated groups. It is largely based on the results of our dated total-evidence analysis (fig. 33), because this shows the greatest congruence with other recent phylogenetic analyses of marsupials, and because it includes both fossil and extant terminals. Except where noted, we follow Voss and Jansa (2009) for names of American marsupial clades and Jackson and Groves (2015) for the names of Sahulian marsupials. For each taxon, we list its contents (restricted to taxa included in this study) and unambiguous craniodental synapomorphies (i.e., those identified under both Accelerated and Delayed Transformations; see Methods) as optimized by parsimony on our dated total-evidence topology (fig. 33).[28] We also list estimated divergence times (median estimates and 95% highest posterior density, HPD) for their divergence from their sister taxa (stem age) and (if comprising more than one terminal) for their first diversification (crown age), also based on the results of our dated total-evidence analysis. Under Comments we compare these age estimates with the fossil record and (where relevant) other studies that have estimated divergence dates within Marsupialia using molecular or total-evidence clock analyses.

Marsupialia, Illiger 1811

Contents: Dasyuromorphia, Didelphimorphia, Diprotodontia, Microbiotheria, Notoryctemorphia, Paucituberculata, Peramelemorphia, and †Yalkaparidontia.

---

[28] Although these accounts include only clades that we consider well supported by available evidence, a list of unambiguous craniodental synapomorphies for all nodes in our dated total-evidence analysis is provided in supplementary file S3.

Stem Age: 59.7 Mya (95% HPD: 55.6–65.8 Mya).

Crown Age: 56.2 Mya (95% HPD: 54.7–58.6 Mya).

Unambiguous Craniodental Synapomorphies: Lower molars without a posterior cingulid (char. 180: 1→0; ci = 0.333).

Comments: As noted in our introduction, most recent authors restrict Marsupialia to the metatherian crown clade, and we follow the node-based definition of Marsupialia proposed by Beck et al. (2014: 131): the least inclusive clade containing *Didelphis marsupialis*, *Caenolestes fuliginosus*, and *Phalanger orientalis*. By contrast, †*Pucadelphys*, †*Mayulestes*, and †*Allqokirus* have consistently fallen outside Marsupialia in most published analyses (Rougier et al., 1998, 2004, 2015; Luo et al., 2003, 2011; Ladevèze and Muizon, 2007; Sánchez-Villagra et al., 2007; Beck et al., 2008a; Horovitz et al., 2008, 2009; Forasiepi, 2009; Ladevèze and Muizon, 2010; Beck, 2012, 2017a; Williamson et al., 2012, 2014; Engelman and Croft, 2014; Forasiepi et al., 2014a; Wilson et al., 2016; Carneiro and Oliveira, 2017a, 2017b; Maga and Beck, 2017; Bi et al., 2018; Carneiro, 2018, 2019; Carneiro et al., 2018; Muizon et al., 2018; Rangel et al., 2019; Ladevèze et al., 2020; Muizon and Ladevèze, 2020. Notable exceptions to this widespread consensus (Goin et al., 2006; Velazco et al., 2022) are discussed in the account for †*Pucadelphys* in appendix 1).

†*Mimoperadectes* also falls outside Marsupialia in all our craniodental (figs. 30, 31) and total-evidence (figs. 32, 33) analyses. This result conflicts with Horovitz et al. (2009), who recovered †*Mimoperadectes* as a stem didelphimorphian, but it agrees with most subsequent studies (Forasiepi, 2009; Beck, 2012; Beck et al., 2014; Engelman and Croft, 2014; Forasiepi et al., 2014a; Suarez et al., 2015; Carneiro, 2018, 2019; Carneiro et al., 2018; Muizon et al., 2018; Rangel et al., 2019; Engelman et al., 2020; Ladevèze et al., 2020; Muizon and Ladevèze, 2020), which have consistently found that †*Mimoperadectes* and other alleged peradectids are outside the

metatherian crown clade.[29] In particular, as we discussed above (see char. 55), †*Mimoperadectes* appears to lack any kind of tympanic process or bulla enclosing the hypotympanic sinus ventrally, as do our outgroup terminals †*Pucadelphys*, †*Mayulestes*, and †*Allqokirus*, plus several other nonmarsupial metatherians not included here (Muizon, 1999; Forasiepi, 2009; Bi et al., 2015; Beck, 2017a; Muizon et al., 2018; Muizon and Ladevèze, 2020). However, the polarity of this feature is debated, and there is clear evidence of homoplasy within Metatheria (Kielan-Jaworowska and Nessov, 1990: 7; Forasiepi, 2009: char. 50; Wilson et al., 2016: supplementary information; Beck, 2017a: 402; Muizon et al., 2018; Muizon and Ladevèze, 2020: 683–684).

Our craniodental and undated total-evidence analyses (figs. 30–32) place †*Herpetotherium* in an unresolved polytomy with Recent marsupials. In contrast to our outgroup terminals and †*Mimoperadectes*, †*Herpetotherium* has an ossified hypotympanic sinus floor, which optimizes as an unambiguous synapomorphy of †*Herpetotherium* + Marsupialia in our results (see supplementary file S3 in the online supplement: https://doi.org/10.5531/sd.sp.54). However, most recent published phylogenetic analyses place †*Herpetotherium* outside Marsupialia (Ladevèze and Muizon, 2007; Sánchez-Villagra et al., 2007; Beck et al., 2008a; Horovitz et al., 2008, 2009; Forasiepi, 2009; Ladevèze and Muizon, 2010; Beck, 2012; Williamson et al., 2012, 2014; Engelman and Croft, 2014; Forasiepi et al., 2014a; Beck, 2017a; Carneiro and Oliveira, 2017a, 2017b; Maga and Beck, 2017; Carneiro, 2018, 2019; Carneiro et al., 2018; Muizon et al., 2018; Rangel et al., 2019; Muizon and Ladevèze, 2020). Based on these studies, and to enable us to calibrate the age of Marsupialia, we constrained †*Herpetotherium* to fall outside the crown clade in our dated total-evidence analysis.

With †*Herpetotherium* constrained to fall outside Marsupialia, only loss of the posterior cingulid optimizes as an unambiguous synapomorphy for the crown clade. Although presence or absence of a posterior cingulid might be a useful criterion for distinguishing marsupials from nonmarsupial marsupialiforms (Voss and Jansa, 2009: 87), this structure was subsequently reacquired by dasyuromorphians (see below) and by the balbarid macropodiform †*Balbaroo* (and other balbarids not included here; see Cooke, 1997a: fig. 7, who referred to the posterior cingulid as the "hypocingulid"). Three fossil Australian taxa that have not been included here due to their incompleteness—†*Djarthia murgonensis* from the early Eocene Tingamarra fauna in northeastern Australia and its probable relatives †*Ankotarinja tirarensis* and †*Keeuna woodburnei* from the late Oligocene Etadunna Formation of central Australia—also have a posterior cingulid and appear to comprise a clade of stem australidelphians (Archer, 1976d; Godthelp et al., 1999; Beck et al., 2008a; Kealy and Beck, 2017), in which case they represent another lineage that independently reacquired this trait. As noted earlier, more or less distinct posterior cingulids have recently been reported in a few extant didelphids (Voss et al., 2018; Voss et al., 2020), thus revealing additional homoplasy.

As already noted (see above and table 6), our late Palaeocene–early Eocene estimate for the age of the most recent common ancestor of Marsupialia is markedly younger than the estimates proposed in several recent molecular clock analyses (Meredith et al., 2009a, 2011; Mitchell et al., 2014; Duchêne et al., 2018) as well as the few other dated total-evidence analyses that have been published to date (Beck et al., 2016; Maga and Beck, 2017). However, it is more congruent with the recent phylogenomic study of Álvarez-Carretero et al. (2021).

Didelphimorphia Gill, 1872

Contents: Didelphidae (see table 2 for included terminal taxa).

Stem Age: 56.2 Mya (95% HPD: 54.7–58.6 Mya).

---

[29] The phylogenetic analysis of Wilson et al. (2016) is a notable exception.

CROWN AGE: 27.1 Mya (95% HPD: 23.7–31.1 Mya).

UNAMBIGUOUS CRANIODENTAL SYNAPOMORPHIES: Premolariform P2 and premolariform P3 subequal in height (char. 119: 21; ci = 0.118); premolariform P3 with well-developed anterior and posterior cutting edges (char. 124: 1→0; ci = 0.667); M4 erupts before P3 (char. 130: 2→0; ci = 0.089); and p2 distinctly taller than p3 (char. 156: 2→0; ci = 0.118).

COMMENTS: As noted by numerous authors (e.g., Aplin and Archer, 1987; Goin, 2003; Forasiepi et al., 2009; Voss and Jansa, 2021), the name "Didelphimorphia" has long been used for a nonmonophyletic assemblage of dentally plesiomorphic metatherians that included both marsupials and stem metatherians. By contrast, we follow the stem-based phylogenetic definition of Didelphimorphia proposed by Beck and Taglioretti (2020), namely, the most inclusive clade containing *Didelphis marsupialis*, but not *Caenolestes fuliginosus* or *Phalanger orientalis*. The family Didelphidae (sensu Voss and Jansa, 2009) comprises the entire didelphimorphian crown clade. All four of our fossil didelphimorphian terminals (†*Hesperocynus*, †*Sparassocynus*, †*Thylatheridium*, and †*Thylophorops*) fall within the crown clade, so craniodental synapomorphies for Didelphimorphia are also synapomorphies of Didelphidae in our applications of these names.

All the craniodental features that optimize as unambiguous synapomorphies of Didelphimorphia/Didelphidae show high levels of homoplasy, as indicated by their low consistency indices (see above). One potential craniodental synapomorphy of Didelphimorphia/Didelphidae that shows less homoplasy is precocious fusion of the suture between the interparietal and supraoccipital (char. 31, state 1). This feature was first noted in this context by Voss and Jansa (2009), who stated that it is unique to didelphids within Marsupialia, but we also observed it in dactylopsiline petaurids (see char. 31). Nevertheless, interparietal-supraoccipital fusion optimizes as a synapomorphy of Didelphimorphia/Didelphidae

only under Accelerated Transformation. The reason is that it could not be scored in key nondidelphimorphian taxa that would help unambiguously resolve the branch along which this feature arose, either because suitably preserved material of an appropriate ontogenetic age is unavailable (e.g., for paucituberculatans, †*Yalkaparidon*, †*Mimoperadectes*, and our outgroup terminals), or because this character is inapplicable (as is the case for †*Herpetotherium*, in which a distinct interparietal appears to be absent; see char. 30).

In agreement with Goin (1991, 1995), our dated total-evidence analysis (fig. 33) indicates that the didelphimorphian crown clade is a relatively young radiation, with its earliest divergence estimated as late Oligocene or early Miocene. This estimate is also broadly congruent with the molecular node-dating analysis of Jansa et al. (2014) and with the total-evidence tip-and-node dating analysis of Beck and Taglioretti (2020); however, it is considerably younger than estimated divergence dates suggested by several other molecular studies, which have dated the last common ancestor of living didelphimorphians to the early Oligocene or Eocene (Steiner et al., 2005; Meredith et al., 2008b; 2011; Mitchell et al., 2014; Vilela et al., 2015; Álvarez-Carretero et al., 2021; see table 6). Our estimated crown age is likewise broadly congruent with the relevant fossil record (reviewed by Beck and Taglioretti, 2020; Castro et al., 2021), in which the oldest known (probable crown-clade) didelphids are from the early Miocene (Colhuehuapian SALMA, ~21.0–20.1 Mya; Goin et al., 2007a; Dunn et al., 2012; Castro et al., 2021).[30]

The comparatively long branch between the divergence of Didelphimorphia from other marsupials and the first diversification of lineages ancestral to living didelphids suggests a long history (presumably largely or entirely South American; Jansa et al., 2014; Voss and

---

[30] Note, however, that these specimens are highly fragmentary (isolated teeth only), and their affinities are correspondingly uncertain (Goin et al., 2007a; Beck and Taglioretti, 2020; Castro et al., 2021).
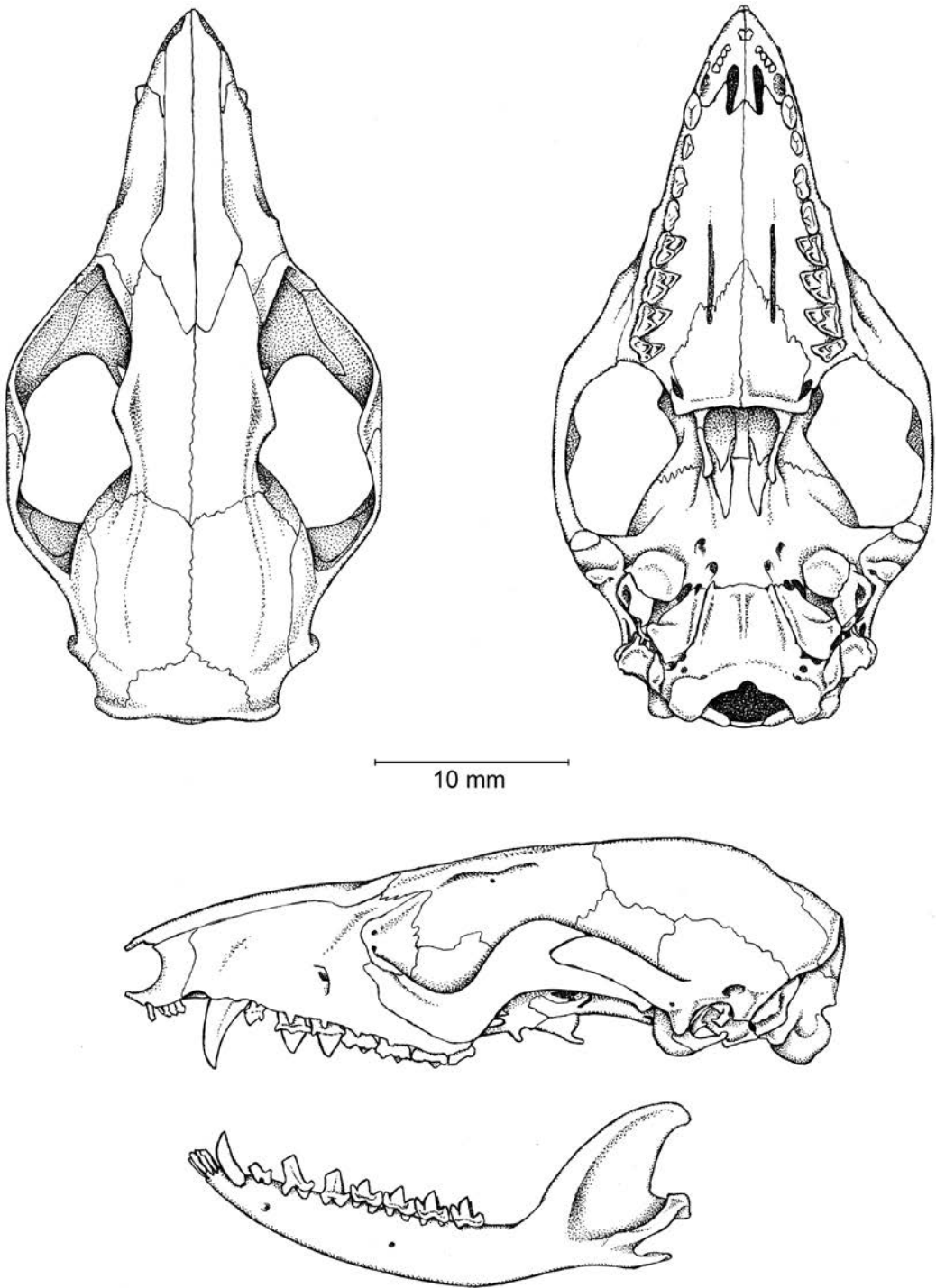
FIG. 34. *Marmosa murina* (Didelphimorphia, Didelphidae; based on AMNH 267368, an adult of unknown sex from French Guiana).

Jansa, 2021) of stem didelphimorphians; because none have been reported to date—in effect, a protracted ghost lineage. However, given the lack of dental synapomorphies characterizing Didelphimorphia (Voss and Jansa, 2009), confidently distinguishing stem didelphimorphians from other dentally plesiomorphic marsupialiforms is likely to be difficult in the absence of well-preserved cranial specimens. Indeed, it seems likely that stem didelphimorphians are represented but remain unidentified among the rich dental record of Palaeogene marsupialiforms from South America (Goin et al., 2016). Postcranial material may prove useful in future attempts to identify stem didelphimorphians, because putative synapomorphies have been identified in the tarsus (Szalay, 1982a; 1994; Szalay and Sargis, 2001; Flores, 2009).

†Yalkaparidontia Archer et al., 1988

CONTENTS: †*Yalkaparidon.*

STEM AGE: 39.9 Mya (95% HPD: 30.7–49.7 Mya).

CROWN AGE: Not applicable.

UNAMBIGUOUS CRANIODENTAL AUTAPOMORPHIES: Postglenoid process greatly reduced or absent (char. 75: 0→1; ci = 0.200); mandible usually with one mental foramen (char. 98: 1→0; ci = 0.063); second and third upper incisors entirely lacking enamel (char. 105: 0→1; ci = 1.000); first upper premolar absent (char. 114: 0→1; ci = 0.200); protocone absent (char. 141: 0→1; ci = 1.000); talonid greatly reduced or absent (char. 166: 0→1; ci = 0.500).

COMMENTS: The peculiar †*Yalkaparidon* is known only from two described species (†*Y. coheni* and †*Y. jonesi*) from late Oligocene to middle Miocene sites at Riversleigh World Heritage Area in northern Australia (Archer et al., 1988; Beck et al., 2014). †*Yalkaparidon coheni* is by far the better known of the two species, being represented by partial cranial material, whereas †*Y. jonesi* is known only from a fragmentary right mandible (Archer et al., 1988;

Beck et al., 2014). †*Yalkaparidon* combines some relatively plesiomorphic features of the skull (particularly of the basicranium) with a highly derived dentition that includes an enlarged "gliriform" anteriormost lower incisor and zalambdodont molars (Archer et al., 1988; Beck, 2009; Beck et al., 2014). Of the other unambiguous craniodental apomorphies identified here, extreme reduction of the postglenoid process likely reflects extensive anteroposterior movement of the lower jaw (a trait also seen, for example, in members of the placental clade Glires; Cope, 1888; Druzinsky, 2015), whereas absence of enamel from I2 and I3 is an autapomorphy that we have not seen in any other metatherian.

Based on its unusual combination of features, we agree with Archer et al. (1988) and Beck et al. (2014) that †*Yalkaparidon* warrants classification within its own family and order. †*Yalkaparidon* is the only definitive member of this order currently known, although the enigmatic †*Yingabalanara richardsoni* (known from two lower molars from the early Miocene of Riversleigh; Archer et al., 1990) may be a dentally plesiomorphic yalkaparidontian (see Beck et al., 2014: 155).

Our undated (fig. 32) and dated (fig. 33) total-evidence analyses both recover a clade that unites †*Yalkaparidon* with paucituberculatans. However, isolated tarsals tentatively referred to †*Yalkaparidon* by Beck et al. (2014) show greater derived similarities to australidelphians than to paucituberculatans and Beck et al.'s (2014) accompanying phylogenetic analyses also supported australidelphian affinities for this taxon (see also Beck et al., 2016). Nevertheless, the subsequent phylogenetic analyses of Beck (2017a) and Zimicz and Goin (2020), which included †*Yalkaparidon* and used character scores from these referred tarsals also placed this taxon in a clade with paucituberculatans (including argyrolagids, a fossil group not included in our study; but see Abello and Candela, 2019). Although this clade is worthy of further investigation, we suspect that placement

of †*Yalkaparidon* with paucituberculatans largely reflects convergent acquisitions of a gliriform lower incisor. Current evidence (including the analyses presented here) indicates that diprotodontians evolved a similar lower incisor independently of paucituberculatans, so it is plausible that †*Yalkaparidon* represents a third origin of this tooth type. Based on our results and those of other recent studies (Beck et al., 2014, 2016; Beck, 2017a; Abello and Candela, 2019; Zimicz and Goin, 2020), we consider the higher-level affinities of †*Yalkaparidon* to be uncertain, beyond its being a member of Marsupialia.

Paucituberculata Ameghino, 1894

CONTENTS: Caenolestidae, †*Evolestes*, †Palaeothentidae, †*Pichipilus*, and †*Stilotherium.*

STEM AGE: 39.9 Mya (95% HPD: 30.7–49.7 Mya).

CROWN AGE: 35.0 Mya (95% HPD: 28.2–44.2 Mya).

UNAMBIGUOUS CRANIODENTAL SYNAPOMORPHIES: None (but see Comments, below).

COMMENTS: †*Evolestes* was not recovered as a member of Paucituberculata in our craniodental analyses (figs. 30, 31) nor in our undated total-evidence analysis (fig. 32), probably due to the relative incompleteness of relevant fossil material (Goin et al., 2007b, 2010): indeed, †*Evolestes* is the least complete of all our terminals, scoreable for only 53 out of the 180 characters (rendering it 29.4% complete; table 4). However, the original descriptions of †*Evolestes* specimens by Goin et al. (2007b, 2010) and in subsequent studies that have examined the phylogenetic relationships of Paucituberculata (Abello, 2013; Forasiepi et al., 2013; Rincón et al., 2015; Engelman et al., 2016; Abello et al., 2020, 2021) collectively present compelling evidence that †*Evolestes* is indeed a paucituberculatan, albeit a dentally plesiomorphic one. For this reason and to enable us to calibrate the age of the Paucituberculata node, we constrained monophyly of Paucituberculata including †*Evolestes* for our dated total-evidence analysis (fig. 33).

However, no craniodental features optimize as an unambiguous synapomorphy for this constrained clade in our dated total-evidence analysis. This is probably due to the incompleteness of †*Evolestes* already mentioned above and to the fact that the immediate sister taxon of Paucituberculata in this analysis is †*Yalkaparidon.* The latter result has two unfortunate consequences: first, some features that might otherwise optimize as paucituberculatan synapomorphies (e.g., a gliriform anteriormost lower incisor) are instead optimized as synapomorphies of Paucituberculata + †*Yalkaparidon* (see file S3 in the online supplement); and second, other traits optimize ambiguously because they are inapplicable in †*Yalkaparidon.* Neverthless, three traits that optimize as paucituberculatan synapomorphies under Accelerated Transformation—subadult fusion of median parietal suture (char. 25: $0 \to 1$; $ci = 0.143$), presence of a large retrodental canal (char. 100: $0 \to 1$; $ci = 1.000$), and m1 paracristid unnotched (char. 160; $ci = 0.125$)—represent distinctive features that are undoubtedly absent in †*Yalkaparidon.* A further three traits that optimize as paucituberculatan synapomorphies under Delayed Transformation—centrocrista discontinuous, with postparacrista and premetacrista terminating in stylar region (char. 140: $2 \to 5$; $ci = 0.333$), upper molar posterolingual cusp formed by metaconule (char. 143: $0 \to 1$; $ci = 0.400$), and paracristids of m2 and m3 deflected posterolingually by hypoconulid of preceding tooth (char. 162: $1 \to 0$; $ci = 1.000$)—are inapplicable in †*Yalkaparidon.*

The relationships within Paucituberculata supported in our dated total-evidence analysis show some differences from those of published phylogenetic analyses of paucituberculatans (Goin et al., 2007b; 2009a; Abello, 2013; Forasiepi et al., 2013; Rincón et al., 2015; Engelman et al., 2016; Abello et al., 2020, 2021). Most notably, †*Pichipilus* (currently classified as a pichipilid palaeothentoid) does not form a clade with the palaeothentids †*Acdestis* and †*Palaeothentes* as found in other studies, but instead is

placed closer to living caenolestids than is the caenolestid †*Stilotherium*. This may be due to the shared presence of an anteorbital vacuity in †*Pichipilus* and extant caenolestids, whereas this structure is definitively absent in †*Acdestis* and †*Palaeothentes* and the condition in †*Stilotherium* is unknown (see char. 4). More generally, these discrepancies could be related to our decision to only include paucituberculatans known from relatively complete craniodental material, and because we did not include many paucituberculatan-specific morphological characters (particularly dental characters) that could not be scored consistently across our broader taxonomic sampling.

Although not included in our analyses, the oldest paucituberculatan described to date is probably †*Bardalestes hunco* from the middle Eocene La Barda locality of Argentina (Goin et al., 2009a). †*Riolestes draco*, from the slightly older (Woodburne et al., 2014a) Itaboraí Local Fauna of Brazil, may be based on a deciduous lower premolar (Goin et al., 2009a; R.M.D.B., personal obs.), and is not unequivocally paucituberculatan. Our estimate for the age of the divergence between †*Evolestes* and our other paucituberculatatan terminals spans a broad range when the 95% HPD is taken into account, from the middle Eocene to the middle Oligocene. However, this is still younger than the ~48 Mya estimate for this split presented by Abello et al. (2020: fig. 2), which was based on *a posteriori* timescaling of a strict consensus of most-parsimonious trees rather than a phylogenetic analysis with a clock model.

†Palaeothentidae (Sinclair, 1906)

Contents: †*Acdestis* and †*Palaeothentes*.
Stem Age: 27.4 Mya (95% HPD: 21.3–34.7 Mya).
Crown Age: 19.8 Mya (95% HPD: 15.3–25.8 Mya).
Unambiguous Craniodental Synapomorphies: Cristid obliqua of m1 contacts metaconid (char. 169: 1→0; ci = 0.250).

Comments: †*Acdestis* and †*Palaeothentes* have been included in our analysis as the two palaeothentids currently best represented by craniodental material (Sinclair, 1906; Marshall, 1980; Goin et al., 2003; Abello, 2007; Forasiepi et al., 2014b; Engelman and Croft, 2016). Monophyly of Palaeothentidae has been consistently supported in published phylogenetic analyses (Goin et al., 2007b, 2009a; Abello, 2013; Forasiepi et al., 2013; Rincón et al., 2015; Engelman et al., 2016; Abello et al., 2020, 2021), but our late Oligocene-early Miocene estimate for the divergence between †*Acdestis* and †*Palaeothentes* is considerably younger than the ~31 Mya estimate for this event in the *a posteriori* time-scaled phylogeny of Abello et al. (2020: fig. 2).

Caenolestidae Trouessart, 1898

Contents: *Caenolestes* (fig. 35), *Lestoros*, and *Rhyncholestes*.
Stem Age: 19.0 Mya (95% HPD: 14.0–23.9 Mya).
Crown Age: 10.0 Mya (95% HPD: 6.6–13.2 Mya).
Unambiguous Craniodental Synapomorphies: None (but see Comments, below).

Comments: As noted above (see Paucituberculata), our dated total-evidence analysis (fig. 33) recovers relationships within Paucituberculata that differ somewhat from other recent studies (Goin et al., 2007b, 2009a; Abello, 2013; Forasiepi et al., 2013; Rincón et al., 2015; Engelman et al., 2016; Abello et al., 2020, 2021), specifically in placing the pichipilid palaeothentoid †*Pichipilus* closer to the extant caenolestid genera *Caenolestes*, *Lestoros*, and *Rhyncholestes* than the fossil caenolestid †*Stilotherium*. Thus, monophyly of Caenolestidae including †*Stilotherium* is not supported here, contra these other studies. However, *Caenolestes*, *Lestoros*, and *Rhyncholestes* form a clade to the exclusion of our fossil terminals in our dated total-evidence analysis, which is congruent with current published evidence. This clade is not supported by any unambiguous synapomorphies, but three traits optimize as synapomorphies under Delayed Transformation:
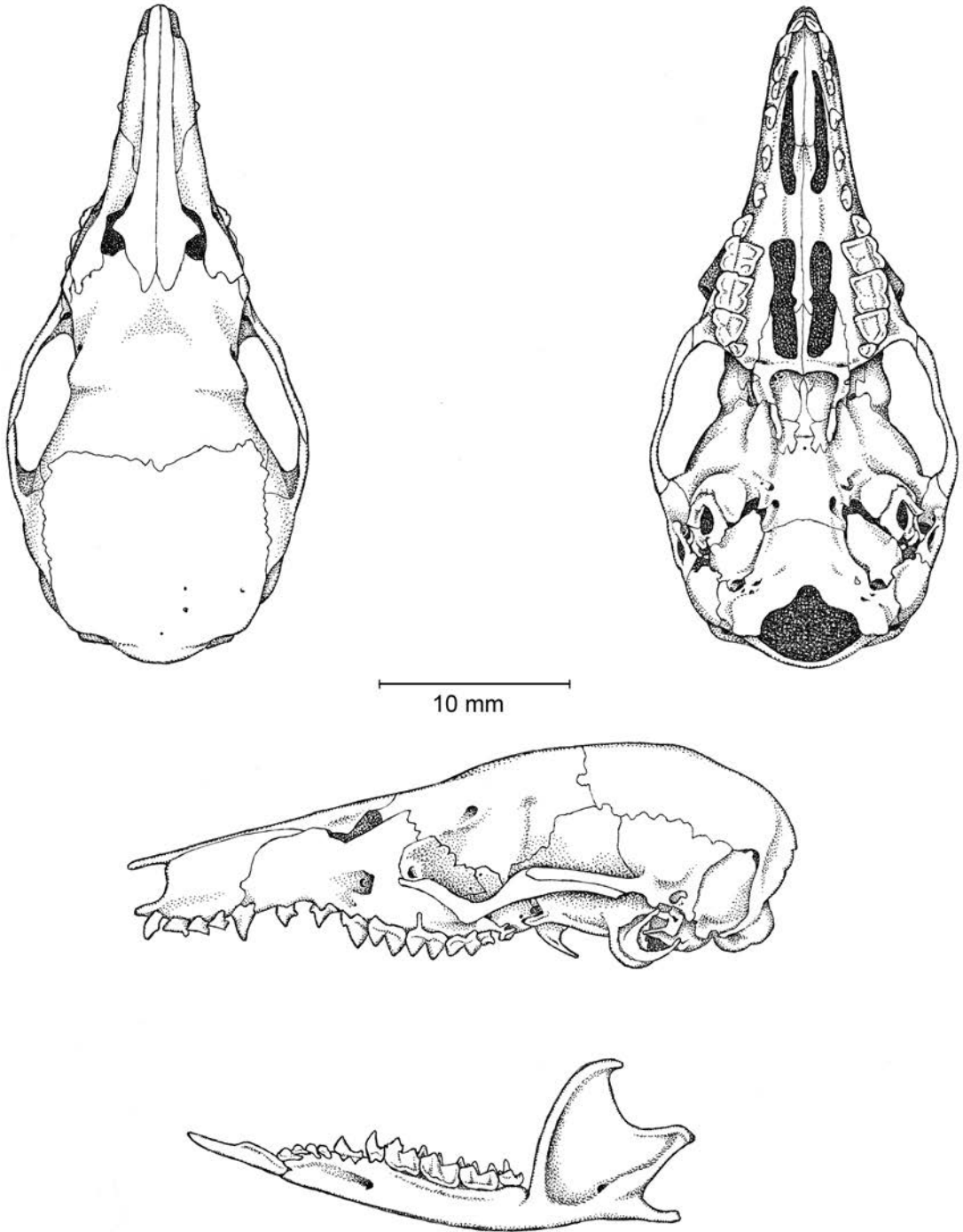
FIG. 35. *Caenolestes fuliginosus* (Paucituberculata, Caenolestidae; based on UMMZ 155581, an adult female from Provincia Napo, Ecuador).

stapes columelliform and microperforate or imperforate (char. 65: 0→1; ci = 0.143; see Gaillard et al., 2021); mastoid fenestra present dorsal and medial to the mastoid exposure of petrosal (char. 91: 0→1; ci = 0.200); and fourth lower molar (m4) trigonid structurally simplified, with only the metaconid distinct (char. 164: 0→1; ci = 0.667).

The three extant caenolestid genera are estimated here as having diverged from each other relatively recently, during the mid to late Miocene, which is somewhat younger than the estimate for this split in the a posteriori time-scaled phylogeny of Abello et al. (2020: fig. 2; ~14 Mya) and the molecular-clock estimate of Mitchell et al. (2014) for the split between *Caenolestes* and *Rhyncholestes* (point estimate: 14.3 Mya; 95% HPD: 12.2–16.0 Mya), but similar to the molecular-clock estimates of Meredith et al. (2009a; 2011). Besides a report of subfossil remains of *Caenolestes fuliginosus*, there is as yet no fossil record of crown-clade Caenolestidae (Abello et al., 2021).

Australidelphia Szalay, 1982

CONTENTS: Dasyuromorphia, Diprotodontia, Microbiotheria, Notoryctemorphia, and Peramelemorphia.

STEM AGE: 55.1 Mya (95% HPD: 54.6–56.6 Mya).

CROWN AGE: 48.0 Mya (95% HPD: 44.3–50.9 Mya).

UNAMBIGUOUS CRANIODENTAL SYNAPOMORPHIES: None.

COMMENTS: Recent phylogenetic analyses based on molecular data (e.g., Phillips et al., 2001; Amrine-Madsen et al., 2003b; Nilsson et al., 2004; Phillips et al., 2006; Beck, 2008a; Meredith et al., 2008b, 2009c, 2011; Nilsson et al., 2010; Mitchell et al., 2014; Gallus et al., 2015a; Duchêne et al., 2018; Álvarez-Carretero et al., 2021) and others based on total-evidence datasets (e.g., Asher et al., 2004; Beck et al., 2008a, 2014, 2016; Horovitz et al., 2009; Beck, 2012; Maga and Beck, 2017) have consistently recovered monophyly of Australidelphia, and australidelphian monophyly has also been found in

most (e.g., Horovitz and Sánchez-Villagra, 2003; Sánchez-Villagra et al., 2007; Horovitz et al., 2008, 2009; Lorente et al., 2016; Carneiro and Oliveira, 2017a; Carneiro et al., 2018; Carneiro, 2019) but not all (e.g., Ladevèze and Muizon, 2010; Wilson et al., 2016) recent morphological analyses. This overall pattern is confirmed here: our morphological analyses did not recover australidelphian monophyly (figs. 30, 31), whereas it was strongly supported in all our molecular (figs. 27–29) and total evidence (figs. 32, 33) analyses. Given that Szalay (1982a) first proposed monophyly of Australidelphia based primarily on shared derived features of the tarsus (specifically the presence of a continuous lower ankle joint, and a tripartite calcaneocuboid facet; see also Szalay, 1994; Beck, 2012), the addition of postcranial characters to our craniodental matrix may ultimately result in morphological support for Australidelphia (as in Horovitz and Sánchez-Villagra, 2003).

No craniodental feature optimizes as an unambiguous synapomorphy of Australidelphia in our dated total-evidence analysis, but three optimize as synapomorphies under Accelerated Transformation—extracranial course of mandibular nerve fully enclosed by medial outgrowths of the auditory bulla (char. 52: 0→1; ci = 0.231); posterior limb of ectotympanic in contact with, but suturally distinct from, pars canalicularis of the petrosal and/or posttympanic process of the squamosal (char. 60: 0→1; ci = 0.333); and prootic canal foramen on tympanic face of petrosal absent (char. 69: 0→1; ci = 0.083)—but all three traits show high levels of homoplasy and undergo subsequent reversals within Australidelphia (see file S3 in the online supplement). Our failure to identify compelling craniodental synapomorphies for Australidelphia likely reflects the fact that the ancestral australidelphian probably had a relatively generalized cranium and dentition that was little different from the plesiomorphic marsupial condition (see Szalay, 1994: 346) and that different lineages within Australidelphia subsequently evolved very disparate apomorphies of

the dentition, cranium, or both (see also comments by Archer, 1984c: 782).

Our estimate for the first split within Australidelphia is in the early to middle Eocene. This is younger than the early or middle Paleocene †*Khasia cordillerensis*, a taxon that was originally described as a microbiotherian (Marshall and Muizon, 1988; see also Muizon, 1991; Goin et al., 2006; Muizon et al., 2018; Muizon and Ladevèze, 2020) and hence a crown-clade australidelphian. However, as noted above, several subsequent authors have argued that †*Khasia* is more likely a "pediomyoid" (Oliveira and Goin, 2006; Goin et al., 2016), a hypothesis supported by the morphological phylogenetic analysis of Carneiro et al. (2018). †*Khasia* has not been included here because it is represented only by dental specimens (Marshall and Muizon, 1988; Muizon, 1991).

If †*Khasia* is discounted, the oldest known australidelphian is probably †*Djarthia murgonensis* from the Tingamarra fossil site in eastern Australia, which has been radiometrically dated as earliest Eocene (~54.6 Mya; (Godthelp et al., 1992; Godthelp et al., 1999; Beck et al., 2008a). We have not included †*Djarthia* here due to its incompleteness (the only craniodental remains are incomplete dental specimens and isolated petrosals; Godthelp et al., 1999; Beck et al., 2008a), but isolated tarsals referred to this taxon exhibit characteristic australidelphian synapomorphies (Beck et al., 2008a). However, †*Djarthia* falls outside crown-clade Australidelphia in most published analyses (with the notable exception of Maga and Beck, 2017: fig. 38, in which it is sister to Dasyuromorphia), and its position is unresolved with respect to the crown clade in others (Beck et al., 2008a, 2014, 2016; Beck, 2012; Lorente et al., 2016; Maga and Beck, 2017).

The next-oldest definitive australidelphian remains are isolated tarsals from the La Barda locality in Argentina, which has been radiometrically dated as middle Eocene (between ~48 and 43 Mya; Tejedor et al., 2009; Lorente et al., 2016). The La Barda australidelphian tarsals fell within Diprotodontia (members of which are otherwise known only from Australia, New Guinea, and adjacent islands) in the phylogenetic analysis of Lorente et al. (2016), but we consider that this biogeographically anomalous relationship warrants further testing.

The woodburnodontid microbiotherian †*Woodburnodon casei* from the Cucullaea I Allomember of the La Meseta Formation on Seymour Island, off the Antarctic Penninsula, is a more compelling candidate for the oldest definitive crown-clade australidelphian because it preserves distinctive dental features that are characteristic of microbiotherians (Goin et al., 2007c), and it has been recovered within Microbiotheria in several phylogenetic analyses (Carneiro and Oliveira, 2017b; Carneiro et al., 2018; Carneiro, 2019). The age of the Cucullaea I Allomember has proved controversial (Crame et al., 2014; Kemp et al., 2014; Gelfo et al., 2017, 2019; Goin et al., 2020), but it now appears to be about 40 Mya (Douglas et al., 2014; Amenábar et al., 2019; Mörs et al., 2020). This postdates our estimate for the first divergence within Australidelphia (see above) and also for the split between Microbiotheria and Diprotodontia (median = 45.6 Mya; 95% HPD: 41.4–48.8 Mya).

Older putative microbiotherians have been reported from the early Eocene (probably 51.4–56.0 Mya; Clyde et al., 2014; Woodburne et al., 2014a, 2014b; Krause et al., 2017) Las Flores Local Fauna of southern Argentina (Goin, 2003; Zimicz, 2012; Woodburne et al., 2014a; Goin et al., 2016), which is incongruent with our estimate for the time of the Microbiotheria-Diprotodontia split, but these potentially important fossils have yet to be described.

Agreodontia Beck et al., 2014

CONTENTS: Dasyuromorphia, Notoryctemorphia, and Peramelemorphia.

STEM AGE: 48.0 Mya (95% HPD: 44.3–50.9 Mya).

CROWN AGE: 45.7 Mya (95% HPD: 42.3–49.2 Mya).

Unambiguous Craniodental Synapomorphies: Median parietal suture at least partially fused in subadults (char. 25: 0→1; ci = 0.143).

Comments: Beck et al. (2014) gave the name Agreodontia to a clade comprising the Australian orders Dasyuromorphia, Peramelemorphia, and Notoryctemorphia, which they defined as the most inclusive clade including *Perameles nasuta*, *Notoryctes typhlops*, and *Dasyurus maculatus*, but excluding *Phalanger orientalis* (Beck et al., 2014: 132). Monophyly of Agreodontia has been consistently supported by analyses of nuclear and combined nuclear and mitochondrial sequence data (e.g., Amrine-Madsen et al., 2003b; Phillips et al., 2006; Beck, 2008a; Meredith et al., 2008b, 2009c, 2011; Mitchell et al., 2014; Duchêne et al., 2018; Álvarez-Carretero et al., 2021), but it is supported only by mitochondrial sequence data when base composition is corrected for (Nilsson et al., 2004; Phillips et al., 2006). A single, uncontradicted retrotransposon insertion also supports agreodontian monophyly, but this does not represent statistically significant support (Nilsson et al., 2010; Gallus et al., 2015a). Recent morphological analyses vary as to whether they recover Agreodontia or not (e.g., Horovitz and Sánchez-Villagra, 2003; Beck et al., 2008a, 2014; Horovitz et al., 2008, 2009; Carneiro and Oliveira, 2017a; Carneiro et al., 2018; Carneiro, 2019), but this clade has been recovered by most total-evidence analyses (Beck et al., 2008a, 2014, 2016; Beck, 2012, 2017a; Maga and Beck, 2017) with the exception of that of Asher et al. (2004).

Our results conform to this general pattern of inconsistent support: whereas our nuclear (fig. 27), combined nuclear and mitochondrial (fig. 29), and total evidence (figs. 32, 33) analyses support monophyly of Agreodontia, our mitochondrial (fig. 28) and morphological (figs. 30, 31) analyses do not. Only partial fusion of the median parietal suture before adulthood optimizes as an unambiguous craniodental synapomorphy of this clade in our dated total-evidence analysis, but this transformation is reversed within Dasyuromorphia.

Putative peramelemorphians have been reported from the earliest Eocene Tingamarra Local Fauna (Godthelp et al., 1992; Archer et al., 1993a; Muirhead, 1994; Archer et al., 1999; Long et al., 2002). Given the published early Eocene (54.6 Mya) radiometric date for Tingamarra (Godthelp et al., 1992), this material would represent the oldest known record of the Agreodontian crown clade and would markedly predate our estimate for the most recent common ancestor of Agreodontia (45.7 Mya; 95% HPD: 42.3–49.2 Mya). However, examination of these Tingamarran specimens by R.M.D.B. revealed some similarities to bunodont, nonperamelemorphian metatherians from the Palaeogene of South America and Australia (e.g., *Chulpasia*, *Rosendolops*; see Archer et al., 1993a; Crochet and Sigé, 1993; Goin and Candela, 1996; Sigé et al., 2009), so we are not convinced that they represent peramelemorphians.

A major gap in the Australian fossil record after the early Eocene (Archer et al., 1999; Long et al., 2002; Woodhead et al., 2014) means that the oldest definitive agreodontians are from the late Oligocene, which is much younger than our estimate for the age of the most recent common ancestor of Agreodontia. Specifically, representatives of Peramelemorphia and Dasyuromorphia are known from multiple late Oligocene sites in central Australia and at Riversleigh World Heritage Area (Long et al., 2002; Wroe, 2003; Archer et al., 2006; Archer and Hand, 2006; Warburton and Travouillon, 2016; Kealy and Beck, 2017; Eldridge et al., 2019). A single partial upper molar of an alleged thylacinid (NTM P2815-10; Murray and Megirian, 2006b) and a single upper molar of a probable notoryctemorphian (NTM P2815-6; Murray and Megirian, 2006b; Beck et al., 2014: 151, 2016: 166) are known from the Pwerte Marnte Marnte Local Fauna in the Northern Territory, which is probably slightly older than the central Australian and Riversleigh sites (Megirian et al., 2010), but which is still late Oligocene.

Notoryctemorphia Kirsch 1977

CONTENTS: *Notoryctes* (fig. 36).

STEM AGE: 45.7 Mya (95% HPD: 42.3–49.2 Mya).

CROWN AGE: N/A.

UNAMBIGUOUS CRANIODENTAL AUTAPOMORPHIES: Nasals truncated anterior to lacrimals (char. 3: 0→1; ci = 0.333); entire orbital mosaic fused (char. 12: 0→2; ci = 1.000); foramen rotundum ventral to sphenorbital fissure (char. 17: 0→2; ci = 0.286); median suture between left and right frontals at least partially fused in subadults (char. 24: 0→1; ci = 0.143); frontal and squamosal in contact on lateral aspect of braincase (char. 26: 0→1; ci = 0.071); auditory bulla large, contacting rostral process of petrosal, or very large, extending posteriorly across the petrosal to contact the exoccipital (char. 55: 1→2 or 1→3; ci = 0.300); ectotympanic concealed from lateral view within bulla (char. 57: 0→1; ci = 0.500); anterior limb of ectotympanic attached firmly to postglenoid process of squamosal (char. 59: 1→2; ci = 0.214); anterior process of malleus entirely absent (char. 64: 0→2; ci = 0.500); rostral and caudal tympanic processes of petrosal seamlessly fused, forming a petrosal plate (char. 68: 0→2; ci = 0.154); postgenoid vein emerges from the postglenoid foramen in the posteromedial corner of the glenoid fossa, medial or anteromedial to the postglenoid process (char. 77: 0→1; ci = 0.250); external auditory meatus ventral to postglenoid fossa (char. 78: 1→2; ci = 1.000); facial nerve exits middle ear via a stylomastoid foramen formed by the ectotympanic, posttympanic process of the squamosal, and pars canalicularis of the petrosal (char. 79: 0→4; ci = 0.625); one hypoglossal foramen present (char. 92: 0→1; ci = 0.500); masseteric fossa perforated by a distinct masseteric foramen (char. 99: 0→1; ci = 0.333); first upper premolar (P1) absent (char. 114: 0→1; ci = 0.200); P2 single-rooted and caniniform or vestigial and occlusally featureless (char. 118: 0→4: ci = 0.444); paracone lost entirely, only metacone present (char. 137: 1→2; ci = 0.400); and talonid greatly reduced or absent (char. 166: 0→1; ci = 0.500).

COMMENTS: *Notoryctes* (the only living representative of the family Notoryctidae and order Nortoryctemorphia) is one of the morphologically most specialized known marsupials. This is reflected in our long list of unambiguous craniodental autapomorphies, which include a number of highly unusual or unique features within Marsupialia, among them: fusion of the entire orbital mosaic, the foramen rotundum positioned ventral (rather than lateral) to the sphenorbital fissure, concealment of the ectotympanic in lateral view by the auditory bulla (convergent with microbiotheriids), complete absence of the anterior process of the malleus, position of the external auditory meatus ventral (rather than posterior) to the glenoid fossa, presence of only a single hypoglossal foramen (convergent with *Tarsipes*), total loss of the paracone, and extreme reduction of the talonid (convergent with †*Yalkaparidon*; Archer et al., 1988, 2011; Asher and Sánchez-Villagra, 2005; Beck et al., 2014).

Our estimated time for the divergence of Notoryctemorphia from other agreodontians dates to the early or middle Eocene, corresponding to a major gap in the fossil record of Australian mammals. †*Naraboryctes philcreaseri* from early Miocene sites at Riversleigh World Heritage Area (Archer et al., 2011; Beck et al., 2016) and a single upper molar of a probable notoryctemorphian from the late Oligocene Pwerte Marnte Marnte Local Fauna in the Northern Territory (NTM P2815-6; Murray and Megirian, 2006b; Beck et al., 2014: 151, 2016: 166) are the only known fossil members of the order. They have not been included in this study due to their incompleteness, but both are dentally markedly more plesiomorphic than *Notoryctes*; most notably, their molars are not fully zalambdodont, as both retain a distinct paracone on their upper molars, and †*Naraboryctes* has an unreduced talonid basin on its lower molars (Murray and Megirian, 2006b; Archer et al., 2011; Beck et al., 2016). Inevitably, our long list of notoryctemorphian synapomorphies will be whittled down as plesiomorphic fossil taxa are added to future analyses, with the probable result that some of these traits may prove to be autapomorphies of *Notoryctes*.

10 mm
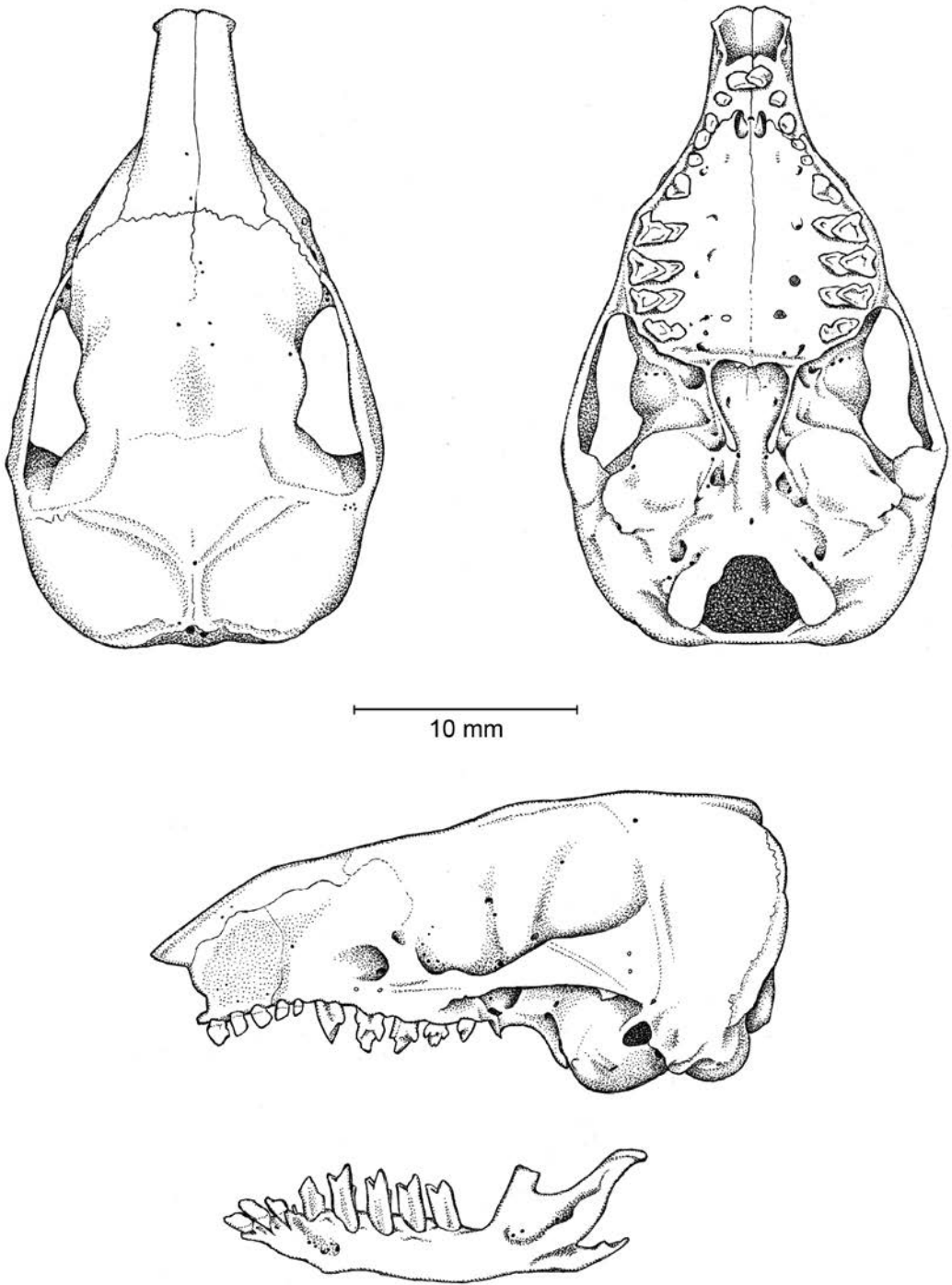
FIG. 36. *Notoryctes typhlops* (Notoryctemorphia, Notoryctidae; based on AMNH 198651, an adult of unknown sex from South Australia).

Peramelemorphia Ameghino, 1889

CONTENTS: †*Bulungu*, †*Galadi*, Perameloidea, and †*Yarala*.

STEM AGE: 43.7 Mya (95% HPD: 39.6–47.4 Mya).

CROWN AGE: 31.4 Mya (95% HPD: 25.3–37.9 Mya).

UNAMBIGUOUS CRANIODENTAL SYNAPOMORPHIES: Facial exposure of jugal deeply bifid, with distinct anterodorsal and anteroventral processes (char. 20: 0→1; $ci = 1.000$); lambdoid sesamoids present (char. 89: 0→1; $ci = 1.000$); M1 preparacrista absent or indistinct (char. 138: 0→1; $ci = 0.333$); M1 pseudopreparacrista present (char. 139: 0→1; $ci = 0.333$); and hypoconulid notch in anterior cingulid of m2–4 absent (char. 158: 0→1; $ci = 0.500$).

COMMENTS: Our estimate for the divergence between Peramelemorphia and Dasyuromorphia dates to the middle Eocene. As mentioned above (see Agreodontia), isolated dental remains from the early Eocene Tingamarra Local Fauna have been identified as putatively peramelemorphian, which would predate our estimate, but the Tingamarran specimens cannot be unequivocally referred to the Peramelemorphia. Instead, the oldest definitive peramelemorphians are late Oligocene (Travouillon et al., 2013a, 2021; Warburton and Travouillon, 2016). The three fossils included here (†*Bulungu*, †*Galadi*, †*Yarala*) are late Oligocene to Miocene taxa (Muirhead and Filan, 1995; Muirhead, 2000; Travouillon et al., 2010, 2013b; Gurovich et al., 2014; Warburton and Travouillon, 2016) and they are recovered outside the peramelemorphian crown clade (Perameloidea; see below) in our analyses, as in previous phylogenetic studies (Travouillon et al., 2010, 2013a, 2013b, 2014a, 2015b, 2019, 2021; Gurovich et al., 2014; Chamberlain et al., 2015; Travouillon and Phillips, 2018). Putative early perameloids are known from the middle Miocene (Travouillon et al., 2014a; see Perameloidea below), but these were not included here because they are only known from isolated teeth.

A recent study by Abello and Candela (2019) included morphological and total evi-
dence phylogenetic analyses that placed members of the South American family †Argyrolagidae in a clade that was sister to Peramelemorphia (represented by *Echymipera* and *Perameles*), but the authors acknowledged that this geographically implausible relationship might reflect convergent evolution of similar derived tarsal features; based on available evidence, argyrolagids are most likely to be paucituberculatans (Sánchez-Villagra, 2001; Beck, 2017a; Zimicz and Goin, 2020) or polydolopimorphians (Goin et al., 2009a; Chornogubsky and Goin, 2015; Carneiro and Oliveira, 2017a, 2017b; Carneiro, 2018, 2019; Carneiro et al., 2018).

Perameloidea Gray, 1825

CONTENTS: Chaeropodidae, Peramelidae, and Thylacomyidae.

STEM AGE: 26.1 Mya (95% HPD: 20.7–31.8 Mya).

CROWN AGE: 20.0 Mya (95% HPD: 15.3–24.5 Mya).

UNAMBIGUOUS CRANIODENTAL SYNAPOMORPHIES: Nasals truncated anterior to lacrimals (char. 3: 0→1; $ci = 0.333$); lacrimal exposure on orbital rim forming a distinct crest (char. 8: 0→2; $ci = 0.118$); frontal and squamosal in contact on lateral aspect of braincase (char. 26: 0→1; $ci = 0.071$); palatine fenestrae present (char. 38: 0→1; $ci = 0.071$); posterior epitympanic sinus of squamosal present, enclosed laterally (char. 84: 0→1; $ci = 0.071$); and entocristid indistinct or absent (char. 176: 0→1; $ci = 0.077$).

COMMENTS: We follow Van Dyck and Strahan's (2008) use of Perameloidea to refer only to the peramelemorphian crown clade, as did Kear et al. (2016). By contrast, other recent studies (e.g., Chamberlain et al., 2015; Warburton and Travouillon, 2016) have used Perameloidea to refer to the crown clade plus all taxa more closely related to it than to the fossil genus †*Yarala*, which has been placed in the family †Yaralidae and superfamily †Yaraloidea (Muirhead, 2000; Warburton and Travouillon, 2016).

Within Parameloidea, all our molecular (figs. 27–29) and total-evidence (figs. 32, 33) analyses support Peramelidae and *Macrotis* (Thylacomyidae) as sister taxa, with *Chaeropus* (Chaeropodidae) the first perameloid family to diverge. This topology is congruent with most other recent molecular and total-evidence phylogenetic analyses (Meredith et al., 2008a; Westerman et al., 2012; Kear et al., 2016; Travouillon and Phillips, 2018). However, the dated total-evidence analysis of Travouillon and Phillips (2018: figs. 1E, 2) placed *Chaeropus* sister to *Macrotis*, the dated total-evidence analyses of Travouillon et al. (2021) placed Thylacomyidae outside *Chaeropus* + Peramelidae,[31] and the molecular phylogenetic analyses of Travouillon et al. (2019) placed *Chaeropus* either sister to *Isoodon* + *Perameles* + *Peroryctes* (in an undated maximum likelihood analysis; Travouillon et al., 2019: fig. 15) or sister to *Isoodon* (in a Bayesian node-dating analysis; Travouillon et al., 2019: fig. 16).

We identified a number of unambiguous cranidodental synapomorphies as characterizing Perameloidea, although most of these are homoplastic. Perhaps the most notable of these is truncation of the nasals anterior to the lacrimals, a trait that is present in all known perameloids (and arose homoplastically in *Notoryctes* and *Potorous*) but that is absent in nonperameloid peramelemorphians, all of which are "short-snouted" (Travouillon et al., 2010, 2013b, 2015b; Gurovich et al., 2014; Chamberlain et al., 2015).

The oldest putative perameloid is †*Bulbadon warburtonae* from the late Oligocene Ditjimanka Local Fauna (Faunal Zone B) of the Etadunna Formation, which is known from a single partial mandible, and has been tentatively identified as a thylacomyid (Travouillon et al., 2021). A best-fit age-model of paleomagnetic data indicates that the Etadunna Formation spans

23.6–26.1 Mya (Metzger and Retallack, 2010), so, if †*Bulbadon* is a thylacomyid, then it predates our estimate for the crown age of Perameloidea. However, †*Bulbadon* did not form a clade with other thylacomyids in the dated total-evidence analyses of Travouillon et al. (2021) and a lack of resolution meant that a position for †*Bulbadon* outside Perameloidea could not be ruled out in their analyses. Two taxa from the middle Miocene of Riversleigh World Heritage Area, both known only from isolated teeth, may also be early perameloids (Travouillon et al., 2014a): †*Crash bandicoot* (which appears to be a peramelid), and †*Liyamayi dayi* (which was described as a thylacomyid, although its position in published phylogenies is highly labile; Travouillon et al., 2014a, 2015b, 2021; Chamberlain et al., 2015; Kear et al., 2016). If †*Crash* and †*Liyamayi* are indeed early perameloids, then their middle Miocene age is broadly congruent with our middle to early Miocene age estimate for the onset of diversfication of Perameloidea.

Chaeropodidae Gill, 1872

Contents: *Chaeropus* (fig. 37).

Stem Age: 20.0 Mya (95% HPD: 15.3–24.5 Mya).

Crown Age: N/A.

Unambiguous Craniodental Autapomorphies: Accessory palatal fenestrae present (char. 35: 0→1; ci = 0.250); auditory bulla large, contacting rostral tympanic process of petrosal (char. 55: 1→2; ci = 0.300); upper canine with distinct anterior cusp only (char. 112: 0→3; ci = 0.375); paracone and metacone subequal (char. 137: 2→1; ci = 0.400); M1 preparacrista present (char. 138: 1→0; ci = 0.333); second lower premolar (p2) distinctly taller than p3 (char. 156: 1→0; ci = 0.118); cristid obliqua on m1 contacts metaconid (char. 169: 1→0; ci = 0.250); and anterior terminus of cristid obliqua of m2–4 bypasses metacristid to terminate at entoconid or entocristid (char. 170: 0→1; ci = 0.500).

---

[31] Note that, contra here, Travouillon et al. (2021) recognized Peroryctidae as a family distinct from Peramelidae (see also Travouillon and Phillips, 2018).
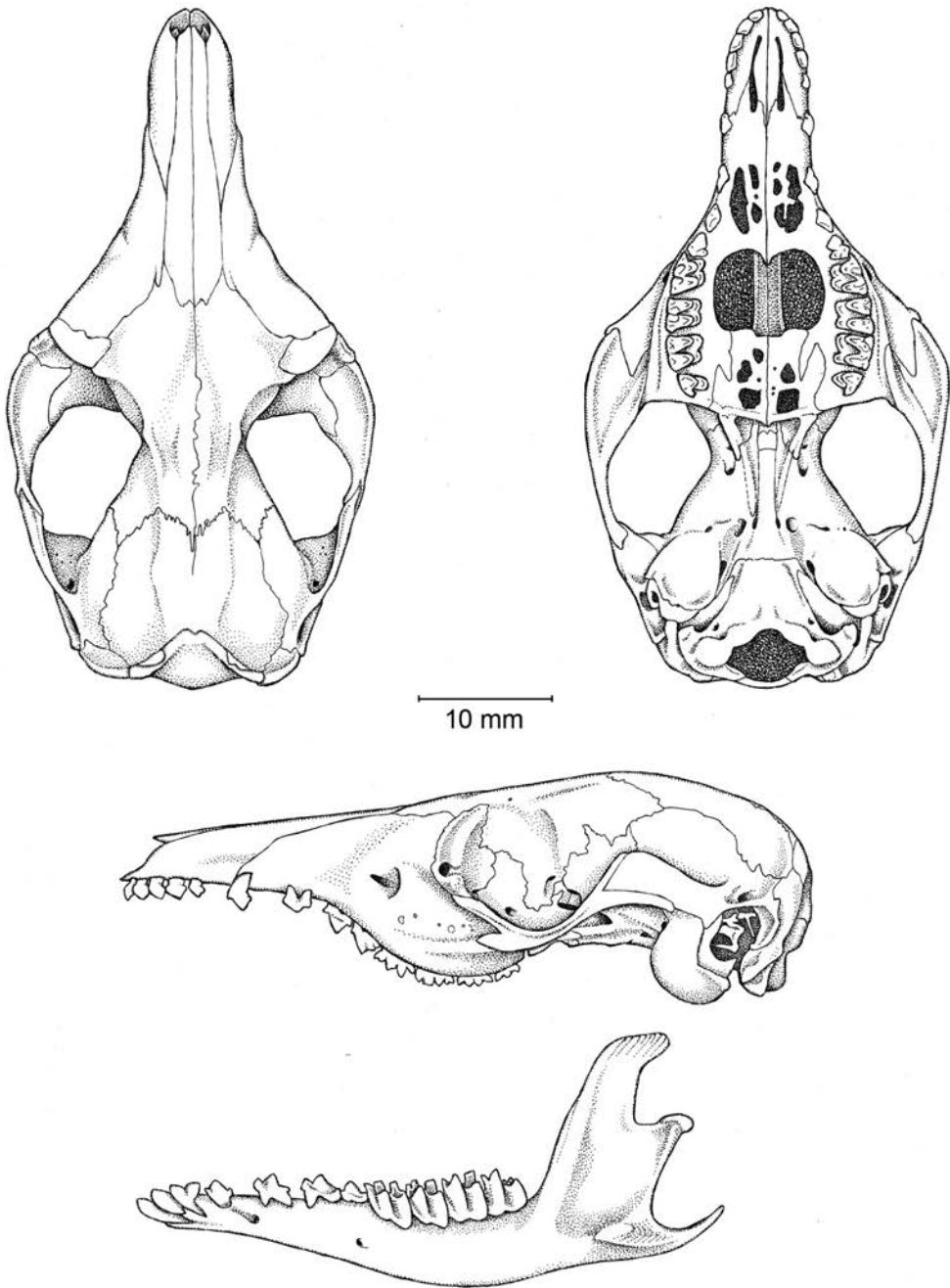
FIG. 37. *Chaeropus* (Peramelemorphia, Chaeropodidae; based primarily on BMNH 1848.1.27.41, an adult female *C. ecaudatus* from New South Wales, but with the morphology of the ear region based on BMNH 1847.8.14.13, an adult *C. ecaudatus* of unknown sex from New South Wales, and the lower dentition based on BMNH 1854.10.24.19, a juvenile *C. yiratji* from northern Australia). Note that the free-standing ventral processes of both pterygoid bones (normally visible in lateral view) had broken away in all the specimens we examined and are not illustrated here.

COMMENTS: *Chaeropus*, the sole known representative of the family Chaeropodidae, is recovered in our molecular (figs. 27–29) and total-evidence (figs. 32, 33) analyses as sister to the remaining perameloids (crown-clade peramelemorphians) as also found in several other recent molecular and total-evidence analyses (Westerman et al., 2012; Kear et al., 2016; Travouillon and Phillips, 2018). However, as already noted (see Perameloidea above), the dated total-evidence analysis of Travouillon and Phillips (2018: figs. 1E, 2) placed *Chaeropus* sister to *Macrotis*, the dated total-evidence analyses of Travouillon et al. (2021) placed *Chaeropus* sister to Peramelidae, and the molecular phylogenetic analyses of Travouillon et al. (2019) placed *Chaeropus* as either sister to *Isoodon* + *Perameles* + *Peroryctes* (in an undated maximum likelihood analysis; Travouillon et al., 2019: fig. 15) or sister to *Isoodon* (in an Bayesian node-dating analysis; Travouillon et al., 2019: fig. 16). The underlying cause(s) of these topological differences warrants further investigation.

Most of the unambiguous cranidodental autapomorphies of Chaeropodidae listed above are homoplastic within Peramelemorphia. However, the paracone and metacone of the upper molars are subequal in height in *Chaeropus* (see Wright et al., 1991: plate 1A), whereas the metacone is distinctly taller in all other known peramelemorphians. The morphology of the m2–4 cristid obliqua is also unusual in *Chaeropus* in that it terminates at the entocristid rather than the metacristid (a morphology also seen in some *Isoodon* specimens). These two dental features may be connected with the predominantly grazing diet of *Chaeropus* by facilitating greater transverse shear (Wright et al., 1991; Travouillon, 2016).

Besides the two Recent species—*Chaeropus ecadautus* and the recently described *C. yirratji* (see Travouillon et al., 2019)—only one other chaeropodid is currently known: *Chaeropus* †*baynesi* from the latest Pliocene or earliest Pleistocene (2.47–2.92 Mya) Fisherman's Cliff Local Fauna in New South Wales (Travouillon, 2016; Travouillon et al., 2017). Thus, Chaeropo-

didae is currently characterized by a lengthy ghost lineage; based on the divergence dates estimated here and in other recent studies (Westerman et al., 2012; Kear et al., 2016; Travouillon and Phillips, 2018), fossil chaeropodids should be expected in fossil Australian deposits from the early-to-middle Miocene onward.

Thylacomyidae Bensley, 1903

CONTENTS: *Macrotis* (fig. 38).

STEM AGE: 16.5 Mya (95% HPD: 12.4–20.6 Mya).

CROWN AGE: N/A.

UNAMBIGUOUS CRANIODENTAL AUTAPOMORPHIES: Two or more discrete lacrimal foramina usually present (char. 10: 1→0; ci = 0.063); at least one lacrimal foramen located within suture between lacrimal and maxilla (char. 11: 0→1; ci = 0.286); pterygoids in midline contact ventral to presphenoid (char. 46: 0→3; ci = 0.111); large, erect paroccipital process directed ventrally (char. 93: 1→2; ci = 0.100); P2 and P3 subequal in height (char. 119: 2→1; ci = 0.118); M1 pseudo-preparacrista absent (char. 139: 1→0; ci = 0.333); upper molar posterolingual cusp is the metacone (char. 143: 1→2; ci = 0.400); lower first molar (m1) paracristid and paraconid both indistinct or absent (char. 159: 0→1; ci = 0.400); neomorphic cuspid(s) in hypoflexid region present (char. 171: 0→1; ci = 0.167); and lower third molar hypoconid lingual to salient protoconid (char. 173: 0→1; ci = 0.045).

COMMENTS: Thylacomyidae, represented here by its sole Recent genus *Macrotis*, is recovered in our molecular (figs. 27–29) and total-evidence (figs. 32, 33) analyses as the next perameloid family to diverge after Chaeropodidae. This topology is also seen in most other recent molecular and total-evidence analyses in which representatives of all extant peramelemorphian families are included (Westerman et al., 2012; Kear et al., 2016; Travouillon and Phillips, 2018: fig. 1B, D; but see Travouillon and Phillips, 2018: figs. 1C, E, 2; Travouillon et al., 2019, 2021).
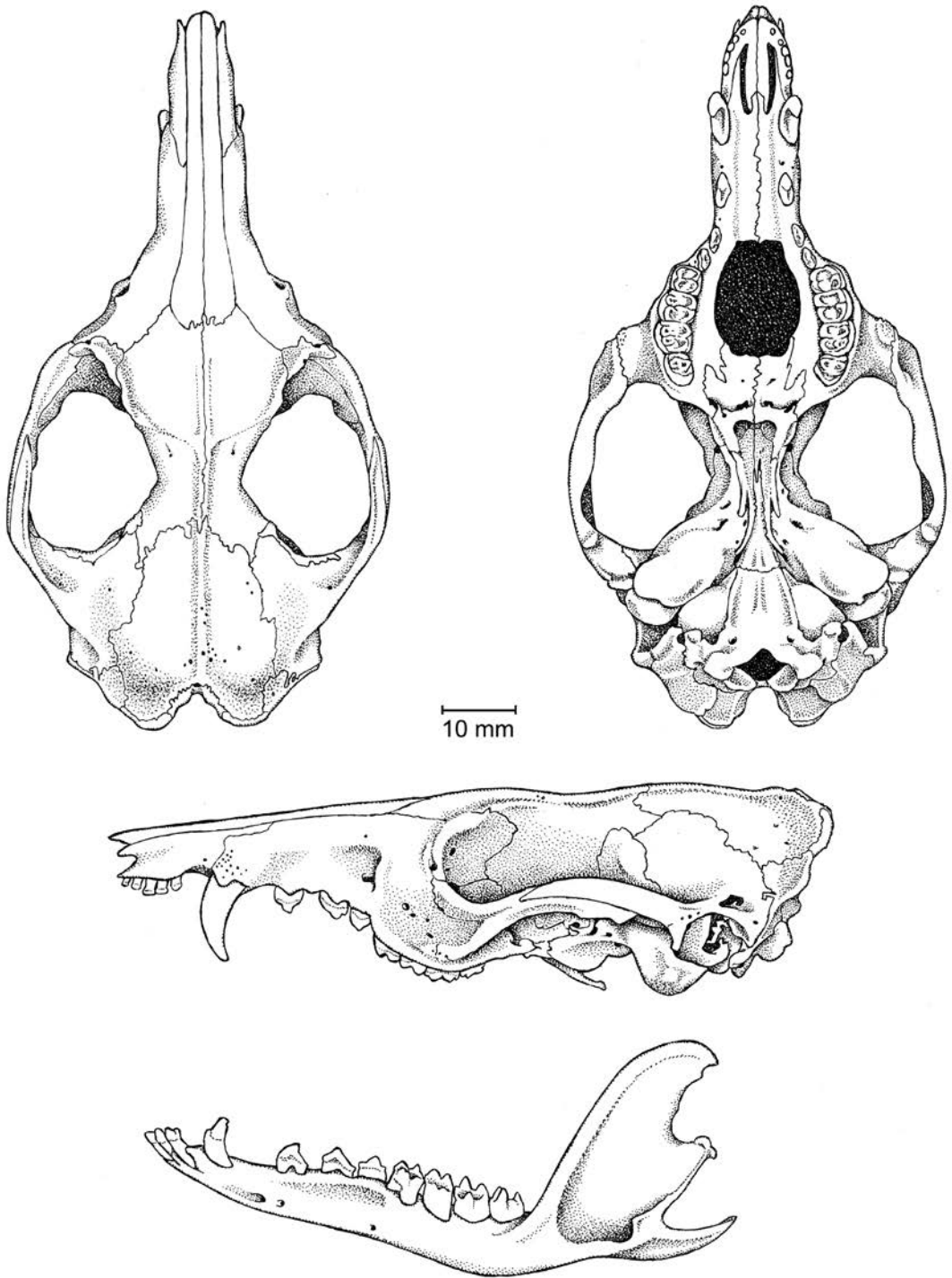
FIG. 38. *Macrotis lagotis* (Peramelemorphia, Thylacomyidae; based on AMNH 35685, an adult male zoo specimen).

Within Peramelemorphia, *Macrotis* is craniodentally distinctive, as demonstrated by the long list of apomorphies identified here; among the most notable of these are the presence of two lacrimal foramina (all other peramelemorphians except some specimens of *Perameles* have a single lacrimal foramen), midline contact between the right and left pterygoids ventral to the presphenoid (also seen in *Isoodon*), the large and erect paroccipital process (also seen in some *Isoodon* specimens), the absence of a pseudopreparacrista on M1 (also seen in some *Isoodon* and *Microperoryctes* specimens), recruitment of the metacone as the posterolingual cusp of the upper molars (rather than, as in all other metatherians with a posterolingual cusp, the metaconule; Bensley, 1903; Archer and Kirsch, 1977), and the absence of a distinct paracristid and paraconid on m1 (as also seen in a few diprotodontians, namely *Burramys*, *Acrobates*, and some specimens of *Distoechurus*).

†*Ischnodon australis* from the Pliocene Tirari Formation at Lake Palankarinna in South Australia, which is known from a single partial right dentary preserving p1–2 and m1–2 (Stirton, 1955; Archer and Kirsch, 1977; Tedford et al., 1992; Travouillon et al., 2017), has been argued to be a thylacomyid, although it is markedly more plesiomorphic than *Macrotis* in retaining a distinct paraconid and paracristid on m1 and in having overall lower-crowned (less hyposodont) molars (Stirton, 1955; Archer and Kirsch, 1977; Travouillon et al., 2017). However, whereas most phylogenetic analyses have placed †*Ischnodon* as sister to *Macrotis* (Travouillon et al., 2014a, 2015b, 2017: [fig. 9B], 2021; Chamberlain et al., 2015) supporting thylacomyid affinities for the former taxon, a few have not (Travouillon et al., 2017: fig. 9A).

As already discussed (see Perameloidea above), †*Bulbadon warburtonae*, known from a single partial mandible, from the late Oligocene Ditjimanka Local Fauna (Faunal Zone B) of the Etadunna Formation, has been described as the oldest known thylacomyid (Travouillon

et al., 2021), but it did not form a clade with other thylacomyids in the dated total-evidence analyses of Travouillon et al. (2021). †*Liyamayi dayi* from the middle Miocene of Riversleigh World Heritage Area has also been described as a thylacomyid (Travouillon et al., 2014a). However, †*L. dayi* is currently known from only two teeth (identified as an M2 and m1) that show striking differences from the homologous teeth of *Macrotis* in, for example, the presence of a distinct metaconule (rather than the metacone) at the posterolingual corner of M2, and a very prominent paraconid and paracristid on m1 (Travouillon et al., 2014a). A number of published phylogenetic analyses have failed to support thylacomyid affinities for †*Liyamayi* (Travouillon et al., 2014a, 2015b; Chamberlain et al., 2015), but most recently the dated total-evidence analyses of Travouillon et al. (2021) placed this taxon sister to *Macrotis* + †*Ischnodon*, suggesting that it is indeed an early thylacomyid.

Peramelidae Gray, 1825

Contents: *Echymipera*, *Isoodon*, *Microperoryctes*, *Perameles* (fig. 39), *Peroryctes*, and *Rhynchomeles*.

Stem Age: 16.5 Mya (95% HPD: 12.4–20.6 Mya).

Crown Age: 8.8 Mya (95% HPD: 6.3–12.3 Mya).

Unambiguous Craniodental Synapomorphies: Orbitosphenoid laterally inapparent or absent (char. 15: 0→1; ci = 1.000), and dP3 very small, nonoccluding, and structurally simplified, or absent (char. 120: 1→2; ci = 0.118).

Comments: Our dated Bayesian total-evidence analysis recovers monophyly of Peramelidae sensu Van Dyck and Strahan, 2008 (= Echymiperinae + Peramelinae + Peroryctinae), to the exclusion of Thylacomyidae and Chaeropodidae (fig. 33), as do our undated Bayesian total-evidence analysis (fig. 32) and all our molecular analyses (figs. 27–29). As already discussed, a similar topology has been recov-
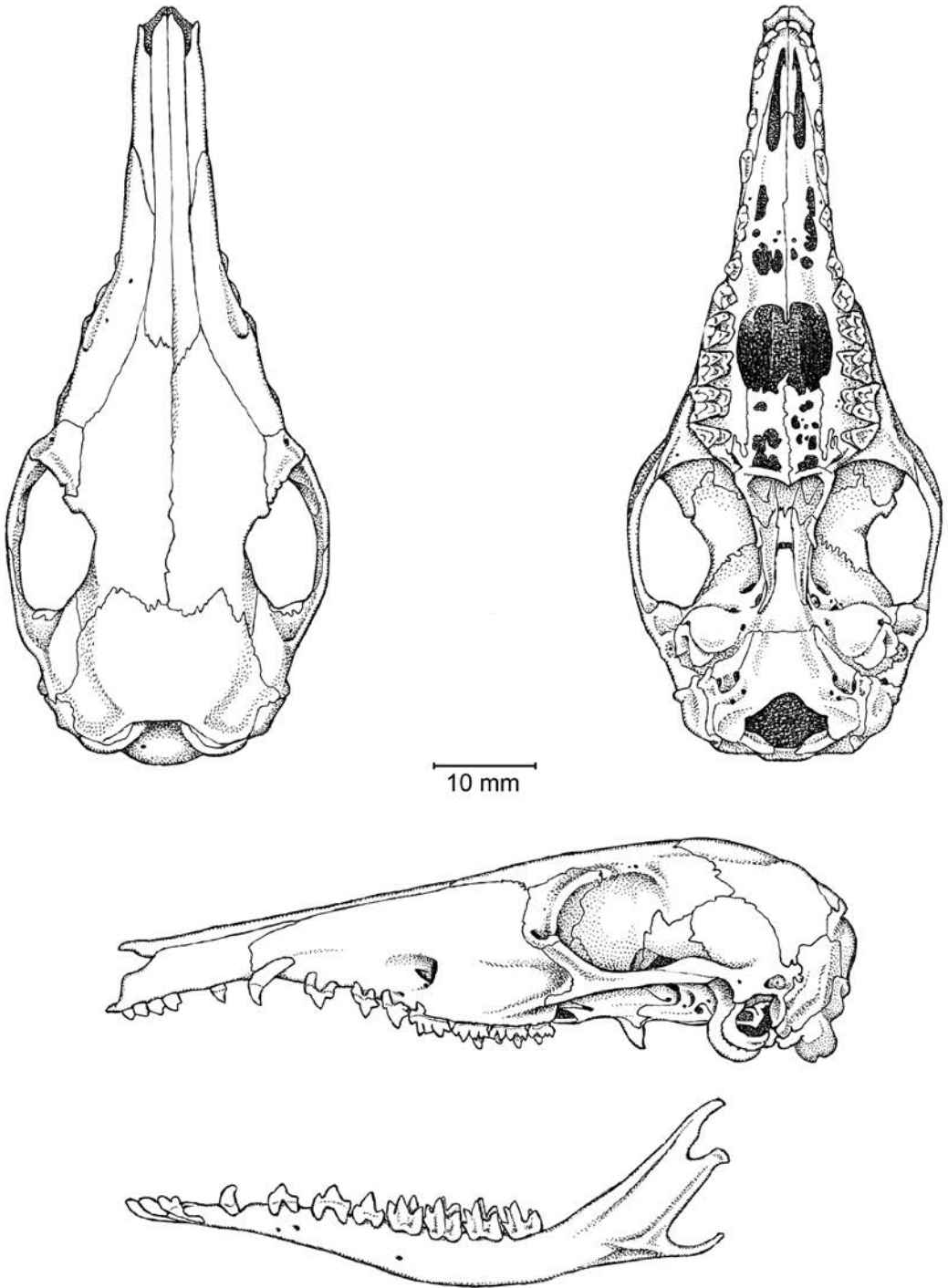
FIG. 39. *Perameles gunnii* (Peramelemorphia, Peramelidae; based on MVZ 127070, an adult male from Tasmania).

ered in most recent molecular and total-evidence analyses (Westerman et al., 2012; Kear et al., 2016; Travouillon and Phillips, 2018). Of the two craniodental features that optimize as unambiguous synapomorphies of Peramelidae, a laterally inapparent or absent orbitosphenoid is unique to this clade and shows no homoplasy among our terminals, whereas presence of a structurally simplified dP3 serves to distinguish peramelids from *Macrotis* and *Chaeropus*, in which dP3 is better developed. However, the morphology of dP3 in †*Bulungu*, †*Galadi* and †*Yarala*, which fall outside the crown clade (Perameloidea) in our analyses, is currently unknown.

†*Crash bandicoot* from the middle Miocene AL90 site (which has been radiometrically dated as ~14.8 Mya; Woodhead et al., 2014) at Riversleigh World Heritage Area was described by Travouillon et al. (2014a) as a member of the peramelid crown group. In support of this, †*Crash* has been recovered in a clade with *Perameles* and *Isoodon* in some recent analyses (Travouillon et al., 2014a, 2015b: fig. 12a; Chamberlain et al., 2015), although not others (Travouillon et al., 2015b: fig. 12b; Kear et al., 2016). However, †*Crash* considerably predates our late Miocene estimate for the most recent common ancestor of Peramelidae. Apart from †*Crash*, the oldest known peramelids are probably early Pliocene taxa that have been referred to *Perameles* (*P.* †*allinghamensis*, *P.* †*bowensis*, and *P.* †*wilkinsorum*; Warburton and Travouillon, 2016; Travouillon et al., 2017).

Dasyuromorphia Gill, 1872

CONTENTS: †*Badjcinus*, †*Barinya*, Dasyuridae, †*Mutpuracinus*, *Myrmecobius*, and Thylacinidae.

STEM AGE: 43.7 Mya (95% HPD: 39.6–47.4 Mya).

CROWN AGE: 31.2 Mya (95% HPD: 26.6–36.5 Mya).

UNAMBIGUOUS CRANIODENTAL SYNAPOMORPHIES: Nasals not produced beyond premaxillary facial processes, incisive foramina exposed in dorsal view (char. 1: 0→1; ci = 1.000); postorbital

processes present (char. 18: 0→1; ci = 0.042); posterolateral palatal foramina absent, posterior margins incomplete (char. 40: 0→1; ci = 0.200); stD taller than stB on M2 (char. 134: 0→1; ci = 0.250); m3 hypoconid lingual to salient protoconid (char. 173: 0→1; ci = 0.045); and lower molars with distinct posterior cingulid (char. 180: 0→1; ci = 0.333).

COMMENTS: Monophyly of Dasyuromorphia sensu Kealy and Beck (2017)—the most inclusive clade including *Dasyurus viverrinus*, but excluding *Perameles nasuta*, *Notoryctes typhlops*, *Phalanger orientalis*, and *Dromiciops gliroides*—is strongly supported in our total-evidence analyses (figs. 32, 33). This clade is supported by six unambiguous craniodental synapomorphies, of which four—nasals not produced beyond premaxillary facial processes, posterolateral palatal foramina absent, stD taller than stB on M2, and lower molars with distinct posterior cingulid present—show little or no homoplasy.

†*Badjcinus turnbulli* from the late Oligocene (Faunal Zone A) of Riversleigh World Heritage area was originally described as a thylacinid (see Muirhead and Wroe, 1998), and it is placed in Thylacinidae sensu Kealy and Beck (2017: table 1) in our undated total-evidence analysis (fig. 32). However, in our dated total-evidence analysis, †*Badjcinus* is placed in a trichotomy with Thylacinidae (†*Nimbacinus* + *Thylacinus*) and a clade comprising our remaining dasyuromorphian terminals (fig. 33). It is, therefore, unclear whether †*Badjcinus* is a member of the dasyuromorphian crown clade (= Dasyuroidea; Kealy and Beck, 2017).[32] In this respect, our results are broadly similar to those of Kealy and Beck (2017), who also failed to unambiguously place

---

[32] †*Badjcinus* exhibits a carnivorously adapted dentition that most closely resembles those of other taxa currently placed in Thylacinidae (see Muirhead and Wroe, 1998), but it has some unusual features—most notably, fusion between stB and the paracone on M1 (char. 136), which is not seen in definitive thylacinids, but which is seen in several dasyurids (e.g., *Dasyurcus*, *Dasyuroides*, *Dasyurus*, *Sarcophilus*)—together with a seemingly plesiomorphic basicranium. Most strikingly, it lacks a posterior squamosal epitympanic sinus (char. 84), a structure that is present in all other known dasyuromorphians (Archer, 1976b; Muirhead and Wroe, 1998).

†*Badjcinus* within Thylacinidae, despite a much denser sampling of dasyuromorphians than that used here; instead, it was placed as sister to all other dasyuromorphians in some analyses, congruent with its antiquity (late Oligocene) and putative basicranial plesiomorphies. Kealy and Beck (2017) argued that †*Badjcinus* is best considered ?Thylacinidae, based on current evidence. By contrast, the phylogenetic analyses of Rovinsky et al. (2019) consistently placed †*Badjcinus* within Thylacinidae, but these employed a less dense sampling of dasyuromorphian taxa than those of Kealy and Beck (2017).

Thylacinidae Bonaparte, 1838

CONTENTS: †*Nimbacinus* and *Thylacinus* (fig. 40).

STEM AGE: 31.2 Mya (95% HPD: 26.6–36.5 Mya).

CROWN AGE: 17.1 Mya (95% HPD: 11.6–24.0 Mya).

UNAMBIGUOUS CRANIODENTAL SYNAPOMORPHIES: Presphenoid exposed in roof of nasopharyngeal fossa above posterior palate (char. 43: 1→0; $ci = 0.091$) and p3 distinctly taller than p2 (char. 156: 0→2; $ci = 0.118$).

COMMENTS: Thylacinidae—defined by Kealy and Beck (2017: table 1) as the most inclusive clade including *Thylacinus cynocephalus*, but excluding *Dasyurus viverrinus* and *Myrmecobius fasciatus*—comprises only *Thylacinus* and †*Nimbacinus* in our dated total-evidence analysis (fig. 33). As already discussed (see Dasyuromorphia above), †*Badjcinus* was originally described as a thylacinid by Muirhead and Wroe (1998) and is placed within Thylacinidae in our undated total-evidence anlaysis (fig. 32) but not in our dated total-evidence analysis (fig. 33). †*Mutpuracinus archibaldi* is another dasyuromorphian that was originally described as a thylacinid (Murray and Megirian, 2000, 2006a), but in our dated total-evidence analysis it is recovered in a clade with another fossil dasyuromorphian, †*Barinya wangala*, and the only extant myrmecobiid, *Myrme-*

cobius; this clade is, in turn, sister to Dasyuridae (fig. 33). †*Barinya* itself was originally described as the oldest and most plesiomorphic known dasyurid (Wroe, 1999), but this inference is not supported here. Again, our results are broadly congruent with those of Kealy and Beck (2017), which likewise did not support thylacinid affinities for †*Mutpuracinus* nor dasyurid affinities for †*Barinya* (see also Eldridge et al., 2019; Rovinsky et al., 2019).

The oldest putative thylacinid remains are a partial upper molar (NTM P2815-10) from the late Oligocene Pwerte Marnte Marnte Local Fauna in the Northern Territory, and a partial lower molar (QM F16809) from the late Oligocene (Faunal Zone A) D-site at Riversleigh that was originally described as a paratype of the thylacinid †*Nimbacinus dicksoni* by Muirhead and Archer (1990), but which Murray and Megirian (2000: 159) concluded "represents a different taxon, probably another genus," Wroe and Musser (2001: 502) considered to be of "uncertain" taxonomic status, and Rovinsky et al. (2019) formally classified as Thylacinidae incertae sedis. Neither specimen has been included in published phylogenetic analyses, so even if they really are thylacinids, their relationship to the two thylacinid terminals included here, †*Nimbacinus* and *Thylacinus*, is unclear. †*Ngamalacinus timmulvaneyi* from the early Miocene (Faunal Zone B) sites at Riversleigh (Muirhead, 1997) has likewise not been included here due to its incompleteness, but it was consistently recovered as a thylacinid in the total-evidence analyses of Kealy and Beck (2017), so we consider it to be the oldest definitive thylacinid currently known.

Our estimate for the divergence between *Thylacinus* and †*Nimbacinus* is latest Oligocene to middle Miocene, congruent with the age of the oldest known representative of the genus *Thylacinus*, *T.* †*macknessi*, which is from middle Miocene (Faunal Zone C) sites at Riversleigh (Muirhead, 1992; Muirhead and Gillespie, 1995; Yates, 2014, 2015a; Rovinsky et al., 2019).

10 mm
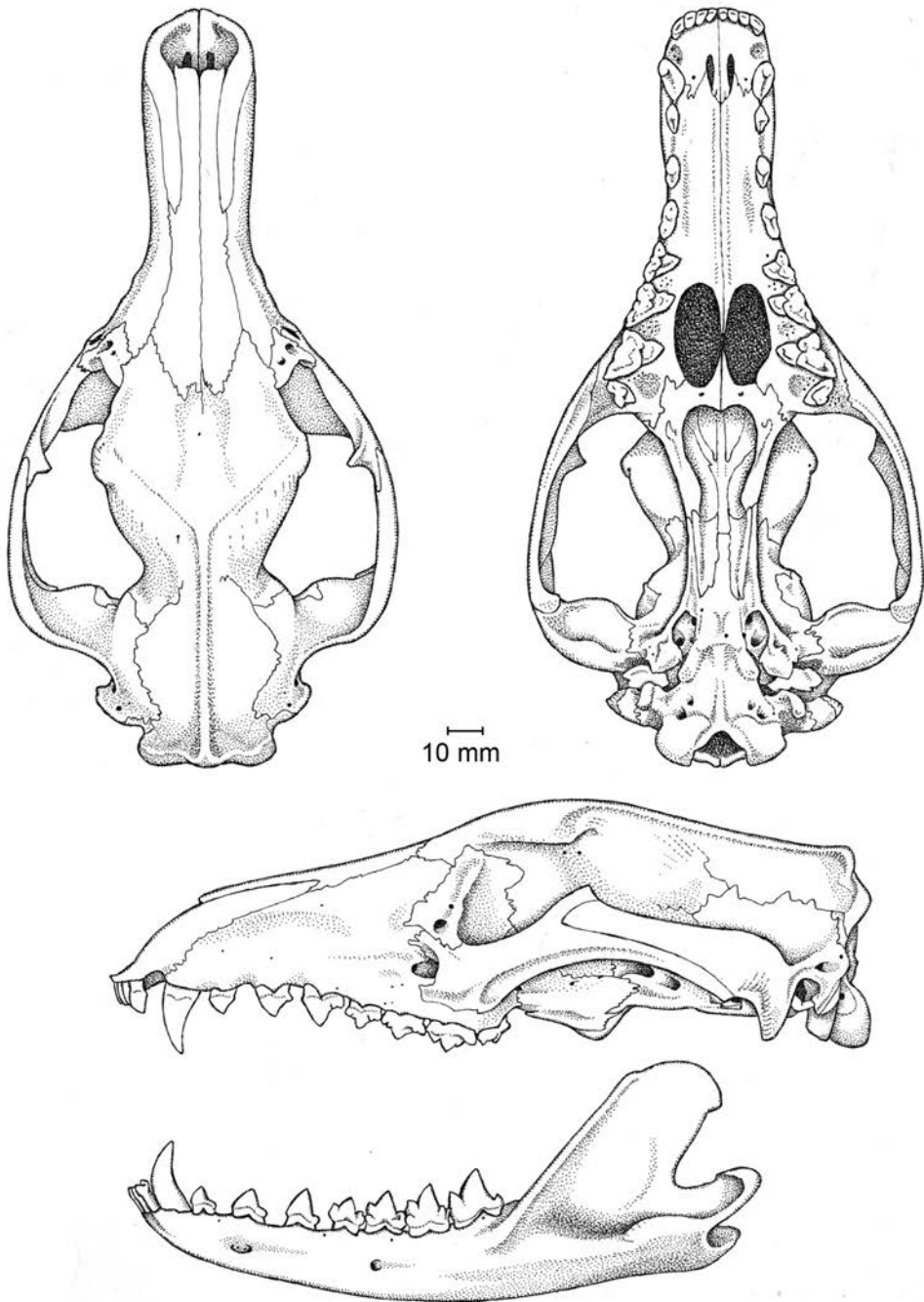
FIG. 40. *Thylacinus cynocephalus* (Dasyuromorphia, Thylacinidae; based primarily on BMNH 1852.1.16.8, an adult female from Tasmania, but with the features of the auditory region reconstructed based on BMNH 1952.1432, an adult of unknown sex (probably also a female, based on its comparatively small and gracile skull) from Tasmania, and with additional information regarding general sutural and pterygoid morphology provided by BMNH 1972.665, an adult male from Tasmania.

Myrmecobiidae Waterhouse, 1841

CONTENTS: *Myrmecobius* (fig. 41).

STEM AGE: 20.2 Mya (95% HPD: 14.4–25.3 Mya).

CROWN AGE: N/A.

UNAMBIGUOUS CRANIODENTAL AUTAPOMORPHIES: Masseteric process present and projecting ventrally below plane of molar alveoli (char. 6: 0→1; ci = 0.125); jugal terminates in a ventrally expanded ectoglenoid crest (char. 22: 0→1; ci = 0.167); glenoid process of alisphenoid absent (char. 23: 1→ 0; ci = 0.125); scars of M. temporalis origin on braincase not fused middorsally to form sagittal crest in adults (char. 27: 1→0; ci = 0.059); maxillopalatine fenestrae consistently absent (char. 36: 1→0; ci = 0.111); posterolateral palatal foramina present, with complete posterior margins (char. 40: 1→0; ci = 0.200); palate extends posterior to presphenoid-basisphenoid suture (char. 42: 0→1; ci = 1.000); pterygoids separated from presphenoid by palatine-basisphenoid contact (char. 46: 0→1; ci = 0.111); pterygoids long, extending posteriorly to sheath the ventral margin of the carotid canal (char. 47: 0→1; ci = 0.333); masseteric fossa perforated by a distinct masseteric foramen (char. 99: 0→1; ci = 0.333); angular process weakly or not inflected (char. 102: 0→1; ci = 0.250); premolariform second upper premolar (P2) distinctly taller than premolariform P3 (char. 119: 2→0; ci = 0.118); i2 alveolus like those of i1 and i3 (char. 149: 0→1; ci = 0.250); paraconid well developed, but paracristid indistinct or absent on m1 (char. 159: 0→2; ci = 0.400); paraconid well developed, but paracristid indistinct or absent on m2 and m3 (char. 161: 0→2; ci = 0.667); cristid obliqua absent or indistinct (char. 167: 0→1; ci = 0.500); hypoconid small and indistinct (char. 172: 0→1; ci = 0.333); and entocristid indistinct or absent (char. 176: 0→1; ci = 0.077).

COMMENTS: Kealy and Beck (2017: table 1) defined Myrmecobiidae as the most inclusive clade including *Myrmecobius fasciatus*, but excluding *Dasyurus viverrinus* and *Thylacinus cynocephalus*. Under this definition, our dated total-evidence analysis (fig. 33) indicates that the fossil dasyuromorphians †*Barinya* and †*Mutpuracinus* are myrmecobiids, as did the dated total-evidence analysis of Kealy and Beck (2017: fig.3). Given our estimate for the age of the split between the *Myrmecobius* lineage and Dasyuridae (median: 24.9 Mya; 95% HPD: 21.8–29.4 Mya) and those of other recent studies (e.g., Mitchell et al., 2014; Westerman et al., 2016; Kealy and Beck, 2017), we would expect stem-myrmecobiids in the fossil record from at least the early Miocene onward; the earliest of these would presumably have had a "typical," unreduced dasyuromorphian dentition, in contrast to the secondarily simplified dentition of *Myrmecobius*. Thus, it is not implausible that †*Barinya* and †*Mutpuracinus* are indeed early myrmecobiids. However, the *Myrmecobius* + *Barinya* + *Mutpuracinus* clade receives only relatively weak support here (BPP = 0.67), and only one craniodental feature optimizes as an unambiguous synapomorphy, namely loss of the posterior cutting edge of P3 (char. 124: 1→2; ci = 0.667), which is clearly the case in †*Barinya* (Wroe, 1999), but which cannot be scored in †*Mutpuracinus* based on available material (Murray and Megirian, 2000; Murray and Megirian, 2006a). We consider the evidence that *Barinya* and *Mutpuracinus* are stem myrmecobiids to be equivocal pending further studies, so we here restrict Myrmecobiidae to *Myrmecobius*.

Myrmecobius is characterized by a long list of craniodental apomorphies not seen in other dasyuromorphians: many of these are dental, but there are also a large number of unusual cranial features (see also Archer, 1976b, 1984c; Archer and Kirsch, 1977; Friend, 1989; Cooper, 2000). At least some of these apomorphies are likely related to myrmecophagy, including several relating to simplification of the molars (reflecting little or no occlusion between the upper and lower dentition; Charles et al., 2013).

Dasyuridae Goldfuss, 1820

CONTENTS: *Antechinomys, Antechinus, Dasycercus, Dasykaluta, Dasyuroides, Dasyurus,*

10 mm
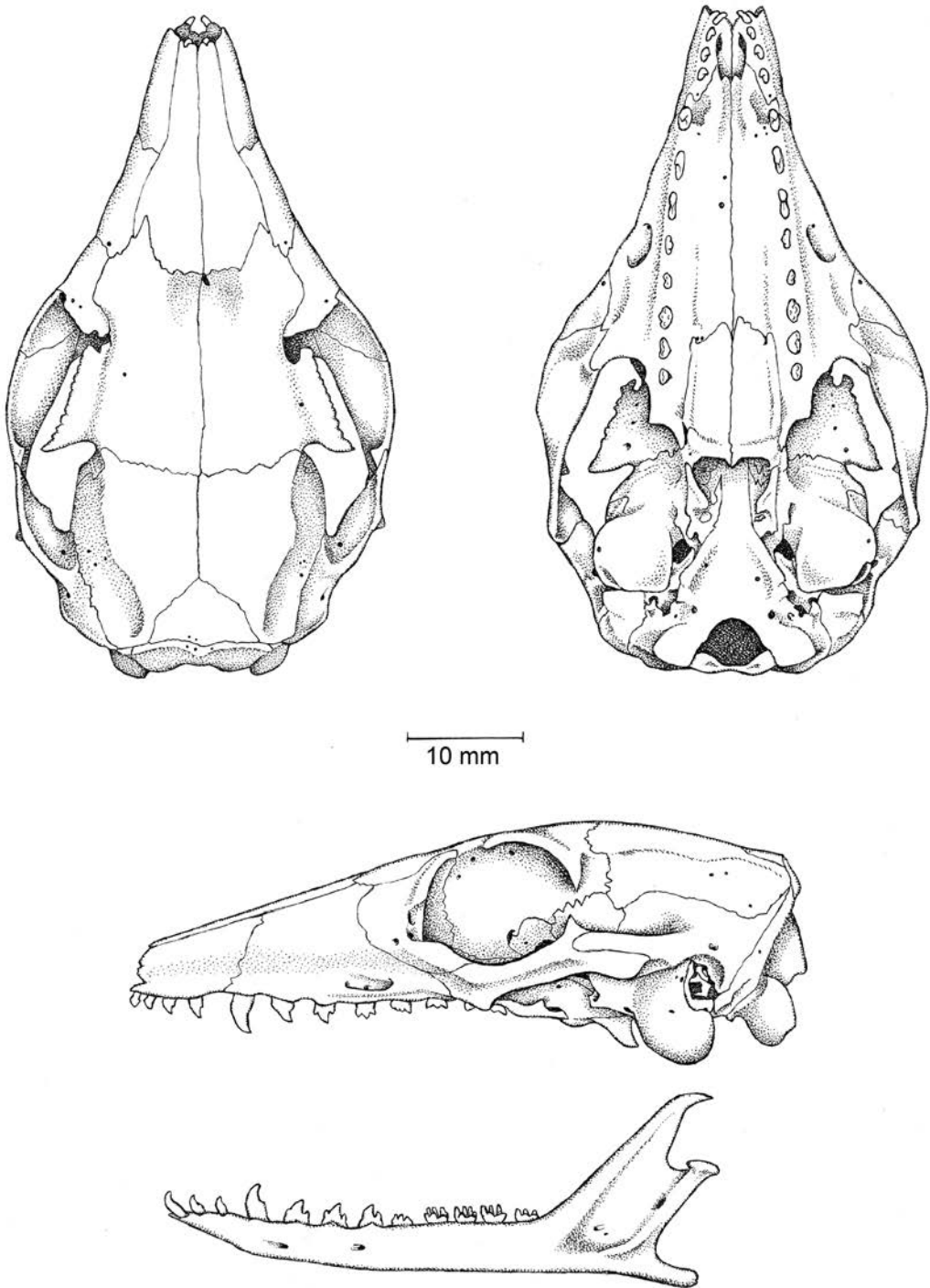
FIG. 41. *Myrmecobius fasciatus* (Dasyuromorphia, Myrmecobiidae; based on WAM M-6668, an adult male from Western Australia).

Micromurexia, *Murexechinus*, *Murexia*, *Myoictis*, *Neophascogale*, *Ningaui*, *Paramurexia*, *Parantechinus*, *Phascogale*, *Phascolosorex*, *Phascomurexia*, *Planigale*, *Pseudantechinus* (fig. 42), *Sarcophilus*, and *Sminthopsis*.

Stem Age: 24.9 Mya (95% HPD: 21.8–29.4 Mya).

Crown Age: 17.8 Mya (95% HPD: 16.1–20.1 Mya).

Unambiguous Craniodental Synapomorphies: Postorbital processes absent or indistinct (char. 18: 1→0; ci = 0.042); scars of M. temporalis origin on braincase not fused middorsally to form sagittal crest in adults (char. 27: 1→0; ci = 0.059); interparietal absent, very small, or polymorphic (char. 30: 1→0; ci = 0.250); palatines separated from presphenoid by vomerine-pterygoid contact (char. 45: 0→1; ci = 0.125) caudal and rostral tympanic processes of petrosal seamlessly fused, forming a petrosal plate (char. 68: 0→2; ci = 0.154); facial nerve exits middle ear via a stylomastoid foramen formed by the rostral and caudal tympanic processes of the petrosal (char. 79: 0→3; ci = 0.625); and P3 erupts after M4 (char. 130: 4→0; ci = 0.089).

Comments: We follow Kealy and Beck's (2017: table 1) definition of Dasyuridae, namely the most inclusive clade including *Dasyurus viverrinus*, but excluding *Myrmecobius fasciatus* and *Thylacinus cynocephalus*. Dasyuridae is characterized by seven unambiguous craniodental synapomorphies, of which perhaps the most striking are the marked reduction in size or loss of the interparietal (this bone is present and markedly larger in other dasyuromorphians), the presence of a petrosal plate (absent in other dasyuromorphians) and presence of a stylomastoid foramen formed by the rostral and caudal tympanic processes of the petrosal (the facial nerve exits the middle ear by a notch rather than a fully enclosed foramen in other dasyuromorphians; Archer, 1976b; Wroe, 1997b, 1999).

The fossil †*Barinya wangala*, from early Miocene (Faunal Zone B) and middle Miocene (Faunal Zone C) sites at Riversleigh World Heritage Area, was described as the most plesiomorphic known dasyurid by Wroe (1999), but it retains a large interparietal and lacks both a petrosal plate and a stylomastoid foramen. As previously discussed, †*Barinya* was recovered by our dated total-evidence analysis (fig. 33) in a clade with *Myrmecobius* and †*Mutpuracinus* (originally described as a thylacinid; Murray and Megirian, 2000; 2006a). Kealy and Beck (2017) likewise found no support for the notion that †*Barinya* is a dasyurid.

Black et al. (2012b: 1020) discussed "probable phascogalines and dasyurines" from the early Miocene (Faunal Zone B) of Riversleigh World Heritage Area; these specimens are potentially significant for understanding the timing of dasyurid diversification, but they have yet to be described. At present, the oldest known definitive dasyurids are probable-Pliocene taxa that have been associated with Recent tribes or genera, including "*Dasyuroides*" †*achilpatna* (which may, in fact, be more closely related to *Dasycercus* than to *Dasyuroides*; Kealy and Beck, 2017) and *Sarcophilus* †*moornaensis* from the Fisherman's Cliff Local Fauna (Archer, 1982b; Crabb, 1982), "*Dasycercus*" †*worboysi* and unnamed "*Antechinus*" and *Sminthopsis* specimens from the Big Sink Local Fauna (Dawson et al., 1999), †*Archerium chinchillaensis* (a probable dasyurin) from the Chinchilla Local Fauna (Wroe and Mackness, 2000a; Louys and Price, 2015), *Dasyurus* †*dunmalli* from multiple Pliocene sites (Bartholomai, 1971a; Archer, 1982b; Wroe and Mackness, 1998, 2000b; Louys and Price, 2015), †*Glaucodon ballaratensis* (a probable relative of *Sarcophilus*) from sites at Smeaton and Batesford in Victoria (Stirton, 1957; Archer, 1982b; Gerdtz and Archbold, 2003; Piper et al., 2006), *Planigale* sp. from the Bluff Downs Local Fauna (Archer, 1982b), and "*Antechinus*" sp. (probably a relative of *Murexia* sensu lato; see Kealy and Beck, [2017: 16]) from the Hamilton Local Fauna (Archer, 1982b).

Within Dasyuridae, our dated total-evidence analysis (fig. 33) is congruent with recent published molecular and total-evidence analyses (Mitchell et al., 2014; May-Collado et

10 mm
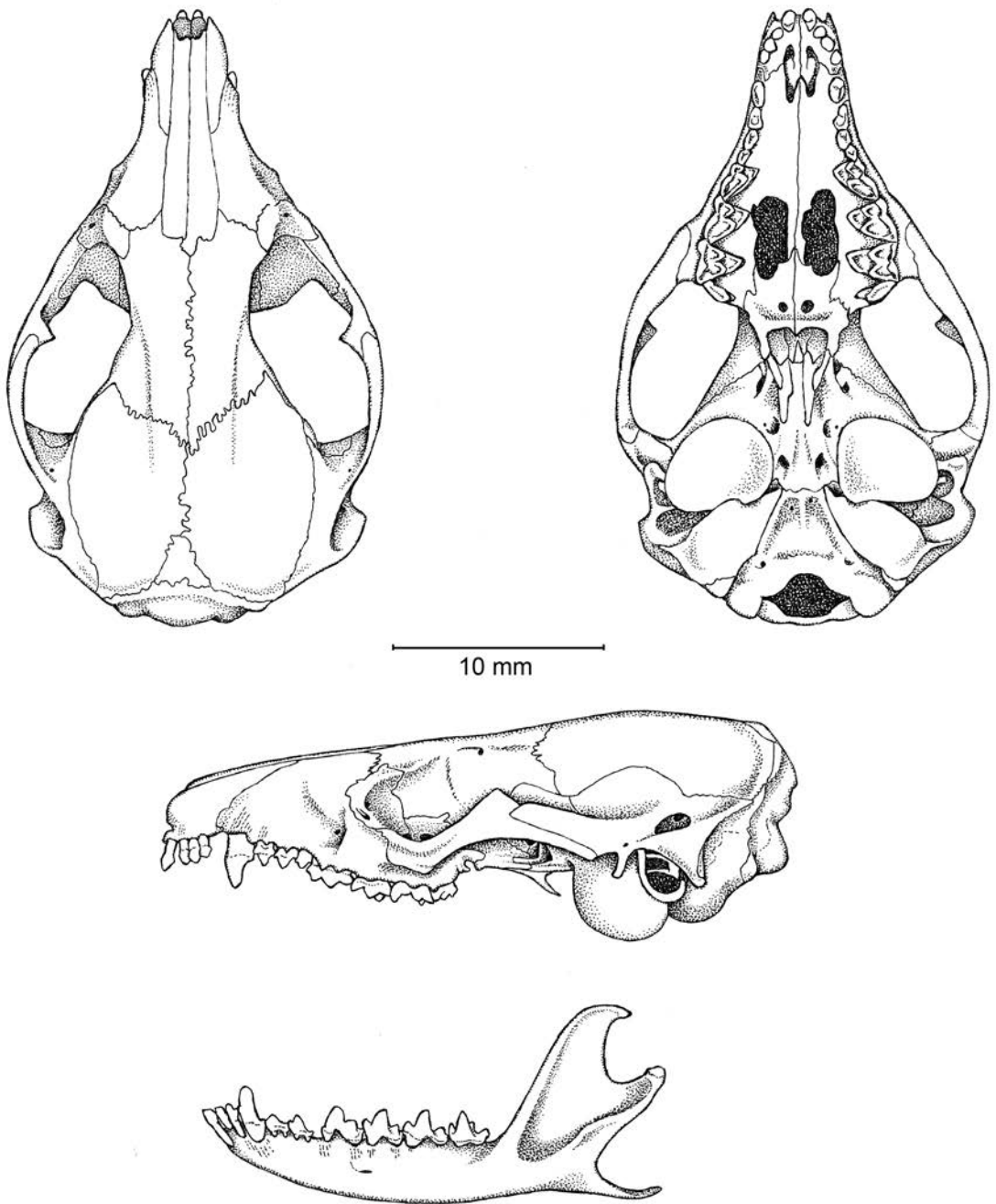
FIG. 42. *Pseudantechinus macdonnellensis* (Dasyuromorphia, Dasyuridae; based on AMNH 196694, an adult female from Western Australia).

al., 2015; Westerman et al., 2016; Kealy and Beck, 2017; García-Navas et al., 2020; Álvarez-Carretero et al., 2021) in supporting a basal split between Dasyurinae and Sminthopsinae, with each of these subfamilies comprised of two tribes: Dasyurini and Phascogalini within Dasyurinae and Sminthopsini and Planigalini within Sminthopsinae. The contents of these tribes and relationships within them recovered by our molecular (figs. 27–29) and total-evidence (figs. 32, 33) analyses are also in agreement with the published results of most recent molecular and total-evidence studies (Mitchell et al., 2014; Westerman et al., 2016; Kealy and Beck, 2017; García-Navas et al., 2020; Álvarez-Carretero et al., 2021)[33].

Our estimated divergence times within Dasyuridae are younger than those estimated by recent molecular-clock studies (Mitchell et al., 2014; Westerman et al., 2016; Álvarez-Carretero et al., 2021) and are younger even than the dated total-evidence analyses of Kealy and Beck (2017), but they are similar to those of the dated total-evidence analysis of García-Navas et al. (2020). If correct, these dates suggest that cladogenesis within modern dasyurid tribes did not occur until the late Miocene onward. This is congruent with the apparently sudden appearance in the fossil record of identifiable representatives of modern dasyurid tribes and and genera in the early Pliocene, as summarized above.

Microbiotheria Ameghino, 1889

Contents: *Dromiciops* (fig. 43) and †*Microbiotherium.*

Stem Age: 45.6 Mya (95% HPD: 41.4–48.8 Mya).

Crown Age: 17.3 Mya (95% HPD: 14.0–21.8 Mya).

Unambiguous Craniodental Synapomorphies: Basisphenoid with a distinct sagittal keel (char. 48: 0→1; ci = 1.000); auditory bulla large,

contacting rostral process of petrosal (char. 55: 1→2; ci = 0.300); caudal and rostral tympanic processes of petrosal seamlessly fused, forming a petrosal plate (char. 68: 0→2; ci = 0.154); and five upper incisors present (char. 103: 2→0; ci = 0.333).

Comments: Of the four unambiguous morphological synapomorphies supporting monophyly of Microbiotheria (equivalent to Microbiotheriidae in our analyses), two occur homoplastically in other marsupial groups and one appears questionable because it is a reversal in the number of upper incisors from three back to the ancestral metatherian complement of five. However, presence of a basisphenoid with a distinct sagittal keel is a distinctive cranial apomorphy that is apparently unique to microbiotherians (Hershkovitz, 1992a; 1999; Giannini et al., 2004; Wible et al., 2018). Although several genera of fossil microbiotherians are known from South America (Marshall, 1982; Goin and Abello, 2013; Goin et al., 2016), all except †*Microbiotherium* (for which cranial material, including a specimen [MACN A 8505] preserving the part of the basisphenoid sagittal keel, is known; Segall, 1969b; Marshall, 1982) are known from dental remains only.

As already discussed (see Australidelphia above), the oldest definitive member of the order described to date is probably the woodburnodontid †*Woodburnodon casei* from the Cucullaea I Allomember of the La Meseta Formation, Seymour Island, off the Antarctic Penninsula. Based on current evidence, the age of †*W. casei* appears to be ~40 Mya (Douglas et al., 2014; Amenábar et al., 2019; Mörs et al., 2020). Most recent studies have concluded that the early or middle Palaeocene †*Khasia cordillerensis* is not a member of Microbiotheria (Oliveira and Goin, 2006; Goin et al., 2016; Carneiro et al., 2018; but see Muizon et al., 2018), and putative microbiotherian specimens reported from the early Eocene Las Flores Fauna (Goin, 2003; Zimicz, 2012; Woodburne et al., 2014a; Goin et al., 2016)

[33] But see Kealy and Beck (2017: 15) regarding anomalous relationships recovered in the molecular analysis of May-Collado et al. (2015).
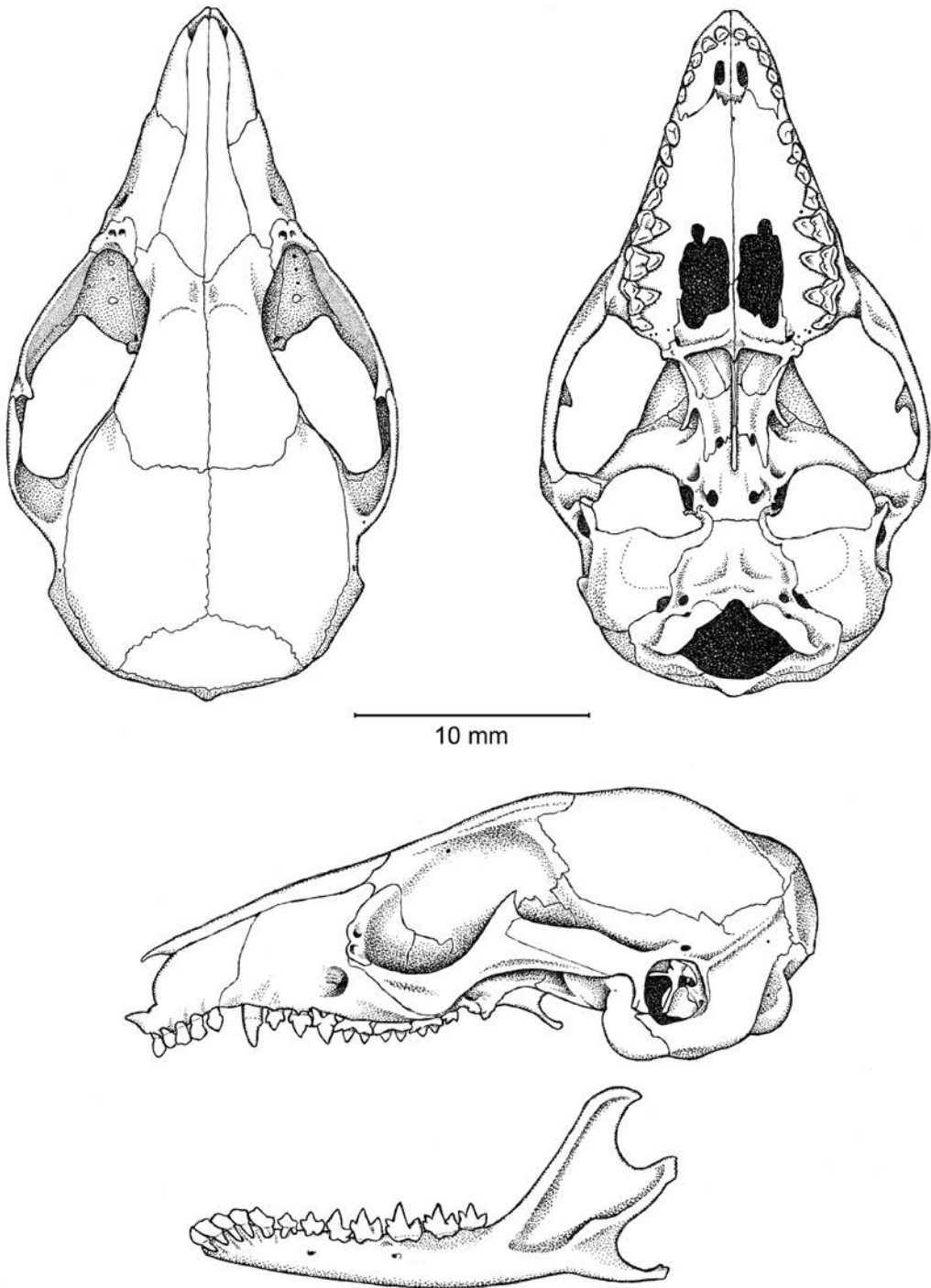
FIG. 43. *Dromiciops gliroides* (Microbiotheria, Microbiotheriidae; based on UWBM 78641, an adult male from Región de La Araucanía, Chile).

have yet to be formally described (see Australidelphia above).

Diprotodontia Owen, 1866

Contents: Acrobatidae, †Balbaridae, Burramyidae, †Diprotodontoidea, †*Ekaltadeta*, Hypsiprymnodontidae, †Ilariidae, Macropodidae, †*Muramura*, †*Namilamadeta*, Petauridae, Phalangeridae, Phascolarctidae, Potoroidae, Pseudocheiridae, Tarsipedidae, †Thylacoleonidae, and Vombatidae.

Stem Age: 45.6 Mya (95% HPD: 41.4–48.8 Mya).

Crown Age: 39.8 Mya (95% HPD: 35.5–45.2 Mya).

Unambiguous Craniodental Synapomorphies: Maxillary foramen contained entirely within the maxilla (char. 14: 0→1; ci = 0.200); glenoid process of alisphenoid absent (char. 23: 1→0; ci = 0.125); sagittal crest small in adults, extending from nuchal crest onto parietals, but not extending onto frontals (char. 27: 0→1; ci = 0.059); pterygoids long, extending posteriorly to sheath the ventral margin of the carotid canal (char. 47: 0→1; ci = 0.333); hypotympanic sinus roof formed by squamosal and petrosal only (char. 54: 0→2; ci = 0.182); posterior squamosal epitympanic sinus distinct and at least partially enclosed laterally (char. 84: 0→1; ci =0.067); zygomatic epitympanic sinus present (char. 85: 0→1; ci = 0.500); P3 semisectorial (char. 123: 0→1; ci = 0.385); P3 erupts before M3 (char. 130: 2→4; ci = 0.089); upper molars without a distinct ectoflexus on any tooth (char. 132: 1→0; ci = 0.333); upper molar posterolingual cusp formed by metaconule (char. 143: 0→1; ci = 0.400); anteriormost lower incisor large, long crowned, and conspicuously procumbent (char. 147: 0→1; ci = 0.500); i2–4 missing (char. 148: 1→3; ci = 0.750); lower canine absent (char. 152: 0→1; ci = 1.000); m1 paracristid unnotched (char. 160: 0→1; ci = 0.125); and hypoconulid absent or indistinct (char. 178: 0→1; ci = 0.333).

Comments: Diprotodontian monophyly is strongly supported in all our molecular (figs. 27–29) and total-evidence (figs. 32, 33) analyses, and a long list craniodental features optimize as unambiguous synapomorphies on our dated total evidence topology (fig. 33). Importantly, although Diprotodontia (homoplastically) shares with †*Yalkaparidon* and paucituberculatans an enlarged, gliriform anteriormost lower incisor, it is characterized by numerous other craniodental synapomorphies that are not seen in these other taxa (see Aplin, 1990: 355–375, for a detailed discussion of the diprotodontian "morphotype"). However, we note that several of these traits are subsequently modified or reversed within Diprotodontia.

Our analyses suggest that Diprotodontia diverged from its sister taxon (Microbiotheria) during the early or middle Eocene and diversified during the middle or late Eocene; this schedule is distinctly later than that proposed by most previous molecular-clock studies (Nilsson et al., 2004; Beck, 2008a; Meredith et al., 2008b, 2009a, 2009c, 2011; Mitchell et al., 2014; Duchêne et al., 2018), but it is similar to the scenario implied by estimated dates in the recent phylogenomic study of Álvarez-Carretero et al. (2021). Regardless of its precise timing, this initial diversification is not preserved in the Australian fossil record due to the long temporal hiatus between the early Eocene Tingamarra Local Fauna (from which diprotodontians have not been identified) and multiple Australian sites known from the late Oligocene, in which definitive diprotodontians (including representatives of many modern diprotodontian families) are known (Archer et al., 1999; Long et al., 2002; Archer and Hand, 2006; Black et al., 2012b).

As already noted (see Australidelphia above), isolated australidelphian tarsals from the middle Eocene La Barda locality in Argentina were placed within Diprotodontia in the morphological phylogenetic analysis of Lorente et al. (2016). However, the relationships supported within Diprotodontia in that analysis are strongly incongruent with the analyses presented here, as well as with the results of other recent molecular studies (e.g., Nilsson et al., 2004; Beck, 2008a; Meredith et al., 2008b, 2009c, 2011; Mitchell et al., 2014; May-Collado et al., 2015; Duchêne et

al., 2018; Álvarez-Carretero et al., 2021); furthermore, dental remains of definitive (crown-clade) diprotodontians have not been described from La Barda or any other fossil locality outside Australia and New Guinea (Goin et al., 2016). Thus, the identity of the La Barda tarsals as diprotodontian (rather than another australidelphian lineage) should be treated as questionable based on available evidence. Instead, the oldest definitive diprotodontians are from the late Oligocene of Australia (Archer et al., 1999; Long et al., 2002; Archer and Hand, 2006; Black et al., 2012b).

†Thylacoleonidae Gill, 1872

Contents: †*Priscileo*, †*Thylacoleo*, and †*Wakaleo.*

Stem Age: 39.8 Mya (95% HPD: 35.5–45.2 Mya).

Crown Age: 29.4 Mya (95% HPD: 21.0–37.7 Mya).

Unambiguous Craniodental Synapomorphies: Presphenoid exposed in roof of nasopharyngeal fossa above posterior palate (char. 43: 1→0; ci = 0.091); neomorphic labial cingulum present on M1–3 (char. 133: 0→1; ci = 0.200); metaconid absent on m1 only (char. 163: 0→1; ci = 0.250); and additional cuspid labial to m1 protoconid present, forming a vertically directed crest (char. 165: 0→2; ci = 0.286).

Comments: Monophyly of †Thylacoleonidae was recovered in all of our morphological (figs. 30, 31) and total-evidence (figs. 32, 33) analyses. In our dated total-evidence analysis (fig. 33), four craniodental features optimize as synapomorphies for the family, three of which are dental. However, the position of †Thylacoleonidae within Vombatiformes is unstable in our analyses, placed as sister to the remainder of Vombatiformes (sensu Beck et al., 2020) in our undated total analysis (fig. 32)—as also found by Gillespie et al. (2016) and Beck et al. (2020)—but forming a trichotomy with Phalangerida and Vombatiformes at the base of Diprotodontia in our dated total-evidence analysis (fig. 33). We suspect the

reason is that early thylacoleonids, such as †*Lekanoleo roskellyae* (see Gillespie, 1997; Gillespie et al., 2020), preserve a plesiomorphic craniodental morphology relative to other diprotodontians. If so, the basicranial features identified by previous authors (Aplin and Archer, 1987; Aplin, 1987) as placing thylacoleonids within Vombatiformes may, in fact, be retained plesiomorphies, in contrast to the more derived basicranial morphologies of phalangeridans (see also Murray et al., 1987).

Postcranial evidence also presents an ambiguous picture: Szalay (1994: 276) suggested that tarsal features present in thylacoleonids and diprotodontoids (e.g., †*Ngapakaldia*) may be synapomorphic, but Munson's (1992) phylogenetic analysis of vombatiforms using postcranial characters placed †Thylacoleonidae as sister to a clade comprising †Diprotodontidae, †Palorchestidae, †Ilariidae, and Vombatidae. On current evidence, we argue that thylacoleonids should be considered Diprotodontia incertae sedis. Ultimately, given that †*Thylacoleo* survived into the late Pleistocene, it may be possible to obtain ancient DNA or ancient protein sequences (e.g., collagen) that might clarify thylacoleonid relationships.

Like most other diprotodontian families, the first record of thylacoleonids is from late Oligocene deposits in central Australia and at Riversleigh (Rauscher, 1987; Archer et al., 1999; Archer and Hand, 2006; Gillespie, 2007; Black et al., 2012b; Gillespie et al., 2017; 2020), so their origin must predate this. Our dated total-evidence analysis estimates that †Thylacoleonidae diverged from other diprotodontians during the middle to late Eocene.

Vombatiformes Woodburne, 1984

Contents: †Diprotodontoidea, †Ilariidae, †*Muramura*, †*Namilamadeta*, Phascolarctidae, and Vombatidae.

Stem Age: 39.8 Mya (95% HPD: 35.5–45.2 Mya).

Crown Age: 32.4 Mya (95% HPD: 29.1–36.4 Mya).

Unambiguous Craniodental Synapomorphies: Lacrimal exposure with one or more distinct tubercles (char. 8: 0→1; ci = 0.118); paroccipital process is a large erect process usually directed ventrally (char. 93: 1→2; ci = 0.100); P1 absent (char. 114: 0→1; ci = 0.200); P2 absent (char. 116: 0→1; ci = 0.333); distinct posterolingual cusp on semi- or fully sectorial P3 present (char. 125: 0→1; ci = 0.250); second lower premolar absent (char. 154: 0→1; ci = 1.000); entostylid labial to the entoconid present and cusplike (char. 174: 0→1; ci = 0.333).

Comments: Beck et al. (2020: table 1) defined Vombatiformes as the most inclusive clade including *Vombatus ursinus* and *Phascolarctos cinereus* but not *Phalanger orientalis*. The family †Thylacoleonidae has usually been considered to be a member of Vombatiformes (e.g., Archer, 1984c; Aplin and Archer, 1987; Aplin, 1987; Marshall et al., 1990; Munson, 1992; Szalay, 1994; Archer and Hand, 2006; Gillespie, 2007; Black et al., 2012a, 2012b; but see Murray et al., 1987, for an alternative view), within which it is usually placed closer to *Vombatus* than to *Phascolarctos*—in other words, as a member of Vombatomorphia sensu Beck et al. (2020; see below). However, as noted above, †Thylacoleonidae was placed as the sister to all other vombatiforms (i.e., outside Vombatomorphia) in our undated total-evidence analysis (fig. 32; a relationship also found by Gillespie et al., 2016; Beck et al., 2020), and it was recovered in a trichotomy at the base of Diprotodontia together with Vombatiformes and Phalangerida in our dated total-evidence analysis (fig. 33). Based on these results, we suggest that †Thylacoleonidae is best considered as Diprotodontia incertae sedis. Thus, in our dated total-evidence analysis, Vombatiformes sensu Beck et al. (2020) is restricted to †Diprotodontoidea, †*Ilaria*, Phascolarctidae, Vombatidae, †*Muramura*, and †*Namilimadeta*. Members of the families †Maradidae, †Palorchestidae, and †Mukupirnidae have not been included here, but have been recovered within Vombatiformes in recent phylogenetic analyses (Black

et al., 2012a; Brewer et al., 2015; Gillespie et al., 2016; Beck et al., 2020). Among the unambiguous synapomorphies of this restricted Vombatiformes are loss of P1, P2, and p2 (see above); all these teeth are retained in plesiomorphic thylacoleonids (Gillespie et al., 2016; Beck et al., 2020).

The oldest known definitive vombatiforms are from the late Oligocene of Australia (Archer et al., 1999; Long et al., 2002; Archer and Hand, 2006; Black et al., 2012b). This is congruent with our estimated divergence dates, which suggest that the initial diversification of vombatiforms took place during the late Eocene or early Oligocene.

Phascolarctomorphia Aplin and Archer, 1987

Contents: †*Litokoala*, †*Nimiokoala*, and *Phascolarctos* (fig. 44).

Stem Age: 32.4 Mya (95% HPD: 29.1–36.4 Mya).

Crown Age: 25.3 Mya (95% HPD: 19.6–30.3 Mya).

Unambiguous Craniodental Synapomorphies: Extracranial course of mandibular nerve traverses a bony canal in the roof of the hypotympanic sinus (char. 52: 1→2; ci = 0.231); postgenoid vein emerges from the postglenoid foramen in the posteromedial corner of the glenoid fossa, medial or anteromedial to the postglenoid process (char. 77: 0→1; ci = 0.250); and additional cuspid labial to m1 protoconid present, forming a cusplike protostylid (char. 165: 0→1; ci = 0.286).

Comments: Phascolarctidae is consistently recovered in our molecular, morphological and total-evidence analyses (figs. 27–33) as sister to the remaining vombatiforms, which collectively comprise Vombatomorphia (note that we consider †Thylacoleonidae to be Diprotodontia incertae sedis and not a member of Vombatiformes; see above). Aplin and Archer (1987) placed Phascolarctidae in its own infraorder, Phascolarctomorphia (coordinate to Vombatomorphia), and it remains the only known phas-
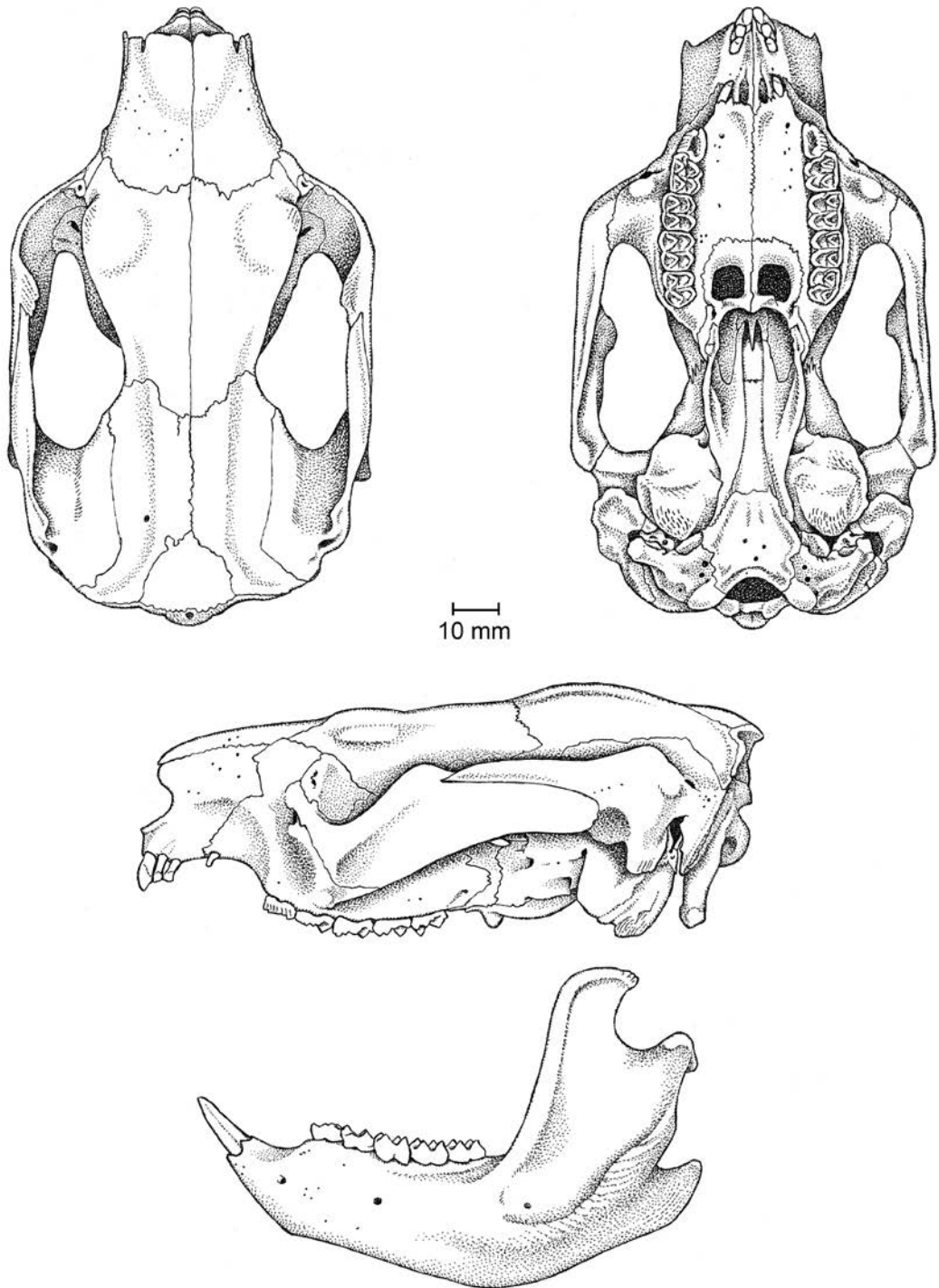
FIG. 44. *Phascolarctos cinereus* (Diprotodontia, Phascolarctidae; based on AMNH 65611, an adult male from Queensland).

colarctomorphian family; thus, the craniodental synapomorphies of Phascolarctidae apply equally to Phascolarctomorphia.

Known phascolarctids are craniodentally distinctive (Sonntag, 1922; Archer, 1984a, 1984c; Aplin, 1987, 1990; Lee and Carrick, 1989; Springer and Woodburne, 1989; Black and Archer, 1997b; Louys et al., 2009; Black et al., 2014a), and monophyly of this clade is supported by three unambiguous craniodental synapomorphies in our analysis, although all show some degree of homoplasy. Perhaps the most striking of these is the extracranial course of the mandibular nerve, which traverses a bony canal in the roof of the hypotympanic sinus in all three of our phascolarctid terminals (†*Litokoala*, †*Nimiokoala* and *Phascolarctos*; Aplin, 1987; 1990; Louys et al., 2009), a feature that (as far as we are aware) occurs in no other metatherians.[34]

In contrast to Black et al. (2012a), we found †*Nimiokoala*, rather than †*Litokoala*, to be more closely related to *Phascolarctos*, with the †*Nimiokoala* + *Phascolarctos* clade supported by a single unambiguous synapomorphy (see file S3 in the online supplement): maxillary and frontal bones in contact on medial orbital wall (char. 13 0→1; c_i = 0.143). Like other vombatiform families, the oldest record of Phascolarctidae is from late Oligocene sites in Australia (Archer et al., 1999; Long et al., 2002; Archer and Hand, 2006; Black et al., 2012b, 2014b).

Vombatomorphia Aplin and Archer, 1987

CONTENTS: †Diprotodontoidea, †Ilariidae, †*Muramura*, †*Namilamadeta*, Phascolarctidae, and Vombatidae.

STEM AGE: 32.4 Mya (95% HPD: 29.1–36.4 Mya).

CROWN AGE: 30.5 Mya (95% HPD: 27.3–34.1 Mya).

_____

[34] By contrast, this nerve traverses a bony canal in the medial wall of the hypotympanic sinus in the sparassocynin didelphids †*Hesperocynus* and †*Sparassocynus* (see char. 52 and Beck and Taglioretti, 2020).

UNAMBIGUOUS CRANIODENTAL SYNAPOMORPHIES: Frontal and squamosal in contact on lateral aspect of braincase (char. 26: 0→1; c_i = 0.071); squamosal prevents parietal-mastoid contact (char. 32: 0→1; c_i = 0.083); subarcuate fossa is a shallow depression (char. 73: 0→1; c_i = 0.500); facial nerve exits the middle ear via a stylomastoid foramen formed by the ectotympanic and pars canalicularis of the petrosal (char. 79: 0→5; c_i = 0.625); zygomatic epitympanic sinus shallow and largely open laterally (char. 86: 1→2; c_i = 0.333); and condylar process transversely elongate and medially extensive (char. 101: 0→1; c_i = 0.333).

COMMENTS: Beck et al. (2020: table 1) defined Vombatomorphia as the most inclusive clade including *Vombatus ursinus* but not *Phascolarctos cinereus*; thus defined, Vombatomorphia comprises all vombatiforms except Phascolarctidae (note that †Thylacoleonidae is considered here Diprotodontia incertae sedis, rather than a member of Vombatiformes; see above). Among the unambiguous craniodental synapomorphies that diagnose this clade is the very shallow subarcuate (or floccular) fossa. The volume of the subarcuate fossa has been suggested to be associated with agility in mammals, with a larger volume indicating greater agility (Olson, 1944; Gannon et al., 1988; Spoor and Leakey, 1996; Jeffery and Spoor, 2006). This hypothesis has not been supported by recent studies (Rodgers, 2011; Ferreira-Cardoso et al., 2017), but there is evidence that, in rodents at least, the petrosal lobules (and the subarcuate fossae that house them) are larger in arboreal forms and smaller in fossorial forms (Arnaudo et al., 2020; Bertrand et al., 2021). Vombatomorphia includes several very large (estimated body mass >100 kg) fossil taxa (Beck et al., 2020), some of which show graviportal adaptations (Camens, 2008; Camens and Wells, 2009) and presumably had low agility. However, †*Muramura* also has a shallow subarcuate fossa, yet was considerably smaller (estimated body mass ~18 kg; Beck et al., 2020: supplementary information), with a relatively gracile postcranial skeleton (Pledge, 2003), and

was presumably much more agile. Pledge (1987: 399) concluded that †*Muramura williamsi* was not fossorial based on its pedal morphology, and postcranial indices for this taxon do not clearly support fossoriality (Beck et al., 2020: table 2). However, in a subsequent paper, Pledge (2003: 554) noted similarities beween the feet of †*Muramura* and fossorially adapted vombatids, suggesting that the second †*Muramura* species known, †*M. pinpensis*, may have been better adapted to burrowing based on its shorter lower limbs.

Definitive vombatomorphians are known from late Oligocene sites in Australia (Archer et al., 1999; Long et al., 2002; Archer and Hand, 2006; Black et al., 2012b), with their initial diversification estimated here as having taken place during the latest Eocene or Oligocene.

†Diprotodontoidea Gill 1872

Contents: †*Neohelos*, †*Ngapakaldia*, †*Nimbadon*, and †*Silvabestius.*

Stem Age: 30.5 Mya (95% HPD: 27.3–34.1 Mya).

Crown Age: 24.4 Mya (95% HPD: 20.2–27.9 Mya).

Unambiguous Craniodental Synapomorphies: Extensive pneumatized endocranial sinuses present within parietal (char. 33: 0→1; ci = 0.500); principal labial and lingual cusps of upper molars connected by well-developed lophs (char. 144: 1→2; ci = 0.200); paraconids and paracristids indistinct or absent on m2 and m3 (char. 161: 0→1; ci = 0.667); cristid obliqua absent or indistinct (char. 167: 0→1; ci = 0.500); and m3 hypoconid lingual to salient protoconid (char. 173: 0→1; ci = 0.045).

Comments: Beck et al. (2020: table 1) defined †Diprotodontoidea as the most inclusive clade including †*Diprotodon opatum*, but not *Phascolarctos cinereus*, *Thylacoleo carnifex* or *Vombatus ursinus*. Following Archer and Bartholomai (1978), the superfamily †Diprotodontoidea is currently considered as comprising the families †Diprotodontidae and †Palorchestidae (see also

Archer, 1984c; Archer et al., 1999; Long et al., 2002; Archer and Hand, 2006; Black, 2008; Black et al., 2012b). We have not included any palorchestids (the so-called marsupial tapirs; Bartholomai, 1978a; Archer, 1984c; Flannery and Archer, 1985; Murray, 1986, 1990; Archer et al., 1999; Long et al., 2002; Archer and Hand, 2006; Black, 2006, 2008; Mackness, 2008; Black et al., 2012b; Trusler, 2016; Trusler and Sharp, 2016; Richards et al., 2019) as terminals here, so we cannot distinguish between craniodental apomorphies for †Diprotodontoidea and those for †Diprotodontidae; however, future inclusion of palorchestids should reveal which apomorphies apply to †Diprotodontidea and which are specific to †Diprotodontidae.

Of the four unambiguous craniodental synapomorphies identified here, three are related to molar morphology, specifically: (1) the presence of well-developed lophs connecting the principal labial and lingual cusps of the upper molars (the fully lophodont condition, also seen in most macropodiforms; char. 144), (2) absence of distinct paraconids or paracristids from m2 and m3 (whereas these structures are retained in fully lophodont macropodiforms; char. 161), and (3) absence of a distinct cristid obliqua (whereas this crest is well developed and forms a midlink on the lower molars of fully lophodont macropodiforms; char. 167).

The oldest diprotodontoids (including members of the family †Diprotodontidae) date to the late Oligocene (Archer et al., 1999; Long et al., 2002; Archer and Hand, 2006; Black, 2008; Black et al., 2012b), and the first diversification among the diprotodontid taxa included here is estimated as having occurred in the late Oligocene or early Miocene. †Diprodontidae includes the largest known marsupials, reaching an extreme with Pleistocene forms such as †*Zygomaturus* and †*Diprotodon*, which have not been included here due to their extremely derived craniodental morphologies (Archer, 1984c; Archer et al., 1999; Long et al., 2002; Wroe et al., 2004; Archer and Hand, 2006; Black, 2008; Price, 2008; Price and Piper, 2009; Black et al., 2012b).

†Ilariidae Tedford and Woodburne, 1987

CONTENTS: †*Ilaria.*

STEM AGE: 30.5 Mya (95% HPD: 27.3–34.1 Mya).

CROWN AGE: N/A.

UNAMBIGUOUS CRANIODENTAL AUTAPOMORPHIES: Mandibular symphysis fused (char. 97: $0 \to 1$; ci = 0.333); masseteric fossa imperforate (char. 99: $1 \to 0$; ci = 0.333); and metacone much larger than paracone (char. 137: $1 \to 2$; ci = 0.400).

COMMENTS: This enigmatic family is currently known from three named species. †*Ilaria illumidens* and †*I. lawsoni* are calf-sized taxa (~150 kg; Beck et al., 2020: supplementary information) from the late Oligocene Pinpa Local Fauna of the Namba Formation, South Australia (Tedford and Woodburne, 1987), whereas †*Kuterintja ngama* is a much smaller taxon (~16 kg; Beck et al., 2020: supplementary information) from sites in South Australia and Queensland (Pledge, 1987a; Myers and Archer, 1997) that are also late Oligocene (Black et al., 2013; Woodhead et al., 2014; Arena et al., 2015). Additionally, an unnamed ilariid, intermediate in size between †*Ilaria* and †*Kuterintja*, is known from the late Oligocene Pwerte Marnte Marnte Fauna of the Northern Territory (Murray and Megirian, 2006b). The apparent absence of representatives of this morphologically distinctive family from sites younger than the late Oligocene suggests that ilariids probably went extinct around the Oligocene-Miocene boundary (Black et al., 2012b).

Only †*Ilaria* has been included as a terminal here, because it is the sole ilariid known from cranial material (Tedford and Woodburne, 1987); other ilariids are known primarily from fragmentary dental material. Ilariids have been universally accepted to be vombatiforms since their original description, but their position within Vombatiformes is controversial (Marshall et al., 1990; Murray, 1998; Archer et al., 1999; Black et al., 2012b) and has varied among phylogenetic analyses (Munson, 1992; Gillespie, 2007; Black, 2008; Black et al., 2012a; Brewer et al., 2015; Gillespie et al., 2016; Beck et al., 2020).

Our undated total-evidence analysis (fig. 32) places †*Ilaria* as sister to †Wynyardiidae (†*Muramura* + †*Namilamadeta*), a result also reported by Black (2008), Black et al. (2012a), and Gillespie et al. (2016). However, our dated total-evidence analysis (fig. 33) places †*Ilaria* in a trichotomy at the base of Vombatomorphia with †Diprotodontidae and Vombatidae + †*Namilamadeta* + †*Muramura* (†Wynyardiidae is paraphyletic in this analysis). The morphological analysis of Beck et al. (2020), meanwhile, placed ilariids as sister to all other vombatomorphians.

The lower molars of ilariids are distinctive (Pledge, 1987a; Tedford and Woodburne, 1987; Myers and Archer, 1997; Murray and Megirian, 2006b). An apparently neomorphic cuspid is present between the protoconid and metaconid, and another is present between the hypoconid and entoconid. We did not score presence of the anterior neomorphic cuspid due to difficulties in defining clearly discrete states (particularly when taking into account the complex trigonid morphology seen in pseudocheirids; Archer, 1984c), but we did score presence/absence and morphology of the posterior neomorphic cuspid, which we refer to as an entostylid (see char. 174). However, presence of a cusplike (versus crestlike) entostylid was not identified as an unambiguous autapomorphy of †Ilariidae in our analyses, presumably because similar structures are also present in †*Namilamadeta* and phascolarctids.

Vombatidae Burnett, 1830

CONTENTS: *Lasiorhinus*, *Vombatus* (fig. 45), and †*Warendja.*

STEM AGE: 22.3 Mya (95% HPD: 17.0–27.9 Mya).

CROWN AGE: 11.4 Mya (95% HPD: 3.7–19.1 Mya).

UNAMBIGUOUS CRANIODENTAL SYNAPOMORPHIES: Masseteric process absent (char. 6: $1 \to 0$; ci = 0.125); hypotympanic sinus floor formed by squamosal only (char. 56: $0 \to 1$; ci = 0.667); post-
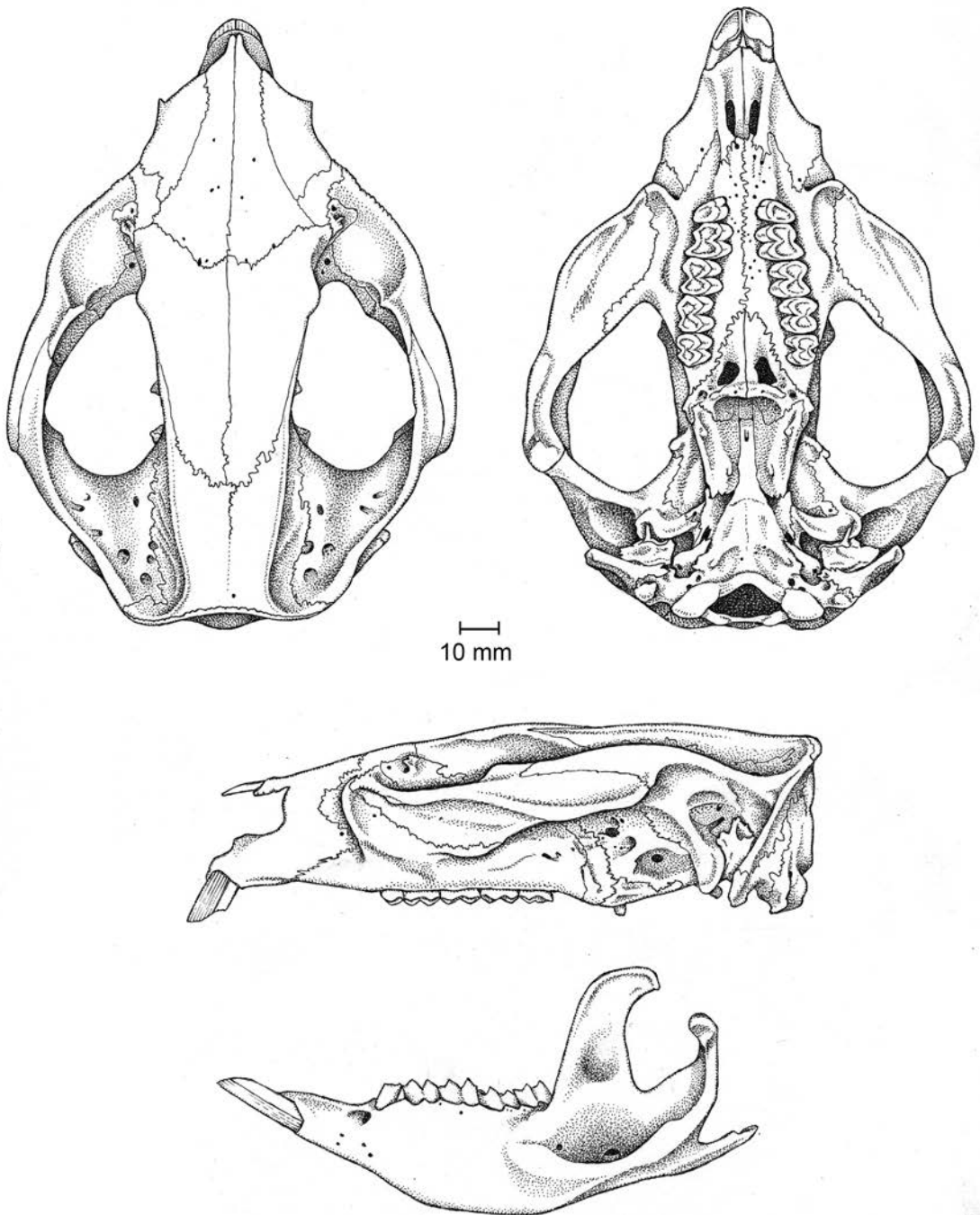
FIG. 45. *Vombatus ursinus* (Diprotodontia, Vombatidae; based on AMNH 200456, an adult of unknown sex from Tasmania, with missing dental elements reconstructed from AMNH 65622, an adult female from Tasmania).

glenoid process of squamosal absent (char. 75: $0{\rightarrow}1$; ci = 0.200); P3 open-rooted (char. 123: $1{\rightarrow}3$; ci = 0.385); and molars with open roots, the crowns growing throughout adulthood (char. 128: $0{\rightarrow}1$; ci = 1.000).

COMMENTS: All our morphological, molecular, and total-evidence analyses recover monophyly of Vombatidae (figs. 27–33). We have included only hypselodont vombatids among our terminals, and hence the presence of open-rooted P3 and open-rooted molars optimize as unambiguous synapomorphies for the family; however, putative vombatids with rooted P3 and rooted molars are known (Stirton et al., 1967b; Murray, 1998; Brewer, 2008; Brewer et al., 2008, 2015, 2018), so the inclusion of such plesiomorphic taxa in future analyses may erode dental character support for the family. The other two unambiguous craniodental synapomorphies identified here are in the glenoid region (namely absence of a masseteric process and absence of a postglenoid process of the squamosal) and are presumably correlated with the unusual masticatory pattern of hypselodont vombatids, in which jaw movement during the power stroke of mastication is primarily or exclusively transverse (Ferreira et al., 1989; Murray, 1998; Crompton et al., 2008; Brewer et al., 2015). The oldest vombatids known from dental material (the early Miocene †*Nimbavombatus* and †*Rhizophascolonus*; Stirton et al., 1967b; Murray, 1998; Brewer et al., 2008, 2015, 2018) are not hypselodont, and they appear to have had an orthal component to their power stroke; however, the morphology of the glenoid region of these taxa, which might be expected to be less specialized than those of hypselodont vombatids, is currently unknown.

Our estimate for the divergence between †*Warendja* and extant vombatids (*Vombatus* and *Lasiorhinus*) is poorly constrained, with the 95% HPD extending into the Pliocene; this raises the possibility that the late Miocene †*Warendja encorensis* may not belong to this genus (see Brewer et al., 2007, 2018: fig. 19).

Phalangerida Aplin and Archer, 1987

CONTENTS: Acrobatidae, †Balbaridae, Burramyidae, †*Ekaltadeta*, Hypsiprymnodontidae, Macropodidae, Petauridae, Phalangeridae, Potoroidae, Pseudocheiridae, and Tarsipedidae.

STEM AGE: 39.8 Mya (95% HPD: 35.5–45.2 Mya).

CROWN AGE: 34.2 Mya (95% HPD: 30.1–38.7 Mya).

UNAMBIGUOUS CRANIODENTAL SYNAPOMORPHIES: Auditory bulla very large, extending posteriorly across the petrosal to contact the exoccipital (char. 55: $1{\rightarrow}3$; ci = 0.300); anterior limb of ectotympanic attached firmly to postglenoid process of squamosal (char. 59: $1{\rightarrow}2$; ci = 0.214); caudal tympanic process of petrosal contacts but not fused with pars cochlearis (char. 68: $0{\rightarrow}1$; ci = 0.154); postgenoid vein emerges from the postglenoid foramen in the posteromedial corner of the glenoid fossa, medial or anteromedial to the postglenoid process (if present) (char. 77: $0{\rightarrow}1$; ci = 0.250); and facial nerve exits middle ear via a a stylomastoid foramen formed by the ectotympanic, posttympanic process of the squamosal and pars canalicularis of the petrosal (char. 79: $0{\rightarrow}4$; ci = 0.625).

COMMENTS: As proposed by Aplin and Archer (1987), the suborder Phalangerida comprises all nonvombatiform diprotodontians (see also Jackson and Groves, 2015: 102–103). All recent molecular and total-evidence phylogenies, including those presented here (figs. 27–29, 32, 33), strongly support monophyly of Phalangerida to the exclusion of living vombatiforms (*Phascolarctos*, *Lasiorhinus*, and *Vombatus*). All five features that optimize as unambiguous craniodental synapomorphies of Phalangerida in our dated total-evidence analysis are in the basicranium, but all show subsequent modifications (including reversals) among different phalangeridan subclades.

Within Phalangerida, our molecular (figs. 27–29) and total-evidence (figs. 32, 33) analyses agree with most recent molecular studies (e.g., Beck, 2008a; Meredith et al., 2008b, 2009a, 2009c,

2011; Phillips and Pratt, 2008; Mitchell et al., 2014; May-Collado et al., 2015; Duchêne et al., 2018; Álvarez-Carretero et al., 2021) in strongly supporting three major clades: Petauroidea (Acrobatidae, Tarsipedidae, Petauridae, and Pseudocheiridae), Burramyoidea + Phalangeroidea, and Macropodiformes. By contrast, the branching relationships among these three clades have proven difficult to resolve. In our molecular and total-evidence analyses we consistently found Petauroidea and Macropodiformes to be sister taxa in agreement with some molecular studies (Meredith et al., 2011; Mitchell et al., 2014; May-Collado et al., 2015) but not others (Phillips and Pratt, 2008; Meredith et al., 2009a, 2009c). Indeed, Meredith et al. (2009a) proposed the name Australoplagiaulacoidea for the Burramyoidea + Phalangeroidea + Macropodoidea clade found in their analyses. However, Duchêne et al. (2018) found that different sets of nuclear genes support alternative resolutions of this trichotomy, a result they attributed to incomplete lineage sorting.

The oldest known phalangeridans include representatives of several already distinct modern families from the late Oligocene of Australia (Flannery and Rich, 1986; Archer et al., 1999; Long et al., 2002; Archer et al., 2006; Archer and Hand, 2006; Black et al., 2012b; Butler et al., 2017). We estimate that Phalangerida began to diversify during the late Eocene or early Oligocene.

Burramyoidea + Phalangeroidea

CONTENTS: Burramyidae and Phalangeridae.
STEM AGE: 34.2 Mya (95% HPD: 30.1–38.7 Mya).
CROWN AGE: 29.9 Mya (95% HPD: 25.8–35.4 Mya).
UNAMBIGUOUS CRANIODENTAL SYNAPOMORPHIES: None.
COMMENTS: Our molecular (figs. 27–29) and total-evidence (figs. 32, 33) analyses agree with most recent molecular studies (e.g., Beck, 2008a; Meredith et al., 2008b, 2009a, 2009c,

2011; Phillips and Pratt, 2008; Mitchell et al., 2014; May-Collado et al., 2015; Duchêne et al., 2018; Álvarez-Carretero et al., 2021) in supporting a clade comprising Phalangeridae (the only extant phalangeroid family) and Burramyidae (the only burramyoid family described to date). However, we found no unambiguous craniodental synapomorphies that support this clade. Two craniodental features optimize as synapomorphies of this clade under Accelerated Transformation only—masseteric fossa imperforate (char. 99: 1→0; $ci = 0.333$) and first lower premolar present (char. 153: 1→0; $ci = 0.500$)—although both of these traits appear to be reversals. A third trait optimizes as a synapomorphy under Delayed Transformation—posterior limb of ectotympanic seamlessly fused with pars canalicularis of the petrosal and/or posttympanic process of the squamosal char. 60: 1→2; $ci = 0.333$.

Aplin and Archer's (1987) concept of Phalangeroidea included Phalangeridae together with two fossil families, †Ektopodontidae and †Miralinidae, that have not been included here due to a lack of well-preserved cranial material. The earliest fossil records of burraymids and phalangeroids are from the late Oligocene of Australia (Archer et al., 1999; Long et al., 2002; Archer and Hand, 2006; Black et al., 2012b), which is broadly congruent with our late Eocene to Oligocene estimate for the divergences among these taxa.

Burramyoidea Broom, 1898

CONTENTS: *Burramys* (fig. 46) and *Cercartetus*.
STEM AGE: 29.9 Mya (95% HPD: 25.8–35.4 Mya).
CROWN AGE: 21.6 Mya (95% HPD: 13.5–26.2 Mya).
UNAMBIGUOUS CRANIODENTAL SYNAPOMORPHIES: Scars of M. temporalis origin on braincase not fused middorsally to form sagittal crest in adults (char. 27: 1→0; $ci = 0.059$) and presphenoid exposed in roof of nasopharyngeal fossa above posterior palate (char. 43: 1→0; $ci = 0.091$).
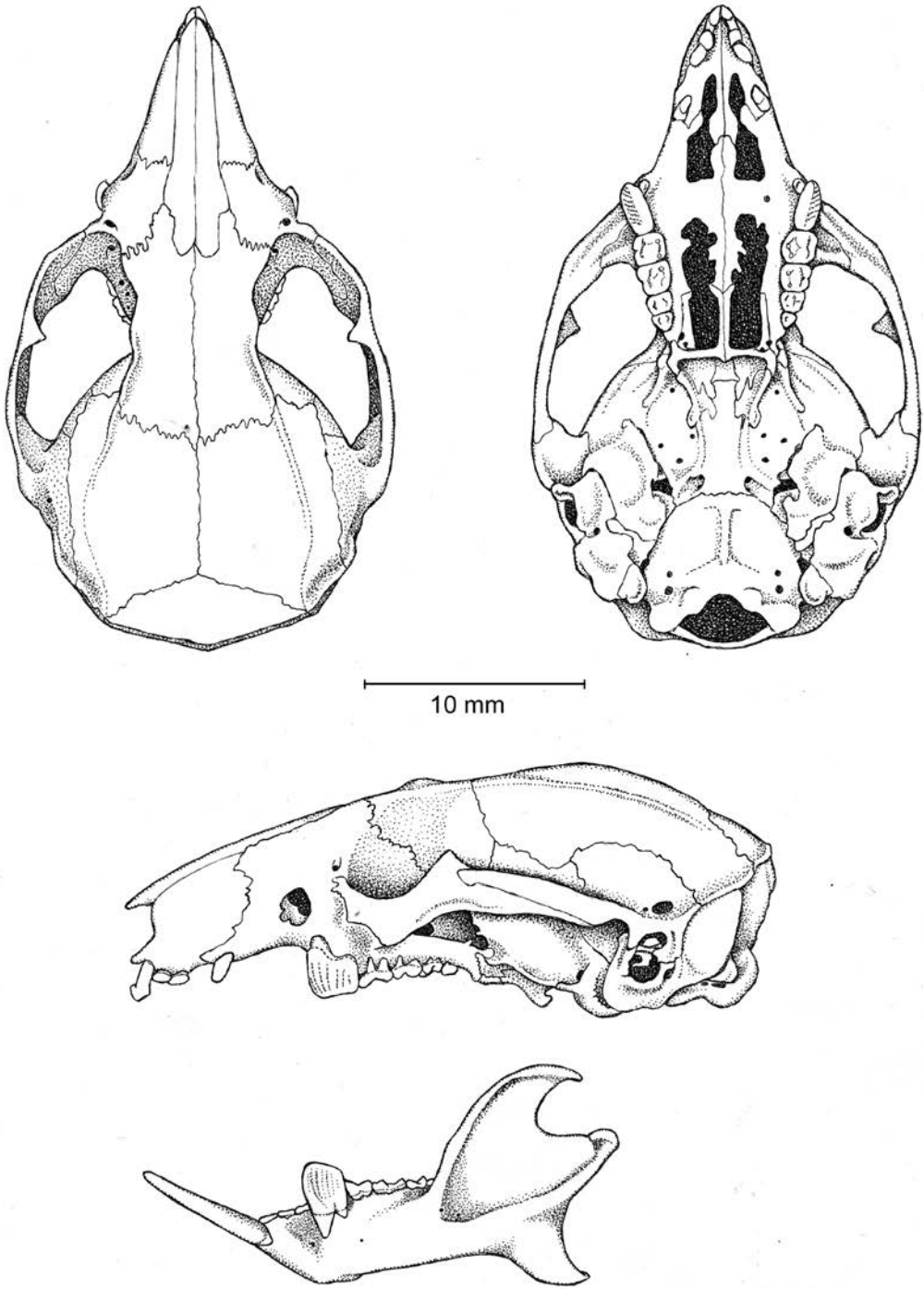
FIG. 46. *Burramys parvus* (Diprotodontia, Burramyidae; based on MVZ 161313, a captive-bred adult of unknown sex).

COMMENTS: Archer (1984c) and Aplin and Archer (1987) gave detailed summaries of the various attempts to unravel the affinities of "pygmy possums." Briefly, Burramyidae was first recognized as a distinct family by Kirsch (1968a, 1968b), who included within it *Burramys*, *Cercartetus*, and *Acrobates*. Kirsch and Calaby (1977) subsequently also classified *Distoechurus* as a burramyid, based on its morphological resemblance to the other three genera. However, Aplin and Archer (1987) removed *Acrobates* and *Distoechurus* to their newly created family Acrobatidae (see Acrobatidae below), leaving *Burramys* and *Cercartetus* as the sole known constituent genera of Burramyidae. Aplin and Archer (1987) placed Burramyidae in its own superfamily, Burramyoidea, based on "the degree of morphological distinction of the burramyids and of their apparently wide phyletic separation from other possums" (Aplin and Archer, 1987: lxi). Aplin and Archer (1987: lx) remarked that monophyly of *Burramys* + *Cercartetus* was "not certainly known" at that time, but subsequent molecular studies have consistently recovered this clade with strong support (Phillips and Pratt, 2008; Meredith et al., 2009a; Mitchell et al., 2014; May-Collado et al., 2015; Duchêne et al., 2018; Álvarez-Carretero et al., 2021), and it is strongly supported in our molecular (figs. 27–29) and total-evidence (figs. 32, 33) analyses, although not in our craniodental analyses (figs. 30, 31).

Fragmentary remains of burramyids are known from the late Oligocene of Australia, and these have been referred to the modern genus *Burramys* (Pledge, 1987b; Brammall and Archer, 1997). Fossil material of *Cercartetus* has not been formally described to date, but fossils have apparently been recovered from early to middle Miocene deposits at Riversleigh World Heritage Area (Brammall and Archer, 1999; Archer and Hand, 2006; Black et al., 2012b). Earlier reports of *Cercartetus*-like fossils from the late Oligocene of central Australia (e.g., Tedford et al., 1977; Rich et al., 1982; Woodburne et al., 1985) actually represent †Pilkipildridae, an extinct phalangeridan family of uncertain relationships (Archer et al., 1987; Brammall and Archer, 1999; Long et al., 2002; Archer and Hand, 2006; Black et al., 2012b). The apparent presence of as yet undescribed *Cercartetus* specimens in the early or middle Miocene, as discussed above, is roughly congruent with our late Oligocene to middle Miocene estimate for the time of divergence between *Burramys* and *Cercartetus*. The late Oligocene *Burramys* specimens may predate our estimate, but their phylogenetic relationship to extant *Burramys* and *Cercartetus* species has not been rigorously tested (the phylogenetic analysis presented by Brammall and Archer, 1997, assumed a priori that *Burramys*, including the fossil species, is monophyletic to the exclusion of *Cercartetus*).

Phalangeroidea Thomas, 1888

CONTENTS: *Ailurops*, †*Onirocuscus*, *Phalanger* (fig. 47), *Spilocuscus*, *Strigocuscus*, *Trichosurus*, "*Trichosurus*" †*dicksoni*, and *Wyulda*.

STEM AGE: 29.9 Mya (95% HPD: 25.8–35.4 Mya).

CROWN AGE: 18.4 Mya (95% HPD: 14.1–23.7 Mya).

UNAMBIGUOUS CRANIODENTAL SYNAPOMORPHIES: One lacrimal foramen usually present (char. 10: 0→1; ci = 0.063); squamosal and pars canalicularis of the petrosal extensively pneumatized and cancellous (char. 87: 0→1; ci = 0.250); mastoid exposure of petrosal restricted to ventralmost part of occiput, not contacting supraoccipital (char. 90: 0→1; ci = 1.000); major crest of semi- or fully sectorial P3 oriented posterolingual to anterolabial (char. 127: 1→0; ci = 0.400); cristid obliqua with strongly developed buccal kink (char. 168: 0→1; ci = 0.333); and entocristid with distinct anterolabial kink (char. 177: 0→2; ci = 0.250).

COMMENTS: Monophyly of the only phalangeroid family included here, namely Phalangeridae, is strongly supported by a number of distinctive craniodental apomorphies, several of which show relatively low homoplasy. Rela-

10 mm
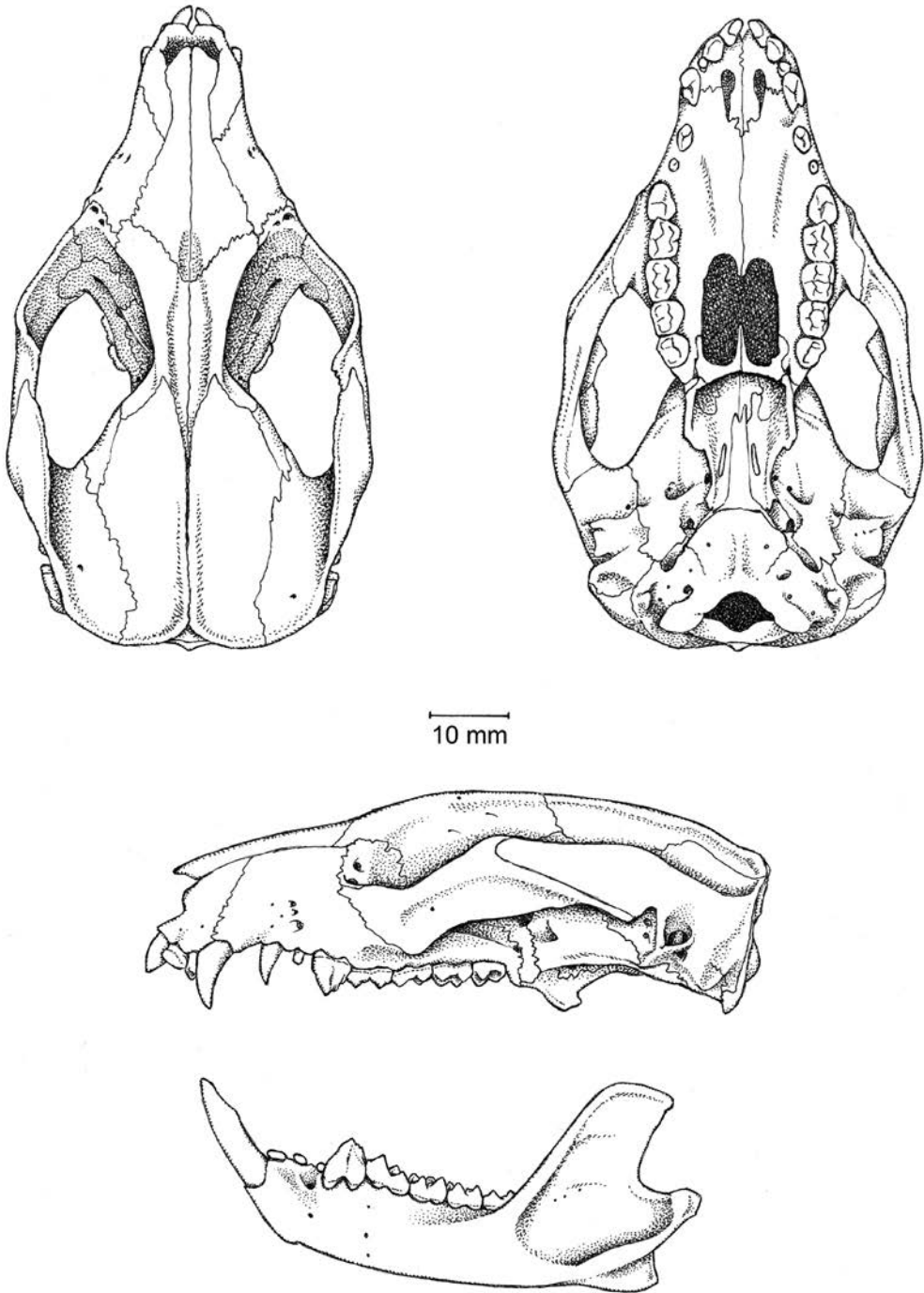
FIG. 47. *Phalanger intercastellanus* (Diprotodontia, Phalangeridae; based on AMNH 157208, an adult male from Milne Bay Province, Papua New Guinea).

tionships among modern phalangerids in our molecular (figs. 27–29) and total-evidence (figs. 32, 33) analyses are congruent with the results of recent molecular studies (Ruedas and Morales, 2005; Raterman et al., 2006; Phillips and Pratt, 2008; Meredith et al., 2009a; Mitchell et al., 2014; May-Collado et al., 2015; Duchêne et al., 2018; Álvarez-Carretero et al., 2021; see also Jackson and Groves, 2015; Eldridge et al., 2019) in supporting a split between *Trichosurus* + *Wyulda* (= Trichosurinae) and the remaining modern genera. Within Phalangerinae, there is support for *Ailurops* + *Strigocuscus* (=Ailuropinae) and *Phalanger* + *Spilocuscus* (= Phalangerinae), again in agreement with recent molecular studies (Ruedas and Morales, 2005; Raterman et al., 2006; Meredith et al., 2009a; Mitchell et al., 2014; May-Collado et al., 2015; Álvarez-Carretero et al., 2021; see also Jackson and Groves, 2015; Eldridge et al., 2019).

The relationships of the two fossil phalangerids included here, "*Trichosurus*" †*dicksoni* and †*Onirocuscus reidi*, differ markedly between the undated and dated total-evidence analyses. In the undated analysis (fig. 32), "*Trichosurus*" †*dicksoni* forms a clade with *Wyulda*, with the modern *Trichosurus* sister to this clade (suggesting that "*T.*" †*dicksoni* is a trichosurine), whereas †*Onirocuscus* is sister to *Strigocuscus* within Ailuropinae; the latter result is notably similar to the relationship originally inferred by Flannery and Archer (Flannery and Archer, 1987a), who placed the species currently known as †*O. reidi* within *Strigocuscus*. By contrast, in the dated analysis (fig. 33), both fossil taxa are placed outside crown-clade Phalangeridae, with †*Onirocuscus* the first to diverge, reflecting the impact that incorporating temporal information can have on tree topology (see also Lee and Yates, 2018; Beck and Taglioretti, 2020; King and Beck, 2020). Crosby's (2007: fig. 7) informal phylogeny also suggests that "*T.*" †*dicksoni* and †*Onirocuscus* are not closely related to the living trichosurines (*Trichosurus* and *Wyulda*) and *Strigocus-*

cus respectively, but it is otherwise incongruent with our molecular and total-evidence results and with other recent molecular studies (Ruedas and Morales, 2005; Raterman et al., 2006; Meredith et al., 2009a; Mitchell et al., 2014; May-Collado et al., 2015; Álvarez-Carretero et al., 2021). With "*T.*" †*dicksoni* and †*Onirocuscus* excluded, our dated total-evidence analysis suggests that the phalangerid crown clade is comparatively young, dating to the middle-to-late Miocene (median estimate: 11.0 Mya; 95% HPD: 8.0–13.1 Mya).

The oldest known fossil phalangerid is †*Eocuscus sarastamppi*, from the late Oligocene Ditjimanka Local Fauna of the Etadunna Fomation in South Australia (Case et al., 2008). This interesting taxon is known from a single right maxilla, and so has not been included in our analyses, but it exhibits a number of dental features that are likely plesiomorphic relative to other phalangerids. These include the morphology of its P3, which has its major cutting crest parallel to the upper molars rather than oriented posterolingual to anterolabially as in most other known phalangerids (see char. 127); additionally, this crest lacks obvious enamel ridges (see char. 126), suggesting that the presence of these ridges (as seen in most phalangerids, *Burramys*, and many macropodiforms) may have arisen multiple times within Phalangerida. Lastly, the protoloph and metaloph of M2 each have a centrally placed cusp in †*E. sarastamppi*; although these central cusps were identified as neomorphs by Case et al. (2008), we consider them homologs of the paracone and metacone for reasons previously discussed at length (see char. 136).

Petauroidea Bonaparte, 1832

Contents: Acrobatidae, Petauridae, Pseudocheiridae, and Tarsipedidae.

Stem Age: 33.0 Mya (95% HPD: 29.3–37.7 Mya).

Crown Age: 29.0 Mya (95% HPD: 26.4–32.7 Mya).

Unambiguous Craniodental Synapomorphies: Maxillary foramen bordered by lacrimal (char. 14: 1→0; ci = 0.200); postorbital process formed by frontal and parietal (char. 19: 1→0; ci = 0.400); scars of M. temporalis origin on braincase not fused middorsally to form sagittal crest in adults (char. 27: 1→0; ci = 0.059); dP3 very small, nonoccluding, and structurally simplified or absent (char. 120: 0→2; ci = 0.118); and third upper premolar (P3) conventionally premolariform (char. 123: 2→0; ci = 0.385).

Comments: The superfamily Petauroidea comprises four morphologically disparate families of phalangeridans: Acrobatidae, Tarsipedidae, Petauridae, and Pseudocheiridae. Nevertheless, petauroid monophyly is strongly supported in our molecular (figs. 27–29) and total-evidence (figs. 32, 33) analyses, as it has also been in other recent molecular studies (Phillips and Pratt, 2008; Meredith et al., 2009a, 2009c, 2011; Mitchell et al., 2014; May-Collado et al., 2015; Duchêne et al., 2018; Álvarez-Carretero et al., 2021). One of the five unambiguous craniodental synapomorphies found to support Petauroidea is a reversal, namely reacquisition of a conventionally premolariform morphology of the third upper premolar from a fully sectorial precursor that is inferred as having evolved deeper within Diprotodontia.

The branching order within Petauroidea recovered in both of our total-evidence analyses (figs. 32, 33)—with Petauridae and Pseudocheiridae forming a clade, Tarsipedidae sister to this, and Acrobatidae the first family to diverge—is congruent with the results of recent molecular studies (Phillips and Pratt, 2008; Meredith et al., 2009a, 2009c, 2011; Mitchell et al., 2014; May-Collado et al., 2015; Duchêne et al., 2018; Álvarez-Carretero et al., 2021). The oldest described petauroids are pseudocheirids from the late Oligocene of central Australia and Riversleigh World Heritage Area (Archer et al., 1999; Long et al., 2002; Archer and Hand, 2006; Roberts, 2008; Roberts et al., 2009; Black et al., 2012b), indicating that the petauroid crown clade had already begun to diversify by this time; our estimated divergence times imply that the first split within Petauroidea occurred during the Oligocene.

Acrobatidae Aplin (in Aplin and Archer), 1987

Contents: *Acrobates* and *Distoechurus* (fig. 48).

Stem Age: 29.0 Mya (95% HPD: 26.4–32.7 Mya).

Crown Age: 14.1 Mya (95% HPD: 10.3–18.1 Mya).

Unambiguous Craniodental Synapomorphies: Foramen for ramus lateralis of mandibular nerve present at anteromedial end of the glenoid fossa (char. 53: 0→1; ci = 1.000); hypotympanic sinus floor formed by petrosal and "entotympanic-like" ossification (char. 56: 0→2; ci = 0.667); ear canal largely occluded by bony disk (char. 62: 0→1; ci = 1.000); malleo-incudal and stapedio-incudal articulations fused, without sutures (char. 63: 0→1; ci = 1.000); stapedial footplate strongly convex (char. 66: 1→2; ci = 0.286); process of the exoccipital extending anterolaterally to the exit of the facial nerve (stylomastoid notch or foramen) present (char. 80: 0→1; ci = 0.500); squamosal and the pars canalicularis of the petrosal seamlessly fused, with no evidence of a suture between the two bones even in juveniles (char. 88: 0→1; ci = 1.000); diastema between C1 and upper incisor row absent (char. 110: 0→1; ci = 0.167); premolariform second upper premolar (P2) distinctly taller than premolariform P3 (char. 119: 2→0; ci = 0.118); M4 absent (char. 129: 0→1; ci = 0.667); and neomorphic labial cingulum present on M1–3 (char. 133: 0→1; ci = 0.200).

Comments: The distinctiveness of *Acrobates* and *Distoechurus* relative to other "possums" was recognized by Aplin and Archer (1983), Archer (1984c), and Baverstock (1984). These two genera were formally referred to their own family, Acrobatidae, by Aplin (in Aplin and Archer, 1987), who identified a long list of distinctive features of the hard and soft tissues shared by *Acrobates* and *Distoechurus*. We also find the family Acrobatidae
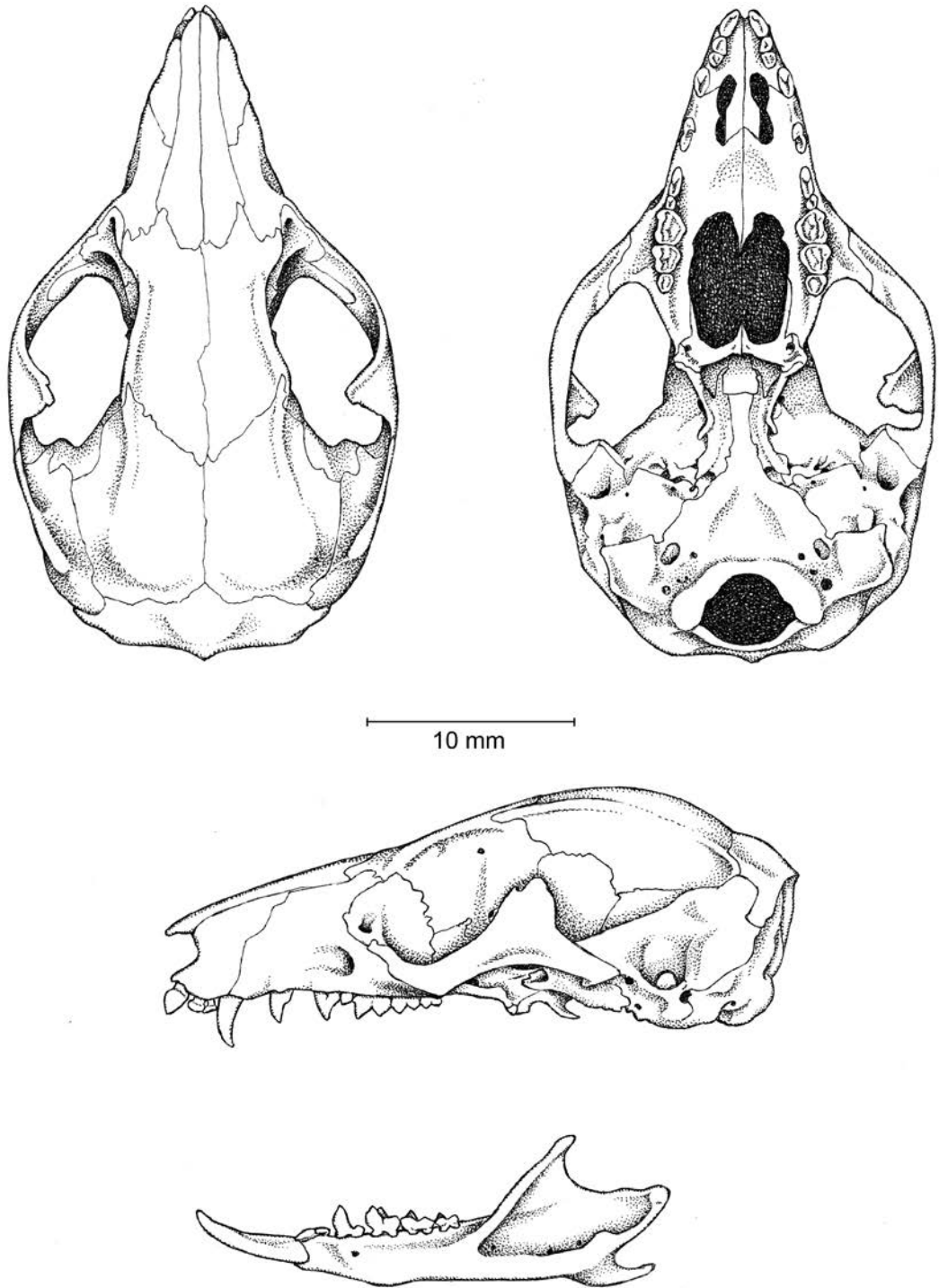
FIG. 48. *Distoechurus pennatus* (Diprotodontia, Acrobatidae; based on AMNH 221721, an adult of unknown sex from Irian Jaya).

to be characterized by numerous craniodental synapomorphies, including several uniquely derived features of the auditory region and associated basicranial structures.

Aplin and Archer (1987: lix–lx) argued that acrobatids share a number of distinctive morphological synapomorphies with *Tarsipes* (the only known representative of the family Tarsipedidae) and that the two families should be placed together in the superfamily Tarsipedoidea, of uncertain relationships to other phalangeridans. However, our molecular (figs. 27–29) and total-evidence (figs. 32, 33) analyses agree with other recent molecular studies in placing Acrobatidae in the superfamily Petauroidea, together with Tarsipedidae, Petauridae, and Pseudocheiridae. A close relationship between Acrobatidae and Tarsipedidae is not supported here or in recent molecular studies (Phillips and Pratt, 2008; Meredith et al., 2009a, 2009c, 2011; Mitchell et al., 2014; May-Collado et al., 2015; Duchêne et al., 2018; Álvarez-Carretero et al., 2021); instead, Acrobatidae is consistently found to be the first petauroid family to diverge, with Tarsipedidae sister to Petauridae + Pseudocheiridae. By implication, the putative synapomorphies shared by acrobatids and *Tarsipes* (Aplin and Archer, 1987) either evolved convergently in those clades, or they are synapomorphies of Petauroidea that were secondarily reversed in the common ancestor of petaurids and pseudocheirids (Phillips and Pratt, 2008: 602). Of these two possibilities, the second appears less likely given the more conventionally phalangeridan morphology of petaurids and pseudocheirids compared to acrobatids and *Tarsipes* (Aplin and Archer, 1987; Aplin, 1987, 1990).

Fossil acrobatids have been found in late Oligocene to middle Miocene sites at Riversleigh World Heritage Area (Brammall and Archer, 1999; Long et al., 2002; Archer and Hand, 2006; Black et al., 2012b; Fabian, 2012). Fabian (2012) concluded that these fossils include early members of both the *Acrobates* and the *Distoechurus* lineages, which, therefore, must have diverged prior to the late Oligocene, a temporal inference

that is congruent with the results of several recent molecular studies (Meredith et al., 2009a; Mitchell et al., 2014; Duchêne et al., 2018). By contrast, our dated total-evidence analysis (fig. 33) supports a somewhat younger (Miocene) date for the *Acrobates-Distoechurus* divergence; if so, then the late Oligocene Riversleigh acrobatids should fall outside the crown clade. However, these potentially important fossils have yet to be formally described.

Also of interest are reports of a currently unnamed "possum" from middle Pleistocene deposits at Mount Etna in Queensland. Hocknull (2005; 2009) considered this mysterious fossil to be superfamily incertae sedis but noted that it has features characteristic of both burramyids and acrobatids. Several authors have concluded that burramyids retain more plesiomorphic craniodental features than other phalangeridans (e.g., Thomas, 1888; Bensley, 1903; Aplin and Archer, 1987; Wroe et al., 1998; but see Winge, 1941; Archer, 1976e), so it is possible that the Mount Etna taxon is a stem acrobatid retaining plesiomorphic similarities to burramyids. However, regardless of its true affinities, the Mount Etna "possum" considerably postdates the inferred origin of the acrobatid crown clade.

Tarsipedidae Gervais and Verreaux, 1842

CONTENTS: *Tarsipes* (fig. 49).

STEM AGE: 27.1 Mya (95% HPD: 24.9–29.6 Mya).

CROWN AGE: N/A.

UNAMBIGUOUS CRANIODENTAL AUTAPOMORPHIES: Nasals very broad posteriorly, contacting lacrimals on each side (char. 2: 1→0; $ci = 0.667$); one lacrimal foramen usually present (char. 10: 0→1; $ci = 0.063$); jugal terminates well anterior to glenoid region (char. 21: 0→1; $ci = 1.000$); transverse canal foramen absent (char. 51: 1→0; $ci = 0.200$); auditory bulla large, contacting rostral tympanic process of petrosal (char. 55: 3→2; $ci = 0.300$); ectotympanic forms a closed tube that completely encircles the ear canal (char. 58: 0→1; $ci = 0.167$); anterior limb of ectotympanic loosely
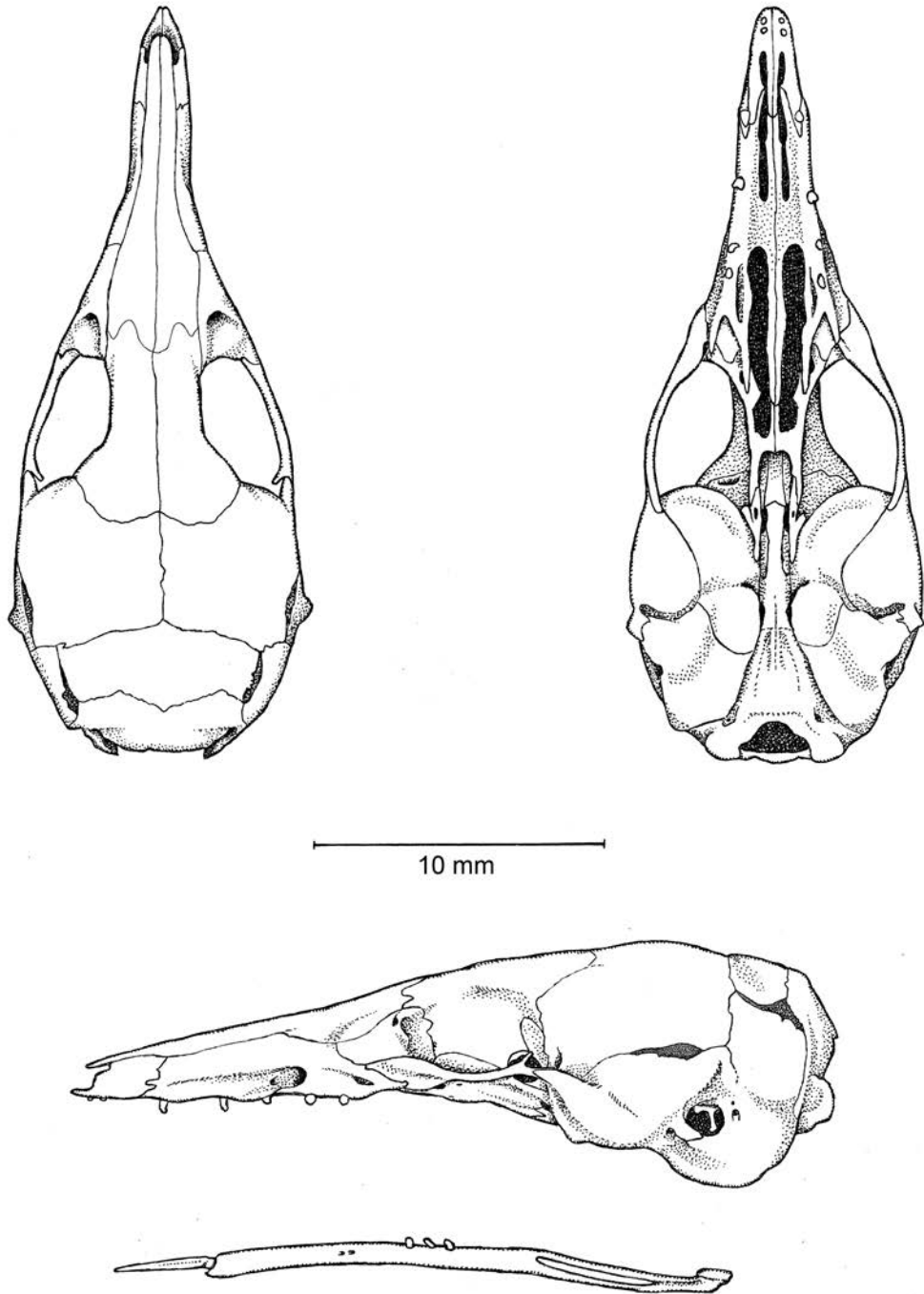
FIG. 49. *Tarsipes rostratus* (Diprotodontia, Tarsipedidae; based primarily on WAM M-6702, an adult male from Western Australia).

attached to the petrosal or squamosal behind postglenoid process (char. 59: 2→1; ci = 0.214); tensor tympani muscle enclosed ventrally by a bridge of bone derived from petrosal (char. 70: 0→1; ci = 1.000); postglenoid process of squamosal absent (char. 75: 0→1; ci = 0.200); postglenoid vein exits skull via the postglenoid foramen above the ear region, posterior or posteromedial to the glenoid fossa (char. 77: 1→0; ci = 0.250); zygomatic epitympanic sinus absent (char. 85: 1→0; ci = 0.500); only one hypoglossal foramen present (char. 92: 0→1; ci = 0.500); mandible much reduced and splintlike, lacking coronoid and angular processes (char. 96: 0→1; ci = 1.000); masseteric fossa perforated by a large unossified vacuity (char. 99: 1→3; ci = 0.333); and postcanine teeth are featureless spicules (char. 113: 0→1; ci = 1.000).

COMMENTS: Aplin and Archer (1987: lii) aptly described *Tarsipes rostratus*, the only known tarsipedid, as the "paragon of autapomorphic specialisation within Diprotodontia," and we identify a correspondingly long list of craniodental apomorphies characterizing this taxon, many of which are unique to *Tarsipes* within Metatheria. There is no known fossil record of *Tarsipes* prior to the latest Pleistocene (Balme et al., 1978; Archer, 1984c; Brammall and Archer, 1999; Long et al., 2002; Archer and Hand, 2006) despite the inferred antiquity of the tarsipedid lineage, which we estimate to have diverged from other petauroids during the Oligocene. However, it is possible that at least some of the specialized features of *Tarsipes* arose comparatively recently, such that plesiomorphic tarsipedids might exist unrecognized among the smaller fossil "possums" known from Oligo-Miocene sites in Australia. Unfortunately, the degenerate postcanine dentition of *Tarsipes* precludes relevant dental comparisons, and none of the currently known fossil "possum" familes are known from well-preserved cranial material (Woodburne and Clemens, 1986c; Archer et al., 1987; Woodburne et al., 1987a; Crosby and Archer, 2000; Crosby, 2002a; Crosby et al., 2004; Schwartz, 2006a; Archer et al., 2018).

Petauridae Bonaparte, 1832

CONTENTS: *Dactylonax*, *Dactylopsila*, *Gymnobelideus*, and *Petaurus* (fig. 50).

STEM AGE: 24.4 Mya (95% HPD: 23.6–26.1 Mya).

CROWN AGE: 18.8 Mya (95% HPD: 15.9–22.4 Mya).

UNAMBIGUOUS CRANIODENTAL SYNAPOMORPHIES: None.

COMMENTS: Monophyly of Petauridae is strongly supported in our molecular (figs. 27–29) and total-evidence (figs. 32, 33) analyses, but we conspicuously failed to identify any unambiguous craniodental synapomorphies for the family. Instead, petaurids apparently retain the plesiomorphic states for many characters that evolved derived conditions along the branch leading to its sister taxon, Pseudocheiridae.[35] Nevertheless, five craniodental features optimize as petaurid synapomorphies under Accelerated Transformation only: the foramen rotundum is laterally exposed and separate from the sphenorbital fissure (char. 17: 1→0; ci = 0.286); postorbital processes are present (char. 18: 0→1; ci = 0.042); the frontal and squamosal are in contact on the lateral aspect of braincase (char. 26: 0→1; ci = 0.071); the presphenoid is exposed in the roof of the nasopharyngeal fossa above the posterior palate (char. 43: 1→0; ci = 0.091); the major crest of the semisectorial or fully sectorial P3 is oriented posterolabial to anterolingual (char. 127: 1→2; ci = 0.400); and the cristid obliqua of m1 contacts the metacristid labial to the metaconid (char. 169: 0→1; ci = 0.250).

Phylogenetic analyses of the fossil petauroid †*Djaludjangi yadjana* (not included in our analyses as it is known from partial dentitions only) suggests that certain dental features of petaurids reconstructed here as plesiomorphic, such as the absence of any trace of selenodonty, may in fact be secondary reversals (Brammall, 1998). Archer

---

[35] Interestingly, Roberts (2008) found the opposite result in some of her phylogenetic analyses of living and fossil pseudocheirids, wherein she failed to identify any unambiguous craniodental synapomorphies for Pseudocheiridae.
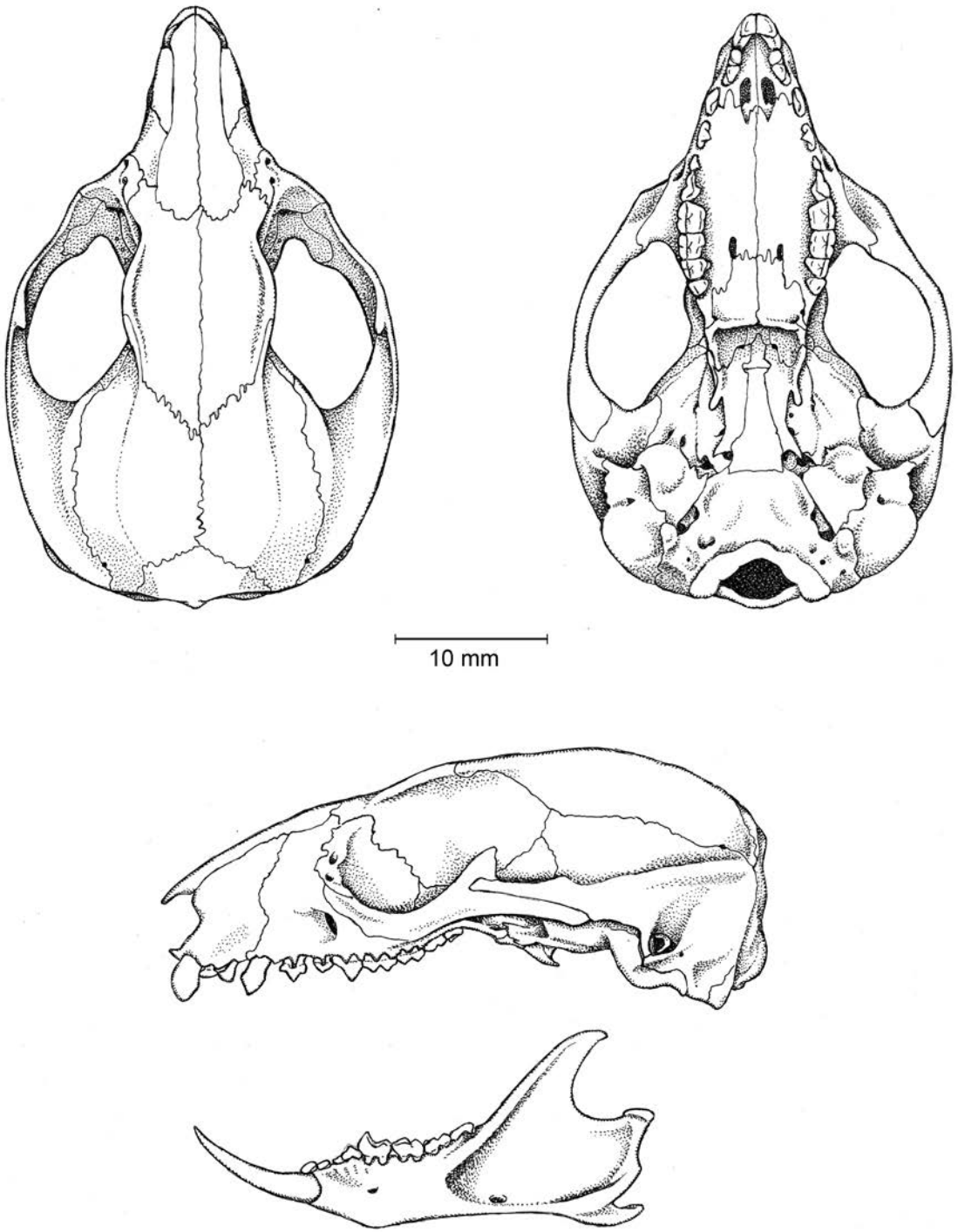
FIG. 50. *Petaurus breviceps* (Diprotodontia, Petauridae; based on AMNH 159481, an adult female from Normanby Island, Papua New Guinea).

(1984c: fig. 189), Archer et al. (1987), and Brammall (1998) listed a number of putative morphological synapomorphies for Petauridae, but, in general, we did not find these to be amenable for scoring as discrete characters. There is a pressing need for detailed studies of fossil and Recent phalangeridans to unravel patterns of craniodental evolution, because it seems plausible that "possum" evolution has been characterized by secondary simplification of certain features (including possible loss of selenodonty in petaurids) as well as the more widely recognized appearance of morphological novelties (Winge, 1941; Archer, 1976e; Archer et al., 1987; Woodburne et al., 1987a; Springer and Woodburne, 1989; Brammall, 1998).

Within Petauridae, all our molecular (figs. 27–29) and total-evidence (figs. 32, 33) analyses placed *Gymnobelideus* in a clade with the dactylopsilines *Dactylopsila* and *Dactylonax*, to the exclusion of *Petaurus*. This arrangement was also recovered by the molecular analyses of Meredith et al. (2009a) and May-Collado et al. (2015), whereas the molecular analyses of Mitchell et al. (2014) and Álvarez-Carretero et al. (2021) found a *Petaurus* + *Gymnobelideus* clade. The cause of this incongruence between studies is unclear, and these different resolutions have important implications for the evolution of gliding adaptations (present in *Petaurus* and *Gymnobelideus*, absent in dactylopsilines) within Petauridae. The topology favored here implies that *Gymnobelideus* and *Petaurus* evolved their gliding patagia independently, or (perhaps less likely) that dactylopsilines have secondarily lost patagia.[36]

Fossil petaurids have been reported from Oligo-Miocene sites in Australia, but much of this material remains undescribed (Brammall, 1998; Archer et al., 1999; Archer and Hand, 2006). †*Djaludjangi yadjana*, mentioned above, shares some putative synapomorphies with petaurids, but this has not been tested via suitably comprehensive phylogenetic analysis (†*Djaludjangi* was

included in the analyses of Roberts, 2008, but these were specifically focused on relationships within Pseudocheiridae), and Brammall's (1998) recommendation that this taxon be treated as Petauroidea incertae sedis has been followed by subsequent authors (Long et al., 2002; Archer and Hand, 2006; Black et al., 2012b).

Tedford et al. (1975) identified fragmentary craniodental remains, including two molars, from the early Miocene Geilston Bay Local Fauna of Tasmania (Tedford et al., 1975; Tedford and Kemp, 1998; Black et al., 2012b; Woodhead et al., 2014) as representing a probable phalangerid, but Tedford and Kemp (1998) subsequently referred them to Petauroidea. Crosby et al. (2001) argued that these molars more likely represent a phalangerid based on the presence of well-developed lophs, but Roberts (2008) continued to refer to them as petauroid, although her phylogenetic analyses did not unambiguously support petauroid affinities for them. Also of interest is Hocknull's (2005, 2009) report of a new, currently unnamed petaurid from middle Pleistocene deposits at Mount Etna in Queensland that appears to retain several dental plesiomorphies relative to Recent petaurids; future phylogenetic analyses including this taxon may help clarify relationships both within the family and between petaurids and other petauroids.

Pseudocheiridae Winge, 1893

CONTENTS: *Petauroides*, *Petropseudes*, *Pseudocheirus*, *Pseudochirops* (fig. 51), and *Pseudochirulus*.

STEM AGE: 24.4 Mya (95% HPD: 23.6–26.1 Mya).

CROWN AGE: 15.8 Mya (95% HPD: 11.7–18.5 Mya).

UNAMBIGUOUS CRANIODENTAL SYNAPOMORPHIES: Paroccipital process a large erect process usually directed ventrally (char. 93: 1→2; c_i = 0.100); mandible usually with two or more mental foramina (char. 98: 0→1; c_i = 0.063); P2 "pseudocheiriform" (char. 118: 0→1; c_i = 0.444); P3

---

[36] See Heritage et al. (2016) and Fabre et al. (2018) for a similar controversy regarding the evolution of gliding adaptations in anomalure rodents.

10 mm
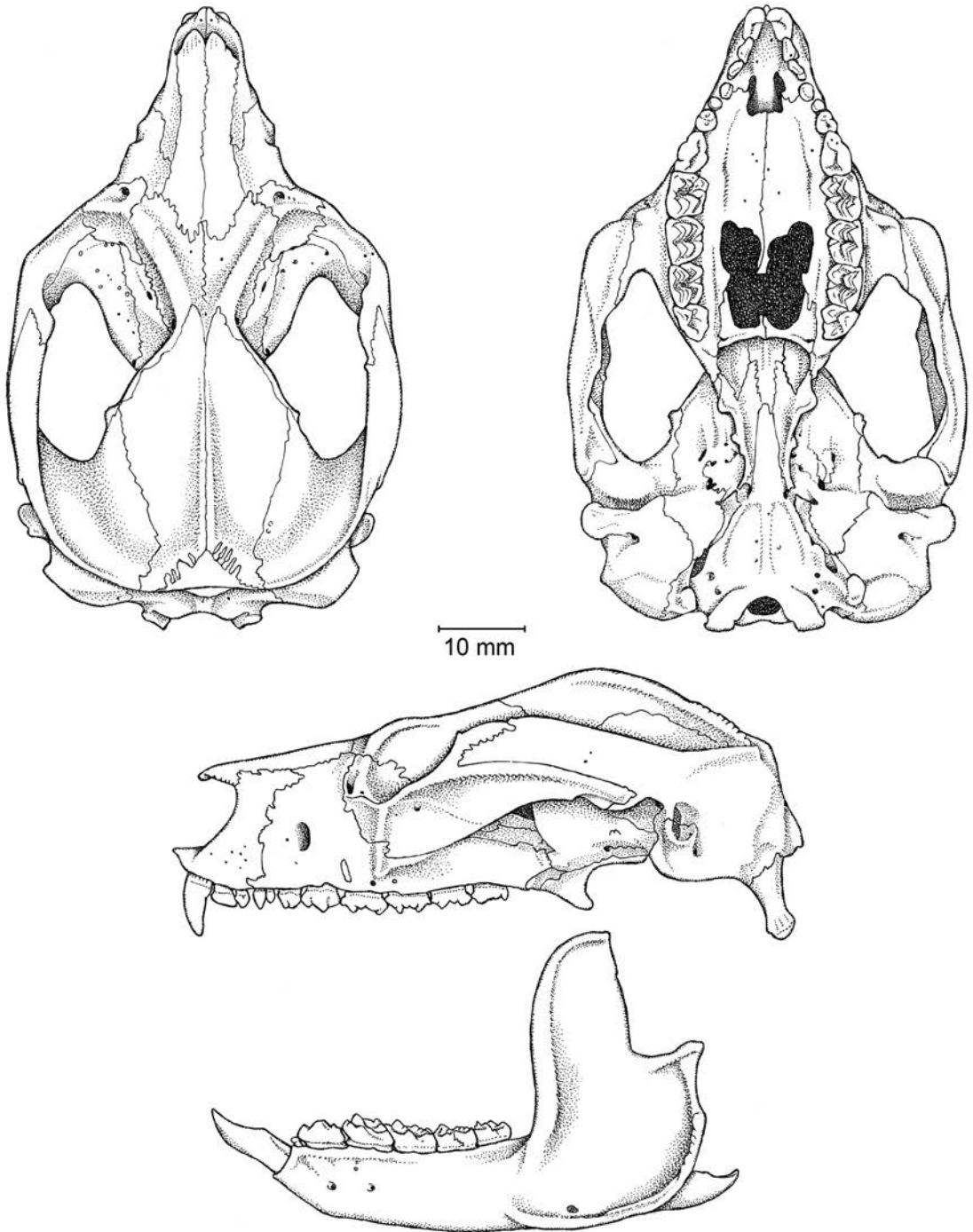
FIG. 51. *Pseudochirops cupreus* (Diprotodontia, Pseudocheiridae; based on AMNH 104149, an adult male from an unknown locality in Papua New Guinea).

semisectorial (char. 123: 0→1; ci = 0.385); paracone not completely fused with any stylar elements (char. 136: 2→0; ci = 0.250); principal labial and lingual cusps of upper molars not connected by transverse lophs (char. 144: 1→0; ci = 0.200); additional cuspid labial to m1 present, forming a cusplike protostylid (char. 165: 0→1; ci = 0.286); entocristid well labial of the lingual margin (char. 177: 0→1; ci = 0.250); and hypoconulid present (char. 178: 1→0; ci = 0.333).

COMMENTS: Monophyly of Pseudocheiridae is strongly supported by our molecular (figs. 27–29), morphological (fig. 30, 31), and total-evidence (figs. 32, 33) analyses, and this clade is associated with a correspondingly long list of unambiguous craniodental (but mostly dental) synapomorphies. This impressive character support is in stark contrast with the previously discussed lack of morphological support for Petauridae and with the unpublished results of Roberts' (2008) analyses. Because the last incorporated numerous fossil pseudocheirids (some of which are known from relatively complete, but currently unpublished, cranial material), it seems likely that adding these and other key fossil petauroids (such as †*Djaludjangi*) to future total-evidence analyses will have a major impact on character polarity within Petauroidea (see discussions in Winge, 1941; Archer, 1976e; Archer et al., 1987; Flannery, 1987; Woodburne et al., 1987a, 1987b; Springer and Woodburne, 1989; Brammall, 1998). Within Pseudocheiridae, we find support for the same three subfamilies—Hemibelideinae (*Hemibelideus* and *Petauroides*), Pseudocheirinae (*Pseudocheirus* and *Pseudochirulus*), and Pseudochiropsinae (*Pseudochirops* and *Petropseudes*)—that have also been supported in recent molecular studies (Meredith et al., 2009a, 2010; Mitchell et al., 2014; May-Collado et al., 2015; Álvarez-Carretero et al., 2021).

Fossil pseudocheirids are first known from the late Oligocene of Australia (Woodburne et al., 1987b; Bassarova and Archer, 1999; Roberts, 2008; Roberts et al., 2009). However, based on largely on the results of recent revisionary work by Roberts (see also Bassarova and Archer, 1999; Long et al.,

2002; Archer and Hand, 2006), the oldest definitive crown-clade pseudocheirids currently known appear to be early Pliocene, namely *Pseudochirops* †*winteri* from the Bluff Downs Local Fauna (Mackness and Archer, 2001) and *Pseudocheirus* †*marshalli* and *Petauroides* †*stirtoni* from the ~4.46 Mya Hamilton Local Fauna (Turnbull and Lundelius, 1970; Archer, 1984c; Turnbull et al., 1987; Bassarova and Archer, 1999; Turnbull et al., 2003), with *Petauroides* †*stirtoni* possibly also present in the early Pliocene Big Sink Fauna (Dawson et al., 1999). This is broadly congruent with our estimated divergence dates, in which crown-clade Pseudocheiridae is inferred as having begun to diversify during the early or middle Miocene.

Macropodiformes Kirsch et al., 1997

CONTENTS: †Balbaridae, †*Ekaltadeta*, Hypsiprymnodontidae, Macropodidae, and Potoroidae.

STEM AGE: 33.0 Mya (95% HPD: 29.3–37.7 Mya).

CROWN AGE: 27.7 Mya (95% HPD: 23.6–32.1 Mya).

UNAMBIGUOUS CRANIODENTAL SYNAPOMORPHIES: Lacrimal exposure with one or more distinct tubercles (char. 8: 0→1; ci = 0.118); maxillary and frontal bones in contact on medial orbital wall (char. 13 0→1; ci = 0.143); maxillary and alisphenoid in contact on orbital floor (char. 16: 0→1; ci = 0.250); frontal and squamosal in contact on lateral aspect of braincase (char. 26: 0→1; ci = 0.071); palatine fenestrae present (char. 38: 0→1; ci = 0.071); pterygoid fossa large, deeply excavated, enclosed laterally by an ectopterygoid crest (char. 49: 0→1; ci = 0.143); masseteric fossa perforated by a masseteric canal (char. 99: 1→2; ci = 0.333); first upper premolar (P1) absent (char. 114: 0→1; ci = 0.200); sectorial P3 with well-developed ridges extending from apex to base of crown (char. 126: 1→2; ci = 0.154); major crest of semi- or fully sectorial P3 oriented posterolingual to anterolabial (char. 127: 1→0; ci = 0.400); and P3 erupts before M4 but after M3 (char. 130: 4→2; ci = 0.089).

COMMENTS: We follow den Boer and Kear (2018) in using Macropodoidea to refer to the crown clade (as defined by the extant families Macropodidae, Potoroidae, and Hypsiprymnodontidae), and Macropodiformes for the total clade, that is to say, the clade comprising macropodoids plus all fossil taxa more closely related to macropodoids than to other extant phalangeridans. Our dated total-evidence analysis (fig. 33) does not resolve whether balbarids and †*Ekaltadeta* fall within Macropodoidea or not, so the unambiguous craniodental synapomorphies identified here apply to Macropodiformes as a whole. Of the craniodental features that optimize as unambiguous synapomorphies, perhaps the most striking is the presence of a masseteric canal perforating the masseteric fossa, a feature that does not occur in any other known metatherian (char. 99; see also Abbie, 1939; Pearson, 1950; Ride, 1959; Woods, 1960; Archer, 1984c; Case, 1984; Flannery, 1984, 1987; Clemens et al., 1989; Warburton, 2009).

Our undated total-evidence analysis (fig. 32) places †*Ekaltadeta* sister to *Hypsiprymnodon*, and the balbarids †*Balbaroo* and †*Ganawayamaya* in a macropodid clade with †*Ganguroo* (a "bulungamayine" [= probable stem] macropodid; Prideaux and Warburton, 2010; Travouillon et al., 2014b; Cooke et al., 2015), †*Hadronomas* and †*Rhizosthenurus* (both plesiomorphic sthenurines; Murray, 1991, 1995; Kear and Cooke, 2001; Kear, 2002; Kirkham, 2004; Prideaux, 2004; Prideaux and Warburton, 2010), *Dorcopsis*, and *Dorcopsulus*. Our dated total-evidence topology (fig. 33) is markedly different, although this is partly the result of topological constraints used to implement node calibrations within Macropodoidea (see Methods and appendix 2). In this reconstruction, there is a polytomy at the base of Macropodoidea, comprising †*Ekaltadeta*, †Balbaridae, Hypsiprymnodontidae (= *Hypsiprymnodon moschatus* + *H.* †*bartholomaii*), and Macropodidae + Potoroidae, whereas †*Ganguroo*, †*Hadronomas*, and †*Rhizosthenurus* are placed as stem macropodids, with †*Hadronomas* and †*Rhizosthenurus* forming a sthenurine clade.

In effect, the dated toplogy is far more similar to other recent published morphological and total-evidence analyses of macropodiform phylogeny that have included some or all of these taxa (Kear et al., 2007; Kear and Pledge, 2008; Prideaux and Warburton, 2010; Prideaux and Tedford, 2012; Black et al., 2014c; Llamas et al., 2015: supplementary material; Travouillon et al., 2014b, 2015a, 2016, 2022; Cooke et al., 2015; Butler et al., 2016, 2018; Cascini et al., 2019). We therefore focus on our dated topology when discussing subclades within Macropodoidea (see below).

The oldest known macropodiforms are from the late Oligocene of Australia (Flannery et al., 1983; Flannery and Rich, 1986; Woodburne et al., 1994; Cooke, 1997a, 2006; Cooke and Kear, 1999; Long et al., 2002; Kear et al., 2007; Kear and Pledge, 2008; Black et al., 2012b, 2014c; Travouillon et al., 2014b, 2015a, 2016; Butler et al., 2016, 2018; den Boer and Kear, 2018). These fossils include at least one probable nonmacropodoid (†*Palaeopotorous priscus*; see den Boer and Kear, 2018); possible macropodoids (e.g., undescribed species of *Hypsiprymnodon* from Faunal Zone A at Riversleigh; Archer et al., 2006; Black et al., 2012b; Butler et al., 2017); and †*Gumardee*, which may be a potoroid (Travouillon et al., 2016; but see Butler et al., 2016, 2018; Travouillon et al., 2022).

Hypsiprymnodontidae Collett, 1887

CONTENTS: *Hypsiprymnodon* †*bartholomaii* and *H. moschatus* (fig. 52).

STEM AGE: 27.7 Mya (95% HPD: 23.6–32.1 Mya).

CROWN AGE: 16.9 Mya (95% HPD: 11.7–22.0 Mya).

UNAMBIGUOUS CRANIODENTAL SYNAPOMORPHIES: Cristid obliqua with strongly developed "buccal kink" (char. 168: 0→1; ci = 0.333).

COMMENTS: Ride (1993) recognized the family Hypsiprymnodontidae as comprising two subfamilies: Hypsiprymnodontinae (for the extant genus *Hypsiprymnodon* only) and †Propleopinae (for †*Ekaltadeta*, †*Jackmahoneya*, and

10 mm
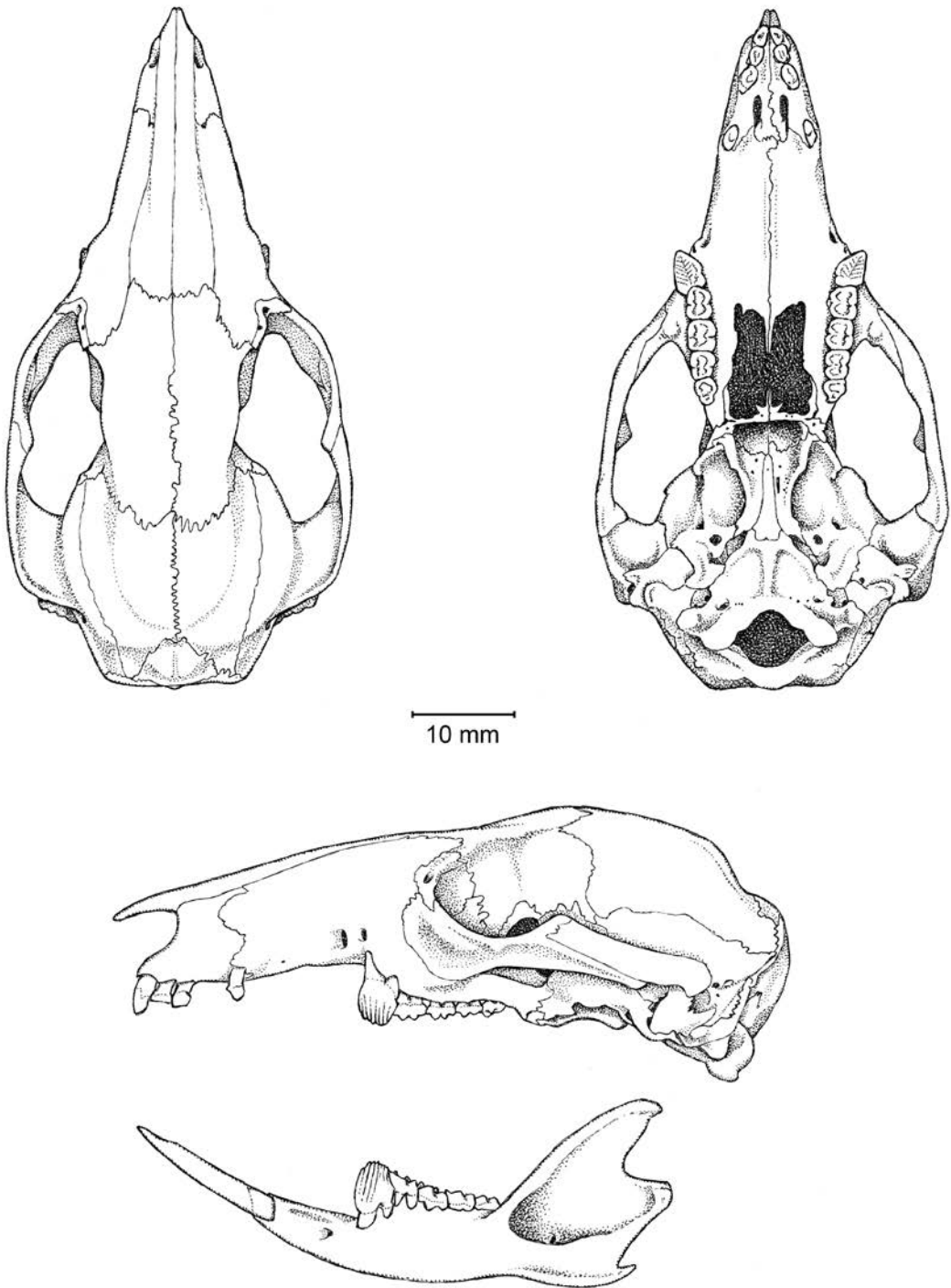
FIG. 52. *Hypsiprymnodon moschatus* (Diprotodontia, Hypsiprymnodontidae; based on AMNH 184580, an adult male from Queensland).

†*Propleopus*). This arrangement has been followed by most subsequent authors (Wroe and Archer, 1995; Kirsch et al., 1997; Ride et al., 1997; Wroe, 1997c; Cooke and Kear, 1999; Kear and Cooke, 2001; Long et al., 2002; Cooke, 2006; Black et al., 2012b; Bates et al., 2014; Jackson and Groves, 2015). However, Wroe et al. (1998) suggested, based on a study of the cranial morphology of †*Ekaltadeta*, that propleopines might be more closely related to balbarids than to *Hypsiprymnodon*. Our dated total-evidence analysis failed to support monophyly of Hypsiprymnodontidae sensu Ride (1993); instead, *Hypsiprymnodon*, †*Ekaltadeta*, †Balbaridae, and Macropodidae + Potoroidae form a polytomy at the base of Macropodiformes. We therefore restrict Hypsiprymnodontidae to *Hypsiprymnodon* only. We note that, of our macropodiform terminals, †*Ekaltadeta* is uniquely plesiomorphic in retaining p2 and P2 into adulthood, whereas these teeth are lost in all the others, including balbarids and *Hypsiprymnodon*; however, *Hypsiprymnodon* is unusual among macropodiforms in retaining P2 for a short period after dP3 has been replaced by P3 (see char. 117).

Monophyly of Hypsiprymnodontidae in this restricted sense (comprising just *Hypsiprymnodon moschatus* and *H.* †*bartholomaii*) is unambiguously supported only by the derived presence of a "buccal kink" in the cristid obliqua of the lower molars. However, this feature is also found in phalangerids, as well as in some fossil phalangeroids, *Dactylopsila*, possibly *Burramys*, and *Pseudochirulus* (see char. 168). Although the presence of a buccally kinked cristid obliqua is interpreted as independently derived in *Hypsiprymnodon* and phalangerids based on our analyses, this interpretation may change if additional fossil phalangeridans (e.g., ektopodontids, miralinids) were to be included in future datasets.

The oldest known hypsiprymnodontid fossils, in our restricted sense of the family, are an undescribed species of *Hypsiprymnodon* from late Oligocene (Faunal Zone A) sites at Riversleigh World Heritage Area (Archer et al., 2006; Black

et al., 2012b; Butler et al., 2017) and "Hypsiprymnodontinae indet." from the late Oligocene Namba Formation (Flannery and Rich, 1986). Both records are congruent with our Oligocene estimate for the divergence of *Hypsiprymnodon* from other macropodoids. However, the presence of probable stem macropodids in the late Oligocene (e.g., *Bulungamaya*, *Cookeroo*, and *Ngamaroo*; Prideaux and Warburton, 2010; Phillips, 2015; Butler et al., 2016, 2017) suggests that the divergence between Macropodidae and Potoroidae had already occurred by this time, in which case our estimate for the divergence between Hypsiprymnodontidae and Macropodidae + Potoroidae, which must have been earlier, would appear to be too young.

†Balbaridae Kear and Cooke, 2001

Contents: †*Balbaroo* and †*Ganawamaya*.

Stem Age: 27.7 Mya (95% HPD: 23.6–32.1 Mya).

Crown Age: 22.5 Mya (95% HPD: 18.7–27.3 Mya).

Unambiguous Craniodental Synapomorphies: Mandible usually with two or more mental foramina (char. 98: 0→1; ci = 0.063), distinct posterolingual cusp on semi- or fully sectorial P3 present (char. 125: 0→1; ci = 0.200); principal labial and lingual cusps of upper molars connected by well-developed lophs (char. 144: 1→2; ci = 0.200); and midpoints of protoloph and metaloph connected by a "midlink" (char. 145: 0→1; ci = 0.500)

Comments: The first balbarids to be described, namely †*Balbaroo camfieldensis* and †*B. gregoriensis*, were originally referred to Macropodidae based largely on their fully lophodont molars (Flannery et al., 1983). However, Cooke (1997a, 1997b, 1997c) showed that balbarids and macropodids appear to have evolved lophodonty independently, and Kear and Cooke (2001) subsequently recognized †Balbaridae as a distinct family.

The position of †Balbaridae has varied in published morphological and total-evidence phylogenetic analyses, and the family has not always been

recovered as monophyletic (Kear et al., 2007; Kear and Pledge, 2008; Black et al., 2014c; Travouillon et al., 2014b, 2015a, 2016; Cooke et al., 2015; Butler et al., 2016, 2018; Cascini et al., 2019). However, both of our total-evidence analyses (figs. 32, 33) support balbarid monophyly. A position for †Balbaridae outside Macropodidae + Potoroidae in our dated analysis (fig. 33) is due to the use of topological constraints required to calibrate selected nodes within Macropodiformes. These constraints may have influenced the character optimizations that indicate that presence of well-developed lophs connecting the principal labial and lingual cusps of the upper molars, and the presence of a midlink connecting these lophs, are both unambiguous synapomorphies of †Balbaridae. Nevertheless, these optimizations are congruent with Cooke's (1997a, 1997b, 1997c) hypothesis that balbarids acquired fully lophodont molars independently of macropodids.

Balbarids were relatively diverse during the late Oligocene, but appear to have declined in diversity from the early Miocene onward, with their last records coming from the late middle or early late Miocene (Faunal Zone D) Encore site at Riversleigh World Heritage area (Butler et al., 2017).

Macropodidae + Potoroidae

CONTENTS: Macropodidae and Potoroidae.

STEM AGE: 27.7 Mya (95% HPD: 23.6–32.1 Mya).

CROWN AGE: 19.3 Mya (95% HPD: 18.0–22.0 Mya).

UNAMBIGUOUS CRANIODENTAL SYNAPOMORPHIES: Presphenoid exposed in roof of nasopharyngeal fossa above posterior palate (char. 43: 1→0; ci = 0.091); anterior limb of ectotympanic loosely attached to the petrosal or squamosal behind postglenoid process (char. 59: 2→1; ci = 0.214); P2 and dP3 simultaneously replaced by P3 (char. 117: 1→2; ci = 0.667); distinct posterolingual cusp on semi- or fully sectorial P3 present (char. 125: 0→1; ci = 0.200); and major crest of semisectorial or fully sectorial P3 parallel to molar row (char. 127: 0→1; ci = 0.400).

COMMENTS: We follow Kear and Cooke (2001; see also Groves, 2005a; Van Dyck and Strahan, 2008; Jackson and Groves, 2015; Eldridge et al., 2019) in recognizing Macropodidae and Potoridae as separate familes (see below). By contrast, Prideaux and collaborators (e.g., Prideaux and Warburton, 2010; Prideaux and Tedford, 2012; McDowell et al., 2015) have recognized these as subfamilies within a more broadly defined Macropodidae.

Monophyly of Macropodidae + Potoroidae to the exclusion of Hypsiprymnodontidae has been a feature of all recent molecular, morphological, and total-evidence analyses of macropodiform phylogeny (Kear et al., 2007; Kear and Pledge, 2008; Meredith et al., 2009a, 2009b, 2009c, 2011; Black et al., 2014c; Llamas et al., 2015; Mitchell et al., 2014; Travouillon et al., 2014b, 2015a, 2016, 2022; Cooke et al., 2015; May-Collado et al., 2015; Butler et al., 2016, 2018; Duchêne et al., 2018; Cascini et al., 2019; Celik et al., 2019; Álvarez-Carretero et al., 2021), although this clade is currently unnamed. This clade is likewise strongly supported in our molecular analyses (figs. 27–29), but as already discussed (see Macropodiformes above), the relationships of some fossil macropodiforms differ markedly between our undated (fig. 32) and dated (fig. 33) total-evidence analyses, as they also do among several recent studies (Kear et al., 2007; Kear and Pledge, 2008; Black et al., 2014c; Llamas et al., 2015: supplementary material; Travouillon et al., 2014b, 2015a, 2016, 2022; Butler et al., 2016, 2018).

Putative macropodids and at least one putative potoroid have been reported from late Oligocene (Faunal Zone A) sites at Riversleigh World Heritage Area (Travouillon et al., 2014b, 2016; Butler et al., 2016; Butler et al., 2017). The former include "bulungamayines" (species of †Bulungamaya, †Cookeroo, †Ganguroo, and †Wabularoo), at least some of which are probably not crown macropodids (Kear et al., 2001a; 2001b, 2007; Kear and Cooke, 2001; Kear, 2002; Kear and Pledge, 2008; Prideaux and Warburton, 2010; Prideaux and Tedford, 2012; Black et al., 2014c; Phillips, 2015; Travouillon et al., 2014b,

2015a, 2016, 2022; Butler et al., 2016, 2018; Cascini et al., 2019; see Macropodidae below). The putative Riversleigh potoroid, meanwhile, is †*Gumardee*, although studies differ as to whether this taxon is indeed a potoroid or a macropodid (Flannery et al., 1983; Butler et al., 2016, 2018; Travouillon et al., 2016, 2022; see Potoroidae below). Flannery and Rich (1986) additionally referred isolated dental specimens from the late Oligocene Namba Formation to †*Gumardee* and "Potoroinae [= Potoroidae here] indet." Collectively, these records suggest that Macropodidae and Potoroidae had diverged from each other by the late Oligocene. However, these fossil taxa have not been included in our analyses, the results of which instead suggest that the macropodid-potoroid split was in the early Miocene.

Macropodidae Gray, 1821

CONTENTS: †*Bohra*, *Dendrolagus*, *Dorcopsis*, *Dorcopsulus*, †*Ganguroo*, †*Hadronomas*, *Lagorchestes*, *Lagostrophus* (fig. 53), *Macropus*, *Notamacropus*, *Onychogalea*, *Osphranter*, *Petrogale*, †*Rhizosthenurus*, *Setonix*, *Thylogale*, and *Wallabia*.

STEM AGE: 19.3 Mya (95% HPD: 18.0–22.0 Mya).

CROWN AGE: 18.2 Mya (95% HPD: 17.8–19.7 Mya).

UNAMBIGUOUS CRANIODENTAL SYNAPOMORPHIES: Parietal and alisphenoid in contact on lateral aspect of braincase (char. 26: 1→0; c_i = 0.071); principal labial and lingual cusps of upper molars connected by well-developed lophs (char. 144: 1→2; c_i = 0.200); midpoints of protoloph and metaloph connected by a "midlink" (char. 145: 0→1; c_i = 0.500); and entocristid indistinct or absent (char. 176: 0→1; c_i = 0.077).

COMMENTS: As already discussed, monophyly of Macropodidae (sensu Kear and Cooke, 2001) was not supported in our undated total-evidence analysis (fig. 32) due to the surprising (and almost certainly erroneous) position of the balbarids †*Balbaroo* and †*Ganawamaya* in a clade with the macropodids *Dorcopsis*, *Dorcopsulus*,

†*Ganguroo*, †*Hadronomas*, and †*Rhizosthenurus*. The following discussion therefore applies to the clade recovered by our dated total-evidence analysis (fig. 33), in which balbarids were constrained to fall outside Macropodidae + Potoroidae, in agreement with all recent published phylogenetic analyses focused on macropodiform relationships (Kear and Cooke, 2001; Cooke, 2006; Kear et al., 2007; Kear and Pledge, 2008; Bates et al., 2014; Black et al., 2014c; Travouillon et al., 2014b, 2015a, 2016, 2022; Cooke et al., 2015; Butler et al., 2016, 2018; den Boer and Kear, 2018). Contact of the parietal and alisphenoid on the lateral aspect of the braincase, which optimizes as an unambiguous synapomorphy of Macropodidae in our dated total-evidence analysis, is a consistent feature among macropodids and its relevance for macropodiform systematics has often been discussed (Pearson, 1950; Archer, 1984c; Case, 1984; Flannery et al., 1984; Flannery and Archer, 1987b, 1987c; Flannery, 1989; Burk et al., 1998; Cooke, 1999, 2000; Kear and Cooke, 2001; Kear et al., 2007; Prideaux and Warburton, 2010). However, alisphenoid-parietal versus frontal-squamosal contact is highly homoplastic within Marsupialia as a whole (see char. 26) with a very low consistency index (0.071, see above), and the presence of alisphenoid-parietal contact in the fossil hypsiprymnodontid *Hypsiprymnodon* †*bartholomaii* indicates that this character is also homoplastic within Macropodiformes (Flannery and Archer, 1987b, 1987c; Flannery, 1989; Burk et al., 1998; Cooke, 1999, 2000; Kear et al., 2007). Presence of well-developed lophs connecting the principal labial and lingual cusps of the upper molars also optimizes as a synapomorphy of Macropodidae, as does presence of a midlink, but this may be influenced by our decision to enforce monophyly of Macropodidae + Potoroidae to the exclusion of Balbaridae (which are also fully lophodont and have a midlink; see chars. 144, 145 and "†Balbaridae" above). Nevertheless, Cooke (1997a, 1997b, 1997c) presented evidence that macropodids and balbarids did indeed independently acquire fully lophodont molars.
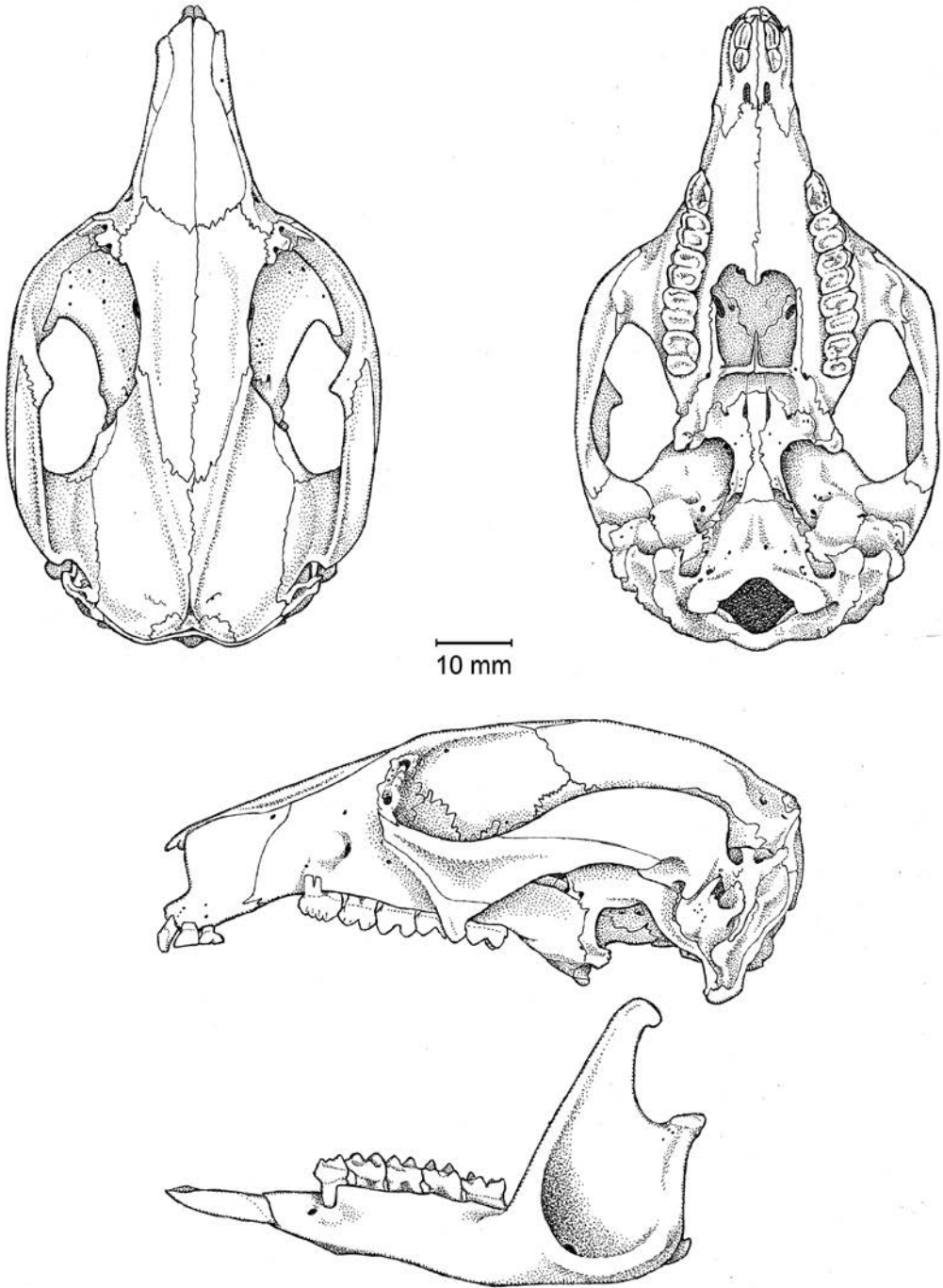
FIG. 53. *Lagostrophus fasciatus* (Diprotodontia, Macropodidae; based on WAM M-6791, a subadult male from Western Australia, with the adult dentition reconstructed from WAM M-3635, an adult female from Western Australia).

Our dated analysis placed the fossil terminals †*Ganguroo*, †*Hadronomas*, and †*Rhizosthenurus* within total-clade Macropodidae but outside the crown clade (= *Lagostrophus* + Macropodinae). Of these, †*Hadronomas* and †*Rhizosthenurus* are currently recognized as plesiomorphic members of the extinct macropodid subfamily †Sthenurinae (Murray, 1991, 1995; Kear and Cooke, 2001; Kear, 2002; Kirkham, 2004; Prideaux, 2004; Prideaux and Warburton, 2010), which achieved considerable diversity during the Plio-Pleistocene (Long et al., 2002; Prideaux, 2004; Prideaux and Warburton, 2010; Black et al., 2012b; Couzens and Prideaux, 2018). The placement of †*Hadronomas* and †*Rhizosthenurus* in a clade that falls outside crown-clade Macropodidae here is congruent with their membership in †Sthenurinae.

Within the macropodid crown clade, we found *Lagostrophus* (the only extant lagostrophine) to be sister to our remaining terminals (which collectively comprise Macropodinae). By contrast, other studies have placed *Lagostrophus* in a clade with sthenurines (Flannery, 1983, 1989; Llamas et al., 2015: fig. 1c; Cascini et al., 2019) or outside †Sthenurine + Macropodinae (Prideaux and Warburton, 2010; Prideaux and Tedford, 2012; Llamas et al., 2015: fig. 1a). The topology found here may be the result of our use of the Fossilized Birth Death model (see Dated Total-Evidence Analysis in the Discussion section for more detail), with †*Rhizosthenurus* (late Miocene) and †*Hadronomas* (late Miocene or earliest Pliocene) recovered as branching deeper within Macropodidae than the extant *Lagostrophus*. This hypothesis could be tested by inclusion of younger sthenurines or older lagostrophines; however, whereas well-preserved remains of sthenurines are known from the Pleistocene (Prideaux, 2004), the oldest known lagostrophine (the Pliocene †*Tjukuru wellsi*) is known only from a single partial lower jaw (Prideaux and Tedford, 2012).

As discussed above (see Macropodidae + Potoroidae), the oldest known macropodids appear to be the "bulungamayines" †*Bulungamaya*, †*Cookeroo*, †*Ganguroo*, and †*Wabularoo*,

which are known from the late Oligocene (Faunal Zone A) sites at Riversleigh World Heritage Area (Cooke, 1997b, 1997c, 2006; Travouillon et al., 2014b; Butler et al., 2016, 2017). However, these taxa consistently fall outside crown-clade Macropodidae (as found for †*Ganguroo* here) in published analyses (Kear et al., 2001a, 2001b, 2007; Kear and Cooke, 2001; Kear, 2002; Kear and Pledge, 2008; Prideaux and Warburton, 2010; Prideaux and Tedford, 2012; Black et al., 2014c; Phillips, 2015; Travouillon et al., 2014b, 2015a, 2016; Butler et al., 2016, 2018; Cascini et al., 2019). Thus, they do not provide insight on the timing of divergences within the macropodid crown clade (Phillips, 2015). We estimate the split between Lagostrophinae and Macropodinae to have occurred during the middle or late Miocene, with Macropodinae beginning to radiate during the late Miocene. These estimated dates are congruent with the known fossil record (Couzens and Prideaux, 2018): the oldest crown-clade macropodid currently known is probably the fossil dorcopsin macropodine †*Dorcopsoides fossilis* from the late Miocene Alcoota Local Fauna in the Northern Territory (Woodburne, 1967; Prideaux and Warburton, 2010; Butler et al., 2018). They are also broadly similar (but overall somewhat younger) to dates from recent molecular- and total-evidence clock analyses (Meredith et al., 2009a, 2009b; Llamas et al., 2015; Mitchell et al., 2014; Dodt et al., 2017; Nilsson et al., 2018; Cascini et al., 2019; Celik et al., 2019; Álvarez-Carretero et al., 2021).

Potoroidae Gray, 1821

CONTENTS: *Aepyprymnus*, *Bettongia*, ?*Bettongia* †*moyesi*, *Caloprymnus*, and *Potorous* (fig. 54).

STEM AGE: 19.3 Mya (95% HPD: 18.0–22.0 Mya).

CROWN AGE: 15.7 Mya (95% HPD: 11.7–22.0 Mya).

UNAMBIGUOUS CRANIODENTAL SYNAPOMORPHIES: None.

COMMENTS: Monophyly of Potoroidae is strongly supported in our molecular (figs. 27–29)
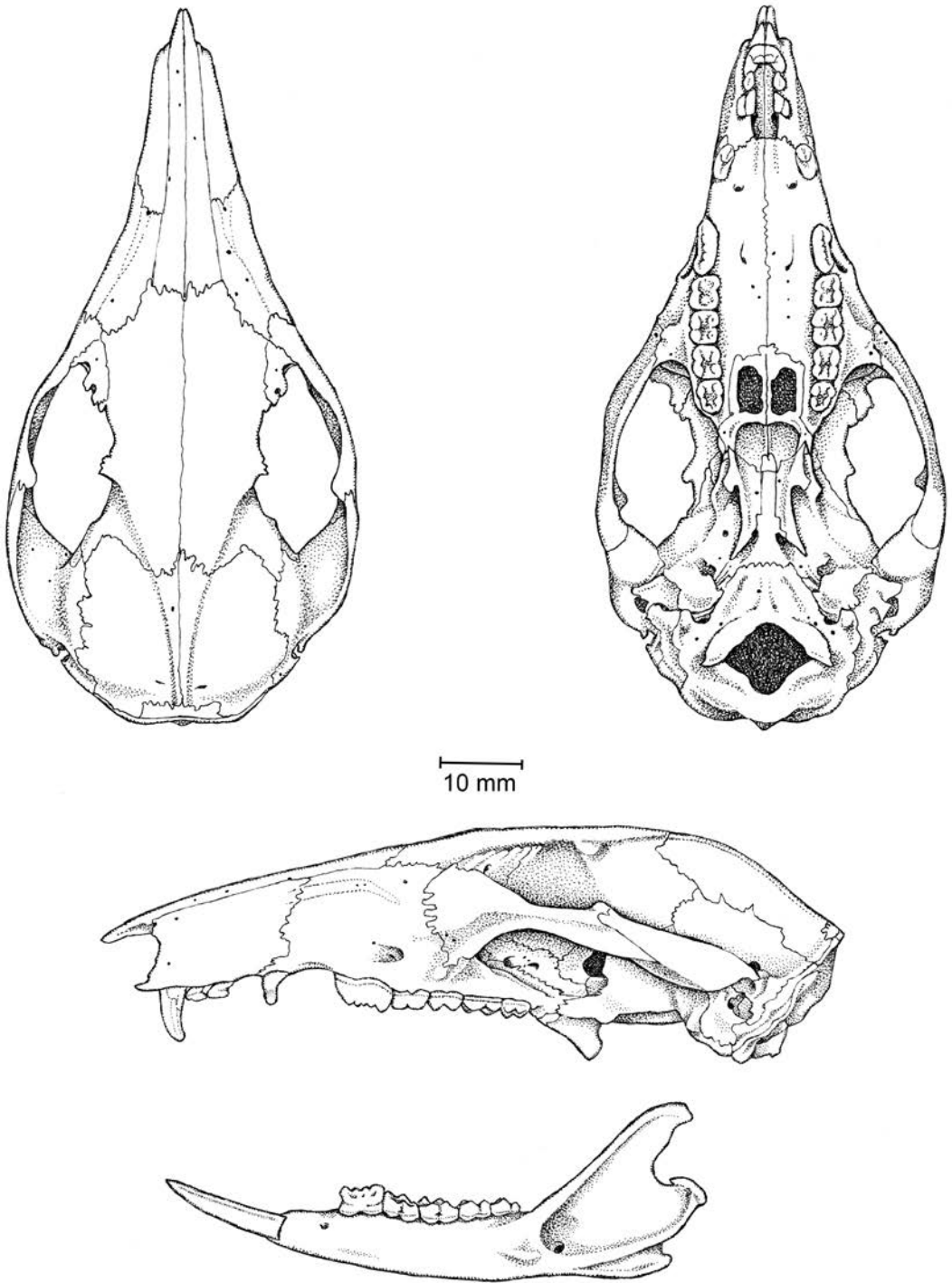
FIG. 54. *Potorous tridactylus* (Diprotodontia, Potoroidae; based on AMNH 66168, an adult male from Tasmania).

and total-evidence (figs. 32, 33) analyses, as it has been in other recent molecular and total-evidence studies (Meredith et al., 2009a, 2009b, 2009c, 2011; Llamas et al., 2015; Mitchell et al., 2014; May-Collado et al., 2015; Duchêne et al., 2018; Cascini et al., 2019; Celik et al., 2019; Álvarez-Carretero et al., 2021). However, morphological studies have failed to consistently support potoroid monophyly (Kear et al., 2007; Kear and Pledge, 2008; Prideaux and Warburton, 2010; Black et al., 2014c; Travouillon et al., 2014b, 2015a, 2016; Cooke et al., 2015; Butler et al., 2016, 2018; Cascini et al., 2019), and our craniodental analyses similarly did not recover a monophyletic Potoroidae (figs. 30, 31). Perhaps unsurprisingly, no craniodental feature optimizes as an unambiguous synapomorphy of Potoroidae in our dated total-evidence analysis. However, one highly homoplastic dental feature optimizes as a potoroid synapomorphy under Delayed Transformation: m3 hypoconid lingual to salient protoconid (char. 173: 0→1; ci = 0.045).

As discussed (see Macropodidae + Potoridae above), at least one putative potoroid— †Gumardee—is known from late Oligocene (Faunal Zone A) sites at Riversleigh World Heritage Area (Flannery et al., 1983; Travouillon et al., 2016) and possibly also from the late Oligocene Namba Formation (Flannery and Rich, 1986). †Gumardee (not included in our analyses due to its fragmentary preservation) has been recovered as a stem potoroid in one published phylogenetic analysis (Travouillon et al., 2016), although not in others (Butler et al., 2016, 2018; Travouillon et al., 2022). Thus, †Gumardee, together with various "bulungamayines" (†Bulungamaya, †Cookeroo, †Ganguroo and †Wabularoo; at least some of which are probably stem macropodids) from Riversleigh Faunal Zone A, and possible additional potoroid material from the Namba Formation (Flannery and Rich, 1986), suggest a late Oligocene split between Macropodidae and Potoroidae. However, we recovered a somewhat younger (early Miocene estimate) for this split in our analyses (see Macropodidae + Potoroidae above), and

even if †Gumardee is a stem potoroid, it is not informative about the timing of divergences within crown-clade Potoroidae. At present, the oldest known crown-clade potoroid is probably †Milliyowi bunganditj from the early Pliocene (~4.46 Mya) Hamilton Local Fauna in Victoria (Flannery et al., 1992; Turnbull et al., 2003), which has not been included in the current analysis. Prideaux (1999) concluded that †Milliyowi is more closely related to Aepyprymnus than to any other extant potoroid genus, although this was not tested using a formal phylogenetic analysis.[37] Nevertheless, this is compatible with our estimated divergence dates, which suggest that crown-clade Potoroidae began to diversify during the middle to late Miocene.

Our undated (fig. 32) and dated (fig. 33) total-evidence analyses disagree with regard to the affinities of the only fossil potoroid that we included, the middle Miocene ?Bettongia †moyesi (described by Flannery and Archer, 1987b): this taxon was found to be sister to Aepyprymnus + Bettongia in our undated analysis, but it falls outside the potoroid crown clade in our dated analysis. Again, this may be the result of our use of the Fossilized Birth Death model in our dated analysis, as this will tend to reconstruct fossil terminals as originating deeper in the tree (see Dated Total-Evidence Analysis in the Discussion section for more detail). However, as already dis-

<hr>

[37] Prideaux (1999) also implied that †Wakiewakie lawsoni (described by Woodburne, 1984a) from the Kutjamarpu Local Fauna of the Wipajiri Formation (which is probably early or middle Miocene; Archer et al., 1997; Travouillon et al., 2006; Black et al., 2012b, 2013, 2014a; Gurovich et al., 2014; Travouillon et al., 2015b; Archer et al., 2018) may be another potential crown-clade potoroid. However, Prideaux's (1999: fig. 3) preferred phylogeny, which was not based on a formal algorithmic analysis of a character matrix, placed Potorous as sister to the remaining extant potoroid genera (Aepyprymnus, Bettongia, and Caloprymnus), which is incongruent with the results of our molecular and total evidence analyses (which instead recover Potorous + Caloprymnus and Aepyprymnus + Bettongia). This raises questions about the polarities of the characters that Prideaux (1999) used to place †Wakiewakie within crown-clade Potoroidae. Subsequent phylogenetic analyses have not supported †Wakiewakie as a member of the crown clade (Kear et al., 2007; Kear and Pledge, 2008; Black et al., 2014c; Travouillon et al., 2014b, 2015a, 2016, 2022; Cooke et al., 2015; Butler et al., 2016, 2018).

cussed, we prefer the results of our dated analysis regarding relationships within Macropodiformes (based on their greater congruence with other recent studies of macropodiform systematics), so we tentatively recognize ?*Bettongia* †*moyesi* as a stem potoroid, as also found by Travouillon et al. (2016). As noted by Flannery and Archer (1987b) in their original description, ?*Bettongia* †*moyesi* closely resembles living *Bettongia* species (particularly *B. lesueur*); if this fossil is, indeed, a stem potoroid, then it seems likely that a *Bettongia*-like morphology may have been ancestral for crown potoroids.

CONCLUSIONS AND THE ROAD AHEAD

This study provides a detailed overview of the macroscopic craniodental morphology of marsupials and several marsupialiform outgroups in the context of a set of discrete characters for which we felt reasonably confident in assigning primary homology (sensu de Pinna, 1991). In compiling these data, we proposed substantially revised hypotheses of homologies of some structures, proposed entirely new hypotheses of homology for others, and noted several examples where homologies remain uncertain. Having explained our interpretation of each problematic case, we now leave it to future researchers to decide whether or not they agree with our coding decisions.

Analyses of our craniodental dataset result in topologies that are reasonably congruent with currently accepted hypotheses of marsupial phylogeny, notably by recovering monophyly of six of the seven Recent orders and of most Recent families. Relationships among ordinal-level taxa recovered by our morphological analyses, however, are often incongruent with currently accepted relationships, most obviously in failing to support monophyly of Australidelphia and in grouping all our ingroup taxa with gliriform lower incisors. Morphological support values are also low for many clades, but this is to be expected for a dataset comprising many taxa but few characters, and with a large proportion of missing data.

By contrast, analyses of our total-evidence dataset result in topologies that are strongly congruent with currently accepted notions of marsupial phylogeny, particularly when we incorporate temporal information in the form of tip-and-node dating. However, even our total-evidence analyses failed to clearly resolve some relationships and supported others that appear anomalous. Such anomalies and other problematic or unresolved relationships discussed above warrant further scrutiny and testing to see whether they are corroborated or rejected by improved datasets.

Our morphological dataset can (and it is hoped will) be expanded by other researchers. Among other omissions, we have not included characters that require CT-scanning—e.g., cranial endocasts, inner-ear morphology, and the turbinals—but such data are becoming increasingly available (e.g., Macrini et al., 2007; Schmelzle et al., 2007; Macrini, 2012, 2014; Alloing-Séguier et al., 2013; Selva and Ladevèze, 2016; Pfaff et al., 2017). Likewise, we have not included characters that require microscopic imaging, such as enamel microstructure (Wood and Rougier, 2005). The postcranial skeleton is another rich source of phylogenetically useful characters, and one that has played a central role in our understanding of marsupial phylogeny (Szalay, 1982a, 1994; Szalay and Sargis, 2001; Horovitz and Sánchez-Villagra, 2003; Szalay and Sargis, 2006; Beck et al., 2008a; Beck, 2012). Indeed, there is a particular need for monographic treatment of marsupial postcranial morphology building on the pioneering work of Szalay (1982a, 1982b, 1993, 1994) and Argot (2001, 2002, 2003; Muizon and Argot, 2003). Soft-tissue characters are another underutilized phylogenetic resource, even though studies to date have shown that such varied systems as sperm ultrastructure (e.g., Temple-Smith, 1994), visceral anatomy (see summary in Aplin and Archer, 1987), neuroanatomy (e.g., Ashwell, 2010; Gurovich and Ashwell, 2020), the integument (e.g., Aplin and Archer, 1987; Voss and Jansa, 2009; 2021; Schneider and Gurovich,

2017; Martin, 2019), reproductive morphology (e.g., Voss and Jansa, 2009; 2021; Schneider and Gurovich, 2017), and the chondrocranium (e.g., Sánchez-Villagra and Forasiepi 2017; Hüppi et al. 2018) appear to show phylogenetic signal within Marsupialia. The muscular anatomy of many marsupials is still incompletely understood, despite a long history of descriptive works reviewed by Aplin (1990) and Warburton (2003). However, because soft-tissue characters are unlikely ever to be fossilised, they are unlikely to help resolve the still ambiguous relationships of many extinct taxa.

Instead, renewed paleontological fieldwork to obtain better-preserved fossil material is a high priority. Of particular importance for future progress will be new fossils preserving intermediate morphologies that may help break up long branches. Inevitably, however, shorter branches will come at the cost of reduced support values, and adding highly incomplete fossils may result in loss of phylogenetic resolution (Horovitz, 1999; Cobbett et al., 2007; Prevosti and Chemisquy, 2010; Pattinson et al., 2015). Therefore, the discovery of relatively complete, well-preserved specimens (not just isolated dental material) will be particularly beneficial. It seems likely that such discoveries will continue to be made in South America, but wide gaps also remain in the Australian fossil record (Woodhead et al., 2014; Beck, 2017b). Unfortunately, filling such gaps has proved difficult, and timely progress in doing so is by no means guaranteed.

Methodological innovations could also contribute to future analyses of expanded morphological datasets. Such analyses might be improved, inter alia, by modelling rate heterogeneity among characters and asymmetries in state changes (Harrison and Larsson, 2015; Wright et al., 2016; Pyron, 2017), and they might also benefit from data partitioning (Rosa et al., 2019). Incorporating temporal information into phylogenetic analyses of morphological and total-evidence data by using clock models (Pyron, 2011; Ronquist, et al. 2012a; Zhang et al., 2016; Gavryushkina et

al., 2017) has been shown to have a major impact on tree topology in a number of cases (e.g., Lee and Yates, 2018; King and Beck, 2020; Beck and Taglioretti, 2020), as was also found in our study. However, the appropriateness of currently available clock models for morphological data, questions about how best to incorporate temporal evidence, and understanding exactly what drives results of analyses that use such models are all topics that need further investigation (Matzke and Wright, 2016; Ronquist et al., 2016; Parins-Fukuchi and Brown, 2017; Turner et al., 2017; Matzke and Irmis, 2018; Cascini et al., 2019; Klopfstein et al., 2019; Püschel et al., 2020; Zhang, 2021). Arguably the most pressing issue is the need to identify and correct for nonindependent morphological characters; considerable progress has been made in this area in recent years (Dávalos et al., 2012, 2014) and, although we have not used such methods here, our craniodental matrix is an obvious candidate for applying them. Continuous morphometric characters may also prove useful in resolving marsupial phylogeny (Parins-Fukuchi, 2018a, 2018b).

Molecular data collection, of course, is certain to proceed more rapidly than marsupial morphological research, and our paltry sequence dataset will undoubtedly soon be surpassed by phylogenomic data obtained by target-sequence capture and other next-generation methods (Mamanova et al., 2010; Bragg et al., 2016; Gasc et al., 2016). Indeed, Duchêne et al.'s (2018) phylogenomic study of marsupials used ~40× the sequence data analyzed in our study, albeit from representatives of only 39 currently recognised Recent genera (versus 97 Recent genera analyzed herein). Nevertheless, considerable further research is needed to determine how best to analyze phylogenomic data (Philippe et al., 2011; Scornavacca et al., 2020), including: (1) whether and how to implement coalescence-based rather than concatenation-based methods (Bryant and Hahn, 2020); (2) whether cases of phylogenetic uncertainty or

conflict are due to inadequate substitution and/ or clock models, homology errors, incomplete lineage sorting, hybridization, or a combination of these factors (Schrempf and Szöllősi, 2020; Simion et al., 2020); and (3) whether whether and how to filter datasets before analysis to maximize phylogenetic signal and ensure model adequacy (Simion et al., 2020; Mongiardino Koch, 2021).

Retroposon insertions (and possibly other types of rare genomic changes; Rokas and Holland, 2000), which have already been used to resolve some relationships within Marsupialia (Nilsson et al., 2010; Zemann et al., 2013; Gallus et al., 2015a, 2015b; Dodt et al., 2017; Feigin et al., 2018), are also likely to play a useful role in further clarifying the branching pattern among Recent species. However, published studies have already found conflicting (homoplastic) retroposon insertion patterns that are probably indicative of incomplete lineage sorting (Gallus et al. 2015a; Feigin et al. 2018), and it seems probable that more will be found as such datasets increase in size.

The ultimate aspiration is, of course, a comprehensive and accurate phylogeny of Marsupialia that includes both living and extinct species, ideally accompanied by accurate estimates of relevant divergence times. This is a worthy and, we think, ultimately achievable goal that will contribute to understanding the biogeographic perigrinations and remarkable adaptive radiations of this fascinating clade. Progress toward this end will require continuing and fruitful collaborations between molecular systematists, comparative morphologists, and palaeontologists, together with some kind of total-evidence approach not altogether unlike that presented here. Despite many challenges ahead, the future of marsupial systematics seems bright.

ACKNOWLEDGMENTS

REFERENCES

Abbie, A.A. 1939. A masticatory adaptation peculiar to some diprotodont marsupials. Proceedings of the Zoological Society of London B109 (2): 261–279.

Abdala, F., D.A. Flores, and N.P. Giannini. 2001. Ontogeny of the skull of *Didelphis albiventris*. Journal of Mammalogy 82 (1): 190–200.

Abello, M.A. 2007. Sistemática y bioestratigrafía de los Paucituberculata (Mammalia, Marsupialia) del Cenozoico de América del Sur. Ph.D. dissertation, Facultad de Ciencias Naturales y Museo, Universidad Nacional de La Plata, La Plata.

Abello, M.A. 2013. Analysis of dental homologies and phylogeny of Paucituberculata (Mammalia: Marsupialia). Biological Journal of the Linnean Society 109 (2): 441–465.

Abello, M.A., and A.M. Candela. 2010. Postcranial skeleton of the Miocene marsupial *Palaeothentes* (Paucituberculata, Palaeothentidae): paleobiology and phylogeny. Journal of Vertebrate Paleontology 30 (5): 1515–1527.

Abello, M.A., and A.M. Candela. 2019. Paleobiology of *Argyrolagus* (Marsupialia, Argyrolagidae): an astonishing case of bipedalism among South American mammals. Journal of Mammalian Evolution 27: 419–444.

Abello, M.A., C.I. Montalvo, and F.J. Goin. 2002. Marsupiales del Mioceno superior de Caleufú (La Pampa, Argentina). Ameghiniana 39 (4): 433–442.

Abello, M.A., et al. 2015. Description of a new species of *Sparassocynus* (Marsupialia: Didelphoidea:

Sparassocynidae) from the late Miocene of Jujuy (Argentina) and taxonomic review of *Sparassocynus heterotopicus* from the Pliocene of Bolivia. Zootaxa 3937 (1): 147–160.

Abello, M.A., N. Toledo, and E. Ortiz-Jaureguizar. 2020. Evolution of South American Paucituberculata (Metatheria: Marsupialia): adaptive radiation and climate changes at the Eocene-Oligocene boundary. Historical Biology 32 (4): 476–493.

Abello, M.A., G.M. Martin, and Y. Cardoso. 2021. Review of the extinct 'shrew-opossums' (Marsupialia: Caenolestidae), with descriptions of two new genera and three new species from the Early Miocene of southern South America. Zoological Journal of the Linnean Society 193 (2): 464–498.

Adkins, R.M., E.L. Gelke, D. Rowe, and R.L. Honeycutt. 2001. Molecular phylogeny and divergence time estimates for major rodent groups: evidence from multiple genes. Molecular Biology and Evolution 18 (5): 777–791.

Adloff, P. 1904. Ueber die Zahnwechsel von *Cavia cobaya*. Anatomischer Anzeiger 25: 141–147.

Aitkin, L.M., and J.E. Nelson. 1989. Peripheral and central auditory specialization in a gliding marsupial, the feathertail glider, *Acrobates pygmaeus*. Brain Behavior and Evolution 33: 325–333.

Albright, L.B., and A.L. Titus. 2016. Magnetostratigraphy of Upper Cretaceous strata in Grand Staircase-Escalante National Monument, southern Utah: the Santonian–Campanian Stage boundary, reassessment of the C33N/C33R magnetochron boundary, and implications for regional sedimentation patterns within the Sevier Foreland Basin. Cretaceous Research 63: 77–94.

Alfaro, M.E., and M.T. Holder. 2006. The posterior and the prior in Bayesian phylogenetics. Annual Review of Ecology, Evolution, and Systematics 37 (1): 19–42.

Allman, E.S., M.T. Holder, and J.A. Rhodes. 2010. Estimating trees from filtered data: identifiability of models for morphological phylogenetics. Journal of Theoretical Biology 263 (1): 108–119.

Alloing-Séguier, L., M.R. Sánchez-Villagra, M.S.Y. Lee, and R. Lebrun. 2013. The bony labyrinth in diprotodontian marsupial mammals: diversity in extant and extinct forms and relationships with size and phylogeny. Journal of Mammalian Evolution 20 (3): 191–198.

Álvarez-Carretero, S., et al. 2021. A species-level timeline of mammal evolution integrating phylogenomic data. Nature 602: 263–267.

Amador, L.I., and N.P. Giannini. 2016. Phylogeny and evolution of body mass in didelphid marsupials (Marsupialia: Didelphimorphia: Didelphidae). Organisms Diversity and Evolution 16 (3): 641–657.

Ameghino, F. 1894. Énumération synoptique des espéces de mammifères fossiles des formations éocènes de Patagonie. Boletín de la Academia Nacional de Ciencias de Córdoba 13: 259–452.

Ameghino, F. 1899. Sinopsis geológico-paleontológica de la República Argentina: suplemento (adiciones y correcciones), La Plata: Imprenta La Libertad.

Ameghino, F. 1904. Nuevas especies de mamíferos cretáceos y terciarios de la República Argentina. Anales de la Sociedad Científica Argentina 56–58: 1–142.

Ameghino, F. 1908. Las formaciones sedimentarias de la región litoral de Mar del Plata y Chapadmalán. Anales del Museo Nacional de Buenos Aires 3: 343–428.

Amenábar, C.R., M. Montes, F. Nozal, and S. Santillana. 2019. Dinoflagellate cysts of the La Meseta Formation (middle to late Eocene), Antarctic Peninsula: implications for biostratigraphy, palaeoceanography and palaeoenvironment. Geological Magazine 157 (3): 351–366.

Amrine-Madsen, H., K.-P. Koepfli, R.K. Wayne, and M.S. Springer. 2003a. A new phylogenetic marker, apolipoprotein B, provides compelling evidence for eutherian relationships. Molecular Phylogenetics and Evolution 28 (2): 225–240.

Amrine-Madsen, H., et al. 2003b. Nuclear gene sequences provide evidence for the monophyly of australidelphian marsupials. Molecular Phylogenetics and Evolution 28 (2): 186–196.

Anderson, C. 1929. Palaeontological notes no. 1. *Macropus titan* Owen and *Thylacoleo carnifex* Owen. Records of the Australian Museum 17 (1): 35–49, plates xvii–xviii.

Anderson, V.J., et al. 2016. Andean topographic growth and basement uplift in southern Colombia: Implications for the evolution of the Magdalena, Orinoco, and Amazon river systems. Geosphere 12 (4): 1235–1256.

Antoine, P.O., et al. 2013. Middle Miocene vertebrates from the Amazonian Madre de Dios Subandean Zone, Peru. Journal of South American Earth Sciences 42: 91–102.

Antoine, P.-O., et al. 2016. A 60-million-year Cenozoic history of western Amazonian ecosystems in Contamana, eastern Peru. Gondwana Research 31: 30–59.

Antoine, P.-O., R. Salas-Gismondi, F. Pujos, M. Ganerød, and L. Marivaux. 2017. Western Amazonia as a hotspot of mammalian biodiversity throughout the Cenozoic. Journal of Mammalian Evolution 24 (1): 5–17.

Aplin, K.P. 1987. Basicranial anatomy of the early Miocene diprotodontian *Wynyardia bassiana* (Marsupialia: Wynyardiidae) and its implications for wynyardiid phylogeny and classification. *In* M. Archer (editor), Possums and opossums: studies in evolution: 369–391. Sydney: Surrey Beatty and Sons.

Aplin, K.P. 1990. Basicranial regions of diprotodontian marsupials: anatomy, ontogeny and phylogeny. Ph.D. dissertation, School of Biological Science, University of New South Wales, Sydney.

Aplin, K.P., and M. Archer. 1983. Review of possum and glider phylogeny: the case for the Phalangeroidea. *In* Abstracts of the 1983 Possums and Gliders Symposium of the Australian Mammal Society: 10–11. Armidale: Australian Mammal Society.

Aplin, K.P., and M. Archer. 1987. Recent advances in marsupial systematics with a new syncretic classification. *In* M. Archer (editor), Possums and opossums: studies in evolution: xv–lxxii. Sydney: Surrey Beatty and Sons.

Aplin, K.P., K.M. Helgen, and D.P. Lunde. 2010. A review of *Peroryctes broadbenti*, the giant bandicoot of Papua New Guinea. American Museum Novitates 3696: 1–41.

Archer, M. 1974a. The development of premolar and molar crowns of *Antechinus flavipes* (Marsupialia, Dasyuridae) and the significance of cusp ontogeny in mammalian teeth. Journal of the Royal Society of Western Australia 57: 118–125.

Archer, M. 1974b. The development of the cheek-teeth in *Antechinus flavipes* (Marsupialia, Dasyuridae). Journal of the Royal Society of Western Australia 57: 54–63.

Archer, M. 1975. *Ningaui*, a new genus of tiny dasyurids (Marsupialia) and two new species, *N. timealeyi* and *N. ridei*, from arid Western Australia. Memoirs of the Queensland Museum 17 (2): 237–249, pls. 227–229.

Archer, M. 1976a. Revision of the marsupial genus *Planigale* Troughton (Dasyuridae). Memoirs of the Queensland Museum 17 (3): 43–51.

Archer, M. 1976b. The basicranial region of marsupicarnivores (Marsupialia), inter-relationships of carnivorous marsupials, and affinities of the insectivorous marsupial peramelids. Zoological Journal of the Linnean Society 59 (3): 217–322.

Archer, M. 1976c. The dasyurid dentition and its relationships to that of didelphids, thylacinids, borhyaenids (Marsupicarnivora) and peramelids (Peramelina: Marsupialia). Australian Journal of Zoology, Supplementary Series S39: 1–34.

Archer, M. 1976d. Miocene marsupicarnivores (Marsupialia) from central South Australia, *Ankotarinja tirarensis* gen. et. sp. nov., *Keeuna woodburnei* gen. et. sp. nov., and their significance in terms of early marsupial radiations. Transactions of the Royal Society of South Australia 100: 53–73.

Archer, M. 1976e. Phascolarctid origins and the potential of the selenodont molar in the evolution of diprotodont marsupials. Memoirs of the Queensland Museum 17 (3): 367–372.

Archer, M. 1977. Revision of the dasyurid marsupial genus *Antechinomys* Krefft. Memoirs of the Queensland Museum 18 (1): 17–29, pls. 18–13.

Archer, M. 1981. Results of the Archbold Expeditions. No. 104. Systematic revision of the marsupial dasyurid genus *Sminthopsis* Thomas. Bulletin of the American Museum of Natural History 168 (2): 61–224.

Archer, M. 1982a. A review of Miocene thylacinids (Thylacinidae, Marsupialia), the phylogenetic position of the Thylacinidae and the problem of apriorisms in character analysis. *In* M. Archer (editor), Carnivorous marsupials: 445–476. Sydney: Royal Zoological Society of New South Wales.

Archer, M. 1982b. Review of the dasyurid (Marsupialia) fossil record, integration of data bearing on phylogenetic interpretation, and suprageneric classification. *In* M. Archer (editor), Carnivorous marsupials: 397–443. Mosman, New South Wales: Royal Zoological Society of New South Wales.

Archer, M. 1984a. On the importance of being a koala. *In* M. Archer and G. Clayton (editors), Vertebrate zoogeography and evolution in Australasia: 809–815. Perth: Hesperian Press.

Archer, M. 1984b. Origins and early radiations of marsupials. *In* M. Archer and G. Clayton (editors), Vertebrate zoogeography and evolution in Australasia: 585–631. Perth: Hesperian Press.

Archer, M. 1984c. The Australian marsupial radiation. *In* M. Archer and G. Clayton (editors), Vertebrate zoogeography and evolution in Australasia: 633–808. Perth: Hesperian Press.

Archer, M., and A. Bartholomai. 1978. Tertiary mammals of Australia: a synoptic review. Alcheringa: an Australasian Journal of Palaeontology 2 (1): 1–19.

Archer, M., and L. Dawson. 1982. Revision of marsupial lions of the genus *Thylacoleo* Gervais (Thylacoleonidae, Marsupialia) and thylacoleonid evolution in the Late Cainozoic. *In* M. Archer (editor), Carnivorous marsupials: 477–494. Mosman, New South Wales: Royal Zoological Society of New South Wales.

Archer, M., and T. Flannery. 1985. Revision of the extinct gigantic rat kangaroos (Potoroidae, Marsupialia), with description of a new Miocene genus and species and a new Pleistocene species of *Propleopus*. Journal of Paleontology 59 (6): 1331–1349.

Archer, M., and S.J. Hand. 2006. The Australian marsupial radiation. *In* J.R. Merrick, M. Archer, G.M. Hickey, and M.S.Y. Lee (editors), Evolution and biogeography of Australasian vertebrates: 575–646. Sydney: Auscipub Pty Ltd.

Archer, M., and J.A.W. Kirsch. 1977. The case for Thylacomyidae and Myrmecobiidae, or why are marsupial families so extended? Proceedings of the Linnean Society of New South Wales 102: 18–25.

Archer, M., and T.H. Rich. 1982. Results of the Ray E. Lemley expeditions. *Wakaleo alcootaensis* n. sp. (Thylacoleonidae, Marsupialia), a new marsupial lion form the Miocene of the Northern Territory with a consideration of early radiation in the family. *In* M. Archer (editor), Carnivorous marsupials: 495–502. Mosman, New South Wales: Royal Zoological Society of New South Wales.

Archer, M., and M. Wade. 1976. Results of the Ray E. Lemley Expeditions, Part I. The Allingham Formation and a new Pliocene vertebrate fauna from northern Australia. Memoirs of the Queensland Museum 17 (3): 379–398.

Archer, M., R.H. Tedford, and T.H. Rich. 1987. The Pilkipildridae, a new family and four new species of ?petauroid possums (Marsupialia: Phalangerida) from the Australian Miocene. *In* M. Archer (editor), Possums and opossums: studies in evolution: 607–627. Sydney: Surrey Beatty and Sons.

Archer, M., S. Hand, and H. Godthelp. 1988. A new order of Tertiary zalambdodont marsupials. Science 239: 1528–1531.

Archer, M., H. Godthelp, S.J. Hand, and D. Megirian. 1989. Fossil mammals of Riversleigh, northwestern Queensland: preliminary overview of biostratigraphy, correlation and environmental change. Australian Zoologist 25: 29–65.

Archer, M., R.G. Every, H. Godthelp, S. Hand, and K. Scally. 1990. Yingabalanaridae, a new family of enigmatic mammals from Tertiary deposits of Riversleigh, northwestern Queensland. Memoirs of the Queensland Museum 28: 193–202.

Archer, M., H. Godthelp, and S.J. Hand. 1993a. Early Eocene marsupial from Australia. Kaupia 3: 193–200.

Archer, M., P. Murray, S.J. Hand, and H. Godthelp. 1993b. Reconsideration of monotreme relationships based on the skull and dentition of the Miocene *Obdurodon dicksoni* (Ornithorhynchidae) from Riversleigh, Queensland, Australia. *In* F.S. Szalay, M.J. Novacek, and M.C. McKenna (editors), Mammal phylogeny, vol 1: Mesozoic differentiation, multituberculates, early therians, and marsupials: 75–94. New York: Springer-Verlag.

Archer, M., S.J. Hand, and H. Godthelp. 1994. Riversleigh: the story of animals in ancient rainforests of inland Australia, Sydney: Reed Books.

Archer, M., S.J. Hand, and H. Godthelp. 1995. Tertiary environmental and biotic change in Australia. *In* E.S. Vrba, G.H. Denton, T.C. Partridge, and L.H. Burckle (editors), Paleoclimate and evolution, with emphasis on human origins: New Haven: Yale University Press.

Archer, M., S.J. Hand, H. Godthelp, and P. Creaser. 1997. Correlation of the Cainozoic sediments of the Riversleigh World Heritage fossil property, Queensland, Australia. *In* J.-P. Aguilar, S. Legendre, and J. Michaux (editors), Actes du Congrès BiochroM'97: 131–152. Montpellier: École Pratique des Hautes Études, Institut de Montpellier.

Archer, M., et al. 1999. The evolutionary history and diversity of Australian mammals. Australian Mammalogy 21: 1–45.

Archer, M., et al. 2006. Current status of species-level representation in faunas from selected fossil localities in the Riversleigh World Heritage Area, northwestern Queensland. Alcheringa: an Australasian Journal of Palaeontology 31 (1): 1–17.

Archer, M., et al. 2011. Australia's first fossil marsupial mole (Notoryctemorphia) resolves controversies about their evolution and palaeoenvironmental origins. Proceedings of the Royal Society of London B, Biological Sciences 278 (1711): 1498–1506.

Archer, M., et al. 2016a. A new family of bizarre durophagous carnivorous marsupials from Miocene deposits in the Riversleigh World Heritage Area, northwestern Queensland. Scientific Reports 6: 26911.

Archer, M., et al. 2016b. Earliest known record of a hypercarnivorous dasyurid (Marsupialia), from newly discovered carbonates beyond the Riversleigh World Heritage Area, north Queensland. Memoirs of Museum Victoria 74: 137–150.

Archer, M., et al. 2018. *Miminipossum notioplanetes*, a Miocene forest-dwelling phalangeridan (Marsupialia; Diprotodontia) from northern and central Australia. Palaeontologia Electronica 21.1.2A: 1–11.

Archer, M., et al. 2019. New Cenozoic acrobatid possums from the Riversleigh World Heritage fossil deposits, Australia, and investigation of their bizarre middle ear structure. Society of Vertebrate Paleontology 79th Annual Meeting Program and Abstracts: 55.

Archibald, J.D. 1998. Archaic ungulates ("Condylarthra"). *In* C.M. Janis, K.M. Scott, and L.L. Jacobs (editors), Evolution of Tertiary mammals of North America, vol. 1. Terrestrial carnivores, ungulates, and ungulatelike mammals: 292–311. Cambridge: Cambridge University Press.

Ardente, N., D. Gettinger, R. Fonseca, H.D.G. Bergallo, and F. Martins-Hatano. 2013. Mammalia, Didelphimorphia, Didelphidae, *Glironia venusta* Thomas, 1912 and *Chironectes minimus* (Zimmermann, 1780): distribution extension for eastern Amazonia. Check List 9 (5): 1104–1107.

Arena, D.A., et al. 2015. Mammalian lineages and the biostratigraphy and biochronology of Cenozoic faunas from the Riversleigh World Heritage Area, Australia. Lethaia 49 (1): 43–60.

Argot, C. 2001. Functional-adaptive anatomy of the forelimb in the Didelphidae, and the paleobiology of the Paleocene marsupials *Mayulestes ferox* and *Pucadelphys andinus*. Journal of Morphology 247 (1): 51–79.

Argot, C. 2002. Functional-adaptive analysis of the hindlimb anatomy of extant marsupials and the paleobiology of the Paleocene marsupials *Mayulestes ferox* and *Pucadelphys andinus*. Journal of Morphology 253: 76–108.

Argot, C. 2003. Functional-adaptive anatomy of the axial skeleton of some extant marsupials and the paleobiology of the Paleocene marsupials *Mayulestes ferox* and *Pucadelphys andinus*. Journal of Morphology 255 (3): 279–300.

Argot, C. 2004. Evolution of South American mammalian predators (Borhyaenoidea): anatomical and palaeobiological implications. Zoological Journal of the Linnean Society 140 (4): 487–521.

Arguero, A., L. Albuja, and J. Brito. 2017. Nuevos registros de *Glironia venusta* Thomas, 1912 (Mammalia, Didelphidae) en el suroriente de Ecuador. Mastozoologia Neotropical 24 (1): 219–225.

Arnaudo, M.E., M. Arnal, and E.G. Ekdale. 2020. The auditory region of a caviomorph rodent (Hystricognathi) from the early Miocene of Patagonia (South America) and evolutionary considerations. Journal of Vertebrate Paleontology 40 (2): e1777557.

Asher, R.J., and M.R. Sánchez-Villagra. 2005. Locking yourself out: diversity among dentally zalambdodont therian mammals. Journal of Mammalian Evolution 12: 265–282.

Asher, R.J., I. Horovitz, and M.R. Sánchez-Villagra. 2004. First combined cladistic analysis of marsupial mammal interrelationships. Molecular Phylogenetics and Evolution 33: 240–250.

Asher, R.J., I. Horovitz, T. Martin, and M.R. Sánchez-Villagra. 2007. Neither a rodent nor a platypus: a reexamination of *Necrolestes patagonensis* Ameghino. American Museum Novitates 3546: 1–40.

Ashwell, K.W.S. 2010. The neurobiology of Australian marsupials: brain evolution in the other mammalian radiation. Melbourne: Cambridge University Press.

Averianov, A.O., J.D. Archibald, and E.G. Ekdale. 2010. New material of the Late Cretaceous deltatheroidan mammal *Sulestes* from Uzbekistan and phylogenetic reassessment of the metatherian-eutherian dichotomy. Journal of Systematic Palaeontology 8 (3): 301–330.

Babot, M.J., J.E. Powell, and Muizon, C. de. 2002. *Callistoe vincei*, a new Proborhyaenidae (Borhyaenoidea, Metatheria, Mammalia) from the early Eocene of Argentina. Geobios 35: 615–629.

Balme, J.M., D. Merrilees, and J.K. Porter. 1978. Late Quaternary mammal remains, spanning about 30 000 years, from excavations in Devil's Lair, Western Australia. Journal of the Royal Society of Western Australia 61 (33–65).

Bapst, D.W. 2013. When can clades be potentially resolved with morphology? PLoS One 8 (4): e62312.

Barba-Montoya, J., M. dos Reis, and Z. Yang. 2017. Comparison of different strategies for using fossil calibrations to generate the time prior in Bayesian molecular clock dating. Molecular Phylogenetics and Evolution 114: 386–400.

Barbour, R.A. 1963. The musculature and limb plexuses of *Trichosurus vulpecula*. Australian Journal of Zoology 11: 488–610.

Bartholomai, A. 1971a. *Dasyurus dunmalli,* a new species of fossil marsupial (Dasyuridae) in the upper Cainozoic deposits of Queensland. Memoirs of the Queensland Museum 16 (1): 19–26.

Bartholomai, A. 1971b. Morphology and variation of the cheek teeth in *Macropus giganteus* Shaw and *Macropus agilis* (Gould). Memoirs of the Queensland Museum 16 (1): 1–18.

Bartholomai, A. 1978a. The rostrum in *Palorchestes* Owen (Marsupialia: Diprotodontidae). Results of the Ray E. Lemley expedition, part 3. Memoirs of the Queensland Museum 18: 145–149.

Bartholomai, A. 1978b. The Macropodidae (Marsupialia) from the Allingham Formation, northern Queensland. Results of the Ray E. Lemley expeditions, Part 2. Memoirs of the Queensland Museum 18 (2): 127–143.

Bassarova, M., and M. Archer. 1999. Living and extinct pseudocheirids (Marsupialia, Pseudocheiridae): Phylogenetic relationships and changes in diversity through time. Australian Mammalogy 21: 25–27.

Bassarova, M., M. Archer, and S.J. Hand. 2001. New Oligo-Miocene pseudocheirids (Marsupialia) of the genus *Paljara* from Riversleigh, northwestern Queensland. Memoirs of the Association of Australasian Palaeontologists 25: 61–75.

Bates, H., et al. 2014. Three new Miocene species of musky rat-kangaroos (Hypsiprymnodontidae, Macropodoidea): description, phylogenetics, and paleoecology. Journal of Vertebrate Paleontology 34 (2): 383–396.

Baverstock, P.R. 1984. The molecular relationships of Australian possums and gliders. *In* A. Smith and I. Hume (editors), Possums and gliders: 1–8. Sydney: Surrey Beatty and Sons.

Beck, R.M.D. 2008a. A dated phylogeny of marsupials using a molecular supermatrix and multiple fossil constraints. Journal of Mammalogy 89 (1): 175–189.

Beck, R.M.D. 2008b. Form, function, phylogeny and biogeography of enigmatic Australian metatherians. Ph.D. dissertation, School of Biological, Earth, and Environmental Sciences, University of New South Wales, Sydney.

Beck, R.M.D. 2009. Was the Oligo-Miocene Australian metatherian *Yalkaparidon* a 'mammalian woodpecker'? Biological Journal of the Linnean Society 97: 1–17.

Beck, R.M.D. 2012. An 'ameridelphian' marsupial from the early Eocene of Australia supports a complex model of Southern Hemisphere marsupial biogeography. Naturwissenschaften 99 (9): 715–729.

Beck, R.M.D. 2015. A peculiar faunivorous metatherian from the early Eocene of Australia. Acta Palaeontologica Polonica 60 (1): 123–129.

Beck, R.M.D. 2017a. The skull of *Epidolops ameghinoi* from the early Eocene Itaboraí fauna, southeastern Brazil, and the affinities of the extinct marsupialiform order Polydolopimorphia. Journal of Mammalian Evolution 24 (4): 373–414.

Beck, R.M.D. 2017b. The biogeographical history of non-marine mammaliaforms in the Sahul region. *In* M.C. Ebach (editor), Handbook of Australasian biogeography: 329–366. Boca Raton: CRC Press.

Beck, R.M.D., and M.L. Taglioretti. 2020. A nearly complete juvenile skull of the marsupial *Sparassocynus derivatus* from the Pliocene of Argentina, the affinities of "sparassocynids," and the diversification of opossums (Marsupialia; Didelphimorphia; Didelphidae). Journal of Mammalian Evolution 27: 385–417.

Beck, R.M.D., H. Godthelp, V. Weisbecker, M. Archer, and S.J. Hand. 2008a. Australia's oldest marsupial fossils and their biogeographical implications. PLoS One 3 (3): e1858.

Beck, R.M.D., et al. 2008b. A bizarre new family of Marsupialia (incertae sedis) from the early Pliocene of northeastern Australia: implications for the phylogeny of bunodont marsupials. Journal of Paleontology 82: 749–762.

Beck, R.M.D., K.J. Travouillon, K.P. Aplin, H. Godthelp, and M. Archer. 2014. The osteology and systematics of the enigmatic Australian Oligo-Miocene metatherian *Yalkaparidon* (Yalkaparidontidae; Yalkaparidontia; ?Australidelphia; Marsupialia). Journal of Mammalian Evolution 21 (2): 127–172.

Beck, R.M.D., N.M. Warburton, M. Archer, S.J. Hand, and K.P. Aplin. 2016. Going underground: postcranial morphology of the early Miocene marsupial mole *Naraboryctes philcreaseri* and the evolution of fossoriality in notoryctemorphians. Memoirs of Museum Victoria 74: 151–171.

Beck, R.M.D., et al. 2020. A new family of diprotodontian marsupials from the latest Oligocene of Australia and the evolution of wombats, koalas, and their relatives (Vombatiformes). Scientific Reports 10: 9741.

Bell, C.J., et al. 2004. The Blancan, Irvingtonian and Rancholabrean mammal ages. *In* M.O. Woodburne (editor), Late Cretaceous and Cenozoic mammals of North America: biostratigraphy and geochronology: 232–314. New York: Columbia University Press.

Bennett, C.V., P. Upchurch, F.J. Goin, and A. Goswami. 2018. Deep time diversity of metatherian mammals: implications for evolutionary history and fossil-record quality. Paleobiology 44 (02): 171–198.

Bensley, B.A. 1903. On the evolution of the Australian Marsupialia, with remarks on the relationships of the marsupials in general. Transactions of the Linnean Society of London (Zoology) 9: 83–217.

Bensley, B.A. 1906. The homologies of the stylar cusps of the upper molars of the Didelphyidae. University of Toronto Studies (Biological Series) 5: 1–13.

Benton, M.J., et al. 2015. Constraints on the timescale of animal evolutionary history. Palaeontologia Electronica 18.1.1FC: 1–106.

Berkovitz, B.K.B. 1966. The homology of the premolar teeth in *Setonix brachyurus* (Macropodidae: Marsupialia). Archives of Oral Biology 11: 1371–1384.

Berkovitz, B.K.B 1968. Some stages in early development of post-incisor dentition of *Trichosurus vulpecula* (Phalangeroidea: Marsupialia). Journal of Zoology, London 154: 403–414.

Berkovitz, B.K.B 1972a. Ontogeny of tooth replacement in the guinea pig (*Cavia cobya*). Archives of Oral Biology 17 (4): 711–718.

Berkovitz, B.K.B 1972b. Tooth development in *Protemnodon eugenii*. Journal of Dental Research 51 (5): 1467–1473.

Berkovitz, B.K.B. 1978. Tooth ontogeny in *Didelphis virginiana* (Marsupialia: Didelphidae). Australian Journal of Zoology 26: 61–68.

Bertrand, O.C., H.P. Püschel, J.A. Schwab, M.T. Silcox, and S.L. Brusatte. 2021. The impact of locomotion on the brain evolution of squirrels and close relatives. Communications Biology 4: 460.

Bi, S., X. Jin, S. Li, and T. Du. 2015. A new Cretaceous metatherian mammal from Henan, China. PeerJ 3: e896.

Bi, S., et al. 2018. An Early Cretaceous eutherian and the placental-marsupial dichotomy. Nature 558 (7710): 390–395.

Black, K.H. 1999. Diversity and relationships of living and extinct koalas (Phascolarctidae, Marsupialia). Australian Mammalogy 21: 16–17.

Black, K.H. 2006. Description of new material for *Propalorchestes novaculacephalus* (Marsupialia: Palorchestidae) from the mid Miocene of Riversleigh, northwestern Queensland. Alcheringa: an Australasian Journal of Palaeontology 30 (2): 351–361.

Black, K.H. 2008. Diversity, phylogeny and biostratigraphy of diprotodontoids (Marsupialia: Diprotodontidae, Palorchestidae) from the Riversleigh World Heritage Area. Ph.D. dissertation, School of Biological, Earth, and Environmental Sciences, University of New South Wales, Sydney.

Black, K.H. 2010. *Ngapakaldia bonythoni* (Marsupialia, Diprotodontidae): new material from Riversleigh, northwestern Queensland, and a reassessment of the genus *Bematherium*. Alcheringa: an Australasian Journal of Palaeontology 34 (4): 471–492.

Black, K.H., and M. Archer. 1997a. *Silvabestius* gen. nov. a primitive zygomaturine (Marsupialia, Diprotodontidae) from Riversleigh, northwestern Queensland. Memoirs of the Queensland Museum 41 (2): 193–208.

Black, K.H., and M. Archer. 1997b. *Nimiokoala* gen. nov. (Marsupialia, Phascolarctidae) from Riversleigh, northwestern Queensland, with a revision of *Litokoala*. Memoirs of the Queensland Museum 41 (2): 209–228.

Black, K.H., and S.J. Hand. 2010. First crania and assessment of species boundaries in *Nimbadon* (Marsupialia: Diprotodontidae) from the middle Miocene of Australia. American Museum Novitates 3678: 1–60.

Black, K.H., and B. Mackness. 1999. Diversity and relationships of diprotodontoid marsupials. Australian Mammalogy 21: 20–21.

Black, K.H., M. Archer, S.J. Hand, and H. Godthelp. 2010. First comprehensive analysis of cranial ontogeny in a fossil marsupial—from a 15-million-year-old cave deposit in northern Australia. Journal of Vertebrate Paleontology 30 (4): 993–1011.

Black, K.H., M. Archer, and S.J. Hand. 2012a. New Tertiary koala (Marsupialia, Phascolarctidae) from Riversleigh, Australia, with a revision of phascolarctid phylogenetics, paleoecology, and paleobiodiversity. Journal of Vertebrate Paleontology 32 (1): 125–138.

Black, K.H., M. Archer, S.J. Hand, and H. Godthelp. 2012b. The rise of Australian marsupials: a synopsis of biostratigraphic, phylogenetic, palaeoecologic and palaeobiogeographic understanding. *In* J.A. Talent (editor), Earth and life: global biodiversity, extinction intervals and biogeographic perturbations through time: 983–1078. Dordrecht: Springer Verlag.

Black, K.H., M. Archer, S.J. Hand, and H. Godthelp. 2013. Revision in the marsupial diprotodontid genus *Neohelos*: systematics and biostratigraphy. Acta Palaeontologica Polonica 58 (4): 679–706.

Black, K.H., J. Louys, and G.J. Price. 2014a. Understanding morphological variation in the extant koala as a framework for identification of species boundaries in extinct koalas (Phascolarctidae; Marsupialia). Journal of Systematic Palaeontology 12 (2): 237–264.

Black, K.H., G.J. Price, M. Archer, and S.J. Hand. 2014b. Bearing up well? Understanding the past, present and future of Australia's koalas. Gondwana Research 25 (3): 1186–1201.

Black, K.H., et al. 2014c. A new species of the basal "kangaroo" *Balbaroo* and a re-evaluation of stem

macropodiform interrelationships. PLoS One 9 (11): e112705.

Blackhart, B.D., et al. 1986. Structure of the human apolipoprotein B gene. Journal of Biological Chemistry 261 (33): 15364–15367.

Blanshard, W.H. 1990. Growth and development of the koala from birth to weaning. *In* M.A.K. Lee, K.A. Handasyde, and G.D. Sanson (editors), Biology of the koala: 193–202. Sydney: Surrey Beatty and Sons.

Boas, J.E.G., and S. Paulli. 1908. The elephant's head. Studies in the comparative anatomy of the organs of the head of the Indian elephant and other mammals. Part I., Copenhagen: Gustav Fisher.

Bolk, L. 1929. Die Gebissentwicklung von *Trichosurus*. Gegenbaurs Morphologisches Jahrbuch 62: 58–178.

Bonaparte, C. 1832. Saggio d'una distribuzione metodica degli animali vertebrati a sangue freddo, Roma: Presso Antonio Boulzaler.

Bonaparte, C. 1838. Synopsis vertebratorum systematis. Annali delle Scienze Naturali, Bologna 2 (1): 105–133.

Bonaparte, J.F. 1990. New Late Cretaceous mammals from the Los Alamitos Formation, northern Patagonia. National Geographic Research 6 (1): 63–93.

Bowen, G.J., and J.I. Bloch. 2002. Petrography and geochemistry of floodplain limestones from the Clarks Fork basin, Wyoming, USA: carbonate deposition and fossil accumulation on a Paleocene-Eocene floodplain. Journal of Sedimentary Research 72 (1): 46–58.

Bown, T.M., and J.G. Fleagle. 1993. Systematics, biostratigraphy, and dental evolution of the Palaeothentidae, later Oligocene to early-middle Miocene (Deseadan-Santacrucian) caenolestoid marsupials of South America. Paleontological Society Memoirs 29: 1–76.

Bown, T.M., and J.G. Fleagle. 1994. New Colhuehuapian and Santacrucian Microbiotheriidae and Caenolestidae from Patagonian Argentina. Journal of Vertebrate Paleontology 11 (Suppl. 3): 17A.

Bown, T.M., and M.J. Kraus. 1979. Origin of the tribosphenic molar and metatherian and eutherian dental formulae. *In* J.A. Lillegraven, Z. Kielan-Jaworowska, and W.A. Clemens (editors), Mesozoic mammals: the first two-thirds of mammalian history: 172–181. Berkeley: University of California Press.

Bown, T.M., and K.D. Rose. 1979. *Mimoperadectes*, a new marsupial, and *Worlandia*, a new dermopteran, from the lower part of the Willwood Formation (early Eocene), Bighorn Basin, Wyoming. Contributions from the Museum of Paleontology University of Michigan 25 (4): 89–104.

Bragg, J.G., S. Potter, K. Bi, and C. Moritz. 2016. Exon capture phylogenomics: efficacy across scales of divergence. Molecular Ecology Resources 16 (5): 1059–1068.

Brammall, J.R. 1998. A new petauroid possum from the Oligo-Miocene of Riversleigh, northwestern Queensland. Alcheringa: an Australasian Journal of Palaeontology 23: 31–50.

Brammall, J.R., and M. Archer. 1997. A new Oligo-Miocene species of *Burramys* (Marsupialia, Burramyidae) from Riversleigh, northwestern Queensland. Memoirs of the Queensland Museum 41: 247–268.

Brammall, J.R., and M. Archer. 1999. Living and extinct petaurids, acrobatids, tarsipedids and burramyids (Marsupialia): relationships and diversity through time. Australian Mammalogy 21: 24–25.

Brewer, P. 2007. New record of *Warendja wakefieldi* (Vombatidae; Marsupialia) from Wombeyan Caves, New South Wales. Alcheringa: an Australasian Journal of Palaeontology 31 (2): 153–171.

Brewer, P. 2008. Palaeontology of primitive wombats. Ph.D. dissertation, School of Biological, Earth, and Environmental Sciences, University of New South Wales, Sydney.

Brewer, P., M. Archer, S. Hand, and H. Godthelp. 2007. A new species of the wombat *Warendja* from late Miocene deposits at Riversleigh, north-west Queensland. Palaeontology 50: 811–828.

Brewer, P., M. Archer, and S. Hand. 2008. Additional specimens of the oldest wombat *Rhizophascolonus crowcrofti* (Vombatidae; Marsupialia) from the Wipajiri Formation, South Australia: an intermediate morphology? Journal of Vertebrate Paleontology 28 (4): 1144–1148.

Brewer, P., M. Archer, S.J. Hand, and R. Abel. 2015. New genus of primitive wombat (Vombatidae, Marsupialia) from Miocene deposits in the Riversleigh World Heritage Area (Queensland, Australia). Palaeontologia Electronica 8.1.9A: 1–40.

Brewer, P., M. Archer, S. Hand, and G. Price. 2018. A new species of Miocene wombat (Marsupialia, Vombatiformes) from Riversleigh, Queensland, Australia, and implications for the evolutionary history of the Vombatidae. Palaeontologia Electronica: 21.2.27A: 1–48.

Brocklehurst, N., and Y. Haridy. 2021. Do meristic characters used in phylogenetic analysis evolve in an ordered manner? Systematic Biology 70 (4): 707–718.

Bromham, L. 2019. Six impossible things before breakfast: Assumptions, models, and belief in molecular dating. Trends in Ecology and Evolution 34 (5): 474–486.

Bromham, L., et al. 2018. Bayesian molecular dating: opening up the black box. Biological Reviews 93 (2): 1165–1191.

Brown, J.W., and S.A. Smith. 2018. The past sure is tense: On interpreting phylogenetic divergence time estimates. Systematic Biology 67 (2): 340–353.

Brown, J.W., C. Parins-Fukuchi, G.W. Stull, O.M. Vargas, and S.A. Smith. 2017. Bayesian and likelihood phylogenetic reconstructions of morphological traits are not discordant when taking uncertainty into consideration: a comment on Puttick *et al.* Proceedings of the Royal Society of London B, Biological Sciences 284 (1864): 20170986.

Bryant, D., and M.W. Hahn. 2020. The concatenation question. *In* C. Scornavacca, F. Delsuc, and N. Galtier (editors), Phylogenetics in the genomic era: 3.4:1–3.4:23. No commercial publisher. [https://hal.inria.fr/PGE/hal-02535651]

Bublitz, J. 1987. Untersuchungen zur Systematik der rezenten Caenolestidae Trouessart, 1898: unter Verwendung craniometerischer Methoden. Bonner Zoologische Monographien 23: 1–96.

Budd, G.E., and R.P. Mann. 2020. Survival and selection biases in early animal evolution and a source of systematic overestimation in molecular clocks. Interface Focus 10 (4): 20190110.

Burgin, C.J., J.P. Colella, P.L. Kahn, and N.S. Upham. 2018. How many species of mammals are there? Journal of Mammalogy 99 (1): 1–14.

Burk, A., M. Westerman, and M. Springer. 1998. The phylogenetic position of the musky rat-kangaroo and the evolution of bipedal hopping in kangaroos (Macropodidae: Diprotodontia). Systematic Biology 47 (3): 457–474.

Burk, A., M. Westerman, D.J. Kao, J.R. Kavanagh, and M.S. Springer. 1999. Analysis of marsupial interordinal relationships based on 12S rRNA, tRNA valine, 16S rRNA, and cytochrome *b* sequences. Journal of Mammalian Evolution 6 (4): 317–334.

Burk, A., E.J.P. Douzery, and M.S. Springer. 2002. The secondary structure of mammalian mitochondrial 16S rRNA molecules: refinements based on a comparative phylogenetic approach. Journal of Mammalian Evolution 9 (3): 225–252.

Burnett, G. 1830. Illustrations of the Quadrupeda, or quadrupeds; being the arrangement of the true four-footed beasts indicated in outline. Quarterly Journal of Science, Literature, and Art (Jul–Dec) 1830: 336–353.

Butler, K., K.J. Travouillon, G.J. Price, M. Archer, and S.J. Hand. 2016. *Cookeroo*, a new genus of fossil kangaroo (Marsupialia, Macropodidae) from the Oligo-Miocene of Riversleigh, northwestern Queensland, Australia. Journal of Vertebrate Paleontology 36 (3): e1083029.

Butler, K., K.J. Travouillon, G.J. Price, M. Archer, and S.J. Hand. 2017. Species abundance, richness and body size evolution of kangaroos (Marsupialia: Macropodiformes) throughout the Oligo-Miocene of Australia. Palaeogeography, Palaeoclimatology, Palaeoecology 487: 25–36.

Butler, K., K.J. Travouillon, G. Price, M. Archer, and S.J. Hand. 2018. Revision of Oligo-Miocene kangaroos, *Ganawamaya* and *Nambaroo* (Marsupialia: Macropodiformes, Balbaridae). Palaeontologia Electronica 21.1.8A: 1–58.

Butler, R.F., L.G. Marshall, R.E. Drake, and G.H. Curtis. 1984. Magnetic polarity stratigraphy and 40K–40Ar dating of late Miocene and early Pliocene continental deposits, Catamarca Province, NW Argentina. Journal of Geology 92: 623–636.

Cabrera, A. 1927. Datos para el conocimiento de los dasyuroideos fósiles argentinos. Revista del Museo de La Plata 30: 271–315.

Camens, A.B. 2008. Systematic and palaeobiological implications of postcranial morphology in the Diprotodontidae (Marsupialia). Ph.D. dissertation, School of Earth and Environmental Sciences, University of Adelaide, Adelaide.

Camens, A.B., and R.T. Wells. 2009. Palaeobiology of *Euowenia grata* (Marsupialia: Diprotodontinae) and its presence in northern South Australia. Journal of Mammalian Evolution 17 (1): 3–19.

Carleton, M.D., and G.G. Musser. 1989. Systematic studies of oryzomyine rodents (Muridae, Sigmodontinae): a synopsis of *Microryzomys*. Bulletin of the American Museum of Natural History 191: 1–83.

Carneiro, L.M. 2018. A new species of *Varalphadon* (Mammalia, Metatheria, Sparassodonta) from the upper Cenomanian of southern Utah, North America: Phylogenetic and biogeographic insights. Cretaceous Research 84: 88–96.

Carneiro, L.M. 2019. A new protodidelphid (Mammalia, Marsupialia, Didelphimorphia) from the Itaboraí Basin and its implications for the evolution of the Protodidelphidae. Anais da Academia Brasileira de Ciencias 91 (Suppl. 2): e20180440.

Carneiro, L.M., and E.V. Oliveira. 2017a. Systematic affinities of the extinct metatherian *Eobrasilia coutoi* Simpson, 1947, a South American early Eocene Stagodontidae: implications for "Eobrasiliinae." Revista Brasileira de Paleontologia 20 (3): 355–372.

Carneiro, L.M., and E.V. Oliveira. 2017b. The Eocene South American metatherian *Zeusdelphys complicatus* is not a protodidelphid but a hatcheriform: Paleobiogeographic implications. Acta Palaeontologica Polonica 62 (3): 497–507.

Carneiro, L.M., É.V. Oliveira, and F.J. Goin. 2018. *Austropediomys marshalli* gen. et sp. nov., a new Pediomyoidea (Mammalia, Metatheria) from the Paleogene of Brazil: paleobiogeographic implications. Revista Brasileira de Paleontologia 21 (2): 120–131.

Cartmill, M. 1974. *Daubentonia*, *Dactylopsila*, woodpeckers, and klinorhynchy. *In* R.D. Martin, G.A. Doyle, and A.C. Walker (editors), Prosimian biology: 655–670. London: Gerald Duckworth and Co. Ltd.

Cartmill, M. 1978. The orbital mosaic in prosimians and the use of variable traits in systematics. Folia Primatologica 30: 89–114.

Cascini, M., K.J. Mitchell, A. Cooper, and M.J. Phillips. 2019. Reconstructing the evolution of giant extinct kangaroos: Comparing the utility of DNA, morphology, and total evidence. Systematic Biology 68 (3): 520–537.

Case, J.A. 1984. A new genus of Potoroinae (Marsupialia: Macropodidae) from the Miocene Ngapakaldi Local Fauna, South Australia, and a definition of the Potoroinae. Journal of Paleontology 58 (4): 1074–1086.

Case, J.A., F.J. Goin, and M.O. Woodburne. 2005. "South American" marsupials from the Late Cretaceous of North America and the origin of marsupial cohorts. Journal of Mammalian Evolution 12 (3-4): 461–494.

Case, J.A., R. Meredith, and J. Person. 2008. A Pre-Neogene phalangerid possum from South Australia. Museum of Northern Arizona Bulletin 65: 659–676.

Castro, M.C., M.J. Dahur, and G.S. Ferreira. 2021. Amazonia as the origin and diversification area of Didelphidae (Mammalia: Metatheria), and a review of the fossil record of the clade. Journal of Mammalian Evolution 28: 583–598.

Celik, M., et al. 2019. A molecular and morphometric assessment of the systematics of the *Macropus* complex clarifies the tempo and mode of kangaroo evolution. Zoological Journal of the Linnean Society 186: 793–812.

Chamberlain, P.M., K.J. Travouillon, M. Archer, and S.J. Hand. 2015. *Kutjamarcoot brevirostrum* gen. et sp. nov., a new short-snouted, early Miocene bandicoot (Marsupialia: Peramelemorphia) from the Kutjamarpu Local Fauna (Wipajiri Formation) in South Australia. Alcheringa: an Australasian Journal of Palaeontology 40 (2): 197–206.

Charles, C., F. Sole, H.G. Rodrigues, and L. Viriot. 2013. Under pressure? Dental adaptations to termitophagy and vermivory among mammals. Evolution 67 (6): 1792–1804.

Chemisquy, M.A. 2015. Peramorphic males and extreme sexual dimorphism in *Monodelphis dimidiata* (Didelphidae). Zoomorphology 134 (4): 587–599.

Chen, S.H., et al. 1986. The complete cDNA and amino acid sequence of human apolipoprotein B-100. Journal of Biological Chemistry 261 (28): 12918–12921.

Chew, A.E., and K.B. Oheim. 2013. Diversity and climate change in the middle-late Wasatchian (early Eocene) Willwood Formation, central Bighorn Basin, Wyoming. Palaeogeography, Palaeoclimatology, Palaeoecology 369: 67–78.

Chornogubsky, L., and F.J. Goin. 2015. A review of the molar morphology and phylogenetic affinities of *Sillustania quechuense* (Metatheria, Polydolopimorphia, Sillustaniidae), from the early Paleogene of Laguna Umayo, southeastern Peru. Journal of Vertebrate Paleontology 35 (6): e983238.

Chornogubsky, L., and A.G. Kramarz. 2012. Nuevos hallazgos de Microbiotheriidae (Mammalia, Marsupialia) en la Formación Pinturas (Mioceno Temprano, Argentina). Ameghiniana 49 (4): 442–450.

Cifelli, R.L., and B.M. Davis. 2015. Tribosphenic mammals from the Lower Cretaceous Cloverly Formation of Montana and Wyoming. Journal of Vertebrate Paleontology 35 (3): e920848.

Cifelli, R.L., and C. de Muizon. 1997. Dentition and jaw of *Kokopellia juddi*, a primitive marsupial or near-marsupial from the Medial Cretaceous of Utah. Journal of Mammalian Evolution 4 (4): 241–258.

Cifelli, R.L., and C. de Muizon. 1998a. Tooth eruption and replacement pattern in early marsupials. Comptes Rendus de l'Académie des Sciences, Paris 326: 215–220.

Cifelli, R.L., and C. de Muizon. 1998b. Marsupial mammal from the Upper Cretaceous North Horn Formation, central Utah. Journal of Paleontology 72 (3): 532–537.

Cione, A.L., G.M. Gasparini, E. Soibelzon, L.H. Soibelzon, and E.P. Tonni. 2015. The Great American

Biotic Interchange: a South American perspective, Dordrecht: Springer.

Cladaras, C., M. Hadzopoulou-Cladaras, R.T. Nolte, D. Atkinson, and V.I. Zannis. 1986. The complete sequence and structural analysis of human apolipoprotein B-100: relationship between apoB-100 and apoB-48 forms. EMBO Journal 5 (13): 3495–3507.

Clark, C.T., and K.K. Smith. 1993. Cranial osteogenesis in *Monodelphis domestica* (Didelphidae) and *Macropus eugenii* (Macropodidae). Journal of Morphology 215: 119–149.

Clemens, W.A. 1966. Fossil mammals of the Type Lance Formation, Wyoming. Part II: Marsupialia. University of California Publications in Geological Sciences 62: 1–122.

Clemens, W.A., and M. Plane. 1974. Mid-Tertiary Thylacoleonidae (Marsupialia, Mammalia). Journal of Paleontology 48 (4): 652–660.

Clemens, W.A., B.J. Richardson, and P.R. Baverstock. 1989. Biogeography and phylogeny of the Metatheria. *In* D.W. Walton, and G.R. Dyne (editors), Fauna of Australia, vol. 1B. Mammalia: 527–548. Canberra: Australian Government Publishing Service.

Clyde, W.C., et al. 2014. New age constraints for the Salamanca Formation and lower Río Chico Group in the western San Jorge Basin, Patagonia, Argentina: implications for Cretaceous-Paleogene extinction recovery and land mammal age correlations. Geological Society of America Bulletin 126 (3-4): 289–306.

Cobbett, A., M. Wilkinson, and M.A. Wills. 2007. Fossils impact as hard as living taxa in parsimony analyses of morphology. Systematic Biology 56 (5): 753–766.

Coccioni, R., et al. 2012. An integrated stratigraphic record of the Palaeocene–lower Eocene at Gubbio (Italy): new insights into the early Palaeogene hyperthermals and carbon isotope excursions. Terra Nova 24: 380–386.

Cohen, K.M., S.C. Finney, P.L. Gibbard, and J. Fan. 2013 [updated]. The ICS International Chronostratigraphic Chart. Episodes 36: 199–204.

Colgan, D., T.F. Flannery, J. Trimble, and K. Aplin. 1993. Electrophoretic and morphological analysis of the systematics of the *Phalanger orientalis* (Marsupialia) species complex in Papua New Guinea and the Solomon Islands. Australian Journal of Zoology 41: 355–378.

Condamine, F.L., N.S. Nagalingum, C.R. Marshall, and H. Morlon. 2015. Origin and diversification of living cycads: a cautionary tale on the impact of the branching process prior in Bayesian molecular dating. BMC Evolutionary Biology 15: 65.

Cooke, B.N. 1997a. Two new balbarine kangaroos and lower molar evolution within the subfamily. Memoirs of the Queensland Museum 41 (2): 269–280.

Cooke, B.N. 1997b. New Miocene bulungamayine kangaroos (Marsupialia: Potoroidae) from Riversleigh, northwestern Queensland. Memoirs of the Queensland Museum 41 (2): 281–294.

Cooke, B.N. 1997c. Researches into fossil kangaroos and kangaroo evolution. Ph.D. dissertation, School of Biological Science, University of New South Wales, Sydney.

Cooke, B.N. 1999. *Wanburoo hilarus* gen. et sp. nov., a lophodont bulungamayine kangaroo (Marsupialia: Macropodoidea: Bulungamayinae) from the Miocene deposits of Riversleigh, northwestern Queensland. Records of the Western Australian Museum, Supplement 57: 239–253.

Cooke, B.N. 2000. Cranial remains of a new species of balbarine kangaroo (Marsupialia: Macropodoidea) from the Oligo-Miocene freshwater limestone deposits of Riversleigh World Heritage area, northern Australia. Journal of Paleontology 74 (2): 317–326.

Cooke, B.N. 2006. Kangaroos. *In* J.R. Merrick, M. Archer, G.M. Hickey, and M.S.Y. Lee (editors), Evolution and biogeography of Australasian vertebrates: 647–672. Sydney: Auscipub Pty Ltd.

Cooke, B.N., and B.P. Kear. 1999. Evolution and diversity of kangaroos (Macropodoidea, Marsupialia). Australian Mammalogy 21: 27–29.

Cooke, B.N., K.J. Travouillon, M. Archer, and S.J. Hand. 2015. *Ganguroo robustiter*, sp. nov. (Macropodoidea, Marsupialia), a middle to early late Miocene basal macropodid from Riversleigh World Heritage Area, Australia. Journal of Vertebrate Paleontology 35 (4): e956879.

Cooper, C.E. 2000. *Myrmecobius fasciatus* (Dasyuromorphia: Myrmecobiidae). Mammalian Species 43 (881): 129–140.

Cooper, N.K., K.P. Aplin, and M. Adams. 2000. A new species of false antechinus (Marsupialia: Dasyuromorphia: Dasyuridae) from the Pilbara region, Western Australia. Records of the Western Australian Museum 20: 115–136.

Cope, E.D. 1880. On the foramina perforating the posterior part of the squamosal bone of the Mammalia. Proceedings of the American Philosophical Society 18: 452–461.

Cope, E.D. 1888. The mechanical causes of the origin of the dentition of the Rodentia. American Naturalist 22: 3–11.

Coues, E. 1872. The osteology and myology of *Didelphys virginiana*. Memoirs of the Boston Society of Natural History 2: 41–154.

Couzens, A.M.C., and G.J. Prideaux. 2018. Rapid Pliocene adaptive radiation of modern kangaroos. Science 362: 72–75.

Cox, P.G. 2006. Character evolution in the orbital region of the Afrotheria. Journal of Zoology 269 (4): 514–526.

Cozzuol, M.A., F. Goin, M. De Los Reyes, and A. Ranzi. 2006. The oldest species of *Didelphis* (Mammalia, Marsupialia, Didelphidae), from the late Miocene of Amazonia. Journal of Mammalogy 87 (4): 663–667.

Crabb, P. 1982. Pleistocene dasyurids from southwestern New South Wales. *In* M. Archer (editor), Carnivorous marsupials: 511–516. Mosman, New South Wales: Royal Zoological Society of New South Wales.

Crame, J.A., et al. 2014. The early origin of the Antarctic marine fauna and its evolutionary implications. PLoS One 9 (12): e114743.

Creaser, P. 1997. Oligocene–Miocene sediments of Riversleigh: the potential significance of topography. Memoirs of the Queensland Museum 41: 303–314.

Crisp, M.D., S.A. Trewick, and L.G. Cook. 2011. Hypothesis testing in biogeography. Trends in Ecology and Evolution 26 (2): 66–72.

Crochet, J.-Y. 1979. Diversité systématique des Didelphidae (Marsupialia) européens tertiaires. Geobios 12 (3): 365–378.

Crochet, J.-Y. 1980. Les marsupiaux du Tertiare d'Europe, Paris: Editions Foundation Singer-Polinac.

Crochet, J.-Y., and B. Sigé. 1993. Les mammifères de Chulpas (Formation Umayo, transition Crétacé-Tertiaire, Pérou). Données préliminaires. Documents du Laboratoire de Géologie de Lyon 125: 97–107.

Croft, D.A. 2007. The middle Miocene (Laventan) Quebrada Honda Fauna, southern Bolivia and a description of its notoungulates. Palaeontology 50 (1): 277–303.

Crompton, A.W., D.E. Lieberman, T. Owerkowicz, R.V. Baudinette, and J. Skinner. 2008. Motor control of masticatory movements in the southern hairy-nosed wombat (*Lasiorhinus latifrons*). *In* C.J. Vinyard, M.J. Ravosa, and C.E. Wall (editors), Primate craniofacial function and biology: 83–111. New York: Springer.

Crompton, A.W., C. Musinsky, G.W. Rougier, B.A.S. Bhullar, and J.A. Miyamae. 2018. Origin of the lateral wall of the mammalian skull: Fossils, monotremes and therians revisited. Journal of Mammalian Evolution 25 (3): 301–313.

Crosby, K. 2002a. A second species of the possum *Durudawiri* (Marsupialia: Miralinidae) from the early Miocene of Riversleigh, northwestern Queensland. Alcheringa: an Australasian Journal of Palaeontology 26: 333–340.

Crosby, K. 2002b. Studies in the diversity and evolution of phalangeroid possums (Marsupialia; Phalangerida; Phalangeroidea). Ph.D. dissertation, School of Biological, Earth, and Environmental Sciences, University of New South Wales, Sydney.

Crosby, K. 2007. Rediagnosis of the fossil species assigned to *Strigocuscus* (Marsupialia, Phalangeridae), with description of a new genus and three new species. Alcheringa: an Australasian Journal of Palaeontology 31: 33–58.

Crosby, K., and M. Archer. 2000. Durudawirines, a new group of phalangeroid marsupials from the Miocene of Riversleigh, northwestern Queensland. Journal of Paleontology 74: 327–335.

Crosby, K., and C.A. Norris. 2003. Periotic morphology in the trichosurin possums *Strigocuscus celebensis* and *Wyulda squamicaudata* (Diprotodontia, Phalangeridae) and a revised diagnosis of the tribe Trichosurini. American Museum Novitates 3414: 1–14.

Crosby, K., M. Nagy, and M. Archer. 2001. *Wyulda asherjoeli*, a new phalangerid (Diprotodontia: Marsupialia) from the early Miocene of Riversleigh, northwestern Queensland. Memoirs of the Association of Australasian Palaeontologists 25: 77–82.

Crosby, K., M. Bassarova, M. Archer, and K. Carbery. 2004. Fossil possums in Australasia: discovery, diversity and evolution. *In* R.L. Goldingray and S.M. Jackson (editors), The biology of Australian possums and gliders: 161–176. Chipping Norton, New South Wales, Australia: Surrey Beatty and Sons.

Czerny, S. 2015. Funktionsmorphologische und phylogenetische Untersuchungen der Mittel- und Innenohrregion ausgewählter "Ameridelphia" und Australidelphia (Metatheria, Mammalia). M.Sc. thesis, Faculty of Life Sciences, University of Vienna, Vienna.

Dávalos, L.M., A.L. Cirranello, J.H. Geisler, and N.B. Simmons. 2012. Understanding phylogenetic incongruence: lessons from phyllostomid bats. Biological Reviews 87 (4): 991–1024.

Dávalos, L.M., P.M. Velazco, O.M. Warsi, P.D. Smits, and N.B. Simmons. 2014. Integrating incomplete

fossils by isolating conflicting signal in saturated and non-independent morphological characters. Systematic Biology 63 (4): 582–600.

Davis, B.M. 2007. A revision of "pediomyid" marsupials from the Late Cretaceous of North America. Acta Palaeontologica Polonica 52: 217–256.

Davis, B.M. 2011. Evolution of the tribosphenic molar pattern in early mammals, with comments on the "dual-origin" hypothesis. Journal of Mammalian Evolution 18: 227–244.

Davis, B.M., and R.L. Cifelli. 2011. Reappraisal of the tribosphenidan mammals from the Trinity Group (Aptian-Albian) of Texas and Oklahoma. Acta Palaeontologica Polonica 56 (3): 441–462.

Davis, B.M., R.L. Cifelli, and Z. Kielan-Jaworowska. 2008. Earliest evidence of Deltatheroida (Mammalia: Metatheria) from the Early Cretaceous of North America. *In* E.J. Sargis and M. Dagosto (editors), Mammalian evolutionary morphology: a tribute to Frederick S. Szalay: 3–24. Dordrecht: Springer.

Dawson, L. 1981. The status of the taxa of extinct giant wombats (Vombatidae: Marsupialia), and a consideration of vombatid phylogeny. Australian Mammalogy 4: 65–79.

Dawson, L. 2004. A new Pliocene tree kangaroo species (Marsupialia, Macropodinae) from the Chinchilla Local Fauna, southeastern Queensland. Alcheringa: an Australasian Journal of Palaeontology 28: 267–273.

Dawson, L., and T. Flannery. 1985. Taxonomic and phylogenetic status of living and fossil kangaroos and wallabies of the genus *Macropus* Shaw (Macropodidae: Marsupialia), with a new subgeneric name for the larger wallabies. Australian Journal of Zoology 33: 473–498.

Dawson, T.J., et al. 1989. Morphology and physiology of the Metatheria. *In* D.W. Walton and G.R. Dyne (editors), Fauna of Australia. vol. 1B. Mammalia: 451–504. Canberra: Australian Government Publishing Service.

Dawson, L., J. Muirhead, and S. Wroe. 1999. The Big Sink Local Fauna: a lower Pliocene mammalian fauna from the Wellington Caves complex, Wellington, New South Wales. Records of the Western Australia Museum, Supplement 57: 265–290.

Dederer, P.H. 1909. Comparison of *Caenolestes* with Polyprotodonta and Diprotodonta. American Naturalist 43 (514): 614–618.

D'Elía, G., N. Hurtado, and A. D'Anatro. 2016. Alpha taxonomy of *Dromiciops* (Microbiotheriidae) with the description of 2 new species of monito del monte. Journal of Mammalogy 97 (4): 1136–1152.

den Boer, W., and B.P. Kear. 2018. Is the fossil rat-kangaroo *Palaeopotorous priscus* the most basally branching stem macropodiform? Journal of Vertebrate Paleontology 38 (2): e1428196.

Dependorf, T. 1898. Zur Entwickelungsgeschichte des Zahnsystems der Marsupialier. Denkschriften der Medicinisch-Naturwissenschaftlichen Gesellschaft zu Jena 6: 243–402.

de Pinna, M.C.C. 1991. Concepts and tests of homology in the cladistic paradigm. Cladistics 7: 367–394.

Dodt, W.G., S. Gallus, M.J. Phillips, and M.A. Nilsson. 2017. Resolving kangaroo phylogeny and overcoming retrotransposon ascertainment bias. Scientific Reports 7 (1): 16811.

Doran, A.H.G. 1878. Morphology of the mammalian *ossicula auditûs*. Transactions of the Linnean Society of London (2nd Series) Zoology 1: 371–497.

Dörner, M., M. Altmann, S. Pääbo, and M. Mörl. 2001. Evidence for import of a lysyl-tRNA into marsupial mitochondria. Molecular Biology of the Cell 12 (9): 2688–2698.

dos Reis, M., et al. 2012. Phylogenomic datasets provide both precision and accuracy in estimating the timescale of placental mammal phylogeny. Proceedings of the Royal Society of London B, Biological Sciences 279 (1742): 3491–3500.

dos Reis, M., P.C. Donoghue, and Z. Yang. 2016. Bayesian molecular clock dating of species divergences in the genomics era. Nature Reviews Genetics 17 (2): 71–80.

Douady, C.J., F. Delsuc, Y. Boucher, W.F. Doolittle, and E.J. Douzery. 2003. Comparison of Bayesian and maximum likelihood bootstrap measures of phylogenetic reliability. Molecular Biology and Evolution 20 (2): 248–254.

Douglas, P.M., et al. 2014. Pronounced zonal heterogeneity in Eocene southern high-latitude sea surface temperatures. Proceedings of the National Academy of Sciences of the United States of America 111 (18): 6582–6587.

Druzinsky, R.E. 2015. The oral apparatus of rodents: variations on the theme of a gnawing machine. *In* P.G. Cox and L. Hautier (editors), Evolution of the rodents: 323–349. Cambridge: Cambridge University Press.

Duchêne, D.A., et al. 2018. Analysis of phylogenomic tree space resolves relationships among marsupial families. Systematic Biology 67 (3): 400–412.

Duchêne, D.A., et al. 2020. Linking branch lengths across sets of loci provides the highest statistical support for phylogenetic inference. Molecular Biology and Evolution 37 (4): 1202–1210.

Dunn, R.E., et al. 2012. A new chronology for middle Eocene–early Miocene South American Land Mammal Ages. Geological Society of America Bulletin 125 (3-4): 539–555.

Eaton, J.G. 2006. Late Cretaceous mammals from Cedar Canyon, southwestern Utah. *In* S.G. Lucas, and R.M. Sullivan (editors), Late Cretaceous Vertebrates from the Western Interior. New Mexico Museum of Natural History and Science Bulletin 35: 1–30.

Ebert, D.L., et al. 1988. Primary structure comparison of the proposed low density lipoprotein (LDL) receptor binding domain of human and pig apolipoprotein B: implications for LDL-receptor interactions. Journal of Lipid Research 29 (11): 1501–1509.

Edgar, R.C. 2004. MUSCLE: multiple sequence alignment with high accuracy and high throughput. Nucleic Acids Research 32 (5): 1792–1797.

Ekdale, E.G., J.D. Archibald, and A.O. Averianov. 2004. Petrosal bones of placental mammals from the Late Cretaceous of Uzbekistan. Acta Palaeontologica Polonica 49 (1): 161–176.

Eldridge, M.D.B., R.M.D. Beck, D.A. Croft, K.J. Travouillon, and B.J. Fox. 2019. An emerging consensus in the evolution, phylogeny, and systematics of marsupials and their fossil relatives (Metatheria). Journal of Mammalogy 100 (3): 802–837.

Engelhardt, H. 1932. Über die Zahnentwicklung bei *Aepyprymnus rufescens*. Gegenbaurs Morphologisches Jahrbuch 71: 77–94.

Engelman, R.K., and D.A. Croft. 2014. A new species of small-bodied sparassodont (Mammalia, Metatheria) from the middle Miocene locality of Quebrada Honda, Bolivia. Journal of Vertebrate Paleontology 34 (3): 672–688.

Engelman, R.K., and D.A. Croft. 2016. Evidence for sexual dimorphism in the early Miocene palaeothentid *Acdestis owenii* (Marsupialia: Paucituberculata). Ameghiniana 53 (4): 444–462.

Engelman, R.K., F. Anaya, and D.A. Croft. 2016. New palaeothentid marsupials (Paucituberculata) from the middle Miocene of Quebrada Honda, Bolivia, and their implications for the palaeoecology, decline and extinction of the Palaeothentoidea. Journal of Systematic Palaeontology 15 (10): 787–820.

Engelman, R.K., F. Anaya, and D.A. Croft. 2020. *Australogale leptognathus*, gen. et sp. nov., a second species of small sparassodont (Mammalia: Metatheria) from the middle Miocene locality of Quebrada Honda, Bolivia. Journal of Mammalian Evolution 27: 37–54.

Erixon, P., B. Svennblad, T. Britton, and B. Oxelman. 2003. Reliability of Bayesian posterior probabilities and bootstrap frequencies in phylogenetics. Systematic Biology 52 (5): 665–673.

Esdaile, P.C. 1916. On the structure and development of the skull and laryngeal cartilages of *Perameles*, with notes on the cranial nerves. Philosophical Transactions of the Royal Society of London B 207: 439–479.

Esteban, G., N. Nasif, and S.M. Georgieff. 2014. Cronobioestratigrafía del Mioceno tardío – Plioceno temprano, Puerta de Corral Quemado y Villavil, provincia de Catamarca, Argentina. Acta Geologica Lilloana 26 (2): 165–192.

Evans, H.E. 1993. Miller's anatomy of the dog, Philadelphia: W.B. Saunders.

Fabian, P.R. 2012. First known Tertiary representatives of the feather-tail possums (Acrobatidae, Marsupialia): palaeobiodiversity, phylogenetics, palaeoecology and palaeogeography. Unpublished Honours thesis, University of New South Wales, Sydney.

Fabre, P.-H., et al. 2018. Flightless scaly-tailed squirrels never learned how to fly: a reappraisal of Anomaluridae phylogeny. Zoologica Scripta 47 (4): 404–417.

Feigin, C.Y., et al. 2018. Genome of the Tasmanian tiger provides insights into the evolution and demography of an extinct marsupial carnivore. Nature Ecology and Evolution 2 (1): 182–192.

Ferreira, J.M., P.P. Phakey, and J. Palamara. 1989. Electron microscopic investigation relating the occlusal morphology to the underlying enamel structure of molar teeth of the wombat (*Vombatus ursinus*). Journal of Morphology 200: 141–149.

Ferreira-Cardoso, S., et al. 2017. Floccular fossa size is not a reliable proxy of ecology and behaviour in vertebrates. Scientific Reports 7: 2005.

Filan, S.L. 1990. Myology of the head and neck of the bandicoot (Marsupialia: Peramelemorphia). Australian Journal of Zoology 38: 617–634.

Finch, E. 1971. *Thylacoleo*. marsupial lion or marsupial sloth? Australian Natural History 17 (1): 7–11.

Finlayson, H.H. 1932. *Caloprymnus campestris*. Its recurrence and characters. Transactions and Proceedings of the Royal Society of South Australia 56: 148–167.

Fitzgerald, E.M.G., and L. Kool. 2015. The first fossil sea turtles (Testudines: Cheloniidae) from the Cenozoic of Australia. Alcheringa: an Australasian Journal of Palaeontology 39 (1): 142–148.

Flannery, T.F. 1983. Revision in the subfamily Sthenurinae (Marsupialia: Macropodoidea) and the rela-

tionships of the species of *Troposodon* and *Lagostrophus*. Australian Mammalogy 6: 15–28.

Flannery, T.F. 1984. Kangaroos: 15 million years of Australian bounders. *In* M. Archer and G. Clayton (editors), Vertebrate zoogeography and evolution in Australasia: 817–835. Perth: Hesperian Press.

Flannery, T.F. 1987. The relationships of the macropodoids (Marsupialia) and the polarity of some morphological features within the Phalangeriformes. *In* M. Archer (editor), Possums and opossums: studies in evolution: 741–747. Sydney: Surrey Beatty and Sons.

Flannery, T.F. 1989. Phylogeny of the Macropodoidea: a study in convergence. *In* G.G. Grigg, P. Jarman, and I. Hume (editors), Kangaroos, wallabies and rat-kangaroos: 1–46. Sydney: Surrey Beatty and Sons.

Flannery, T.F. 1995a. Mammals of the south-west Pacific and Moluccan islands. Chatswood, Australia: Reed Books.

Flannery, T.F. 1995b. Mammals of New Guinea, Chatswood, NSW: Reed Books.

Flannery, T.F., and M. Archer. 1984. The macropodoids (Marsupialia) of the early Pliocene Bow Local Fauna, central eastern New South Wales. Australian Zoologist 21 (4-5): 357–383.

Flannery, T.F., and M. Archer. 1985. *Palorchestes* Owen, 1874. Large and small palorchestids. *In* P. Rich and G. Van Tets (editors), Kadimakara: extinct vertebrates of Australia: 234–239. Lilydale: Pioneer Design Studio.

Flannery, T.F., and M. Archer. 1987a. *Strigocuscus reidi* and *Trichosurus dicksoni*, two new fossil phalangerids (Marsupialia: Phalangeridae) from the Miocene of northwestern Queensland. *In* M. Archer (editor), Possums and opossums: studies in evolution: 527–536. Sydney: Surrey Beatty and Sons.

Flannery, T.F., and M. Archer. 1987b. *Bettongia moyesi*, a new and plesiomorphic kangaroo (Marsupialia: Potoroidae) from Miocene sediments of northwestern Queensland. *In* M. Archer (editor), Possums and opossums: studies in evolution: 759–767. Sydney: Surrey Beatty and Sons.

Flannery, T.F., and M. Archer. 1987c. *Hypsiprymnodon bartholomaii* (Potoroidae: Marsupialia), a new species from the Miocene Dwornamor Local Fauna and a reassessment of the phylogenetic position of *H. moschatus*. *In* M. Archer (editor), Possums and opossums: studies in evolution: 749–758. Sydney: Surrey Beatty and Sons.

Flannery, T.F., and J.H. Calaby. 1987. Notes on the species of *Spilocuscus* (Marsupialia: Phalangeridae) from northern New Guinea and the Admirality and St. Matthias Island groups. *In* M. Archer (editor), Possums and opossums: studies in evolution: 547–557. Sydney: Surrey Beatty and Sons.

Flannery, T.F., and N.S. Pledge. 1987. Specimens of *Warendja wakefieldi* (Vombatidae: Marsupialia) from the Pleistocene of South Australia. *In* M. Archer (editor), Possums and opossums: studies in evolution: 365–368. Sydney: Surrey Beatty and Sons.

Flannery, T.F., and T.H.V. Rich. 1986. Macropodoids from the middle Miocene Namba Formation, South Australia, and the homology of some dental structures in kangaroos. Journal of Paleontology 60 (2): 418–447.

Flannery, T.F., and F.S. Szalay. 1982. *Bohra paulae*, a new giant fossil tree kangaroo (Marsupialia: Macropodidae) from New South Wales, Australia. Australian Mammalogy 5: 83–94.

Flannery, T.F., M. Archer, and M. Plane. 1983. Middle Miocene kangaroos (Macropodoidea: Marsupialia) from three localities in northern Australia, with a description of two new subfamilies. Journal of Australian Geology and Geophysics 7: 287–302.

Flannery, T.F., M. Archer, and M. Plane. 1984. Phylogenetic relationships and a reconsideration of higher level systematics within the Potoroidae (Marsupialia). Journal of Paleontology 58 (4): 1087–1097.

Flannery, T.F., M. Archer, and J. Maynes. 1987. The phylogenetic relationships of living phalangerids (Phalangeroidea: Marsupialia) with a suggested new taxonomy. *In* M. Archer (editor), Possums and opossums: studies in evolution: 477–506. Sydney: Surrey Beatty and Sons.

Flannery, T.F., T.H. Rich, W.D. Turnbull, and E.L. Lundelius Jr. 1992. The Macropodoidea (Marsupialia) of the early Pliocene Hamilton local fauna, Victoria, Australia. Fieldiana: Geology 25: 1–37.

Flores, D.A. 2009. Phylogenetic analyses of postcranial skeletal morphology in didelphid marsupials. Bulletin of the American Museum of Natural History 320: 1–81.

Flores, D.A., and F. Abdala. 2001. Diferencias morfológicas de cráneo y dentición en *Didelphis albiventris* y *D. marsupialis* (Didelphimorphia: Didelphidae) de Argentina y Bolivia. Comunicações do Museu de Ciências da PUCRS (Série Zoologia) 14: 101–110.

Flores, D.A., N.P. Giannini, and F. Abdala. 2003. Cranial ontogeny of *Lutreolina crassicaudata* (Didelphidae): a comparison with *Didelphis albiventris*. Acta Theriologica 48 (1): 1–9.

Flores, D.A., N. Giannini, and F. Abdala. 2006. Comparative postnatal ontogeny of the skull in the australidelphian metatherian *Dasyurus albopunctatus*

(Marsupialia: Dasyuromorpha: Dasyuridae). Journal of Morphology 267 (4): 426–440.

Flores, D.A., F. Abdala, and N. Giannini. 2010. Cranial ontogeny of *Caluromys philander* (Didelphidae: Caluromyinae): a qualitative and quantitative approach. Journal of Mammalogy 91 (3): 539–550.

Flores, D.A., F. Abdala, and N.P. Giannini. 2013. Postweaning cranial ontogeny in two bandicoots (Mammalia, Peramelomorphia, Peramelidae) and comparison with carnivorous marsupials. Zoology (Jena) 116 (6): 372–384.

Flower, W.H. 1866. On the development and succession of the teeth in the Marsupialia. Proceedings of the Royal Society of London 15: 463–468.

Flower, W.H. 1867. On the development and succession of the teeth in the Marsupialia. Philosophical Transactions of the Royal Society of London 157: 631–641.

Flynn, J.J., and A.R. Wyss. 1999. New marsupials from the Eocene-Oligocene transition of the Andean Main Range, Chile. Journal of Vertebrate Paleontology 19 (3): 533–549.

Flynn, J.J., J. Guerrero, and C.C. Swisher III. 1997. Geochronology of the Honda Group. *In* R.F. Kay, R.H. Madden, R.L. Cifelli, and J.J. Flynn (editors), Vertebrate paleontology in the Neotropics: the Miocene fauna of La Venta, Colombia: 44–60. Washington: Smithsonian Institution Press.

Forasiepi, A.M. 2009. Osteology of *Arctodictis sinclairi* (Mammalia, Metatheria, Sparassodonta) and phylogeny of Cenozoic metatherian carnivores from South America. Monografías del Museo Argentino de Ciencias Naturales 6: 1–174.

Forasiepi, A., M., and M.R. Sánchez-Villagra. 2014. Heterochrony, dental ontogenetic diversity, and the circumvention of constraints in marsupial mammals and extinct relatives. Paleobiology 40 (2): 222–237.

Forasiepi, A.M., F. Goin, and A.G. Martinelli. 2009. Contribution to the knowledge of the Sparassocynidae (Mammalia, Metatheria, Didelphoidea), with comments on the age of the Aisol Formation (Neogene), Mendoza Province, Argentina. Journal of Vertebrate Paleontology 29 (4): 1252–1263.

Forasiepi, A.M., A.G. Martinelli, M.S. de la Fuente, S. Dieguez, and M. Bond. 2011. Paleontology and stratigraphy of the Aisol Formation (Neogene), San Rafael, Mendoza. *In* J. Salfity and R.A. Marquillas (editors), Cenozoic geology of the Central Andes of Argentina: 135–154. Salta: SCS Publisher.

Forasiepi, A.M., F.J. Goin, M.A. Abello, and E. Cerdeño. 2013. A unique, late Oligocene shrew-like marsupial from western Argentina and the evolution of dental morphology. Journal of Systematic Palaeontology 12 (5): 549–564.

Forasiepi, A.M., M.J. Babot, and N. Zimicz. 2014a. *Australohyaena antiqua* (Mammalia, Metatheria, Sparassodonta), a large predator from the late Oligocene of Patagonia. Journal of Systematic Palaeontology 13 (6): 503–525.

Forasiepi, A.M., M.R. Sánchez-Villagra, T. Schmelzle, S. Ladevèze, and R.F. Kay. 2014b. An exceptionally well-preserved skeleton of *Palaeothentes* from the early Miocene of Patagonia, Argentina: new insights into the anatomy of extinct paucituberculatan marsupials. Swiss Journal of Palaeontology 133 (1): 1–21.

Forasiepi, A., M., R.D.E. MacPhee, and S.E. Hernández del Pino. 2019. Caudal cranium of *Thylacosmilus atrox* (Mammalia, Metatheria, Sparassodonta), a South American predaceous sabertooth. Bulletin of the American Museum of Natural History 433: 1–64.

Fortelius, M. 1985. Ungulate cheek teeth: developmental, functional, and evolutionary interrelations. Acta Zoologica Fennica 180: 1–76.

Fosse, G. 1969. Development of the teeth in a pouch-young specimen of *Antechinus stuartii* and a pouch-young specimen of *Sminthopsis crassicaudata*. Dasyuridae: Marsupialia. Archives of Oral Biology 14 (2): 207–218.

Fosse, G., and S. Risnes. 1972. Development of the teeth in a pouch-young specimen of *Isoodon obesulus* and one of *Perameles gunnii* (Peramedidae: Marsupialia). Archives of Oral Biology 17 (5): 829–838.

Fox, R.C. 1983. Notes on the North American Tertiary marsupials *Herpetotherium* and *Peradectes*. Canadian Journal of Earth Sciences 20: 1565–1578.

Fox, R.C., and B.G. Naylor. 2006. Stagodontid marsupials from the Late Cretaceous of Canada and their systematic and functional implications. Acta Palaeontologica Polonica 51 (1): 13–36.

Freedman, L. 1967. Skull and tooth variation in the genus *Perameles*. Part I. Anatomical features. Records of the Australian Museum 27: 147–165.

Friend, J.A. 1989. 22. Myrmecobiidae. *In* D.W. Walton and B.J. Richardson (editors), Fauna of Australia, vol. 1B. Mammalia: 1–18. Canberra: AGPS.

Frigo, L., and P.A. Woolley. 1996. Development of the skeleton of the stripe-faced dunnart, *Sminthopsis macroura* (Marsupialia: Dasyuridae). Australian Journal of Zoology 44: 155–164.

Fujino, T., N. Navaratnam, A. Jarmuz, A. von Haeseler, and J. Scott. 1999. C→U editing of apolipoprotein B

mRNA in marsupials: identification and characterisation of APOBEC–1 from the American opossum *Monodelphus domestica*. Nucleic Acids Research 27 (13): 2662–2671.

Gabbert, S. 1998. Basicranial anatomy of *Herpetotherium* (Marsupialia: Didelphimorphia) from the Eocene of Wyoming. American Museum Novitates 3235: 1–13.

Gadow, H. 1892. On the systematic position of *Notoryctes typhlops*. Proceedings of the Zoological Society of London 1892: 361–370.

Gaillard, C., R.D.E. MacPhee, and A.M. Forasiepi. 2021. The stapes of stem and extinct Marsupialia: implications for the ancestral condition. Journal of Vertebrate Paleontology 41 (2): e1924761.

Gallus, S., A. Janke, V. Kumar, and M.A. Nilsson. 2015a. Disentangling the relationship of the Australian marsupial orders using retrotransposon and evolutionary network analyses. Genome Biology and Evolution 7 (4): 985–992.

Gallus, S., et al. 2015b. Evolutionary histories of transposable elements in the genome of the largest living marsupial carnivore, the Tasmanian devil. Molecular Biology and Evolution 32 (5): 1268–1283.

Gannon, P.J., A.R. Eden, and J.T. Laitman. 1988. The subarcuate fossa and cerebellum of extant primates: comparative study of a skull-brain interface. American Journal of Physical Anthropology 77: 143–164.

García-Navas, V., B.P. Kear, and M. Westerman. 2020. The geography of speciation in dasyurid marsupials. Journal of Biogeography 47 (9): 2042–2053.

García-Sandoval, R. 2014. Why some clades have low bootstrap frequencies and high Bayesian posterior probabilities. Israel Journal of Ecology and Evolution 60 (1): 41–44.

Gardner, A.L. 1973. The systematics of the genus *Didelphis* (Marsupialia: Didelphidae) in North and Middle America. Special Publications, Museum, Texas Tech University 4: 1–81.

Gardner, A.L. (editor), 2008. Mammals of South America. Vol. 1. Marsupials, xenarthrans, shrews, and bats. Chicago: Chicago University Press.

Garrido, A.C., G.F. Turazzini, M. Bond, G. Aguirrezabala, and A.M. Forasiepi. 2014. Estratigrafía, vertebrados fósiles y evolución tectosedimentaria de los depósitos neógenos del Bloque de San Rafael (Mioceno-Plioceno), Mendoza, Argentina. Acta Geologica Lilloana 26 (2): 133–164.

Gasc, C., E. Peyretaillade, and P. Peyret. 2016. Sequence capture by hybridization to explore modern and ancient genomic diversity in model and nonmodel organisms. Nucleic Acids Research 44 (10): 4504–4518.

Gaudin, T.J., J.R. Wible, J.A. Hopson, and W.D. Turnbull. 1996. Reexamination of the morphological evidence for the cohort Epitheria (Mammalia, Eutheria). Journal of Mammalian Evolution 3 (1): 31–79.

Gavryushkina, A., et al. 2017. Bayesian total-evidence dating reveals the recent crown radiation of penguins. Systematic Biology 66 (1): 57–73.

Gelfo, J.N., F.J. Goin, M.O. Woodburne, and C. de Muizon. 2009. Biochronological relationships of the earliest South American Paleogene mammalian faunas. Palaeontology 52 (1): 251–269.

Gelfo, J.N., G.M. López, and S.N. Santillana. 2017. Eocene ungulate mammals from west Antarctica: implications from their fossil record and a new species. Antarctic Science 29 (05): 445–455.

Gelfo, J.N., F.J. Goin, N. Bauzá, and M. Reguero. 2019. The fossil record of Antarctic land mammals: commented review and hypotheses for future research. Advances in Polar Science 30 (3): 274–292.

Gerdtz, W.D., and N.W. Archbold. 2003. *Glaucodon ballaratensis* (Marsupialia, Dasyuridae), a late Pliocene 'devil' from Batesford, Victoria. Proceedings of the Royal Society of Victoria 115: 35–44.

Gheerbrant, E., A. Filippo, and A. Schmitt. 2016. Convergence of afrotherian and laurasiatherian ungulate-like mammals: First morphological evidence from the Paleocene of Morocco. PLoS One 11 (7): e0157556.

Giannini, N.P., F. Abdala, and D.A. Flores. 2004. Comparative postnatal ontogeny of the skull in *Dromiciops gliroides* (Marsupialia: Microbiotheriidae). American Museum Novitates 3460: 1–17.

Giannini, N.P., J.R. Wible, and N.B. Simmons. 2006. On the cranial osteology of Chiroptera. I. *Pteropus* (Megachiroptera: Pteropodidae). Bulletin of the American Museum of Natural History 295: 1–134.

Gill, E.D. 1957. The stratigraphical occurrence and palaeoecology of some Australian Tertiary marsupials. Memoirs of Museum Victoria 21: 135–203.

Gill, T. 1872. Arrangement of the families of mammals with analytical tables. Smithsonian Miscellaneous Collections 11 (1): 1–98.

Gillespie, A.K. 1997. *Priscileo roskellyae* sp. nov. (Thylacoleonidae, Marsupialia) from Riversleigh, northwestern Queensland. Memoirs of the Queensland Museum 41: 321–328.

Gillespie, A.K. 1999. Diversity and evolutionary relationships of marsupial lions. Australian Mammalogy 21: 21–22.

Gillespie, A.K. 2007. Diversity and systematics of marsupial lions from the Riversleigh World Heritage Area and the evolution of the Thylacoleonidae. Ph.D. dissertation, School of Biological, Earth, and Environmental Sciences, University of New South Wales, Sydney.

Gillespie, A.K., M. Archer, S.J. Hand, and K.H. Black. 2014. New material referable to *Wakaleo* (Marsupialia: Thylacoleonidae) from the Riversleigh World Heritage Area, northwestern Queensland: revising species boundaries and distributions in Oligo/Miocene marsupial lions. Alcheringa: an Australasian Journal of Palaeontology 38 (4): 513–527.

Gillespie, A.K., M. Archer, and S.J. Hand. 2016. A tiny new marsupial lion (Marsupialia, Thylacoleonidae) from the early Miocene of Australia. Palaeontologia Electronica 9.2.26A: 1–26.

Gillespie, A.K., M. Archer, and S.J. Hand. 2017. A new Oligo–Miocene marsupial lion from Australia and revision of the family Thylacoleonidae. Journal of Systematic Palaeontology 17 (1): 59–89.

Gillespie, A.K., M. Archer, and S.J. Hand. 2020. *Lekaneleo*, a new genus of marsupial lion (Marsupialia, Thylacoleonidae) from the Oligocene–Miocene of Australia, and the craniodental morphology of *L. roskellyae*, comb. nov. Journal of Vertebrate Paleontology 39 (5): e1703722.

Gingerich, P.D. 1971. Cranium of *Plesiadapis*. Nature 232: 566.

Gingerich, P.D. 2001. Biostratigraphy of the continental Paleocene-Eocene boundary interval on Polecat Bench in the northern Bighorn Basin. University of Michigan Papers on Paleontology 33: 37–71.

Godowski, P.J., et al. 1989. Characterization of the human growth hormone receptor gene and demonstration of a partial gene deletion in two patients with Laron-type dwarfism. Proceedings of the National Academy of Sciences of the United States of America 86 (20): 8083–8087.

Godthelp, H., M. Archer, R.L. Cifelli, S.J. Hand, and C.F. Gilkeson. 1992. Earliest known Australian Tertiary mammal fauna. Nature 356: 514–516.

Godthelp, H., S. Wroe, and M. Archer. 1999. A new marsupial from the early Eocene Tingamarra Local Fauna of Murgon, southeastern Queensland: a prototypical Australian marsupial? Journal of Mammalian Evolution 6 (3): 289–313.

Goin, F.J. 1991. Los Didelphoidea (Mammalia, Marsupialia) del Cenozoico tardío de la región Pampeana. Ph.D. dissertation, Facultad de Ciencias Naturales y Museo, Universidad Nacional de La Plata, La Plata.

Goin, F.J. 1995. Los marsupiales. *In* M.T. Alberdi, G. Leone, and E.P. Tonni (editors), Evolución biológica y climática de la región pampeana durante los últimos cinco millones de años: Un ensayo de correlación con el Mediterráneo occidental: 165–179. Madrid: Museo Nacional de Ciencias Naturales.

Goin, F.J. 1997a. New clues for understanding Neogene marsupial radiations. *In* R.F. Kay, R.H. Madden, R.L. Cifelli, and J.J. Flynn (editors), Vertebrate paleontology in the Neotropics: the Miocene fauna of La Venta, Colombia: 187–206. Washington: Smithsonian Institution Press.

Goin, F.J. 1997b. *Thylamys zettii*, nueva especie de marmosino (Marsupialia, Didelphidae) del Cenozoico de la región pampeana. Ameghiniana 34: 481–484.

Goin, F.J. 2003. Early marsupial radiations in South America. *In* M. Jones, C. Dickman, and M. Archer (editors), Predators with pouches: the biology of carnivorous marsupials: 30–42. Collingwood, Australia: CSIRO (Commonwealth Scientific and Industrial Research Organization).

Goin, F.J., and M.A. Abello. 2013. Los Metatheria sudamericanos de comienzos del Neógeno (Mioceno temprano, edad mamífero Colhuehuapense). Parte 2: Microbiotheria y Polydolopimorphia. Ameghiniana 50 (1): 51–78.

Goin, F.J., and A.M. Candela. 1996. A new early Eocene polydolopimorphian (Mammalia, Marsupialia) from Patagonia. Journal of Vertebrate Paleontology 16 (2): 292–296.

Goin, F.J., and A.M. Candela. 1998. Dos nuevos marsupiales "pseudodiprotodontes" del Eoceno de Patagonia, Argentina. Publicación Especial de la Asociación Paleontológica Argentina 5: 79–84.

Goin, F.J., and A.M. Candela. 2004. New Paleogene marsupials from the Amazon Basin of eastern Peru. *In* K.E. Campbell, Jr. (editor), The Paleogene Mammalian Fauna of Santa Rosa, Amazonian Peru: 15–60. Los Angeles: Natural History Museum of Los Angeles County.

Goin, F.J., and A.A. Carlini. 1995. An Early Tertiary microbiotheriid marsupial from Antarctica. Journal of Vertebrate Paleontology 15: 205–207.

Goin, F.J., and C.I. Montalvo. 1988. Revisión sistemática y reconocimiento de una nueva especie del género *Thylatheridium* Reig (Marsupialia, Didelphidae). Ameghiniana 25: 161–167.

Goin, F.J., and U.F.J. Pardiñas. 1996. Revisión de las especies del género *Hyperdidelphys* Ameghino, 1904 (Mammalia, Marsupialia, Didelphidae), su significado filogenético, estratigráfico y adaptativo en el

Neógeno del Cono Sur Sudamericano. Estudios Geológicos 52: 327–359.

Goin, F.J., and P. Rey. 1997. Sobre las afinidades de *Monodelphis* Burnett, 1830 (Mammalia: Marsupialia: Didelphidae: Marmosinae). Neotropica 43: 93–98.

Goin, F.J., and M. de los Reyes. 2011. Contribución al conocimiento de los representantes extintos de *Lutreolina* Thomas, 1910 (Mammalia, Marsupialia, Didelphidae). Historia Natural 1 (2): 15–25.

Goin, F.J., U.F.J. Pardiñas, and M.J. Lezcano. 1994. Un nuevo resto del cenoléstido *Pliolestes* Reig, 1955 (Mammalia, Marsupialia) del Plioceno de la Provincia de Buenos Aires (Argentina). Ameghiniana 31: 15–21.

Goin, F.J., J.A. Case, M.O. Woodburne, S.F. Vizcaino, and M.A. Reguero. 1999. New discoveries of "opossum-like" marsupials from Antarctica (Seymour Island, Medial Eocene). Journal of Mammalian Evolution 6 (4): 335–365.

Goin, F.J., C. Montalvo, and G. Visconti. 2000. Los marsupiales (Mammalia) del Mioceno superior de la Formación Cerro Azul (Provincia de La Pampa, Argentina). Revista Española de Geología 56: 101–126.

Goin, F.J., M.R. Sánchez-Villagra, R.F. Kay, F. Anaya-Daza, and M. Takai. 2003. New palaeothentid marsupial from the middle Miocene of Bolivia. Palaeontology 46 (2): 307–315.

Goin, F.J., et al. 2006. The earliest Tertiary therian mammal from South America. Journal of Vertebrate Paleontology 26 (2): 505–510.

Goin, F., et al. 2007a. Los Metatheria sudamericanos de comienzos del Neógeno (Mioceno Temprano, Edad-mamífero Colhuehuapense). Parte I: Introducción, Didelphimorphia y Sparassodonta. Ameghiniana 44 (1): 29–71.

Goin, F.J., M.R. Sánchez-Villagra, A. Abello, and R.F. Kay. 2007b. A new generalized paucituberculatan marsupial from the Oligocene of Bolivia and the origin of 'shrew-like' opossums. Palaeontology 50: 1267–1276.

Goin, F.J., et al. 2007c. New marsupial (Mammalia) from the Eocene of Antarctica, and the origins and affinities of the Microbiotheria. Revista de la Asociacion Geologica Argentina 62 (4): 597–603.

Goin, F.J., A.M. Candela, M.A. Abello, and E.V. Oliveira. 2009a. Earliest South American paucituberculatans and their significance in the understanding of 'pseudodiprotodont' marsupial radiations. Zoological Journal of the Linnean Society 155: 867–884.

Goin, F.J., N. Zimicz, M. de Los Reyes, and L. Soibelzon. 2009b. A new large didelphid of the genus *Thy-lophorops* (Mammalia: Didelphimorphia: Didelphidae), from the late Tertiary of the Pampean Region (Argentina). Zootaxa 2005: 35–46.

Goin, F.J., M.A. Abello, and L. Chornogubsky. 2010. Middle Tertiary marsupials from central Patagonia (early Oligocene of Gran Barranca): understanding South America's *Grande Coupure*. *In* R.H. Madden, A.A. Carlini, M.G. Vucetich, and R.F. Kay (editors), The paleontology of Gran Barranca: evolution and environmental change through the middle Cenozoic of Patagonia: 71–107. Cambridge: Cambridge University Press.

Goin, F.J., J.N. Gelfo, L. Chornogubsky, M.O. Woodburne, and T. Martin. 2012. Origins, radiations, and distribution of South American mammals: from greenhouse to icehouse worlds. *In* B.D. Patterson and L.P. Costa (editors), Bones, clones, and biomes: an 80-million year history of modern Neotropical mammals: 20–50. Chicago: University of Chicago Press.

Goin, F.J., J.I. Noriega, and M. de los Reyes. 2013. Los Metatheria (Mammalia) del "Mesopotamiense" (Mioceno Tardío) de la Provincia de Entre Ríos, Argentina, y una reconsideración de *Philander entrerianus* (Ameghino, 1899). *In* D. Brandoni and J.I. Noriega (editors), El Neógeno de la Mesopotamia argentina: 109–117. Buenos Aires: Asociación Paleontológica Argentina.

Goin, F.J., M.O. Woodburne, A.N. Zimicz, G.M. Martin, and L. Chornogubsky. 2016. A brief history of South American metatherians: Evolutionary contexts and intercontinental dispersals. Dordrecht: Springer.

Goin, F.J., et al. 2020. New metatherian mammal from the early Eocene of Antarctica. Journal of Mammalian Evolution 27: 17–36.

Goldfuss, G. 1820. Handbuch der Zoologie. Abteilung II. Nürnberg: Johan Leonhard Schrag.

Goloboff, P.A., and J.S. Arias. 2019. Likelihood approximations of implied weights parsimony can be selected over the Mk model by the Akaike information criterion. Cladistics 35 (6): 695–716.

Goloboff, P.A., and S.A. Catalano. 2016. TNT version 1.5, including a full implementation of phylogenetic morphometrics. Cladistics 32: 221–238.

Goloboff, P.A., J.S. Farris, and K.C. Nixon. 2008. TNT, a free program for phylogenetic analysis. Cladistics 24 (5): 774–786.

Goloboff, P.A., A.T. Galvis, and J.S. Arias. 2018a. Parsimony and model-based phylogenetic methods for morphological data: comments on O'Reilly et al. Palaeontology 61 (4): 625–630.

Goloboff, P.A., A. Torres, and J.S. Arias. 2018b. Weighted parsimony outperforms other methods of phylogenetic inference under models appropriate for morphology. Cladistics 34 (4): 407–437.

Goloboff, P.A., M. Pittman, D. Pol, and X. Xu. 2019. Morphological data sets fit a common mechanism much more poorly than DNA sequences and call into question the Mkv model. Systematic Biology 68 (3): 494–504.

González, B., F. Brook, and G.M. Martin. 2020. Variability and variation in *Rhyncholestes raphanurus* Osgood (Paucituberculata, Caenolestidae). Revista Chilena de Historia Natural 93: 1.

Gould, J. 1863. The mammals of Australia. London: J. Gould.

Gray, J.E. 1821. On the natural arrangement of vertebrose animals. London Medical Repository 15: 296–310.

Gray, J.E. 1825. An outline of an attempt at the disposition of the Mammalia into tribes and families with a list of the genera apparently appertaining to each tribe. Annals of Philosophy 10 (2): 337–344.

Green, R.H., and J.L. Rainbird. 1987. The common wombat *Vombatus ursinus* (Shaw 1800) in Northern Tasmania—part 1. Breeding, growth and development. Records of the Queen Victoria Museum 91: 1–19.

Gregory, W.K. 1910. The orders of mammals. Bulletin of the American Museum of Natural History 27: 1–524.

Gregory, W.K. 1920. Studies in comparative myology and osteology: no. IV – a review of the lacrymal bone of vertebrates with special reference to that of mammals. Bulletin of the American Museum of Natural History 42: 95–263.

Griffiths, T.A. 1978. Modification of M. cricothyroideus and the larynx in the Mormoopidae, with reference to amplification of high-frequency pulses. Journal of Mammalogy 59 (4): 724–730.

Groves, C.P. 1987. On the cuscuses (Marsupialia: Phalangeridae) of the *Phalanger orientalis* group from Indonesian territory. *In* M. Archer (editor), Possums and opossums: studies in evolution: 569–579. Sydney: Surrey Beatty and Sons.

Groves, C.P. 2005. Order Diprotodontia. *In* D.E., Wilson and D.M. Reeder (editors), Mammal species of the world: a taxonomic and geographic reference, 3rd ed.: 43–70. Baltimore: Johns Hopkins University Press.

Groves, C.P., and T.F. Flannery. 1990. Revision of the families and genera of bandicoots. *In* J.H. Seebeck, R.L. Wallis, P.R. Brown, and C.M. Kemper (editors), Bandicoots and bilbies: 1–11. Sydney: Surrey Beatty and Sons.

Gruber, K.F., R.S. Voss, and S.A. Jansa. 2007. Base-compositional heterogeneity in the RAG1 locus among didelphid marsupials: implications for phylogenetic inference and the evolution of GC content. Systematic Biology 56 (1): 83–96.

Guerrero, J. 1993. Magnetostratigraphy of the upper part of the Honda Group and Neiva Formation, Miocene uplift of the Colombian Andes. Ph.D. dissertation, Department of Geology, Duke University, Durham, North Carolina.

Guerrero, J. 1997. Stratigraphy, sedimentary environments, and the Miocene uplift of the Colombian Andes. *In* R.F. Kay, R.H. Madden, R.L. Cifelli, and J.J. Flynn (editors), Vertebrate paleontology in the Neotropics: the Miocene fauna of La Venta, Colombia: 15–43. Washington: Smithsonian Institution Press.

Gurovich, Y., and K.W.S. Ashwell. 2020. Brain and behavior of *Dromiciops gliroides*. Journal of Mammalian Evolution 27: 177–197.

Gurovich, Y., K.J. Travouillon, R.M.D. Beck, J. Muirhead, and M. Archer. 2014. Biogeographical implications of a new mouse-sized fossil bandicoot (Marsupialia: Peramelemorphia) occupying a dasyurid-like ecological niche across Australia. Journal of Systematic Palaeontology 12 (3): 265–290.

Haight, J.R., and P.F. Murray. 1981. The cranial endocast of the early Miocene marsupial, *Wynyardia bassiana*: an assessment of taxonomic relationships based upon comparisons with recent forms. Brain Behavior and Evolution 19 (1-2): 17–36.

Hand, S.J., M. Archer, H. Godthelp, T.H. Rich, and N.S. Pledge. 1993. *Nimbadon*, a new genus and three new species of Tertiary zygomaturines (Marsupialia: Diprotodontidae) from northern Australia, with a reassessment of *Neohelos*. Memoirs of the Queensland Museum 33 (1): 193–210.

Harman, M.T., and A. Smith. 1936. Some observations on the development of the teeth of *Cavia cobaya*. Anatomical Record 66 (1): 97–111.

Harris, J.M. 2015. *Acrobates pygmaeus* (Diprotodontia: Acrobatidae). Mammalian Species 47 (920): 32–44.

Harrison, L.B., and H.C.E. Larsson. 2015. Among-character rate variation distributions in phylogenetic analysis of discrete morphological characters. Systematic Biology 64 (2): 307–324.

Hayes, F.G. 2005. Arikareean (Oligocene–Miocene) *Herpetotherium* (Marsupialia, Didelphidae) form

Nebraska and Florida. Bulletin of the Florida Museum of Natural History 45: 341–360.

Heath, T.A., J.P. Huelsenbeck, and T. Stadler. 2014. The fossilized birth-death process for coherent calibration of divergence-time estimates. Proceedings of the National Academy of Sciences of the United States of America 111 (29): E2957–2966.

Helgen, K.M., and T.F. Flannery. 2004. Notes on the phalangerid marsupial genus *Spilocuscus*, with description of a new species from Papua. Journal of Mammalogy 85 (5): 825–833.

Heritage, S., et al. 2016. Ancient phylogenetic divergence of the enigmatic African rodent *Zenkerella* and the origin of anomalurid gliding. PeerJ 4: e2320.

Hershkovitz, P. 1982. The staggered marsupial lower third incisor (I_3). Geobios, mémoire special 6: 191–200.

Hershkovitz, P. 1992a. Ankle bones: the Chilean opossum *Dromiciops gliroides* Thomas, and marsupial phylogeny. Bonner Zoologische Beiträge 43: 181–213.

Hershkovitz, P. 1992b. The South American gracile mouse opossums, genus *Gracilinanus* Gardner and Creighton, 1989 (Marmosidae, Marsupialia): a taxonomic review with notes on general morphology and relationships. Fieldiana Zoology (New Series) 39: i–vi, 1–56.

Hershkovitz, P. 1995. The staggered marsupial third lower incisor: hallmark of cohort Didelphimorphia, and description of a new genus and species with staggered i3 from the Albian (Lower Cretaceous) of Texas. Bonner Zoologische Beitrage 45: 153–169.

Hershkovitz, P. 1997. Composition of the family Didelphidae Gray, 1821 (Didelphoidea: Marsupialia), with a review of the morphology and behavior of the included four-eyed pouched opossums of the genus *Philander* Tiedemann, 1808. Fieldiana Zoology (New Series) 86: 1–103.

Hershkovitz, P. 1999. *Dromiciops gliroides* Thomas, 1894, last of the Microbiotheria (Marsupialia), with a review of the family Microbiotheriidae. Fieldiana Zoology 93: 1–60.

Hiiemae, K., and F.A. Jenkins Jr. 1969. The anatomy and internal architecture of the muscles of mastication in *Didelphis marsupialis*. Postilla 140: 1–49.

Hillis, D.M., and J.J. Bull. 1993. An empirical-test of bootstrapping as a method for assessing confidence in phylogenetic analysis. Systematic Biology 42 (2): 182–192.

Ho, S.Y., and M.J. Phillips. 2009. Accounting for calibration uncertainty in phylogenetic estimation of evolutionary divergence times. Systematic Biology 58 (3): 367–380.

Hocknull, S.A. 2005. Ecological succession during the late Cainozoic of central eastern Queensland: extinction of a diverse rainforest community. Memoirs of the Queensland Museum 51 (1): 39–122.

Hocknull, S.A. 2009. Late Cainozoic rainforest vertebrates from Australopapua: evolution, biogeography and extinction. Ph.D. dissertation, School of Biological, Earth, and Environmental Sciences, University of New South Wales, Sydney.

Hoffstetter, R., and G. Petter. 1983. *Paraborhyaena boliviana* et *Andinogale sallensis*, deux marsupiaux (Borhyaenidae) nouveaux du Déséadien (Oligocène inférieur) de Salla (Bolivie). Comptes-Rendus des Seances de l'Academie des Sciences, Serie 2: Mecanique-Physique, Chimie, Sciences de l'Univers, Sciences de la Terre 296: 205–208.

Hoffstetter, R., and C. Villarroel. 1974. Découverte d'un marsupial microtragulidé (= argyrolagidé) dans le Pliocène de l'Altiplano bolivien. Comptes Rendus de l'Académie des Sciences, Paris 278: 1947–1950.

Hooker, J.J., et al. 2008. The origin of Afro-Arabian 'didelphimorph' marsupials. Palaeontology 51 (3): 635–648.

Hope, J.H., and H.E. Wilkinson. 1982. *Warendja wakefieldi*, a new genus of wombat (Marsupialia: Vombatidae) from Pleistocene sediments in McEacherns Cave, western Victoria. Memoirs of the National Museum of Victoria 43 (2): 109–120.

Hopewell-Smith, A., and H.W. Marett Tims. 1911. Tooth-germs in the wallaby *Macropus billardieri*. Proceedings of the Zoological Society of London 81 (4): 926–942.

Horovitz, I. 1999. A phylogenetic study of living and fossil platyrrhines. American Museum Novitates 3269: 1–40.

Horovitz, I. 2000. The tarsus of *Ukhaatherium nessovi* (Eutheria, Mammalia) from the Late Cretaceous of Mongolia: an appraisal of the evolution of the ankle in basal therians. Journal of Vertebrate Paleontology 20 (3): 547–560.

Horovitz, I., and M.R. Sánchez-Villagra. 2003. A morphological analysis of marsupial mammal higher-level phylogenetic relationships. Cladistics 19: 181–212.

Horovitz, I., et al. 2008. The anatomy of *Herpetotherium* cf. *fugax* Cope, 1873, a metatherian from the Oligocene of North America. Palaeontographica Abteilung A 284 (4-6): 109–141.

Horovitz, I., et al. 2009. Cranial anatomy of the earliest marsupials and the origin of opossums. PLoS One 4 (12): e8278.

Hospattankar, A.V., S.W. Law, K. Lackner, and H.B. Brewer, Jr. 1986. Identification of low density lipoprotein receptor binding domains of human apolipoprotein B-100: a proposed consensus LDL receptor binding sequence of apoB-100. Biochemical and Biophysical Research Communications 139 (3): 1078–1085.

Hunter, J.P., and J. Jernvall. 1995. The hypocone as a key innovation in mammalian evolution. Proceedings of the National Academy of Sciences of the United States of America 92 (23): 10718–10722.

Hüppi, E., M.R. Sánchez-Villagra, A.C. Tzika, and I. Werneburg. 2018. Ontogeny and phylogeny of the mammalian chondrocranium: the cupula nasi anterior and associated structures of the anterior head region. Zoological Letters 4: 29.

Hyrtl, J. 1845. Verleichende-Anatomische Untersuchungen über das innere Gehörorgan des Menschen und der Säugethiere. Prague: Friedrich Ehrlich.

Illiger, J. 1811. Prodromus systematis mammalium et avium additis terminis zoographicis utriusque classis, eorumque versione Germanica. Berlin: C. Salfeld.

International Committee on Veterinary Gross Anatomical Nomenclature (NAV). 2017. Nomina anatomica veterinaria, 6th ed. Online resource (http://www.wava-amav.org/wava-documents.html).

Isla, F., M. Taglioretti, and A. Dondas. 2015. Revisión y nuevos aportes sobre la estratigrafía y sedimentología de los acantilados entre Mar de Cobo y Miramar, provincia de Buenos Aires. Revista de la Asociacion Geologica Argentina 72 (2): 235–250.

Jackson, S., and C. Groves. 2015. Taxonomy of Australian mammals, Clayton: CSIRO Publishing.

Jaillard, E., et al. 1993. Sedimentology, palaeontology, biostratigraphy and correlation of the Late Cretaceous Vilquechico Group of southern Peru. Cretaceous Research 14 (6): 623–661.

Janke, A., G. Feldmaier-Fuchs, W.K. Thomas, A. von Haeseler, and S. Pääbo. 1994. The marsupial mitochondrial genome and the evolution of placental mammals. Genetics 137 (1): 243–256.

Janke, A., X. Xu, and U. Arnason. 1997. The complete mitochondrial genome of the wallaroo (Macropus robustus) and the phylogenetic relationship among Monotremata, Marsupialia, and Eutheria. Proceedings of the National Academy of Sciences of the United States of America 94: 1276–1281.

Jansa, S.A., and R.S. Voss. 2000. Phylogenetic studies on didelphid marsupials I. Introduction and prelimi-nary results from nuclear IRBP gene sequences. Journal of Mammalian Evolution 7 (1): 43–77.

Jansa, S.A., and R.S. Voss. 2005. Phylogenetic relationships of the marsupial genus Hyladelphys based on nuclear gene sequences and morphology. Journal of Mammalogy 86 (5): 853–865.

Jansa, S.A., J.F. Forsman, and R.S. Voss. 2006. Different patterns of selection on the nuclear genes IRBP and DMP-1 affect the efficiency but not the outcome of phylogeny estimation for didelphid marsupials. Molecular Phylogenetics and Evolution 38: 363–380.

Jansa, S.A., F.K. Barker, and R.S. Voss. 2014. The early diversification history of didelphid marsupials: a window into South America's "splendid isolation." Evolution 68 (3): 684–695.

Jeffery, N., and F. Spoor. 2006. The primate subarcuate fossa and its relationship to the semicircular canals part I: prenatal growth. Journal of Human Evolution 51 (5): 537–549.

Jehle, S., A. Bornemann, A.F. Lagel, A. Deprez, and R.P. Speijer. 2019. Paleoceanographic changes across the Latest Danian Event in the South Atlantic Ocean and planktic foraminiferal response. Palaeogeography, Palaeoclimatology, Palaeoecology 525: 1–13.

Jia, F., N. Lo, and S.Y. Ho. 2014. The impact of modelling rate heterogeneity among sites on phylogenetic estimates of intraspecific evolutionary rates and timescales. PLoS One 9 (5): e95722.

Johanson, Z. 1996a. Revision of the Late Cretaceous North American marsupial genus Alphadon. Palaeontographica Abteilung A 242: 127–184.

Johanson, Z. 1996b. New marsupial from the Fort Union Formation, Swain Quarry, Wyoming. Journal of Paleontology 70 (6): 1023–1031.

Johnson, P.M., and R. Strahan. 1982. A further description of the musky rat kangaroo, Hysiprymnodon moschatus Ramsay, 1876 (Marsupialia, Potoroidae), with notes on its biology. Australian Zoologist 21: 27–46.

Jones, F.W. 1930. A re-examination of the skeletal characters of Wynyardia bassiana, an extinct Tasmanian marsupial. Papers and Proceedings of the Royal Society of Tasmania 1930: 96–115.

Jones, F.W. 1949. The study of a generalized marsupial (Dasycercus cristicauda Krefft). Transactions of the Zoological Society of London 26: 409–501.

Jones, K.E., et al. 2009. PanTHERIA: a species-level database of life history, ecology, and geography of extant and recently extinct mammals. Ecology 9: 2648.

Kay, R.F., B.J. MacFadden, R.H. Madden, H. Sandeman, and F. Anaya. 1998. Revised age of the Salla beds,

Bolivia, and its bearing on the age of the Deseadan South American Land Mammal "Age." Journal of Vertebrate Paleontology 18 (1): 189–199.

Kealy, S., and R.M.D. Beck. 2017. Total evidence phylogeny and evolutionary timescale for Australian faunivorous marsupials (Dasyuromorphia). BMC Evolutionary Biology 17 (1): 240.

Kealy, S., et al. 2019. Phylogenetic relationships of the cuscuses (Diprotodontia: Phalangeridae) of island Southeast Asia and Melanesia based on the mitochondrial ND2 gene. Australian Mammalogy 42 (3): 266–276.

Kear, B.P. 2002. Phylogenetic implications of macropodid (Marsupialia: Macropodoidea) postcranial remains from Miocene deposits of Riversleigh, northwestern Queensland. Alcheringa: an Australasian Journal of Palaeontology 26 (2): 299–318.

Kear, B.P., and B.N. Cooke. 2001. A review of macropodoid (Marsupialia) systematics with the inclusion of a new family. Memoirs of the Association of Australasian Palaeontologists 25: 83–101.

Kear, B.P., and N.S. Pledge. 2008. A new fossil kangaroo from the Oligocene-Miocene Etadunna Formation of Ngama Quarry, Lake Palankarinna, South Australia. Australian Journal of Zoology 55 (6): 331–339.

Kear, B.P., M. Archer, and T.F. Flannery. 2001a. Bulungamayine (Marsupialia: Macropodoidea) postcranial remains from the late Miocene of Riversleigh, northwestern Queensland. Memoir of the Association of Australasian Palaeontologists 25: 103–122.

Kear, B.P., M. Archer, and T.F. Flannery. 2001b. Postcranial morphology of *Ganguroo bilamina* Cooke, 1997 (Marsupialia: Macropodidae) from the middle Miocene of Riversleigh, northwestern Queensland. Memoir of the Association of Australasian Palaeontologists 25: 123–138.

Kear, B.P., B.N. Cooke, M. Archer, and T.F. Flannery. 2007. Implications of a new species of the Oligo-Miocene kangaroo (Marsupialia: Macropodoidea) *Nambaroo*, from the Riversleigh World Heritage Area, Queensland, Australia. Journal of Paleontology 81 (6): 1147–1167.

Kear, B.P., K.P. Aplin, and M. Westerman. 2016. Bandicoot fossils and DNA elucidate lineage antiquity amongst xeric-adapted Australasian marsupials. Scientific Reports 6: 37537.

Kemp, D.B., et al. 2014. A cool temperate climate on the Antarctic Peninsula through the latest Cretaceous to early Paleogene. Geology 42 (7): 583–586.

Kido, N., S. Tanaka, Y. Wada, S. Sato, and T. Omiya. 2018. Molar eruption and identification of the eastern grey kangaroo (*Macropus giganteus*) at different ages. Journal of Veterinary Medical Science 80 (4): 648–652.

Kielan-Jaworowska, Z., and L.A. Nessov. 1990. On the metatherian nature of the Deltatheroida, a sister group of the Marsupialia. Lethaia 23 (1): 1–10.

Kielan-Jaworowska, Z., R.L. Cifelli, and Z.-X. Luo. 2004. Mammals from the age of dinosaurs: origins, evolution, and structure. New York: Columbia University Press.

King, B. 2021. Bayesian tip-dated phylogenetics in paleontology: Topological effects and stratigraphic fit. Systematic Biology 70 (2): 283–294.

King, B., and R.M.D. Beck. 2020. Tip dating supports novel resolutions of controversial relationships among early mammals. Proceedings of the Royal Society of London B, Biological Sciences 287 (1928): 20200943.

Kirkham, Z. 2004. The cranial description of the primitive macropodid *Rhizosthenurus flanneryi* and its phylogeny based on cranial and postcranial characters. Honours thesis, School of Biological, Earth, and Environmental Sciences, University of New South Wales, Sydney.

Kirkland, J.I., M. Suarez, C. Suarez, and R. Hunt-Foster. 2016. The Lower Cretaceous in east-central Utah—The Cedar Mountain Formation and its bounding strata. Geology of the Intermountain West 3: 101–228.

Kirkpatrick, T.H. 1969. The dentition of the marsupial family Macropodidae with particular reference to tooth development in the grey kangaroo *Macropus giganteus* Shaw. Ph.D. dissertation, Department of Zoology, University of Queensland, Brisbane.

Kirkpatrick, T.H. 1978. The development of the dentition of *Macropus giganteus* (Shaw): an attempt to interpret the marsupial dentition. Australian Mammalogy 2: 29–36.

Kirsch, J.A.W. 1968a. The serological affinities of *Burramys* and related possums (Marsupialia: Phalangeroidea). Australian Journal of Science 31: 43–45.

Kirsch, J.A.W. 1968b. Prodromus of the comparative serology of Marsupialia. Nature 217: 418–420.

Kirsch, J.A.W., and M. Archer. 1982. Polythetic cladistics, or, when parsimony's not enough: the relationships of carnivorous marsupials. *In* M. Archer (editor), Carnivorous marsupials: 595–619. Mosman, Australia: Royal Zoological Society of New South Wales.

Kirsch, J.A.W., and J.H. Calaby. 1977. The species of living marsupials: an annotated list. *In* B. Stone-

house and D. Gilmore (editors), The biology of marsupials: 9–26. New York: Macmillan Press Ltd.

Kirsch, J.A.W., A.W. Dickerman, O.A. Reig, and M.S. Springer. 1991. DNA hybridization evidence for the Australasian affinity of the American marsupial *Dromiciops australis*. Proceedings of the National Academy of Sciences of the United States of America 88: 10465–10469.

Kirsch, J.A.W., F.J. Lapointe, and M.S. Springer. 1997. DNA-hybridization studies of marsupials and their implications for metatherian classification. Australian Journal of Zoology 45: 211–280.

Kitchener, D.J., J. Stoddart, and J. Henry. 1983. A taxonomic appraisal of the genus *Ningaui* Archer (Marsupialia: Dasyuridae), including description of a new species. Australian Journal of Zoology 31: 361–379.

Klopfstein, S. 2020. The age of insects and the revival of the minimum age tree. Austral Entomology 60 (1): 138–146.

Klopfstein, S., R. Ryer, M. Coiro, and T. Spasojevic. 2019. Mismatch of the morphology model is mostly unproblematic in total-evidence dating: insights from an extensive simulation study. bioRxiv preprint 679084.

Koch, J.M., and M.T. Holder. 2012. An algorithm for calculating the probability of classes of data patterns on a genealogy. PLoS Currents Tree of Life 4: e4fd1286980c1286908.

Koenigswald, W. von, and G. Storch. 1988. Messeler Beuteltiere – unauffällige Beutelratten. *In* S. Schaal and W. Ziegler (editors), Ein Schaufenster in die Geschichte der Erde und des Lebens: 155–158. Frankfurt a.M.: Verlag Waldemar Kramer.

Korth, W.W. 1994. Middle Tertiary marsupials (Mammalia) from North America. Journal of Paleontology 68 (2): 376–397.

Korth, W.W. 2008. Marsupialia. *In* C.M. Janis, G.F. Gunnell, and M.D. Uhen (editors), Evolution of Tertiary mammals of North America, vol. 2. Small mammals, xenarthrans, and marine mammals: 39–48. Cambridge: Cambridge University Press.

Korth, W.W. 2018. Review of the marsupials (Mammalia: Metatheria) from the late Paleogene (Chadronian-Arikareean: late Eocene-late Oligocene) of North America. PalZ 92 (3): 499–523.

Koyabu, D., W. Maier, and M.R. Sánchez-Villagra. 2012. Paleontological and developmental evidence resolve the homology and dual embryonic origin of a mammalian skull bone, the interparietal. Proceedings of the National Academy of Sciences of the United States of America 109 (35): 14075–14080.

Krajewski, C., L. Buckley, and M. Westerman. 1997. DNA phylogeny of the marsupial wolf resolved. Proceedings of the Royal Society of London B, Biological Sciences 264 (1383): 911–917.

Krajewski, C., G.R. Moyer, J.T. Sipiorski, M.G. Fain, and M. Westerman. 2004. Molecular systematics of the enigmatic 'phascolosoricine' marsupials of New Guinea. Australian Journal of Zoology 52 (4): 389–415.

Krajewski, C., R. Torunsky, J.T. Sipiorski, and M. Westerman. 2007. Phylogenetic relationships of the dasyurid marsupial genus *Murexia*. Journal of Mammalogy 88 (3): 696–705.

Krause, J.M., et al. 2017. New age constraints for early Paleogene strata of central Patagonia, Argentina: Implications for the timing of South American Land Mammal Ages. Geological Society of America Bulletin 129 (7-8): 886–903.

Krishtalka, L., and R.K. Stucky. 1983. Paleocene and Eocene marsupials of North America. Annals of Carnegie Museum 52 (10): 229–263.

Kurz, C. 2001. Osteologie einer Beutelratte (Didelphimorphia, Marsupialia, Mammalia) aus dem Mitteleozän der Grube Messel bei Darmstadt. Kaupia 11: 83–109.

Kurz, C. 2005. Ecomorphology of opossum-like marsupials from the Tertiary of Europe and a comparison with selected taxa. Kaupia 14: 21–26.

Kurz, C. 2007. The opossum-like marsupials (Didelphimorphia and Peradectia, Marsupialia, Mammalia) from the Eocene of Messel and Geiseltal—ecomorphology, diversity and palaeogeography. Kaupia 15: 3–64.

Kurz, C., and J. Habersetzer. 2004. Untersuchungen der Zahnmorphologie von Beutelratten aus Messel mit der Mikroröntgenmethode CORR. Courier Forschungsinstitut Senckenberg 252: 13–21.

Ladevèze, S. 2004. Metatherian petrosals from the late Paleocene of Itaboraí (Brazil), and their phylogenetic implications. Journal of Vertebrate Paleontology 24: 202–213.

Ladevèze, S. 2005. La région auditive des métathériens (Mammalia, Metatheria) du Tertiaire inférieur d'Amérique du Sud. Incidence sur l'origine phylogénétique et la systématique des Notometatheria (métathériens d'Australie et d'Amérique du Sud. Ph.D. dissertation, École Doctorale Sciences de la Nature et de l'Homme (ED 0227), Muséum National d'Histoire Naturelle, Paris.

Ladevèze, S., and C. de Muizon. 2007. The auditory region of early Paleocene Pucadelphydae (Mamma-

lia, Metatheria) from Tiupampa, Bolivia, with phylogenetic implications. Palaeontology 50 (5): 1123–1154.

Ladevèze, S., and C. de Muizon. 2010. Evidence of early evolution of Australidelphia (Metatheria, Mammalia) in South America: phylogenetic relationships of the metatherians from the late Palaeocene of Itaboraí (Brazil) based on teeth and petrosal bones. Zoological Journal of the Linnean Society 159 (3): 746–784.

Ladevèze, S., R.J. Asher, and M.R. Sánchez-Villagra. 2008. Petrosal anatomy in the fossil mammal *Necrolestes*: evidence for metatherian affinities and comparisons with the extant marsupial mole. Journal of Anatomy 213 (6): 686–697.

Ladevèze, S., P. Missiaen, and T. Smith. 2010. First skull of *Orthaspidotherium edwardsi* (Mammalia, "Condylarthra") from the late Paleocene of Berru (France) and phylogenetic affinities of the enigmatic European family Pleuraspidotheriidae. Journal of Vertebrate Paleontology 30 (5): 1559–1578.

Ladevèze, S., C. de Muizon, R.M.D. Beck, D. Germain, and R. Cespedes-Paz. 2011. Earliest evidence of mammalian social behaviour in the basal Tertiary of Bolivia. Nature 474: 83–86.

Ladevèze, S., R. Smith, and T. Smith. 2012. Reassessment of the morphology and taxonomic status of the earliest herpetotheriid marsupials of Europe. Journal of Mammalian Evolution 19 (4): 249–261.

Ladevèze, S., C. Selva, and C. de Muizon. 2020. What are "opossum-like" fossils? The phylogeny of herpetotheriid and peradectid metatherians, based on new features from the petrosal anatomy. Journal of Systematic Palaeontology 18 (17): 1463–1479.

Lanfear, R. 2016. PartitionFinder2 Manual. [http://www.robertlanfear.com/partitionfinder/assets/Manual_v2.1.x.pdf]

Lanfear, R., B. Calcott, S.Y. Ho, and S. Guindon. 2012. Partitionfinder: combined selection of partitioning schemes and substitution models for phylogenetic analyses. Molecular Biology and Evolution 29 (6): 1695–1701.

Lanfear, R., P.B. Frandsen, A.M. Wright, T. Senfeld, and B. Calcott. 2017. Partitionfinder 2: new methods for selecting partitioned models of evolution for molecular and morphological phylogenetic analyses. Molecular Biology and Evolution 34 (3): 772–773.

Latorre, C., J. Quade, and W.C. McIntosh. 1997. The expansion of C_4 grasses and global change in the late Miocene: Stable isotope evidence from the Americas. Earth and Planetary Science Letters 146 (1-2): 83–96.

Leche, W. 1891. Beitrage zur Anatomie des *Myrmecobius fasciatus*. Biologiska Foreningens Forhandlingar 3: 136–154.

Lee, A.K., and F.N. Carrick. 1989. 31. Phascolarctidae. *In* D.W. Walton and B.J. Richardson (editors), Fauna of Australia, vol. 1B. Mammalia: 1–31. Canberra: AGPS.

Lee, M.S.Y., and A. Palci. 2015. Morphological phylogenetics in the genomic age. Current Biology 25 (19): R922–929.

Lee, M.S.Y., and A.M. Yates. 2018. Tip-dating and homoplasy: reconciling the shallow molecular divergences of modern gharials with their long fossil record. Proceedings of the Royal Society of London B, Biological Sciences 285 (1881): 20181071.

Lentle, R.G., and I. Hume. 2010. Mesial drift and mesial shift in the molars of four species of wallaby: the influence of chewing mechanics on tooth movement in a group of species with an unusual mode of jaw action. *In* G. Coulson and M. Eldridge (editors), Macropods: the biology of kangaroos, wallabies and rat-kangaroos: 127–137. Collingwood, Australia: CSIRO Publishing.

Lepage, T., D. Bryant, H. Philippe, and N. Lartillot. 2007. A general comparison of relaxed molecular clock models. Molecular Biology and Evolution 24 (12): 2669–2680.

Lewis, P.O. 2001. A likelihood approach to estimating phylogeny from discrete morphological character data. Systematic Biology 50: 913–925.

Linnaeus, C. 1758. Systema naturae per regna tria naturae, secundum classes, ordines, genera, species, cum characteribus, differentiis, synonymis, locis. 10th ed., tomus 1. Holmiae [Stockholm]: Laurentii Salvii.

Llamas, B., et al. 2015. Late Pleistocene Australian marsupial DNA clarifies the affinities of extinct megafaunal kangaroos and wallabies. Molecular Biology and Evolution 32 (3): 574–584.

Long, J.A., M. Archer, T.F. Flannery, and S.J. Hand. 2002. Prehistoric mammals of Australia and New Guinea: one hundred million years of evolution, Sydney: UNSW Press.

Loomis, F.B. 1925. Dentition of artiodactyls. Geological Society of America Bulletin 36 (4): 583–604.

Lorente, M., L. Chornogubsky, and F.J. Goin. 2016. On the existence of non-microbiotherian australidelphian marsupials (Diprotodontia) in the Eocene of Patagonia. Palaeontology 59 (4): 533–547.

Louys, J., and G. Price. 2015. The Chinchilla Local Fauna: an exceptionally rich and well-preserved

Pliocene vertebrate assemblage from fluviatile deposits of south-eastern Queensland, Australia. Acta Palaeontologica Polonica 60 (3): 551–572.

Louys, J., K. Black, M. Archer, S.J. Hand, and H. Godthelp. 2007. Descriptions of koala fossils from the Miocene of Riversleigh, northwestern Queensland and implications for *Litokoala* (Marsupialia, Phascolarctidae). Alcheringa: an Australasian Journal of Palaeontology 31: 99–110.

Louys, J., K.P. Aplin, R.M.D. Beck, and M. Archer. 2009. Cranial anatomy of Oligo-Miocene koalas (Diprotodontia: Phascolarctidae): stages in the evolution of an extreme leaf-eating specialization. Journal of Vertebrate Paleontology 29 (4): 981–992.

Luckett, W.P. 1985. Superordinal and intraordinal affinities of rodents: Developmental evidence from the dentition and placentation. *In* W.P. Luckett and J.-L. Hartenberger (editors), Evolutionary relationships among rodents: a multidisciplinary analysis: 227–276. New York: Springer.

Luckett, W.P. 1993a. Ontogenetic staging of the mammalian dentition, and its value for assessment of homology and heterochrony. Journal of Mammalian Evolution 1 (4): 269–282.

Luckett, W.P. 1993b. An ontogenetic assessment of dental homologies in therian mammals. *In* F.S. Szalay, M.J. Novacek, and M.C. McKenna (editors), Mammal phylogeny, vol. 1. Mesozoic differentiation, multituberculates, monotremes, early therians, and marsupials: 182–204. New York: Springer Verlag.

Luckett, W.P. 1994. Suprafamilial relationships within Marsupialia: resolution and discordance from multidisciplinary data. Journal of Mammalian Evolution 2 (4): 255–283.

Luckett, W.P., and N. Hong. 2000. Ontogenetic evidence for dental homologies and premolar replacement in fossil and extant caenolestids (Marsupialia). Journal of Mammalian Evolution 7 (2): 109–127.

Luckett, W.P., and P.A. Woolley. 1996. Ontogeny and homology of the dentition in dasyurid marsupials: Development in *Sminthopsis virginiae*. Journal of Mammalian Evolution 3 (4): 327–364.

Luckett, W.P., N. Hong Luckett, and T. Harper. 2019. Microscopic analysis of the developing dentition in the pouch young of the extinct marsupial *Thylacinus cynocephalus*, with an assessment of other developmental stages and eruption. Memoirs of Museum Victoria 78: 1–21.

Lundelius, E.L.J. 1983. Climatic implications of late Pleistocene and Holocene faunal associations in Australia. Alcheringa: an Australasian Journal of Palaeontology 7: 125–149.

Luo, A., et al. 2010. Performance of criteria for selecting evolutionary models in phylogenetics: a comprehensive study based on simulated datasets. BMC Evolutionary Biology 10: 242.

Luo, A., D.A. Duchêne, C. Zhang, C.-D. Zhu, and S.Y.W. Ho. 2020. A simulation-based evaluation of tip-dating under the fossilized birth–death process. Systematic Biology 69 (2): 325–344.

Luo, Z.-X., Q. Ji, J.R. Wible, and C.-X. Yuan. 2003. An Early Cretaceous tribosphenic mammal and metatherian evolution. Science 302: 1934–1940.

Luo, Z.-X., Z. Kielan-Jaworowska, and R.L. Cifelli. 2004. Evolution of dental replacement in mammals. Bulletin of Carnegie Museum of Natural History 36: 159–175.

Luo, Z.-X., C.X. Yuan, Q.J. Meng, and Q. Ji. 2011. A Jurassic eutherian mammal and divergence of marsupials and placentals. Nature 476: 442–445.

Lyne, A.G., and P.A. Mort. 1981. A comparison of skull morphology in the marsupial bandicoot genus *Isoodon*: its taxonomic implications and notes on a newspecies, *Isoodon arnhemensis*. Australian Mammalogy 4: 107–133.

Macalister, A. 1872. The muscular anatomy of the koala (*Phascolarctos cinereus*). Annals and Magazine of Natural History (Series 4) 10: 127–134.

MacFadden, B.J., et al. 1990. Late Cenozoic paleomagnetism and chronology of Andean basins of Bolivia: evidence for possible oroclinal bending. Journal of Geology 98: 541–555.

MacIntyre, G.T. 1967. Foramen pseudovale and quasi-mammals. Evolution 21: 834–841.

Mackness, B.S. 2008. Reconstructing *Palorchestes* (Marsupialia: Palorchestidae) – from giant kangaroo to marsupial 'tapir'. Proceedings of the Linnean Society of New South Wales 130: 21–36.

Mackness, B.S., and M. Archer. 2001. A new petauroid possum (Marsupialia, Pseudocheiridae) from the Pliocene Bluff Downs Local Fauna, northern Queensland. Alcheringa: an Australasian Journal of Palaeontology 25 (3-4): 439–444.

Mackness, B.S., P.W. Whitehead, and G.C. McNamara. 2000. New potassium-argon basalt date in relation to the Pliocene Bluff Downs Local Fauna, Northern Australia. Australian Journal of Earth Sciences 47 (4): 807–811.

MacPhee, R.D.E. 1979. Entotympanics, ontogeny and primates. Folia Primatologica 31: 23–47.

MacPhee, R.D.E. 1981. Auditory regions of primates and eutherian insectivores: Morphology, ontogeny,

and character analysis. Contributions to Primatology 18: 1–282.

Macrini, T.E. 2012. Comparative morphology of the internal nasal skeleton of adult marsupials based on X-ray computed tomography. Bulletin of the American Museum of Natural History 365: 1–91.

Macrini, T.E. 2014. Development of the ethmoid in *Caluromys philander* (Didelphidae, Marsupialia) with a discussion on the homology of the turbinal elements in marsupials. Anatomical Record 297 (11): 2007–2017.

Macrini, T.E., Muizon, C. de, R.L. Cifelli, and T. Rowe. 2007. Digital cranial endocast of *Pucadelphys andinus*, a Paleocene metatherian. Journal of Vertebrate Paleontology 27 (1): 99–107.

Maeda, N., et al. 1988. Molecular genetics of the apolipoprotein B gene in pigs in relation to atherosclerosis. Gene 70 (2): 213–229.

Maga, A.M., and R.M.D. Beck. 2017. Skeleton of an unusual, cat-sized marsupial relative (Metatheria: Marsupialiformes) from the middle Eocene (Lutetian: 44–43 million years ago) of Turkey. PLoS One 12 (8): e0181712.

Maier, W. 1987. The ontogenetic development of the orbitotemporal region in the skull of *Monodelphis domestica* (Didelphidae, Marsupialia), and the problem of the mammalian alisphenoid. *In* H.J. Kuhn and U. Zeller (editors), Morphogenesis of the mammalian skull: 71–90. Hamburg and Berlin: V.P. Parey.

Mamanova, L., et al. 2010. Target-enrichment strategies for next-generation sequencing. Nature Methods 7 (2): 111–118.

Mammal Diversity Database. 2021. Mammal diversity database (version 1.5). Online resource (https://www.mammaldiversity.org), accessed March 3, 2022.

Marshall, L.G. 1973. Fossil vertebrate faunas from the Lake Victoria region, S.W. New South Wales, Australia. Memoirs of Musem Victoria 34: 15–172.

Marshall, L.G. 1976. New didelphine marsupials from the La Venta Fauna (Miocene) of Colombia, South America. Journal of Paleontology 50: 402–418.

Marshall, L.G. 1977. Cladistic analysis of borhyaenoid, dasyuroid, didelphoid, and thylacinid (Marsupialia: Mammalia) affinity. Systematic Zoology 26 (4): 410–425.

Marshall, L.G. 1978. *Glironia venusta*. Mammalian Species 107: 1–3.

Marshall, L.G. 1979. Evolution of metatherian and eutherian (mammalian) characters: a review based on cladistic methodology. Zoological Journal of the Linnean Society 66: 369–410.

Marshall, L.G. 1980. Systematics of the South American marsupial family Caenolestidae. Fieldiana Geology (new series) 5: i–viii, 1–145.

Marshall, L.G. 1982. Systematics of the South American marsupial family Microbiotheriidae. Fieldiana Geology 10: 1–75.

Marshall, L.G. 1987. Systematics of Itaboraian (middle Paleocene) age "opossum-like" marsupials from the limestone quarry at São José de Itaboraí, Brazil. *In* M. Archer (editor), Possums and opossums: studies in evolution: 91–160. Sydney: Surrey Beatty and Sons.

Marshall, L.G. 1990. Fossil Marsupialia from the type Friasian land mammal age (Miocene), Alto Rio Cisnes, Aisen, Chile. Revista Geologica de Chile 17: 19–55.

Marshall, L.G., and C. de Muizon. 1988. The dawn of the age of mammals in South America. National Geographic Research 4 (1): 23–55.

Marshall, L.G., and C. de Muizon. 1995. Part II: The skull. *In* C. de Muizon (editor), *Pucadelphys andinus* (Marsupialia, Mammalia) from the early Paleocene of Bolivia (Memoires du Muséum national d'Histoire naturelle 165): 21–90. Paris: Muséum national d'Histoire naturelle.

Marshall, L.G., and R. Pascual. 1977. Nuevos marsupiales Caenolestidae del 'Piso Notohipidense' (SW de Santa Cruz, Patagonia) de Ameghino. Sus aportaciones a la cronología y evolución de las comunidades de mamíferos sudamericanos. Publicaciones del Museo Municipal de Ciencias Naturales de Mar del Plata 'Lorenzo Scaglia' 2: 91–122.

Marshall, L.G., and D. Sigogneau-Russell. 1995. Part III: Postcranial skeleton. *In* C. de Muizon (editor) *Pucadelphys andinus* (Marsupialia, Mammalia) from the early Palaeocene of Bolivia (Mémoires du Muséum national d'Histoire naturelle 165): 91–164. Paris: Muséum national d'Histoire naturelle.

Marshall, L.G., C. de Muizon, and B. Sigé. 1983. Late Cretaceous mammals (Marsupialia) from Bolivia. Geobios 16: 739–745.

Marshall, L.G., J.A. Case, and M.O. Woodburne. 1990. Phylogenetic relationships of the families of marsupials. Current Mammalogy 2: 433–505.

Marshall, L.G., T. Sempere, and R.F. Butler. 1997. Chronostratigraphy of the mammal-bearing Paleocene of South America. Journal of South American Earth Sciences 10 (1): 49–70.

Martin, G. 2005. Intraspecific variation in *Lestodelphys halli* (Marsupialia: Didelphimorphia). Journal of Mammalogy 86 (4): 793–802.

Martin, G.M. 2007. Dental anomalies in *Dromiciops gliroides* (Microbiotheria, Microbiotheriidae), *Cae-*

nolestes fuliginosus and *Rhyncholestes raphanurus* (Paucituberculata, Caenolestidae). Revista Chilena de Historia Natural 80 (4): 393–406.

Martin, G.M. 2013. Intraspecific variability in *Lestoros inca* (Paucituberculata, Caenolestidae), with reports on dental anomalies and eruption pattern. Journal of Mammalogy 94 (3): 601–617.

Martin, G.M. 2018. Variability and variation in *Dromiciops* Thomas, 1894 (Marsupialia, Microbiotheria, Microbiotheriidae). Journal of Mammalogy 99 (1): 159–173.

Martin, G.M. 2019. The palmar and plantar anatomy of *Dromiciops gliroides* Thomas, 1894 (Marsupialia, Microbiotheria) and its relationship to Australian marsupials. Journal of Mammalian Evolution 26 (1): 51–60.

Martin, J.E., J.A. Case, J.W.M. Jagt, A.S. Schulp, and E.W.A. Mulder. 2005. A new European marsupial indicates a Late Cretaceous high-latitude transatlantic dispersal route. Journal of Mammalian Evolution 12 (3-4): 495–511.

Martin, R., K. Handasyde, and A. Krockenburger. 2008. Koala *Phascolarctos cinereus*. *In* S. Van Dyck and R. Strahan (editors), The mammals of Australia: 198–201. Sydney: New Holland.

Martinez-Lanfranco, J.A., D. Flores, J.P. Jayat, and G. D'Elia. 2014. A new species of lutrine opossum, genus *Lutreolina* Thomas (Didelphidae), from the South American Yungas. Journal of Mammalogy 95 (2): 225–240.

Mason, M.J. 2001. Middle ear structures in fossorial mammals: a comparison with non-fossorial species. Journal of Zoology, London 255: 467–486.

Matzke, N.J. 2016. The evolution of antievolution policies after Kitzmiller versus Dover. Science 351: 28–30.

Matzke, N.J., and R.B. Irmis. 2018. Including autapomorphies is important for paleontological tip-dating with clocklike data, but not with non-clock data. PeerJ 6: e4553.

Matzke, N.J., and A. Wright. 2016. Inferring node dates from tip dates in fossil Canidae: the importance of tree priors. Biological Letters 12 (8): 20160328.

May-Collado, L.J., C.W. Kilpatrick, and I. Agnarsson. 2015. Mammals from 'down under': a multi-gene species-level phylogeny of marsupial mammals (Mammalia, Metatheria). PeerJ 3: e805.

McDowell, M.C., et al. 2015. Morphological and molecular evidence supports specific recognition of the recently extinct *Bettongia anhydra* (Marsupialia: Macropodidae). Journal of Mammalogy 96 (2): 287–296.

Megirian, D. 1986. The dentary of *Wakaleo vanderleueri* (Thylacoleonidae: Marsupialia). Beagle, Occasional Papers of the Northern Territory Museum of Arts and Sciences 3 (1): 71–79.

Megirian, D., G.J. Prideaux, P.F. Murray, and N. Smit. 2010. An Australian land mammal age biochronological scheme. Paleobiology 36 (4): 658–671.

Meng, J. 2014. Mesozoic mammals of China: implications for phylogeny and early evolution of mammals. National Science Review 1: 521–542.

Mercerat, A. 1899. Sur de nouveaux restes fossiles de carnassiers primitifs de Monte Hermoso. Anales de la Sociedad Científica Argentina 47: 56–60.

Meredith, R.W., M. Westerman, and M.S. Springer. 2008a. A timescale and phylogeny for "bandicoots" (Peramelemorphia: Marsupialia) based on sequences for five nuclear genes. Molecular Phylogenetics and Evolution 47 (1): 1–20.

Meredith, R.W., M. Westerman, J.A. Case, and M.S. Springer. 2008b. A phylogeny and timescale for marsupial evolution based on sequences for five nuclear genes. Journal of Mammalian Evolution 15 (1): 1–36.

Meredith, R.W., M. Westerman, and M.S. Springer. 2009a. A phylogeny of Diprotodontia (Marsupialia) based on sequences for five nuclear genes. Molecular Phylogenetics and Evolution 51 (3): 554–571.

Meredith, R.W., M. Westerman, and M.S. Springer. 2009b. A phylogeny and timescale for the living genera of kangaroos and kin (Macropodiformes: Marsupialia) based on nuclear DNA sequences. Australian Journal of Zoology 56: 395–410.

Meredith, R.W., C. Krajewski, M. Westerman, and M.S. Springer. 2009c. Relationships and divergence times among the orders and families of Marsupialia. Museum of Northern Arizona Bulletin 65: 383–406.

Meredith, R.W., M.A. Mendoza, K.K. Roberts, M. Westerman, and M.S. Springer. 2010. A phylogeny and timescale for the evolution of Pseudocheiridae (Marsupialia: Diprotodontia) in Australia and New Guinea. Journal of Mammalian Evolution 17 (2): 75–99.

Meredith, R.W., et al. 2011. Impacts of the Cretaceous Terrestrial Revolution and KPg extinction on mammal diversification. Science 334: 521–524.

Métais, G., et al. 2018. Eocene metatherians from Anatolia illuminate the assembly of an island fauna during Deep Time. PLoS One 13 (11): e0206181.

Metzger, C.A., and G.J. Retallack. 2010. Paleosol record of Neogene climate change in the Australian outback. Australian Journal of Earth Sciences 57: 871–885.

Miller, W., et al. 2009. The mitochondrial genome sequence of the Tasmanian tiger (*Thylacinus cynocephalus*). Genome Research 19: 213–220.

Miller, M.A., W. Pfeiffer, and T. Schwartz. 2010. Creating the CIPRES Science Gateway for inference of large phylogenetic trees. *In* Conference Proceedings of the 2010 Gateway Computing Environments Workshop (GCE 2010): 1–8.

Mitchell, K.J., et al. 2014. Molecular phylogeny, biogeography, and habitat preference evolution of marsupials. Molecular Biology and Evolution 31 (9): 2322–2330.

Mones, A. 1982. An equivocal nomenclature: what means hypsodonty? Paläontologische Zeitschrift 56: 107–111.

Mongiardino Koch, N. 2021. Phylogenomic subsampling and the search for phylogenetically reliable loci. Molecular Biology and Evolution 38 (9): 4025–4038.

Montanari, S., J. Louys, and G.J. Price. 2013. Pliocene paleoenvironments of southeastern Queensland, Australia inferred from stable isotopes of marsupial tooth enamel. PLoS One 8 (6): e66221.

Morgan, G.S. 2018. Vertebrate fauna and geochronology of the Great American Biotic Interchange in North America. *In* S.G. Lucas, G.S. Morgan, J.A. Spielmann, and D.R. Prothero (editors), Neogene mammals. New Mexico Museum of Natural History and Science Bulletin 44: 93–140.

Morlo, M., S. Schaal, G. Mayr, and C. Seiffert. 2004. An annotated taxonomic list of the middle Eocene (MP 11) Vertebrata of Messel. Courier Forschungsinstitut Senckenberg 252: 95–108.

Mörs, T., M. Reguero, and D. Vasilyan. 2020. First fossil frog from Antarctica: implications for Eocene high latitude climate conditions and Gondwanan cosmopolitanism of Australobatrachia. Scientific Reports 10: 5051.

Muirhead, J. 1992. A specialized thylacinid, *Thylacinus macknessi*, (Marsupialia: Thylacinidae) from Miocene deposits of Riversleigh, northwestern Queensland. Australian Mammalogy 15: 67–76.

Muirhead, J. 1994. Systematics, evolution and palaeobiology of recent and fossil bandicoots (Marsupialia: Peramelemorphia). Ph.D. dissertation, School of Biological Science, University of New South Wales, Sydney.

Muirhead, J. 1997. Two new early Miocene thylacines from Riversleigh, northwestern Queensland. Memoirs of the Queensland Museum 41 (2): 367–377.

Muirhead, J. 2000. Yaraloidea (Marsupialia, Peramelemorphia), a new superfamily of marsupial and a description and analysis of the cranium of the Miocene of *Yarala burchfieldi*. Journal of Paleontology 74 (3): 512–523.

Muirhead, J., and M. Archer. 1990. *Nimbacinus dicksoni*, a plesiomorphic thylacine (Marsupialia, Thylacinidae) from Tertiary deposits of Queensland and the Northern Territory. Memoirs of the Queensland Museum 28: 203–221.

Muirhead, J., and S. Filan. 1995. *Yarala burchfieldi* (Peramelemorphia) from Oligo-Miocene deposits of Riversleigh, northwestern Queensland. Journal of Paleontology 69 (1): 127–134.

Muirhead, J., and A.K. Gillespie. 1995. Additional parts of the type specimen of *Thylacinus macknessi* (Marsupialia: Thylacinidae) from Miocene deposits of Riversleigh, northwestern Queensland. Australian Mammalogy 18: 55–60.

Muirhead, J., and S. Wroe. 1998. A new genus and species, *Badjcinus turnbulli* (Thylacinidae: Marsupialia), from the late Oligocene of Riversleigh, northern Australia, and an investigation of thylacinid phylogeny. Journal of Vertebrate Paleontology 18: 612–626.

Muizon, C. de. 1991. La fauna de mamíferos de Tiupampa (Paleoceno Inferior, Formacion Santa Lucia), Bolivia. *In* R. Suarez-Soruco (editor), Fósiles y facies de Bolivia, vol. 1. Vertebrados: 575–624. Santa Cruz, Bolivia: Revista Technica de Yacimientos Petroliferos Fiscales Bolivianos.

Muizon, C. de. 1994. A new carnivorous marsupial from the Palaeocene of Bolivia and the problem of marsupial monophyly. Nature 370: 208–211.

Muizon, C. de. 1998. *Mayulestes ferox*, a borhyaenoid (Metatheria, Mammalia) from the early Palaeocene of Bolivia: phylogenetic and palaeobiologic implications. Geodiversitas 20 (1): 19–142.

Muizon, C. de. 1999. Marsupial skulls from the Deseadan (late Oligocene) of Bolivia and phylogenetic analysis of the Borhyaenoidea (Marsupialia, Mammalia). Geobios 32 (3): 483–509.

Muizon, C. de, and C. Argot. 2003. Comparative anatomy of the Tiupampa didelphimorphs: an approach to locomotory habits of early marsupials. *In* M. Jones, C. Dickman, and M. Archer (editors), Predators with pouches: the biology of carnivorous marsupials: 43–62. Collingwood, Australia: CSIRO Publishing.

Muizon, C. de, and R.L. Cifelli. 2000. The "condylarths" (archaic Ungulata, Mammalia) from the early Palaeocene of Tiupampa (Bolivia): implications on the origin of the South American ungulates. Geodiversitas 22 (1): 47–150.

Muizon, C. de, and S. Ladevèze. 2020. Cranial anatomy of *Andinodelphys cochabambensis*, a stem metatherian from the early Palaeocene of Bolivia. Geodiversitas 42 (30): 597–739.

Muizon, C. de, and B. Lange-Badré. 1997. Carnivorous dental adaptations in tribosphenic mammals and phylogenetic reconstruction. Lethaia 30: 353–366.

Muizon, C. de, et al. 1983. Late Cretaceous vertebrates including mammals from Bolivia. Geobios 16 (6): 747–753.

Muizon, C. de, L.G. Marshall, and B. Sigé. 1984. The mammal fauna from the El Molino Formation (Late Cretaceous-Maastrichtian) at Tiupampa, southcentral Bolivia. Bulletin du Muséum national d'Histoire naturelle Paris 4e série, section C 6 (4): 315–327.

Muizon, C. de, R.L. Cifelli, and R. Céspedes Paz. 1997. The origin of the dog-like borhyaenoid marsupials of South America. Nature 389: 486–489.

Muizon, C. de, G. Billet, C. Argot, S. Ladevèze, and F. Goussard. 2015. *Alcidedorbignya inopinata*, a basal pantodont (Placentalia, Mammalia) from the early Palaeocene of Bolivia: anatomy, phylogeny and palaeobiology. Geodiversitas 37 (4): 397–634.

Muizon, C. de, S. Ladevèze, C. Selva, R. Vignaud, and F. Goussard. 2018. *Allqokirus australis* (Sparassodonta, Metatheria) from the early Palaeocene of Tiupampa (Bolivia) and the rise of the metatherian carnivorous radiation in South America. Geodiversitas 40 (16): 363–459.

Muller, J. 1934. The orbitotemporal region of the skull of the Mammalia. Archives Néerlandaises de Zoologie 1 (1): 118–259.

Müller, J., and R.R. Reisz. 2006. The phylogeny of early eureptiles: comparing parsimony and Bayesian approaches in the investigation of a basal fossil clade. Systematic Biology 55 (3): 503–511.

Munson, C.J. 1992. Postcranial descriptions of *Ilaria* and *Ngapakaldia* (Vombatiformes, Marsupialia) and the phylogeny of the vombatiforms based on postcranial morphology. University of California Publications in Zoology 125: 1–99.

Murray, P.F. 1986. *Propalorchestes novaculacephalus* gen. sp.nov., a new palorchestid (Diprotodontoidea: Marsupialia) from the middle Miocene Camfield Beds, Northern Territory, Australia. Beagle, Occasional Papers of the Northern Territory Museum of Arts and Sciences 3 (1): 195–211.

Murray, P.F. 1989. The cranium of *Hadronomus puckridgi* Woodburne, 1967 (Macropodoidea: Macropodidae) a primitive macropodid kangaroo from the late Miocene Alcoota Fauna of the Northern Territory. Beagle, Records of the Museums and Art Galleries of the Northern Territory 6 (1): 115–132.

Murray, P.F. 1990. Primitive marsupial tapirs (*Propalorchestes novaculacephalus* Murray and *P. ponticulus* sp. nov.) from the mid-Miocene of north Australia (Marsupialia: Palorchestidae). Beagle, Records of the Northern Territory Museum of Arts and Sciences 7 (2): 39–51.

Murray, P.F. 1991. The sthenurine affinity of the late Miocene kangaroo, *Hadronomas puckridgi* Woodburne (Marsupialia, Macropodidae). Alcheringa: an Australasian Journal of Palaeontology 15: 255–283.

Murray, P.F. 1992. Thinheads, thickheads and airheads—functional craniology of some diprotodontian marsupials. Beagle, Records of the Northern Territory Museum of Arts and Sciences 9 (1): 825–833.

Murray, P.F. 1995. The postcranial skeleton of the Miocene kangaroo, *Hadronomas puckridgi* Woodburne (Marsupialia, Macropodidae). Alcheringa: an Australasian Journal of Palaeontology 19: 119–170.

Murray, P.F. 1998. Palaeontology and palaeobiology of wombats. *In* R.T. Wells and P.A. Pridmore (editors), Wombats: 1–33. Chipping Norton: Surrey Beatty and Sons.

Murray, P.F., and D. Megirian. 1990. Further observations on the morphology of *Wakaleo vanderleueri* (Marsupialia:Thylacoleonidae) from the mid-Miocene Camfield Beds, Northern Territory. Beagle, Records of the Museums and Art Galleries of the Northern Territory 7 (1): 91–102.

Murray, P.F., and D. Megirian. 1992. Continuity and contrast in middle and late Miocene vertebrate communities from the Northern Territory. Beagle, Records of the Northern Territory Museum of Arts and Science 9 (1): 195–218.

Murray, P.F., and D. Megirian. 2000. Two new genera and three new species of Thylacinidae (Marsupialia) from the Miocene of the Northern Territory, Australia. Beagle, Records of the Museums and Art Galleries of the Northern Territory 16: 145–162.

Murray, P.F., and D. Megirian. 2006a. Cranial morphology of the Miocene thylacinid *Mutpuracinus archibaldi* (Thylacinidae, Marsupialia) and relationships within the Dasyuromorphia. Alcheringa: an Australasian Journal of Palaeontology Special Issue 1: 229–276.

Murray, P.F., and D. Megirian. 2006b. The Pwerte Marnte Marnte Local Fauna: a new vertebrate assemblage of presumed Oligocene age from the Northern Territory of Australia. Alcheringa: an Australasian Journal of Palaeontology Special Issue 1: 211–228.

Murray, P.F., R. Wells, and M. Plane. 1987. The cranium of the Miocene thylacoleonid, *Wakaleo vanderleuri*: click go the shears – a fresh bite at thylacoleonid systematics. *In* M. Archer (editor), Possums and opossums: studies in evolution: 433–466. Sydney: Surrey Beatty and Sons.

Murray, P.F., et al. 2000a. Morphology, systematics and evolution of the marsupial genus *Neohelos* Stirton (Diprotodontidae, Zygomaturinae). Museums and Art Galleries of the Northern Territory Research Report 6: 1–141.

Murray, P.F., D. Megirian, T. Rich, M. Plane, and P. Vickers-Rich. 2000b. *Neohelos stirtoni*, a new species of Zygomaturinae (Diprotodontidae: Marsupialia) from the mid-Tertiary of northern Australia. Memoirs of the Queen Victoria Museum 105: 1–47.

Myers, T.J., and M. Archer. 1997. *Kuterintja ngama* (Marsupialia, Ilariidae): a revised systematic analysis based on material from the late Oligocene of Riversleigh, northwestern Queensland. Memoirs of the Queensland Museum 41 (2): 379–392.

Myers, T., K. Crosby, M. Archer, and M. Tyler. 2001. The Encore Local Fauna, a late Miocene assemblage from Riversleigh, northwestern Queensland. Memoirs of the Association of Australasian Palaeontologists 25: 147–154.

Nasrullah, Q., M.B. Renfree, and A.R. Evans. 2018. Three-dimensional mammalian tooth development using diceCT. Archives of Oral Biology 85: 183–191.

Nesslinger, C.L. 1956. Ossification centers and skeletal development in the postnatal Virginia opossum. Journal of Mammalogy 37: 382–394.

Neumann, J.S., et al. 2021. Morphological characters can strongly influence early animal relationships inferred from phylogenomic data sets. Systematic Biology 70 (2): 360–375.

Newton, A.H., et al. 2018. Letting the 'cat' out of the bag: pouch young development of the extinct Tasmanian tiger revealed by X-ray computed tomography. Royal Society Open Science 5 (2): 171914.

Ni, X., et al. 2016. A late Paleocene probable metatherian (?deltatheroidan) survivor of the Cretaceous mass extinction. Scientific Reports 6: 38547.

Nilsson, M.A., A. Gullberg, A.E. Spotorno, U. Arnason, and A. Janke. 2003. Radiation of extant marsupials after the K/T boundary: evidence from complete mitochondrial genomes. Journal of Molecular Evolution 57: S3–S12.

Nilsson, M.A., U. Arnason, P.B.S. Spencer, and A. Janke. 2004. Marsupial relationships and a timeline for marsupial radiation in South Gondwana. Gene 340: 189–196.

Nilsson, M.A., et al. 2010. Tracking marsupial evolution using archaic genomic retroposon insertions. PLoS Biology 8 (7): e1000436.

Nilsson, M.A., Y. Zheng, V. Kumar, M.J. Phillips, and A. Janke. 2018. Speciation generates mosaic genomes in kangaroos. Genome Biology and Evolution 10 (1): 33–44.

Norris, C.A. 1993. Changes in the composition of the auditory bulla in southern Solomon Islands populations of the grey cuscus, *Phalanger orientalis breviceps* (Marsupialia, Phalangeridae). Zoological Journal of the Linnean Society 107: 93–106.

Norris, C.A. 1994. The periotic bones of possums and cuscuses: cuscus polyphyly and the division of the marsupial family Phalangeridae. Zoological Journal of the Linnean Society 111: 73–98.

Norris, C.A., and G.G. Musser. 2001. Systematic revision within the *Phalanger orientalis* complex (Diprotodontia, Phalangeridae): a third species of lowland gray cuscus from New Guinea and Australia. American Museum Novitates 3356: 1–20.

Novacek, M.J. 1993. Patterns of diversity in the mammalian skull. *In* J. Hanken and B.K. Hall (editors), The skull, vol. 2: 438–545. Chicago: University of Chicago Press.

Novacek, M.J., and A. Wyss. 1986. Origin and transformation of the mammalian stapes. Contributions to Geology, University of Wyoming, Special Paper 3: 35–53.

Nylander, J.A.A., F. Ronquist, J.P. Huelsenbeck, and J.L. Nieves-Aldrey. 2004. Bayesian phylogenetic analysis of combined data. Systematic Biology 53 (1): 47–67.

O'Leary, M.A., et al. 2013. The placental mammal ancestor and the post-K-Pg radiation of placentals. Science 339: 662–667.

O'Meara, R.N., and R.S. Thompson. 2014. Were there Miocene meridiolestidans? Assessing the phylogenetic placement of *Necrolestes patagonensis* and the presence of a 40 million year meridiolestidan ghost lineage. Journal of Mammalian Evolution 21 (3): 271–284.

O'Reilly, J.E., and P.C.J. Donoghue. 2016. Tips and nodes are complementary not competing approaches to the calibration of molecular clocks. Biology Letters 12 (4): 20150975.

O'Reilly, J.E., and P.C.J. Donoghue. 2020. The effect of fossil sampling on the estimation of divergence times with the Fossilized Birth–Death process. Systematic Biology 69 (1): 124–138.

O'Reilly, J.E., M. dos Reis, and P.C. Donoghue. 2015. Dating tips for divergence-time estimation. Trends in Genetics 31 (11): 637–650.

O'Reilly, J.E., et al. 2016. Bayesian methods outperform parsimony but at the expense of precision in the estimation of phylogeny from discrete morphological data. Biology Letters 12 (4): 20160081.

O'Reilly, J.E., M.N. Puttick, D. Pisani, and P.C.J. Donoghue. 2018. Probabilistic methods surpass parsimony when assessing clade support in phylogenetic analyses of discrete morphological data. Palaeontology 61 (1): 105–118.

Ojala-Barbour, R., et al. 2013. A new species of shrew-opossum (Paucituberculata: Caenolestidae) with a phylogeny of extant caenolestids. Journal of Mammalogy 94 (5): 967–982.

Oliveira, E.V., and F.J. Goin. 2006. Marsupiais do início do Terciário do Brasil: origem, irradiação e história biogeográfica. *In* N.C. Cáceres and E.L.A. Monteiro Filho (editors), Os Marsupiais do Brasil: biologia, ecologia e evolução: 299–320. Campo Grande: UFMS.

Olson, E.C. 1944. Origin of mammals based upon cranial morphology of the therapsid suborders. Geological Society of America Special Papers 55: 1–130.

Ortiz Jaureguizar, E. 1997. Análisis cladístico, paleoecología y extinción de la subfamilia Pichipilinae (Marsupialia, Caenolestidae). Estudios Geológicos 53: 55–67.

Osgood, W.H. 1921. A monographic study of the American marsupial *Caenolestes*. Field Museum of Natural History Zoological Series 14: 1–156.

Osgood, W.H. 1924. Review of living caenolestids with description of a new genus from Chile. Field Museum of Natural History Publication 207 (Zoological Series 14): 163–172, pl. 123.

Owen, R. 1839. Outlines of a classification of the Marsupialia. Transactions of the Zoological Society of London 2 (4): 315–333.

Owen, R. 1859. On the fossil mammals of Australia.— Part I. Description of a mutilated skull of a large marsupial carnivore (*Thylacoleo carnifex*, Owen), from a calcareous conglomerate stratum, eighty miles S.W. of Melbourne, Victoria. Philosophical Transactions of the Royal Society of London 149: 309–322.

Owen, R. 1866. Anatomy of vertebrates. Vol. II. Birds and mammals, London: Longman, Green and Co.

Pallas, P.S. 1766. Miscellanea zoologica, quibus novæ imprimis atque obscuræ animalum species describuntur et observationibus iconibusque illustrantur. The Hague: Petrum van Cleef.

Palma, R.E., and A.E. Spotorno. 1999. Molecular systematics of marsupials based on the rRNA 12S

mitochondrial gene: the phylogeny of Didelphimorphia and of the living fossil microbiotheriid *Dromiciops gliroides* Thomas. Molecular Phylogenetics and Evolution 13 (3): 525–535.

Pantel, J., et al. 2000. Species-specific alternative splice mimicry at the growth hormone receptor locus revealed by the lineage of retroelements during primate evolution. Journal of Biological Chemistry 275 (25): 18664–18669.

Parins-Fukuchi, C. 2018a. Bayesian placement of fossils on phylogenies using quantitative morphometric data. Evolution 72 (9): 1801–1814.

Parins-Fukuchi, C. 2018b. Use of continuous traits can improve morphological phylogenetics. Systematic Biology 67 (2): 328–339.

Parins-Fukuchi, C., and J.W. Brown. 2017. What drives results in Bayesian morphological clock analyses? bioRxiv preprint 219048.

Parker, W.K. 1890. On the skull of *Tarsipes rostratus*. Studies from the Museum of Zoology in University College, Dundee 1: 79–84.

Parsons, F.G. 1896. On the anatomy of *Petrogale xanthopus*, compared with that of other kangaroos. Proceedings of the Zoological Society of London 1896: 683–714.

Pascual, R. 2006. Evolution and geography: the biogeographic history of South American land mammals. Annals of the Missouri Botanical Garden 93 (2): 209–230.

Pascual, R., and E. Ortiz-Jaureguizar. 2007. The Gondwanan and South American episodes: two major and unrelated moments in the history of the South American mammals. Journal of Mammalian Evolution 14 (2): 75–137.

Patterson, B. 1956. Early Cretaceous mammals and the evolution of mammalian molar teeth. Fieldiana: Geology 13: 1–105.

Patterson, B. 1965. The auditory region of the borhyaenid marsupial *Cladosictis*. Breviora 217: 1–9.

Patterson, B.D., and M.H. Gallardo. 1987. *Rhyncholestes raphanurus*. Mammalian Species 286: 1–5.

Patterson, C. 1982. Morphological characters and homology. *In* K.A. Joysey and A.E. Friday (editors), Problems of phylogenetic reconstruction: 21–74. London: Academic Press.

Pattinson, D.J., R.S. Thompson, A.K. Piotrowski, and R.J. Asher. 2015. Phylogeny, paleontology, and primates: do incomplete fossils bias the tree of life? Systematic Biology 64 (2): 169–186.

Pavan, S.E., and R.S. Voss. 2016. A revised subgeneric classification of short-tailed opossums (Didelphi-

dae: *Monodelphis*). American Museum Novitates 3868: 1–44.

Pearson, J. 1950. The relationships of the Potoroidae to the Macropodidae (Marsupialia). Paper of the Royal Society of Tasmania 1950: 211–229.

Perkins, M.E., et al. 2012. Tephrochronology of the Miocene Santa Cruz and Pinturas formations, Argentina. *In* S.F. Vizcaíno, R.F. Kay, and M.S. Bargo (editors), Early Miocene paleobiology in Patagonia: high-latitude paleocommunities of the Santa Cruz Formation: 23–40. Cambridge: Cambridge University Press.

Pfaff, C., S. Czerny, D. Nagel, and J. Kriwet. 2017. Functional morphological adaptations of the bony labyrinth in marsupials (Mammalia, Theria). Journal of Morphology 278 (6): 742–749.

Philippe, H., et al. 2011. Resolving difficult phylogenetic questions: why more sequences are not enough. PLoS Biology 9 (3): e1000602.

Phillips, M.J. 2015. Four mammal fossil calibrations: balancing competing palaeontological and molecular considerations. Palaeontologia Electronica 18.1.5FC: 1–16.

Phillips, M.J., and R.C. Pratt. 2008. Family-level relationships among the Australasian marsupial "herbivores" (Diprotodontia: koala, wombats, kangaroos and possums). Molecular Phylogenetics and Evolution 46: 594–605.

Phillips, M.J., Y.H. Lin, G.L. Harrison, and D. Penny. 2001. Mitochondrial genomes of a bandicoot and a brushtail possum confirm the monophyly of australidelphian marsupials. Proceedings of the Royal Society of London B, Biological Sciences 268 (1475): 1533–1538.

Phillips, M.J., P.A. McLenachan, C. Down, G.C. Gibb, and D. Penny. 2006. Combined mitochondrial and nuclear DNA sequences resolve the interrelations of the major Australasian marsupial radiations. Systematic Biology 55 (1): 122–137.

Phillips, M.J., D. Haouchar, R.C. Pratt, G.C. Gibb, and M. Bunce. 2013. Inferring kangaroo phylogeny from incongruent nuclear and mitochondrial genes. PLoS One 8 (2): e57745.

Pine, R.H., P.L. Dalby, and J.O. Matson. 1985. Ecology, postnatal development, morphometrics, and taxonomic status of the short-tailed opossum, *Monodelphis dimidiata,* an apparently semelparous annual marsupial. Annals of Carnegie Museum 54 (6): 195–231.

Piper, K.J., E.M.G. Fitzgerald, and T.H. Rich. 2006. Mesozoic to early Quaternary mammal faunas of Victoria, south-east Australia. Palaeontology 49 (6): 1237–1262.

Pledge, N.S. 1975. A new species of *Thylacoleo* (Marsupialia: Thylacoleonidae) with notes on the occurrences and distribution of Thylacoleonidae in South Australia. Records of the South Australian Museum 17: 261–267.

Pledge, N.S. 1987a. *Kuterintja ngama*, a new genus and species of primitive vombatoid marsupial from the medial Miocene Ngama Local Fauna of South Australia. *In* M. Archer (editor), Possums and opossums: studies in evolution: 419–422. Sydney: Surrey Beatty and Sons.

Pledge, N.S. 1987b. A new species of *Burramys* Broom (Marsupialia: Burramyidae) from the middle Miocene of South Australia. *In* M. Archer (editor), Possums and opossums: studies in evolution: 725–728. Sydney: Surrey Beatty and Sons.

Pledge, N.S. 1987c. *Muramura williamsi*, a new genus and species of ?wynyardiid (Marsupialia; Vombatoidea) from the Middle Miocene Etadunna Formation of South Australia. *In* M. Archer (editor), Possums and opossums: studies in evolution: 393–400. Sydney: Surrey Beatty and Sons.

Pledge, N.S. 1992. The weird wonderful wombat *Warendja wakefieldi* Hope and Wilkinson. Beagle, Records of the Northern Territory Museum of Arts and Sciences 9: 111–114.

Pledge, N.S. 2003. A new species of *Muramura* Pledge (Wynyardiidae: Marsupialia) from the middle Tertiary of the Callabonna Basin, northeastern South Australia. *In* L.J. Flynn (editor), Vertebrate fossils and their context: contributions in honor of Richard H. Tedford. Bulletin of the American Museum of Natural History 279: 541–555.

Pledge, N.S. 2005. The Riversleigh wynyardiids. Memoirs of the Queensland Museum 51 (1): 135–169.

Pledge, N.S. 2010. A new koala (Marsupialia: Phascolarctidae) from the late Oligocene Etadunna Formation, Lake Eyre Basin, South Australia. Australian Mammalogy 32: 79–86.

Prevosti, F.J., and M.A. Chemisquy. 2010. The impact of missing data on real morphological phylogenies: influence of the number and distribution of missing entries. Cladistics 26 (3): 326–339.

Prevosti, F.J., and A.M. Forasiepi. 2018. Evolution of South American mammalian predators during the Cenozoic: Paleobiogeographic and paleoenvironmental contingencies. Cham, Switzerland: Springer International Publishing.

Price, G.J. 2008. Taxonomy and palaeobiology of the largest-ever marsupial, *Diprotodon* Owen, 1838 (Diprotodontidae, Marsupialia). Zoological Journal of the Linnean Society 153: 369–397.

Price, G.J., and K.J. Piper. 2009. Gigantism of the Australian *Diprotodon* Owen 1838 (Marsupialia, Diprotodontoidea) through the Pleistocene. Journal of Quaternary Science 24 (8): 1029–1038.

Price, G.J., and I.H. Sobbe. 2011. Morphological variation within an individual Pleistocene *Diprotodon optatum* Owen, 1838 (Diprotodontinae; Marsupialia): implications for taxonomy within diprotodontoids. Alcheringa: an Australasian Journal of Palaeontology 35 (1): 21–29.

Prideaux, G.J. 1999. *Borungaboodie hatcheri* gen. et sp. nov., a very large bettong (Marsupialia: Macropodoidea) from the Pleistocene of southwestern Australia. Records of the Western Australian Museum Supplement 57: 317–329.

Prideaux, G.J. 2004. Systematics and evolution of the sthenurine kangaroos. University of California Publications in Geological Sciences 146: 1–622.

Prideaux, G.J., and R.H. Tedford. 2012. *Tjukuru wellsi,* gen. et sp. nov., a lagostrophine kangaroo (Diprotodontia, Macropodidae) from the Pliocene (Tirarian) of northern South Australia. Journal of Vertebrate Paleontology 32 (3): 717–721.

Prideaux, G.J., and N.M. Warburton. 2008. A new Pleistocene tree-kangaroo (Diprotodontia: Macropodidae) from the Nullarbor Plain of south-central Australia. Journal of Vertebrate Paleontology 28 (2): 463–478.

Prideaux, G.J., and N. Warburton. 2009. *Bohra nullarbora* sp. nov., a second tree-kangaroo (Marsupialia: Macropodidae) from the Pleistocene of the Nullarbor Plain, Western Australia. Records of the Western Australian Museum 25: 165–179.

Prideaux, G.J., and N.M. Warburton. 2010. An osteology-based appraisal of the phylogeny and evolution of kangaroos and wallabies (Macropodidae: Marsupialia). Zoological Journal of the Linnean Society 159: 954–987.

Prideaux, G.J., et al. 2007. An arid-adapted middle Pleistocene vertebrate fauna from south-central Australia. Nature 445: 422–425.

Prothero, D.R., and R.J. Emry. 2004. The Chadronian, Orellan, and Whitneyan North American Land Mammal Ages. *In* M.O. Woodburne (editor) Late Cretaceous and Cenozoic mammals of North America: biostratigraphy and geochronology: 157–168. New York: Columbia University Press.

Prothero, D.R., and S.E. Foss (editors). 2007. The evolution of artiodactyls. Baltimore: Johns Hopkins University Press.

Püschel, H.P., J.E. O'Reilly, D. Pisani, and P.C.J. Donoghue. 2020. The impact of fossil stratigraphic ranges on tip-calibration, and the accuracy and precision of divergence time estimates. Palaeontology 63 (1): 67–83.

Puttick, M.N. 2019. MCMCtreeR: functions to prepare MCMCtree analyses and visualize posterior ages on trees. Bioinformatics 35 (24): 5321–5322.

Puttick, M.N., et al. 2017a. Uncertain-tree: discriminating among competing approaches to the phylogenetic analysis of phenotype data. Proceedings of the Royal Society of London B, Biological Sciences 284: 20162290.

Puttick, M.N., et al. 2017b. Parsimony and maximum-likelihood phylogenetic analyses of morphology do not generally integrate uncertainty in inferring evolutionary history: a response to Brown et al. Proceedings of the Royal Society of London B, Biological Sciences 284: 20171636.

Pütz, J., B. Dupuis, M. Sissler, and C. Florentz. 2007. Mamit-tRNA, a database of mammalian mitochondrial tRNA primary and secondary structures. RNA 13 (8): 1184–1190.

Pyron, R.A. 2011. Divergence time estimation using fossils as terminal taxa and the origins of Lissamphibia. Systematic Biology 60 (4): 466–481.

Pyron, R.A. 2017. Novel approaches for phylogenetic inference from morphological data and total-evidence dating in squamate reptiles (lizards, snakes, and amphisbaenians). Systematic Biology 66 (1): 38–56.

Quintero-Galvis, J.F., et al. 2021. The biogeography of *Dromiciops* in southern South America: Middle Miocene transgressions, speciation and associations with *Nothofagus*. Molecular Phylogenetics and Evolution 163: 107234.

Quintero-Galvis, J.F., et al. 2022. Genomic diversity and demographic history of the *Dromiciops* genus (Marsupialia: Microbiotheriidae). Molecular Phylogenetics and Evolution 168: 107405.

Rabosky, D.L. 2010. Extinction rates should not be estimated from molecular phylogenies. Evolution 64 (6): 1816–1824.

Rabosky, D.L. 2016. Challenges in the estimation of extinction from molecular phylogenies: A response to Beaulieu and O'Meara. Evolution 70 (1): 218–228.

Rae, T.C., T.M. Bown, and J.G. Fleagle. 1996. New palaeothentid marsupials (Caenolestoidea) from the

early Miocene of Patagonian Argentina. American Museum Novitates 3165: 1–10.

Rambaut, A., M.A. Suchard, D. Xie, and A.J. Drummond. 2014. Tracer v1.6.

Rangel, C.C., et al. 2019. Diversity, affinities and adaptations of the basal sparassodont *Patene* (Mammalia, Metatheria). Ameghiniana 56 (4): 263–289.

Raterman, D., R.W. Meredith, L.A. Ruedas, and M.S. Springer. 2006. Phylogenetic relationships of the cuscuses and brushtail possums (Marsupialia:Phalangeridae) using the nuclear gene BRCA1. Australian Journal of Zoology 54: 353–361.

Rauscher, B. 1987. *Priscileo pitkantensis*, a new genus and species of thylacoleonid marsupial (Marsupialia: Thylacoleonidae) from the Miocene Etadunna Formation, South Australia. *In* M. Archer (editor), Possums and opossums: studies in evolution: 423–432. Sydney: Surrey Beatty.

Ré, G.H., et al. 2010. A geochronology for the Sarmiento Formation at Gran Barranca. *In* R.H. Madden, A.A. Carlini, M.G. Vucetich, and R.F. Kay (editors), The paleontology of Gran Barranca: Evolution and environmental change through the middle Cenozoic of Patagonia: 46–60. Cambridge: Cambridge University Press.

Reig, O.A. 1952. Descripcion previa de nuevos ungulados y marsupiales fosiles del Plioceno y del Eocuartario Argentinos. Revista del Museo Municipal de Ciencias Naturales y Tradicional de Mar del Plata 1: 119–129.

Reig, O.A. 1958a. Notas para una actualizacion del conocimiento de la fauna de la formacion Chapadmalal. II. Amphibia, Reptilia, Aves, Mammalia (Marsupialia: Didelphidae, Borhyaenidae). Acta Geologica Lilloana 2: 255–283.

Reig, O.A. 1958b. Comunicación preliminar sobre nuevas especies del género *Thylatheridium* Reig (Mammalia, Didelphidae). Neotropica 4: 89–95.

Reig, O.A., and G.G. Simpson. 1972. *Sparassocynus* (Marsupialia, Didelphidae), a peculiar mammal from the late Cenozoic of Argentina. Journal of Zoology 167 (Aug): 511–539.

Reig, O.A., J.A.W. Kirsch, and L.G. Marshall. 1987. Systematic relationships of the living and Neocenozoic American "opossum-like" marsupials (suborder Didelphimorphia), with comments on the classification of these and the Cretaceous and Paleogene New World and European metatherians. *In* M. Archer (editor), Possums and opossums: studies in evolution: 1–89. Sydney: Surrey Beatty and Sons.

Rich, T.H., and M. Archer. 1979. *Namilamadeta snideri*, a new diprotodontan (Marsupialia, Vombatoidea) from the medial Miocene of South Australia. Alcheringa: an Australasian Journal of Palaeontology 3: 197–208.

Rich, T.H., and P. Vickers-Rich. 1987. New specimens of *Ngapakaldia* (Marsupialia: Diprotodontoidea) and taxonomic diversity in medial Miocene palorchestids. *In* M. Archer (editor) Possums and opossums: studies in evolution: 467–476. Sydney: Surrey Beatty and Sons.

Rich, T.H., et al. 1982. Australian Tertiary mammal localities. *In* P.V. Rich and E.V. Thompson (editors), The fossil vertebrate record of Australasia: 526–572. Clayton: Monash University Offset Printing.

Richards, H.L., R.T. Wells, A.R. Evans, E.M.G. Fitzgerald, and J.W. Adams. 2019. The extraordinary osteology and functional morphology of the limbs in Palorchestidae, a family of strange extinct marsupial giants. PLoS One 14 (9): e0221824.

Ride, W.D.L. 1956. The affinities of *Burramys parvus* Broom a fossil phalangeroid marsupial. Proceedings of the Zoological Society of London 127 (3): 413–429.

Ride, W.D.L. 1957. *Protemnodon parma* (Waterhouse) and the classification of related wallabies (*Protemnodon*, *Thylogale*, and *Setonix*). Journal of Zoology 128 (3): 327–346.

Ride, W.D.L. 1959. Mastication and taxonomy in the macropodine skull. Systematics Association Publication 3: 33–59.

Ride, W.D.L. 1961. The cheek-teeth of *Hypsiprymnodon moschatus* Ramsay 1876 (Macropodidae: Marsupialia). Journal of the Royal Society of Western Australia 44: 53–60.

Ride, W.D.L. 1962. On the evolution of Australian marsupials. *In* G.W. Leeper (editor), The evolution of living organisms: 281–306. Melbourne: Melbourne University Press.

Ride, W.D.L. 1964a. A review of Australian fossil marsupials. Journal and Proceedings of the Royal Society of Western Australia 47: 97–131.

Ride, W.D.L. 1964b. *Antechinus rosamondae*, a new species of dasyurid marsupial from the Pilbara District of Western Australia; with remarks on the classification of *Antechinus*. Western Australian Naturalist 9: 58–65.

Ride, W.D.L. 1971. On the fossil evidence of the evolution of the Macropodidae. Australian Zoologist 16 (1): 6–16.

Ride, W.D.L. 1993. *Jackmahoneya* gen. nov. and the genesis of the macropodiform molar. Memoir of the

Association of Australasian Palaeontologists 15: 441–459.

Ride, W.D.L., P.A. Pridmore, R.E. Barwick, R.T. Wells, and R.D. Heady. 1997. Towards a biology of *Propleopus oscillans* (Marsupialia: Propleopinae, Hypsiprymnodontidae). Proceedings of the Linnean Society of New South Wales 117: 243–328.

Riggs, E.S., and B. Patterson. 1939. Stratigraphy of late Miocene and Pliocene deposits of the Province of Catamarca (Argentina) with notes on the faunae. Physis 14: 143–162.

Rincón, A.D., B.J. Shockey, F. Anaya, and A. Solórzano. 2015. Palaeothentid marsupials of the Salla Beds of Bolivia (late Oligocene): two new species and insights into the post-Eocene radiation of palaeothentoids. Journal of Mammalian Evolution 22 (4): 455–471.

Roberts, K.K. 2008. Oligo-Miocene pseudocheirid diversity and the early evolution of ringtail possums (Marsupialia). Ph.D. dissertation, School of Biological, Earth, and Environmental Sciences, University of New South Wales, Sydney.

Roberts, K.K., M. Archer, S.J. Hand, and H. Godthelp. 2007. New genus and species of extinct Miocene ringtail possums (Marsupialia: Pseudocheiridae). American Museum Novitates 3560: 1–15.

Roberts, K.K., M. Bassarova, and M. Archer. 2008. Oligo-Miocene ringtail possums of the genus *Paljara* (Pseudocheiridae: Marsupialia) from Queensland, Australia. Geobios 41 (6): 833–844.

Roberts, K.K., M. Archer, S.J. Hand, and H. Godthelp. 2009. New Australian Oligocene to Miocene ringtail possums (Pseudocheiridae) and revision of the genus *Marlu*. Palaeontology 52: 441–456.

Rodgers, J.C. 2011. Comparative morphology of the vestibular semicircular canals in therian mammals. Ph.D. dissertation, Faculty of the Graduate School, University of Texas at Austin, Austin.

Rodrigues, H.G., L. Hautier, and A.R. Evans. 2017. Convergent traits in mammals associated with divergent behaviors: The case of the continuous dental replacement in rock-wallabies and african mole-rats. Journal of Mammalian Evolution 24 (3): 261–274.

Rokas, A., and P.W.H. Holland. 2000. Rare genomic changes as a tool for phylogenetics. Trends in Ecology and Evolution 15: 454–459.

Ronquist, F., and J.P. Huelsenbeck. 2003. MrBayes 3: Bayesian phylogenetic inference under mixed models. Bioinformatics 19 (12): 1572–1574.

Ronquist, F., J.P. Huelsenbeck, and P. van der Mark. 2005. MrBayes 3.1 manual.

Ronquist, F., J. Huelsenbeck, and M. Teslenko. 2011. MrBayes version 3.2 manual: tutorials and model summaries.

Ronquist, F., et al. 2012a. A total-evidence approach to dating with fossils, applied to the early radiation of the Hymenoptera. Systematic Biology 61 (6): 973–999.

Ronquist, F., et al. 2012b. MrBayes 3.2: efficient Bayesian phylogenetic inference and model choice across a large model space. Systematic Biology 61 (3): 539–542.

Ronquist, F., N. Lartillot, and M.J. Phillips. 2016. Closing the gap between rocks and clocks using total-evidence dating. Philosophical Transactions of the Royal Society of London B, Biological Sciences 371 (1699): 20150136.

Rosa, B.B., G.A.R. Melo, and M.S. Barbeitos. 2019. Homoplasy-based partitioning outperforms alternatives in Bayesian analysis of discrete morphological data. Systematic Biology 68 (4): 657–671.

Röse, C. 1893. Über die Zahnentwickelung von *Phascolomys* Wombat. Deutsche Akademie der Wissenschaften zu Berlin Physikalisch-Mathematische Klasse: 749–755.

Rose, K.D., et al. 2012. Earliest Eocene mammalian fauna from the Paleocene-Eocene Thermal Maximum at Sand Creek Divide, southern Bighorn Basin, Wyoming. University of Michigan Papers on Paleontology 36: 1–121.

Rose, R.K., D.A. Pemberton, N.J. Mooney, and M.E. Jones. 2017. *Sarcophilus harrisii* (Dasyuromorphia: Dasyuridae). Mammalian Species 49 (942): 1–17.

Rosenberg, H.I., and K.C. Richardson. 1995. Cephalic morphology of the honey possum, *Tarsipes rostratus* (Marsupialia: Tarsipedidae); an obligate nectarivore. Journal of Morphology 223 (3): 303–323.

Rothecker, J., and J.E. Storer. 1996. The marsupials of the Lac Pelletier Lower Fauna, middle Eocene (Duchesnean) of Saskatchewan. Journal of Vertebrate Paleontology 16 (4): 770–774.

Rougier, G.W., and J.R. Wible. 2006. Major changes in the ear region and basicranium of early mammals. *In* M.T. Carrano, T.J. Gaudin, R.W. Blob, and J.R. Wible (editors), Amniote paleobiology: perspectives on the evolution of mammals, birds, and reptiles: 269–311. Chicago: University of Chicago Press.

Rougier, G.W., J.R. Wible, and J.A. Hopson. 1992. Reconstruction of the cranial vessels in the Early Cretaceous mammal *Vincelestes neuquenianus*: implications for the evolution of the mammalian cranial vascular system. Journal of Vertebrate Paleontology 12 (2): 188–216.

Rougier, G.W., J.R. Wible, and M.J. Novacek. 1998. Implications of *Deltatheridium* specimens for early marsupial history. Nature 396: 459–463.

Rougier, G.W., J.R. Wible, and M.J. Novacek. 2004. New specimens of *Deltatheroides cretacicus* (Metatheria, Deltatheroida) from the Late Cretaceous of Mongolia. Bulletin of Carnegie Museum of Natural History 36 (1): 245–266.

Rougier, G.W., A.M. Forasiepi, R.V. Hill, and M. Novacek. 2009a. New mammalian remains from the Late Cretaceous La Colonia Formation, Patagonia, Argentina. Acta Palaeontologica Polonica 54 (2): 195–212.

Rougier, G.W., L. Chornogubsky, S. Casadio, N.P. Arango, and A. Giallombardo. 2009b. Mammals from the Allen Formation, Late Cretaceous, Argentina. Cretaceous Research 30 (1): 223–238.

Rougier, G.W., L.C. Gaetano, B. Drury, N. Paéz Arango, and R. Colella. 2011. A review of the Mesozoic mammalian record of South America. *In* J. Calvo, J. Porfiri, B. Gonzales Riga, and D. Dos Santos (editors), Paleontología y dinosaurios desde América Latina: 195–214. Mendoza, Argentina: Editorial de la Universidad Nacional de Cuyo e EDIUNC.

Rougier, G.W., J.R. Wible, R.M.D. Beck, and S. Apesteguia. 2012. The Miocene mammal *Necrolestes* demonstrates the survival of a Mesozoic nontherian lineage into the late Cenozoic of South America. Proceedings of the National Academy of Sciences of the United States of America 109 (49): 20053–20058.

Rougier, G.W., B.M. Davis, and M.J. Novacek. 2015. A deltatheroidan mammal from the Upper Cretaceous Baynshiree Formation, eastern Mongolia. Cretaceous Research 52: 167–177.

Rovinsky, D.S., A.R. Evans, and J.W. Adams. 2019. The pre-Pleistocene fossil thylacinids (Dasyuromorphia: Thylacinidae) and the evolutionary context of the modern thylacine. PeerJ 7: e7457.

Ruedas, L.A., and J.C. Morales. 2005. Evolutionary relationships among genera of Phalangeridae (Metatheria: Diprotodontia) inferred from mitochondrial DNA. Journal of Mammalogy 86: 353–365.

Russell, E.M., and M.B. Renfree. 1989. Tarsipedidae. *In* D.W. Walton and B.J. Richardson (editors), Fauna of Australia Mammalia: 769–782. Canberra: AGPS.

Sakai, T., and H. Yamada. 1992. Molar structure in Australian marsupials. *In* P. Smith and E. Tchernov (editors), Structure, function and evolution of teeth: 103–114. Tel Aviv: Freund Publishing House.

Sánchez-Villagra, M.R. 1998. Patterns of morphological change in the ontogeny and phylogeny of the mar-supial skull. Ph.D. dissertation, Department of Biological Anthropology and Anatomy, Duke University, Durham.

Sánchez-Villagra, M.R. 2001. The phylogenetic relationships of argyrolagid marsupials. Zoological Journal of the Linnean Society 131: 481–496.

Sánchez-Villagra, M.R. 2002. The cerebellar parafloc-culus and the subarcuate fossa in *Monodelphis domestica* and other marsupial mammals – ontogeny and phylogeny of a brain-skull interaction. Acta Theriologica 47 (1): 1–14.

Sánchez-Villagra, M.R., and R.J. Asher. 2002. Craniosensory adaptations in small, faunivorous mammals, with special reference to olfaction and the trigeminal system. Mammalia 66 (1): 93–109.

Sánchez-Villagra, M.R., and A.M. Forasiepi. 2017. On the development of the chondrocranium and the histological anatomy of the head in perinatal stages of marsupial mammals. Zoological Letters 3: 1.

Sánchez-Villagra, M.R., and R.F. Kay. 1996. Do phalan-geriforms (Marsupialia: Diprotodontia) have a 'hypocone'? Australian Journal of Zoology 44 (5): 461–467.

Sánchez-Villagra, M.R., and S. Nummela. 2001. Bullate stapedes in some phalangeriform marsupials. Mammalian Biology 66: 174–177.

Sánchez-Villagra, M.R., and K.K. Smith. 1997. Diversity and evolution of the marsupial mandibular angular process. Journal of Mammalian Evolution 4 (2): 119–144.

Sánchez-Villagra, M.R., and J.R. Wible. 2002. Patterns of evolutionary transformation in the petrosal bone and some basicranial features in marsupial mammals, with special reference to didelphids. Journal of Zoological Systematics and Evolutionary Research 40: 26–45.

Sánchez-Villagra, M.R., R.F. Kay, and F. Anaya-Daza. 2000. Cranial anatomy and palaeobiology of the Miocene marsupial *Hondalagus altiplanensis* and a phylogeny of argyrolagids. Palaeontology 43 (2): 287–301.

Sánchez-Villagra, M.R., S. Gemballa, S. Nummela, K.K. Smith, and W. Maier. 2002. Ontogenetic and phylogenetic transformations of the ear ossicles in marsupial mammals. Journal of Morphology 251 (3): 219–238.

Sánchez-Villagra, M.R., et al. 2007. Exceptionally preserved North American Paleogene metatherians: adaptations and discovery of a major gap in the opossum fossil record. Biology Letters 3 (3): 318–322.

Sansom, R.S., P.G. Choate, J.N. Keating, and E. Randle. 2018. Parsimony, not Bayesian analysis, recovers more stratigraphically congruent phylogenetic trees. Biological Letters 14 (6): 20180263.

Sanson, G.D. 1980. The morphology and occlusion of the molariform cheek teeth in some Macropodinae (Marsupialia; Macropodidae). Australian Journal of Zoology 28: 341–365.

Sanson, G.D. 1989. Morphological adaptations of teeth to diets and feeding in the Macropodoidea. *In* G.C. Grigg, P.J. Jarman, and I.D. Hume (editors), Kangaroos, wallabies and rat-kangaroos: 151–168. Sydney: Surrey Beatty and Sons.

Scapino, R. 1981. Morphological investigation into functions of the jaw symphysis in carnivorans. Journal of Morphology 167: 339–375.

Scarpetta, S.G. 2020. Combined-evidence analyses of ultraconserved elements and morphological data: an empirical example in iguanian lizards. Biology Letters 16 (8): 20200356.

Schmelzle, T., S. Nummela, and M.R. Sánchez-Villagra. 2005. Phylogenetic transformations of the ear ossicles in marsupial mammals, with special reference to diprotodontians: a character analysis. Annals of Carnegie Museum 74 (3): 189–200.

Schmelzle, T., M.R. Sánchez-Villagra, and W. Maier. 2007. Vestibular labyrinth diversity in diprotodontian marsupial mammals. Mammal Study 32: 83–97.

Schneider, N.Y., and Y. Gurovich. 2017. Morphology and evolution of the oral shield in marsupial neonates including the newborn monito del monte (*Dromiciops gliroides*, Marsupialia Microbiotheria) pouch young. Journal of Anatomy 231 (1): 59–83.

Schrago, C.G., B.O. Aguiar, and B. Mello. 2018. Comparative evaluation of maximum parsimony and Bayesian phylogenetic reconstruction using empirical morphological data. Journal of Evolutionary Biology 31 (10): 1477–1484.

Schrempf, D., and G. Szöllősi. 2020. The sources of phylogenetic conflicts. *In* C. Scornavacca, F. Delsuc, and N. Galtier (editors), Phylogenetics in the genomic era: 3.1:1–3.1:23. No commercial publisher.

Schultz, P.H., M. Zarate, W. Hames, C. Camilion, and J. King. 1998. A 3.3-Ma impact in Argentina and possible consequences. Science 282: 2061–2063.

Schultz, P.H., et al. 2006. The record of Miocene impacts in the Argentine Pampas. Meteoritics and Planetary Science 41: 749–771.

Schwartz, L.R.S. 2006a. Miralinidae (Marsupialia: Phalangeroidea) from northern Australia, including the youngest occurrence of the family. Alcheringa: an Australasian Journal of Palaeontology 30 (2): 343–350.

Schwartz, L.R.S. 2006b. A new species of bandicoot from the Oligocene of northern Australia and implications of bandicoots for correlating Australian Tertiary mammal faunas. Palaeontology 49 (5): 991–998.

Schwartz, L.R.S. 2016. A revised faunal list and geological setting for Bullock Creek, a Camfieldian site from the Northern Territory of Australia. Memoirs of Museum Victoria 74: 263–290.

Scornavacca, C., F. Delsuc, and N. Galtier (editors). 2020. Phylogenetics in the genomic era. No commercial publisher.

Scott, J.E., A.S. Hogue, and M.J. Ravosa. 2012. The adaptive significance of mandibular symphyseal fusion in mammals. Journal of Evolutionary Biology 25 (4): 661–673.

Segall, W. 1969a. The auditory ossicles (malleus, incus) and their relationships to the tympanic: in marsupials. Acta Anatomica 73: 176–191.

Segall, W. 1969b. The middle ear region of *Dromiciops*. Acta Anatomica 73: 489–501.

Segall, W. 1970. Morphological parallelisms of the bulla and auditory ossicles in some insectivores and marsupials. Fieldiana Zoology 51: 169–205.

Segall, W. 1971. The auditory region (ossicles, sinuses) gliding mammals and selected representatives of non-gliding genera. Fieldiana Zoology 58 (5): 27–59.

Selva, C., and S. Ladevèze. 2016. Computed microtomography investigation of the skull of Cuvier's famous 'opossum' (Marsupialiformes, Herpetotheriidae) from the Eocene of Montmartre. Zoological Journal of the Linnean Society 180 (3): 672–693.

Sempere, T., et al. 1997. Stratigraphy and chronology of Upper Cretaceous-lower Paleogene strata in Bolivia and northwest Argentina. Geological Society of America Bulletin 109 (6): 709–727.

Sereno, P.C. 2006. Shoulder girdle and forelimb in multituberculates: evolution of parasagittal forelimb posture in mammals. *In* M.T. Carrano, T.J. Gaudin, R.W. Blob, and J.R. Wible (editors), Amniote paleobiology: perspectives on the evolution of mammals, birds, and reptiles: 315–366. Chicago: University of Chicago Press.

Sigé, B. 1971. Les Didelphoidea de Laguna Umayo (formation Vilquechico, Crétacé supérieur, Pérou), et le peuplement marsupial d'Amérique du Sud. Comptes Rendus de l'Académie des Sciences de Paris 273: 2479–2481.

Sigé, B. 1972. La faunule de mammifères du Crétacé supérieur de Laguna Umayo (Andes péruviennes). Bulletin du Muséum National d'Histoire Naturelle de Paris 99 (3): 375–405.

Sigé, B., T. Sempere, R.F. Butler, L.G. Marshall, and J.-Y. Crochet. 2004. Age and stratigraphic reassessment of the fossil-bearing Laguna Umayo red mudstone unit, SE Peru, from regional stratigraphy, fossil record, and paleomagnetism. Geobios 37 (6): 771–794.

Sigé, B., et al. 2009. *Chulpasia* and *Thylacotinga*, late Paleocene-earliest Eocene trans-Antarctic Gondwanan bunodont marsupials: New data from Australia. Geobios 42 (6): 813–823.

Simion, P., F. Delsuc, and H. Philippe. 2020. To what extent current limits of phylogenomics can be overcome? *In* C. Scornavacca, F. Delsuc, and N. Galtier (editors), Phylogenetics in the genomic era: 2.1:1–2.1:34. No commercial publisher.

Simpson, G.G. 1933. The "plagiaulacoid" type of mammalian dentition a study of convergence. Journal of Mammalogy 14 (2): 97–107.

Simpson, G.G. 1936. Studies of the earliest mammalian dentitions. Dental Cosmos 78: 791–800, 940–953.

Simpson, G.G. 1970. Addition to the knowledge of *Groeberia* (Mammalia, Marsupialia) from the mid-Cenozoic of Argentina. Breviora 362: 1–17.

Simpson, G.G. 1972. Didelphidae from the Chapadmalal Formation in the Museo Municipal de Ciencias Naturales de Mar del Plata. Revista del Museo Municipal de Ciencias Naturales de Mar del Plata 2: 1–40.

Simpson, G.G. 1974. Notes on Didelphidae (Mammalia, Marsupialia) from the Huayquerian (Pliocene) of Argentina. American Museum Novitates 2559: 1–15.

Sinclair, W.J. 1906. Mammalia of the Santa Cruz Beds (Marsupialia). Reports of the Princeton University Expeditions to Patagonia 4 (3): 333–460.

Slater, G.J., L.J. Harmon, and M.E. Alfaro. 2012. Integrating fossils with molecular phylogenies improves inference of trait evolution. Evolution 66 (12): 3931–3944.

Smith, M.R. 2019. Bayesian and parsimony approaches reconstruct informative trees from simulated morphological datasets. Biological Letters 15 (2): 20180632.

Smits, P.D., and A.R. Evans. 2012. Functional constraints on tooth morphology in carnivorous mammals. BMC Evolutionary Biology 12: 146.

Solé, F., and S. Ladevèze. 2017. Evolution of the hypercarnivorous dentition in mammals (Metatheria, Eutheria) and its bearing on the development of tribosphenic molars. Evolution and Development 19 (2): 56–68.

Sonntag, C.F. 1922. On the myology and classification of the wombat, koala, and phalangers. Proceedings of the Zoological Society of London 92 (4): 863–896.

Speijer, R.P., H. Pälike, C.J. Hollis, J.J. Hooker, and J.G. Ogg. 2020. The Paleogene Period. *In* Geologic time scale 2020: 1087–1140. Amsterdam: Elsevier.

Spencer, B. 1896. Mammalia. *In* B. Spencer (editor), Report on the work of the Horn Scientific Expedition to Central Australia Part 2–Zoology: 1–52. Melbourne: Melville, Mullen and Slade.

Spencer, W.B. 1901. A description of *Wynyardia bassiana*, a fossil marsupial from the Tertiary beds of Table Cape, Tasmania. Proceedings of the Zoological Society of London 1900: 776–794.

Spoor, F., and M. Leakey. 1996. Absence of the subarcuate fossa in cercopithecids. Journal of Human Evolution 31: 569–575.

Sprain, C.J., P.R. Renne, G.P. Wilson, and W.A. Clemens. 2015. Paleogene transition and recovery interval in the Hell Creek region, Montana. Geological Society of America Bulletin 127: 393–409.

Springer, M.S. 1987. Lower molars of *Litokoala* (Marsupialia: Phascolarctidae) and their bearing on phascolarctid evolution. *In* M. Archer (editor), Possums and opossums: studies in evolution: 319–325. Sydney: Surrey Beatty and Sons.

Springer, M.S. 1993. Phylogeny and rates of character evolution among ringtail possums (Pseudocheiridae, Marsupialia). Australian Journal of Zoology 41 (3): 273–291.

Springer, M.S., and E. Douzery. 1996. Secondary structure and patterns of evolution among mammalian mitochondrial 12S rRNA molecules. Journal of Molecular Evolution 43 (4): 357–373.

Springer, M.S., and M.O. Woodburne. 1989. The distribution of some basicranial characters within the Marsupialia and a phylogeny of the Phalangeriformes. Journal of Vertebrate Paleontology 9 (2): 210–221.

Springer, M.S., J.A.W. Kirsch, and J.A. Case. 1997. The chronicle of marsupial evolution. *In* T. Givnish and K. Sytsma (editors), Molecular evolution and adaptive radiation: 129–161. New York: Cambridge University Press.

Springer, M.S., et al. 1998. The origin of the Australasian marsupial fauna and the phylogenetic affinities of the enigmatic monito del monte and marsupial

mole. Proceedings of the Royal Society of London B, Biological Sciences 265 (1413): 2381–2386.

Steiner, C., M.-k. Tilak, E.J.P. Douzery, and F.M. Catzeflis. 2005. New DNA data from a transthyretin nuclear intron suggest an Oligocene to Miocene diversification of living South America opossums (Marsupialia: Didelphidae). Molecular Phylogenetics and Evolution 35: 363–379.

Stirton, R.A. 1955. Late Tertiary marsupials from South Australia. Records of the South Australian Museum 11: 247–268.

Stirton, R.A. 1957. Tertiary marsupials from Victoria, Australia. Memoirs of the National Museum of Victoria 21: 121–134.

Stirton, R.A. 1967. The Diprotodontidae from the Ngapakaldia Fauna, South Australia. Bureau of Mineral Resources, Geology and Geophysics, Australia, Bulletin 85: 1–44.

Stirton, R.A., M.O. Woodburne, and M.D. Plane. 1967a. A phylogeny of the Tertiary Diprotodontidae and its significance in correlation. Bureau of Mineral Resources, Geology and Geophysics, Australia, Bulletin 85: 149–160.

Stirton, R.A., R.H. Tedford, and M.O. Woodburne. 1967b. A new Tertiary formation and fauna from the Tirari Desert, South Australia. Records of the South Australian Museum 15: 427–461.

Storch, G. 2001. Paleobiological implications of the Messel mammalian assemblage. In G.F. Gunnell (editor), Eocene biodiversity: unusual occurrences and rarely sampled habitats – topics in geobiology, 18: 215–235. New York: Kluwer Academic/Plenum Publishers.

Suarez, C., A.M. Forasiepi, F.J. Goin, and C. Jaramillo. 2015. Insights into the Neotropics prior to the Great American Biotic Interchange: new evidence of mammalian predators from the Miocene of Northern Colombia. Journal of Vertebrate Paleontology 36 (1): e1029581.

Suárez Gómez, S.C. 2019. Estudios taxonómicos y paleobiológicos sobre los Metatheria (Mammalia) del Mioceno medio de La Venta, Colombia. Ph.D. dissertation, Facultad de Ciencias Naturales y Museo, Universidad Nacional de La Plata, La Plata.

Suárez-Villota, E.Y., et al. 2018. Monotypic status of the South American relictual marsupial Dromiciops gliroides (Microbiotheria). Journal of Mammalogy 99 (4): 803–812.

Sullivan, C., et al. 2014. The vertebrates of the Jurassic Daohugou Biota of northeastern China. Journal of Vertebrate Paleontology 34 (2): 243–280.

Sullivan, J., and P. Joyce. 2005. Model selection in phylogenetics. Annual Review of Ecology, Evolution, and Systematics 36: 445–466.

Suzuki, Y., G.V. Glazko, and M. Nei. 2002. Overcredibility of molecular phylogenies obtained by Bayesian phylogenetics. Proceedings of the National Academy of Sciences of the United States of America 99: 16138–16143.

Swofford, D.L. 2003. PAUP*: phylogenetic analysis using parsimony (*and other methods).

Szalay, F.S. 1982a. A new appraisal of marsupial phylogeny and classification. In M. Archer (editor), Carnivorous marsupials: 621–640. Mosman, New South Wales: Royal Zoological Society of New South Wales.

Szalay, F.S. 1982b. Phylogenetic relationships of the marsupials. Geobios 15 (Supplement 1): 177–190.

Szalay, F.S. 1993. Metatherian taxon phylogeny: Evidence and interpretation from the cranioskeletal system. In F.S. Szalay, M.J. Novacek, and M.C. McKenna (editors), Mammal phylogeny, vol. 1. Mesozoic differentiation, multituberculates, early therians, and marsupials: 216–242. New York: Springer-Verlag.

Szalay, F.S. 1994. Evolutionary history of the marsupials and an analysis of osteological characters, Cambridge: Cambridge University Press.

Szalay, F.S., and E.J. Sargis. 2001. Model-based analysis of postcranial osteology of marsupials from the Palaeocene of Itaboraí (Brazil) and the phylogenetics and biogeography of Metatheria. Geodiversitas 23 (2): 139–302.

Szalay, F.S., and E.J. Sargis. 2006. Cretaceous therian tarsals and the metatherian-eutherian dichotomy. Journal of Mammalian Evolution 13: 171–210.

Takahashi, F. 1974. Variaçao morfológica de incisivos em didelfídeos (Marsupialia, Didelphinae). Anais Academia Brasileira de Ciencias 46: 413–416.

Tamura, K., G. Stecher, D. Peterson, A. Filipski, and S. Kumar. 2013. MEGA6: Molecular Evolutionary Genetics Analysis version 6.0. Molecular Biology and Evolution 30 (12): 2725–2729.

Tarver, J.E., et al. 2016. The interrelationships of placental mammals and the limits of phylogenetic inference. Genome Biology and Evolution 8 (2): 330–344.

Tate, G.H.H. 1933. A systematic revision of the marsupial genus Marmosa with a discussion of the adaptive radiation of the murine opossums (Marmosa). Bulletin of the American Museum of Natural History 66 (1): 1–250.

Tate, G.H.H. 1947. Results of the Archbold Expeditions. No. 56. On the anatomy and classification of

the Dasyuridae (Marsupialia). Bulletin of the American Museum of Natural History 88 (3): 97–156.

Tate, G.H.H. 1948. Results of the Archbold Expeditions. No. 59. Studies on the anatomy and phylogeny of the Macropodidae (Marsupialia). Bulletin of the American Museum of Natural History 91 (2): 233–351.

Tate, G.H.H. 1951. The banded anteater, *Myrmecobius* Waterhouse (Marsupialia). American Museum Novitates 1521: 1–8.

Tedford, R.H. 1966. A review of the macropodid genus *Sthenurus*. University of California Publications in Geological Sciences 57: 1–72.

Tedford, R.H., and N.R. Kemp. 1998. Oligocene marsupials of the Geilston Bay local fauna, Tasmania. American Museum Novitates 3244: 1–22.

Tedford, R.H., and M.O. Woodburne. 1987. The Ilariidae, a new family of vombatiform marsupials from Miocene strata of South Australia and an evaluation of the homology of molar cusps in the Diprotodonta. *In* M. Archer (editor), Possums and opossums: studies in evolution: 401–418. Sydney: Surrey Beatty.

Tedford, R.H., and M.O. Woodburne. 1998. The diprotodontian 'hypocone' revisited. Australian Journal of Zoology 46 (3): 249–250.

Tedford, R.H., M.R. Banks, N.R. Kemp, I. McDougall, and F.L. Sutherland. 1975. Recognition of the oldest known fossil marsupials from Australia. Nature 225: 141–142.

Tedford, R.H., et al. 1977. The discovery of Miocene vertebrates, Lake Frome area, South Australia. Bureau of Mineral Resources Journal of Australian Geology and Geophysics 2: 53–57.

Tedford, R.H., R.T. Wells, and S.F. Barghoorn. 1992. Tirari Formation and contained faunas, Pliocene of the Lake Eyre Basin, South Australia. Beagle, Records of the Northern Territory Museum of Arts and Sciences 9 (1): 173–194.

Tejedor, M.F., et al. 2009. New early Eocene mammalian fauna from western Patagonia, Argentina. American Museum Novitates 3638: 1–43.

Temple-Smith, P.D. 1994. Comparative structure and function of marsupial spermatozoa. Reproduction Fertility and Development 6 (4): 421–435.

Thomas, O. 1887a. On the homologies and succession of the teeth in the Dasyuridae, with an attempt to trace the history of the evolution of mammalian teeth in general. Philosophical Transactions of the Royal Society of London B 178: 443–462.

Thomas, O. 1887b. On the milk-dentition of the koala. Proceedings of the Zoological Society of London 1887: 338–339.

Thomas, O. 1888. Catalogue of the Marsupialia and Monotremata in the collection of the British Museum (Natural History), London: Trustees of the British Museum (Natural History).

Thomas, O. 1895. On *Caenolestes*, a still existing survivor of the Epanorthidae of Ameghino, and the representative of a new family of Recent marsupials. Proceedings of the Zoological Society of London 1895: 870–878.

Thomas, O. 1904. On a collection of mammals made by Mr. J.T. Tunney in Arnhem Land, Northern Territory of South Australia. Novitates Zoologicae 11: 222–229.

Thomas, O. 1910. A new genus for *Dactylopsila palpator*. Annals and Magazine of Natural History 6 (36): 610.

Thomas, O. 1920. *Notoryctes* in north-west Australia. Annals and Magazine of Natural History 6: 111–113.

Tomassini, R.L., C.I. Montalvo, C.M. Deschamps, and T. Manera. 2013. Biostratigraphy and biochronology of the Monte Hermoso Formation (early Pliocene) at its type locality, Buenos Aires Province, Argentina. Journal of South American Earth Sciences 48: 31–42.

Tomes, R.F. 1863. Notice of a new American form of marsupial. Proceedings of the Zoological Society of London 1863: 50–51.

Tomo, S., I. Tomo, G.C. Townsend, and K. Hirata. 2007. Masticatory muscles of the great-gray kangaroo (*Macropus giganteus*). Anatomical Record 290 (4): 382–388.

Travouillon, K.J. 2016. Oldest fossil remains of the enigmatic pig-footed bandicoot show rapid herbivorous evolution. Royal Society Open Science 3 (8): 160089.

Travouillon, K.J., and M.J. Phillips. 2018. Total evidence analysis of the phylogenetic relationships of bandicoots and bilbies (Marsupialia: Peramelemorphia): reassessment of two species and description of a new species. Zootaxa 4378 (2): 224–256.

Travouillon, K.J., M. Archer, S.J. Hand, and H. Godthelp. 2006. Multivariate analyses of Cenozoic mammalian faunas from Riversleigh, northwestern Queensland. Alcheringa: an Australasian Journal of Palaeontology Special Issue 1: Proceedings of CAVEPS 2005: 323–349.

Travouillon, K.J., S. Legendre, M. Archer, and S.J. Hand. 2009. Palaeoecological analyses of Riversleigh's Oligo-Miocene sites: implications for Oligo-Miocene climate change in Australia. Palaeogeography, Palaeoclimatology, Palaeoecology 276 (1-4): 24–37.

Travouillon, K.J., Y. Gurovich, R.M.D. Beck, and J. Muirhead. 2010. An exceptionally well-preserved short-snouted bandicoot (Marsupialia; Peramelemorphia) from Riversleigh's Oligo-Miocene deposits, northwestern Queensland, Australia. Journal of Vertebrate Paleontology 30 (5): 1528–1546.

Travouillon, K.J., R.M.D. Beck, S.J. Hand, and M. Archer. 2013a. The oldest fossil record of bandicoots (Marsupialia; Peramelemorphia) from the late Oligocene of Australia. Palaeontologia Electronica 16 (2): 13A.

Travouillon, K.J., Y. Gurovich, M. Archer, S.J. Hand, and J. Muirhead. 2013b. The genus *Galadi*: three new bandicoots (Marsupialia, Peramelemorphia) from Riversleigh's Miocene deposits, Northwestern Queensland, Australia. Journal of Vertebrate Paleontology 33 (1): 153–168.

Travouillon, K.J., S.J. Hand, M. Archer, and K.H. Black. 2014a. Earliest modern bandicoot and bilby (Marsupialia, Peramelidae and Thylacomyidae) from the Miocene of the Riversleigh World Heritage Area, northwestern Queensland, Australia. Journal of Vertebrate Paleontology 34 (2): 375–382.

Travouillon, K.J., B.N. Cooke, M. Archer, and S.J. Hand. 2014b. Revision of basal macropodids from the Riversleigh World Heritage Area with descriptions of new material of *Ganguroo bilamina* Cooke, 1997 and a new species. Palaeontologia Electronica 17 (1): 20A.

Travouillon, K.J., M. Archer, and S.J. Hand. 2015a. Revision of *Wabularoo*, an early macropodid kangaroo from mid-Cenozoic deposits of the Riversleigh World Heritage Area, Queensland, Australia. Alcheringa: an Australasian Journal of Palaeontology 39 (2): 274–286.

Travouillon, K.J., M. Archer, S.J. Hand, and J. Muirhead. 2015b. Sexually dimorphic bandicoots (Marsupialia: Peramelemorphia) from the Oligo-Miocene of Australia, first cranial ontogeny for fossil bandicoots and new species descriptions. Journal of Mammalian Evolution 22: 141–167.

Travouillon, K.J., K. Butler, M. Archer, and S.J. Hand. 2016. New material of *Gumardee pascuali* Flannery et al., 1983 (Marsupialia: Macropodiformes) and two new species from the Riversleigh World Heritage Area, Queensland, Australia. Memoirs of Museum Victoria 74: 189–207.

Travouillon, K.J., et al. 2017. A review of the Pliocene bandicoots of Australia, and descriptions of new genus and species. Journal of Vertebrate Paleontology: e1360894.

Travouillon, K.J., et al. 2019. Hidden in plain sight: reassessment of the pig-footed bandicoot, *Chaeropus ecaudatus* (Peramelemorphia, Chaeropodidae), with a description of a new species from central Australia, and use of the fossil record to trace its past distribution. Zootaxa 4566: 1.

Travouillon, K.J., R.M.D. Beck, and J.A. Case. 2021. Upper Oligocene–lower-Middle Miocene peramelemorphians from the Etadunna, Namba and Wipajiri formations of South Australia. Alcheringa: an Australasian Journal of Palaeontology 45 (1): 109–125.

Travouillon, K.J., K. Butler, M. Archer, and S.J. Hand. 2022. Two new species of the genus *Gumardee* (Marsupialia, Macropodiformes) reveal the repeated evolution of bilophodonty in kangaroos. Alcheringa: an Australasian Journal of Palaeontology 46 (1): 105–128.

Tribe, C.J. 1990. Dental age classes in *Marmosa incana* and other didelphoids. Journal of Mammalogy 71: 566–569.

Triggs, B. 2009. Wombats. Collingwood, Australia: CSIRO Publishing.

Trouessart, E.-L. 1898. Catalogus mammalium tam viventium quam fossilium. Fasciculus V. Sirenia, Cetacea, Edentata, Marsupialia, Allotheria, Monotremata, Berolini: R. Friedländer and Sohn.

Trusler, P. 2016. Cranial reconstruction of *Palorchestes azael*. Ph.D. dissertation, Faculty of Science, Monash University, Clayton.

Trusler, P.W., and A.C. Sharp. 2016. Description of new cranial material of *Propalorchestes* (Marsupialia: Palorchestidae) from the middle Miocene Camfield Beds, Northern Territory, Australia. Memoirs of Museum Victoria 74: 291–324.

Turnbull, W.D. 1970. Mammalian masticatory apparatus. Fieldiana: Geology 18: 149–356.

Turnbull, W.D., and E.L.J. Lundelius. 1970. The Hamilton fauna. A late Pliocene mammalian fauna from the Grange Burn, Victoria, Australia. Fieldiana: Geology 19: 1–163.

Turnbull, W.D., and F.R. Schram. 1973. Broom Cave *Cercartetus*: with observations on pygmy possum dental morphology, variation, and taxonomy. Records of the Australian Museum 28 (19): 437–464.

Turnbull, W.D., T.H.V. Rich, and E.L.J. Lundelius. 1987. Pseudocheirids (Marsupialia: Pseudocheiridae) of the early Pliocene Hamilton Local Fauna, southwestern Victoria. *In* M. Archer (editor), Possums and opossums: studies in evolution: 693–713. Sydney: Surrey Beatty and Sons.

Turnbull, W.D., E.L. Lundelius Jr., and M. Archer. 2003. Dasyurids, perameloids, phalangeroids, and vombatoids from the Early Pliocene Hamilton Fauna, Victoria, Australia. *In* L.J. Flynn (editor), Vertebrate fossils and their context: contributions in honor of Richard H. Tedford. Bulletin of the American Museum of Natural History 279: 513–540.

Turner, A.H., A.C. Pritchard, and N.J. Matzke. 2017. Empirical and Bayesian approaches to fossil-only divergence times: a study across three reptile clades. PLoS One 12 (2): e0169885.

Tyndale-Biscoe, C.H., and R.B. MacKenzie. 1976. Reproduction in *Didelphis marsupialis* and *D. albiventris* in Colombia. Journal of Mammalogy 57 (2): 249–265.

Urbanek, M., J.N. MacLeod, N.E. Cooke, and S.A. Liebhaber. 1992. Expression of a human growth hormone (hGH) receptor isoform is predicted by tissue-specific alternative splicing of exon 3 of the hGH receptor gene transcript. Molecular Endocrinology 6 (2): 279–287.

Valladares-Gómez, A., J.L. Celis-Diez, R.E. Palma, and G.S. Manríquez. 2017. Cranial morphological variation of *Dromiciops gliroides* (Microbiotheria) along its geographical distribution in south-central Chile: A three-dimensional analysis. Mammalian Biology 87: 107–117.

van der Klaauw, C.J. 1931. The auditory bulla in some fossil mammals with a general introduction to this region of the skull. Bulletin of the American Museum of Natural History 62: 1–352.

Van Dyck, S. 2002. Morphology-based revision of *Murexia* and *Antechinus* (Marsupialia: Dasyuridae). Memoirs of the Queensland Museum 48: 239–330.

Van Dyck, S., and R. Strahan (editors). 2008. The mammals of Australia, 3rd ed. Sydney: New Holland Publishers.

van Nievelt, A.F.H. 2002. Dental development in *Monodelphis domestica* (Marsupialia:Didelphidae) and the evolution of tooth replacement in mammals. Ph.D. dissertation, Department of Biological Anthropology and Anatomy, Duke University, Durham.

van Nievelt, A.F.H., and K.K. Smith. 2005a. Tooth eruption in *Monodelphis domestica* and its significance for phylogeny and natural history. Journal of Mammalogy 86 (2): 333–341.

van Nievelt, A.F.H., and K.K. Smith. 2005b. To replace or not to replace: the significance of reduced tooth replacement in marsupial and placental mammals. Paleobiology 31 (2): 324–346.

Van Valen, L. 1966. Deltatheridia, a new order of mammals. Bulletin of the American Museum of Natural History 132 (1): 1–126.

Velazco, P.M., et al. 2022. Combined data analysis of fossil and living mammals: a Paleogene sister taxon of Placentalia and the antiquity of Marsupialia. Cladistics [Early view: https://doi.org/10.1111/cla.12499]

Vilela, J.F., J.A. De Oliveira, and C.A.D. Russo. 2015. The diversification of the genus *Monodelphis* and the chronology of Didelphidae (Didelphimorphia). Zoological Journal of the Linnean Society 174 (2): 414–427.

Voss, R.S. 2022. An annotated checklist of Recent opossums (Mammalia: Didelphidae). Bulletin of the American Museum of Natural History 455: 1–74.

Voss, R.S., and S.A. Jansa. 2003. Phylogenetic studies on didelphid marsupials II. Nonmolecular data and new IRBP sequences: separate and combined analyses of didelphine relationships with denser taxon sampling. Bulletin of the American Museum of Natural History 276: 1–82.

Voss, R.S., and S.A. Jansa. 2009. Phylogenetic relationships and classification of didelphid marsupials, an extant radiation of New World metatherian mammals. Bulletin of the American Museum of Natural History 322: 1–177.

Voss, R.S., and S.A. Jansa. 2021. Opossums: an adaptive radiation of New World marsupials, Baltimore: Johns Hopkins University Press.

Voss, R.S., D.P. Lunde, and N.B. Simmons. 2001. The mammals of Paracou, French Guiana: a Neotropical rainforest fauna. Part 2. Nonvolant species. Bulletin of the American Museum of Natural History 263: 1–236.

Voss, R.S., J.F. Díaz-Nieto, and S.A. Jansa. 2018. A revision of *Philander* (Marsupialia: Didelphidae), Part 1: *P. quica*, *P. canus*, and a new species from Amazonia. American Museum Novitates 3891: 1–70.

Voss, R.S., T.C. Giarla, J.F. Díaz-Nieto, and S.A. Jansa. 2020. A revision of the didelphid marsupial genus *Marmosa* Part 2. Species of the Rapposa Group (subgenus *Micoureus*). Bulletin of the American Museum of Natural History 439 (1): 1–60.

Vullo, R., E. Gheerbrant, C. de Muizon, and D. Neraudeau. 2009. The oldest modern therian mammal from Europe and its bearing on stem marsupial paleobiogeography. Proceedings of the National Academy of Sciences of the United States of America 106 (47): 19910–19915.

Warburton, N.M. 2003. Functional morphology and evolution of marsupial moles (Marsupialia; Noto-

ryctemorphia). Ph.D. dissertation, School of Animal Biology, University of Western Australia, Perth.

Warburton, N.M. 2009. Comparative jaw muscle anatomy in kangaroos, wallabies, and rat-kangaroos (Marsupialia: Macropodoidea). Anatomical Record 292 (6): 875–884.

Warburton, N.M., and K.J. Travouillon. 2016. The biology and palaeontology of the Peramelemorphia: a review of current knowledge and future research directions. Australian Journal of Zoology 64 (3): 151–181.

Warburton, N.M., K.J. Travouillon, and A.B. Camens. 2019. Skeletal atlas of the thylacine (*Thylacinus cynocephalus*). Palaeontologia Electronica 22.2.29A: 1–56.

Ward, S.J., and D.P. Woodside. 2008. Feathertail glider. *In* S. Van Dyck and R. Strahan (editors), The mammals of Australia Third edition: 261–264. Sydney: New Holland Publishers.

Warnock, R.C., Z. Yang, and P.C. Donoghue. 2012. Exploring uncertainty in the calibration of the molecular clock. Biology Letters 8 (1): 156–159.

Warnock, R.C., J.F. Parham, W.G. Joyce, T.R. Lyson, and P.C. Donoghue. 2015. Calibration uncertainty in molecular dating analyses: there is no substitute for the prior evaluation of time priors. Proceedings of the Royal Society of London B, Biological Sciences 282 (1798): 20141013.

Watanabe, A. 2015. The impact of poor sampling of polymorphism on cladistic analysis. Cladistics 32 (3): 317–334.

Waterhouse, G.R. 1841a. The natural history of Marsupialia or pouched animals. Edinburgh: W.H. Lizars.

Waterhouse, G.R. 1841b. Description of a new genus of mammiferous animals from Australia, belonging probably to the order Marsupialia. Transactions of the Zoological Society of London 2: 149–154, plates 127–128.

Webster, D.B., and M. Webster. 1975. Auditory systems of Heteromyidae: functional morphology and evolution of the middle ear. Journal of Morphology 146: 343–376.

Weisbecker, V., and R.M.D. Beck. 2015. Marsupial and monotreme evolution and biogeography. *In* A. Klieve, L. Hogan, S. Johnston, and P. Murray (editors), Marsupials and monotremes: Nature's enigmatic mammals: 1–31. Hauppauge, New York: Nova Science.

Wells, R.T., and R.H. Tedford. 1995. *Sthenurus* (Macropodidae: Marsupialia) from the Pleistocene of Lake Callabonna, South Australia. Bulletin of the American Museum of Natural History 225: 1–111.

Westerman, M., et al. 2012. Phylogenetic relationships of living and recently extinct bandicoots based on nuclear and mitochondrial DNA sequences. Molecular Phylogenetics and Evolution 62 (1): 97–108.

Westerman, M., et al. 2016. Phylogenetic relationships of dasyuromorphian marsupials revisited. Zoological Journal of the Linnean Society 176 (3): 686–701.

Whitelaw, M.J. 1991a. Magnetic polarity stratigraphy of Pliocene and Pleistocene fossil vertebrate localities in southeastern Australia. Geological Society of America Bulletin 103 (11): 1493–1503.

Whitelaw, M.J. 1991b. Magnetic polarity stratigraphy of the Fisherman's Cliff and Bone Gulch vertebrate fossil faunas from the Murray Basin, New South Wales, Australia Earth and Planetary Science Letters 104 (2-4): 417–423.

Wible, J.R. 1990. Late Cretaceous marsupial petrosal bones from North America and a cladistic analysis of the petrosal in therian mammals. Journal of Vertebrate Paleontology 10: 183–205.

Wible, J.R. 2003. On the cranial osteology of the short-tailed opossum *Monodelphis brevicaudata* (Marsupialia, Didelphidae). Annals of Carnegie Museum 72 (3): 137–202.

Wible, J.R. 2008. On the cranial osteology of the Hispaniolan solenodon, *Solenodon paradoxus* Brandt, 1833 (Mammalia, Lipotyphla, Solenodontidae). Annals of Carnegie Museum 77 (3): 321–402.

Wible, J.R. 2009. The ear region of the pen-tailed treeshrew, *Ptilocercus lowii* Gray, 1848 (Placentalia, Scandentia, Ptilocercidae). Journal of Mammalian Evolution 16 (3): 199–233.

Wible, J.R. 2010. Petrosal anatomy of the nine-banded armadillo, *Dasypus novemcinctus* Linnaeus, 1758 (Mammalia, Xenarthra, Dasypodidae). Annals of Carnegie Museum 79 (1): 1–28.

Wible, J.R. 2011. On the treeshrew skull (Mammalia, Placentalia, Scandentia). Annals of Carnegie Museum 79 (3): 149–238.

Wible, J.R., and T.J. Gaudin. 2004. On the cranial osteology of the yellow armadillo *Euphractus sexcinctus* (Dasypodidae, Xenarthra, Placentalia). Annals of Carnegie Museum 73 (3): 117–196.

Wible, J.R., and J.A. Hopson. 1993. Basicranial evidence for early mammal phylogeny. *In* F.S. Szalay, M.J. Novacek, and M.C. McKenna (editors), Mammal phylogeny, vol 1. Mesozoic differentiation, multituberculates, early therians, and marsupials: 45–62. New York: Springer-Verlag.

Wible, J.R., and J.A. Hopson. 1995. Homologies of the prootic canal in mammals and non-mammalian

cynodonts. Journal of Vertebrate Paleontology 15 (2): 331–356.

Wible, J.R., and M. Spaulding. 2013. On the cranial osteology of the African palm civet, *Nandinia binotata* (Gray, 1830) (Mammalia, Carnivora, Feliformia). Annals of Carnegie Museum 82 (1): 1–114.

Wible, J.R., G.W. Rougier, M.J. Novacek, and M.C. McKenna. 2001. Earliest eutherian ear region: a petrosal referred to *Prokennalestes* from the Early Cretaceous of Mongolia. American Museum Novitates 3322: 1–44.

Wible, J.R., M.J. Novacek, and G.W. Rougier. 2004. New data on the skull and dentition in the Mongolian Late Cretaceous eutherian mammal *Zalambdalestes*. Bulletin of the American Museum of Natural History 281: 1–144.

Wible, J.R., G.W. Rougier, and M.J. Novacek. 2005. Anatomical evidence for superordinal/ordinal eutherian taxa in the Cretaceous. *In* K.D. Rose and J.D. Archibald (editors), The rise of placental mammals: Origins and relationships of the major extant clades: 15–36. Baltimore: Johns Hopkins University Press.

Wible, J.R., G.W. Rougier, M.J. Novacek, and R.J. Asher. 2009. The eutherian mammal *Maelestes gobiensis* from the Late Cretaceous of Mongolia and the phylogeny of Cretaceous Eutheria. Bulletin of the American Museum of Natural History 327: 1–123.

Wible, J.R., S.L. Shelley, and G.W. Rougier. 2018. The mammalian parasphenoid: Its occurrence in marsupials. Annals of Carnegie Museum 85 (2): 113–164.

Wible, J.R., S.L. Shelley, and C. Belz. 2021. The element of Paaw in marsupials and the ear region of *Philander opossum* (Linnaeus, 1758) (Didelphimorphia, Didelphidae). Annals of Carnegie Museum 87 (1): 1–35.

Wiens, J.J. 2000. Coding morphological variation within species and higher taxa for phylogenetic analysis. *In* J.J. Wiens (editor), Phylogenetic analysis of morphological data: 115–145. Washington, D.C.: Smithsonian Institution Press.

Wiens, J.J. 2001. Character analysis in morphological phylogenetics: problems and solutions. Systematic Biology 50 (5): 689–699.

Wilcox, T. 2002. Phylogenetic relationships of the dwarf boas and a comparison of Bayesian and bootstrap measures of phylogenetic support. Molecular Phylogenetics and Evolution 25 (2): 361–371.

Wilkins, K.T., J.C. Roberts, C.S. Roorda, and J.E. Hawkins. 1999. Morphometrics and functional morphology of middle ears of extant pocket gophers (Rodentia, Geomyidae). Journal of Mammalogy 80: 180–198.

Wilkinson, M. 2003. Missing entries and multiple trees: instability, relationships, and support in parsimony analysis. Journal of Vertebrate Paleontology 23 (4): 986–986.

Williamson, T.E., and T.J. Carr. 2007. *Bomburia* and *Ellipsodon* (Mammalia: Mioclaenidae) from the early Paleocene of New Mexico. Journal of Paleontology 81 (5): 966–985.

Williamson, T.E., and L.H. Taylor. 2011. New species of *Peradectes* and *Swaindelphys* (Mammalia: Metatheria) from the early Paleocene (Torrejonian) Nacimiento Formation, San Juan Basin, New Mexico, USA. Palaeontologia Electronica 14 (3): 23A.

Williamson, T.E., S.L. Brusatte, T.D. Carr, A. Weil, and B.R. Standhardt. 2012. The phylogeny and evolution of Cretaceous-Palaeogene metatherians: cladistic analysis and description of new early Palaeocene specimens from the Nacimiento Formation, New Mexico. Journal of Systematic Palaeontology 10 (4): 625–651.

Williamson, T.E., S.L. Brusatte, and G.P. Wilson. 2014. The origin and early evolution of metatherian mammals: the Cretaceous record. Zookeys 465: 1–76.

Wilson, D.E., and D.M. Reeder. 2005. Mammal species of the world: a taxonomic and geographic reference, 3rd ed. Baltimore: John Hopkins University Press.

Wilson, G.P., E.G. Ekdale, J.W. Hoganson, J.J. Calede, and A. Vander Linden. 2016. A large carnivorous mammal from the Late Cretaceous and the North American origin of marsupials. Nature Communications 7: 13734.

Wilson, J.T., and J.P. Hill. 1897. Observations upon the development and succession of the teeth in *Perameles*; together with a contribution to the discussion of the homologies of the teeth in marsupial animals. Quarterly Journal of Microscopical Science 39: 427–588.

Winge, H. 1882. Om Pattedyrenes Tandskifte, isaer med Hensyn til Taendernes Former. Videnskabelige Meddelelser Dansk Naturhistorisk Forening Copenhagen 4: 15–67.

Winge, H. 1893. Jordfunde og nulevende Pungdyr (Marsupialia) fra Lagoa Santa, Monas Geraes, Brasilien. E Museo Lundii – En Samling af Afhandlinger 2 (2): 1–133.

Winge, H. 1941. The interrelationships of the mammalian genera. vol. 1. Monotremata, Marsupialia, Insectivora, Chiroptera, Edentata. (translated from the 1923 Danish original by E. Deichmann and G.M. Allen), Copenhagen: C.A. Reitzels Forlag.

Wood, C.B., and G.W. Rougier. 2005. Updating and recoding enamel microstructure in Mesozoic mammals: In search of discrete characters for phylogenetic reconstruction. Journal of Mammalian Evolution 12 (3-4): 433–459.

Woodburne, M.O. 1967. The Alcoota Fauna, central Australia. Bulletin of the Bureau of Mineral Resources Geology and Geophysics, Australia 87: 1–187.

Woodburne, M.O. 1984a. *Wakiewakie lawsoni*, a new genus and species of Potoroinae (Marsupialia: Macropodidae) of medial Miocene age, South Australia. Journal of Paleontology 58 (4): 1062–1073.

Woodburne, M.O. 1984b. Families of marsupials: Relationships, evolution and biogeography. *In* T.W. Broadhead (editor), Mammals: notes for a short course: 48–71. Knoxville: University of Tennessee.

Woodburne, M.O. 2010. The Great American Biotic Interchange: dispersals, tectonics, climate, sea level and holding pens. Journal of Mammalian Evolution 17: 245–264.

Woodburne, M.O., and J.A. Case. 1996. Dispersal, vicariance, and the Late Cretaceous to early Tertiary land mammal biogeography from South America to Australia. Journal of Mammalian Evolution 3: 121–161.

Woodburne, M.O., and W.A. Clemens. 1986a. Phyletic analysis and conclusions. *In* M.O. Woodburne and W.A. Clemens (editors), Revision of the Ektopodontidae (Mammalia; Marsupialia, Phalangeroidea) of the Australian Neogene University of California Publications in Geological Sciences, vol. 131: 94–102. Berkeley: University of California Press.

Woodburne, M.O., and W.A. Clemens. 1986b. A new genus of Ektopodontidae and additional comments on *Ektopodon serratus*. *In* M.O. Woodburne and W.A. Clemens (editors), Revision of the Ektopodontidae (Mammalia; Marsupialia, Phalangeroidea) of the Australian Neogene University of California Publications in Geological Sciences, vol. 131: 10–42. Berkeley: University of California Press.

Woodburne, M.O., and W.A. Clemens. 1986c. Revision of the Ektopodontidae (Mammalia; Marsupialia, Phalangeroidea) of the Australian Neogene (University of California Publications in Geological Sciences, vol. 131). Berkeley: University of California Press.

Woodburne, M.O., et al. 1985. Biochronology of the continental mammal record of Australia and New Guinea. South Australian Department of Mines and Energy Special Publication 5: 347–365.

Woodburne, M.O., N.S. Pledge, and M. Archer. 1987a. The Miralinidae, a new family and two new species of phalangeroid marsupials from Miocene strata of South Australia. *In* M. Archer (editor), Possums and opossums: studies in evolution: 581–602. Sydney: Surrey Beatty and Sons.

Woodburne, M.O., R.H. Tedford, and M. Archer. 1987b. New Miocene ringtail possums (Marsupialia: Pseudocheiridae) from South Australia. *In* M. Archer (editor), Possums and opossums: studies in evolution: 639–679. Sydney: Surrey Beatty and Sons.

Woodburne, M.O., R.H. Tedford, M. Archer, and N.S. Pledge. 1987c. *Madakoala*, a new genus and two species of Miocene koalas (Marsupialia: Phascolarctidae) from South Australia, and a new species of *Perikoala*. *In* M. Archer (editor), Possums and opossums: studies in evolution: 293–317. Sydney: Surrey Beatty and Sons.

Woodburne, M.O., et al. 1994. Land mammal biostratigraphy and magnetostratigraphy of the Etadunna Formation (Late Oligocene) of South Australia. Journal of Vertebrate Paleontology 13: 483–515.

Woodburne, M.O., et al. 2014a. Revised timing of the South American early Paleogene land mammal ages. Journal of South American Earth Sciences 54: 109–119.

Woodburne, M.O., et al. 2014b. Paleogene land mammal faunas of South America; a response to global climatic changes and indigenous floral diversity. Journal of Mammalian Evolution 21 (1): 1–73.

Woodhead, J., et al. 2014. Developing a radiometrically-dated chronologic sequence for Neogene biotic change in Australia, from the Riversleigh World Heritage Area of Queensland. Gondwana Research 29 (1): 153–167.

Woods, J.T. 1956. The skull of *Thylacoleo carnifex*. Memoirs of the Queensland Museum 113: 125–140.

Woods, J.T. 1960. The genera *Propleopus* and *Hypsiprymnodon* and their position in the Macropodidae. Memoirs of the Queensland Museum 13: 199–221.

Woodward, M.F. 1893. Contributions to the study of mammalian dentition. Part 1. On the development of the teeth of the Macropodidæ. Proceedings of the Zoological Society of London 1893: 450–473.

Woodward, M.F. 1896. On the teeth of the Marsupialia, with especial eeference to the premilk dentition. Anatomischer Anzeiger 12 (12-13): 281–291.

Woolley, P.A. 2005a. Revision of the three-striped dasyures, genus *Myoictis* (Marsupialia: Dasyuridae), of New Guinea, with description of a new species. Records of the Australian Museum 57: 321–340.

Woolley, P.A. 2005b. The species of *Dasycercus* Peters, 1875 (Marsupialia: Dasyuridae). Memoirs of Museum Victoria 62 (2): 213–221.

Woolley, P.A. 2011. *Pseudantechinus mimulus*: a little known dasyurid marsupial. Australian Mammalogy 33: 57–67.

Woolley, P.A., A. Haslem, and M. Westerman. 2013. Past and present distribution of *Dasycercus*: toward a better understanding of the identity of specimens in cave deposits and the conservation status of the currently recognized species *D. blythi* and *D. cristicauda* (Marsupialia: Dasyuridae). Australian Journal of Zoology 61 (4): 281–290.

Wortman, J.L. 1902. Studies of Eocene Mammalia in the Marsh collection, Peabody Museum. American Journal of Science (Series 4) 13: 433–448.

Wright, A.M., and D.M. Hillis. 2014. Bayesian analysis using a simple likelihood model outperforms parsimony for estimation of phylogeny from discrete morphological data. PLoS One 9 (10): e109210.

Wright, A.M., G.T. Lloyd, and D.M. Hillis. 2016. Modeling character change heterogeneity in phylogenetic analyses of morphology through the use of priors. Systematic Biology 65 (4): 602–611.

Wright, W., G.D. Sanson, and C. McArthur. 1991. The diet of the extinct bandicoot *Chaeropus ecaudatus*. *In* P. Vickers-Rich, J.M. Monaghan, R.F. Baird, and T.H. Rich (editors), Vertebrate palaeontology of Australasia: 229–245. Lilydale, Victoria: Pioneer Design Studio.

Wroe, S. 1996a. *Muribacinus gadiyuli* (Thylacinidae, Marsupialia), a very plesiomorphic thylacinid from the Miocene of Riversleigh, northwestern Queensland, and the problem of paraphyly for the Dasyuridae. Journal of Paleontology 70 (6): 1032–1044.

Wroe, S. 1996b. An investigation of phylogeny in the giant extinct rat kangaroo *Ekaltadeta* (Propleopinae, Potoroidae, Marsupialia). Journal of Paleontology 70 (4): 681–690.

Wroe, S. 1997a. *Mayigriphus orbus* gen. et sp. nov. a Miocene dasyuromorphian from Riversleigh, northwestern Queensland. Memoirs of the Queensland Museum 41 (2): 439–448.

Wroe, S. 1997b. A reexamination of proposed morphology-based synapomorphies for the families of Dasyuromorphia (Marsupialia). 1. Dasyuridae. Journal of Mammalian Evolution 4 (1): 19–52.

Wroe, S. 1997c. Stratigraphy and phylogeny of the giant extinct rat-kangaroos (Propleopinae, Hypsiprymnodontidae, Marsupialia). Memoirs of the Queensland Museum 41 (2): 449–456.

Wroe, S. 1998. A new 'bone-cracking' dasyurid (Marsupialia), from the Miocene of Riversleigh, northwestern Queensland. Alcheringa: an Australasian Journal of Palaeontology 22: 277–284.

Wroe, S. 1999. The geologically oldest dasyurid (Marsupialia), from the Miocene Riversleigh, northwestern Queensland. Palaeontology 42: 1–27.

Wroe, S. 2003. Australian marsupial carnivores: recent advances in palaeontology. *In* M. Jones, C. Dickman, and M. Archer (editors), Predators with pouches: the biology of marsupial carnivores: 102–123. Collingwood, Australia: CSIRO Publishing.

Wroe, S., and M. Archer. 1995. Extraordinary diphyodonty-related change in dental function for a tooth of the extinct marsupial *Ekaltadeta ima* (Propleopinae, Hypsiprymnodontidae). Archives of Oral Biology 40 (7): 597–603.

Wroe, S., and B.S. Mackness. 1998. Revision of the Pliocene dasyurid, *Dasyurus dunmalli* (Dasyuridae: Marsupialia). Memoirs of the Queensland Museum 42 (2): 605–612.

Wroe, S., and B.S. Mackness. 2000a. A new genus and species of dasyurid from the Pliocene Chinchilla Local Fauna of south-eastern Queensland. Alcheringa: an Australasian Journal of Palaeontology 24 (4): 319–326.

Wroe, S., and B.S. Mackness. 2000b. Additional material of *Dasyurus dunmalli* from the Pliocene Chinchilla Local Fauna of Queensland and its phylogenetic implications. Memoirs of the Queensland Museum 45 (2): 641–645.

Wroe, S., and A. Musser. 2001. The skull of *Nimbacinus dicksoni* (Thylacinidae: Marsupialia). Australian Journal of Zoology 49 (5): 487–514.

Wroe, S., J. Brammall, and B.N. Cooke. 1998. The skull of *Ekaltadeta ima* (Marsupialia, Hypsiprymnodontidae?): an analysis of some cranial features within Marsupialia and a re-investigation of propleopine phylogeny; with notes on the inference of carnivory among mammals. Journal of Paleontology 72 (4): 738–751.

Wroe, S., T.J. Myers, R.T. Wells, and A. Gillespie. 1999. Estimating the weight of the Pleistocene marsupial lion, *Thylacoleo carnifex* (Thylacoleonidae: Marsupialia): implications for the ecomorphology of a marsupial super-predator and hypotheses of impoverishment of Australian marsupial carnivore faunas. Australian Journal of Zoology 47: 489–498.

Wroe, S., M. Ebach, S. Ahyong, C. de Muizon, and J. Muirhead. 2000. Cladistic analysis of dasyuromorphian (Marsupialia) phylogeny using cranial and

dental characters. Journal of Mammalogy 81 (4): 1008–1024.

Wroe, S., et al. 2003. An alternative method for predicting body mass: the case of the Pleistocene marsupial lion. Paleobiology 29 (3): 403–411.

Wroe, S., M. Crowther, J. Dortch, and J. Chong. 2004. The size of the largest marsupial and why it matters. Proceedings of the Royal Society of London B, Biological Sciences 271 Suppl 3: S34–36.

Yang, C.Y., et al. 1986. Sequence, structure, receptor-binding domains and internal repeats of human apolipoprotein B-100. Nature 323: 738–742.

Yang, Z. 2006. Computational molecular evolution. Oxford: Oxford University Press.

Yates, A.M. 2014. New craniodental remains of *Thylacinus potens* (Dasyuromorphia: Thylacinidae), a carnivorous marsupial from the late Miocene Alcoota Local Fauna of central Australia. PeerJ 2: e547.

Yates, A.M. 2015a. *Thylacinus* (Marsupialia: Thylacinidae) from the Mio-Pliocene boundary and the diversity of late Neogene thylacinids in Australia. PeerJ 3: e931.

Yates, A.M. 2015b. New craniodental remains of *Wakaleo alcootaensis* (Diprotodontia: Thylacoleonidae) a carnivorous marsupial from the late Miocene Alcoota Local Fauna of the Northern Territory, Australia. PeerJ 3: e1408.

Yates, B., et al. 2017. Genenames.org: the HGNC and VGNC resources in 2017. Nucleic Acids Research 45 (D1): D619–D625.

Young, S.G. 1990. Recent progress in understanding apolipoprotein B. Circulation 82 (5): 1574–1594.

Yu, G. 2020. Using ggtree to visualize data on tree-like structures. Current Protocols in Bioinformatics 69: e96.

Yu, G., et al. 2016. ggtree: an R package for visualization and annotation of phylogenetic trees with their covariates and other associated data. Methods in Ecology and Evolution 8 (1): 28–36.

Zack, S.P. 2010. The phylogeny of eutherian mammals: A new analysis emphasizing dental and postcranial morphology of Paleogene taxa. Ph.D. dissertation, School of Medicine, Johns Hopkins University, Baltimore.

Zack, S.P., T.A. Penkrot, D.W. Krause, and M.C. Maas. 2005. A new apheliscine "condylarth" mammal from the late Paleocene of Montana and Alberta and the phylogeny of "hyopsodontids." Acta Palaeontologica Polonica 50 (4): 809–830.

Zanazzi, A., M.J. Kohn, and D.O.J. Terry. 2009. Biostratigraphy and paleoclimatology of the Eocene-Oligocene boundary section at Toadstool Park, northwestern Nebraska, USA. The Geological Society of America Special Paper 452: 197–214.

Zárate, M. 2005. El Cenozoico tardío continental de la provincia de Buenos Aires. *In* R.E. Barrio, R.O. Etcheverry, M.F. Caballé, and E. Llambías (editors), Geología y Recursos Minerales de la Provincia de Buenos Aires: 139–158. La Plata: XVI Congreso Geológico Argentino.

Zemann, A., et al. 2013. Ancestry of the Australian termitivorous numbat. Molecular Biology and Evolution 30 (5): 1041–1045.

Zhang, C. 2021. Selecting and averaging relaxed clock models in Bayesian tip dating of Mesozoic birds. Paleobiology: 1–13 [doi:10.1017/pab.2021.42].

Zhang, C., T. Stadler, S. Klopfstein, T.A. Heath, and F. Ronquist. 2016. Total-evidence dating under the fossilized birth-death process. Systematic Biology 65 (2): 228–249.

Ziegler, A.C. 1971. A theory of the evolution of therian dental formulas and replacement patterns. Quarterly Review of Biology 46 (3): 226–249.

Zimicz, A.N. 2012. Ecomorfología de los marsupiales paleógenos de América del Sur. Ph.D. dissertation, Facultad de Ciencias Naturales y Museo, Universidad Nacional de La Plata, La Plata.

Zimicz, A.N., and F.J. Goin. 2020. A reassessment of the genus *Groeberia* Patterson, 1952 (Mammalia, Metatheria): functional and phylogenetic implications. Journal of Systematic Palaeontology 18 (12): 975–992.

Zimicz, A.N., et al. 2020. *Archaeogaia macachaae* gen. et sp. nov., one of the oldest Notoungulata Roth, 1903 from the early-middle Paleocene Mealla Formation (Central Andes, Argentina) with insights into the Paleocene-Eocene South American biochronology. Journal of South American Earth Sciences 103: 102772.

APPENDIX 1

Fossil Metatherian Terminal Taxa and Their Provenance

Below we summarize relevant information about the fossil metatherians we scored as terminal taxa, including the species scored for each genus, locality information, the probable ages of the specimens we examined, and the age range assumed in our tip-dating analyses. Because we did not use every known specimen to score character data for this study, the localities and ages listed may not include all known records of a specific taxon. Where applicable, however, we briefly note the localities of additional specimens (not used for scoring purposes), and we discuss previous studies that are important for placing these taxa in phylogenetic context.

OUTGROUP TAXA

†*Pucadelphys*

Species Scored: †*Pucadelphys andinus* (type and only described species).

Geological Provenance of Scored Specimens: Tiupampa, Santa Lucía Formation, Bolivia.

Age of Scored Specimens: The fossil-bearing beds at Tiupampa are within a reversed magnetostratigraphic polarity unit (Marshall et al., 1997; Sempere et al., 1997). Based on a range of geological evidence, Marshall et al. (1997) and Sempere et al. (1997) identified this reversal as corresponding to chron 26r, which spans from the late Danian (~62.15 Mya; Jehle et al., 2019) to the Selandian-Thanetian boundary (61.6 Mya; Coccioni et al., 2012: fig. 2; Cohen et al., 2013 [updated]). This interpretation was followed by Zimicz et al. (2020).

However, the study by Gelfo et al. (2009) and several subsequent studies (Woodburne et al., 2014a, 2014b; Muizon et al., 2015, 2018; Muizon and Ladevèze, 2020) have instead associated this reversal with the earlier chron 28r, which spans from 65.118 to 64.866 Mya (Sprain et al., 2015).

This was driven in large part by the results of various cluster analyses presented by Gelfo et al. (2009), in which the Tiupampan mammal fauna grouped with North American early Paleocene (Puercan) faunas, to the exclusion of other South American Paleocene and Eocene mammal faunas. We critically review the evidence presented by Gelfo et al. (2009) in detail here (see also Zimicz et al., 2020).

The grouping of the Tiupampa and North American Puercan mammal faunas found by Gelfo et al. (2009) was largely due to the shared presence of the metatherian †*Peradectes*. However, this is problematic for a number of reasons. The Tiupampan †*Peradectes* is currently known from a single damaged upper molar (YPFB Pal 6132; Marshall and Muizon, 1988: fig. 12) and has not, to our knowledge, been included in a formal phylogenetic analysis to test whether it is indeed a member of this genus. The only other South American record of †*Peradectes* is †*P. austrinum*—which is the species to which Marshall and Muizon (1988) originally referred the Tiupampan specimen, although Muizon (1992) subsequently referred it to †*P.* cf. *austrinum* (see also Jaillard et al., 1993: 656)—from Laguna Umayo in Peru (Sigé, 1971; 1972; Crochet, 1980). Sigé et al. (2004) concluded that Laguna Umayo is either Chron 26r or Chron 24r (late Thanetian to early Ypresian; Coccioni et al., 2012), in which case †*Peradectes* survived in South America until at least the late Paleocene; thus, the presence of †*Peradectes* at Tiupampa does not clearly support an early Paleocene age. The Puercan (earliest Paleocene) faunas were the only North American mammal faunas considered by Gelfo et al. (2009), but the North American record of †*Peradectes* extends until the end of the Eocene (Korth, 2008; 2018), and so again the shared presence of †*Peradectes* at Tiupampa and in the Puercan of North America does not directly support an early Paleocene age for the former. Furthermore, the North American Puercan "†*Peradectes*" does not unambiguously group with †*Peradectes* sensu stricto in the phylogenetic analyses of Williamson et al. (2012; 2014), and some of these Puercan specimens are now recognized as

belonging to a different genus, †*Thylacodon* (Williamson et al., 2012; 2014); this casts further doubt on whether the Tiupampan and Puercan taxa are closely related, particularly in the absence of a formal phylogenetic analysis that includes the Tiupampan †*Peradectes* specimen.

The only other taxa shared by Tiumpampa and the Puercan faunas in Gelfo et al.'s (2009) dataset are "Didelphimorphia," "Didelphidae," and "Condylarthra"—all of which are arguably inappropriate to use in clustering analyses because they are clearly nonmonophyletic (at least as used by Gelfo et al., 2009)—and the "condylarth" family †Mioclaenidae (see Muizon and Cifelli, 2000). Zack et al. (2005; see also Zack, 2010) considered †Mioclaenidae to be equivalent to †Hyopsodontidae, and placed the Tiupampan and other South American members of this group within the hyopsodontid subfamily Kollpaninae (Zack et al., 2005: table 4). Regardless, mioclaenids/hyopsodontids survived in North America after the Puercan (Archibald, 1998; Williamson and Carr, 2007), and so their presence at Tiupampa is not clearly supportive of a Puercan age for the latter. Thus, evidence from these other taxa likewise does not clearly support an early Paleocene age for Tiupampa (Zimicz et al., 2020).

Muizon and Ladevèze (2020: 600–609) restated the evidence in favor of an early Paleocene (chron 28r) age for Tiupampa, and argued that the "primitiveness" of various Tiupampan mammals compared to relatives at other fossil sites in North and South America provides further support for this age interpretation. However, Muizon and Ladevèze (2020) did not provide any phylogenetic or other quantitative analyses in support of their arguments, and such "stage of evolution" evidence is not (in our opinion) compelling, given that the comparisons are made between fossil sites at very different paleolatitudes and on different continents (see also Zimicz et al., 2020).

In summary, while an early Paleocene age for Tiupampa is plausible, we do not find the evidence for correlating this fauna with chron 28r, rather than chron 26r, to be overwhelming (contra Gelfo et al., 2009; Muizon et al., 2015, 2018; Muizon and Ladevèze, 2020). Instead, we take a compromise position, and assign †*Pucadelphys* and the other Tiupampan terminals included here (†*Mayulestes* and †*Allqokirus*; see below) an age range corresponding to the maximum age of chron 28r (65.118 Mya; Sprain et al., 2015) and the minimum age of chron 26r, which corresponds to the Seldandian-Thanetian boundary (59.2 Mya; Coccioni et al., 2012; Cohen et al., 2013 [updated]).

ASSIGNED AGE RANGE: 65.118–59.200 Mya.

REMARKS: †*Pucadelphys andinus* is represented by abundant, excellently preserved cranial and postcranial material from the Tiupampa Fauna in Bolivia (Marshall and Muizon, 1995; Ladevèze and Muizon, 2007; Ladevèze et al., 2011). As discussed above, the age of the Tiupampa Fauna, which is within the Santa Lucía Formation, remains somewhat controversial: originally suggested to be Late Cretaceous (Marshall et al., 1983; Muizon et al., 1983, 1984; Marshall and Muizon, 1988), it now appears to be either middle Paleocene (Marshall et al., 1997; Sempere et al., 1997; Zimicz et al., 2020) or early Paleocene (Gelfo et al., 2009; Woodburne et al., 2014a; Muizon et al., 2015, 2018; Muizon and Ladevèze, 2020). Twenty-two individuals of †*P. andinus* (12 adult females, six adult males, and four subadults) are known from mostly intact crania and mandibles, and numerous other individuals (including a single juvenile) are known from more fragmentary remains (Marshall and Muizon, 1995; Ladevèze and Muizon, 2007; Ladevèze et al., 2011). These specimens indicate the presence of marked sexual dimorphism and also a surprising degree of variation in molar morphology (Ladevèze et al., 2011).

Although †*Pucadelphys* was originally classified as a "didelphid" (Marshall and Muizon, 1988; 1995), it differs from crown-clade didelphimorphians (Didelphidae sensu Voss and Jansa, 2009) in numerous morphological features, including absence of an ossified hypotympanic sinus floor, presence of a medial process of the squamosal,

absence of a distinct rostral tympanic process of the petrosal, presence of posterior cingulids on the lower molars, absence of a proximal calcaneo-cuboid facet on the ventral surface of the calcaneus, and presence of a third trochanter of the femur, among others (Marshall and Muizon, 1988; 1995; Marshall and Sigogneau-Russell, 1995; Muizon et al., 1997; Argot, 2002; Muizon and Argot, 2003; Ladevèze and Muizon, 2007).

In fact, †*Pucadelphys* has consistently been recovered within Marsupialiformes sensu Beck (2017a; see also Vullo et al., 2009) but outside Marsupialia in published phylogenetic analyses based on morphology (Rougier et al., 1998, 2004, 2015; Luo et al., 2003, 2011; Asher et al., 2004; Ladevèze and Muizon, 2007; Sánchez-Villagra et al., 2007; Beck et al., 2008; Horovitz et al., 2008, 2009; Forasiepi, 2009; Ladevèze and Muizon, 2010; Williamson et al., 2012, 2014; Engelman and Croft, 2014; Forasiepi et al., 2014a; Suarez et al., 2015; Ni et al., 2016; Wilson et al., 2016; Beck, 2017b; Carneiro and Oliveira, 2017a, 2017b; Maga and Beck, 2017; Bi et al., 2018; Carneiro et al., 2018; Muizon et al., 2018; Carneiro, 2019; Rangel et al., 2019; Engelman et al., 2020; Ladevèze et al., 2020; Muizon and Ladevèze, 2020; Zimicz and Goin, 2020), total evidence (Asher et al., 2004; Beck et al., 2014; Beck, 2017b; Maga and Beck, 2017; Abello and Candela, 2019), and molecular-scaffold (Beck, 2012) datasets.

Two notable exceptions to this general consensus are the studies of Goin et al. (2006) and Velazco et al. (2022), both of which reported phylogenetic analyses that placed †*Pucadelphys* within Marsupialia. Goin et al.'s (2006) analysis is problematic in several respects, inter alia: (1) their study was based almost exclusively on dental characters; (2) plesiomorphic absence versus secondary loss of certain features was determined a priori (e.g., chars. 13, 16, 18); (3) fossil taxa were scored for unpreserved characters (e.g., sperm-pairing was scored as absent in †*Kokopellia* but present in †*Itaboraidelphys*), and (4) the monophyly of several clades was enforced a priori using topological constraints (Goin et al.,

2006: supplementary data). Parsimony analysis of a corrected version of the Goin et al. (2006) resulted in a largely unresolved strict consensus with no support for †*Pucadelphys* within Marsupialia (R.M.D.B., personal obs.).

Velazco et al. (2022) used an expanded version of the "phenomic" morphological matrix of O'Leary et al. (2013), comprising 4541 osteological and soft tissue characters, which they analyzed in combination with 37 kb of DNA sequence data from 27 nuclear genes, using both maximum parsimony and maximum likelihood. These analyses placed †*Pucadelphys* sister to †*Deltatheridium* from the Late Cretaceous of Mongolia, with this clade sister to the Recent didelphid *Didelphis*, and the Recent microbiotheriid *Dromiciops* in turn sister to †*Pucadelphys* + †*Deltatheridium* + *Didelphis*. This topology implies that both †*Pucadelphys* and †*Deltatheridium* are marsupials, rather than (as was previously generally accepted) nonmarsupial metatherians. This surprising result warrants further scrutiny; in particular, Velazco et al. (2022) included only two Recent marsupials (*Didelphis virginiana* and *Dromiciops gliroides*) in their study, and it remains to be seen what impact the addition of more Recent marsupials would have. We also note that at least some of the synapomorphies identified by Velazco et al. (2022: 7) as supporting a †*Pucadelphys* + †*Deltatheridium* + *Didelphis* clade to the exclusion of *Dromiciops* appear to be questionable. The fossil microbiotheriid †*Microbiotherium* has a paracanine fossa (see char. 34), suggesting that its absence in *Dromiciops* may be secondary rather than plesiomorphic, and evidence from other fossil microbiotheriids (in particular, †*Woodburnodon*; Goin et al., 2007c) indicates that the absence of well-developed stylar cusps in *Dromiciops* is likewise secondary. In addition, contact between the fibula and calcaneus is present in †*Pucadelphys* (Muizon, 1998; Argot, 2002; Szalay and Sargis, 2006) and †*Deltatheridium* (Horovitz, 2000: fig. 9), whereas it is absent in *Dromiciops* (Szalay, 1994; Szalay and Sargis, 2006) contra Velazco et al. (2022).

We consider that the majority of current evidence indicates that †*Pucadelphys* is a nonmarsupial metatherian contra Goin et al. (2006) and Velazco et al. (2022), and we follow the classification of Muizon et al. (2018), in which it is a member of the family †Pucadelphyidae, within the superorder †Pucadelphyda (which includes the order †Sparassodonta; see †*Mayulestes* and †*Allqokirus* below). As such, we consider †*Pucadelphys* suitable for use as an outgroup taxon for our morphological and total-evidence analyses.

†*Mayulestes*

Species Scored: †*Mayulestes ferox* (type and only described species).

Geological Provenance of Scored Specimens: Tiupampa, Santa Lucía Formation, Bolivia.

Age of Scored Specimens: Early or middle Paleocene (see †*Pucadelphys* above).

Assigned Age Range: 65.118–59.200 Mya.

Remarks: †*Mayulestes ferox* was described by Muizon (1994; 1998) as the earliest and most plesiomorphic known member of the order †Sparassodonta (= "Borhyaenoidea" in Muizon's [1994, 1998] usage), an exclusively South American clade of carnivorously adapted forms that survived until the Pliocene (Argot, 2004; Prevosti and Forasiepi, 2018). A number of phylogenetic analyses have failed to recover †*Mayulestes* within †Sparassodonta (Rougier et al., 1998, 2004, 2015; Forasiepi, 2009; Engelman and Croft, 2014; Forasiepi et al., 2014a; Suarez et al., 2015; Ni et al., 2016; Wilson et al., 2016; Engelman et al., 2020). However, Muizon et al. (2018) argued strongly in favor of †*Mayulestes* as a plesiomorphic sparassodont, which they placed together with †*Allqokirus* (see below) and †*Patene* in the family †Mayulestidae. We follow Muizon et al. (2018) in considering †*Mayulestes* to be a member of †Sparassodonta, within the superorder †Pucadelphyda (see †*Pucadelphys* above).

Like †*Pucadelphys* (see above), †*Mayulestes* has been consistently recovered inside Marsupialiformes sensu Beck (2017a; see also Vullo et al.,

2009) but outside Marsupialia in published phylogenetic analyses, regardless of whether it has been placed within †Sparassodonta or not (Rougier et al., 1998, 2004, 2015; Luo et al., 2003, 2011; Asher et al., 2004; Ladevèze and Muizon, 2007; Sánchez-Villagra et al., 2007; Beck et al., 2008, 2014; Horovitz et al., 2008, 2009; Forasiepi, 2009; Ladevèze and Muizon, 2010; Luo et al., 2011; Beck, 2012, 2017b; Williamson et al., 2012, 2014; Engelman and Croft, 2014; Forasiepi et al., 2014a; Suarez et al., 2015; Lorente et al., 2016; Ni et al., 2016; Wilson et al., 2016; Carneiro and Oliveira, 2017a, 2017b; Maga and Beck, 2017; Bi et al., 2018; Carneiro et al., 2018; Muizon et al., 2018; Abello and Candela, 2019; Carneiro, 2019; Rangel et al., 2019; Engelman et al., 2020; Ladevèze et al., 2020; Muizon and Ladevèze, 2020; Zimicz and Goin, 2020). This, together with the excellent preservation of the holotype and only known specimen— MNHC 1249, which comprises a nearly complete cranium and associated left and right mandibles (Muizon, 1994, 1998)—renders it a suitable outgroup taxon for our study.

†*Allqokirus*

Species Scored: †*Allqokirus australis* (type and only described species).

Geological Provenance of Scored Specimens: Tiupampa, Santa Lucía Formation, Bolivia.

Age of Scored Specimens: Early or middle Paleocene (see †*Pucadelphys* above).

Assigned Age Range: 65.118–59.200 Mya.

Remarks: †*Allqokirus australis* is another metatherian from Tiupampa that is known from relatively complete cranial material, specifically specimen MNHC 8267, a well-preserved but partially disarticulated cranium and associated left and right mandibles of a subadult individual (P3/p3 and M4/m4 are not fully erupted; Muizon et al., 2018). Part of MNHC 8267 was illustrated by Cifelli and Muizon (1998a: fig. 2G, H), who identified it as †*Mayulestes ferox*, but subsequently the entire specimen was described in detail as †*Allqokirus australis* by Muizon et al.

(2018). Based on its known morphology, †*Allqokirus* appears to be an early member of †Sparassodonta (Muizon et al., 2018). We follow Muizon et al. (2018) in placing it in the sparassodont family †Mayulestidae. As discussed (see †*Mayulestes*, above), †Sparassodonta has been consistently recovered outside Marsupialia in published phylogenetic analyses.

INGROUP TAXA

†*Herpetotherium*

Species Scored: †*Herpetotherium fugax* (type species), †*H.* cf. *fugax*.

Geological Provenance of Scored Specimens: White River Formation, Wyoming.

Age of Scored Specimens: All examined specimens come from the Orellan North American Land Mammal Age, which is currently estimated as spanning from 33.9 to 32.0 Mya (Prothero and Emry, 2004; Zanazzi et al., 2009).

Assigned Age Range: 33.900–32.000 Mya.

Remarks: †*Herpetotherium fugax* is known from numerous specimens from the White River Formation, including well-preserved skulls and associated postcranial material (Gabbert, 1998; Sánchez-Villagra et al., 2007; Horovitz et al., 2008). Sánchez-Villagra et al. (2007) included †*Herpetotherium* in a comprehensive morphological phylogenetic analysis of marsupials and relatives, and found that this taxon fell outside (crown-clade) Marsupialia. Most subsequent morphological and total-evidence analyses have found a similar result, in which †*Herpetotherium* either falls outside Marsupialia or is not unambiguously a member of this clade (Beck et al., 2008, 2014, 2016; Horovitz et al., 2008, 2009; Beck, 2012, 2017b; Forasiepi et al., 2014a; Suarez et al., 2015; Lorente et al., 2016; Carneiro and Oliveira, 2017a, 2017b; Maga and Beck, 2017; Carneiro, 2018, 2019; Carneiro et al., 2018; Engelman et al., 2020; Muizon et al., 2018; Abello and Candela, 2019; Rangel et al., 2019; Ladevèze et al., 2020; Muizon and Ladevèze, 2020; Zimicz and Goin, 2020). However, a few recent pub-

lished phylogenetic analyses—namely, the morphological analyses of Forasiepi (2009: fig. 51), Engelman and Croft (2014: fig. 6), and Wilson et al. (2016: fig. 3), and the tip-and-node dated total evidence analysis of Maga and Beck (2017: fig. 39)—have found †*Herpetotherium* within Marsupialia, so some questions remain regarding its affinities.

†*Mimoperadectes*

Species Scored: †*Mimoperadectes labrus* (type species), †*M. houdei*.

Geological Provenance of Scored Specimens: UM Locality SC-69, lower part of Willwood Formation, Park County, Wyoming (†*Mimoperadectes labrus*); UM Locality SC-133, lower part of Willwood Formation, Park County, Clark Fork Basin, Wyoming (†*M. houdei*).

Age of Scored Specimens: UM Locality SC-69 is within Zone Wa-0 of the Wasatchian North American Land Mammal Age (Gingerich, 2001: fig. 11), whereas UM Locality SC-133 is within Zone Wa-2 (Bowen and Bloch, 2002: fig. 2, table 2); the maximum bound of Wa-0 is approximately 55.8 Mya, and the minimum bound of Wa-2 is approximately 55.1 Mya (Chew and Oheim, 2013: fig. 2).

Assigned age range: 55.800–55.100 Mya.

Remarks: Bown and Rose (1979) described †*Mimoperadectes labrus* based on incomplete, predominantly dental, specimens from the earliest Eocene of the Willwood Formation, and referred it to the family Didelphidae. Horovitz et al. (2009) described a broken but nearly complete cranium of †*Mimoperadectes* (USNM 482355) from a slightly younger site in the Willwood Formation, referred it to a new species, †*M. houdei*, and referred †*Mimoperadectes* to the family †Peradectidae. In the same year, Beard and Dawson (2009) described a third species, †*M. sowasheenis*, from the early Wasatchian Red Hot Local Fauna, Uppermost Tuscahoma Formation, Lauderdale County, Mississippi. Subsequently, Rose et al. (2012) described additional specimens (including an isolated astragalus) of

the type species, †*M. labrus*, from the Wa-0 Sand Creek Divide Fauna in the Willwood Formation, and argued that the validity of †*M. houdei* as a distinct species should be reassessed (Rose et al., 2012: 22). Of this material, only the specimens described by Bown and Rose (1979) and Horovitz et al. (2009) have been used for scoring purposes here.

Horovitz et al. (2009) presented a morphological phylogenetic analysis that included a terminal combining craniodental character scores for †*Mimoperadectes labrus* and †*M. houdei* with dental character scores from †*Peradectes* spp. and three postcranial character scores from "a *Peradectes*-like species from the Middle Eocene of Messel, Germany, which may belong to this same genus or alternatively may be closely related to it" (Horovitz et al., 2009: supporting information). In their analysis, the "*Mimoperadectes-Peradectes*" terminal was recovered as sister to a clade comprising the living didelphids *Monodelphis* and *Didelphis*, suggesting that it was a crown-clade marsupial and a member of the order Didelphimorphia. The morphological analysis of Wilson et al. (2016) also included a "*Mimoperadectes-Peradectes*" terminal, which again fell inside Marsupialia, as sister to †*Herpetotherium*, with this clade sister to Didelphidae + Dasyuridae, and *Dromiciops* outside this. However, the relationships among extant marsupials found by Wilson et al. (2016) are in clear conflict with molecular, total-evidence, and most morphological analyses (e.g., Phillips et al., 2001; Amrine-Madsen et al., 2003b; Horovitz and Sánchez-Villagra, 2003; Asher et al., 2004; Nilsson et al., 2004, 2010; Phillips et al., 2006; Sánchez-Villagra et al., 2007; Beck, 2008, 2012; Beck et al., 2008, 2014, 2016; Horovitz et al., 2008, 2009; Meredith et al., 2008, 2009c, 2011; Mitchell et al., 2014; Gallus et al., 2015a; May-Collado et al., 2015; Lorente et al., 2016; Carneiro and Oliveira, 2017b; Maga and Beck, 2017; Carneiro et al., 2018; Duchêne et al., 2018; Abello and Candela, 2019; Carneiro, 2019; Zimicz and Goin, 2020; Álvarez-Carretero et al., 2021) in failing to support monophyly of Australidelphia.

An implicit assumption of the analyses of Horovitz et al. (2009) and Wilson et al. (2016) is that the taxa they used to score their "*Mimoperadectes-Peradectes*" terminal (i.e., †*Mimoperadectes labrus*, †*M. houdei*, †*Peradectes* spp., and the "*Peradectes*-like species" from Messel) form a clade to the exclusion of their other terminals. However, evidence in support of this assumption is not particularly strong. The phylogenetic analyses of Williamson et al. (2012; 2014) recovered †*Mimoperadectes labrus* and †*M. houdei* as sister taxa in a clade that also included †*Peradectes chesteri* and †*P. protinnominatus* (as well as †*Armintodelphys blacki* and †*A. dawsoni*), which supports a close relationship between †*Mimoperadectes* and these particular †*Peradectes* species. However, other †*Peradectes* species included by Williamson et al. (2012, 2014)—namely †*P. minor* (the type species), †*P. californicus*, †*P. coproxeches* (= †*Peradectes*, sp. nov., in Williamson et al., 2012; see Williamson and Taylor, 2011), †*P. elegans*, and †*P. gulottai*—were not resolved as members of this clade, but instead formed part of a polytomy (within which †*P. elegans* and †*P. californicus* were sister taxa) that also included the †*Mimoperadectes* + †*Armintodelphys* + †*P. chesteri* + †*P. protinnominatus* clade discussed above, †*Maastrichtidelphys*, †*Pucadelphys*, †*Szalinia*, and †Pediomyidae. Thus, the analyses of Williamson et al. (2012; 2014) do not unambiguously support monophyly of †*Peradectes* nor monophyly of †*Mimoperadectes* + †*Peradectes*. Williamson et al. (2012; 2014) referred to the taxa forming this polytomy, but excluding †Pediomyidae, as "Peradectidae sensu lato," and Williamson et al. (2012: 629) specifically argued that future studies would place at least some of these taxa within a monophyletic †Peradectidae sensu stricto, which they defined as "the most inclusive clade containing *Peradectes elegans*, but not *Herpetotherium fugax*, *Pediomys elegans* or *Didelphis virginiana*" (Williamson et al., 2012: 629).

Carneiro and Oliveira (2017b) and Carneiro (2018) recovered a clade comprising †*Mimoperadectes*, †*Peradectes*, and †*Thylacodon* (the last

genus having been regarded as synonymous with †*Peradectes* by some authors; see Williamson et al., 2012), although they did not specify exactly which species they used to score these terminals. In two other papers, Carneiro et al. (2018) and Carneiro (2019) found a clade that they called †Peradectidae comprising †*Mimoperadectes*; †*Peradectes*; †*Thylacodon*; the North American taxa †*Golderdelphys*, †*Nanodelphys*, and †*Didelphidectes*; †*Siamoperadectes* from Thailand; and an unnamed taxon from the Itaboraí Local Fauna of Brazil. Rangel et al. (2019), meanwhile, also found a †*Mimoperadectes* + †*Peradectes* clade (they did not include †*Thylacodon* or the other putative peradectids used by Carneiro et al. [2018] and Carneiro [2019]), but again it is unclear exactly which species were used for scoring purposes.

The "*Peradectes*-like species" from Messel, meanwhile, has never had its relationship to definitive †*Peradectes* species formally tested, largely because the known specimens of the Messel taxon (although preserved as largely complete, articulated skeletons with some soft-tissue preservation) are heavily crushed, and details of the dentition that could be compared with known specimens of †*Peradectes* and similar taxa (most of which are known from dental material only) are not easily visible (Koenigswald and Storch, 1988; Kurz, 2001, 2005, 2007; Storch, 2001; Kurz and Habersetzer, 2004). Indeed, Horovitz et al. (2009: supplementary information) were able to score only three characters from the Messel specimens, all of which were from the postcranial skeleton. Kurz and Habersetzer (2004) used "continuous online recalibrated radiography" (CORR) to view the occlusal surfaces of the postcanine teeth of the Messel specimens, noting that the centrocrista of the molars is only slightly curved and that the paracone and metacone are similar in size (Kurz and Habersetzer, 2004: 18), features that have traditionally been used to distinguish peradectids from herpetotheriids, with the latter characterized has having a distinctly V-shaped centrocrista and a metacone that is markedly larger

than the paracone (e.g., Crochet, 1979, 1980; Krishtalka and Stucky, 1983; Korth, 1994, 2008; Johanson, 1996b; Case et al., 2005; Hooker et al., 2008). However, the phylogenetic analysis of Williamson et al. (2012: 634) implies that a V-shaped centrocrista has evolved at least five times within Metatheria, so the presence of a relatively straight centrocrista (which is likely plesiomorphic for both Metatheria and Marsupialiformes) in the Messel specimens is not compelling evidence that they represent †*Peradectes*. Indeed, Morlo et al. (2004: footnote 79) remarked that "As the taxonomy is unclear, Storch (2001) and Kurz (unpublished data) regard the specimens as "*Peradectes*," in the sense of a primitive didelphimorphian from the Palaeocene of Europe"—we note here that "didelphimorphian" is presumably used by Morlo et al. (2004) to mean a dentally generalized marsupialiform, rather than a close relative of Didelphidae.

Williamson et al. (2012; 2014) did not include representatives of Didelphidae or any other extant marsupial family in the published versions of their analyses, so they did not test the relationship of †*Mimoperadectes*, †*Peradectes*, and other "peradectids" to Didelphidae, nor to crown-clade Marsupialia. Williamson et al. (2012: 631–632) reported that they had included extant didelphid *Didelphis virginiana* as an "experimental exercise," but found that its inclusion led to a considerable loss of resolution in the resultant phylogeny. Beck (2012) used a modified version of Horovitz et al.'s (2009) matrix, but modified their "*Mimoperadectes-Peradectes*" terminal (which he renamed †Peradectidae) by deleting the three postcranial character scores taken from the "*Peradectes*-like species" from Messel and revising some character scores. In particular, Beck (2012: electronic supplementary material) scored his †Peradectidae terminal as lacking an alisphenoid tympanic wing, based on personal observations by R.S.V. of the holotype and only known specimen of †*Mimoperadectes houdei* (USNM 482355; see also Horovitz et al., 2009: fig. S3). Muizon et al. (2018: 402) maintained that a "small tympanic process is…likely to have

been present in *Mimoperadectes*," but did not provide any supporting evidence. In fact, †*M. houdei* appears to entirely lack an ossified hypotympanic sinus floor (see char. 55). Beck's (2012) maximum parsimony and Bayesian analyses of his revised morphological matrix using a molecular scaffold placed †Peradectidae outside Marsupialia (Beck, 2012: fig. 6), and subsequent morphological and total-evidence analyses that have used versions of his matrix have either found †*Mimoperadectes*/†Peradectidae to fall outside Marsupialia (Beck et al., 2014, 2016; Lorente et al., 2016; Maga and Beck, 2017; Abello and Candela, 2019; Zimicz and Goin, 2020) or have found this relationship to be unresolved (Beck, 2017b). Numerous recent studies that have used rather different morphological datasets from Beck's (2012) have also found †*Mimoperadectes* or †Peradectidae outside Marsupialia (Forasiepi, 2009; Engelman and Croft, 2014; Forasiepi et al., 2014a; Suarez et al., 2015; Carneiro and Oliveira, 2017b; Carneiro, 2018; Carneiro et al., 2018; Muizon et al., 2018; Carneiro, 2019; Rangel et al., 2019; Engelman et al., 2020; Ladevèze et al., 2020; Muizon and Ladevèze, 2020).

In summary, the composition of †Peradectidae remains unsettled, but most phylogenetic analyses that have included †*Mimoperadectes* or a composite peradectid terminal that combines character scores from †*Mimoperadectes* and †*Peradectes* have found that this taxon falls outside Marsupialia (contra Horovitz et al., 2009; Wilson et al., 2016), The current study represents a further test of the relationship of †*Mimoperadectes* to the marsupial crown clade.

†*Sparassocynus*

SPECIES SCORED: †*Sparassocynus bahiai* (type species), †*S. derivatus.*

GEOLOGICAL PROVENANCE OF SCORED SPECIMENS: All examined specimens of †*Sparassocynus bahiai* were collected in the vicinity of Monte Hermoso in Buenos Aires Province, Argentina, presumably from the coastal Monte Hermoso

Formation (Farola Monte Hermoso; Tomassini et al., 2013). Examined specimens of †*S. derivatus* are from the Chapadmalal Formation, which is exposed along the coastline between Miramar and Mar del Plata, also in Buenos Aires Province, Argentina (Isla et al., 2015).

AGE OF SCORED SPECIMENS: The fossil-bearing sediments near Monte Hermoso are the type locality of the Montehermosan South American Land Mammal Age (SALMA) and are estimated to be younger than 5.28 ± 0.04 Mya based on radiometric dating of impact glasses and older than 4.5 or 5.0 Mya based on magnetostratigraphy (Zárate, 2005; Schultz et al., 2006; Tomassini et al., 2013). Impact glasses from the top of the Chapadmalal Formation, type locality of the Chapadmalalan SALMA, yield radiometric dates of 3.3 ± 0.2 Mya (Schultz et al., 1998), a plausible minimum age for the material we examined from this formation, for which Woodburne (2010: fig. 3) suggested a maximum age of about 5 Mya (see also Prevosti and Forasiepi, 2018: table 1.1).

ASSIGNED AGE RANGE: 5.320–3.100 Mya.

REMARKS: Originally described by Mercerat (1899) as a sparassodont based on fragmentary dental remains from the Monte Hermoso Formation (see also Ameghino, 1899: 7; Cabrera, 1927: 306), †*Sparassocynus* was later referred to the didelphid subfamily Sparassocyninae by Reig (1958b). This arrangement was maintained by Reig and Simpson (1972) in their description of additional well-preserved cranial material of the genus. However, Reig et al. (1987) and several subsequent authors (e.g., Goin, 1991, 1995; Forasiepi et al., 2009; Abello et al., 2015) classified †*Sparassocynus* and a second fossil taxon, †*Hesperocynus* (see below) in a separate family, †Sparassocynidae, which they placed together with Didelphidae (sensu Voss and Jansa, 2009) in the superfamily Didelphoidea.

Beck and Taglioretti (2020) described the skull of a well-preserved, late-stage juvenile of †*Sparassocynus derivatus* (MMP M-5292, collected from the Chapadmalal Formation), which revealed the presence of a distinctive cranial apo-

morphy of Didelphidae (early fusion between the interparietal and supraoccipital; see char. 31), as well as other apparently apomorphic craniodental features characteristic of subclades within Didelphidae. The latter include a posterior palatal margin (postpalatal torus) with distinct "corners" (found in all Recent didelphids except *Caluromys*, *Caluromysiops*, and *Glironia*; Voss and Jansa, 2003; 2009), contact between the maxilla and alisphenoid in the ventral floor of the orbit (also present in *Lutreolina*, *Monodelphis*, and †*Thylatheridium*; Voss and Jansa, 2003, 2009; see char. 16), and fusion in subadults of the midfrontal suture (as found in *Chironectes*, *Didelphis*, *Lutreolina*, and *Philander*; Voss and Jansa, 2003, 2009; see char. 24). Beck and Taglioretti (2020) also reinterpreted the specialized, highly inflated auditory region of †*Sparassocynus*, documenting the presence of an enormously expanded hypotympanic sinus (part of which was identified as an epitympanic sinus by Reig and Simpson, 1972; see also comments by Forasiepi et al., 2009: 1256), a posterior squamosal epitympanic sinus (see char. 84), and an unusual course for the mandibular division of the trigeminal nerve (within a bony canal in the medial wall of the hypotympanic sinus; see char. 52). Of these, the last two also appear to be present in †*Hesperocynus* (see below), whereas the first cannot be assessed based on available material.

The total-evidence Bayesian phylogenetic analyses of Beck and Taglioretti (2020), which used a dataset modified from Voss and Jansa (2009), recovered †*Sparassocynus* and †*Hesperocynus* as sister taxa within Didelphidae, either inside the genus *Monodelphis* (in the undated analysis) or, perhaps more plausibly, sister to *Monodelphis* (in the tip-and-node dating analysis). Beck and Taglioretti (2020) argued that †*Sparassocynus* and †*Hesperocynus* warranted distinction at the tribal level within Didelphidae (as †Sparassocynini). The analyses presented here represent a further test of the phylogenetic relationships of †*Sparassocynus* and †*Hesperocynus* based on an expanded and revised character set and a wider sampling of marsupials and non-marsupial metatherian outgroup taxa.

Although we scored †*Sparassocynus* based on craniodental material traditionally identified as †*S. bahiai* (from the Monte Hermoso Formation) and †*S. derivatus* (from the Chapadmalal Formation), these nominal species were distinguished only by Reig and Simpson (1972: 515) based on minor dental differences, and they do not differ in size (Abello et al., 2015); they could plausibly be synonymized.

†*Hesperocynus*

SPECIES SCORED: †*Hesperocynus dolgopolae* (type and only described species).

GEOLOGICAL PROVENANCE OF SCORED SPECIMENS: Level 20 (sensu Stahlecker; see Riggs and Patterson, 1939) of the Andalhuala Formation, Catamarca Province, Argentina; Arroyo Seco de la Frazada, La Huertita Formation (previously middle section of the Aisol Formation; Forasiepi et al., 2009, 2011; Garrido et al., 2014), Mendoza Province, Argentina.

AGE OF SCORED SPECIMENS: Esteban et al. (2014: fig. 2) summarized the stratigraphy of the Andalhuala Formation and published radiometric dates for the various Levels sensu Stahlecker (see Riggs and Patterson, 1939). Of these, Butler et al. (1984) gave a radiometric date of 6.70 ± 0.05 Mya for Level 15, while Latorre et al. (1997) presented a radiometric date of 5.64 ± 0.16 Mya for Level 23, which collectively bracket Level 20, from which the Andalhuala *Hesperocynus* specimen was collected. This falls within the late Miocene Huayquerian SALMA (9–5.28 Mya; Prevosti and Forasiepi, 2018: table 1.1). Garrido et al. (2014) renamed the "middle section of the Aisol Formation" as the La Huertita Formation and identified it as Montehermosan-Chapadmalalan based on biostratigraphy. The ages of the Montehermosan and Chapadmalalan SALMAs are discussed above (see †*Sparassocynus*).

ASSIGNED AGE RANGE: 6.750–3.100 Mya.

REMARKS: Based largely on information provided by a partial skull from the La Huertita For-

mation (MHNSR-PV 1046), Forasiepi et al. (2009) erected the genus †*Hesperocynus* to include specimens originally referred to †*Thylatheridium dolgopolae* (Reig, 1958a; Goin and Montalvo, 1988; Goin et al., 2000). Forasiepi et al. (2009) noted that †*H. dolgopolae* shares derived craniodental similarities with †*Sparassocynus* (a partial posterior braincase of †*H. dolgopolae*, FMNH P-15225, had previously been identified as †*Sparassocynus* sp. by previous authors; Reig, 1958b; Reig and Simpson, 1972; Simpson, 1974), but is somewhat more plesiomorphic, and they classified both genera within Sparassocynidae. As already discussed (see †*Sparassocynus*, above), the total-evidence analyses of Beck and Taglioretti (2020) recovered †*Hesperocynus* and †*Sparassocynus* as a tribal-level clade within Didelphidae (Sparassocynini). Our analyses provide an additional test of the relationship between †*Hesperocynus* and †*Sparassocynus* and Recent didelphids.

We were able to examine FMNH P-15225, a partial posterior braincase of †*H. dolgopolae* from the Andalhuala Formation (see Simpson, 1974: figs. 7–10), but not the well-preserved skull from the Aisol Formation (MHNSR–PV 1046) described by Forasiepi et al. (2009). A number of character scores (particularly those relating to the dentition) have therefore been taken directly from Forasiepi et al.'s (2009) description and figures. As well as the Andalhuala and Aisol formations, †*H. dolgopolae* specimens have been collected from the Cerro Azul Formation (La Pampa Province, Argentina; Goin et al., 2000; Abello et al., 2002; Forasiepi et al., 2009), but this last material has not been used for scoring purposes here and was not used to inform the assigned age range of our †*Hesperocynus* terminal (see Püschel et al., 2020).

†*Thylatheridium*

Species Scored: †*Thylatheridium cristatum* (type species).

Geological Provenance of Scored Specimens: Barranca de los Lobos Formation and Chapadmalal Formation (including "Playa Estafeta," "nivel VI-VII," "Los Acantilados," and "Las Palomas"), Mar del Plata, Buenos Aires Province, Argentina.

Age of Scored Specimens: The Barranca de los Lobos Formation is considered to represent the Barrancalobian substage of the Marplatan stage/age (Cione et al., 2015: fig. 2; Beck and Taglioretti, 2020), which is about 2.9–3.3 Mya (Woodburne, 2010: fig. 3; Prevosti and Forasiepi, 2018: table 1.1). As noted above (see †*Sparassocynus*), the Chapadmalal Formation is thought to fall within the interval from 3.3 to about 5 Mya.

Assigned Age Range: 5.000–2.900 Mya.

Remarks: Reig (1952) erected the genus †*Thylatheridium* and described a single species, †*T. cristatum*, based on a well-preserved skull (MACN 6442) and additional specimens collected from late Pliocene localities near Chapadmalal, Mar del Plata. Two other species have been named—†*T. hudsoni* and †*T. pascuali* (see Reig, 1952; Goin and Montalvo, 1988)—although the latter was described as "dubious" by Forasiepi et al. (2009). †*Hesperocynus dolgopolae* was also originally described as a species of †*Thylatheridium* (see †*Hesperocynus* above). †*Thylatheridium* has been considered by most authors to be most closely related to the Recent didelphid *Monodelphis* (Reig, 1952; Reig et al., 1987; Goin and Montalvo, 1988; Goin, 1991, 1995; Goin and Rey, 1997; Goin et al., 2000; Voss and Jansa, 2009). This hypothesis was formalized by Voss and Jansa (2009), who referred †*Thylatheridium* to the didelphid tribe Marmosini, together with *Marmosa*, *Monodelphis*, and *Tlacuatzin*. Beck and Taglioretti (2020) proposed restricting the name Marmosini to the *Marmosa* lineage only (or possibly to *Marmosa* + *Tlacuatzin*, if these two genera form a clade), and using Monodelphini to refer to the *Monodelphis* lineage (see also Goin, 1991, 1995; Goin and Rey, 1997; Goin et al., 2000), in which case *Thylatheridium* may also be a monodelphin. Indeed, it is possible that †*Thylatheridium* is actually nested within *Monodelphis* (Reig, 1958: 90; Voss and Jansa, 2009: 101).

By contrast, Simpson (1972) argued in favor of a closer relationship between †*Thylatheridium* and *Lestodelphys* (a member of the Recent didelphid tribe Thylamyini), and some of the phylogenetic analyses of Reig et al. (1987: figs. 65, 67) placed †*Thylatheridium* in a clade with both *Lestodelphys* and *Thylamys*, to the exclusion of *Monodelphis*. Regardless, it seems certain that †*Thylatheridium* is a member of Didelphidae sensu Voss and Jansa (2009).

†*Thylophorops*

Species Scored: †*Thylophorops chapalmalensis* (type species).

Geological Provenance of Scored Specimens: "Barranca Parodi," Chapadmalal Formation; but several specimens that we examined to score this taxon lack locality data.

Age of Scored Specimens: As noted above (in the account for †*Sparassocynus*), the Chapadmalal Formation is thought to fall within the interval from 3.3 ± 0.2 Mya to about 5 Mya.

Assigned Age Range: 5.000–3.100 Mya.

Remarks: †*Thylophorops chapalmalensis* was originally described as *Didelphys* †*chapalmalense* by Ameghino (1908), but it was referred to the newly erected genus †*Thylophorops* by Reig (1952). Goin and Pardiñas (1996) subsequently referred a second species—originally described by Ameghino (1904) as *D.* †*perplana*—to †*Thylophorops*. Goin et al. (2009b) described a third species, †*T. lorenzinii*, which is the largest known didelphid described to date, with an estimated body mass of 4.8–7.4 kg. †*Thylophorops chapalmalensis*, the only species we examined to score character data, had an estimated body mass of 3.1–3.4 kg (Goin et al., 2009b), which overlaps the known range of body mass for the largest living didelphid, *Didelphis virginiana* (see Jones et al., 2009).

Most authors (Simpson, 1972; Reig et al., 1987; Goin, 1991; Goin et al., 2009b; Voss and Jansa, 2009) have considered †*Thylophorops* to belong to the extant didelphid tribe Didelphini sensu Voss and Jansa (2009), which also includes *Chironectes*, *Didelphis*, *Lutreolina*, and *Philander*. Reig et al. (1987: 73) suggested a close relationship between †*Thylophorops* and *Lutreolina*, a possibility also acknowledged by Simpson (1972: 15), who wrote that "classification of *chapalmalensis* as a fairly robust species of *Lutreolina* is not ruled out by the available information." By contrast, Goin (1991) and Goin et al. (2009b) argued for closer affinities with *Didelphis* and *Philander*.

†*Evolestes*

Species Scored: †*Evolestes hadrommatos* (type and only described species), †*Evolestes* sp.

Geological Provenance of Scored Specimens: Unit 6 of the Salla Beds, La Paz Department, Bolivia (†*Evolestes hadrommatos*); GBV-19 ("La Cantera" locality), Unit 3, Upper Puesto Almendra Member, Sarmiento Formation, Gran Barranca south of Lake Colhue-Huapi, Sarmiento Department, Chubut Province, Argentina (†*Evolestes* sp.).

Age of Scored Specimens: Unit 6 (= "the Upper White interval") of the Salla Beds is 25.82–25.89 Mya (i.e., late Oligocene) based on radiometric and magnetostratigraphic evidence (Kay et al., 1998: 191, fig. 2), whereas the "La Cantera" fossil locality is 29.5–31.1 Mya based on magnetostratigraphy (Ré et al., 2010: 57).

Assigned Age Range: 31.100–25.820 Mya.

Remarks: †*Evolestes hadrommatos* is known from a single partial cranium (the holotype MNHN-BOL-V-004017 [previously MNHN-BOL-96-400]; Goin et al., 2007). Of particular interest for this study, this specimen exhibits a molar dentition that is markedly more plesiomorphic than that of any extant paucituberculatan (Abello, 2007; Goin et al., 2007, 2010; Abello, 2013). Subsequently, additional dental material assignable to †*Evolestes* and possibly representing a new species was described from the "La Cantera" locality at the Gran Barranca in Argentina (Goin et al., 2010; Abello, 2013). The La Cantera material is important because it includes lower molars, which have not been

described for †*E. hadrommatos*. Goin et al. (2010) thought that †*Evolestes* might be a caenolestid, but such a familial assignment is not supported by published phylogenetic analyses (Goin et al., 2007, 2009a; Abello, 2013; Forasiepi et al., 2013; Rincón et al., 2015; Engelman et al., 2016; Abello et al., 2020), which instead suggest that †*Evolestes* represents an early-branching lineage within Paucituberculata.

†*Stilotherium*

Species Scored: †*Stilotherium dissimile* (type species).

Geological Provenance of Scored Specimens: Santa Cruz Formation, Santa Cruz Province, Argentina.

Age of Scored Specimens: The Santa Cruz Formation contains the type fauna of the Santacrucian SALMA, which is estimated to span about 16–18 Mya in the Atlantic coastal plain and about 14–19 Mya in the Andean foothills based on tephrochronology (Perkins et al., 2012).

Assigned Age Range: 19.000–14.000 Mya.

Remarks: †*Stilotherium dissimile* is represented by abundant dental specimens from the Santa Cruz Formation, which we used to score this taxon. Unfortunately, well-preserved cranial material is as yet unknown. Specimens of †*S. dissimile* (including some material originally referred to "*Garzonia*" and "*Halmarhipus*"; see Marshall, 1980; Abello, 2007) have played a key role in discussions regarding antemolar homologies in paucituberculatans (e.g., Sinclair, 1906: 417; Osgood, 1921: 112–116; Ride, 1962; Marshall, 1980: 113–114; Abello, 2007, 2013). †*Stilotherium* is currently classified as a member of the extant paucituberculatan family Caenolestidae, within the superfamily Caenolestoidea (e.g., Abello, 2007, 2013; Goin et al., 2009a: table 3; Rincón et al., 2015; Abello et al., 2020: fig. 2), and published phylogenetic analyses consistently support a close relationship between †*Stilotherium* (and another fossil taxon, †*Pliolestes*) and extant caenolestids (Goin et al., 2007, 2009a; Abello, 2013; Forasiepi et al.,

2013; Rincón et al., 2015; Engelman et al., 2016; Abello et al., 2020).

†*Pichipilus*

Species Scored: †*Pichipilus osborni* (type species), †*P. centinelus*, †*P. riggsi*.

Geological Provenance of Scored Specimens: Santa Cruz Formation, Santa Cruz Province, Argentina (†*Pichipilus osborni* and †*P. centinelus*); Sarmiento Formation, Colué-Huapí Member, Gran Barranca, Chubut Province, Argentina (†*P. riggsi*).

Age of Scored Specimens: Examined specimens of †*Pichipilus osborni* and †*P. centinelus* are from "Notohippidian" ("Notohippidense") sites in the Santa Cruz Formation, which appear to represent the early part of the Santacrucian SALMA (about14–19 Mya; see †*Stilotherium*, above). By contrast, the Colué-Huapí fauna of the Sarmiento Formation, the type fauna of the Colhuehuapian SALMA and source of our material of †*P. riggsi*, is estimated to span the interval from 20.0 to 20.4 Mya (i.e., early Miocene) based on radiometric and magnetostratigraphic evidence (Ré et al., 2010).

Assigned Age Range: 20.400–14.000 Mya.

Remarks: The holotype and only known specimen of †*Pichipilus centinelus*, a partial cranium and associated partial left mandible (MLP-68-I-17-204) described by Marshall and Pascual (1977; see also Goin et al., 2003, 2007b), is one of only a handful of fossil paucituberculatan skulls currently known. Conflicting opinions have been expressed as to whether this specimen preserves evidence of an anteorbital vacuity between the nasal, frontal, and maxillary bones, a distinctive cranial feature that is unique to caenolestids among extant marsupials (Thomas, 1895; Osgood, 1921, 1924; Bublitz, 1987; Patterson and Gallardo, 1987; Goin et al., 2003, 2007; Abello, 2007). Most of our character data for †*Pichipilus* is based on MLP-68-I-17-204. However, we also used specimens of †*P. osborni* (known only from the holotype, a partial mandible) and †*P. riggsi* for scoring dental characters

(see Abello, 2007). †*Pichipilus* was referred by Goin et al. (2009a) to the family †Pichipilidae, which falls within the larger clade Palaeothentoidea in recent large-scale phylogenetic analyses of Paucituberculata (Abello, 2013; Rincón et al., 2015; Engelman et al., 2016; Abello et al., 2020).

†*Palaeothentes*

SPECIES SCORED: †*Palaeothentes minutus*, †*P. lemoinei*.

GEOLOGICAL PROVENANCE OF SCORED SPECIMENS: Santa Cruz Formation, Santa Cruz Province, Argentina.

AGE OF SCORED SPECIMENS: the Santa Cruz Formation spans a maximum of 14 to 19 Mya (see †*Stilotherium* above).

ASSIGNED AGE RANGE: 19.000–14.000 Mya.

REMARKS: We scored †*Palaeothentes minutus* based on abundant but mostly fragmentary specimens collected by Carlos Ameghino from several localities in the early Miocene Santa Cruz Formation; this material has been revised by Marshall (1980) and Abello (2007). Bown and Fleagle (1993) subsequently collected considerable additional dental material of †*P. minutus* from localities in the Santa Cruz and Pinturas formations, and Marshall (1990) identified this species from the ?middle Miocene (Friasian SALMA) Río Frias Formation in Chile; however, we did not use these additional specimens for scoring purposes. Croft (2007: table 3) reported †*P. minutus* from the middle Miocene (Laventan SALMA) Quebrada Honda Fauna in southern Bolivia, but Engelman et al. (2016) subsequently referred this material to two new species (†*P. serratus* and †*P. relictus*), and we did not use it to score our †*Palaeothentes* terminal.

Well-preserved cranial material of †*Palaeothentes minutus* is unavailable, but Forasiepi et al. (2014b) described a well-preserved skull and partial skeleton (MPM-PV 3566) of a congeneric species, †*P. lemoinei*, also from the Santa Cruz Formation. Monophyly of †*Palaeothentes* (excluding "†*Palaeothentes*" *primus*) has been found in all recent large-scale phylogenetic analyses of Paucituberculata (Abello, 2013; Rincón et al., 2015; Engelman et al., 2016; Abello et al., 2020), so we used Forasiepi et al.'s (2014b) description of the skull of †*P. lemoinei* to score cranial characters for our †*Palaeothentes* terminal. †*Palaeothentes* is the type genus of the family †Palaeothentidae, which is a member of the superfamily †Palaeothentoidea (Abello, 2007, 2013; Goin et al., 2009a; Rincón et al., 2015; Engelman et al., 2016; Abello et al., 2020).

†*Acdestis*

SPECIES SCORED: †*Acdestis maddeni*, †*A. owenii* (type species), †*A. spegazzinii*.

GEOLOGICAL PROVENANCE OF SCORED SPECIMENS: "Nivel I–II" of the Río Rosario Local Fauna and Willajara locality, and "Nivel I" of the Quebrada Honda Local Fauna, both part of the Honda Group, Tarija Department, Bolivia (†*A. maddeni*); Santa Cruz Formation, Santa Cruz Province, Argentina (†*A. owenii* and †*A. spegazzinii*).

AGE OF SCORED SPECIMENS: The Río Rosario and Quebrada Honda Local Faunas both belong to the Honda Group and are collectively estimated to span 12.5–13.0 Mya (late middle Miocene) based on radiometric and magnetostratigraphic data (MacFadden et al., 1990). The Santa Cruz Formation spans a maximum of 14–19 Mya (see †*Stilotherium* above).

ASSIGNED AGE RANGE: 19.000–12.500 Mya.

REMARKS: Goin et al. (2003) described the fossil paucituberculatan †*Acdestis maddeni* based on a partial cranium (MNHN-Pal-Bol-V-004000) that includes a well-preserved basicranium, and an additional partial maxilla (MNHN-Pal-Bol-V-003689), both from middle Miocene (11.9–15.4 Mya) deposits in southernmost Bolivia. We used this material to obtain most of the character scores for our †*Acdestis* terminal, but a number of dental characters (particularly those of the lower dentition, which is not preserved in known remains of †*A. maddeni*) were scored from specimens of †*A. owenii* (the type species) and †*A. spegazzinii*, both of which are known from abun-

dant albeit fragmentary dental material from the Santa Cruz Formation (Marshall, 1980; Bown and Fleagle, 1993; Rae et al., 1996; Abello, 2007; Engelman and Croft, 2016). Engelman and Croft (2016) concluded that †*Acdestis owenii* probably represents males, and the somewhat smaller and more gracile †*A. spegazzinii* represents females, of a single taxon (for which the name †*A. owenii* would have priority), but this inference was disputed by Abello et al. (2020: supplemental material).

†*Acdestis* is currently classified as a member of the family †Palaeothentidae, within the superfamily †Palaeothentoidea (Abello, 2007, 2013; Goin et al., 2009a; Rincón et al., 2015; Engelman et al., 2016; Abello et al., 2020).

†*Microbiotherium*

Species Scored: †*Microbiotherium tehuelchum*.

Geological Provenance of Scored Specimens: Santa Cruz Formation, Santa Cruz Province, Argentina.

Age of Scored Specimens: The Santa Cruz Formation spans a maximum of 14–19 Mya (see account for †*Stilotherium*, above).

Assigned Age Range: 19.000–14.000 Mya.

Remarks: †*Microbiotherium tehuelchum* is the only fossil microbiotheriid currently known from anything other than isolated dental remains (Segall, 1969; Marshall, 1982). Of particular importance is a partial auditory region (PU 15038) that exhibits a number of distinctive cranial features that are seen only in *Dromiciops* among living marsupials (Segall, 1969). We scored our †*Microbiotherium* terminal based solely on specimens of †*M. tehuelchum* from the Santa Cruz Formation (Segall, 1969; Marshall, 1982). However, material from the ?middle Miocene (Friasian SALMA) Río Frias Formation in Chile (Marshall, 1990) and the early Miocene Pinturas Formation in Argentina (Bown and Fleagle, 1994; Chornogubsky and Kramarz, 2012) has also been referred to †*M. tehuelchum*. Goin and Abello (2013) presented a phylogenetic

analysis of Microbiotheriidae, including †*M. tehuelchum*, based on 20 dental characters.

†*Badjcinus*

Species Scored: †*Badjcinus turnbulli* (type and only described species).

Geological Provenance of Scored Specimens: White Hunter Site (Riversleigh Faunal Zone A), Riversleigh World Heritage Area, Queensland, Australia.

Age of Scored Specimens: Riversleigh Faunal Zone A is currently interpreted to be late Oligocene based on biostratigraphy (Archer et al., 1989, 1994, 1995, 1997, 2006; Creaser, 1997; Myers and Archer, 1997; Travouillon et al., 2006; Black, 2010; Black et al., 2012b, 2013; Woodhead et al., 2014; Arena et al., 2015). Specifically, Myers and Archer (1997) correlated it with the Ngama Local Fauna, which occurs in Zone D of the Etadunna Formation at Mammalon Hill, South Australia, based on the shared presence of the ilariid †*Kuterintja ngama*. Based on palaeomagnetic data presented by Woodburne et al. (1994), Metzger and Retallack (2010) estimated the Etadunna Formation to span 26.1–23.6 Mya, so a similar age range for Riversleigh Faunal Zone A seems plausible. However, pending the publication of absolute dates, a more conservative approach is to use the entire range of the late Oligocene (Chattian; Cohen et al., 2013 [updated]) for this taxon.

Assigned Age Range: 27.820–23.030 Mya.

Remarks: †*Badjcinus turnbulli* is the oldest fossil dasyuromorphian represented by relatively well-preserved craniodental material. It is currently known from a single partial cranium that includes a well-preserved auditory region (QM F30408) and additional dental specimens (Muirhead and Wroe, 1998). †*Badjcinus turnbulli* differs from all other known dasyuromorphians in lacking both a squamosal epitympanic sinus and a distinct rostral tympanic process of the petrosal, although there is some debate as to whether these features are plesiomorphic or apomorphic (Muirhead and Wroe, 1998; Murray and Megirian, 2006a).

Muirhead and Wroe (1998) identified †*Badjcinus* as a thylacinid, and thylacinid affinities for this taxon have been supported in most phylogenetic analyses (Wroe and Musser, 2001; Murray and Megirian, 2006a; Yates, 2014, 2015b; Archer et al., 2016; Kealy and Beck, 2017; Rovinsky et al., 2019). However, the craniodental analysis of Wroe et al. (2000) placed †*Badjcinus* closer to Dasyuridae than to *Thylacinus*, and the dated total evidence analyses of Kealy and Beck (2017) recovered †*Badjcinus* as sister to all other dasyuromorphians, and hence outside the crown clade (Dasyuroidea sensu Kealy and Beck, 2017: table 1). We therefore follow Kealy and Beck (2017) as classifying †*Badjcinus* as ?Thylacinidae.

†*Mutpuracinus*

SPECIES SCORED: †*Mutpuracinus archibaldi* (type and only described species).

GEOLOGICAL PROVENANCE OF SCORED SPECIMENS: Bullock Creek Local Fauna, Camfield Beds, Northern Territory, Australia; Jaw Junction Site (Riversleigh Faunal Zone D), Riversleigh World Heritage Area, Queensland, Australia.

AGE OF SCORED SPECIMENS: based on biostratigraphy, the Bullock Creek Local Fauna is interpreted to be middle Miocene (Murray and Megirian, 1992; Megirian et al., 2010; Black et al., 2013; Schwartz, 2016; Trusler and Sharp, 2016), whereas Riversleigh Faunal Zone D is considered to be somewhat younger, namely early late Miocene, perhaps 10–12 Mya (Archer et al., 1989, 1994, 1995; Myers et al., 2001; Black et al., 2012b, 2013; Woodhead et al., 2014; Arena et al., 2015). In the absence of direct dates, we have conservatively assumed the entire span of the middle to late Miocene (Langhian to Messinian; Cohen et al., 2013 [updated]) for this taxon.

ASSIGNED AGE RANGE: 15.970–5.333 Mya.

REMARKS: †*Mutpuracinus archibaldi* was originally described by Murray and Megirian (2000) based on fragmentary craniodental material from the Bullock Creek Local Fauna. Subsequently, a relatively complete, albeit somewhat disarticulated, skull (NTM P91168-5) was recovered from the Jaw Junction Site at Riversleigh (Murray and Megirian, 2006a). Murray and Megirian (2000, 2006a) identified †*Mutpuracinus* as a thylacinid, but its position was unstable in their phylogenetic analyses (Murray and Megirian, 2006a: appendix 2, figs. 2–4); notably, it was recovered as closer to Recent dasyurids than to thylacinids when added to the craniodental character matrix of Wroe and Musser (2001; see Murray and Megirian, 2006a: appendix 2 fig. 2B). The phylogenetic analyses of Archer et al. (2016), Kealy and Beck (2017), and Rovinsky et al. (2019) also did not support thylacinid affinities for †*Mutpuracinus*, and we follow the last two studies in considering this taxon to be Dasyuromorphia *incertae sedis*. Regardless of its true phylogenetic relationships, the craniodental morphology of †*Mutpuracinus* implies previously unsuspected dasyuromorphian homoplasy in either the dentition or auditory region, or both (Murray and Megirian, 2006a).

†*Nimbacinus*

SPECIES SCORED: †*Nimbacinus dicksoni* (type species).

GEOLOGICAL PROVENANCE OF SCORED SPECIMENS: AL90 and Henk's Hollow sites (Riversleigh Faunal Zone C), Riversleigh World Heritage Area, Queensland, Australia.

AGE OF SCORED SPECIMENS: Riversleigh Faunal Zone C is interpreted to be middle Miocene based on biostratigraphy (Archer et al., 1989, 1994, 1995, 1997, 2006; Creaser, 1997;; Travouillon et al., 2006; Black et al., 2012b, 2013; Woodhead et al., 2014; Arena et al., 2015). AL90 site has been radiometrically dated as 14.17–15.11 Mya (Woodhead et al., 2014), but such dates are currently unavailable for Henk's Hollow site, so we conservatively assume the entire span of the middle Miocene (Langhian-Serravallian; Cohen et al., 2013 [updated]) for this taxon.

ASSIGNED AGE RANGE: 15.970–11.630 Mya.

REMARKS: †*Nimbacinus dicksoni* was originally described by Muirhead and Archer (1990) based on fragmentary dental material, most of it

from the Riversleigh Henk's Hollow site. Subsequently, a nearly complete cranium and associated mandibles (QM F36357) from the Riversleigh AL90 site were described by Wroe and Musser (2001); this specimen also includes an associated skeleton (Long et al., 2002: 61), which remains undescribed. Muirhead and Archer (1990) also identified a broken m2 from D Site at Riversleigh (Faunal Zone A, probably late Oligocene; see †*Badjcinus* above) and a partial right mandible from the Bullock Creek Local Fauna (probably middle Miocene; see †*Mutpuracinus* above) in the Northern Territory as representing †*N. dicksoni*. Subsequently, Murray and Megirian (2000) referred the Bullock Creek specimen mentioned by Muirhead and Archer (1990) to a new species, †*N. richi*, together with several additional Bullock Creek thylacinid specimens. Murray and Megirian (2000) also suggested that the D Site specimen represents a third distinct taxon. Wroe and Musser (2001) agreed with Murray and Megirian (2000) that the D Site specimen is probably not †*N. dicksoni*, but they questioned whether †*N. richi* should be recognized as a distinct species. Most recently, Rovinsky et al. (2019) concluded that †*N. richi* is probably synonymous with †*N. dicksoni*, and considered the D Site specimen referred to *N. dicksoni* by Muirhead and Archer (1990) to be Thylacinidae incertae sedis. Only specimens of †*N. dicksoni* from the Riversleigh Henk's Hollow and AL90 sites have been used for scoring purposes here.

Published phylogenetic analyses consistently support thylacinid affinities for †*Nimbacinus* (Wroe and Musser, 2001; Murray and Megirian, 2006a; Yates, 2014, 2015b; Archer et al., 2016; Kealy and Beck, 2017; Rovinsky et al., 2019).

†*Barinya*

Species Scored: †*Barinya wangala* (type species).

Geological Provenance of Scored Specimens: Neville's Garden, Bite's Antennary and Upper sites (Riversleigh Faunal Zone B), and Henk's Hollow and Jim's Jaw sites (Riversleigh Faunal Zone C), Riversleigh World Heritage Area, Queensland, Australia.

Age of Scored Specimens: Based on biostratigraphy, Riversleigh Faunal Zone B is interpreted to be early Miocene (Archer et al., 1989, 1994, 1995, 1997, 2006; Creaser, 1997; Travouillon et al., 2006; Black et al., 2012b, 2013; Woodhead et al., 2014; Arena et al., 2015), and Faunal Zone C is interpreted to be middle Miocene (see †*Nimbacinus* above). Radiometric dates from Woodhead et al. (2014) are 17.72–18.53 Mya for Neville's Garden Site and 16.84–17.38 Mya for Bite's Antennary Site, but the other sites lack dates, so we have conservatively assumed the entire span of the early to middle Miocene (Aquitanian to Serravallian; Cohen et al., 2013 [updated]) for this taxon.

Assigned Age Range: 23.030–11.630 Mya.

Remarks: Wroe (1999) described †*Barinya wangala* as the oldest known dasyurid based on two relatively complete skulls (QM F31408 and F314089) plus additional dental specimens. Wroe (1999) identified a number of putative dasyurid apomorphies in the auditory region, but Murray and Megirian (2006a) subsequently argued that at least some of these features may have been secondarily lost in thylacinids. Among dasyuromorphians, †*B. wangala* is dentally autapomorphic in exhibiting a very large bulbous P3, somewhat reminiscent of the enlarged P3 seen in males of some Recent peramelemorphians (see Aplin et al., 2010: 26–31). A second species, †*B. kutjamarpensis*, was described by Binfield et al. (2016), based on a single partial right dentary (SAM P53348) from the the ?early-middle Miocene Leaf Locality of the Kutjamarpu Local Fauna in the Wipajiri Formation, Lake Ngapakaldi, Tirari Desert, Lake Eyre Basin, South Australia (Woodburne et al., 1994; Archer et al., 1997; Travouillon et al., 2006; Megirian et al., 2010; Black et al., 2012b, 2013, 2014a; Gurovich et al., 2014); however, †*B. kutjamarpensis* has not been used for scoring purposes here.

†*Barinya* was recovered as a dasyurid in the phylogenetic analyses of Wroe et al. (2000), Wroe

and Musser (2001), and Murray and Megirian (2006a), but not in those of Archer et al. (2016) or Kealy and Beck (2017), and in only some of those by Rovinsky et al. (2019); we therefore follow Kealy and Beck (2017) in considering this taxon Daysuromorphia incertae sedis.

†*Bulungu*

SPECIES SCORED: †*Bulungu palara* (type species).

GEOLOGICAL PROVENANCE OF SCORED SPECIMENS: Lee Sye's Outlook (LSO) Site (Riversleigh Faunal Zone A), Boid Site East, Camel Sputum, Dirk's Towers, Inabeyance, Judith's Horizontalis, Mike's Potato Patch, Neville's Garden, Outasite, Price Is Right, Quantum Leap, Rat Vomit, RSO, Upper, and Wayne's Wok sites (Riversleigh Faunal Zone B); and AL90, Gag, Gotham City, Henk's Hollow, Rick's Sausage, Ringtail, Two Trees, and Wang sites (Riversleigh Faunal Zone C), Riversleigh World Heritage Area, Queensland, Australia.

AGE OF SCORED SPECIMENS: Riversleigh Faunal zones A, B, and C are interpreted to be late Oligocene, early Miocene, and middle Miocene, respectively, based on biostratigraphy (see previous accounts above). Radiometric dates from Woodhead et al. (Woodhead et al., 2014) are 16.97–18.53 Mya for Camel Sputum Site, 17.72–18.53 Mya for Neville's Garden Site, 17.76–18.26 Mya for Outasite, 16.24–16.86 Mya for RSO Site, 14.17–15.11 Mya for AL90 Site, and 14.23–12.89 Mya for Ringtail Site, but the other sites lack dates, so we have conservatively assumed the entire span of the late Oligocene to middle Miocene (Chattian to Serravallian; Cohen et al., 2013 [updated]) for this taxon.

ASSIGNED AGE RANGE: 27.820–11.630 Mya.

REMARKS: Gurovich et al. (2014) described a single well-preserved skull of †*Bulungu palara* (QM F23437) from Upper Site at Riversleigh and they also referred additional fragmentary specimens from multiple other sites spanning Riversleigh Faunal zones A, B, and C to this taxon. Gurovich et al. (2014) additionally referred two specimens from the ?early-middle Miocene Leaf Locality of the Kutjamarpu Local Fauna in the Wipajiri Formation of South Australia (see †*Barinya* above) to †*B. palara*, but we did not examine these for scoring character data. Travouillon et al. (2013a) described an additional two species of †*Bulungu* from the Etadunna Formation of South Australia (†*B. muirheadae*, from the Ditjimanka Local Fauna, and †*B. campbelli*, from the Ngapakaldi Local Fauna), which we likewise did not use for scoring characters. Based on QM F23437, †*B. palara* differs from all Recent peramelemorphians in exhibiting a number of putatively plesiomorphic craniodental features, such as alisphenoid-parietal (rather than frontal-squamosal) contact on the lateral wall of the braincase, and nasals that extend posteriorly beyond the anterior margin of the orbits (Gurovich et al., 2014). It consistently falls outside the peramelemorphian crown-clade (= Perameloidea) in published phylogenetic analyses (Travouillon et al., 2013a, 2014a, 2015b, 2017, 2019; Gurovich et al., 2014; Chamberlain et al., 2015; Kear et al., 2016; Travouillon and Phillips, 2018).

†*Galadi*

SPECIES SCORED: †*Galadi speciosus* (type species).

GEOLOGICAL PROVENANCE OF SCORED SPECIMENS: Boid, Camel Sputum, Judith's Horizontalis, Microsite, Mike's Menagerie, Neville's Garden, Quantum Leap, Upper, and Wayne's Wok sites (Riversleigh Faunal Zone B), Riversleigh World Heritage Area, Queensland, Australia.

AGE OF SCORED SPECIMENS: Riversleigh Faunal Zone B is interpreted to be early Miocene based on biostratigraphy (see above); radiometric dates from Woodhead et al. (2014) are 16.97–18.53 Mya for Camel Sputum Site and 17.72–18.53 Mya for Neville's Garden Site, but the other sites lack dates, so we have conservatively assumed the entire span of the early Miocene (Aquitanian to Burdigalian; Cohen et al., 2013 [updated]) for this taxon.

ASSIGNED AGE RANGE: 23.030–15.970 Mya.

Remarks: †*Galadi speciosus* was described by Travouillon et al. (2010) based on well-preserved craniodental specimens (notably the holotype, QM F23393, an almost perfect cranium and associated partial dentaries) from Riversleigh Faunal zones A and B. Later, a three further species (†*G. adversus*, †*G. amplus*, and †*G. grandis*) were described from Riversleigh Faunal zones B and C (Travouillon et al., 2013b), but we did not use these to score character data for this study. Like †*Bulungu*, †*Galadi* appears to be craniodentally more plesiomorphic than Recent peramelemorphians, and it has been recovered outside the peramelemorphian crown clade in published phylogenetic analyses (Travouillon et al., 2010, 2013a, 2013b, 2014a, 2105b, 2017, 2019; Gurovich et al., 2014; Chamberlain et al., 2015; Kear et al., 2016; Travouillon and Phillips, 2018). The proportionally brevirostral skull of †*G. speciosus* also suggests that it may have fed on larger prey items than do modern peramelemorphians (Travouillon et al., 2010).

†*Yarala*

Species Scored: †*Yarala burchfieldi* (type species).

Geological Provenance of Scored Specimens: Camel Sputum and Upper sites (Riversleigh Faunal Zone B), Riversleigh World Heritage Area, Queensland, Australia.

Age of Scored Specimens: Riversleigh Faunal Zone B is interpreted to be early Miocene based on biostratigraphy (see above). Camel Sputum Site has been radiometrically as 16.97–18.53 Mya (Woodhead et al., 2014), but a radiometric date is unavailable for Upper Site, so we have used the entire range of the early Miocene (Aquitanian to Burdigalian; Cohen et al., 2013 [updated]) for this taxon.

Assigned Age Range: 23.030–15.970 Mya.

Remarks: †*Yarala burchfieldi* was the first fossil peramelemorphian to be known from relatively well-preserved cranial material (Muirhead, 2000). Like †*Bulungu* and †*Galadi*, it appears to be markedly more plesiomorphic than Recent peramelemorphians (Muirhead and Filan, 1995; Muirhead, 2000), and it consistently falls outside the peramelemorphian crown clade in published phylogenetic analyses (Travouillon et al., 2010, 2013a, 2013b, 2014a, 2017, 2019; Gurovich et al., 2014; Chamberlain et al., 2015; Kear et al., 2016; Travouillon and Phillips, 2018). †*Yarala burchfieldi* is also notable in that it is the smallest peramelemorphian known, either living or extinct, with an estimated body mass of about 65 g (Travouillon et al., 2009, 2010). Two further †*Yarala* species— †*Y. kida* and an as yet unnamed taxon—have been identified based on fragmentary dental material from the late Oligocene or early Miocene Kangaroo Well Local Fauna in the Northern Territory of Australia (Schwartz, 2006b; 2016), but we did not use it to score character data for this study.

†*Litokoala*

Species Scored: †*Litokoala kutjamarpensis* (type species), †*L. dicksmithi*.

Geological Provenance of Scored Specimens: UCR Locality RV-8453 (Kanunka North Local Fauna), Etadunna Formation, Lake Kanunka, South Australia, Australia (†*L. kutjamarpensis*); Jim's Carousel, Henk's Hollow, Dwornamor, and Gotham sites (Riversleigh Faunal Zone C), Riversleigh World Heritage Area, Queensland, Australia (†*L. kutjamarpensis*); Ross Scott-Orr Site (Riversleigh Faunal Zone B), Riversleigh World Heritage Area, Queensland, Australia (†*L. dicksmithi*).

Age of Scored Specimens: Based on the paleomagnetic data of Woodburne et al. (1994), Metzger and Retallack (2010) estimated the Etadunna Formation to span 26.1–23.6 Mya. Riversleigh Faunal Zone B and C are interpreted to be early and middle Miocene, respectively, based on biostratigraphy (see above), but only Ross Scott-Orr (RSO) Site has a radiometric date, of 16.24–16.86 Mya (Woodhead et al., 2014). We conservatively assign an age range of the entire late Oligocene to middle Miocene (Chattian to Serravalian; Cohen et al., 2013 [updated]) for this taxon.

Assigned Age Range: 27.820–11.630 Mya.

Remarks: †*Litokoala* is one of only two fossil phascolarctids known from relatively complete craniodental material (Louys et al., 2009; Black et al., 2014a), but its taxonomic history is complex and remains controversial. †*Litokoala kutjamarpensis* was described by Stirton et al. (1967a) based on a single M1 from the Kutjamarpu Local Fauna, Wipajiri Formation, Lake Ngapakaldi, South Australia. Springer (1987) then described a second species, †*L. kanunkaensis*, based on two isolated lower molars and two partial upper molars from the Kanunka North Local Fauna, Etadunna Formation, Lake Kanunka, South Australia. Black and Archer (1997b) subsequently referred several phascolarctid dental specimens from a number of Riversleigh Faunal Zone C sites to †*L. kanunkaensis*. However, based on study of the dentition of a new, well-preserved partial cranium (QM F51382) from the Riversleigh Faunal Zone C JC Site, Louys et al. (2007) concluded that †*L. kanunkaensis* is a junior synonym of †*L. kutjamarpensis*. Louys et al. (2007) also named a new species, †*L. garyjohnstoni*, based on a partial maxilla and isolated M4 from the Riversleigh Faunal Zone B Outasite Site. Louys et al. (2009) subsequently gave a detailed description of the cranial morphology of QM F51382, which they maintained represents †*L. kutjamarpensis*.

Pledge (2010), however, retained †*L. kanunkaensis* as a separate species for the isolated molars from the Kanunka North Local Fauna described by Springer (1987), referred the Riversleigh Faunal Zone C specimens (including QM F51382) to a new species, †*L. dicktedfordi*, and named a further species, †*L. thurmerae*, based on an isolated M3 from the ?late Oligocene Ngama Local Fauna, Lake Palankarinna, South Australia. Thus, Pledge (2010) recognized five species: †*L. kutjamarpensis* (Kutjamarpu Local Fauna; ?early or middle Miocene), †*L. kanunkaensis* (Kanunka North Local Fauna; ?late Oligocene), †*L. garyjohnstoni* (Riversleigh Faunal Zone B; ?early Miocene), †*L. dicktedfordi* (Riversleigh Faunal Zone C; ?middle Miocene),

and †*L. thurmerae* (Ngama Local Fauna; ?late Oligocene). Most recently, Black et al. (2014a, 2014b) reaffirmed that †*L. kanunkaensis* (including the Riversleigh Faunal Zone C species referred to †*L. dicktedfordi* by Pledge, 2010) is a junior synonym of †*L. kutjamarpensis*, considered †*L. thurmerae* to be a nomen dubium, and named yet another new species, †*L. dicksmithi*, based on a well-preserved rostral fragment (QM F54567). Here we follow the taxonomy of Louys et al. (2007, 2009) and Black et al. (2014a, 2014b), who recognized only two species within the genus: the type species, †*Litokoala kutjamarpensis*, and †*L. dicksmithi*.

We scored our †*Litokoala* terminal based on specimens of †*L. kutjamarpensis* from both the Kanunka North Local Fauna and Riversleigh Faunal Zone C sites, and also on the only known specimen (QM F54567) of †*L. dicksmithi*. Based on this material, †*Litokoala* appears to have lacked masticatory specializations seen in *Phascolarctos* (Louys et al., 2009). In addition, estimated body masses for †*Litokoala* species (2.4–4.6 kg; Black et al., 2014a; 2014b) are considerably less than those of *P. cinereus* (4.1–13.5 kg; Martin et al., 2008). Nevertheless, phylogenetic analyses of vombatiform relationships based on 71 craniodental characters by Black et al. (2012a) supported a sister-group relationship between †*Litokoala* and *Phascolarctos* to the exclusion of the other currently named fossil phascolarctid genera, and Beck et al. (2020 fig. 5) found †*Litokoala* to be paraphyletic with respect to *Phascolarctos*, with †*L. kutjamarpensis* and *Phascolarctos* forming a clade to the exclusion of †*L. dicksmithi*. However, an undescribed new genus and species of phascolarctid from the Riversleigh Faunal Zone D Encore Site, previously identified as *Phascolarctos* sp. by Myers et al. (2001), may be more closely related to the living genus than is †*Litokoala* (Black et al., 2014b).

†*Nimiokoala*

Species Scored: †*Nimiokoala greystanei* (type and only described species).

Geological Provenance of Scored Specimens: Boid Site East (BSE) (Riversleigh Faunal Zone A or B), Riversleigh World Heritage Area, Queensland, Australia; Camel Sputum, Inabeyance, Neville's Garden, Rat Vomit, Dirk's Towers, and Upper sites (Riversleigh Faunal Zone B), Riversleigh World Heritage Area, Queensland, Australia.

Age of Scored Specimens: Arena et al. (2015) concluded that Boid Site East (BSE) was either Riversleigh Faunal Zone A or B; all other †*N. greystanei* specimens used here are from Riversleigh Faunal Zone B sites (Arena et al., 2015; Travouillon et al., 2006; Woodhead et al., 2014). Based on biostratigraphy, Riversleigh Faunal Zone A is interpreted to be late Oligocene, and Riversleigh Faunal Zone B is interpreted to be early Miocene (see above).

Assigned Age Range: 27.820–15.970 Mya.

Remarks: †*Nimiokoala greystanei* is the second fossil phascolarctid for which relatively well-preserved craniodental material is available, namely a partial cranium (QM F30483) that was described in detail by Louys et al. (2009). Black and Archer (1997b) described the dentition of †*N. greystanei*, based on QM F30483 and several other, less complete specimens. QM F30483 is from Boid Site East (BSE), which is part of Riversleigh Faunal Zone A or B (Arena et al., 2015; Travouillon et al., 2006; Woodhead et al., 2014), whereas the remaining specimens are from Faunal Zone B sites. Like †*Litokoala* (see above), †*N. greystanei* was smaller (estimated body mass of 2.6–4.1 kg; Black et al., 2014b) and appears to have had a less derived masticatory system (Louys et al., 2009) than the Recent koala *Phascolarctos cinereus*. In the phylogenetic analyses of Black et al. (2012a) and Beck et al. (2020), †*Nimiokoala* was recovered as sister to a clade that included *Phascolarctos* and †*Litokoala*.

†*Warendja*

Species Scored: †*Warendja wakefieldi* (type species).

Geological Provenance of Scored Specimens: McEacherns Cave, Victoria, Australia; Comaum Forest Cave, South Australia, Australia; Wombeyan Caves, New South Wales, Australia.

Age of Scored Specimens: The deposits containing specimens of †*Warendja wakefieldi* at McEacherns Cave, Comaum Forest Cave, and Wombeyan Caves are all estimated to be Pleistocene based on faunal composition (Hope and Wilkinson, 1982; Lundelius, 1983; Flannery and Pledge, 1987). We have assigned an age range of the entire Pleistocene (Cohen et al., 2013 [updated]) to this terminal.

Assigned Age Range: 2.580–0.012 Mya.

Remarks: †*Warendja wakefieldi* was originally described based on two mandibles and six isolated teeth from McEacherns Cave, Victoria (Hope and Wilkinson, 1982). These specimens preserve characteristic vombatid apomorphies, most notably open-rooted (hypselodont) molars, but nevertheless appear distinctly more plesiomorphic than those of other known vombatids. Additional cranial material and teeth were subsequently recovered from Comaum Forest Cave, South Australia (Flannery and Pledge, 1987; Pledge, 1992), enabling reconstruction of a partial cranium (Pledge, 1992). Based on these specimens, the cranial morphology of †*W. wakefieldi* appears markedly more gracile than that of living vombatids (Pledge, 1992; Murray, 1998). Brewer (2007) described additional specimens of †*W. wakefieldi* from Wombeyan Caves, New South Wales, and we used her description to score some characters for this terminal. Brewer et al. (2007) described another species (†*W. encorensis*) based on fragmentary dental remains from the Riversleigh Faunal Zone D (?late Miocene) Encore Site at Riversleigh, but we did not use those specimens for scoring purposes.

†*Neohelos*

Species Scored: †*Neohelos stirtoni*.

Geological Provenance of Scored Specimens: Bullock Creek Local Fauna, Camfield Beds, Northern Territory, Australia.

AGE OF SCORED SPECIMENS: the Bullock Creek Local Fauna is interpreted to be middle Miocene based on biostratigraphy (see †*Mutpuracinus* above).

ASSIGNED AGE RANGE: 15.970–11.630 Mya.

REMARKS: The diprotodontid †*Neohelos stirtoni* is represented by multiple well-preserved individuals, including juveniles, from the Bullock Creek Local Fauna (Murray et al., 2000a, 200b). Black (2008) and Black et al. (2013) reported the presence of †*N. stirtoni* in a number of Riversleigh Fanal Zone C sites, but this material is considerably less complete, and only Bullock Creek specimens have been used for scoring purposes here. †*Neohelos* is usually considered to be a member of the diprotodontid subfamily †Zygomaturinae (e.g., Stirton et al., 1967b; Black and Mackness, 1999; Murray et al., 2000a, 2000b; Black et al., 2013). However, the traditional subdivision of †Diprotodontidae into †Zygomaturinae and †Diprotodontinae is primarily based on features of P3 morphology that now appear to be more variable than previously suspected (Murray et al., 2000b; Price, 2008; Black and Hand, 2010; Price and Sobbe, 2011; Black et al., 2013).

†*Ngapakaldia*

SPECIES SCORED: †*Ngapakaldia tedfordi* (type species), †*N. bonythoni*; †*Ngapakaldia* sp.

GEOLOGICAL PROVENANCE OF SCORED SPECIMENS: Ngapakaldi Local Fauna, Etadunna Formation, Lake Ngapakaldi, South Australia, Australia (†*Ngapakaldia bonythoni*, †*N. tedfordi*, and †*Ngapakaldia* sp.); AL Site, D Site, Hiatus, Hiatus South, Jeanette's Amphitheatre, Lee Sye's Outlook (LSO), Sticky Beak, Upper Burnt Offering, and White Hunter sites (Riversleigh Faunal Zone A), and Bone Reef, Camel Sputum, Dirk's Towers, Dunsinane, and Mike's Potato Patch sites (Riversleigh Faunal Zone B), Riversleigh World Heritage Area, Queensland Australia (†*N. bonythoni*).

AGES OF SCORED SPECIMENS: Based on palaeomagnetic data, Metzger and Retallack (2010) estimated the Etadunna Formation to span 26.1–23.6 Mya. Riversleigh Faunal zones A and B are interpreted as late Oligocene and early Miocene, respectively, based on biostratigraphy (see above).

ASSIGNED AGE RANGE: 27.820–15.970 Mya.

REMARKS: In his original description of †*Ngapakaldia tedfordi* and †*N. bonythoni*, Stirton (1967) suggested a close relationship between these taxa and †*Palorchestes*, placing them together in the diprotodontid subfamily †Palorchestinae. More recent studies (e.g., Murray, 1990; Black and Archer, 1997a; Black, 2010) have suggested that †*Ngapakaldia* is more appropriately placed in the subfamily †Diprotodontinae and that the similarities between †*Ngapakaldia* and †*Palorchestes* (now usually placed in a separate family, †Palorchestidae) are plesiomorphies. Both †*N. tedfordi* and †*N. bonythoni* were originally described based on material from the †Ngapakaldi Local Fauna (Faunal Zone C of the Etadunna Formation; Stirton, 1967; Woodburne et al., 1994), but Black (2010) referred additional specimens from Riversleigh Faunal zones A and B to †*N. bonythoni*. We used Ngapakaldi specimens of †*N. tedfordi*, and Ngapakaldi and Riversleigh specimens of †*N. bonythoni*, to score a composite †*Ngapakaldia* terminal. Rich and Vicker-Rich (1987) listed additional fragmentary specimens of both species from various sites in the Etadunna and Namba formations, but we did not use this material for scoring purposes.

†*Nimbadon*

SPECIES SCORED: †*Nimbadon lavarackorum* (type and only described species).

GEOLOGICAL PROVENANCE OF SCORED SPECIMENS: AL90 Site (Riversleigh Faunal Zone C), Riversleigh World Heritage Area, Queensland, Australia.

AGE OF SCORED SPECIMENS: The AL90 Site is considered to be part of Riversleigh Faunal Zone C, which is interpreted to be middle Miocene based on biostratigraphy (see above). Radiometric dates for the AL90 Site span 14.17–15.11 Mya.

ASSIGNED AGE RANGE: 15.110–14.170 Mya.

Remarks: †*Nimbadon lavarackorum* is represented by a remarkable series of well-preserved individuals from the AL90 Site at Riversleigh, which have been used for scoring purposes here, plus additional less-well-preserved specimens from other Riversleigh Faunal Zone C sites that were not scored (Hand et al., 1993; Black, 2008; Black et al., 2010; Black and Hand, 2010). The AL90 specimens range in ontogenetic stage from pouch young to old adults, represent both putative males and females, and include multiple intact skulls (Hand et al., 1993; Black, 2008; Black et al., 2010; Black and Hand, 2010). †*Nimbadon* is currently placed within the diprotodontid subfamily †Zygomaturinae based largely on P3 morphology (Hand et al., 1993; Murray et al., 2000b; Black, 2008; Black et al., 2010; Black and Hand, 2010).

†*Silvabestius*

Species Scored: †*Silvabestius johnnilandi* (type species), †*S. michaelbirti.*

Geological Provenance of Scored Specimens: Hiatus South Site (Riversleigh Faunal Zone A) and VIP Site (Riversleigh Faunal Zone A or B), Riversleigh World Heritage Area, Queensland, Australia.

Age of Specimens Scored: Riversleigh Faunal zones A and B are interpreted as late Oligocene and early Miocene respectively, based on biostratigraphy (see above). We have assigned the entire age range of the late Oligocene to early Miocene (Chattian to Burdigalian; Cohen et al., 2013 [updated]) for this taxon.

Assigned Age Range: 27.820–15.970 Mya.

Remarks: Two species, †*Silvabestius johnnilandi* and †*S. michaelbirti*, were described by Black and Archer (1997a) based on specimens from the VIP and Hiatus South sites. The VIP Site has been identified as part of Riversleigh Faunal Zone A, but may in fact belong to Faunal Zone B (K.H. Black, personal commun.). Both species are represented by relatively complete cranial material (e.g., the holotype of †*S.*

jonhnnilandi is a well-preserved juvenile skull), but only dental descriptions of these specimens have been formally published to date (Black and Archer, 1997a); however, the unpublished thesis of Black (2008) includes cranial descriptions. We used this Riversleigh material of both species to score a composite †*Silvabestius* terminal.

†*Lekanoleo*

Species Scored: †*Lekanoleo roskellyae* (type and only described species).

Geological Provenance of Scored Specimens: White Hunter site (Riversleigh Faunal Zone A), and Upper, Dirk's Towers, and Camel Sputum sites (Riversleigh Faunal Zone B), Riversleigh World Heritage Area, Queensland, Australia.

Age of Scored Specimens: Riversleigh Faunal zones A and B are interpreted to be late Oligocene and early Miocene respectively, based on biostratigraphy (see above). We have assigned the entire age range of the late Oligocene to early Miocene (Chattian to Serravallian; Cohen et al., 2013 [updated]).

Assigned Age Range: 27.820–15.970 Mya.

Remarks: †*Lekanoleo roskellyae* is one of the oldest thylacoleonids known from relatively complete craniodental material, with a single well-preserved cranium (QM F23453) collected from Upper Site in Riversleigh Faunal Zone B, and additional craniodental fragments known from sites in Riversleigh Faunal zones A and B (Gillespie, 1997, 2007; Gillespie et al., 2020). In her original description, which was of the upper dentition of QM F23453 only, Gillespie (1997) referred this taxon to the existing genus †*Priscileo*. More recently, Gillespie et al. (2020) described the cranial morphology of QM F23453, provided additional information on the dentition, and referred this taxon to a new genus, †*Lekanoleo*. †*Lekanoleo roskellyae* is notable for its small size relative to most other known thylacoleonids, with an estimated body mass of 1.8 kg based on dental

measurements (Gillespie et al., 2016) and 2.7–3.1 kg based on skull length (Gillespie et al., 2020); however, †*Microleo attenboroughi*, from the early Miocene (Riversleigh Faunal Zone B) Neville's Garden site at Riverseigh, which is known from much less complete remains, and so has not been included in this study, is even smaller, with an estimated body mass of 590 g based on dental measurements (Gillespie et al., 2016).

†*Thylacoleo*

Species Scored: †*Thylacoleo carnifex* (type species).

Geological Provenance of Scored Specimens: Multiple Pleistocene sites in South Australia.

Age of Scored Specimens: Pleistocene.

Assigned Age Range: 2.580–0.012 Mya.

Remarks: †*Thylacoleo carnifex* was the largest (with some individuals possibly >100 kg; Wroe et al., 1999; 2003; Richards et al., 2019), morphologically most specialized, and last surviving thylacoleonid (Gillespie, 1999; Long et al., 2002; Gillespie, 2007). It is known from abundant craniodental and postcranial material from various Pleistocene deposits around Australia (Gillespie, 2007).

†*Wakaleo*

Species Scored: †*Wakaleo vanderleueri* (type species).

Geological Provenance of Scored Specimens: Bullock Creek Local Fauna, Northern Territory; Encore site (Riversleigh Faunal Zone D), Riversleigh World Heritage Area, Queensland, Australia.

Age of Scored Specimens: The Bullock Creek Local Fauna is interpreted to be middle Miocene based on biostratigraphy, whereas Riversleigh Faunal Zone D is estimated to be early late Miocene, also based on biostratigraphy (see above). In the absence of radiometric dates, we have assumed the entire span of the middle to late Miocene (Langhian to Messinian; Cohen et al., 2013 [updated]) for this terminal.

Assigned Age Range: 15.970–5.333 Mya.

Remarks: †*Wakaleo vanderleueri* is known from a single exceptionally well-preserved holotype cranium (CPC 26604, which was described in detail by Murray et al., 1987) and additional dental material from the middle Miocene Bullock Creek Local Fauna (Clemens and Plane, 1974; Megirian, 1986; Murray and Megirian, 1990). We used these Bullock Creek specimens to score character data, together with additional dental specimens from the Encore Site of Riversleigh Faunal Zone D that were also referred to †*W. vanderleuri* by Gillespie et al. (2014). A single isolated M3 (QM F36466) from the Golden Steph (GS) site of Riversleigh Faunal Zone C was identified by Gillespie et al. (2014) as representing †*W. vanderleuri*, but this specimen has not been used for scoring purposes here.

†*Ilaria*

Species Scored: †*Ilaria illumidens* (type species), †*I. lawsoni*.

Geological Provenance of Scored Specimens: AMNH site B, Zone B (Pinpa Local Fauna) Namba Formation, Lake Pinpa, South Australia (†*I. illumidens*); AMNH SIAM locality, unit 6, Zone B (Ditjimanka Local Fauna), Lake Palankarinna, Etadunna Formation, South Australia (†*I. lawsoni*);

Age of Scored Specimens: Based on palaeomagnetic data, Metzger and Retallack (2010) estimated the Etadunna Formation to span 26.1–23.6 Mya. Zone A of the Etadunna Formation and the Pinpa Local Fauna of the Namba Formation appear to be stratigraphic equivalents (Woodburne et al., 1994). However, in the absence of radiometric dates, we have assumed the entire span of the late Oligocene (Chattian; Cohen et al., 2013 [updated]) for this terminal.

Assigned Age Range: 27.820–23.030 Mya.

Remarks: †*Ilaria illumidens* is represented by craniodental and associated postcranial elements of several individuals, while the slightly larger †*I.*

lawsoni is known from a single partial right dentary only (Tedford and Woodburne, 1987). Both species are characterized by large size (estimated body mass of †*Ilaria illumidens* is ~215 kg; Beck et al., 2020) and several unusual craniodental features. The upper molars are strongly selenodont, while the lower molars are incipiently lophodont with prominent neomorphic cuspids present; Tedford and Woodburne (1987) identified the "central cuspid" between the metaconid and protoconid, and a second between the hypconid and entoconid, as neomorphic, but could not rule out the possibility that it is in fact the lingual cuspids (the putative "metaconid" and "entoconid") are the neomorphs (Tedford and Woodburne, 1987: 415), and we have treated the homologies of these structures as unknown in this study. †*Ilaria* is also unusual in that the mandibular symphysis is fused, a feature otherwise seen only in a few other vombatiforms (see char. 97). Another ilariid, the much smaller (estimated body mass ~16 kg; Beck et al., 2020) †*Kuterintja ngama*, is known from the Ngama Local Fauna (Zone D of the Etadunna Formation; Pledge, 1987b; Woodburne et al., 1994) and the Riversleigh Faunal Zone A White Hunter Site (Myers and Archer, 1997), both of which are late Oligocene (see above); however, †*K. ngama* specimens is currently represented by fragmentary dental material only, and so has not been included here.

†*Muramura*

Species Scored: †*Muramura williamsi* (type species), †*M. pinpensis*.

Geological Provenance of Scored Specimens: SAM PL 8307 (Member 5) locality, Zone A ("Minkina" or "wynyardiid" Local Fauna), Lake Palankarinna, Etadunna Formation, South Australia (†*M. williamsi*); AMNH site B, Zone B (Pinpa Local Fauna) Namba Formation, Lake Pinpa, South Australia (†*M. pinpensis*).

Age of Scored Specimens: See †*Ilaria* above, for a discussion of the ages of the Etadunna and Namba formations. In the absence of radiometric dates, we have assumed the entire span of the late Oligocene (Chattian; Cohen et al., 2013 [updated]) for this terminal.

Assigned Age Range: 27.820–23.030 Mya.

Remarks: The diprotodontian family †Wynyardiidae takes its name from †*Wynyardia bassiana*, which is known from a single incomplete skull and associated partial postcranial skeleton collected from Table Cape (near Wynyard) in Tasmania some time before 1876 (Spencer, 1901). Unfortunately, this specimen had lost its entire dentition through erosion prior to discovery. Largely as a result of this lack of dental evidence, the relationships of †*Wynyardia* were controversial for many years (Spencer, 1901; Osgood, 1921; Jones, 1930; Gill, 1957; Ride, 1964; Haight and Murray, 1981). However, Aplin's (1987) careful study of the well-preserved auditory region of the holotype clearly supports diprotodontian, and most likely vombatiform, affinities. Tedford et al. (1977) tentatively referred a number of fossil diprotodontian specimens from Lake Pinpa to †Wynyardiidae based on postcranial similarities to †*W. bassiana*; this material was ultimately described as †*Muramura pinpensis* by Pledge (2003). Prior to this, Pledge (1987a) had described †*Muramura williamsi* based on two virtually complete skeletons from the Minkina Local Fauna, Lake Palankarinna, in the Etadunna Formation. We used specimens of both †*M. pinpensis* and †*M. williamsi* to score a composite †*Muramura* terminal. The cranial morphology of †*Muramura* has yet to be described in detail, but the molar dentition is noteworthy (as is that of the second wynyardiid included here, †*Namilamadeta*; see below) in that it appears to be intermediate between selenodont and lophodont-type morphologies (Pledge, 1987a: fig. 2; 2003: fig. 19.2; Beck et al., 2020). Doubts have been expressed as to whether †Wynyardiidae (comprising the genera †*Wynyardia*, †*Muramura*, and †*Namilamadeta*) is monophyletic (Aplin and Archer, 1987: xlviii; Long et al., 2002: 117). However, the phylogenetic analyses of Pledge (2005)—who included all three genera—and Beck et al. (2020)—who did not include †*Wynyardia* due to the poor preservation of the only known specimen—both supported the monophyly of †*Muramura* + †*Namilamadeta*.

†*Namilamadeta*

Species Scored: †*Namilamadeta albivenator*, †*N. crassirostrum*, †*N. superior*.

Geological Provenance of Scored Specimens: Riversleigh Faunal zones A and B, Riversleigh World Heritage Area, Queensland, Australia.

Age of Scored Specimens: Riversleigh Faunal zones A and B are interpreted to be late Oligocene and early Miocene, respectively, based on biostratigraphy (see above). In the absence of radiometric dates, we have assumed the entire span of the late Oligocene to early Miocene (Chattian to Burdigalian; Cohen et al., 2013 [updated]) for this terminal.

Assigned Age Range: 27.820–15.970 Mya.

Remarks: †*Namilamadeta* was tentatively referred to †Wynyardiidae by Rich and Archer (1979) based on a number of cranial similarities to †*Wynyardia bassiana*. The type species, †*N. snideri*, is only known from fragmentary craniodental material from the Namba Formation at Lake Tarkarooloo (Rich and Archer, 1979), but we did not use this material for scoring purposes. Instead, we scored a composite †*Namilamadeta* terminal from well-preserved skulls and additional dental specimens of the three Riversleigh species recently described by Pledge (2005). For discussion of the phylogenetic affinities of †Wynyardiidae, see †*Muramura* above.

†*Onirocuscus*

Species Scored: †*Onirocuscus reidi* (type species).

Geological Provenance of Scored Specimens: Riversleigh Faunal Zone C, Riversleigh World Heritage Area, Queensland, Australia.

Age of Scored Specimens: Riversleigh Faunal Zone C is interpreted to be middle Miocene based on biostratigraphy (see above). In the absence of radiometric dates, we have assumed the entire span of the middle Miocene (Langhian to Serravallian; Cohen et al., 2013 [updated]) for this terminal.

Assigned Age Range: 15.970–11.630 Mya.

Remarks: †*Onirocuscus reidi* was originally described as a fossil species of *Strigocuscus* by Flannery and Archer (1987c), who highlighted similarities with the ground cuscus *Phalanger gymnotis* (formerly also classified in the genus *Strigocuscus* sensu Flannery et al., 1987). However, based on evidence from a subsequently discovered and substantially complete cranium, Crosby (2007) referred *reidi* to a new genus, †*Onirocuscus*, which she placed in the phalangerid tribe Trichosurini. Crosby (2007) also described four other species of †*Onirocuscus*, but we did not use them for scoring purposes. Crosby's (2007: fig. 7) phylogenetic hypothesis suggests that †*Onirocuscus* is closely related to "*Trichosurus*" †*dicksoni*, another fossil phalangerid from Riversleigh (see below). However, her phylogeny was not the result of analyzing a published data matrix and it endorsed some relationships—such as a basal position for *Ailurops* within Phalangeridae and *Strigocuscus celebensis* within Trichosurini (see also Crosby and Norris, 2003)—that are contradicted by recent molecular analyses (Ruedas and Morales, 2005; Raterman et al., 2006; Meredith et al., 2009b; Mitchell et al., 2014; Kealy et al., 2019).

"*Trichosurus*"

Species Scored: "*Trichosurus*" †*dicksoni*.

Geological Provenance of Scored Specimens: Riversleigh Faunal Zone C, Riversleigh World Heritage Area, Queensland, Australia.

Age of Scored Specimens: Riversleigh Faunal Zone C is interpreted to be middle Miocene based on biostratigraphy (see above). In the absence of radiometric dates, we have assumed the entire span of the middle Miocene (Langhian to Serravallian; Cohen et al., 2013 [updated]) for this terminal.

Assigned Age Range: 15.970–11.630 Mya.

Remarks: "*Trichosurus*" †*dicksoni* was described by Flannery and Archer (1987c) as the oldest fossil member of the Recent phalangerid genus *Trichosurus*, based on specimens from Riv-

ersleigh Faunal Zone C (?middle Miocene) sites. If correct, this implies that *Trichosurus* had diverged from its extant sister taxon, *Wyulda*, prior to the ?middle Miocene. However, in her unpublished Ph.D. thesis, Crosby (2002b) concluded that "*T.*" †*dicksoni* is not, in fact, referable to *Trichosurus*, but warrants referral to a separate, entirely extinct, genus. Crosby (2007: fig. 7) presented an informal phylogeny that placed "*T.*" †*dicksoni* closer to †*Onirocuscus* (see above) than to Recent trichosurins, but this was not based on a formal, algorithmic analysis of character data. Crosby (2002b), however, did present formal phylogenetic analyses of phalangerid relationships that failed to support a close relationship between "*T.*" †*dicksoni* and extant *Trichosurus* species.

It is also noteworthy that some recent molecular studies (Meredith et al., 2009b; Mitchell et al., 2014) estimated that *Trichosurus* and *Wyulda* did not diverge from each other until the late Miocene, i.e., after the inferred age of "*Trichosurus*" †*dicksoni*, although others suggested that the *Trichosurus-Wyulda* split may have occurred prior to this (Ruedas and Morales, 2005; Kealy et al., 2019). Regardless, all recent molecular-clock analyses indicated that the *Wyulda* + *Trichosurus* lineage (= Trichosurini) had diverged from the rest of Phalangeridae by the middle Miocene or earlier (Ruedas and Morales, 2005; Raterman et al., 2006; Meredith et al., 2009b; Mitchell et al., 2014; Kealy et al., 2019).

†*Ekaltadeta*

Species Scored: †*Ekaltadeta ima* (type species).

Geological Provenance of Scored Specimens: Riversleigh Faunal zones A, B, and C, Riversleigh World Heritage Area, Queensland, Australia.

Age of Scored Specimens: Riversleigh Faunal zones A, B, and C are interpreted to be late Oligocene, early Miocene, and middle Miocene, respectively, based on biostratigraphy (see above). In the absence of radiometric dates, we have assumed the entire span of the large Oligocene to the middle Miocene (Chat-

tian to Serravallian; Cohen et al., 2013 [updated]) for this terminal.

Assigned Age Range: 27.820–11.630 Mya.

Remarks: †*Ekaltadeta ima* is known from numerous craniodental specimens, including two well-preserved crania (QM F14236 and F36330; Wroe et al., 1998). These specimens exhibit a number of plesiomorphic features, notably retention of the second upper and lower premolars throughout adulthood (Wroe and Archer, 1995), whereas all other known macropodiforms lose these teeth over the course of ontogeny (see char. 117). A second species, †*E. jamiemulvaneyi*, was described from Riversleigh Faunal Zone C by Wroe (1996b), but we did not score character data from that taxon. Currently, †*Ekaltadeta*, the Pliocene †*Jackmahoneya*, and the Plio-Pleistocene †*Propleopus* are usually classified as members of a distinct subfamily (†Propleopinae) within Hypsiprymnodontidae (e.g., Wroe and Archer, 1995; Ride et al., 1997; Wroe, 1997; Wroe et al., 1998; Kear and Cooke, 2001; Long et al., 2002; Black et al., 2012b). However, some recent phylogenetic analyses suggest that †*Ekaltadeta* and other propleopines may be more closely related to taxa currently classified as members of the family †Balbaridae than to *Hypsiprymnodon* (Kear et al., 2007; Kear and Pledge, 2008; Travouillon et al., 2014b, 2015a; Cooke et al., 2015; Butler et al., 2016, 2018; den Boer and Kear, 2018: supplemental data). The analysis of Travouillon et al. (2016), however, recovered a clade comprising Recent and fossil species of *Hypsiprymnodon*, †*Ekaltadeta*, †*Jackmahoneya* and †*Propleopus* that was sister to all other macropodiforms they included.

Hypsiprymnodon

Species Scored: *Hypsiprymnodon* †*bartholomaii*.

Geological Provenance of Scored Specimens: Riversleigh Faunal Zone C, Riversleigh World Heritage Area, Queensland, Australia.

Ages of Scored Specimens: Riversleigh Faunal Zone C is interpreted to be middle Miocene

based on biostratigraphy (see above). In the absence of radiometric dates, we have assumed the entire span of the middle Miocene (Langhian to Serravallian; Cohen et al., 2013 [updated]) for this terminal.

ASSIGNED AGE RANGE: 15.97–11.63 Mya.

REMARKS: *Hypsiprymnodon* †*bartholomaii* was described by Flannery and Archer (1987a) based on a partial cranium and two isolated molars, all from the Gag Site, which is part of Riversleigh Faunal Zone C. If this taxon is indeed referable to *Hypsiprymnodon*, then it indicates that the genus originated prior to the middle Miocene. However, Flannery and Archer (1987a) noted a number of striking craniodental differences between *H.* †*bartholomaii* and the Recent species *H. moschatus*, notably parietal-alisphenoid versus frontal-squamosal contact and presence versus absence of a distinct postglenoid process. Three further fossil *Hypsiprymnodon* species have recently been described from Riversleigh Faunal zones B and C sites (Bates et al., 2014), but we did not examine these for scoring purposes. Some phylogenetic analyses have found *Hypsiprymnodon* to be polyphyletic (Black et al., 2014c; den Boer and Kear, 2018: fig. S11), others have found it to be paraphyletic (den Boer and Kear, 2018: figs. S9–10), and still others have failed to unambiguously support its monophyly (Bates et al., 2014; Butler et al., 2016, 2018; den Boer and Kear, 2018: supplemental data), but that of Travouillon et al. (2016) placed Recent and fossil *Hypsiprymnodon* species in a clade that also included the propleopines, †*Ekaltadeta*, †*Jackmahoneya*, and †*Propleopus*.

?*Bettongia*

SPECIES SCORED: ?*Bettongia* †*moyesi*.

GEOLOGICAL PROVENANCE OF SCORED SPECIMENS: Henk's Hollow and Two Trees sites (Riversleigh Faunal Zone C), Riversleigh World Heritage Area, Queensland, Australia.

AGE OF SCORED SPECIMENS: Riversleigh Faunal Zone C is interpreted to be middle Miocene based on biostratigraphy (see above). In the absence of radiometric dates, we have assumed the entire span of the middle Miocene (Langhian to Serravallian; Cohen et al., 2013 [updated]) for this terminal.

ASSIGNED AGE RANGE: 15.970–11.630 Mya.

REMARKS: Flannery and Archer (1987b) referred this fossil taxon, which is represented by a partial skull and associated mandibles plus an additional left mandibular fragment, to the Recent potoroid genus *Bettongia*, but we consider it only questionably a member of this genus based on available evidence, which we summarize briefly here. Flannery and Archer (1987b) noted particular similarities between ?*B.* †*moyesi* and the living *B. lesueur*. The phylogenetic analysis of Kear et al. (2007) recovered a sister-group relationship between ?*B.* †*moyesi* and the extant potoroid *Potorous tridactylus* to the exclusion of other macropodiforms in their taxon sample, supporting the potoroid affinities of ?*B.* †*moyesi*. However, *P. tridactylus* was the sole Recent potoroid included by Kear et al. (2007), so the precise position of ?*B.* †*moyesi* within Potoroidae (and, particularly, its relationship to recent *Bettongia* species) remained uncertain in this analysis. The phylogenetic analysis of Travouillon et al. (2016), meanwhile, recovered ?*B.* †*moyesi* within Potoroidae but outside the crown clade. Some other published analyses have failed to place ?*B.* †*moyesi* within Potoroidae (Travouillon et al., 2015a: fig. 5A; Butler et al., 2016, 2018; den Boer and Kear, 2018: supplemental data), or have found its relationship relative to Macropodidae and Potoroidae to be largely unresolved (Bates et al., 2014; Black et al., 2014c; Travouillon et al., 2014b, 2015a: fig. 5B; Cooke et al., 2015; den Boer and Kear, 2018: supplemental data).

†*Bohra*

SPECIES SCORED: †*Bohra illuminata*.

GEOLOGICAL PROVENANCE OF SCORED SPECIMENS: Last Tree Cave, Nullarbor Plain, southeastern Western Australia.

AGE OF SCORED SPECIMENS: Prideaux et al. (2007) identified fossils from the Last Tree Cave

as early middle Pleistocene; we have interpreted this as corresponding to the first half of the Chibanian stage (Cohen et al., 2013 [updated]).

ASSIGNED AGE RANGE: 0.774–0.452 Mya.

REMARKS: †*Bohra paulae* was originally described and identified as a plesiomorphic tree kangaroo by Flannery and Szalay (1982) based on postcranial elements from Plio-Pleistocene deposits from Wellington Caves in New South Wales. A second species, †*B. wilkinsonorum*, was named by Dawson (2004) based on a single partial juvenile maxilla from the late Pliocene Chinchilla Local Fauna in southeastern Queensland. Prideaux and Warburton (2008) described a third species, †*B. illuminata*, based on exceptionally well-preserved craniodental material from early middle Pleistocene cave deposits in the Nullarbor Plain. A fourth species, †*B. nullarbora*, has also been described, again based on specimens from early middle Pleistocene cave deposits in the Nullarbor Plain (Prideaux and Warburton, 2009). Prideaux and Warburton (2008) noted that some aspects of the craniodental morphology of †*B. illuminata* are more similar to extant *Petrogale* species (particularly *P. brachyotis*), than to extant *Dendrolagus* species. In their subsequent phylogenetic analysis, Prideaux and Warburton (2010) recovered †*B. illuminata* as the sister taxon to *Dendrolagus*, with *P. brachyotis* (the sole *Petrogale* species included in their matrix) as sister to this clade, and referred to the †*Bohra-Dendrolagus-Petrogale* clade as Dendrolagini (see also Jackson and Groves, 2015). By contrast, Flannery (1989) and Kear and Cooke (2001) restricted Dendrolagini to †*Bohra* and *Dendrolagus* only. Recent molecular and total-evidence phylogenies consistently support a sister-group relationship between *Petrogale* (sensu Groves, 2005, i.e., including *Peradorcas*) and *Dendrolagus* (see, e.g., Meredith et al., 2009a, 2009b; Phillips et al., 2013; Llamas et al., 2015; Mitchell et al., 2014; Dodt et al., 2017; Cascini et al., 2019; Celik et al., 2019; Álvarez-Carretero et al., 2021).

†*Gangaroo*

SPECIES SCORED: †*Gangaroo bilamina* (type species), †*G. bites*, †*G. robustiter*.

GEOLOGICAL PROVENANCE OF SCORED SPECIMENS: Riversleigh Faunal zones B and C, Riversleigh World Heritage Area, Queensland, Australia.

AGE OF SCORED SPECIMENS: Riversleigh Faunal zones B and C are interpreted to be early Miocene and middle Miocene respectively, based on biostratigraphy (see above). In the absence of radiometric dates, we have assumed the entire span of the early and middle Miocene (Aquitanian to Serravallian; Cohen et al., 2013 [updated]) for this terminal.

ASSIGNED AGE RANGE: 23.030–11.630 Mya.

REMARKS: Cooke (1997a) described †*Gangaroo bilamina* based on isolated mandibles from several sites in Riversleigh Faunal Zone B and referred this taxon to the macropodiform subfamily †Bulungamayinae, which was erected by Flannery et al. (1983) and placed by those authors within Potoroidae. Subsequent studies have suggested that †*Gangaroo* and other "bulungamayines" are not in fact potoroids, but instead likely form a paraphyletic assemblage at the base of Macropodidae (Cooke, 1997a, 1997b, 2006; Cooke and Kear, 1999; Kear and Cooke, 2001; Prideaux, 2004; Kear et al., 2007; Kear and Pledge, 2008; Prideaux and Warburton, 2010; Black et al., 2014c; Phillips, 2015; Travouillon et al., 2014b, 2015a, 2016; Cooke et al., 2015; Butler et al., 2016, 2018; den Boer and Kear, 2018: supplemental data; Cascini et al., 2019).

Well-preserved craniodental material of †*Ganguroo bilamina* is known from Riversleigh Faunal Zone B sites (Cooke, 1997b; Travouillon et al., 2014b), with a second species, †*G. robustiter*, known from Riversleigh Faunal zones C and D (Cooke et al., 2015). A third species, †*G. bites*, is known only from lower jaw material from Faunal Zone B (Travouillon et al., 2014b). Specimens of all three species were used to code this terminal, but we only examined the Riversleigh Faunal Zone C specimens of †*G. robusti-*

ter, so we restrict the assigned age range of our †*Ganguroo* terminal to early to middle Miocene (see above).

†*Hadronomas*

SPECIES SCORED: †*Hadronomas puckridgi* (type and only described species).

GEOLOGICAL PROVENANCE OF SCORED SPECIMENS: Alcoota Local Fauna, Alcoota Station, Northern Territory, Australia.

AGE OF SCORED SPECIMENS: Black et al. (2013: 1036) summarized evidence regarding the age of the Alcoota Local Fauna, which may be late Miocene ("Mitchellian," ~8.2–10.8 Mya; Piper et al., 2006) or latest late Miocene to earliest Pliocene ("Cheltenhamian," ~4.5–6.5 Mya; Fitzgerald and Kool, 2015). Congruent with this, Megirian et al. (2010) placed the Alcoota Local Fauna within their "Waitean" Australian Land Mammal Age, for which they gave boundary estimates of 5 and 12 Mya. This age range has been assumed in subsequent papers on the Alcoota Local Fauna (e.g., Yates, 2014; 2015a) and has been followed here.

ASSIGNED AGE RANGE: 12.000–5.000 Mya.

REMARKS: Woodburne (1967) described †*Hadronomas puckridgi* based on fragmentary dental and mandibular specimens from the Alcoota Local Fauna, identifying it as a macropodid of uncertain affinities. Subsequent discovery of more complete cranial and also postcranial material led Murray (1989, 1991, 1995) to propose a close relationship between this taxon and sthenurine macropodids. Prideaux (2004) similarly concluded that †*H. puckridgi* is an early sthenurine, and this hypothesis has been supported in numerous subsequent phylogenetic analyses (Kear et al., 2007; Prideaux and Warburton, 2010; Prideaux and Tedford, 2012; Bates et al., 2014; Black et al., 2014c; Llamas et al., 2015: supplementary material; Travouillon et al., 2014b, 2015a, 2016; Cooke et al., 2015; Butler et al., 2018; den Boer and Kear, 2018: supplemental data; Cascini et al., 2019).

†*Rhizosthenurus*

SPECIES SCORED: †*Rhizosthenurus flanneryi* (type and only described species).

GEOLOGICAL PROVENANCE OF SCORED SPECIMENS: Encore Site, Riversleigh Faunal Zone D, Riversleigh World Heritage Area, Queensland, Australia.

AGE OF SCORED SPECIMENS: Riversleigh Faunal Zone D is estimated to be early late Miocene based on biostratigraphy (see above). In the absence of radiometric dates, however, we have assumed the entire span of the late Miocene (Tortonian to Messinian; Cohen et al., 2013 [updated]) for this terminal.

ASSIGNED AGE RANGE: 11.630–5.333 Mya.

REMARKS: Kear et al. (2001a) described macropodiform postcranial remains from the Encore Site of Riversleigh Faunal Zone D, which they interpreted as representing an unidentified species of the "bulungamayine" genus †*Wanburoo*. In a subsequent paper, Kear (2002) reallocated this material to a new species, †*Rhizosthenurus flanneryi*. The sthenurine affinities of †*R. flanneryi* were supported by Kear et al.'s (2001a) and Kear's (2002) phylogenetic analyses of postcranial characters, and by subsequent analyses of combined craniodental and postcranial evidence (Kear et al., 2007; Bates et al., 2014; Black et al., 2014c; Travouillon et al., 2014b, 2015a; Cooke et al., 2015). A well-preserved skull is associated with the holotype postcranial skeleton of †*R. flanneryi* (QM F31456), and additional isolated teeth from the Encore site have also been referred to this taxon in an unpublished thesis (Kirkham, 2004). We examined these craniodental specimens of †*R. flanneryi* (which have yet to be formally described) to score character data for this study.

†*Balbaroo*

SPECIES SCORED: †*Balbaroo fangaroo*.

GEOLOGICAL PROVENANCE OF SCORED SPECIMENS: Riversleigh Faunal zones A and B, Riversleigh World Heritage Area, Queensland, Australia.

AGES OF SCORED SPECIMENS: Riversleigh Faunal zones A and B are interpreted to be late Oligocene and early Miocene, respectively, based on biostratigraphy (see above). In the absence of radiometric dates, we have assumed the entire span of the late Oligocene to the early Miocene (Chattian to Burdigalian; Cohen et al., 2013 [updated]) for this terminal.

ASSIGNED AGE RANGE: 27.820–15.970 Mya.

REMARKS: Flannery et al. (1983) described †*Balbaroo camfieldensis* (the type species) from the ?middle Miocene Bullock Creek Local Fauna, and †*B. gregoriensis* from the G Site of Riversleigh Faunal Zone A, and referred them to a new macropodid subfamily, †Balbarinae. Flannery et al. (1983: 295) concluded that "balbarines appear to represent the most primitive macropodids known." Later, Kear and Cooke (2001) ranked balbarines as a family-level clade based on the work of Cooke (1997a, 1997b, 1997c), which indicated that balbarids evolved fully lophodont molars independently from macropodids. Subsequent phylogenetic analyses have typically recovered †Balbaridae outside a clade that includes the extant macropodoid families Macropodidae and Potoroidae (Kear et al., 2007; Kear and Pledge, 2008; Bates et al., 2014; Black et al., 2014c; Travouillon et al., 2014b, 2015a, 2016; Cooke et al., 2015; Butler et al., 2016, 2018). However, the affinities of balbarids are otherwise somewhat unstable, with different analyses finding a close relationship with †*Ekaltadeta* and (when included) other propleopines (Kear et al., 2007; Kear and Pledge, 2008; Butler et al., 2016, 2018), with both †*Ekaltadeta* (and other propleopines, if included) and *Hypsiprymnodon* (Travouillon et al., 2014b, 2015a; Cooke et al., 2015; den Boer and Kear, 2018: figs. S5, S9-S11), or with neither (Travouillon et al., 2016; den Boer and Kear, 2018: figs. S4, S6, S8). The morphological analysis of Travouillon (2016: fig. 7) and the tip-and-node dated total-evidence analysis of Cascini et al. (2019: fig. 5) differ from other published analyses in finding †Balbaridae to be paraphyletic rather than monophyletic, and, in Cascini et al.'s (2019: fig. 5) analysis only, closer to Macropodidae than to Potoroidae.

Cooke (2000) described relatively complete craniodental material of two individuals of †*Balbaroo fangaroo*, both of which we examined to score this taxon. One specimen (QM F30456) reveals the presence of hypertrophied upper canines, a surprising morphology apparently convergent on that seen in some extant artiodactyls (e.g., *Tragulus* and *Moschus*), in which this feature is sexually dimorphic. The two other species †*Balbaroo* species described by Flannery et al. (1983) —†*B. camfieldensis* and †*B. gregoriensis*—have not been used for scoring purposes here.

†*Ganawamaya*

SPECIES SCORED: †*Ganawamaya gillespieae*.

GEOLOGICAL PROVENANCE OF SCORED SPECIMENS: Quantum Leap Site (Riversleigh Faunal Zone B), Riversleigh World Heritage Area, Queensland, Australia.

AGE OF SCORED SPECIMENS: Riversleigh Faunal Zone B is interpreted to be early Miocene based on biostratigraphy (see above). In the absence of radiometric dates, we have assumed the entire span of the early Miocene (Aquitanian to Burdigalian; Cohen et al., 2013 [updated]) for this terminal.

ASSIGNED AGE RANGE: 23.030–15.970 Mya.

REMARKS: We scored †*Ganawamaya gillespieae*, the second balbarid included in our taxon sample, based on the holotype (QM F35432), an almost complete cranium and associated mandibles from the Quantum Leap Site of Riversleigh Faunal Zone B (Kear et al., 2007). One of the two paratypes of †*G. gillespieae* (AR 15347) is known from the older (Riversleigh Faunal Zone A) White Hunter Site, but neither this nor the other paratype (AR 12829) from the Riversleigh Faunal Zone B Wayne's Wok Site was consulted for scoring purposes here. Kear et al. (2007) originally described this taxon as a species of †*Nambaroo*, but we follow Butler et al. (2018), who assigned it to †*Ganawamaya*. Our current understanding of the evolutionary relationships of balbarids is summarized above (see †*Balbaroo*).

†*Yalkaparidon*

Species Scored: †*Yalkaparidon coheni* (type species), †*Yalkaparidon.* sp.

Geological Provenance of Scored Specimens: Riversleigh Faunal Zone B, Riversleigh World Heritage Area, Queensland, Australia.

Age of Scored Specimens: Riversleigh Faunal Zone B is interpreted to be early Miocene, based on biostratigraphy (see above). In the absence of radiometric dates, we have assumed the entire span of the early Miocene (Aquitanian to Burdigalian; Cohen et al., 2013 [updated]) for this terminal.

Assigned Age Range: 23.030–15.970 Mya.

Remarks: †*Yalkaparidon* is unique among Australian fossil metatherians in that it is known from extensive craniodental material, including a well-preserved partial skull (QM F13008, the holotype of †*Y. coheni*), and yet cannot be confidently referred to one of the seven extant Australian marsupial orders (Archer et al., 1988; Beck et al., 2014). This is due to its unique combination of dental features, including hypselodont first upper and lower incisors; a procumbent, gliriform lower first incisor; zalambdodont molars; and a cranial morphology that appears plesiomorphic compared with other known Australian marsupials yet also exhibits some striking apomorphic features (such as a very reduced postglenoid process, a transverse canal foramen that is posterior to the carotid foramen, and very robust and posteriorly extensive entopterygoid crests; Archer et al., 1988; Beck, 2009; Beck et al., 2014). Marshall et al. (1990) and Szalay (1994) suggested that †*Yalkaparidon* is a member of Diprotodontia, whereas Woodburne and Case (1996) placed it in Notoryctemorphia. However, the most detailed studies of †*Yalkaparidon* to date suggest that it be placed in its own order, †Yalkaparidontia (Archer et al., 1988; Beck et al., 2014). Isolated tarsals tentatively referred to †*Yalkaparidon* preserve apomorphic features that appear to be characteristic of australidelphians (Beck et al., 2014), and some phylogenetic analyses have placed †*Yalkaparidon* within Australidelphia (Beck et al., 2014; Beck et al., 2016); however, other analyses have placed †*Yalkaparidon* in a clade with paucituberculatans (Beck, 2017b; Zimicz and Goin, 2020), with which it shares presence of a gliriform lower first incisor.

Archer et al. (1988) described two species, both from Riversleigh: †*Yalkaparidon coheni* (based on specimens from Faunal Zone B) and †*Y. jonesi* (based on specimens from Faunal Zone C). Beck et al. (2014) examined all known material of †*Yalkaparidon* collected to date from Riversleigh, and identified additional specimens of †*Y. coheni* and other †*Yalkaparidon* material not identifiable to species level from one Riversleigh Faunal Zone A site (White Hunter) and multiple Faunal Zone B sites (see Beck et al., 2014: electronic supplementary material); only Faunal Zone B specimens have been used for scoring purposes here. We did not score character data from specimens of †*Y. jonesi*, which appears to be more derived than †*Y. coheni* in lacking any teeth between the enlarged procumbent anteriormost lower incisor and the tooth that Archer et al. (1988) referred to as p3 but which Beck et al. (2014) argued is m1.

APPENDIX 2

Minimum and Maximum Bounds for Calibrated Nodes

Following O'Reilly and Donoghue (2016), we elected to use a combined tip-and-node dating approach for our total-evidence dating analyses, in which temporal information is incorporated by assigned ages (or age ranges) for terminal taxa, and by setting constraints on the minimum and maximum ages of selected internal nodes (as in, e.g., Kealy and Beck, 2017; Maga and Beck, 2017; Travouillon and Phillips, 2018; Cascini et al., 2019; Beck and Taglioretti, 2020). In a Bayesian context, these constraints can be specified using a range of different prior distributions (e.g., uniform, exponential, lognormal), which reflect different assumptions regarding the information provided by the fossil record (Ho and Phillips, 2009). If multiple node calibrations are specified, these can interact with each other, as well as with any other specified priors (e.g., the ages of the tips and the tree prior, which specifies the branching process), such that the joint (effective) prior age constraints on those nodes differ—sometimes quite markedly—from the originally specified prior constraints (Warnock et al., 2012, 2015; Barba-Montoya et al., 2017; Brown and Smith, 2018).

We attempted to take a conservative approach to node calibration by using deliberately broad age ranges specified as uniform distributions for our calibrated nodes (Ho and Phillips, 2009). Ideally, this should mean that posterior divergence date estimates are largely driven by our character data, and, if the signal in our character data is weak, the posterior divergence date estimates should be correspondingly broad. To investigate how our priors on node ages interact with each other and with our other priors to generate joint (effective) prior age constraints for those nodes (Warnock et al., 2012, 2015; Barba-Montoya et al., 2017; Bromham et al., 2018; Brown and Smith, 2018), we ran one analysis without data but using otherwise identical analytical settings in MrBayes 3.2.7 (see Materials

and Methods). This approach also allows us to investigate whether our posterior estimates for those calibrated nodes differ appreciably from the priors, which should indicate the extent to which there is temporal signal in our data (Parins-Fukuchi and Brown, 2017; Brown and Smith, 2018). Table 6 summarizes the posterior age estimates for these nodes, together with posterior age estimate from four recent molecular clock studies of marsupials (Meredith et al., 2009, 2011; Mitchell et al., 2014; Álvarez-Carretero et al., 2021).

Our calibrated nodes are listed below. For each node, we list the contents and our specified minimum[38] and maximum bounds, as well as the median effective prior (with the 95% Highest Posterior Density [HPD] interval given in parentheses) inferred using a MrBayes 3.2.7 analysis run without data. We also provide a full justification for our chosen minimum and maximum bounds. It is a requirement of MrBayes 3.2.7 that calibrated nodes are constrained to be monophyletic, so we also summarise evidence supporting the monophyly of our calibrated nodes, both from our undated analyses and from other studies.

Node: Root

CONTENTS: All ingroup and outgroup terminals.

MINIMUM BOUND: 59.2 Mya.

MAXIMUM BOUND: 109.0 Mya.

MEDIAN EFFECTIVE PRIOR (AND 95% HPD): 71.9 Mya (63.6–83.1 Mya).

JUSTIFICATION: The minimum bound is the minimum age of Tiupampa (see the account for †*Pucadelphys* in appendix 1), which is the source of our oldest terminals, namely the outgroup taxa †*Pucadelphys*, †*Mayulestes*, and †*Allqokirus*. Carneiro (2018) identified †*Varalphadon janetae*,

---

[38] Note that in several cases (e.g., the root node), the minimum bound enforced in our analysis was very slightly larger (0.001, 0.002, or 0.003 Ma; see table 6) than that listed here; this was necessary to account for the use of additional nested calibrations that use the same minimum bound and without which MrBayes 3.2.7 would not run (see Beck and Lee, 2014: electronic supplementary material).

from the upper Cenomanian (95–93 Mya) Naturita Formation (Kirkland et al., 2016) and lower Conacian "upper" Straight Cliffs Formation (Eaton, 2006; Albright and Titus, 2016) of southern Utah as the oldest known member of †Sparassodonta (which also includes †*Mayulestes* and †*Allqokirus*); if correct, this would indicate that the divergence between †*Pucadelphys* and the sparassodonts †*Mayulestes* and †*Allqokirus* had already occurred by 93 Mya, and hence the age of our root divergence must predate this. However, Carneiro's (2018) identification of †*V. janetae* as a sparassodont was criticized by Muizon et al. (2018: 430), and we do not follow it here.

Specifying a maximum bound is difficult due to uncertainty regarding the relationship of Cretaceous North American marsupialiaforms to South American taxa (including crown marsupials), as well as to Cenozoic northern hemisphere taxa traditionally referred to the families †Herpetotheriidae (such as †*Herpetotherium*, included as a terminal here) and †Peradectidae (such as †*Mimoperadectes*, included as a terminal here), as discussed by Williamson et al. (2012; 2014). As our maximum bound, we use the maximum age of the oldest known marsupialiform fossil, a single partial lower molar (OMNH 62432) of an unnamed taxon from deposits in the Cloverly Formation, Montana, that date to 104–109 Mya (Cifelli and Davis, 2015).

Node: †Pucadelphyda

CONTENTS: †*Pucadelphys*, and †Mayulestidae.
MINIMUM BOUND: 59.2 Mya.
MAXIMUM BOUND: 83.6 Mya.
MEDIAN EFFECTIVE PRIOR (AND 95% HPD): 67.0 Mya (62.0–74.9 Mya).

JUSTIFICATION: The phylogenetic analyses of Muizon et al. (2018) indicated that †*Pucadelphys* is part of a clade that also includes sparassodonts such †*Mayulestes* and †*Allqokirus*; Muizon et al. (2018) named this clade the superorder †Pucadelphyda, and we assume that it is monophyletic here for calibration purposes. The minimum bound is the minimum age of Tiupampa (see the account for

†*Pucadelphys* in appendix 1), which is the source of all three of the pucadelphydans included here.

As discussed above (see Node: Root, above), Carneiro (2018) identified the upper Cenomanian–lower Coniacian North American taxon †*Varalphadon janetae* as the earliest known sparassodont, in which case the divergence between †*Pucadelphys* and †Sparassodonta must have occurred by ~93 Mya. However, we follow Muizon et al. (2018: 430) in rejecting this hypothesis. Instead, we agree with Muizon et al. (2018) that †Pucadelphyda likely represents a South American radiation, and we consider further that the close cranial similarities between †*Pucadelphys*, †*Mayulestes*, and †*Allqokirus* (Muizon, 1994, 1998; Marshall and Muizon, 1995; Muizon et al., 1997, 2018) suggest that these Tiupampan taxa document the early stages of this radiation. The youngest Mesozoic mammals from South America are from the Allenian (or Alamitian South American Land Mammal Age) faunas of Patagonia, which are Campanian-Maastrichtian and appear to lack therian mammals, despite their taxonomic richness (Bonaparte, 1990; Kielan-Jaworowska et al., 2004; Rougier et al., 2009a, 2009b, 2011). We follow numerous previous authors in concluding that this indicates that neither metatherians nor eutherians had dispersed to South America from North America by this time (e.g., Szalay, 1994; Pascual, 2006; Pascual and Ortiz-Jaureguizar, 2007; Beck, 2008b; Goin et al., 2012, 2016; Woodburne et al., 2014; Beck, 2017b). If so, and if †Pucadelphyda is indeed a purely South American radiation, then the origin of †Pucadelphyda must postdate these Allenian/Alamitian faunas. Thus, we use maximum age of the Campanian (Cohen et al., 2013 [updated]) as a maximum bound on this node.

Node: †Mayulestidae

CONTENTS: †*Allqokirus*, and †*Mayulestes*.
MINIMUM BOUND: 59.2 Mya.
MAXIMUM BOUND: 83.6 Mya.
MEDIAN EFFECTIVE PRIOR (AND 95% HPD): 64.7 Mya (60.7–69.7 Mya).

JUSTIFICATION: Based on the results of their phylogenetic analyses, Muizon et al. (2018) placed †*Mayulestes* and †*Allqokirus* within the sparassodont family †Mayulestidae (which also includes the slightly younger †*Patene*). We assume monophyly of †Mayulestidae here for calibration purposes, and assume a minimum bound of 59.2 Mya based on the age of †*Mayulestes* and †*Allqokirus* (see above), and the same maximum bound as for †Pucadelphyda, again based on the assumption that †Mayulestidae is a South American radiation that postdates the entry of metatherians into South America (see †Pucadelphyda above).

Node: Marsupialia

CONTENTS: Dasyuromorphia, Didelphimorphia, Diprotodontia, Microbiotheria, Notoryctemorphia, Paucituberculata, Peramelemorphia, and †Yalkaparidontia.
MINIMUM BOUND: 54.55 Mya.
MAXIMUM BOUND: 83.6 Mya.
MEDIAN EFFECTIVE PRIOR: 59.6 Mya (54.8–68.3 Mya).
JUSTIFICATION: Although our morphological and undated total-evidence analyses do not clearly resolve the relationship of †*Herpetotherium* to definitive crown-clade marsupials, most recent published phylogenetic analyses place †*Herpetotherium* outside Marsupialia (Ladevèze and Muizon, 2007; Sánchez-Villagra et al., 2007; Beck et al., 2008; Horovitz et al., 2008, 2009; Forasiepi, 2009; Ladevèze and Muizon, 2010; Beck, 2012, 2017a; Williamson et al., 2012, 2014; Engelman and Croft, 2014; Forasiepi et al., 2014; Carneiro and Oliveira, 2017a, 2017b; Maga and Beck, 2017; Carneiro, 2018, 2019; Carneiro et al., 2018; Muizon et al., 2018; Rangel et al., 2019; Muizon and Ladevèze, 2020), so we constrained Marsupialia to exclude †*Herpetotherium* here.

The age of the oldest definitive crown-clade marsupials is controversial, as summarized by Eldridge et al. (2019). These authors concluded that two taxa from the Tingamarra Local Fauna of northeastern Australia (which has been radio-metrically dated as 54.6 Mya; Godthelp et al., 1992) are the oldest definitive crown-clade marsupials currently known: the plesiomorphic australidelphian †*Djarthia* (Godthelp et al., 1999; Beck et al., 2008) and an isolated marsupial calcaneus (QM F30060) described by Beck (2012) that is transitional between "ameridelphian" and australidelphian tarsal morphologies (Szalay, 1982; 1994; Beck et al., 2008; Beck, 2012). The Tingamarra Local Fauna has been radiometrically dated as having a "minimum age of 54.6 ± 0.05" Mya (Godthelp et al., 1992: 514), so we use 54.55 Mya as our minimum bound for this node. This radiometric dating was carried out nearly 30 years ago, using K-Ar dating (which has largely been superseded by more accurate methods such as Ar-Ar and U-Pb dating) on authigenic illite-smectite clays (Godthelp et al., 1992), for which dates are likely to be less reliable than for volcanic minerals (J.J. Flynn, personal commun.). Attempts to redate the site have so far proven unsuccessful (R.M.D.B., personal obs.). However, the known fossil fauna of Tingamarra is compatible with an early Eocene age (Beck et al., 2008: supporting information), and there is no direct evidence contradicting the published date. Thus, we use the minimum age of Tingamarra as the minimum bound on the age of Marsupialia.

Our maximum bound is the same as that used for †Pucadelphyda and †Mayulestidae (see above), namely the maximum age of the Campanian and, for a similar reason, i.e., the earliest splits within Marsupialia probably did not occur prior to the arrival of metatherians in South America (see also Jansa et al., 2014: supporting information; Beck, 2017b; Eldridge et al., 2019), which presumably took place no earlier than the Campanian.

Node: Paucituberculata + Australidelphia + †Yalkaparidontia

CONTENTS: Dasyuromorphia, Diprotodontia, Microbiotheria, Notoryctemorphia, Paucituberculata, Peramelemorphia, and †Yalkaparidontia.
MINIMUM BOUND: 54.55 Mya.

MAXIMUM BOUND: 83.6 Mya.

MEDIAN EFFECTIVE PRIOR: 59.6 Mya (54.8–68.3 Mya).

JUSTIFICATION: Although our our molecular analyses consistently place the marsupial root between Paucituberculata and Didelphimorphia + Australidelphia (figs. 27–29), we constrained Didelphimorphia to be the sister to a clade comprising the remaining marsupial orders, given the statistically significant support for this topology provided by retrotransposon insertions (Gallus et al., 2015a). We included †*Yalkaparidon* (†Yalkaparidontia) in the nondidelphimorphian marsupial clade, because our morphological and undated total-evidence analyses place this fossil taxon with paucituberculatans, as do several other published phylogenetic analyses (Beck, 2017a; Abello and Candela, 2019; Zimicz and Goin, 2020), while yet others place it within Australidelphia (Beck et al., 2014, 2016; Abello and Candela, 2019). Our maximum and minimum bounds are the same as for Marsupialia (see above). Isolated tarsal remains referred to †*Djarthia murgonensis* from the Tingamarra Local Fauna by Beck et al. (2008) preserve the "continuous lower ankle joint pattern" that was originally identified by Szalay (1982; 1994) as a distinctive australidelphian synapomorphy, and phylogenetic analyses consistently place †*Djarthia* within Australidelphia (Beck et al., 2008, 2016; Beck, 2012; Lorente et al., 2016; Maga and Beck, 2017; Abello and Candela, 2019; Zimicz and Goin, 2020); thus, the Tingamarran †*Djarthia* must postdate the divergence of Australidelphia from its sister taxon. Based on available evidence, we do not think that the maximum bound for this node can be estimated more precisely than that for Marsupialia.

Node: Didelphimorphia

CONTENTS: *Caluromys*, *Caluromysiops*, *Chacodelphys*, *Chironectes*, *Cryptonanus*, *Didelphis*, *Glironia*, *Gracilinanus*, †*Hesperocynus*, *Hyladelphys*, *Lestodelphys*, *Lutreolina*, *Marmosa*, *Marmosops*, *Metachirus*, *Monodelphis*, *Philander*, †*Sparassocynus*, *Thylamys*, †*Thylatheridium*, †*Thylophorops*, and *Tlacuatzin*.

MINIMUM BOUND: 12.5 Mya.

MAXIMUM BOUND: 65.118 Mya.

MEDIAN EFFECTIVE PRIOR (AND 95% HPD): 20.1 Mya (12.5–35.7 Mya).

JUSTIFICATION: Goin (1997a) described representatives of the extant didelphid genera *Marmosa* ("*Micoureus*" sensu Goin, 1997a; see Voss and Jansa, 2009; Suárez Gómez, 2019) and *Thylamys* from the 13.8–11.6 Mya (Guerrero, 1993; Flynn et al., 1997; Guerrero, 1997; Anderson et al., 2016) Honda Group at La Venta, Colombia, based on isolated dental remains. In an unpublished thesis, Suárez Gómez (2019) revised the La Venta metatherian fauna, upholding Goin's (1997a) identification of *Marmosa* and *Thylamys* and also identifying other specimens as representing the extant didelphid genus *Tlacuatzin* or a closely related taxon. The La Venta specimens are extremely fragmentary, and the reported presence of *Thylamys* is potentially problematic because the molecular-clock analysis of Jansa et al. (2014) and the total-evidence clock analysis of Beck and Taglioretti (2020) both suggest that *Thylamys* did not diverge from *Lestodelphys* until the latest Miocene or Pliocene (but see Vilela et al., 2015). However, phylogenetic analyses presented by Suárez Gómez (2019) placed these La Venta taxa within the didelphimorphian crown clade, i.e., Didelphidae, so we consider them suitable for use for calibration purposes here.

Within the Honda Group, the La Victoria Formation underlies the younger Villavieja Formation (Guerrero, 1993; Flynn et al., 1997; Guerrero, 1997; Anderson et al., 2016). Although most of the didelphid material described by Goin (1997a) and Suárez Gómez (2019) is from the Villavieja Formation, they reported specimens of *Marmosa* †*laventica* from the La Victoria Formation. The contact between the La Victoria and Villavieja specimens is estimated to be 12.5 Mya (Guerrero, 1993; Flynn et al., 1997; Guerrero, 1997; Anderson et al., 2016), so we use this as a minimum bound on the diversification of Didelphidae.

Assigning a maximum bound for this node is difficult, given the lack of obvious dental apomorphies that would distinguish (crown-clade) didelphids from nondidelphid didelphimorphians and other dentally plesiomorphic marsupialiforms (Voss and Jansa, 2009; this study). We use the maximum age of Tiupampa as a maximum bound (see the account for †*Pucadelphys* in appendix 1), on the assumption that Didelphidae originated in South America (Jansa et al., 2014) and that Tiupampa documents the early stages of the South American marsupialiform radiation. We note that this markedly predates all recent published molecular and total-evidence clock estimates for the age of Didelphidae (Steiner et al., 2005; Meredith et al., 2011; Jansa et al., 2014; Mitchell et al., 2014; Vilela et al., 2015; Beck and Taglioretti, 2020).

Node: *Didelphis + Philander*

CONTENTS: *Didelphis*, and *Philander*.
MINIMUM BOUND: 3.3 Mya.
MAXIMUM BOUND: 21.0 Mya.
MEDIAN EFFECTIVE PRIOR (AND 95% HPD): 4.2 Mya (3.3–7.4 Mya).

JUSTIFICATION: The minimum bound for this node follows Jansa et al. (2014: supporting information) and is based specifically on a well-preserved (nearly complete) skull of *Didelphis* †*brachydonta* (MMP 879M; Simpson, 1972) from the Chapadmalal Formation in Argentina that preserves unambiguously diagnostic generic synapomorphies of *Didelphis* (Jansa et al., 2014: supporting information; see the account for †*Sparassocynus* in appendix 1 of this report for a justification of the age assigned to the Chapadmalal Formation). Again, assigning a maximum bound for this node is difficult; we have used the maximum age of the oldest putative (crown-clade) didelphids, described by Goin et al. (2007a; see also Beck and Taglioretti, 2020; Castro et al., 2021), and we note that this markedly predates all recent published molecular and total-evidence clock estimates for this divergence (Steiner et al., 2005; Meredith et al., 2011; Jansa et al., 2014;

Mitchell et al., 2014; Vilela et al., 2015; Beck and Taglioretti, 2020; Álvarez-Carretero et al., 2021).

Node: Paucituberculata

CONTENTS: †*Acdestis*, *Caenolestes*, †*Evolestes*, *Lestoros*, †*Palaeothentes*, †*Pichipilus*, *Rhyncholestes*, and †*Stilotherium*.
MINIMUM BOUND: 25.82 Mya.
MAXIMUM BOUND: 65.118 Mya.
MEDIAN EFFECTIVE PRIOR (AND 95% HPD): 31.9 Mya (26.7–39.4 Mya).

JUSTIFICATION: †*Evolestes* was originally described as a plesiomorphic paucituberculatan (Goin et al., 2007b), but our undated total-evidence analysis fails to unambiguously group this taxon with other members of Paucituberculata to the exclusion of †*Yalkaparidon* (which we do not consider to be a paucituberculatan; see Beck et al., 2014). However, other published phylogenetic analyses that have focused on paucituberculatan relationships have consistently placed †*Evolestes* within Paucituberculata (Abello, 2007, 2013; Goin et al., 2007b, 2009, 2010; Forasiepi et al., 2013; Rincón et al., 2015; Engelman et al., 2016; Abello et al., 2020). Thus, we have enforced †*Evolestes* as a member of Paucituberculata (to the exclusion of †*Yalkaparidon*) in our dated total-evidence analysis, so that we can calibrate this node. Our minimum bound for the node is the minimum age of †*Evolestes* (see appendix 1), as this is the oldest member of this clade. The maximum bound is the same as for Didelphidae (see above), and follows a similar reasoning, namely that Paucituberculata likely originated in South America and that Tiupampa documents the early stages of the South American marsupialiform radiation; the a posteriori time-scaled morphological phylogenies of Abello (2013: fig. 8) and Abello et al. (2020: fig. 2) suggested that Paucituberculata began to radiate during the late Paleocene (i.e., considerably after our proposed maximum bound).

Node: Peramelidae

CONTENTS: *Echymipera*, *Isoodon*, *Microperoryctes*, *Perameles*, *Peroryctes*, and *Rhynchomeles*.

Minimum Bound: 3.62 Mya.

Maximum Bound: 27.82 Mya.

Median Effective Prior (and 95% HPD): 5.6 Mya (3.6–15.6) Mya.

Justification: Based on current evidence, we consider the oldest definitive crown-clade peramelid to be *Perameles* †*allinghamensis* from the Bluff Downs Local Fauna (Archer and Wade, 1976; Travouillon et al., 2017). We therefore use as our minimum bound for the first divergence within Peramelidae the minimum age (based on radiometric dating) of the Bluff Downs Local Fauna (Mackness et al., 2000). As a maximum bound, we use the maximum age of Riversleigh Faunal Zone A, which is currently interpreted to be late Oligocene based on biostratigraphic evidence (Black et al., 2012b, 2013; Woodhead et al., 2014; Arena et al., 2015), and from which multiple nonperameloid (i.e., non-crown-clade) peramelemorphian taxa are known, but no crown-clade forms (Travouillon et al., 2010, 2013, 2015b; Gurovich et al., 2014; Warburton and Travouillon, 2016). Currently, the oldest known probable perameloids are middle Miocene in age (Travouillon et al., 2014a; Warburton and Travouillon, 2016).

Node: Dasyuromorphia

Contents: †*Badjcinus*, †*Barinya*, Dasyuridae, †*Mutpuracinus*, *Myrmecobius*, and Thylacinidae.

Minimum Bound: 23.03 Mya.

Maximum Bound: 65.118 Mya.

Median Effective Prior (and 95% HPD): 28.9 Mya (24.2–35.7 Mya).

Justification: The minimum bound is the minimum age of the oldest dasyuromorphian in our taxon sample, namely †*Badjcinus turnbulli* from the White Hunter Site at Riversleigh, which (along with other sites in Riversleigh Faunal Zone A) is interpreted to be late Oligocene based on biostratigraphic evidence (Black et al., 2012; Woodhead et al., 2014; Arena et al., 2015). The only pre-Oligocene Australian site known to preserve metatherians is Tingamarra, which has been radiometrically dated as 54.6 Mya (see

Marsupialia above), and from which no definitive representative of any modern Australian order (including Dasyuromorphia) is currently known (R.M.D.B, personal obs.). However, the Tingamarra mammal fauna is highly fragmentary, with only a few taxa having been described to date (Godthelp et al., 1992, 1999; Archer et al., 1993; Beck et al., 2008; Sigé et al., 2009; Beck, 2012; 2015); thus, we do not use it as a maximum bound. Instead, we follow a similar approach for our nodes calibrations for Didelphidae and Paucituberculata (excluding †*Evolestes*) and use the maximum age of Tiupampa as a maximum bound (see above). This is on the assumption that the modern Australian marsupial radiation (including Dasyuromorphia) is the result of dispersal from South America, via Antarctica (Beck, 2008b, 2012; 2017b; Beck et al., 2008), and that Tiupampa documents the early stages of the South American marsupialiform radiation (see above).

Node: Dasyurinae

Contents: *Antechinus*, *Dasycercus*, *Dasykaluta*, *Dasyuroides*, *Dasyurus*, *Micromurexia*, *Murexechinus*, *Murexia*, *Myoictis*, *Neophascogale*, *Paramurexia*, *Parantechinus*, *Phascogale*, *Phascolosorex*, *Phascomurexia*, *Pseudantechinus*, *Sarcophilus*.

Minimum Bound: 3.4 Mya.

Maximum Bound: 65.118 Mya.

Median Effective Prior (and 95% HPD): 7.4 Mya (3.4–15.9 Mya).

Justification: *Dasyurus* †*dunmalli* and †*Archerium chinchillensis* from the Chinchilla Local Fauna (Bartholomai, 1971; Wroe and Mackness, 1998, 2000a, 2000b; Louys and Price, 2015) appear to be members of the tribe Dasyurini sensu Kealy and Beck (2017: table 1), in which case they must postdate the first split within Dasyurinae, which is between Dasyurini and Phascogalini. The Chinchilla Local Fauna is estimated to date to approximately 3.4 Mya based on biostratigraphy (Tedford et al., 1992; Montanari et al., 2013), so this provides our

minimum bound for this node. Black et al. (2012: 1020) reported that "probable phascogalines and dasyurines" (= phascogalins and dasyurins sensu Kealy and Beck, 2017: table 1) have been collected from Riversleigh Faunal Zone B (early Miocene) sites, but these specimens have not been described, and so we have not used them to inform our minimum bound here.

Most dasyuromorphians are known from isolated fragmentary dental remains (Archer, 1982, 1984; Long et al., 2002; Wroe, 2003; Archer and Hand, 2006), and there is a lack of compelling dental apomorphies that unambiguously distinguish dasyurins from phascogalins (Archer, 1976, 1982; Kirsch and Archer, 1982; Wroe and Mackness, 1998, 2000a, 2000b; Wroe et al., 2000; Van Dyck, 2002; Krajewski et al., 2004, 2007; Kealy and Beck, 2017). For this reason, and given Black et al.'s (2012: 1020) report of putative early Miocene phascogalins and dasyurins, we use the same maximum bound as for Dasyuromorphia (see above), namely the maximum age of Tiupampa.

Node: Dasyurini

Contents: *Dasycercus*, *Dasykaluta*, *Dasyuroides*, *Dasyurus*, *Myoictis*, *Neophascogale*, *Parantechinus*, *Phascolosorex*, *Pseudantechinus*, *Sarcophilus*.

Minimum Bound: 2.42 Mya.

Maximum Bound: 27.82 Mya.

Median Effective Prior (and 95% HPD): 4.1 Mya (2.4–7.9 Mya).

Justification: Our minimum bound is the minimum age for the Fisherman's Cliff Local Fauna (Whitelaw, 1991a; 1991b), from which putative representatives of extant dasyurin genera are known, namely *Dasyuroides* †*achilpatna* and *Sarcophilus* †*moornaensis* (Marshall, 1973; Archer, 1982; Crabb, 1982). Of these, *Dasyuroides* †*achilpatna* was consistently recovered within Dasyurini (albeit closer to *Dasycercus cristicauda* than to *Dasyuroides byrnei*) in the phylogenetic analyses of Kealy and Beck (2017), and so can be used to place a minimum bound

on the diversification of Dasyurini. *Dasyurus* †*dunmalli* is known from older sites (including the Chinchilla Local Fauna; see Dasyurini + Phascogalini above) but, unlike all extant *Dasyurus* species, this taxon retains P3, raising some questions as to whether it belongs to this genus; we therefore do not use *D.* †*dunmalli* to calibrate this node.

Black et al. (2012: 1020) stated that "probable phascogalines and dasyurines" (= phascogalins and dasyurins sensu Kealy and Beck, 2017: table 1) are present in Riversleigh Faunal Zone B (early Miocene) sites, so the Dasyurini-Phascogalini split may have occurred prior to the early Miocene. Given this, we use the maximum age of the late Oligocene as a conservative maximum bound on the diversification of Dasyurini. Although several dasyuromorphians have been described from late Oligocene Australian sites, none appear to be crown-clade dasyurids (Long et al., 2002; Wroe, 2003; Archer and Hand, 2006; Black et al., 2012; Kealy and Beck, 2017).

Node: †Thylacoleonidae

Contents: †*Lekanoleo*, †*Thylacoleo*, †*Wakaleo*.

Minimum Bound: 15.97 Mya.

Maximum Bound: 65.118 Mya.

Median Effective Prior (and 95% HPD): 24.7 Mya (17.6–33.8 Mya).

Justification: The minimum bound is the minimum age of our oldest thylacoleonid terminal, namely †*Lekanoleo* (see appendix 1). Thylacoleonids, including species of †*Priscileo* and †*Wakaleo*, are known from late Oligocene sites in Australia, indicating that the family had already begun to radiate by this time (Gillespie, 1999; Long et al., 2002; Wroe, 2003; Archer and Hand, 2006; Gillespie, 2007; Black et al., 2012). We use the maximum age of Tiupampa as our maximum bound, following the same rationale used to specify the maximum bound for Dasyuromorphia (see Node: Dasyuromorphia above).

Node: Phascolarctidae

CONTENTS: †*Litokoala*, †*Nimiokoala*, *Phascolarctos*.

MINIMUM BOUND: 15.97 Mya.

MAXIMUM BOUND: 65.118 Mya.

MEDIAN EFFECTIVE PRIOR (AND 95% HPD): 26.9 Mya (18.9–36.3 Mya).

JUSTIFICATION: The minimum bound is the minimum age of our oldest phascolarctid terminal, namely †*Nimiokoala* (see appendix 1). Fossil phascolarctids are known from late Oligocene sites in Australia, indicating that the family had already begun to radiate by this time (Black, 1999; Long et al., 2002; Archer and Hand, 2006; Black et al., 2012, 2014a). We use the maximum age of Tiupampa as our maximum bound, following the same rationale used to specify the maximum bound for Dasyuromorphia (see above).

Node: *Lasiorhinus* + *Vombatus* + †*Warendja*

CONTENTS: *Lasiorhinus*, *Vombatus*, †*Warendja*.

MINIMUM BOUND: 3.62 Mya.

MAXIMUM BOUND: 27.82 Mya.

MEDIAN EFFECTIVE PRIOR (AND 95% HPD): 5.2 Mya (3.6–10.4 Mya).

JUSTIFICATION: The minimum bound is the minimum age of the Bluff Downs Local Fauna (see Peramelidae above), from which the fossil vombatid †*Ramsayia lemleyi* is known (Archer and Wade, 1976; Dawson, 1981; Murray, 1998). Although we have not included †*Ramsayia* as a terminal here, the phylogenetic analyses of Brewer et al. (2018) and Beck et al. (2020) suggested that it is more closely related to the modern genera *Vombatus* and *Lasiorhinus* than to the fossil †*Warendja*. If so, then †*R. lemleyi* must postdate the divergence between †*Warendja* and the *Vombatus-Lasiorhinus* lineage. We have not used the Riversleigh Faunal Zone D (late Miocene) †*Warendja encorensis* described by Brewer et al. (2007) to calibrate this divergence because that taxon is known only from isolated teeth and its similarities

to the Pleistocene †*W. wakefieldi* may be plesiomorphic; indeed, †*W. encorensis* and †*W. wakefieldi* did not consistently form a clade in the phylogenetic analysis of Brewer et al. (2018).

All three vombatid terminals included here, namely *Lasiorhinus*, *Vombatus*, and *Warendja*, are hypselodont. Assuming a single origin of hypselodonty within Vombatidae (Brewer, 2008; Brewer et al., 2015, 2018; Beck et al., 2020), these three taxa cannot have diverged prior to the acquisition of hypselodonty in Vombatidae. The oldest hypselodont vombatid, †*Warendja encorensis*, is late Miocene in age (Brewer et al., 2007), providing a minimum age for the origin of vombatid hypselodonty. Several older, nonhypselodont vombatids are known, the oldest of which may be late Oligocene in age (Brewer, 2008; Brewer et al., 2018). Based on this, we use the maximum age of the late Oligocene (Cohen et al., 2013 [updated]) as a maximum bound.

Node: †Diprotodontidae

CONTENTS: †*Neohelos*, †*Ngapakaldia*, †*Nimbadon*, †*Silvabestius*.

MINIMUM BOUND: 15.97 Mya.

MAXIMUM BOUND: 65.118 Mya.

MEDIAN EFFECTIVE PRIOR (AND 95% HPD): 27.2 Mya (19.6–36.1 Mya).

JUSTIFICATION: The minimum bound is the minimum age of our oldest diprotodontid terminals, namely †*Ngapakaldia* and †*Silvabestius* (see appendix 1). Diprotodontids are known from late Oligocene sites in Australia, indicating that the family had already begun to radiate by this time (Black and Mackness, 1999; Long et al., 2002; Archer and Hand, 2006; Black, 2008; Black et al., 2012). We use the maximum age of Tiupampa as our maximum bound, following the same rationale used to specify the maximum bound for Dasyuromorphia (see above).

Node: Macropodiformes

CONTENTS: †Balbaridae, †*Ekaltadeta*, Hypsiprymnodontidae, Macropodidae, and Potoroidae.

Minimum Bound: 23.6 Mya.

Maximum Bound: 65.118 Mya.

Median Effective Prior (and 95% HPD): 30.5 Mya (23.6–40.1 Mya).

Justification: We scored our balbarid macropodiform terminal †*Ganawamaya* based on material of †*G. gillespiae* from Riversleigh Faunal Zone B (early Miocene) sites (see appendix 1). However, an older species, †*G. couperi*, is known from the late Oligocene, namely the Riversleigh Faunal Zone A White Hunter site and the Ngapakaldi Local Fauna in the Etadunna Formation of South Australia (Cooke, 1997a; Butler et al., 2018). Metzger and Retallack (2010) estimated the Etadunna Formation to span 26.1–23.6 Mya; we use the minimum age as our minimum bound for the diversification of Macropodiformes sensu den Boer and Kear (2018). Numerous other fossil macropodiforms are known from late Oligocene Australian sites, indicating that the clade had already begun to radiate by this time (Flannery and Rich, 1986; Long et al., 2002; Cooke, 2006; Butler et al., 2017; den Boer and Kear, 2018). We use the maximum age of Tiupampa as our maximum bound, following the same rationale used to specify the maximum bound for Dasyuromorphia (see above).

Node: Macropodidae + Potoroidae

Contents: Macropodidae, and Potoroidae.

Minimum Bound: 17.790 Mya.

Maximum Bound: 65.118 Mya.

Median Effective Prior (and 95% HPD): 23.3 Mya (18.4–29.7 Mya).

Justification: Calibrating divergences within Macropodiformes is difficult because of ongoing uncertainty regarding relationships of various fossil taxa to the three crown lineages: Macropodidae, Potoroidae, and the sole extant hypsiprymnodontid, *Hypsiprymnodon moschatus*. However, the fossil "bulungamayine" macropodiform †*Ganguroo bilamina* has been recovered as a macropodid (and usually outside crown-clade Macropodidae) in most published phylogenetic analyses (Kear et al., 2007;

Kear and Pledge, 2008; Prideaux and Warburton, 2010; Prideaux and Tedford, 2012; Black et al., 2014b; Phillips, 2014; Cooke et al., 2015; Travouillon et al., 2015a, 2016, 2022; Butler et al., 2016, 2018; Cascini et al., 2019). We scored our †*Ganguroo* terminal based on specimens of †*G. bilamina* from Riversleigh Faunal zones B and C (see appendix 1), and therefore assigned it an age range spanning the entire early and middle Miocene, following the recommendations of Püschel et al. (2020). However, one of the Riversleigh Faunal Zone B sites from which †*G. bilamina* is known, Neville's Garden Site (Travouillon et al., 2014b; Butler et al., 2017), has been radiometrically dated as 17.85 ± 0.06 Mya (Woodhead et al., 2014), and we use the minimum age for this site as the minimum bound for the divergence between Macropodidae and Potoridae.

Butler et al. (2017: supplementary data file 3) listed a new species of †*Ganguroo* as present in Riversleigh Faunal Zone A White Hunter Site, which is currently interpreted as late Oligocene (see appendix 1). Also of relevance is the fossil macropodiform †*Gumardee*, which has been proposed to be potoroid (Flannery et al., 1983, 1984; Travouillon et al., 2016), and species of which are known from Riversleigh Faunal Zone A sites (Flannery et al., 1983, 1984; Travouillon et al., 2016). Thus, the divergence between Macropodidae and Potoroidae may date to the late Oligocene or earlier. However, the White Hunter †*Ganguroo* species is currently undescribed, and monophyly of †*Ganguroo* has not been supported in published phylogenetic analyses (Travouillon et al., 2014b, 2016; Butler et al., 2016, 2018), while the position of †*Gumardee* varies in published phylogenetic analyses (Butler et al., 2016, 2018; Travouillon et al., 2016); thus, we have not used these late Oligocene taxa for calibration purposes here. Nevertheless, it is plausible that this node predates the late Oligocene, and so we use the maximum age of Tiupampa as our maximum bound, following the same rationale used to specify the maximum bound for Dasyuromorphia (see above).

Node: Macropodidae

CONTENTS: †*Bohra*, *Dendrolagus*, *Dorcopsis*, *Dorcopsulus*, †*Ganguroo*, †*Hadronomas*, *Lagorchestes*, *Lagostrophus*, *Macropus*, *Notamacropus*, *Onychogalea*, *Osphranter*, *Petrogale*, †*Rhizosthenurus*, *Setonix*, *Thylogale*, and *Wallabia*.

MINIMUM BOUND: 17.79 Mya.

MAXIMUM BOUND: 65.118 Mya.

MEDIAN EFFECTIVE PRIOR (AND 95% HPD): 20.0 Mya (17.8–24.7 Mya).

JUSTIFICATION: We use the same minimum bound for Macropodidae as for Macropodidae + Potoroidae (see above), based on the minimum radiometric age of material of the "bulungamayine" macropodid †*Ganguroo bilamina* from Neville's Garden Site at Riversleigh World Heritage Area (Travouillon et al., 2014b; Woodhead et al., 2014; Butler et al., 2017). Butler et al.'s (2017: supplementary data file 3) report of an undescribed species of †*Ganguroo* from Riversleigh Faunal Zone A White Hunter Site. This means that diversification of the macropodid taxa included in our analysis could have begun in the late Oligocene or earlier, but we do not use the White Hunter †*Ganguroo* species for calibration purposes here, for the same reasons discussed for Macropodidae + Potoroidae (see above). Nevertheless, it is plausible that this node (like Macropodidae + Potoroidae) predates the late Oligocene, and so we use the maximum age of Tiupampa as our maximum bound, following the same rationale used to specify the maximum bound for Dasyuromorphia (see above).

Node: Macropodinae

CONTENTS: †*Bohra*, *Dendrolagus*, *Dorcopsis*, *Dorcopsulus*, *Lagorchestes*, *Macropus*, *Notamacropus*, *Onychogalea*, *Osphranter*, *Petrogale*, *Setonix*, *Thylogale*, and *Wallabia*.

MINIMUM BOUND: 4.45 Mya.

MAXIMUM BOUND: 27.82 Mya.

MEDIAN EFFECTIVE PRIOR (AND 95% HPD): 8.2 Mya (4.5–14.8 Mya).

JUSTIFICATION: Fossil representatives of modern macropodine genera (e.g., *Thylogale* †*ignis*) have been described from the Hamilton Local Fauna (Flannery et al., 1992), which has a minimum age of 4.46 ± 0.1 Mya based on potassium-argon dating of an overlying basalt (Turnbull et al., 2003); we use this as a minimum bound here. As noted above (see Macropodidae + Potoroidae and Macropodidae), an undescribed species of the probable stem-macropodid †*Ganguroo* has been reported from the Riversleigh Faunal Zone A White Hunter Site, suggesting that Macropodidae and Potoroidae may have diverged by the late Oligocene. However, the oldest confidently attested macropodine that has been reported to date is much younger, namely the probable dorcopsin †*Dorcopsoides fossilis* from the late Miocene Alcoota Local Fauna (Woodburne, 1967; Prideaux and Warburton, 2010). We use the maximum age of the late Oligocene (Cohen et al., 2013 [updated]) as the maximum bound here.

Node: *Macropus* sensu lato

CONTENTS: *Macropus*, *Notamacropus*, *Osphranter*, *Wallabia*.

MINIMUM BOUND: 3.62 Mya.

MAXIMUM BOUND: 11.63 Mya.

MEDIAN EFFECTIVE PRIOR (AND 95% HPD): 4.6 Mya (3–6.7.1 Mya).

JUSTIFICATION: *Osphranter* †*pavana*, is known from the Bluff Downs Local Fauna (Bartholomai, 1978b; Flannery and Archer, 1984; Dawson and Flannery, 1985), which has been dated as a minimum of 3.62 Mya (Mackness et al., 2000) and so provides a minimum bound on the diversification of *Macropus* sensu lato. Numerous macropodids have been described from the Miocene (Cooke, 1997b; Cooke and Kear, 1999; Kear and Cooke, 2001; Long et al., 2002; Prideaux, 2004; Cooke, 2006; Black et al., 2012; Butler et al., 2017; Couzens and Prideaux, 2018), but none are members of *Macropus* sensu lato, and Couzens and Prideaux (2018) argued based on fossil evidence that the modern macropodin genera (the *Macropus* sensu lato genera *Macropus*, *Notamacropus*, *Osphranter*, and *Wallabia*, plus *Lago-*

rchestes, *Onychogalea*, and *Setonix*) probably originated during the early Pliocene. As discussed above (see Macropodinae), the oldest well-attested crown-clade macropodid is the late Miocene †*Dorcopsoides fossilis*, and so we use the maximum age of the late Miocene (Cohen et al., 2013 [updated]) as the maximum bound for this node.

Node: Phalangeridae + Burramyidae

Contents: Burramyidae, and Phalangeridae.
Minimum Bound: 23.6 Mya.
Maximum Bound: 65.118 Mya.
Median Effective Prior (and 95% HPD): 25.7 Mya (23.6–32.0 Mya).
Justification: The oldest definitive phalangerid is †*Eocuscus sarastamppi* from the Ditjimanka Local Fauna, in Faunal Zone B of the Etadunna Formation (Case et al., 2008). As discussed above (see Macropodiformes), Metzger and Retallack (2010) estimated the Etadunna Formation as spanning 26.1–23.6 Mya, and we use the minimum age as our minimum bound here. We use the maximum age of Tiupampa as our maximum bound, following the same rationale used to specify the maximum bound for Dasyuromorphia (see above).

Node: Petauroidea

Contents: Acrobatidae, Petauridae, Pseudocheiridae, and Tarsipedidae.
Minimum Bound: 23.6 Mya.
Maximum Bound: 65.118 Mya.
Median Effective Prior (and 95% HPD): 28.0 Mya (23.9–35.5 Mya).
Justification: Pseudocheirids are known from the Etadunna Formation (Woodburne et al., 1987; Roberts, 2008; Roberts et al., 2009), so we use the same minimum and maximum bounds as for Phalangeridae + Burramyidae (see above).

Node: Petauridae + Pseudocheiridae

Contents: Petauridae, and Pseudocheiridae.
Minimum Bound: 23.600 Mya.
Maximum Bound: 65.118 Mya.
Median Effective Prior (and 95% HPD): 25.1 Mya (23.6–28.8 Mya).
Justification: Pseudocheirids are known from the Etadunna Formation (Woodburne et al., 1987; Roberts, 2008; Roberts et al., 2009), so we use the same minimum and maximum bounds as for Phalangeridae + Burramyidae (see above).

Node: Pseudocheiridae

Contents: *Hemibelideus*, *Petauroides*, *Petropseudes*, *Pseudocheirus*, *Pseudochirops archeri*, *Pseudochirops cupreus*, *Pseudochirulus*.
Minimum Bound: 4.45 Mya.
Maximum Bound: 27.82 Mya.
Median Effective Prior (and 95% HPD): 7.1 Mya (4.5–16.8 Mya).
Justification: Revisionary work by Roberts (2008) in her unpublished Ph.D. thesis indicates that the oldest definitive crown-clade pseudocheirids are from the Hamilton Local Fauna (Turnbull and Lundelius, 1970), which has a minimum age of 4.45 Mya (see Macropodinae above) and therefore provides a minimum bound for this node. We use the maximum age of the late Oligocene as a conservative maximum bound, as all late Oligocene pseudocheirids appear to be stem forms (Roberts, 2008) and this markedly predates the maximum estimate for the age of this divergence from published molecular-clock studies (e.g., Meredith et al., 2009, 2010; Mitchell et al., 2014).

ON THE COVER: THE RED KANGAROO (*OSPHRANTER RUFUS*) IS THE LARGEST LIVING MARSUPIAL AND AN ICON OF THE SAHULIAN MARSUPIAL RADIATION (ILLUSTRATION FROM GOULD, 1863).